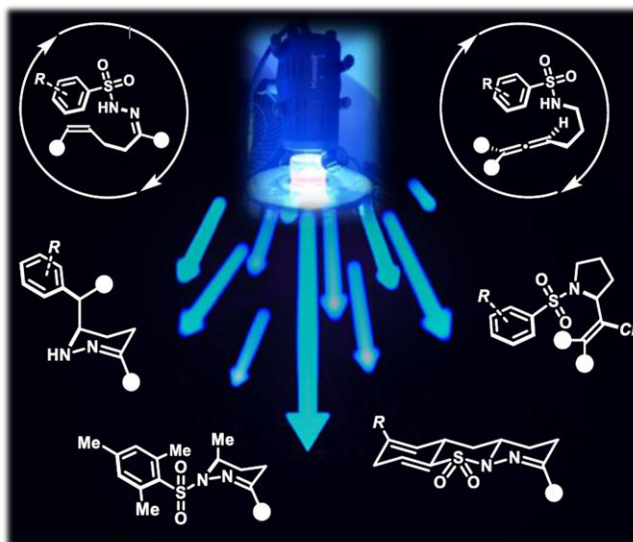**Università degli Studi di Torino**
Doctoral School of the University of Torino
PhD Programme in Chemical and Materials Sciences XXXIV Cycle

Visible-Light Mediated Reactivity of γ,δ-Unsaturated *N*-Arylsulfonylhydrazones and *N*-Allenylsulfonylamides: an Approach to Structurally Diverse Tetrahydropyridazines and Chlorovinylpyrrolidines

Emanuele Azzi

Supervisor:
Prof. Annamaria Deagostino

Università degli Studi di Torino

Doctoral School of the University of Torino
PhD Programme in Chemical and Materials Sciences XXXIV cycle

Candidate: **Emanuele Azzi**

Supervisor: Prof. **Annamaria Deagostino**

Jury Members: Prof. **Cristina Prandi**
                     Università di Torino
                     Dipartimento di Chimica

                     Prof. **Pier Giorgio Cozzi**
                     Università di Bologna Alma Mater Studiorum
                     Dipartimento di Chimica "Giacomo Ciamician"

                     Dr. **Manuel Nappi**
                     Universidade de Santiago de Compostela
                     Centro Singular de Investigación en Química Biológica y
                     Materiales Moleculares (CIQUS)

Head of the Doctoral School: Prof. Alberto Rizzuti
PhD Programme Coordinator: Prof. Bartolomeo Civalleri

Torino, 2022

"One has to be sane to think clearly, but one can think deeply and be quite insane"

Nikola Tesla

TABLE OF CONTENTS

V

PREFACE

The dissertation herein presented describes the results of my PhD project aiming to demonstrate the potentiality of light generated nitrogen centered radical intermediates in the synthesis of saturated heterocycles. Two main projects defined my doctoral studies: the cyclization of *N*-arylsulfonylhydrazones under photoredox conditions and the photocatalytic chlorocyclization of sulfonylamidoallenes. Both projects relied on the use of photocatalysis to achieve nitrogen centered radical species delivering (partially) saturated nitrogen containing heterocycles upon intramolecular C-N bond formation. Consequently, the general introduction is divided in two chapters. The first provides the general principles of photocatalysis, starting from light-matter interaction, explaining the general principles of transformations involving the excited state of a molecule, to move then to the modern concepts of photoredox chemistry and finally summarizing the generation of radical species under visible light, with dedicated focus on nitrogen centered radicals. The brief second introductory chapter describes the synthetic targets of my studies instead, the nitrogen containing heterocycles. A general explanation of their desirable biological features and a presentation of the classical, non-radical, strategies commonly employed for their synthesis is furnished.

The antithesis between the radical chemistry presented in the first chapter and the polar chemistry of the second one is debated throughout this thesis. The fundamental role of light and photocatalysis in the development of a parallel chemistry disclosing otherwise inaccessible pathways and outcomes is defined. Therefore, at the beginning of each chapter, a more detailed introduction on the specific topic will be provided, and both thermal and radical methodologies to achieve the target molecular scaffold will be reported.

CHAPTER ONE:

INTRODUCTION

ح

حمم

PHOTOCHEMISTRY FOR ORGANIC SYNTHESIS

CHAPTER 1 INTRODUCTION - PHOTOCHEMISTRY FOR ORGANIC SYNTHESIS

1.1 Photochemistry

The primary feature that distinguishes photochemistry from the other branches of chemistry is the generation of an electronically excited molecular species upon photon absorption.[1] Thus, photochemistry can be defined as a description of the chemical and physical changes originated by interactions between matter and light.[2,3] The Grötthus-Draper Law (also called "the Principle of Photochemical Activation") and the Stark-Einstein Law are the two fundamental principles of photochemistry adopted to rationalize every photochemical transformation:

Grötthus-Draper Law: "*Only the light which is absorbed by a chemical entity is effective in bringing about chemical change*"[1]

Stark-Einstein Law: "*The primary act of light absorption by a molecule is a one quantum process*" or "*Each quantum of light that is absorbed by a molecule will cause a (primary) chemical or physical reaction in that molecule*"[4]

In addition to these two main principles, the formulation and the development of quantum theory provided the essential means to describe and predict such changes.

1.1.1 Interaction between organic molecules and light

The underlying phenomenon of every photochemical transformation is the absorption of light by the matter. Given the dual nature of electrons in matter, being characterized by both wavelike and particle like properties, such event is described as the encounter of a photon with a molecule of matter.

---

[1] Wardle, B., *Principles and Applications of Photochemistry*. John Wiley & Sons: Manchester **2009**.
[2] McNaught, M.; Wilkinson, A., *IUPAC. Compendium of Chemical Terminology ("Gold Book")*. Blackwell Scientific Publications: Oxford **1997**.
[3] Braslavsky, S. E. *Pure Appl. Chem.* **2007**, *79*, 293-465.
[4] Cox, A.; Kemp, T. J., *Introductory Photochemistry*. McGraw-Hill: London **1971**.

The photon, also defined as light quantum, is a particle possessing a quantum of energy of the electromagnetic radiation and when this energy value is coincident to the energy difference between two electronic states of the absorbing species of matter, the absorption of light occurs. Thus, the quantum of energy carried by the photon is completely consumed to transfer an electron from a lower energy level of the absorbing molecule to a higher one. Consequently, an electronically excited species is generated, and the energy of the photon becomes part of the total energy of such species. It means that absorbing molecules are characterized with electronically excited states endowed with an excess of energy. The lifetime of these excited states is short, and this excess of energy is dissipated by the system to return to a ground state electronic configuration.[1,5]

1.1.1.1 Deactivation processes of excited organic molecules

Dissipative events involving an excited state are defined as deactivation processes which occur with the return of the excited species to its original ground state as a purely physical dissipative process. However, dissipative processes leading to the formation of a new molecular species, thus providing a chemical change are also possible. To the aim of this paragraph, the focus is set on the physical deactivation of excited states of organic molecules. These relaxation processes are classified as intramolecular and intermolecular processes.

Intramolecular processes are divided in radiative transitions (involving emission of electromagnetic radiation as dissipation of energy) originating luminescence phenomenon (fluorescence and phosphorescence) and radiationless transitions.

Intermolecular processes include instead vibrational relaxation, energy transfer and electron transfer.

Vibrational relaxation describes the deactivation process induced by the collisions of the molecules having an excess of vibrational energy with one another and with solvent molecules, thus producing molecules collocated in the lowest vibrational level of a determined electronic energy level.

The electron transfer event or photoinduced electron transfer (PET) is a photophysical process occurring when the photoexcited molecule interacts with another molecule in the ground state. The photo-promoted electron in

---

[5] Wayne, C. E.; Wayne, R. P., *Photochemistry*. Oxford University Press: **2005**.

the upper state might be transferred to another molecule in the ground state. On the other hand, the electron vacancy in the lower energy state generated upon photoinduced promotion might be occupied by an electron transferred from another molecule in the ground state. In both cases an ion pair originates.

The energy transfer allows instead the deactivation by the direct transfer of energy from the species in the electronically excited state acting as the energy donor to another species in its ground state acting as the acceptor. The latter is itself promoted to a higher electronic state and may undergo the same photophysical deactivation events described so far.
Energy Transfer and Electron Transfer are the two main deactivation processes exploited in photochemistry and photoredox chemistry to trigger organic reactions and will be discussed in detail in this dissertation.

1.1.1.2 The Jablonski Diagram

The Jablonski diagram (Scheme 1.1) appropriately describes and summarizes the deactivation processes and the behavior of molecules in their excited states.[1,6,7]

The diagram depicts the electronic states (and their relative energies) of a given species. Upon light absorption, the molecule is promoted from its singlet ground state S_0 (v=0) to an upper excited state (a singlet S_2 state in the case depicted). The reached electronically excited state may be a "vibrationally-hot" (v>0) level. In this case, this excited molecule is associated with an energy value given by the sum of its electronic energy and the excess of vibrational energy. The molecule will then dissipate this exceeding vibrational energy as heat *via* vibrational relaxation. This process is represented with vertical wavy arrows going from a level with v>0 to a level with v=0 (e.g. from S_2(v=5) to S_2(v=0)) and occurs when the excited molecule collides with other species. This process occurs in a 10^{-13}-10^{-9} seconds timescale.

---

[6] Jablonski, A. *Nature* **1933,** *131*, 839-840.
[7] Zimmermann, J.; Zeug, A.; Röder, B. *Phys. Chem. Chem. Phys.* **2003,** *5*, 2964-2969.
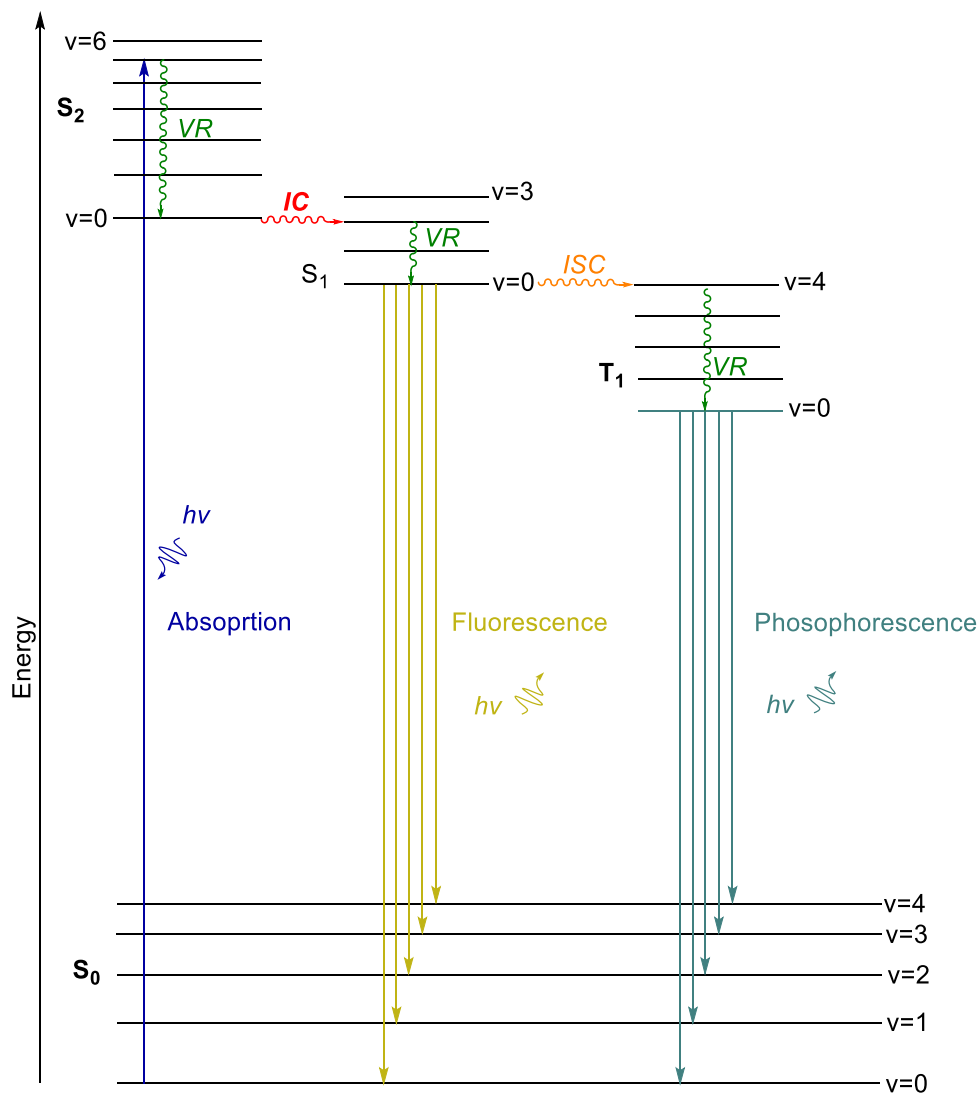
Scheme 1.1 Jablonski Diagram depicting photo physical deactivation of excited states of organic molecules. Singlet electronic states indicated as S_0, S_1, S_2, triplet electronic states indicated as T_1. Vibrational levels associated with each state is indicated as v=0, v=1, v=2, in order of increasing energy. Radiative Transitions are drawn as straight vertical arrows, radiationless transitions are drawn as horizontal (internal conversion IC and intersystem crossing ISC) or vertical (vibration relaxation VR) wavy arrows.

Given the relatively small difference in energy between vibronic states of the excited states, it might be possible for two vibronic states of the same total energy of two different upper excited states with the same spin multiplicity to have the same total energy (isoenergetic, e.g. $S_2(v=0)$ and $S_1(v=2)$). Thus, the radiationless transition of internal conversion (IC) occurs leading to energy transfer between these two electronic levels and is represented with a horizontal wavy arrow. The timescales for these transitions between excited state are in the order of 10^{-14}-10^{-11} seconds, dramatically increasing for internal conversion from S_1 to ground state S_0 (10^{-9}-10^{-7} seconds).

It is noteworthy that vibrational relaxation still occurs in each excited state. This leads to the observation of another kind of radiationless intramolecular transition between isoenergetic states: intersystem crossing (ISC), occurring between two vibronic states with different spin multiplicity but same total energy (e.g. $S_1(v=0)$ and $T_1(v=4)$) with timescale of 10^{-11} - 10^{-8} seconds.

According to the timescales of the transitions observed so far, it is important to highline how, regardless of which excited state is generated upon light absorption, internal conversion and vibrational relaxation processes are so rapid that the excited species will inevitably relax to the most persistent $S_1(v=0)$ excited state. From this state, the radiative processes of fluorescence and the radiationless ISC become competitive. Consequently, luminescence emissions and chemical reactions induced by photoexcited species are ascribable to the v=0 level of the lowest excited singlet S_1 or triplet T_1 excited state, given the quick rate of deactivation of the upper vibrational states. This paradigm is known as the Kasha's Rule,[8,9,10] stating that:

"*Polyatomic molecular entities luminesce with appreciable yield occurs only from the lowest excited state of a given multiplicity. There are exceptions to this rule.*" [11]

---

[8] Kasha, M. *Chem. Rev.* **1947,** *41*, 401-419.
[9] Kasha, M. *Discuss. Faraday Soc.* **1950,** *9*, 14-19.
[10] Kasha, M. *J. Chem. Educ.* **1984,** *61*, 204.
[11] Braslavsky, S. E. *Pure Appl. Chem.* **2007,** *79*, 293-465.

The luminescence processes allow the deactivation of the excited species by photon emission with the unique difference that fluorescence is spin-allowed and occurs between states of the same multiplicity (e.g. from $S_1(v=0)$ to $S_0(v=n)$, timescales 10^{-12}-10^{-6} seconds) whereas phosphorescence is spin forbidden and slower (e.g. from $T_1(v=0)$ to $S_0(v=n)$, timescales 10^{-3}-10^2 seconds):

Fluorescence: $S_1(v=0) \rightarrow S_0 + h\nu$

Phosphorescence: $T_1(v=0) \rightarrow S_0 + h\nu$
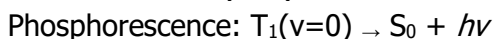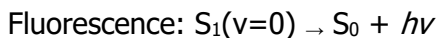
Table 1.1 Summary of timescales for photophysical processes[12]

Process	Type	Time Scale ($t = 1/k_{process}$) seconds
Absorption	Radiative	10^{-15}
Internal Conversion *IC* (between excited states)	Radiationless	$10^{-14} - 10^{-11}$
Internal Conversion *IC* ($S_1 \rightarrow S_0$)	Radiationless	$10^{-9} - 10^{-7}$
Intersystem Crossing *ISC* ($S \rightarrow T$)	Radiationless	$10^{-11} - 10^{-8}$
Vibrational Relaxation *VR*	Radiationless	$10^{-13} - 10^{-9}$
Fluorescence	Radiative	$10^{-12} - 10^{-6}$
Phosphorescence	Radiative	$10^{-3} - 10^2$

1.1.2 Intermolecular processes of excited states

The study of Jablonski Diagram predicts and describes all the possible physical pathways leading to the deactivation of a photoexcited species. Nevertheless, these radiationless and radiative events of deactivation are unimolecular processes. An extensive range of deactivation processes is provided when interactions with another molecule are considered. Every molecular species able to increase the deactivation rate of an electronically excited species is defined as a "quencher", thus this intermolecular deactivation is known as "quenching".

1.1.2.1 Intermolecular Energy Transfer (EnT)

In an intermolecular Energy Transfer (EnT), a photoexcited species indicated as Donor D, transfer its exceeding energy to another species defined as acceptor A. A is the quencher, and it is therefore promoted to an excited state, while D dissipates the energy reaching a lower electronic energy thanks

---

[12] Valeur, B., *Molecular Fluorescence: Principles and Applications*. Wiley-VCH Verlag GmbH: Weinheim **2001**.

to this transfer (Scheme 1.2). The process is also defined as the photosensitization of A, since the photoexcitation of D is transferred to A.

a) $D^* + A \longrightarrow D + A^*$

b) $^1D^* + {}^1A \longrightarrow {}^1D + {}^1A^*$

c) $^3D^* + {}^1A \longrightarrow {}^1D + {}^3A^*$
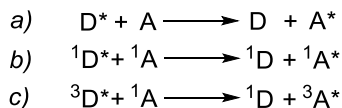
Scheme 1.2 *a)* general reaction of energy transfer; *b)* singlet-singlet energy transfer; *c)* triplet-triplet energy transfer process[13]

A particular kind of energy transfer, called "trivial" mechanism, might occur when the emission from the excited donor matches the energy gap between the ground state and an upper excited state of the acceptor A resulting in the absorption of this radiation emitted from the donor D by the acceptor A. Nevertheless, the most common energy transfer processes proceed through nonradiative interactions and are indicated as Förster (through-space) and Dexter (through-bond or "exchange") energy transfer. Despite the different primary physical origins of the reactions, both these mechanisms yield the same couple of products D and A* (Scheme 1.3).[14]
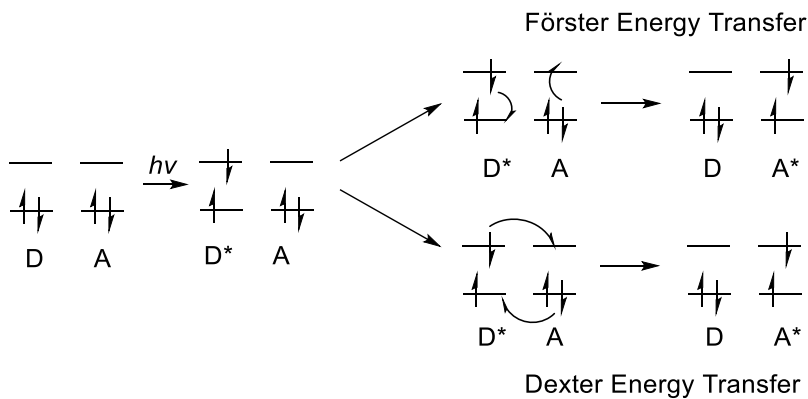
Scheme 1.3 Förster and Dexter energy transfer mechanisms

The Förster energy[15] transfer is driven by a Coulombic interaction and operates up to 10 nm.[16] As D* relaxes to D, the dipole moment created by

---

[13] Wilkinson, F. *J. Phys. Chem* **1962,** *66*, 2569-2574.

[14] Arnaut, L.; Formosinho, S.; Burrows, H., *Chemical Kinetics. From Molecular Structure to Chemical Reactivity*. Elsevier: Amsterdam **2007**.

[15] Főrster, T. *Discuss. Faraday Soc.* **1959,** *27*, 7-17.

[16] Sahoo, H. *J. Photochem. Photobiol. C: Photochem. Rev.* **2011,** *12*, 20-30.

this transition couples with that concomitantly originated by A to A*
transition. The energies of these coupled transitions must be equivalent,
therefore a good spectral overlap between the absorption spectrum of A and
the emitted fluorescence of the D is required determining a resonance
condition. Thus, Förster energy transfer is also indicated as Förster resonance
energy transfer or FRET.

On the contrary, in the Dexter mechanism[17] two simultaneous electron
transfer reactions occur with a through-bond mechanism. Consequently,
Dexter electron transfer is observed only when an orbital overlap between A
and D is possible, circumscribing this interaction to maximum 10 Å distances.
Namely, Dexter process requires physical contacts between A and D, so that
the two species approach until overlap of the two different electron densities,
making electrons exchange possible.[18]

1.1.2.2 Photoinduced Electron Transfer (PET)

The photoinduced electron transfer (PET) is a consequence of a
change in the redox properties due to light absorption. The light-induced
excitation of an electron to an upper electronic energy state has two
consequences: it creates a vacancy in the highest occupied molecular orbital
(HOMO) while concomitantly moving a single electron to the lowest
unoccupied molecular orbital (LUMO). The excited species becomes a better
reducing agent (or electron donor) because of the electron in the LUMO and
at the same a better oxidizing agent (or electron acceptor) due to the vacancy
in the HOMO.[18] Therefore, differently from the molecule in its ground state,
the photoexcited molecule R* might interact with another molecule M to
accept or donate an electron (Scheme 1.4). This is the general mechanism of
an electron transfer, where no formation or breaking of bonds is observed.
Such transformation is defined as an "outer-sphere" electron transfer. In a
PET this electron is transferred between the excited molecule and the ground-
state one, thus requiring the orbital overlap of the two species. In both
oxidative and reductive PET event, an ionic pair is formed.

The interpretations and predictions of PET outcomes are provided by
Marcus Theory of Electron Transfer[19] (Figure 1.1), that describes this

---

[17] Dexter, D. L. *J. Chem. Phys.* **1953,** *21*, 836-850.
[18] Scandola, F.; Indelli, M. T.; Chiorboli, C.; Bignozzi, C. A., *Photoinduced electron and energy transfer in polynuclear complexes*. Springer Berlin **1990**.
[19] Marcus, R. A. *Angew. Chem. Int. Ed.* **1993,** *32*, 1111-1121.

interaction considering the kinetic of the process, the variation of potential energy surfaces and the reorganization energy of the system for bimolecular systems.
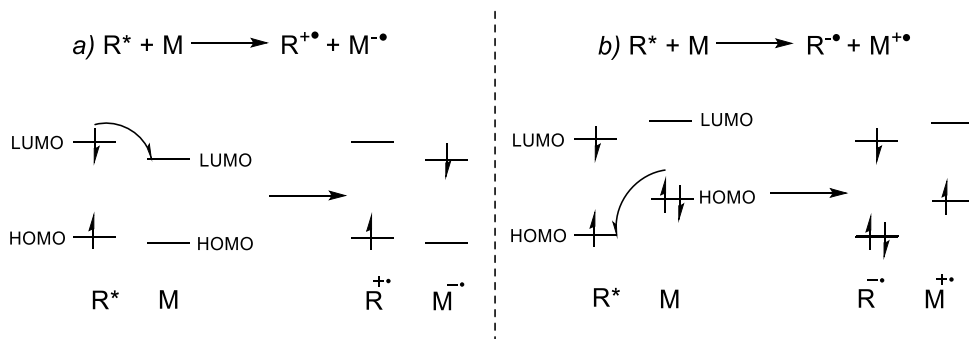
Scheme 1.4 a) Oxidative electron Transfer with representation of molecular orbitals; b) Reductive electron transfer with representation of molecular orbitals

$$k_{eT} = \frac{2\pi}{\hbar} \left|H_{AB}\right|^2 \frac{1}{\sqrt{4\pi\lambda k_B T}} \exp\left[\frac{(-\Delta G^\circ + \lambda)^2}{4\lambda k_B T}\right]$$

λ = reorganization energy
k_B = Boltzmann costant
h = Planck costant
T = Temperature in Kelvin
ΔG° = thermodynamic driving force for electron transfer
H_{AB} = electronic coupling between the donor and the acceptor

Figure 1.1 Electron Transfer Rate according to Marcus Theory

PET and Dexter EnT are almost analogous, anyway, three main differences must be noted. First, the products of Dexter EnT are an excited species and a ground state one, with no charge separation, whereas PET leads to the formation of an ionic pair. Moreover, given the new charge distribution originated in PET, the reorganization energy (involving solvent contributes) has a stronger influence in PET than in Dexter EnT. Finally, Dexter EnT involves the concomitant transfer and exchange of two electrons, hence the distance dependence of the process rate is larger (e^{-2r} for EnT vs e^{-r} for PET).[18]

1.1.3 Selection Rules

Both organic and inorganic molecules can absorb a photon and be promoted to an excited state. However, not all molecules get to their excited states upon absorption of light, even when the energy of the photon matches the gap between the ground state and the upper electronic excited state of the molecular entity considered. Indeed, transitions between energy levels are subject to specific requirements and constraints, referred to as selection rules. That is the reason why not all colored molecules (that are therefore able to visible light) always get to the corresponding excited state upon interaction with light.[1,4,5]

1.1.3.1 Selection Rules for Organic Molecules

The absorption bands in organic molecules result from transitions between molecular orbitals (MO). MO are categorized by the molecular-orbital symmetry labels σ (sigma), π (pi), non-bonding (n) and anti-bonding orbitals indicated with *. There are, in principle, six types of electronic transition, designated σ→ σ*, σ→π*, π→π*, π→σ*, n→σ* and n→π*. However the ones concerning molecular organic photochemistry are the π→π* and n→π* transitions, which produce electronically-excited states (π, π*) and (n, π*), respectively. The intensity of a transition, that is directly associated with the intensity of the absorption peak, is governed by selection rules. For organic molecules, and π→π* and n→π* transitions two main selection rules are applied: the spin selection rule and the orbital symmetry rule. [1,4,5]

The spin selection rule states that an electronic transition takes place with no change in the total electron spin, thus singlet-triplet transitions (e.g. $S_0 \rightarrow T_1$). This rule is derived from quantum mechanical calculations and is affected by the fact that such calculation does not consider the interactions of electrons with other electrons or with nuclei in a molecule. However, the spin of an electron is influenced by its orbital motion, with a phenomena described as Spin–orbit coupling. Consequently, a singlet state can be said to have some triplet character and a triplet state some singlet character with resulting mixing of the states. Therefore, the spin selection rule is not rigidly applied especially in the case of molecules containing atoms of high atomic mass (heavy atom effect). Indeed, an internal heavy atom effect occur when the heavy atom is incorporated in the molecule, thus influencing the spin character of the molecule and enhancing $S_0 \rightarrow T_1$ absorption due to spin–orbit

coupling. An external heavy atom effect could be instead observed when the heavy atom is part of a solvent molecule.

The orbital symmetry selection rule derives from that paradigm of the quantum theory that explains the intensity of absorption by molecules considering the wavefunctions of the initial and final states (ψ and ψ^*, respectively). The rate of absorption is greatest when the coupling between the initial and final states is strongest. Consequently, an electronic transition will proceed most rapidly when ψ and ψ^* most closely resemble each other. Thus, transitions involving a large change in the region of space that the electron occupies are forbidden. It means that an allowed transition will exhibit a large orbital overlap between the ground state and excited state. This explains for instance why π→π* transitions are allowed. Indeed, π and π* orbitals occupy the same regions of space, so overlap between them is large. On the contrary, the orbital overlap between n and π* orbitals that are perpendicular to each other is smaller. n→π* transitions are therefore forbidden. However, as this rule derives from quantum calculations that includes Born–Oppenheimer approximation, it can be broken. Indeed, nuclei of the molecules are not steady, thus, coupling of vibrational and electronic motions can occur. This so-called vibronic coupling provides explanation for transitions prohibited by orbital symmetry.

1.1.3.2 Selection Rules for Inorganic Molecules

Concerning inorganic complexes, the metal complexes of the *d*-block elements are object of this dissertation. They can absorb light due to electronic transitions occurring between *d* orbitals of the metal species (*d-d* transitions), or because of charge transfer within the complex (metal to ligand charge transfer, MLCT, or ligand to metal charge transfer, LMCT).

For a free *d* block atom, all five *d* orbitals are degenerate (all five have the same energy) but for metal complexes of these atoms a difference is observed. Due to the ligand field, the complexes will assume a specific geometrical disposition. For octahedral complexes the five *d*-orbitals are split into two sets: a triply degenerate, lower energy set (t_{2g}) and a doubly degenerate, higher energy set (e_g). As for organic molecules, the intensity of the transitions is dictated by selection rules. For inorganic molecules three rules exist: the spin-, the angular momentum- and the Laporte selection rule.[1,4,5]

The spin selection rule, as reported above, implies that there should be no change in the spin multiplicity albeit weak spin-forbidden bands may occur when spin–orbit coupling is possible. For inorganic complexes, since atoms heavier than the ones usually incorporated in organic molecules (if halogen atoms are not considered) are involved, heavy atoms effect are also relevant. Thus large spin–orbit couplings occur in complexes of heavy metals and intense spin-forbidden transitions are observed.

The angular momentum selection rule states that there should a change in angular momentum quantum number by 1 for a transition to be allowed. Thus *p↔d or d↔f* for instance are allowed, whereas *d↔d* transitions are not allowed.

Finally, the Laporte selection rule is applied to those metal complexes possessing a center of symmetry and forbids transitions between energy levels with the same symmetry with respect to the center of inversion. Thus, transitions such as $t_{2g} \rightarrow e_g$ are not allowed.

These two rules seem to exclude any possibility for *d-d* transitions; and it seems that they should not be indicated as a reason for absorption. However, the Laporte selection rule could not be rigorously applied since some ligands around the metal might disrupt the perfect symmetry theorized in the ligand field theory or if, once again, we consider that molecules are not steady and can vibrates to remove the center of symmetry. The interaction between electronic and vibrational modes is another example of vibronic coupling and means that *d–d* occur, although weakly absorbing. Complexes with tetrahedral symmetry, lacking a center of inversion, allow an easier mixing of the levels, giving more intense transitions.

The other way in which a metal complex absorb light is by charge-transfer transitions, where transfer of an electron from the *d* orbitals of the metal to the ligand or *viceversa* occurs. $Ru(bpy)_3^{2+}$ is a metal complex that will be largely debated in this dissertation and provides an example of MLCT. Upon photoexcitation, a *d* electron is transferred from the ruthenium into the antibonding π* orbitals of a bipyridyl ligand. This transition is allowed by both angular momentum selection rule and Laporte rule. The broad MLCT absorbance results in a good overlap with the wavelength characterizing visible light, thus vast research were dedicated to the study of photophysical behavior of $Ru(bpy)_3^{2+}$.

1.1.4 Pathways of photochemical reactions
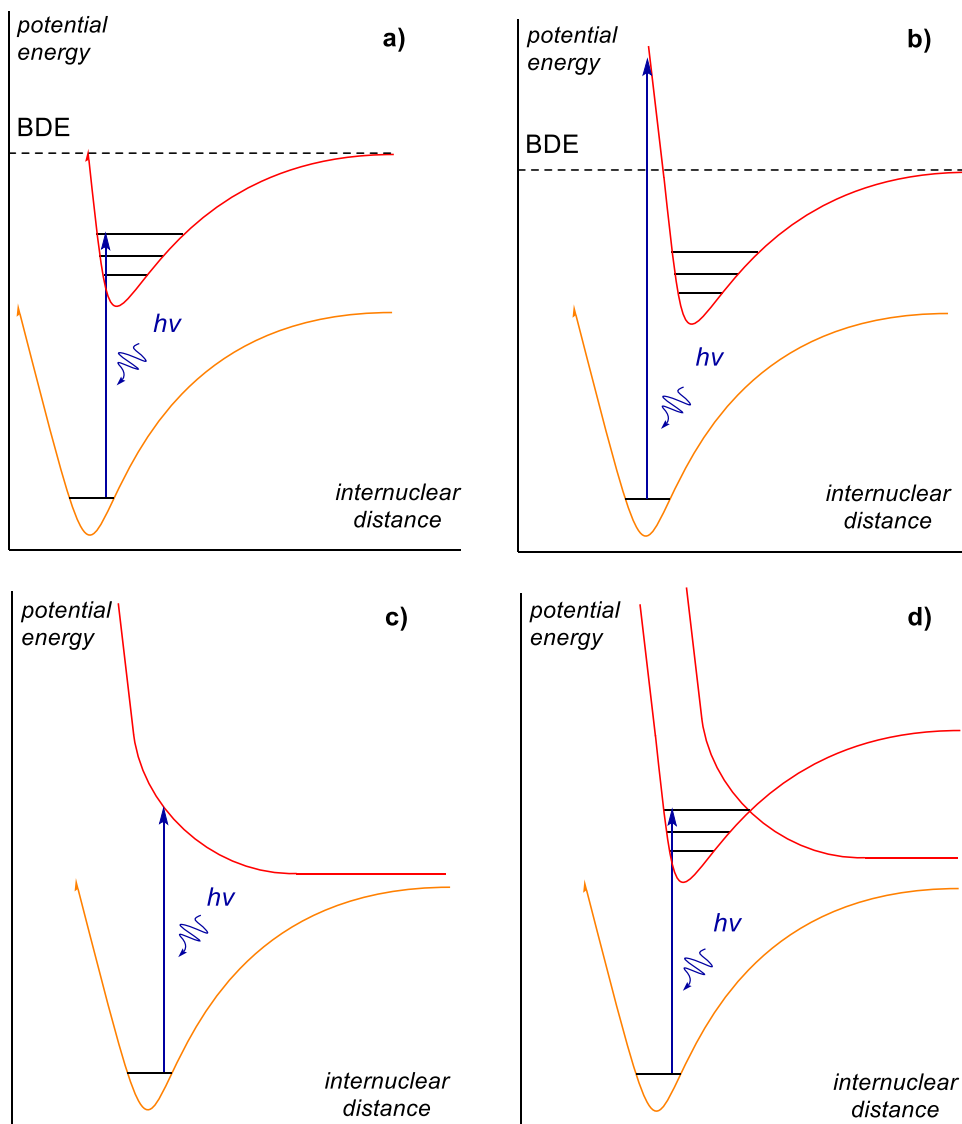
Scheme 1.5 Photon absorption behavior for diatomic molecules represented with Morse Curve: *a)* absorption to upper stable state: vibronic transition; *b)* absorption to a bound excited state with energy greater than the bond dissociation energy (BDE); *c)* absorption to a dissociative state *d)* predissociation: absorption to a stable state followed by crossing to a dissociative one

As stated in Grotthus-Draper and Stark-Einstein Laws, every reaction in photochemistry is initiated by the absorption of a photon. As a result, the reactant entity of a photochemical transformation is a species raised to a higher energy level. Anyhow, this excitation has different final outcomes, that strictly depend on the nature of electronic states of the considered molecule.

The study of Morse curves for diatomic molecules is a good approximation that avoids the use of complex multidimensional potential energy surfaces and allow the identifications of four general types of absorption behaviors (Scheme 1.5).

The simplest case (Scheme 1.5 a) is an electronic transition that promotes the molecule to an excited vibrational state ($v \neq 0$) of an upper electronic state indicated as reported in Scheme 1.6

$$R(v=0) + h\nu \longrightarrow R^*(v=n)$$
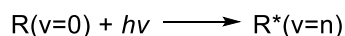
Scheme 1.6 Reaction of photon absorption for R

In a second case (Scheme 1.5 b), the bond in the molecule is cleaved due to light absorption. Indeed, upon promotion, the species reaches a potential energy that is higher that the bond dissociation energy (the value of energy is larger than the one associated with the maximum vibrational level of the molecule) and the first vibration will result in bond rupture.

Another behavior (Scheme 1.5 c) might lead as well to the bond cleavage. When the excited molecule is promoted to an electronic state with no vibrational levels, it has reached the dissociative state. This upper electronic state is characterized by the absence of a minimum and is therefore unstable resulting in bond rupture.

Finally, a molecule might also be promoted to a stable upper electronic state (Scheme 1.5 d). Nevertheless, if another upper electronic state which is unstable (like the dissociative state observed in previous case) exists and if the energy of this state is close to the stable one, the curves for these two electronic states cross at a certain coordinate of internuclear distance. The vibration of the excited molecule will result in meeting this crossing point, thus moving the species to the unstable state. Such behavior is defined as predissociation.

The first behavior (Scheme 1.5 a) is the pathway that leads to the excited molecule and to the several deactivation events described in paragraphs above. The remaining options (Scheme 1.5 b-d) always lead to

bond cleavage. However, these events need to be described considering the Morse potential curve of both the ground state of the molecule and its excited one. Consequently, a single energy surface (or potential curve) is not adequate to represent a photochemical reaction pathway as it might be instead for ground-state reactions. A more detailed representations is given plotting the potential energy surfaces for reactants, intermediates, transition states and products both in the ground-state (R) and in the excited state (R*) *versus* the reaction coordinate (Scheme 1.7).
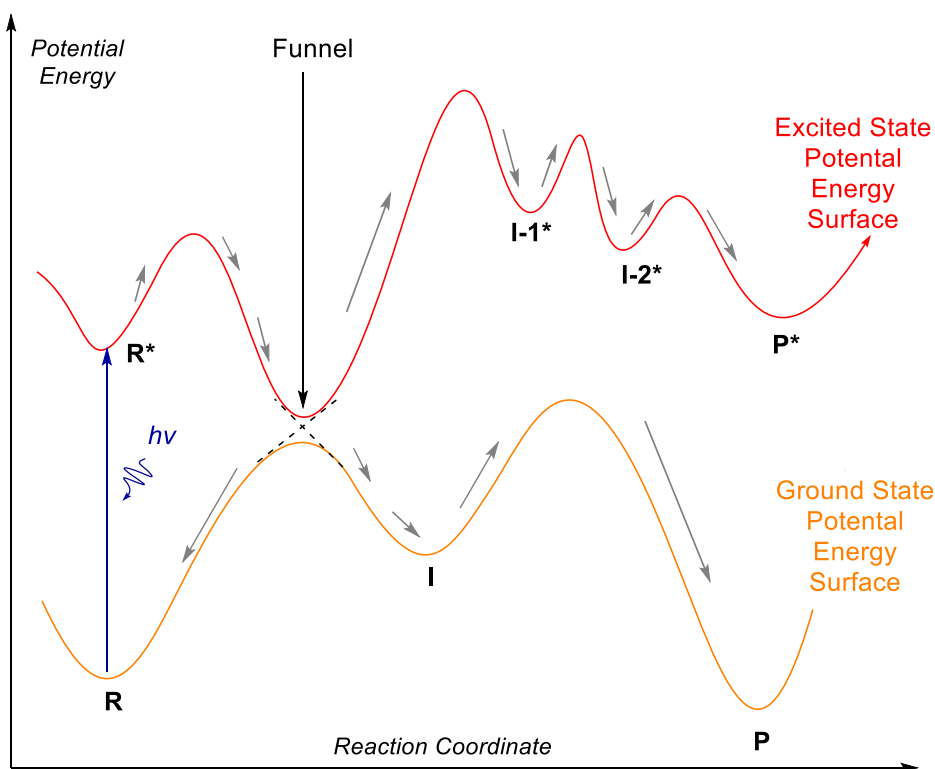
Scheme 1.7 Representation of the potential energy surface (PES) for excited state (red curve) and ground state (orange curve) molecules, providing a conical intersection (CI). PES are simplified as potential curves. The route of a molecule along the reaction coordinate is represented by small grey arrows. R, I, P indicate reagents, intermediates, and products. * indicates a species in the excited state.

The scheme depicts how a photochemical transformation delivering a product in its ground state requires a peculiar crossing from the excited state to the ground state. When the complex and multidimensional potential energy surfaces PES are considered, this crossing is not a point but a region. In such region, the equations for the two surfaces are represented as two geometrical (almost) touching cones. Thus, it is identified as a Conical Intersection (CI) or indicated as the photochemical funnel, providing the delivery to the ground state of an excited intermediate or excited reactant so that it evolves to the ground state product from there.[20] Notably, when the excited molecule **R*** reaches the CI, an alternative pathway where the molecule go backwards towards the reagent R in the ground state is also possible.[21,22]

The pathway of a photochemical reaction is then always initiated by the absorption of a photon from a reactant species **R** that is promoted to an electronically excited state **R***. From this latter, two primary photochemical processes might occur. Either the conversion o **R*** to a product **P** (e.g. some pericyclic reactions, evolving from the singlet state and moving through a cyclic transition state with the concomitant formation and cleavage of both σ- and π-bonds) or the formation of reactive intermediate **I** (or reactive intermediates) that will further react to deliver reaction products. From **I** secondary photochemical processes (also called dark processes) originate, including reactions of radical species, that correspond to the focus of this dissertation.

1.1.5 Comparison between photochemical and thermal reactions

The energy profile of a thermal reaction proceeds starting from a reagent in its ground state that must surmount an energy barrier to provide the product. Along the reaction path, the reagent might climb a first barrier to deliver a reaction intermediate, that upon the overcoming of a second one evolves to the product (Scheme 1.8 a and Scheme 1.8 b).
For thermal transformations, the generation of such intermediates is provided by heating or by treatment with another chemical reactant.

---

[20] Robb, M. A.; Bernardi, F.; Olivucci, M. *Pure Appl. Chem.* **1995,** *67*, 783-789.
[21] Martinez, T. J. *Nature* **2010,** *467*, 412-413.
[22] Polli, D.; Altoè, P.; Weingart, O.; Spillane, K. M.; Manzoni, C.; Brida, D.; Tomasello, G.; Orlandi, G.; Kukura, P.; Mathies, R. A.; Garavelli, M.; Cerullo, G. *Nature* **2010,** *467*, 440-443.
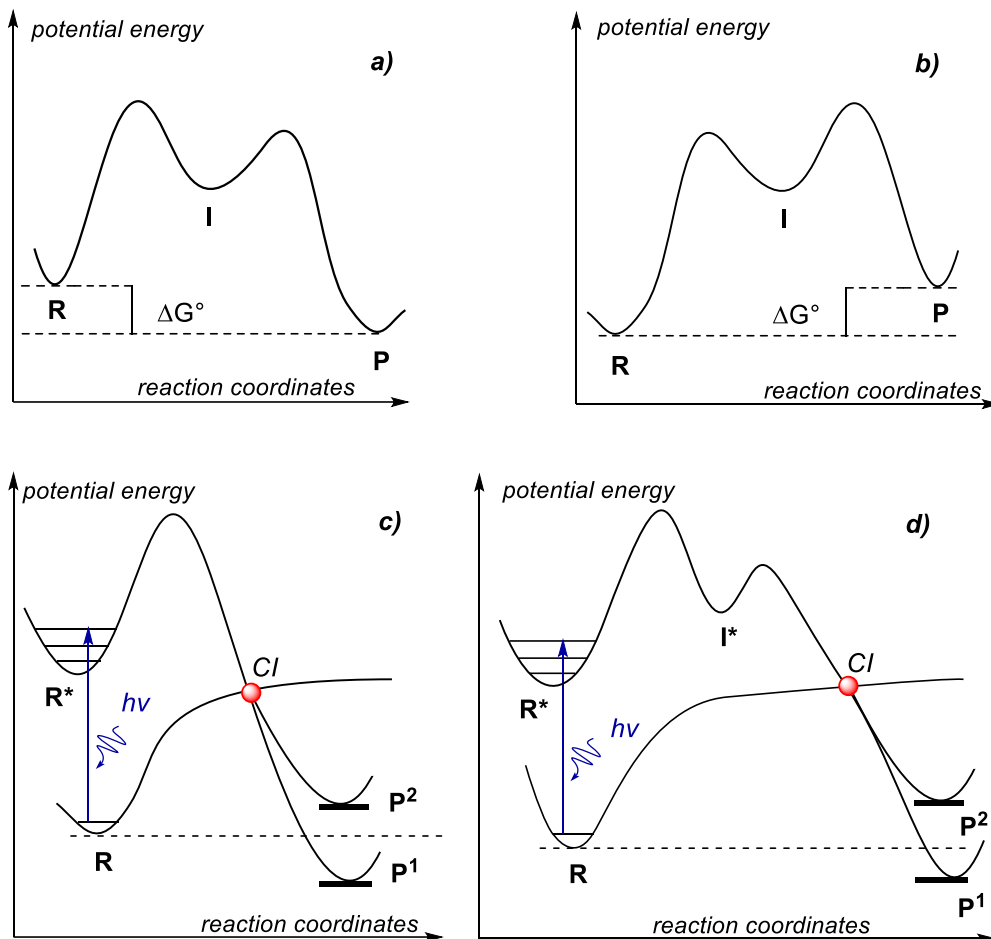
Scheme 1.8 Comparison between energy profiles for a thermal reaction and for photochemical reactions (PES are simplified as potential curves, R=reagent, I=intermediate, P=Product, *=species in the excited state): *a)* energy profile for a favored thermal reaction; *b)* energy profile for an unfavored thermal reaction; *c)* energy profile for a photochemical reaction where R is promoted to R* and may return to the ground state PES through a conical intersection (CI) reaching product P^1, thermodynamically favored, but also P^2 thermodynamically unfavored; *d)* energy profile for a photochemical reaction, similar to the previous case, but R is promoted to R* and needs to pass through the formation of an intermediate I* on the excited state PES to reach the CI

However, it is important to point out that whatever the barrier to overcome is encountered by the chemical system, the latter will always evolve to a configuration associated to the lowest possible energy level. A photochemical transformation is, in contrast, initiated by a reagent reaching its excited state,

thus meaning this species is associated with an energy that is, by definition above, the lowest energy possible for its atomic configuration. The reagent will persist in the excited state, moving along the corresponding PES of the excited state that is characterized by higher energy configurations. It will never reach a configuration associated to the lowest energy level, unless it encounters a CI, allowing to funnel back to the PES of the ground state (Scheme 1.8 c). Note that the pathway where **R*** might rearrange to a high energy intermediate on the PES of the excited state to reach the CI is also possible (Scheme 1.8 d). Notably, in both cases the reaction might deliver both thermodynamically favored and unfavored products.

This leads to three important considerations. First, the promotion to the excited state allows the reagents to reach high energy levels, from where also products that are associated to a value of energy that is higher than that of the ground state reagents are accessible. Thus, even though no heating is provided, thermodynamically unfavored transformations ($\Delta G°>0$) might be observed. Second, moving along the PES of the excited state might lead to the generation of intermediates that are so high in energy, that they would never be observed in thermal conditions. Instead, in photochemical conditions, highly energetic intermediates are observed. This leads to the final consideration, that is at the base of this dissertation and the modern use of photochemistry to generate radical intermediates. Indeed, upon funneling back to the ground state PES, a molecule might reach the configuration of an intermediate **I** that could also be obtained under thermal conditions (Scheme 1.9). It means that photochemistry also allows thermal reaction *via* **I** whose generation would be thermodynamically too expensive. In fact, such **I** is accessible *via* thermal pathway, but that would imply geometrical changes in the configuration of the atoms of the molecule (stretching and breaking of bonds) that only high amount of thermal energy would make possible. Thus, given the large quantity of heat that needs to be provided to the molecule, the generation of such **I** would be slow. On the contrary, photochemical transformations are initiated setting R on a very high energy level upon conversion to its excited state **R***. Moving along the excited state PES, high energy level configurations of the atoms can be considered. In other words, since the starting point (the electronic excited state) is very high in energy, and since that energy is larger than the value required to break covalent bonds between atoms, **R*** lays above the high-energy **I** of thermal

transformation, making them thermodynamically accessible within the short timescales of a photochemical process.[23]

Of course, in this case a new graphical coordinate must be introduced, in order to provide an accurate albeit still simplified description of the energy profile of the reaction.
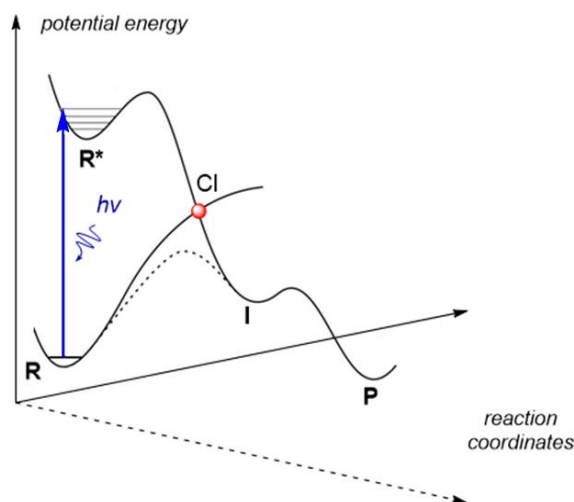
Scheme 1.9 A particular case of a photochemical reaction that shows the need for a further reaction coordinate: R is promoted to the excited state R* and when it crosses the CI, the photochemical path leads to the configuration of an intermediate **I** that can also be formed through a thermal process

1.1.5.1 Main differences between photochemical and thermal reactions

The different representation required to describe a reaction profile is the first main difference reported comparing thermal and photochemical reactions and it reflects many of the dissimilarities between these two classes of transformations.

First, photochemical reactions involve transformations of excited states and are initiated by photon absorption, while thermal ones involve ground-state molecules and are initiated by heat. Consequently, photochemical processes might occur at low temperature since the energy provided by photon absorption is similar to the activation energy for ground-

---

[23] Albini, A.; Fagnoni, M., *Photochemically-Generated Intermediates in Synthesis*. John Wiley & Sons: Hoboken, New Jersey **2013**.

state transformations, which can instead only rely on heat to overcome that barrier.

Second, a photoinduced transition to an electronic excited state entails a different electronic distribution, hence a different geometry of the molecule when compared to its ground state. Generally, a photoinduced promotion of an electron populates an antibonding molecular orbital. Thus, elongated and easier to cleave bonds are provided in the excited species.

Moreover, as reported above, moving an electron to an upper state implies the alteration of the redox properties of the molecule, that becomes a better electron donor and a better electron acceptor in comparison to the corresponding species in the ground state.

Furthermore, from a thermodynamical point of view the promotion of a reactant species R to an excited R* increases the library of accessible products. Indeed, a reaction is thermodynamically favored when the value of Gibbs free energy for the products P is lower than the one for the reactants R. Since photoexcitation implies acquisition of exceeding energy the G° value for reactant R raises becoming R*. This latter has now a G° value that is higher than several products making favored the transformation towards such products.

Finally, photochemistry allows the reaching of a new level of selectivity in chemical transformations. While in thermal processes heat is indiscriminately applied to all reagents, products and media, the quantum nature of light absorption and the wise use of light sources (e.g. monochromatic light) allows selective excitation of a single particular species among all the reaction components.

To conclude, it can be stated that photochemical transformations and photochemical activations of reactant molecules impart reactivity pathways and selectivity strategies that are complementary to the reaction paradigms of thermal processes and that would remain otherwise undisclosed without the use of light.

Remarking the words of the Nobel laureate Noyori, "*photo-synthetic catalysts*" should be developed "*to enhance the power of chemical synthesis by removing current thermodynamic restrictions*" thus facilitating "*thermally unachievable, energetically uphill reaction*".[24]

---

[24] Noyori, R. *Tetrahedron* **2010,** *66*, 1028.

1.2 Organic Photochemistry

The use of light as an essential tool to disclose new reactivities has not been ignored by organic chemists. Together with the fascination due to the new synthetic possibilities provided, the exploitation of light to promote chemical processes has also been contributing to the modern quest towards a "greener" approach to organic transformations. This idea of converting electromagnetic radiation, and in particular solar light into chemical energy, to replace more pollutant energy sources is always associated with the vision anticipated by G. Ciamician more than a century ago:

"On the arid lands there will spring up industrial colonies without smoke and without smokestacks; forests of glass tubes will extend over the plains and lass buildings will rise everywhere; inside of these will take place the photochemical processes that hitherto have been the guarded secret of the plants, but that will have been mastered by human industry which will know how to make them bear even more abundant fruit than nature, for nature is not in a hurry and mankind is. And if in a distant future the supply of coal becomes completely exhausted, civilization will not be checked by that, for life and civilization will continue as long as the sun shines!"[25]

Guided by this inspiration, organic chemistry has recently observed a continuous implementation of photochemical methodologies to deliver synthetic targets. Such methodologies enjoy the green benefits of exploiting the large amount of energy associated to the photons without any production of waste by this radiative energy.

Given the different source and amount of energy involved in photochemical transformations, when compared to thermal ones, new terminologies and definitions must be employed to provide accurate descriptions of these phenomena. Accordingly, a general classification is required for the various chemical pathways that a light-initiated organic reaction might follow.

Historically, a first main division occurred between the *photochemical* process and the *photocatalytic* processes. This distinction was based on the effect of light on the thermodynamic of the chemical transformations. Thus, when light was accelerating a thermodynamically favored process, that would

---

[25] Ciamician, G. *Science* **1912,** *36*, 385-394.

have anyway occurred in the dark, the reaction was indicated as *photocatalytic*. On the other hand, if supplementary energy was required to promote an otherwise thermodynamically unfavored process, and that energy was provided by light and incorporated in the product (which possess a higher G° value than that of the reactant) the reaction was indicated as *photochemical* (Scheme 1.10).[26]

$$R \xrightleftharpoons{h\nu} P \qquad \begin{array}{l} \Delta G < 0 = \textit{Photocatalytic} \\ \Delta G > 0 = \textit{Photochemical} \end{array}$$
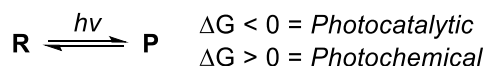
Scheme 1.10 Historical definition of *photocatalytic* and *photochemical* processes based on the effect of light on equilibrium[26]

However, nowadays the term *photocatalysis* is not used antithetically to *photochemistry*, but it indicates instead a subgroup of it. Indeed, photocatalytic processes are photochemical reactions where both light and a chemical entity acting as a catalyst are required. In turn, this latter might be identified as a photocatalyst or as a photosensitizer. A *photocatalyst* is a species that upon light absorption can directly chemically activate a reactant molecule (e.g. by electron transfer). A *photosensitizer* is a molecule that absorbs light and gain an excess of energy that is then physically transferred to a reactant non-absorbing molecule.[27] It is noteworthy that direct photoexcitation and photosensitization both result in the final excitation of a reagent as outcome, even though the second mechanism provides this excitation indirectly.

As previously reported (paragraph 1.1.4), the photoexcitation of the reagent might lead to the formation of a product or to the generation of a reactive intermediate. Whether it is a direct photochemical excitation or a photocatalytic transformation that is analyzed, the energy delivered through the absorption of a photon allows in both cases the generation of very reactive intermediate species from otherwise less reactive or unreactive substrates. Besides, these reactive intermediates are delivered in mild conditions, since all the energy is provided by light and no thermal heating is required.

---

[26] Benrath, A. *Z. Phys. Chem.* **1910,** *74U*, 115-124.
[27] Ravelli, D.; Protti, S.; Albini, A. *Molecules* **2015,** *20*, 1527-1542.

1.2.1. Photogeneration of reactive intermediates

The photochemical approach towards the generation of incipient reactive species brings a major benefit. Since no harsh conditions are required, a better control on the generation of intermediates and in avoiding degradation reactions is possible. Examples of the highly reactive species that can be obtained are radicals, biradicals, radical ions (radical cations or anions) and carbenes;[28] although zwitterions,[28] 1,3-dipoles,[28] as well as unusual species like quinodimethanes[29] and quinone methides[30] are also reported. Carbon-based species might be originated and exploited to provide direct construction of carbon-based molecular bonds and molecular backbones. However also heteroatom-based reactive intermediates can be photogenerated, thus allowing the direct installation of functional groups.

To the aim of this dissertation, only photogeneration of radicals and radical ions will mainly be considered, with a more specific insight into the generation of nitrogen centered radical species.

1.2.2 From traditional thermal radical generation to modern photoinduced radical generation

Open-shell intermediates in organic processes are generally obtained by the homolysis of covalent bonds. This transient species containing an unpaired electron shows an enhanced reactivity due to its instability. Nevertheless, designing an organic transformation aiming to exploit the formation of a radical intermediate to enhance the reactivity of the process might be difficult. Indeed, the classic methods of radical generation always come with some downside.

Commonly, the use of a radical initiator like 2,2'-azobis(isobutyronitrile) (AIBN), organic peroxides, or triethylborane B(Et)$_3$ (in open vessel, air exposure conditions) is required (Scheme 1.11).[31,32] These hazardous initiators might be explosive at high temperature and they are characterized by at least one weak atom-atom bond that can be homolytically cleaved by heating, thus generating a radical species. This latter then triggers a radical chain process leading to the generation of reactive intermediates

---

[28] Ravelli, D.; Protti, S.; Fagnoni, M. *Chem. Rev.* **2016,** *116*, 9850-9913.
[29] Segura, J. L.; Martín, N. *Chem. Rev.* **1999,** *99*, 3199-3246.
[30] Toteva, M. M.; Richard, J. P. *Adv. Phys. Org. Chem.* **2011,** *45*, 39-91.
[31] Curran, D. P. *Synthesis* **1988,** *1988*, 417-439.
[32] O'Mahony, G. *Synlett* **2004,** *2004*, 572-573.

upon the exploitation of the reported radical reactivity: radical additions, radical abstractions or radical eliminations (Scheme 1.12).

a) AIBN thermal decomposition
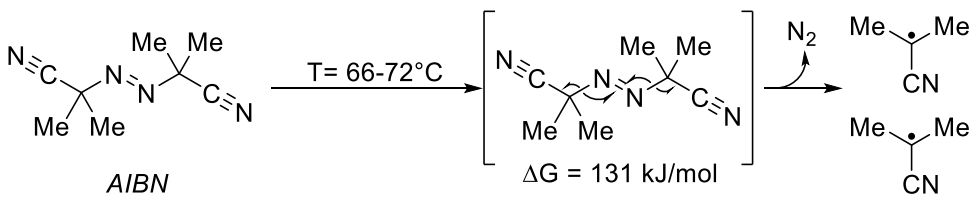
b) organic peroxides thermal decomposition
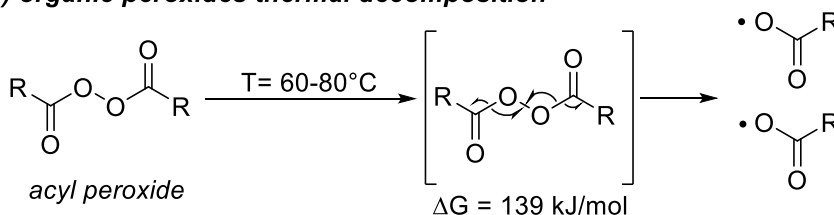
c) autoxidation of triethylborane
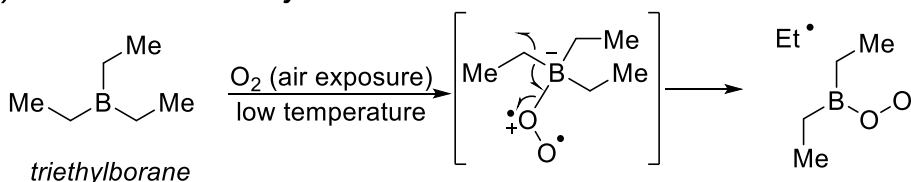
Scheme 1.11 Mode of action (initiation reactions) of common thermal radical initiators

Nevertheless, the initiator often persists in the reaction mean as a waste or might interact with the radical chain providing undesired reactive pathways. Besides, the heating required for homolysis cannot be selectively directed to the initiator, instead it affects all the reaction participants (other reagents, intermediates, products, and reaction mean).

Sometimes, for particular transformations like the radical substitution of a halogen with a hydrogen atom (radical dehalogenation) or the radical addition of a single electron to a spin-paired molecule, toxic and air-unstable reagents like tributyltin hydride (Bu$_3$SnH) and Group I metals are needed (Scheme 1.13).

a) radical generation by substitution (abstraction)
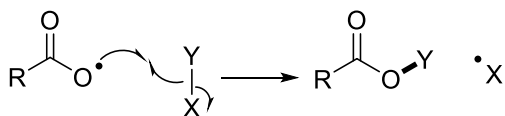
b) radical generation by addition
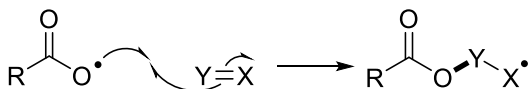
c) radical generation by elimination (homolysis)
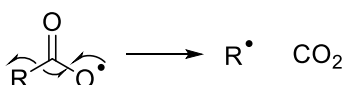
Scheme 1.12 Methods of chain propagation for radical generations from other radicals (obtained upon initiation by organic acyl peroxides in these examples): *a)* substitution (abstraction); *b)* addition; *c)* elimination (homolysis)

a) particular case: addition of an electron (reduction)
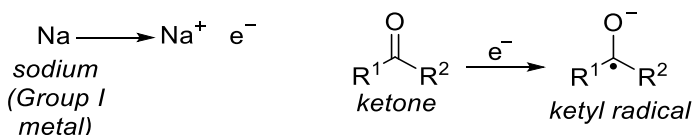
b) particular case: substitution of halogen by H
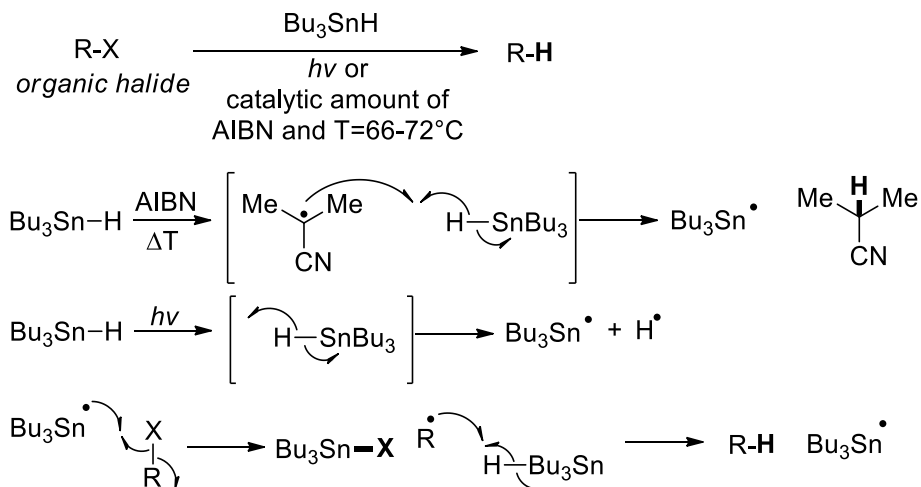
Scheme 1.13 Radical generation in particular cases: *a)* by the addition of an electron; *b)* by the substitution of halogen by a hydrogen atom

In other cases, the generation of radical species avoiding the use of radical initiators relies on very high temperatures. Thanks to the advent of photochemistry and its implementation among the other synthetic strategies, the use of light has become a valid alternative for radical generation under more controlled conditions. Indeed, it is a mean for delivering large amounts of energy to a specific molecule to cause homolytic rupture of a chemical bond. Photolysis and photoredox catalysis constitute two examples of these alternative strategies.

1.2.3 Photolysis

Sometimes the energy value characterizing a covalent chemical bond of a given molecule is in the same order of magnitude of the energy carried by the ultraviolet portion of visible light. Thus, absorption of a photon might result in the generation of an excited species fated to cleave in two parts upon rupture of a covalent bond. This process is known as photolysis, or photodissociation. The homolytic cleavage causes the electron pair (that was shared by the two atoms connected) to be relocated to each of the two atoms, and two radical species are formed.

UV light induced photolysis is anyhow still considered a classical method for radical generation albeit difficult to control. Indeed, the high energy associated with UV light is in the same order of magnitude of a C-C bond therefore it might lead to dissociation and carbon backbone degradation reactions (especially with molecules bearing strained structural complexities). Nevertheless, visible light might still represent a thoughtful choice to induce photolysis in those substrates bearing a weaker heteroatom-heteroatom bond, or a carbon-heteroatom bond (Table 1.2). Since most of common organic molecules do not absorb in the visible region, they could be reacted with the radical intermediates generated by visible light induced photolysis of such weaker bonds.

Table 1.2 Selected examples of Bond Dissociation Energies [33, 34, 35]

Bond X-Y	ΔG for X-Y→ X• + Y• (kJ/mol)
UV Light (200nm) associated energy = 586 kJ/mol	
OH-H	498
H_3C-H	435
Cl-H	431
Sn-Cl	406
Sn-F	467
Cl-N	389
H_3C-OH	383
H_3C- H_3C	368
Br-H	366
H_3C-Cl	349
Sn-Br	339
I-H	298
Blue Light associated energy = 293 kJ/mol	
H_3C-Br	293
N-Br	276
Sn-H	267
Cl-NH_2	251
Cl-Cl	243
H_3C-I	234
Sn-I	234
HO-OH	213
HO-NCH	209
Br-Br	192
Red Light associated energy = 167 kJ/mol	
I-I	151
MeO-OMe	151
Cl-NO	159

[33] Cottrell, T. L., *The Strengths of Chemical Bonds*. Butterworth: London **1958**.
[34] Kerr, J. A. *Chem. Rev.* **1966**, 465-500.
[35] Benson, S. W. *J. Chem. Ed.* **1965,** *42*, 502-518.

1.2.4 Photoredox catalysis

The photoinduced generation of an excited species leads to the change of the redox properties of such absorbing molecule. When this chemical entity acts as a catalyst and dissipates its excess energy generating reactive intermediates, the reaction is photocatalyzed. Particularly, if this catalyst, upon excitation, can accept or remove an electron from an organic or organometallic substrate in a redox event of single electron transfer (SET), the reaction is described as "photoredox catalyzed".

Notably, the first photoredox catalysts (PC) were metallo-polipyridyl complexes (Figure 1.2 and Figure 1.3) and were developed in the first part of the previous century for inorganic applications such as carbon dioxide reduction[36], water splitting,[37,38] or as solar-cell materials[39]. However, in the last two decades, many organic synthesis research groups managed to master these principles and converted the employment of such catalysts to the generation of radical species in mild conditions.

[Ru(bpy)₃]Cl₂ **[Ru(bpy)₃](PF₆)₂** **[Ru(phen)₃](PF₆)₂** **[Ru(bpz)₃](PF₆)₂**
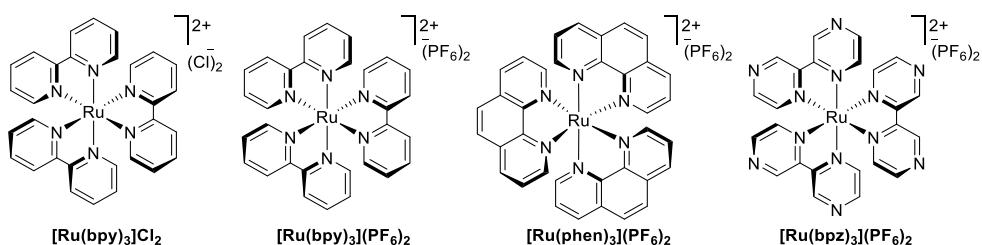
Figure 1.2 Examples of typical Ru(II) complexes commonly employed as PCs

fac-**[Ir(ppy)₃]** **[Ir(ppy)₂(dtbbpy)](PF₆)** **[Ir(dF{CF₃}ppy)₂(dtbbpy)]⁺(PF₆)**
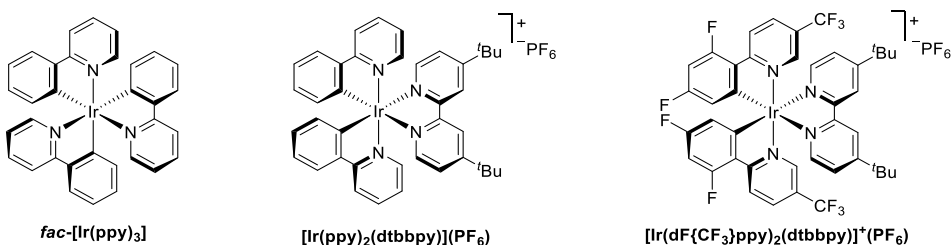
Figure 1.3 Examples of typical Ir(III) complexes commonly employed as PCs

36 Takeda, H.; Ishitani, O. *Coord. Chem. Rev.* **2010,** *254*, 346-354.
37 Lowry, M. S.; Bernhard, S. *Chem. Eur. J.* **2006,** *12*, 7970-7977.
38 Graetzel, M. *Acc. Chem Res.* **1981,** *14*, 376-384.
39 Kalyanasundaram, K.; Grätzel, M. *Coord. Chem. Rev.* **1998,** *177*, 347-414.

Despite some pioneering reports describing the use of Ru(bpy)$_3^{2+}$ and visible light to synthetize new organic bonds which appeared throughout late 70's and early 90's,[40,41,42,43,44] the groundbreaking works that gave birth to organic photoredox catalysis date back to 2008-2009 by MacMillan,[45] Yoon[46] and Stephenson[47] (Scheme 1.14).

The strength of photoredox catalysis lies primarily in the possibility of delivering reactive open shell intermediates or activating other catalysts (that would be ineffective in the absence of the PC and/or visible light) both in controlled manner and under mild conditions. Such synthetic innovation is due to the functional core and main character of a photoredox process: the photoredox catalyst (PC). Its direct interaction with otherwise unreactive organic or organometallic substrates leads to their transformation into highly reactive radical intermediates. The fact that the generation process of these intermediates is mediated by this intermediary allows a reaction set up where light is tuned to excite uniquely the PC. This prevents the excitation of species that could be negatively affected by photon absorption, like intermediates or reaction products that might be consumed absorbing light that is too energetic. Indeed, with organic photoredox catalysis, visible light irradiation is used, and the photons employed are characterized by wavelength where absorption by common organic molecules does not occur.

Moreover, despite the generation of radicals by ultraviolet (UV) light irradiation might still represent an alternative, the selective use of a lower energy wavelength avoids side-processes leading to competitive or degradation pathways due to an excessive delivery of energy.

[40] Van Bergen, T. J.; Hedstrand, D. M.; Kruizinga, W. H.; Kellogg, R. M. *J. Org. Chem.* **1979,** *44*, 4953-4962.

[41] Pac, C.; Ihama, M.; Yasuda, M.; Miyauchi, Y.; Sakurai, H. *J. Am. Chem. Soc.* **1981,** *103*, 6495-6497.

[42] Cano-Yelo, H.; Deronzier, A. *Tetrahedron Lett.* **1984,** *25*, 5517-5520. Cano-Yelo, H.; Deronzier, A. *J. Photochem.* **1987,** *37*, 315-321.

[43] Fukuzumi, S.; Koumitsu, S.; Hironaka, K.; Tanaka, T. *J. Am. Chem. Soc.* **1987,** *109*, 305-316.

[44] Okada, K.; Okamoto, K.; Morita, N.; Okubo, K.; Oda, M. *J. Am. Chem. Soc.* **1991,** *113*, 9401-9402.

[45] Nicewicz, D. A.; MacMillan, D. W. C. *Science* **2008,** *322*, 75-80.

[46] Ischay, M. A.; Anzovino, M. E.; Du, J.; Yoon, T. P. *J. Am. Chem. Soc.* **2008,** *130*, 12886-12887.

[47] Narayanam, J. M. R.; Tucker, J. W.; Stephenson, C. R. J. *J. Am. Chem. Soc.* **2009,** *131*, 8756-8757.

(a) Yoon, 2008 - [2+2] Enone cycloadditions

[Ru(bpy)$_3$]Cl$_2$ (5 mol%)
LiBF$_4$ (2.0 eq.),
i-Pr$_2$NEt (2.0 eq.),
MeCN, rt, 275 W CFL

bis(enone)

13 examples
58-98% yield, 4:1 to 10:1 dr
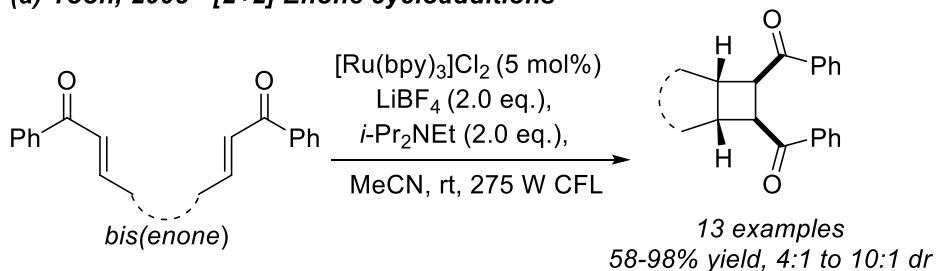
(b) MacMillan, 2008 - asymmetric catalytic α-alkylation of aldehydes

alkyl bromide

·HOTf

aldehyde (2.0 eq.)

organocatalyst (0.2 eq.)
[Ru(bpy)$_3$]Cl$_2$ (0.5 mol%)
2,6-Lutidine (2.0 eq.)
DMF, 23°C, 15 W CFL

12 examples
63-93% yield, 88-99% ee
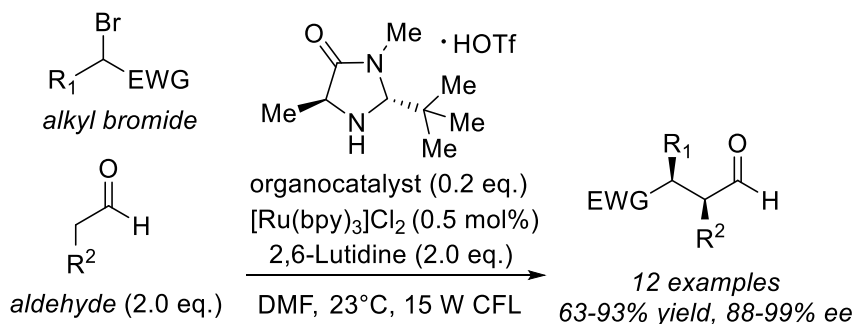
(c) Stephenson, 2009 - reductive dehalogenation of activated alkyl halides

activated alkyl halides employed:

PG= amine protective group

alkyl bromide

[Ru(bpy)$_3$]Cl$_2$ (2.5 mol%)
i-Pr$_2$NEt (10.0 eq.)
HCOOH (10.0 eq.)
DMF, rt, 14 W CFL

6 examples
80-95% yield

alkyl chloride

[Ru(bpy)$_3$]Cl$_2$ (2.5 mol%)
i-Pr$_2$NEt (2.0 eq.)
Hantzsch ester (1.1 eq.)
DMF, rt, 14 W CFL

4 examples
78-89% yield
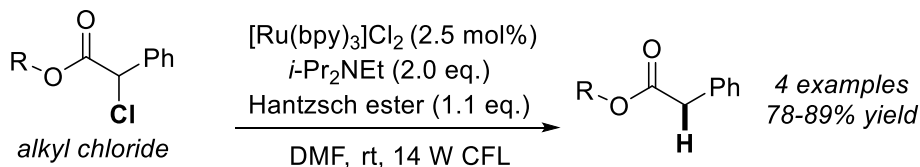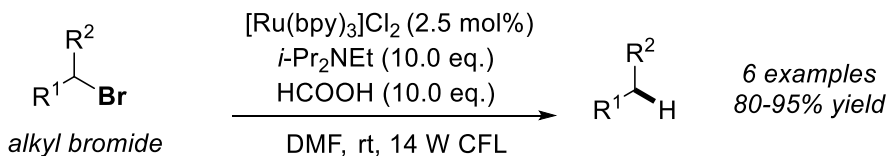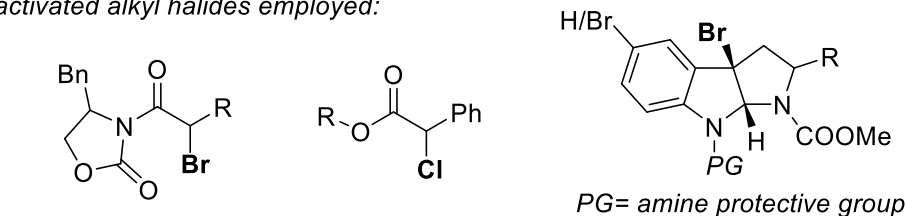
Scheme 1.14 Yoon *(a)*, MacMillan *(b)*, and Stephenson *(c)* seminal works with light and Ru(bpy)$_3$Cl$_2$: the advent of modern organic photoredox catalysis.

Besides, a PC might simultaneously provide both oxidation and reduction of such substrates. This allows an inimitable feature for photoredox processes, the ability of bestowing both an oxidative and a reductive reaction environment. In contrast to the traditional redox processes which exploit only oxidative or only reductive conditions, photoredox catalysis might disclose inaccessible redox-neutral reactions, thanks to the unique redox behavior of a PC. This is the reason why the photoredox catalytic cycle and the general design of a PC will be discussed in detail in the following paragraphs.

1.2.4.1 Photoredox catalyst

A point of debate is the employment of the appropriate term for the catalyst of a photoredox reaction. Typically *photosensitizer* and *photocatalyst* are used as synonyms, however Nicewicz and Yoon defined a more specific class *photoredox catalyst*.[48,49] According to the authors, a *sensitizer* should only indicate a molecule that operates an energy transfer sensitization while the word *photocatalyst* should intend a catalytic involvement of photons, that is observed only when light-triggered chain processes are considered. However, in recent papers the term *photocatalyst* is still used to indicate a species used in low loadings that allow the transformation to occur upon light absoprtion. Thus, photoredox catalyst (PC) has become as a more specific term indicating a subclass of photocatalysts. A PC is a molecule which interacts with other molecules *via* redox reactions in its excited state (reached upon absorption of a photon) and is regenerated to its ground state in the following turnover step thus defining a catalytic cycle.

The general behavior of a PC is therefore uncommon, since in a single cycle many chemically different processes can occur, such as the excitation of the catalyst, redox events (PET or SET)[50] with the final regeneration of the ground state PC. A general depiction is given in Scheme 1.15. The **PC** can be a metal complex or a colored organic molecule (organic dye able to absorb

---

[48] Romero, N. A.; Nicewicz, D. A. *Chem. Rev.* **2016,** *116*, 10075-10166.
[49] Kozlowski, M.; Yoon, T. P. *J. Org. Chem.* **2016,** *81*, 6895-6897.
[50] Photoinduced Electron Transfer (PET) and Single Electron Transfer (SET) may appear as interchangeable along the dissertation. However, the use of PET will be related only to those ET involving the excited state of a molecule, with a direct interaction of the excited state of a PC. SET, as a more general definition indicating all kind of electron transfers, will be used to indicate a general redox event with the transfer of a single electron.

light thus reaching its excited state. When the PC reaches its excited state and is indicated as **PC*,** two possible PET might occur, therefore two catalytic cycles are possible: the *oxidative quenching cycle* and the *reductive quenching cycle*.
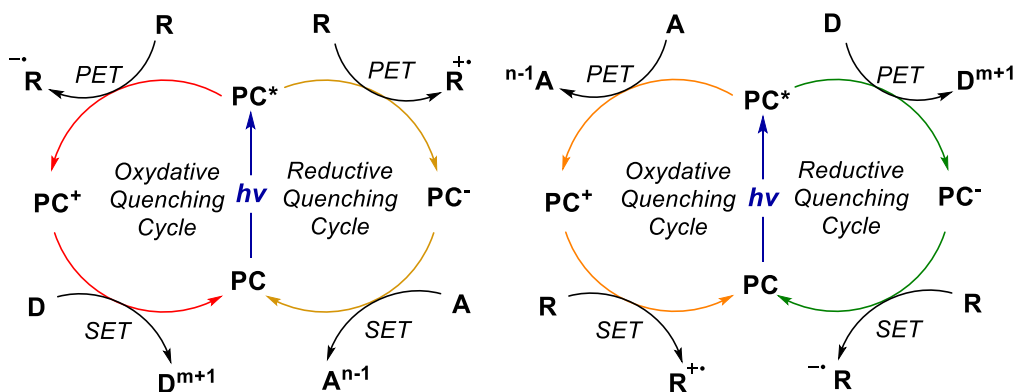
Scheme 1.15 General catalytic cycle of a photoredox catalyst: oxidative quenching cycle *versus* reductive quenching cycle.

When The **PC*** act as an electron donor, the photo promoted electron is transferred to an acceptor substrate that is therefore reduced while PC is oxidized, meaning that an oxidative quenching cycle is occurring. The acceptor molecule can be either neutral or a charged species, whose reduction generates a reactive neutral radical or an ionic radical species respectively (since ionic radicals are the ones that are typically generated, radical (ionic) species will be indicated as **R$^{\bullet-}$** or **R$^{\bullet+}$** in the Scheme 1.15: **R$^{\bullet-}$** if the radical is generated upon the reduction of the starting material, **R$^{\bullet+}$** if the radical is generated upon the oxidation of the starting material).

Depending on the nature of the acceptor, two possible options arise. If the acceptor is a reagent substrate, indicated as **R**, its evolution to a radical intermediate **R$^{\bullet-}$** triggers further transformations towards the reaction products. In this case, a molecule in the reaction mean (that might even be one of the reaction products or intermediates) should act as an electron donor **D** providing a reduction of the intermediate **PC$^+$** in the turnover step (becoming the oxidized species **D^{m+1}** upon loss of a single electron in a SET), thus regenerating the ground state **PC** (red path, Scheme 1.15, see Scheme 1.16 for an applied example). Alternatively, the presence of a sacrificial acceptor **A** quenches the **PC*** leading to generation of the **PC$^+$** (while A becomes a reduced species acquiring a single electron **A^{n-1}** in a SET), that only after this transformation possesses the feasible redox potential to react

with **R** in order to deliver a reactive **R•+** and regenerating the **PC** in its ground state (orange path, Scheme 1.15).

In the reductive quenching state, the **PC*** is quenched by a donor substrate, by the transfer of an electron to the catalyst, producing the **PC⁻** intermediate. When this PET event involves the reagent **R** as the donor, **R•+** is consequently generated and a sacrificial electron acceptor **A** is needed to close PC cycle, oxidizing **PC⁻** (gold path in Scheme 1.15, see Scheme 1.17 for an applied example). Otherwise, **R** might have a potential that allow a radical species to be formed by the interaction with the **PC**. Thus, at first a sacrificial **D** quenches the **PC*** delivering **PC⁻** and only at this point **R** can be involved in a SET event, evolving to **R•⁻** in the turnover step that closes the PC cycle (green path Scheme 1.15).[51,52,53] Concerning Ru(II) salt as PC, two applications of its oxidative and reductive quenching cycle are described in Scheme 1.16 and Scheme 1.17 (focus is dedicated to the fate of the PC while radical transformations are avoided for the aim of this paragraph).[54,55] In the first case, the light triggers the PC cycle, promoting Ru(II) to its excited state. *Ru(II) is quenched by the substrate **1a**, an aryldiazonium salt, delivering the oxidized Ru(III) species and the corresponding aryl radical **1-I** from reduction of **1a** upon loss of nitrogen and . The radical coupling of **1-I** with styrene provides a radical **1-II** which acts as the donor species being oxidized to the cation **1-III** while regenerating the ground state PC Ru(II). In the second example, the excited *Ru(II) salt is instead a reductant for the alkylaniline **2a** which is converted to the a radical cation species **2-I** while delivering Ru(I). A radical cascade process occur converting **2-I** to **2-IV** upon reaction with styrene and the resulting radical cation **2-IV** react as the acceptor in the turnover step of the PC cycle to obtain the product **2-P** concomitantly repristinating Ru(II).

Examining these general photoredox catalytic cycles, a general observation emerges. A PC carries out its cycle exploiting only the PET among all the possible deactivation mechanisms previously described, thus avoiding any

---

[51] Stephenson, C. R. J.; Yoon, T. P.; Macmillan, D. W. C., *Visible light photocatalysis in organic chemistry*. Wiley-VCH Verlag GmbH: Weinheim **2018**.

[52] Arias-Rotondo, D. M.; McCusker, J. K. *Chem. Soc. Rev.* **2016,** *45*, 5803-5820.

[53] Zeitler, K. *Angew. Chem. Int. Ed.* **2009,** *48*, 9785-9789.

[54] Crespi, S.; Jäger, S.; König, B.; Fagnoni, M. *Eur. J. Org. Chem.* **2017,** *2017*, 2147-2153.

[55] Maity, S.; Zhu, M.; Shinabery, R. S.; Zheng, N. *Angew. Chem. Int. Ed.* **2012,** *51*, 222-226.

EnT process. This statement is only partially true and comes with some precautions that should be taken while designing a photoredox organic transformation. First, Dexter Energy transfer might easily occur with the oxygen as the quencher, especially when the PC is a metal complex.[56,57] Consequently, some photoredox catalysed transformations might not occur unless deoxygenated solutions are used, and anoxic conditions of the reaction system are set. Second, most organic molecules studied in photoredox conditions are carefully chosen among those which not absorb visible light (to avoid collateral reactions). Hence, the spectral overlap among PC emission and substrates absorption should not exist, and Förster energy transfer should not represent a deactivation mechanism for the excited PC.

Nevertheless, some examples in which organic dyes are used as PCs, report the deactivation of PC* and generation or reactive radical intermediates *via* EnT mechanism (discussed in paragraph 1.2.4.1.2).

Finally, it is important to point out the singularity of PCs among all kind of catalysts. As long as the irradiation of the reaction persists, the excited-state catalyst is incessantly regenerated. This avoids the decrease in yield due to unproductive PETs or parasite reactions in which the excited state is quenched leading to no formation of desired products. Indeed, after the parasite quenching occurs, the photocatalyst will be re-excited until the required quenching *en route* to the final product will occur, and even after such desired event and consequent return to its ground state, the PC can still be re-excited.

Given all the observation resulting from the analysis of the singular catalytic cycle described by a PC, a list of the most desirable features for a PC can be drawn up:[51,52]

- PC must absorb light in the visible region, even better if in a region where both reagents and products could be irradiated with no consequences.
- PC must be stable in solution so that the catalytic cycle could persist after hours of irradiation, while the reaction occurs.
- PC must persist in its excited-state long enough to interact with other molecules in PET event (excited lifetime timescale higher than 10^{-9} -10^{-8} seconds).

---

[56] Demas, J. N.; Harris, E. W.; McBride, R. P. *J. Am. Chem. Soc.* **1977,** *99*, 3547-3551.
[57] Brunschwig, B.; Sutin, N. *J. Am. Chem. Soc.* **1978,** *100*, 7568-7577.

- PC most possess a reversible redox behavior to establish the catalytic cycle
- All the above-mentioned features must be tunable with slight chemical modifications of the model PC.
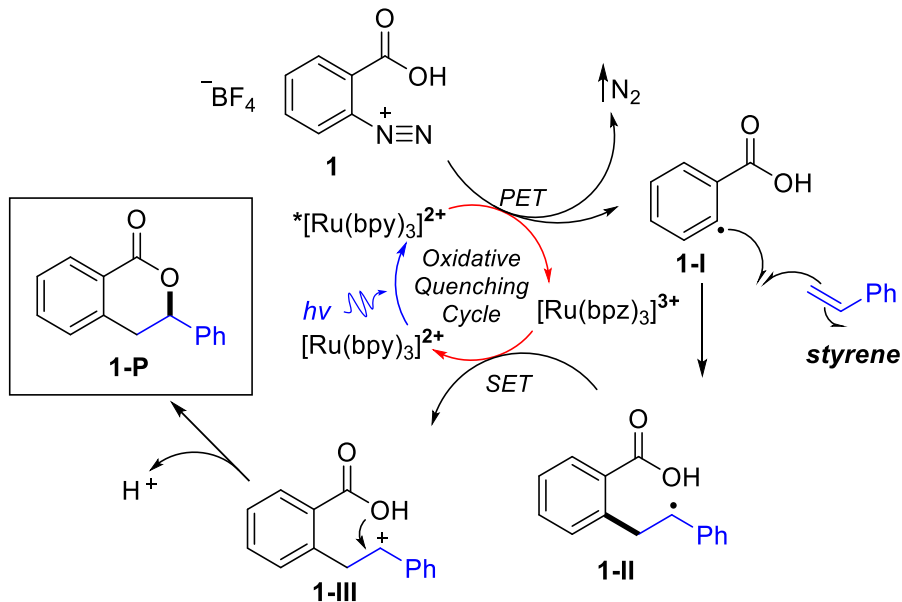
Scheme 1.16 Example of a photoredox transformation exploiting the oxidative quenching cycle of a Ru(II) PC[54]
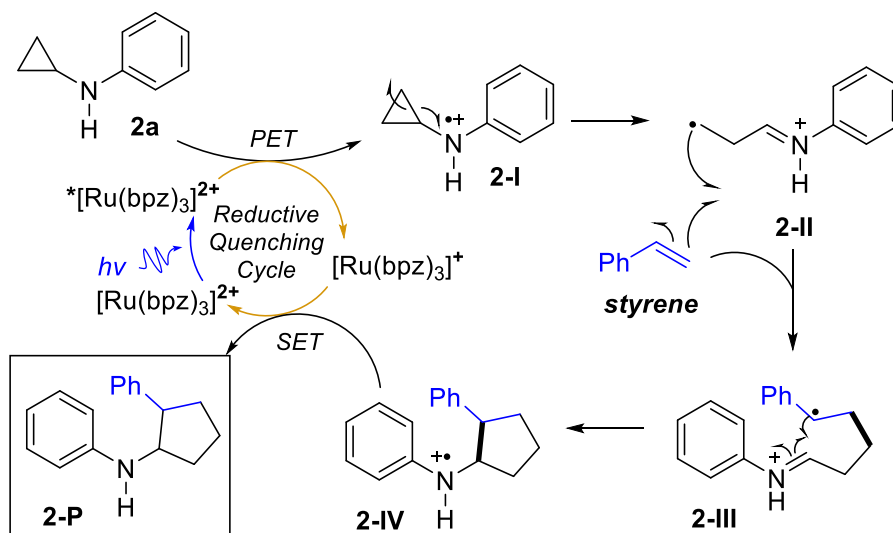
Scheme 1.17 Example of a photoredox transformation exploiting the reductive quenching cycle of a Ru(II) PC[55]

1.2.4.1.1 Transition metal complex-based photoredox catalysts

Since the initial reports[40-44] and the seminal works of 2008[45-47] the polypyridyl complexes of Ruthenium have shown their versatility as PCs. Among them, $[Ru(bpy)_3]^{2+}$ is the one whose properties have been studied for the longest time and is then used as a prototype to describe the behavior of metal complexes-based PCs.

The wavelength for the $[Ru(bpy)_3]^{2+}$ maximum of absorption is located at 452 nm, corresponding to the maximum emission associated to blue light (490–450 nm). Absorption of light in the case of $[Ru(bpy)_3]^{2+}$ corresponds to the excitation of the metal complexes identified as metal to ligand charge transfer (MLCT).

Indeed, reaching the excited state with the generation of $*[Ru(bpy)_3]^2$ implies the promotion of a single electron from the HOMO of the metal-centered t_{2g} orbital to a ligand-centered $\pi*$ orbital. Thus, the molecule is set on the singlet S_1 excited state with a vacancy in the former HOMO and a new occupied molecular orbital, the former LUMO that now is the SOMO. As previously explained for general cases, this transfer of electrons, due to MLCT for metal complexes, makes the PC both an oxidant and a reductant. In particular, one electron has been transferred from a metal-centered orbital leading to the formation of a Ru(III) metal center that is a better oxidant. At the same time, such electron has been placed in a ligand central orbital, thus making the ligand a negatively overcharged reductant. Notably, the overall charge of the complex is still unchanged. The singlet-excited state is anyhow unstable and rapidly yields the lowest energy triplet-excited state T_1 by ISC causing the spin flip of the electron in the $\pi*$ orbital (Scheme 1.18).

The first triplet excited state of the molecule persists for about 1100 ns.[58,59] Such long life allows the engagement of the excited $*[Ru(bpy)_3]^{2+}$ species in SET events (Scheme 1.19).[51,52] As described in the previous paragraph, PET event might now occur from molecules in the reaction mean and $*[Ru(bpy)_3]^{2+}$ leading to the formation of $[Ru(bpy)_3]^{+}$ in the reductive quenching cycle or to the formation of $[Ru(bpy)_3]^{3+}$ in the oxidative quenching cycle. The resulting oxidized or reduced form of the PC is now characterized by a strong thermodynamic push towards its ground state

---

[58] McCusker, J. K. *Acc. Chem Res.* **2003,** *36*, 876-887.

[59] Campagna, S.; Puntoriero, F.; Nastasi, F.; Bergamini, G.; Balzani, V., *Photochemistry and Photophysics of Coordination Compounds I*. Springer: Berlin **2007**.

original oxidation state. Thus, a second SET event will occur to regenerate the catalyst, highlighting once again the ability for the single PC to operate in net redox-neutral conditions.
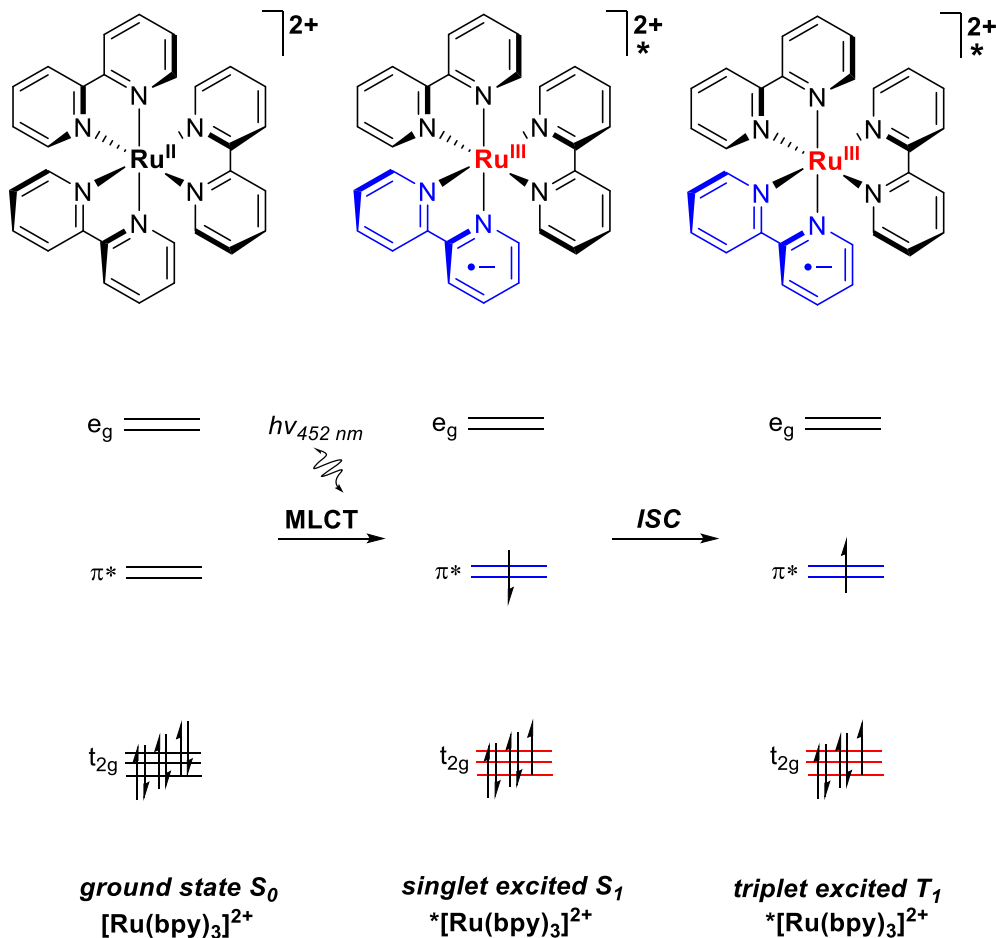
Scheme 1.18 Simplified molecular orbital scheme of the prototypical polypyridyl transition-metal based photoredox catalyst Ru(bpy)$_3^{2+}$ for MLCT and ISC events upon visible-light irradiation.
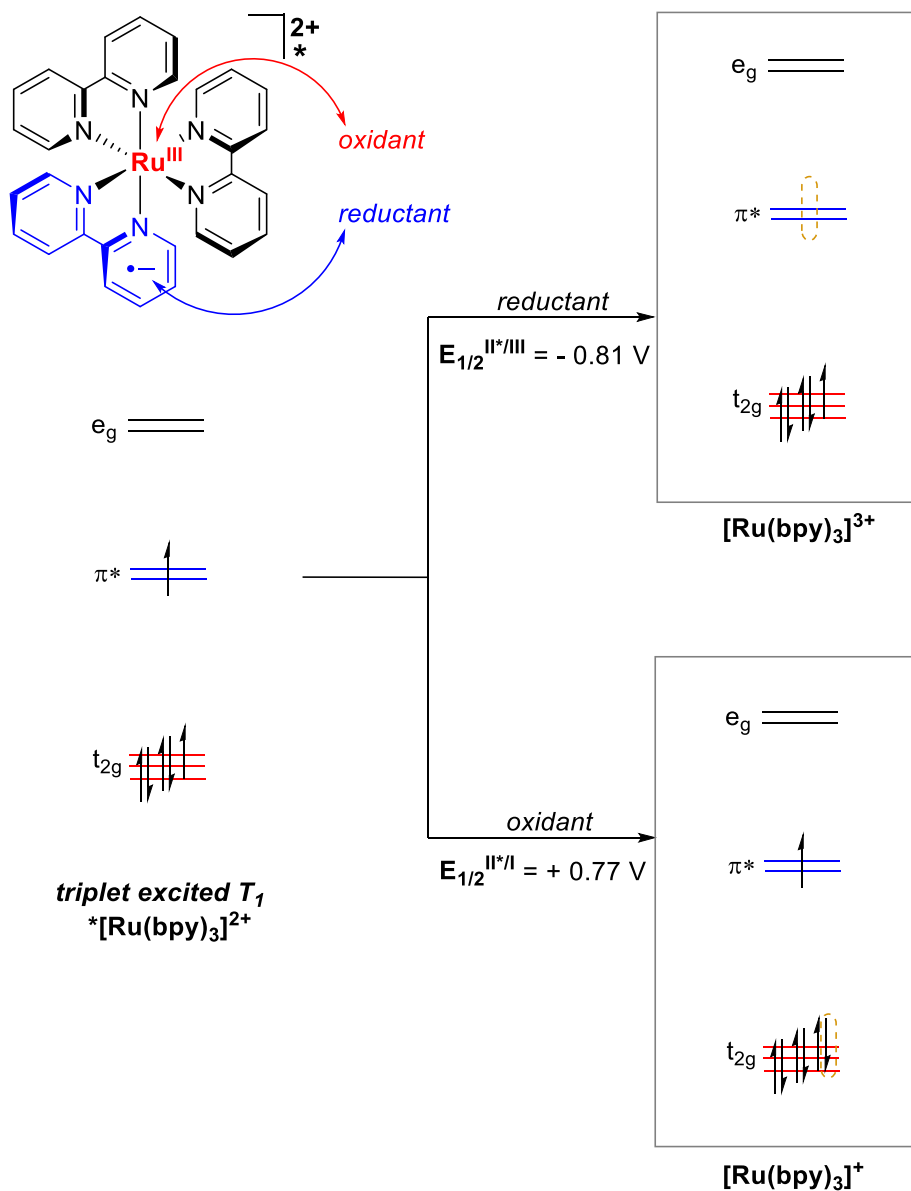
Scheme 1.19 Simplified molecular orbital scheme of Ru(bpy)$_3^{2+}$ describing its excited state photoredox reactivity

Metal complexes are efficient catalysts and one of the main advantages of their employment is the possible tunability of their properties. As a result, the photoredox properties of the PC, such as the wavelength of absorption and

the potentials governing each PET and SET of the catalytic cycle, might be tailored with the variation of the metal centers (using different metal atoms) and the ligands (e.g. using phenylpyridyl instead bipyridyl ligand) and on the ligands (adding substituent groups on the aromatic rings).

Table 1.3 Selected examples of Iridium PCs and their redox properties.
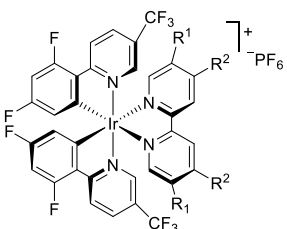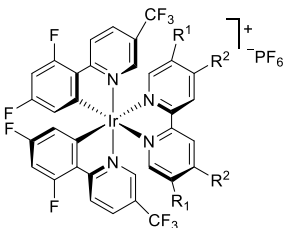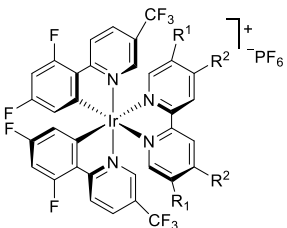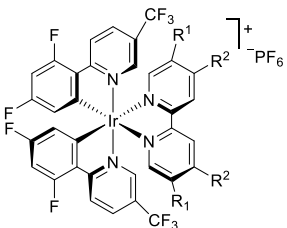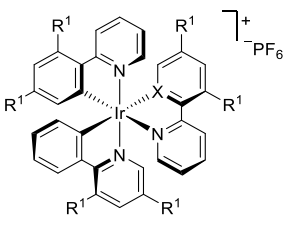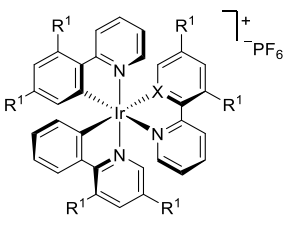
Iridium Photoredox Catalyst	
	[Ir(dFCF₃ppy)₂(dtbbpy)](PF₆) R^1=H , R^2=^{t}Bu $E_{1/2}$(*PC/PC⁻) = +1.21 V vs SCE $E_{1/2}$(PC/PC⁻) = -1.37 V vs SCE $E_{1/2}$(PC⁺/*PC⁻) = -0.89 V vs SCE $E_{1/2}$(PC⁺/PC) = +1.69 V vs SCE **[Ir(dFCF₃ppy)₂(bpy)](PF₆)** R^1=H , R^2=H $E_{1/2}$(*PC/PC⁻) = +1.32 V vs SCE $E_{1/2}$(PC/PC⁻) = -1.37 V vs SCE $E_{1/2}$(PC⁺/*PC⁻) = -1.00 V vs SCE $E_{1/2}$(PC⁺/PC) = +1.69 V vs SCE
	[Ir(dFCF₃ppy)₂(4,4'-dCF₃bpy)](PF₆) R^1=H , R^2=CF₃ $E_{1/2}$(*PC/PC⁻) = +1.65 V vs SCE $E_{1/2}$(PC/PC⁻) = -0.79 V vs SCE $E_{1/2}$(PC⁺/*PC⁻) = -0.51 V vs SCE $E_{1/2}$(PC⁺/PC) = +1.93 V vs SCE **[Ir(dFCF₃ppy)₂(5,5'-dCF₃bpy)](PF₆)** R^1=CF₃ , R^2=H $E_{1/2}$(*PC/PC⁻) = +1.68 V vs SCE $E_{1/2}$(PC/PC⁻) = -0.69 V vs SCE $E_{1/2}$(PC⁺/*PC⁻) = -0.43 V vs SCE $E_{1/2}$(PC⁺/PC) = +1.94 V vs SCE
	[Ir(ppy)₂(bpy)](PF₆) R^1=H , R^2=H, X=N $E_{1/2}$(*PC/PC⁻) = +1.22 V vs SCE $E_{1/2}$(PC/PC⁻) = -1.44 V vs SCE $E_{1/2}$(PC⁺/*PC⁻) = -1.17 V vs SCE $E_{1/2}$(PC⁺/PC) = +1.49 V vs SCE ***fac*-Ir(ppy)₃** R^1=H , R^2=H, X=C $E_{1/2}$(*PC/PC⁻) = +0.31 V vs SCE $E_{1/2}$(PC/PC⁻) = -2.19 V vs SCE $E_{1/2}$(PC⁺/*PC⁻) = -1.73 V vs SCE $E_{1/2}$(PC⁺/PC) = +0.77 V vs SCE

Table 1.4 Selected examples of Ruthenium PCs and their redox properties.

Ruthenium Photoredox Catalyst	
	Ru(bpy)$_3$(PF$_6$)$_2$ **X= PF$_6$** $E_{1/2}$(*PC/PC$^-$) = +0.77 V vs SCE $E_{1/2}$(PC/PC$^-$) = -1.33 V vs SCE $E_{1/2}$(PC$^+$/*PC$^-$) = -0.81 V vs SCE $E_{1/2}$(PC$^+$/PC) = +1.29 V vs SCE **Ru(bpy)$_3$(Cl)$_2$** **X=Cl** $E_{1/2}$(*PC/PC$^-$) = +0.78 V vs SCE $E_{1/2}$(PC/PC$^-$) = -1.35 V vs SCE $E_{1/2}$(PC$^+$/*PC$^-$) = -0.87 V vs SCE $E_{1/2}$(PC$^+$/PC) = +1.26 V vs SCE
	Ru(phen)$_3$(PF$_6$)$_2$ $E_{1/2}$(*PC/PC$^-$) = +0.82 V vs SCE $E_{1/2}$(PC/PC$^-$) = -1.36 V vs SCE $E_{1/2}$(PC$^+$/*PC$^-$) = -0.87 V vs SCE $E_{1/2}$(PC$^+$/PC) = +1.26 V vs SCE
	Ru(bpz)$_3$(PF$_6$)$_2$ $E_{1/2}$(*PC/PC$^-$) = +1.45 V vs SCE $E_{1/2}$(PC/PC$^-$) = -0.80 V vs SCE $E_{1/2}$(PC$^+$/*PC$^-$) = -0.26 V vs SCE $E_{1/2}$(PC$^+$/PC) = +1.86 V vs SCE
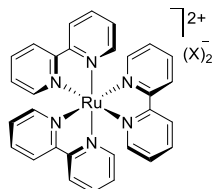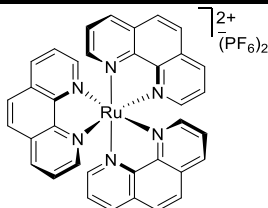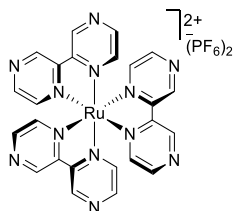
Since the first reports, the most studied alternatives always referred to the variation of the ligands installed on Ir(III) or Ru(II) metal centers (Table 1.3 and Table 1.4).[60]

Nevertheless, being these two elements some of the rarest metal on Earth, some downsides in terms of scalability limit their employment. Thus, modern organic photo-redox chemistry is considering the idea of replacing these expensive metal centers with different more Earth abundant-metals. Several

---

[60] Teegardin, K.; Day, J. I.; Chan, J.; Weaver, J. *Org. Process Res. Dev.* **2016,** *20,* 1156-1163.

transition metals have been investigated and their successful employment as PCs have been reviewed.[61,62,63]

1.2.4.1.2 Organic photoredox catalysts

Given the need for designing PCs based on less rare metals and the necessity for the development of metal-free processes in industrial fields where the toxicity of metals must be strictly avoided, research interest in photoredox catalysis has moved towards the development of purely organic PCs.[48,64,65] The most suitable candidates have been found among those organic dyes absorbing light in the visible region. When compared to their metal complexes counterparts, such organic molecules might be considered as less photostable and associated with shorter excited lifetime. In contrast to this putative photo-weakness a comparison between $Ru(bpy)_3^{2+}$ and Eosin Y is reported in Scheme 1.20.
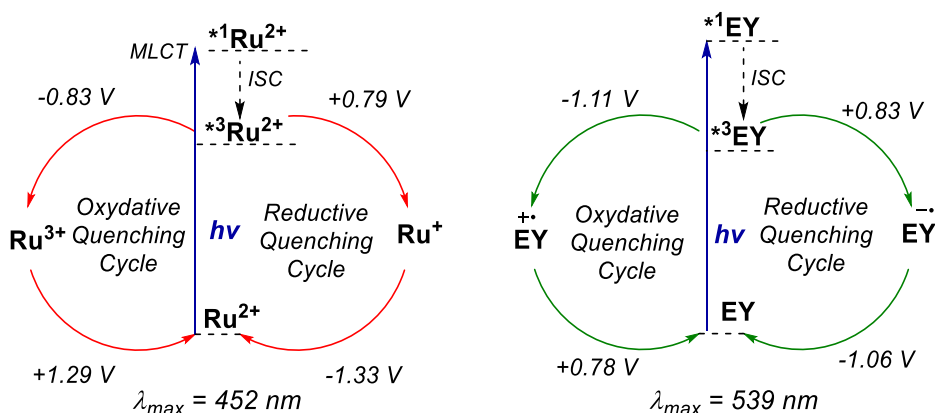
Scheme 1.20 Comparison between the photo-redox properties of a model metal-based PC $Ru(bpy)_3^{2+}$ and an organic PC Eosin Y (EY).

Eosin Y (EY) photoredox behavior is comparable to that of a metal complex,[66,67] being involved in the same PET and SET events that characterize

[61] Larsen, C. B.; Wenger, O. S. *Chem. Eur. J.* **2018,** *24*, 2039-2058.
[62] Hockin, B. M.; Li, C.; Robertson, N.; Zysman-Colman, E. *Catal. Sci. Technol.* **2019,** *9*, 889-915.
[63] Glaser, F.; Wenger, O. S. *Coord. Chem. Rev.* **2020,** *405*, 213129.
[64] Nicewicz, D. A.; Nguyen, T. M. *ACS Catal.* **2014,** *4*, 355-360.
[65] Fukuzumi, S.; Ohkubo, K. *Org. Biomol. Chem.* **2014,** *12*, 6059-6071.
[66] Hari, D. P.; König, B. *Chem. Commun.* **2014,** *50*, 6688-6699.
[67] Majek, M.; Filace, F.; Wangelin, A. J. v. *Beilstein J. Org. Chem.* **2014,** *10*, 981-989.

the general cycle of a PC with the unique difference that in the case of metal complexes, excitation to the triplet state occurs upon MLCT. Concerning the lifetime of excited Eosin Y, the enhanced spin-orbit coupling provided by the Bromine (heavy atom effect) allows ISC the triplet state of the molecule to be reached, ensuring long lifetime of the excited state. This demonstrates that organic molecules might work as organic photoredox catalysts.[51,66,67] Being the triplet T^1 state the lower excited state, to ensure photocatalytic behavior, such chromophores requires two features. First, singlet S^1 state should be associated to relatively low energies. Second, the triplet T^1 state should be associated to relative high energy level and to long life thus making high ISC rates possible. That is indeed the case of heavy atom-substituted dyes like Eosin Y, but also carbonyl compounds, enones, cyanoarenes and so on.[48]

Organic molecules that might act as PCs are in general bench stable, wide available and less expensive when compared to metal complexes. Moreover, the wide availability of organic transformations that can be applied to the functional groups of the archetypical organic PC allows the selective tuning of the redox properties of the dyes. Thus, organic PCs, as well as metal-based ones, can be classified and selected according to the redox potential required in the PET and SET events of the planned reaction.

Besides, cyanoarenes, quinones, anthraquinones, methylquinolinium, pyrylium salts, aryl ketones and xanthones are well-known colored molecules whose excited state properties were historically exploited using UV irradiation, given the short availability of alternative light sources.[68,69] The minor absorbing ability in the visible region (wavelength above 400 nm) have been ignored until the last decades. With UV irradiation and the highly energetic correlated photons, the irradiation of organic dyes has disclosed their potential use as *photosensitizers.* Indeed, organic molecules excited with the energy of a UV photon might reach the triplet state and perform a triplet-triplet sensitization thus exciting an organic substrate by EnT mechanism.[13,68,69] The classical photochemistry of methylene blue, rose Bengal, and benzophenone which are characterized by long triplet lifetimes relies on such behavior, transferring the excited state to other organic molecules which might then undergo homolysis to generate radical species. However, if the energy associated with a photon absorbed in the visible

---

[68] Albini, A. *Synthesis* **1981,** *1981*, 249-264.
[69] Zhao, J.; Wu, W.; Sun, J.; Guo, S. *Chem. Soc. Rev.* **2013,** *42*, 5323-5351.

region (we can take a λ=400nm value that gives an energy of 300 kJ/mol) is considered, it will be noticed that the triplet energy of organic molecules is exceeded also with visible light irradiation.[70] It means that some organic photocatalysts might work as photosensitizers even under visible light irradiation, exploiting an EnT deactivation mechanism with triplet sensitization as successfully demonstrated with mechanistic insights in some methodological works.[71,72,73]

To conclude, despite the putative weakness theorized, colored organic molecules are emerging as efficient catalysts in photoredox catalysis offering both a metal-free alternative to metal complexes and a complementary reactivity thanks to EnT deactivation mechanism. Therefore, during the optimization study of a photoredox process, their employment must always be considered.

1.2.4.1.3 Singlet vs triplet excited states of PC*

Given the fact that T_1 is generally associated to lower energy values than S_1 (see the Jablonski Diagram, Scheme 1.1), PC* in the singlet state are virtually more potent oxidants and reductants than the corresponding PC* in the triplet state.[48] It means that the singlet state has a wider potential of being involved in SET event with organic substrates. However, a deeper inquire into such statement must be provided.

When the contact between PC* species and the organic substrates occurs, leading to PET, the kinetic of the process is ruled by a constant molecular rate, similar for both S_1 and T_1 when the ΔG of the process is large. In both cases however, the close distance between the two species (PC and substrate **R**) might lead to a back electron transfer (BET) event determining a difference in the rate of this process.

Scheme 1.21 describes the case of a reductive quenching of the PC. Indeed, when the two species are in contact, a new single species that is a radical (ion) pair is incipiently formed. This latter will retain the same overall spin multiplicity of the excited state catalyst PC* meaning that **^{3}PC*** will originate a triplet contact radical ion pair **TCRIP** while **^{1}PC*** will originate a singlet

---

[70] Ni, T.; Caldwell, R. A.; Melton, L. A. *J. Am. Chem. Soc.* **1989,** *111*, 457-464.

[71] Arceo, E.; Montroni, E.; Melchiorre, P. *Angew. Chem. Int. Ed.* **2014,** *53*, 12064-12068.

[72] Alonso, R.; Bach, T. *Angew. Chem. Int. Ed.* **2014,** *53*, 4368-4371.

[73] Metternich, J. B.; Gilmour, R. *J. Am. Chem. Soc.* **2015,** *137*, 11254-11257.

contact radical ion pair **SCRIP**. Both these radical ion pairs can either undergo the photoredox-desired radical intermediate formation. The PC can be reduced to **PC⁻•** or suffer from BET leading to the regeneration of the ground state **PC** and the ground state substrate **R**. However, the BET for the **TCRIP** is a slower process because it requires an intersystem crossing (the electron in the radical (ion) pair needs to flip its spin to be donated back).
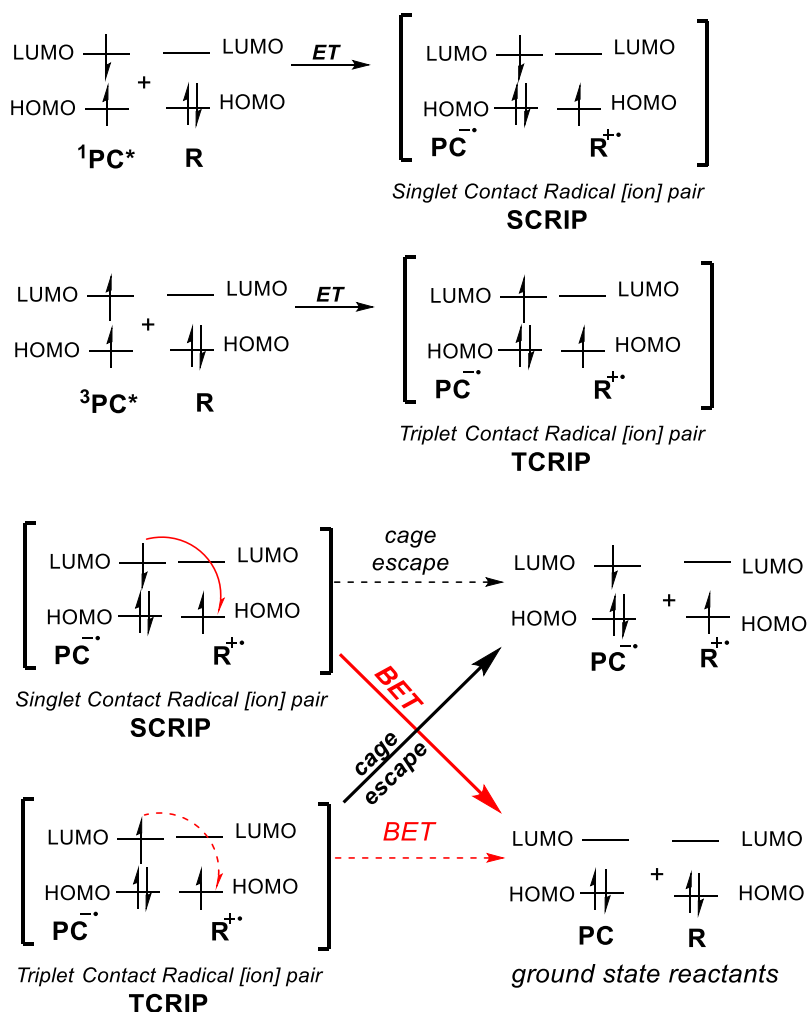
Scheme 1.21 The formation of Radical (Ion) pair upon ET from triplet and singlet excited state of the PC and Back Electron Transfer (BET). Dashed arrows indicate spin-forbidden ET

This leads to the assumption that the triplet state of the PC is the main actor in the photoredox catalytic cycle (in those processes where a BET might

occur). Such statement is further confirmed by two experimental studies comparing the production of free ions occurring from $^1PC^*$ and $^3PC^*$. In the second case, the free ion generation is more efficient and larger.[74,75]

1.2.4.1.4 Redox properties of the PCs.

The viability of a photoredox reactions depends on the redox potentials of the substrate that needs to be reduced or oxidized to form a radical species. That means that the E_{RED} (R/R$^{•-}$) and E_{ox} (R/R$^{•-}$) must be compared to those of the chosen organic photocatalyst in the excited state to understand whether the redox event might occur. When a photoredox catalyst is synthesized for the first time, it is commonly totally characterized including the crucial reduction E_{RED} (PC*/PC$^-$) or oxidation E_{ox}(PC*/PC+) values related to the excited state of the catalyst. The extensive reviewing work about photoredox catalysis of the last decade has provided a series of charts comparing such electrochemical potentials of the available PCs with the electrochemical potentials of classes of substrates. These practical tools can be consulted to identify and design the ideal PC for delivering a radical intermediate from a chosen substrate.

A brief representative depiction based on such charts is reported in Scheme 1.22 and some general observations might be reported. Stabilized anions (carboxylates, thiolates) and amines are good electron donor E_{ox} (R/R$^{•+}$) = ca 1V *versus* the saturated calomel electrode (SCE) so they will be easily oxidized by most of the PCs with E_{RED} (PC*/PC$^-$) above +1. Unsubstituted functional groups like alcohols, ethers, ketones, nitriles are instead very difficult to oxidize. Other classes of substrates are instead more prone to reduction. Positively charged aryl diazonium salts are easily reduced and as well as α-bromo carbonyls or aromatic halides.

For saturated hydrocarbons oxidation by PC* is almost unachievable. On the contrary olefins can be both reduced and oxidized depending on the substituents, electron-poor olefins require quite strong oxidant (E_{ox} (R/R$^{•-}$) of at least +2 V vs SCE) as they have a E_{RED} (R/R$^{•-}$) = ca. −2 V vs SCE to be reduced, while electron rich olefins (with tri- o tetra- alkylated olefins or

---

[74] Yasunao, K.; Tatsuo, A.; Hirochika, S.; Katsumi, T. *Chem. Lett.* **1988,** *17*, 1193-1196.
[75] Akaba, R.; Ohshima, K.; Kawai, Y.; Obuchi, Y.; Negishi, A.; Sakuragi, H.; Tokumaru, K. *Tetrahedron Lett.* **1991,** *32*, 109-112.

substituted with an electrondonating group (as for vinylethers) are easily oxidated having of E_{ox} (R/R$^{\bullet+}$) ranging from +1 to +2 vs SCE.

Concerning the PC, notably organic PCs, as previously anticipated, allows a wide range of transformations otherwise unachievable. Examples in this sense are given by cyanoarenes (the powerful oxidants with E_{RED} (PC*/PC$^-$) above +3 V vs SCE), pyridinium and acridinium salts (with E_{RED} (PC*/PC$^-$) above +2 V). However, despite common Ir(III) and Ru(II) might seem smooth oxidants and reductants, the ligands substitution dramatically affects their redox potential.
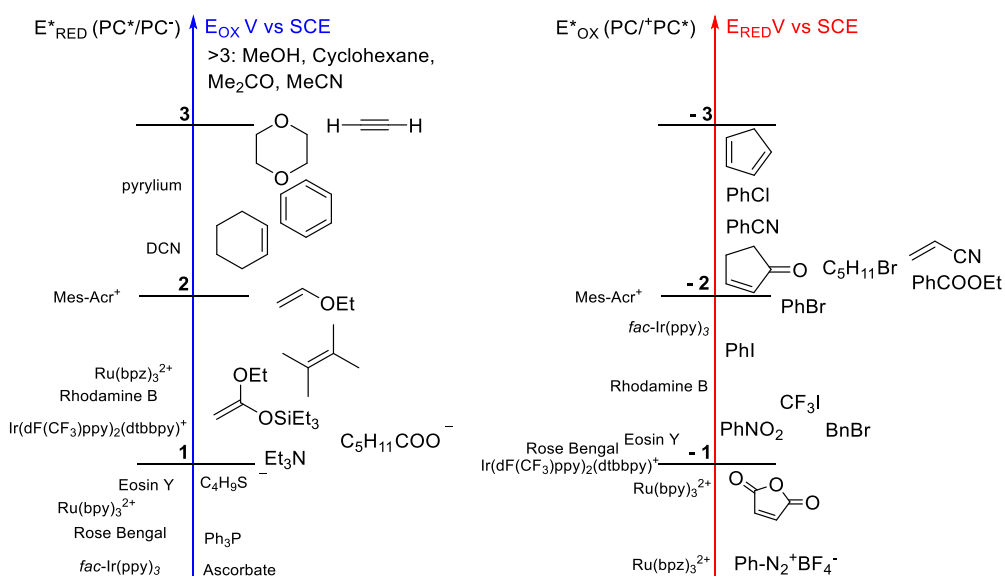
Scheme 1.22 Qualitative depiction of comparison between reduction potential in the excited state of common PCs and the oxidation potential of selected functional groups (left) and between the oxidation potential in the excited state of common PCs and the reduction potential of selected functional groups (right)

The study of the electrochemical potentials of PCs and substrates involved in the reactions allows its design. Nevertheless, such electrochemical features are deeply influenced by all the participants of the photoredox process, like solvents, temperature, and intrinsic conditions of the reaction mean. Thus, a complementary optimization study based on empirical evidence is always required to discover the best conditions for a photoredox reaction.

1.2.4.2 Photoredox catalysis complementarity to thermal reactivity

The use of radical species generated by photoredox catalysis can influence the reaction outcome leading to synthetic targets otherwise unreachable with common thermal methodologies (Scheme 1.23). After its milestone works of 2008,[46] Yoon's research group studied the influence of photoredox catalysis on Diels-Alder cycloadditions. Surprisingly, a photoredox-generated cationic radical species yielded a product **5b** with reversed regioselectivity when compared to the same thermal 4+2 Diels-Alder product **5a**. Indeed, the radical cation generation leads to a formal umpolung, inverting the electronic character of the dienophile and therefore the regioselectivity of cyclization.[76] Some months later, once again *via* a radical cation species, Nicewicz's group[77] demonstrated that photoredox-generated intermediates led to the opposite outcome typically observed for hydroetherification reactions under thermal conditions. In this case the anti-Markovnikov regioselectivity dictated by the radical intermediate in the intermolecular hydroetherification of a 5-hydroxy-alkene **6** provided a 6-membered heterocycle **7**, instead of the 5-membered one **8** that would be obtained with the common acid catalyzed electrophilic addition.[77] A further example of different regioselectivity was discovered by MacMillan[79] while continuing its investigation about the simultaneous employment of organocatalysis and photoredox. The possibility of alkylating an aldehyde in the β position (delivering **11**) instead of in the α position (as commonly implied employing enamine catalysis[78], yielding **12**) was disclosed once again upon the photo-redox generation of a radical intermediate, a β-enaminyl radical in this case.[79]

The previously described works (Scheme 1.23) constitutes an exemplificative glimpse on the entire range of alternative reactivities that might be disclosed using photoredox catalysis. Synthetic organic chemists have constantly foraged new photoredox methodologies over the last decade to provide new elements to this groundbreaking idea of a complementary reactivity.

---

[76] Lin, S.; Ischay, M. A.; Fry, C. G.; Yoon, T. P. *J. Am. Chem. Soc.* **2011,** *133*, 19350-19353.
[77] Hamilton, D. S.; Nicewicz, D. A. *J. Am. Chem. Soc.* **2012,** *134*, 18577-18580.
[78] Mukherjee, S.; Yang, J. W.; Hoffmann, S.; List, B. *Chem. Rev.* **2007,** *107*, 5471-5569.
[79] Terrett, J. A.; Clift, M. D.; MacMillan, D. W. C. *J. Am. Chem. Soc.* **2014,** *136*, 6858-6861.
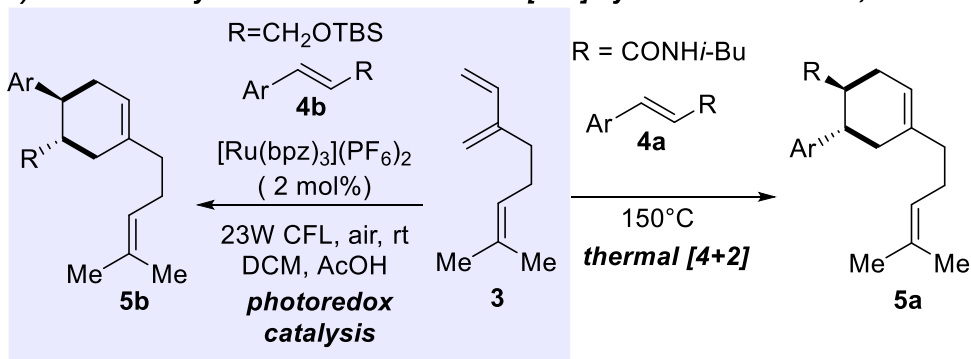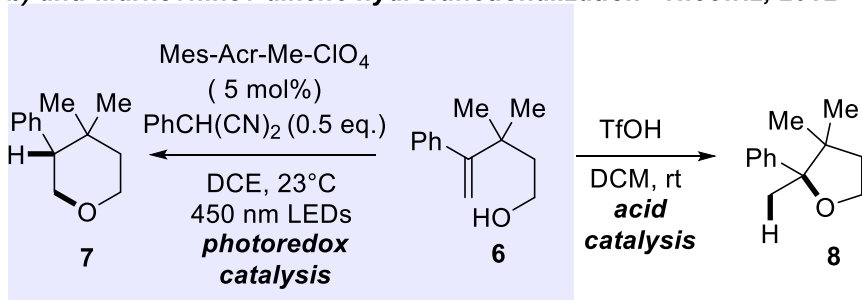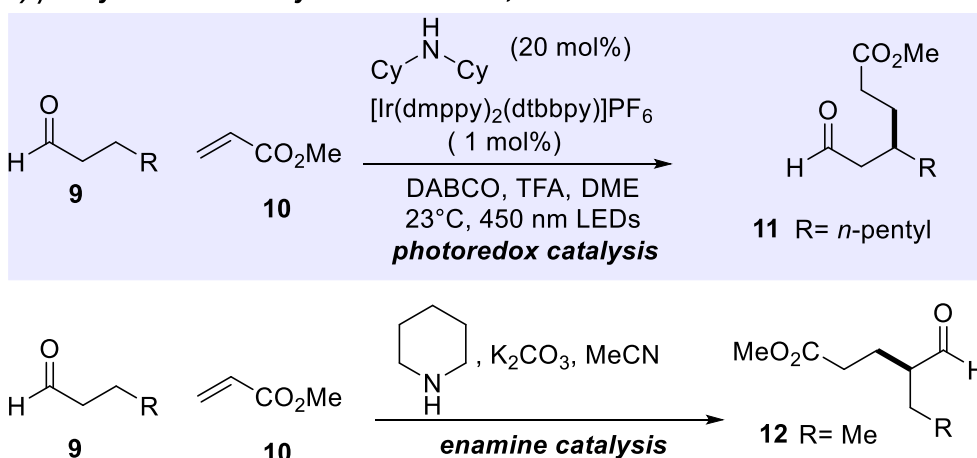
Scheme 1.23 Selected examples of complementarity between photoredox catalysis and thermal reactivity

49

These continuously growing efforts have been gathered in some seminal reviews.[80,81,82,83,84] However, organic photoredox catalysis has become a branch of organic chemistry that is getting more and more diversified every year. Thus, the focus of the review papers has become more specific, analyzing specific classes of transformations allowed by photoredox catalysis: for example transformations promoted by organic PC,[48] or processes that merge two different catalytical approaches like organocatalysis and photoredox catalysis[85] or transition metal catalysis and photoredox catalysis[86]. Throughout the years the topic photoredox-catalysis has furtherly diversified, with new emerging topics as enantioselective or asymmetric photoredox catalysis, photoredox catalysis for specific C-H activation, for biomacromolecules modification, applied to polymer science and to the synthesis of natural products; all gathered in dedicated special issues of review-based high impact journals.[87,88,89]

Alternatively, the reviewing works concerning photoredox catalysis have evolved to provide an easy tool to consult ultimately leading to the implementation of photoredox catalyzed steps in virtually each synthetic plan.[90,91,92,93]

[80] Narayanam, J. M. R.; Stephenson, C. R. J. *Chem. Soc. Rev.* **2011,** *40*, 102-113.

[81] Xuan, J.; Xiao, W.-J. *Angew. Chem. Int. Ed.* **2012,** *51*, 6828-6838.

[82] Prier, C. K.; Rankic, D. A.; MacMillan, D. W. C. *Chem. Rev.* **2013,** *113*, 5322-5363.

[83] Skubi, K. L.; Blum, T. R.; Yoon, T. P. *Chem. Rev.* **2016,** *116*, 10035-10074.

[84] Shaw, M. H.; Twilton, J.; MacMillan, D. W. C. *J. Org. Chem.* **2016,** *81*, 6898-6926.

[85] Ravelli, D.; Fagnoni, M.; Albini, A. *Chem. Soc. Rev.* **2013,** *42*, 97-113.

[86] Twilton, J.; Le, C.; Zhang, P.; Shaw, M. H.; Evans, R. W.; MacMillan, D. W. C. *Nat. Rev. Chem.* **2017,** *1*, 0052 (0051-0018).

[87] *Photochemistry in Organic Synthesis [Special Issue]*. *Chem. Rev.,* American Chemical Society: **2016,** *116,* 17

[88] *Photoredox Catalysis in Organic Chemistry [Special Issue]*. *Acc. Chem. Res.,* American Chemical Society: **2016,** *49,* 7-10

[89] *Photochemical Catalytic Processes [Special Issue]*. *Chem. Rev.,* American Chemical Society: **2022,** *122,* 2

[90] Douglas, J. J.; Sevrin, M. J.; Stephenson, C. R. J. *Org. Process Res. Dev.* **2016,** *20*, 1134-1147.

[91] Marzo, L.; Pagire, S. K.; Reiser, O.; König, B. *Angew. Chem. Int. Ed.* **2018,** *57*, 10034-10072.

[92] Petzold, D.; Giedyk, M.; Chatterjee, A.; König, B. *Eur. J. Org. Chem.* **2020,** *2020*, 1193-1244.

[93] Pitre, S. P.; Overman, L. E. *Chem. Rev.* **2022,** *122*, 1717-1751.

1.2.5 Photogeneration of radical and radical ions species

This paragraph provides a summary of the main methods that exploit visible light both to achieve photolysis of chemical bond and to apply photoredox catalysis with the final aim of generating radical and radical ion species.

$$R^1\text{-}X \quad + \quad R^2\text{-}Y$$

$$h\nu \downarrow \qquad\qquad \downarrow h\nu$$

$${}^*R^1\text{-}X \qquad R^2\text{-}Y^*$$

$$R^2\text{-}Y \qquad\qquad R^1\text{-}X$$

$$\boxed{R^1\text{-}X^{-\bullet} \quad R^2\text{-}Y^{+\bullet}}$$
radical ion pair

$$R^1\text{-}X + R^2\text{-}Y \qquad X^- \qquad Y^+ \qquad R^1\text{-}X\text{-}R^2\text{-}Y$$

radical substitution addition/ elimination $\quad \bullet R^1 \qquad \bullet R^2 \quad$ radical substitution/ addition/ elimination

$$R^2\text{-}Y^{+\bullet} \qquad R^1\text{-}X^{-\bullet}$$

$$Y^+ \qquad\qquad X^-$$

$$R^1\text{-}R^2 \qquad\qquad R^1\text{-}R^2$$
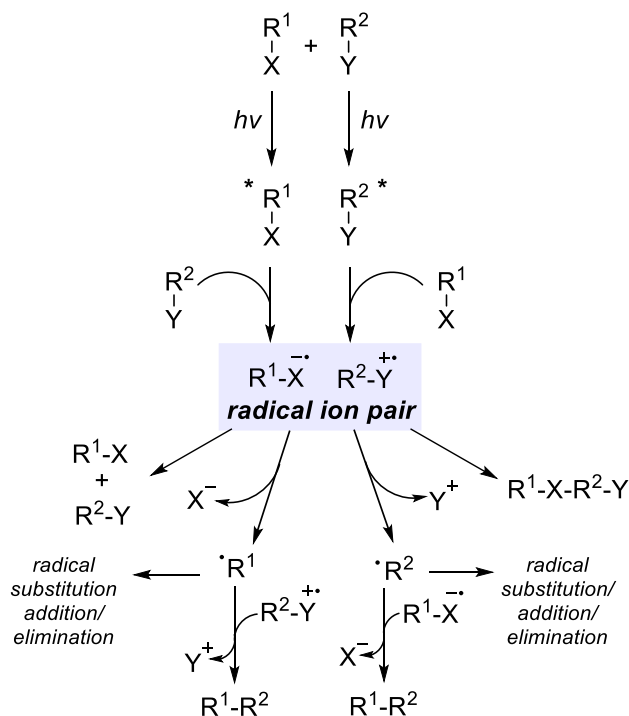
Scheme 1.24 Photogeneration and reactivity or radical ion pair formation by the direct irradiation of organic molecules

Concerning radical ions, the typical photochemical approach to their generation is the irradiation of one of the two organic molecules **R¹-X** and **R²-X**. The promotion to the excited state yields the species **R¹-X*** that can now interact with the ground state of **R²-X** as described in the typical mechanism of a photoinduced electron transfer (Scheme 1.4), leading to the formation of a radical ions pair. Depending on the nature of the PET (oxidative or reductive) both [(R¹-X)•⁺(R²-Y)•⁻] and [(R¹-X)•⁻(R²-Y)•⁺] pairs can be generated. For the purposes of a general description, only the formation of **[(R¹-X)•⁻(R²-Y)•⁺]** will be considered. From this latter, many outcomes can occur. BET would yield the two initial species back to the ground state, preventing any chemical transformation. A desirable outcome would instead

occur when one of the radical ions is a stable species whereas the other one evolves to a radical intermediate **R•**. This happens when **X** is a nucleofugal group in the radical anion **R¹-X•⁻** or when **Y** is an electrofugal group in the radical cation **R²-Y•⁺**. In both cases, upon the release of such groups (as **X⁻** and **Y⁺**, respectively), the desired **R•** is obtained and can in turn react in radical substitution, addition, or elimination reactions. Alternatively, it can also be trapped by the remaining radical ion, providing a reaction of *iso* substitution. A final rare outcome is represented by the formation of the chemical adduct between the two ionic species **R¹-X-R²-Y** (Scheme 1.24).[28]

However, the modern prominent strategy way to obtain radical ions intermediates (**R•⁺** and **R•⁻**) is the use of photoredox catalysis, relying on the exploitation of PET reactions provided by an excited **PC** to deliver such species, as thoroughly described in Scheme 1.15. Once generated, **R•⁺** and **R•⁻** might then directly react as radical ions and then yield the reaction products. Alternatively, they might be converted to a radical species **R•** if they bear a nucleo- or electro-fugal group, as described above. Notably, a carbon-based reactive radical ion intermediate can be generated in photoredox conditions when an unsaturated organic molecule is directly engaged in the PET (Scheme 1.25).
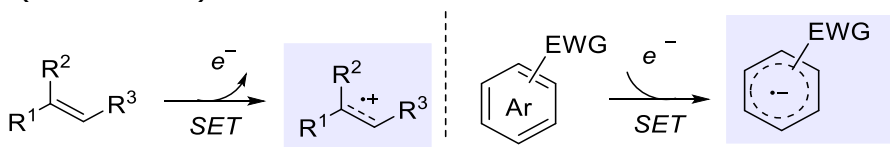
Scheme 1.25 Selected examples of photoredox mediated generation of radical ion pair by SET involving unsaturated systems. See also Scheme 1.15 for the general photoredox mediated generation of radical ion pair

Concerning neutral radicals, organic chemistry has mainly focused on the generation of carbon radicals, since the guided and selective construction of C-C bonds is the final aim of every synthetic process.

In this context, photolysis was among the first strategy used to deliver heteroatom centered radicals **Z•** that were then exploited to generate carbon centered radical species. Previously in this dissertation, the use of photolysis has been shown as an alternative to AIBN activation of Bu₃Sn-H. Table 1.2 shows that many organic bonds might be subjected to photolysis even under visible light conditions. Molecules bearing N-halo (particularly in amides), S−S disulfides, X-X dihalogens (the photoinduced halogenation of alkanes is one of the best-known examples), or N−O bonds are easily cleaved yielding

heteroatom centered radicals **Z•** that may further interact with organic substrates.

However, the most desirable homolysis of Z−H bond is still impractical in most cases, and only S-H or P-H bond can be successfully broken exploiting photolysis. Nevertheless, some examples of homolytical cleavage of photoinitiators **PI** upon irradiation yielding an activated species that can abstract a hydrogen from a Z-H bond are reported.

Photoredox catalysis represents an alternative to this strategy, since, for example, amide N-H bond rupture can be obtained through a proton coupled electron transfer (PCET) delivering a N centered amidyl radical[94] (Scheme 1.26). However, specific methods of visible light induced generation of nitrogen center radical will be discussed in the next paragraph of this dissertation.
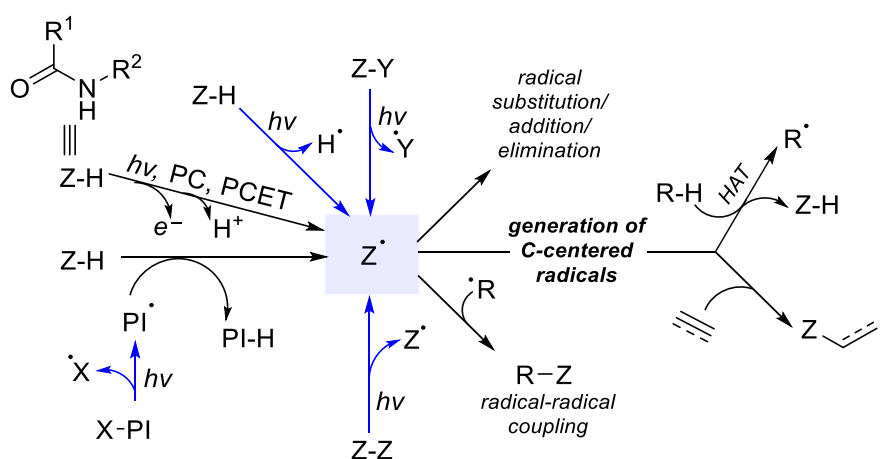
Z= heteroatom: tipically P, S, N, O
Y= heteroatom different from Z
X= halogen

Scheme 1.26 The photogeneration and reactivity of neutral heteroatom centered radicals. Blue arrows indicate photolysis paths. PC=photoredox catalyst, PCET=proton coupled electron transfer

The direct carbon-heteroatom photolysis is possible, although the **R-Z** species presenting suitable matching between bond strength and visible light associated energy are usually also associated with poor light absorption.

---

[94] Choi, G. J.; Knowles, R. R. *J. Am. Chem. Soc.* **2015,** *137*, 9226-9229.

Besides, a competitive heterolytic pathway may arise from the same species yielding an ion pair (R^+ and Z^-). Thus, alternative targets for a photolysis mechanism yielding $R^{\bullet}$ have been proposed. Upon the direct and high yielding modification of a starting carboxylic acid **13**, *N*-hydroxy-2-thiopyridone (Barton) ester **14** can easily be obtained. This latter, upon irradiation with UV or violet light experiences a photofragmentation initiated by the photolysis of N-O bond delivering $R^{\bullet}$ upon loss of CO_2. However, despite the straightforward synthetic availability, Barton esters are associated with difficult handling and storage.
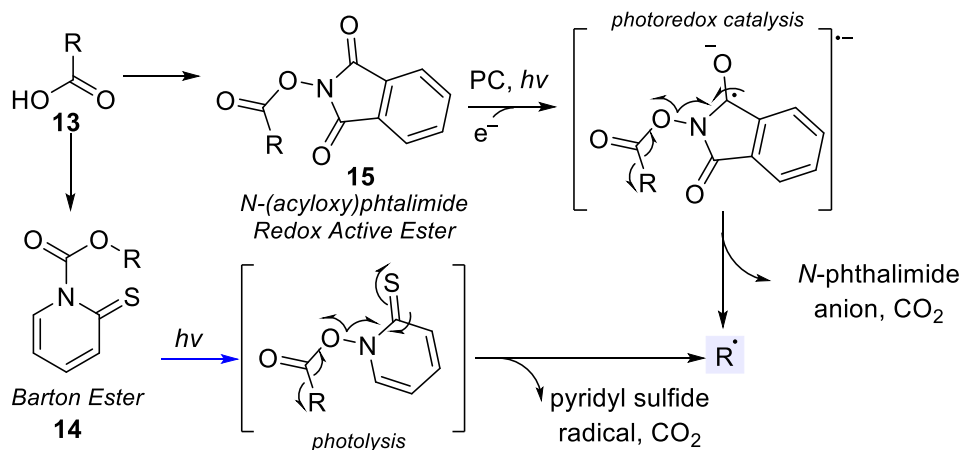
Scheme 1.27 The photogeneration of carbon centered radicals from **13** treated to obtain Barton Esters **14** or Redox Active Esters **15**. Blue arrow indicates photolysis path. PC=photoredox catalyst

However, the development of photoredox catalysis has disclosed the employment of *N*-(Acyloxy)phthalimides ester or Redox Active Esters RAE **15** as an alternative. Under photoredox conditions, such esters are reduced in a PET event yielding a radical anion that undergoes a similar photofragmentation initiated by N-O cleavage that finally delivers $R^{\bullet}$ (Scheme 1.27).[95]

A further ideal alternative to achieve neutral carbon centered radicals is represented by the selective breaking of a C-H bond. This process, when intended as the main way to produce a $R^{\bullet}$ species, is identified as Hydrogen Atom Transfer (HAT).[96] Indeed, when a species in its excited state or a pre-

[95] Murarka, S. *Adv. Synth. Catal.* **2018,** *360*, 1735-1753.
[96] Capaldo, L.; Ravelli, D.; Fagnoni, M. *Chem. Rev.* **2022,** *122*, 1875-1924.

formed radical can perform a radical substitution of a hydrogen atom from a R-H species (namely a hydrogen atom abstraction) producing a **R$^\bullet$** intermediate, such process is classified as HAT. HAT processes are in turn divided into Direct Hydrogen Atom Transfer (*d*-HAT) and Indirect Hydrogen Atom Transfer (*i*-HAT).

In the first case, a light-absorbing molecule with particular features acts as a catalyst **C$_{HAT}$** for the process. Such features are represented by the presence of an oxo group moiety (C=O or Z=O), that upon light absorption by the molecule, get the oxygen atom to acquire a radical character in the excited state. Thus, the excited catalyst **C$_{HAT}$*** is similar to an alkoxyl radical that might act as a hydrogen abstractor breaking a R-H bond to yield **R$^\bullet$** while being reduced to **C$_{HAT}$$^\bullet$-H** by hydrogen transfer. A back-HAT step is required to regenerate the catalyst. The hydrogen acceptor might be a sacrificial molecule in the reaction mean, that should accept both an electron and a proton from the reduced catalyst (in PCET process) or the final radical intermediate *en route* to the product that would terminate its radical chain reactivity in this way (net back hydrogen transfer) (Scheme 1.28 right). Proper HAT catalysts among organic molecules are represented by those aldehydes and ketones usually employed as dyes, colored dyes, α-diketones, α-ketoacids, and (anthra)quinones. Some inorganic variations include the decatungstate anion $[W_{10}O_{32}]^{4-}$, the uranyl cation $[UO_2]^{2+}$ (Z = U) and antimony oxo porphyrin complexes.

In the case of an *i*-HAT, instead, an excited molecule, that in most of the cases is actually a photoredox catalyst **PC**, promotes the generation of a radical or radical **Z$^\bullet$** ionic species (**Z$^{\bullet+}$** or **Z$^{\bullet-}$**) that can act as a hydrogen atom abstractor upon SET. The regeneration of the **PC** follows the paths already described in Scheme 1.15, whereas the **R$^\bullet$** obtained by HAT can react in the desired fashion. Common radical species **Z$^\bullet$** acting in HAT are alkoxyl radicals, aminoxyl radicals, amidyl radicals, thyil radicals, halogen atoms, and of course other sacrificial *C*-centered radicals. Amine radical cations are the most exploited among radical ions, while some neutral species like dioxiranes or metal-oxo species can also be employed (Scheme 1.28 left).

Although **C$_{HAT}$** and **PC** might seem similar, it is important to highline that HAT photocatalytic cycle involves the transfer of a hydrogen atom, hence radical substitution reactions, whereas a photoredox catalytic cycle involves the transfer of an electron, hence redox processes.
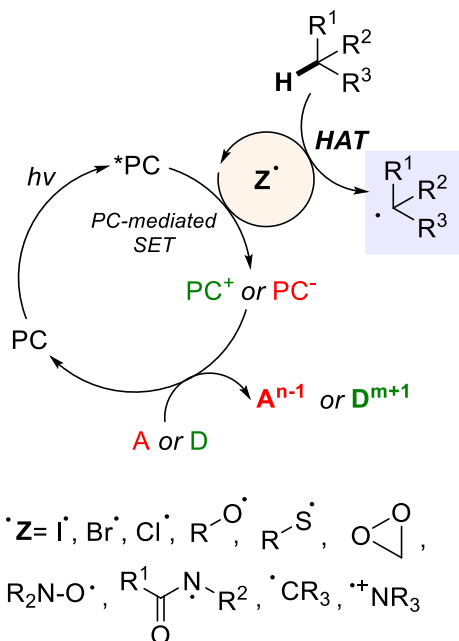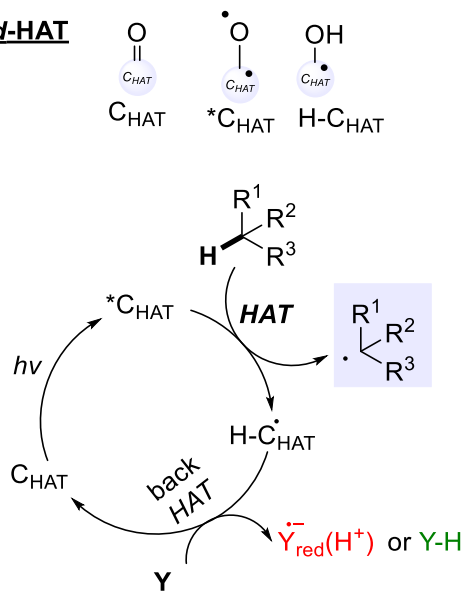
Scheme 1.28 General mechanism of indirect hydrogen atom transfer (i-HAT), left; and of direct hydrogen atom transfer (d-HAT), right

Photoredox catalysis might provide direct strategies to obtain neutral carbon centered radicals **R•** upon SET promoted by the PC cycle   This represents an alternative to the photofragmentation of RAE and i-HAT. Stabilized anionic species like carboxylates **17** might be employed and engaged in oxidative SET events, leading to a neutral carbon centered radical species **18** upon loss of CO_2.[97] Alternatively, a C-halogen bond, instead of being broken upon direct photolysis, might be broken by the intermediation of the excited **PC** in a reductive SET, leading to the generation of **18** upon release of the halide from **16**.[47,98] A further alternative offered by the exploitation of photoredox SET is, as described above, for heteroatom centered radical, the PCET. Phenones **19** might be reduced to the corresponding secondary alcohol that upon loss of hydrogen yield a hydroxy-

[97] Chu, L.; Ohta, C.; Zuo, Z.; MacMillan, D. W. C. *J. Am. Chem. Soc.* **2014,** *136*, 10886-10889.
[98] Nguyen, J. D.; D'Amato, E. M.; Narayanam, J. M. R.; Stephenson, C. R. J. *Nat. Chem.* **2012,** *4*, 854-859.

substituted carbon centered radical species (namely, ketyl radical **20**).[99] Besides, the formation of a radical ion pair centered on a hetoroatom **21**, typically nitrogen, might also evolve in the generation of a carbon centered species **22**.[100] For example, if the carbon atom adjacent to the nitrogen center carrying the ionic radical functionality is deprotonated (Scheme 1.29).

fragmentation (halides and carboxylates)
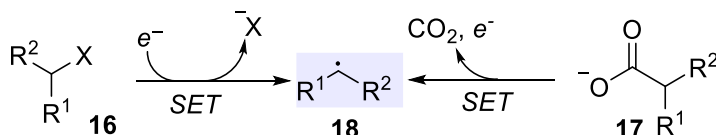
proton coupled electron transfer
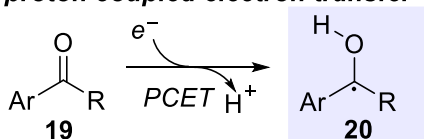
sequential oxidation/deprotonation
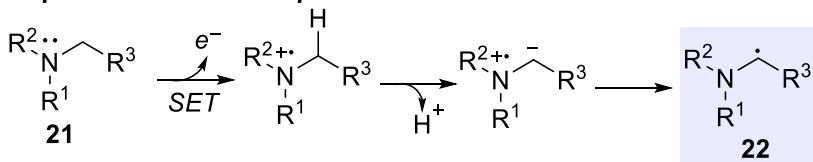
Scheme 1.29 Selected examples of strategies that relies on photoredox catalysis to generate neutral carbon centered radicals

To conclude, it is important to remember that radical intermediates **R•** whether photo- or thermally generated, heteroatom- or carbon-based, might all react in radical substitution, addition, or elimination reactions (Scheme 1.12). Consequently, the general reactivity of a radical is itself a way to generate other radical species.

[99] Tarantino, K. T.; Liu, P.; Knowles, R. R. *J. Am. Chem. Soc.* **2013,** *135*, 10022-10025.
[100] Prier, C. K.; MacMillan, D. W. C. *Chem. Sci.* **2014,** *5*, 4173-4178.
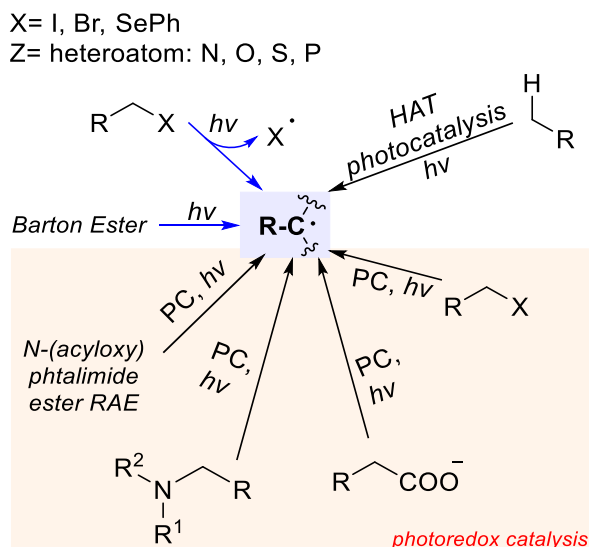
Scheme 1.30 Summary of the photogeneration of carbon centered radicals. Blue arrows indicate photolysis paths. PC= photoredox catalyst

1.3 Nitrogen Centered Radicals (NCRs)

To the aim of this dissertation, nitrogen centered radicals (NCRs) and their generation under thermal, photocatalytic and photoredox conditions are brought into focus, with dedicated emphasis on their reactivity concerning the addition to unsaturated systems delivering nitrogen-based heterocycles. As emerging topic in current organic chemistry, it is important to highline that NCRs might also be obtained *via* electrochemical processes.[101,102] However, to the aim of this dissertation, mainly photochemical methods of generation of NCRs will be discussed, while thermal methods will be only briefly cited as seminal examples and point of comparison regarding the modern photogeneration of NCRs.

1.3.1 Generation of NCRs

NCRs can be generated in two different fashions: *via* the direct homolysis of a N-X bond or *via* SET event, a category that is in turn divided into SET in oxidative conditions, SET in reductive conditions and PCET. (Scheme 1.31).

---

[101] Chen, N.; Xu, H.-C. *Green Synth. Catal.* **2021,** *2*, 165-178.
[102] Xiong, P.; Xu, H.-C. *Acc. Chem Res.* **2019,** *52*, 3339-3350.

a) homolytic cleavage

b) oxidative conditions

b¹) SET

b²) SET

c) reductive conditions

c¹) SET

c²) SET

d) oxidative PCET

SET and loss of H⁺
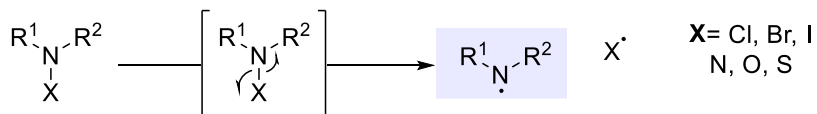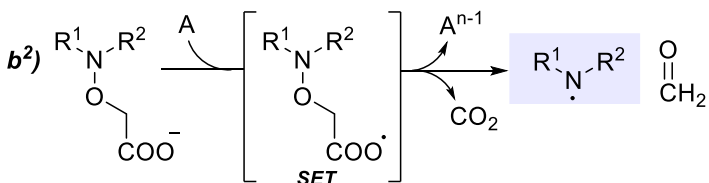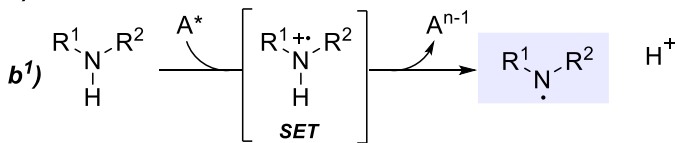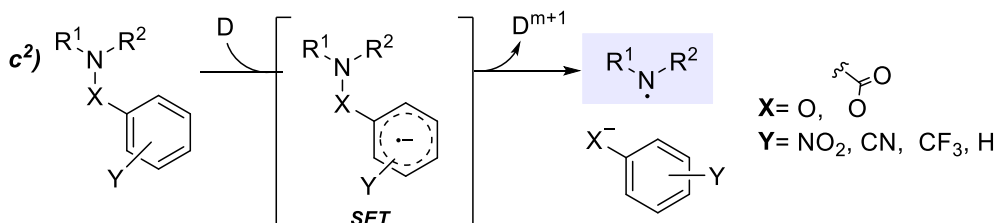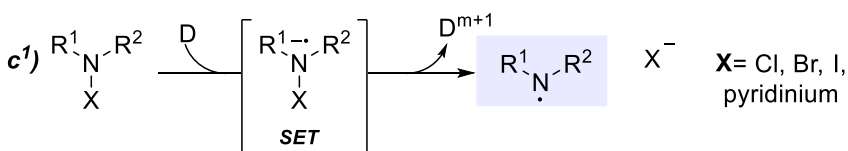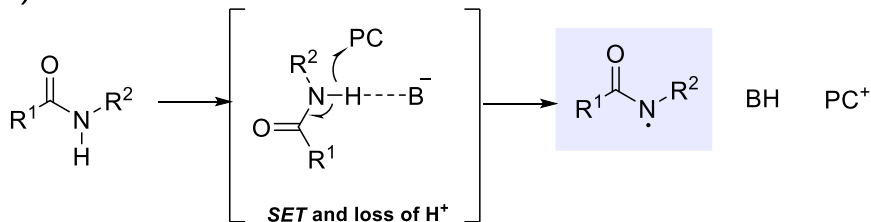
Scheme 1.31 The generation of NCRs. A=generic molecule acting as Acceptor, D=generic molecule acting as Donor, PC=photoredox catalyst

Homolysis is commonly achieved upon UV-light irradiation; thus, the photolytic cleavage of the N-X bond delivers two neutral radicals (Scheme 1.31 a).

SET in oxidative conditions is observed when the molecules bearing the nitrogen functionality donate an electron to another species. This might in turn happens in two ways, the one involving a nitrogen cation and the peripherally induced photofragmentation. The generation of the nitrogen radical cation is observed when the oxidative SET occurs directly from the HOMO centered on the nitrogen atom to an acceptor species. This nitrogen radical cationic intermediate can then react as a radical ion or undergo fragmentation with loss of H^+ delivering a neutral NCR. This well-known strategy relies, under thermal conditions, on the use of sacrificial acceptors working as oxidants employed in stoichiometric quantities. Typical examples are hypervalent iodine compounds or *tert*-butyl hypochlorite.[103,104]

As previously noticed, the use of modern photoredox catalysis, on the other hand, allows this oxidative electron transfer to occur as a SET in the PC cycle thus delivering a nitrogen radical cation (Scheme 1.31 b[1]).

The peripherally induced photofragmentation occurs instead when the oxidative SET involves another functional group of the same molecule carrying the nitrogen functionality. The oxidation of such group triggers a photofragmentation usually driven by the favored release of a neutral molecule (typically CO_2) resulting in the final cleavage of a N-X bond that delivers the neutral NCR. This strategy was first disclosed to achieve iminyl radicals under thermal conditions in the '70s (using oximinoacetic or -propanoic acids in the presence of persulfate as the oxidant)[105] and extensively studied and extended to obtain amidyl and aminyl NCRs by Zard's research group (using O-carboxymethyl oximes) under UV irradiation (Scheme 1.31 b[2]).[106]

---

[103] Togo, H.; Harada, Y.; Yokoyama, M. *J. Org. Chem.* **2000,** *65*, 926-929. Togo, H.; Hoshina, Y.; Muraki, T.; Nakayama, H.; Yokoyama, M. *J. Org. Chem.* **1998,** *63*, 5193-5200.

[104] Barton, D. H. R.; Beckwith, A. L. J.; Goosen, A. *J. Chem. Soc. (Resumed)* **1965**, 181-190.

[105] Forrester, A. R.; Gill, M.; Sadd, J. S.; Thomson, R. H. *J. Chem. Soc., Chem. Commun.* **1975**, 291-292.

[106] Callier-Dublanchet, A.-C.; Quiclet-Sire, B.; Zard, S. Z. *Tetrahedron Lett.* **1995,** *36*, 8791-8794. Boivin, J.; Callier-Dublanchet, A.-C.; Quiclet-Sire, B.; Schiano, A.-M.; Zard, S. Z. *Tetrahedron* **1995,** *51*, 6517-6528. Boivin, J.; Fouquet, E.; Schiano, A.-M.; Zard, S. Z. *Tetrahedron* **1994,** *50*, 1769-1776.

SET in reductive conditions occurs when an electron is transferred to the molecule bearing the nitrogen functionality. As in the previous case, this reduction might either directly occur on the nitrogen functionality, or on a peripheral moiety of the molecule thus inducing a reductive cascade fragmentation.

In the first case, the electron is transferred to the σ* MO of the N-X bond, delivering a nitrogen centered radical anion. When X⁻ is a nucleofugal group, fragmentation leads to the neutral NCR. This transformation, already reported more than 50 years ago, was achieved under thermal conditions using stoichiometric amount of transition metal-based compounds with strong reducing activities like Fe(0) or Ti(III) (Scheme 1.31 c^1).[107]

In the second case, the electron is transferred instead to an unsaturated moiety of the molecule, in the π* orbital of an aromatic or double bond system directly linked to the X moiety of the N-X functionalities. This triggers a cascade photofragmentation that ultimately results in the homolytic cleavage of *N*-X delivering the NCR. Such fragmentation might be successfully achieved under photoredox conditions (Scheme 1.31 c^2).[108]

As emerged from the previous investigations, both mechanisms of SET reductions and SET oxidations proceed through the formation of a charged species, a radical ion intermediate, that subsequently evolves to the neutral NCR (with the exception of photofragmentation that typically arises from an already charged species like a carboxylate). Thanks to the pioneering works of Knowles' research group,[109] it is possible to circumvent the radical ion formation with the oxidative PCET strategy. Indeed, when a protic *N*-H group is in the presence of a base and a PC under irradiation, the deprotonation by the former and a concomitant SET event triggered by the catalytic cycle of the latter lead to the formal homolytic cleavage of N-H. PCET strategy, only recently established and enabled by photoredox catalysis, demonstrates a groundbreaking potential, since no prefunctionalization of the nitrogen center is required Scheme 1.31 d).

[107] Neale, R. S. *Synthesis* **1971,** *1971*, 1-15.
[108] Kärkäs, M. D. *ACS Catal.* **2017,** *7*, 4999-5022.
[109] Gentry, E. C.; Knowles, R. R. *Acc. Chem Res.* **2016,** *49*, 1546-1556. Murray, P. R. D.; Cox, J. H.; Chiappini, N. D.; Roos, C. B.; McLoughlin, E. A.; Hejna, B. G.; Nguyen, S. T.; Ripberger, H. H.; Ganley, J. M.; Tsui, E.; Shin, N. Y.; Koronkiewicz, B.; Qiu, G.; Knowles, R. R. *Chem. Rev.* **2022,** *122*, 2017-2291.

1.3.2 Types of *N*-centered radicals

Depending on the substrates bearing the nitrogen centers, four main different classes of corresponding NCR intermediates can be obtained: iminyl, aminyl, amidiyl and aminium radicals (classification introduced by Leonori).[110]

These four different classes of radicals exhibit unique and different reactivities determined by the geometrical disposition of the atoms characterizing the functional group bearing the nitrogen center (Scheme 1.32). Such feature strictly depends on the orbital where the unpaired electron is located, thus the MO structure is a criterion that determines the reactivity of NCR. Besides, such intermediates might also be classified in terms of "radical philicity"[111,112] thus defining the relative "nucleophilic" or "electrophilic" nature of the radical by comparison with its reactive partner. This terminology must be cautiously employed since it derives from empirical rationalization of the product outcomes from NCR and a coupling partner.

Iminyl radicals, coming from the corresponding imine, are defined as ambiphilic meaning that can react both with electrophilic and nucleophilic coupling partners. They are characterized by a planar structure due to the double bond C=N, thus the electron is located in a sp^2 orbital. Among NCRs, they are to the most similar to carbon centered radicals.

Amidyl radicals come from amides and are also characterized by a sp^2 hybridized *N* atom, but the unpaired electron of the radical occupies a p orbital, thus they are π-radicals. Amidyl are considered electrophilic in nature relatively to the other NCRs.

The remaining classes, aminyl radicals and their protonated analogues aminium radicals, come both from amines and are π-radicals, too.
Aminyls are considered the most nucleophilic between NCRs.   On   the contrary, aminium radicals are the result of a SET oxidation of an amine leading to the formation of a nitrogen centered radical cation and given their positive charge, they are the most electrophilic of the four classes.
Other types of nitrogen radicals exist but their reactivity can be exemplified using these four general classes (e.g., carbamoyl radicals and *N*-Ts radicals are consistent with the behavior of amidyl radicals). Indeed, together with

---

[110] Davies, J.; Morcillo, S. P.; Douglas, J. J.; Leonori, D. *Chem. Eur. J.* **2018,** *24*, 12154-12163.
[111] Héberger, K.; Lopata, A. *J. Org. Chem.* **1998,** *63*, 8646-8653.
[112] De Vleeschouwer, F.; Van Speybroeck, V.; Waroquier, M.; Geerlings, P.; De Proft, F. *Org. Lett.* **2007,** *9*, 2721-2724.

these principal classes, other NCRs are reported like cyanoamidyl and sulfonamidyl and hydrazonyl radicals (Scheme 1.32).[113] Their reactivity is considered consistent with that of amidyl radicals[110] and possess π-electronic structures.

main types of NCRs
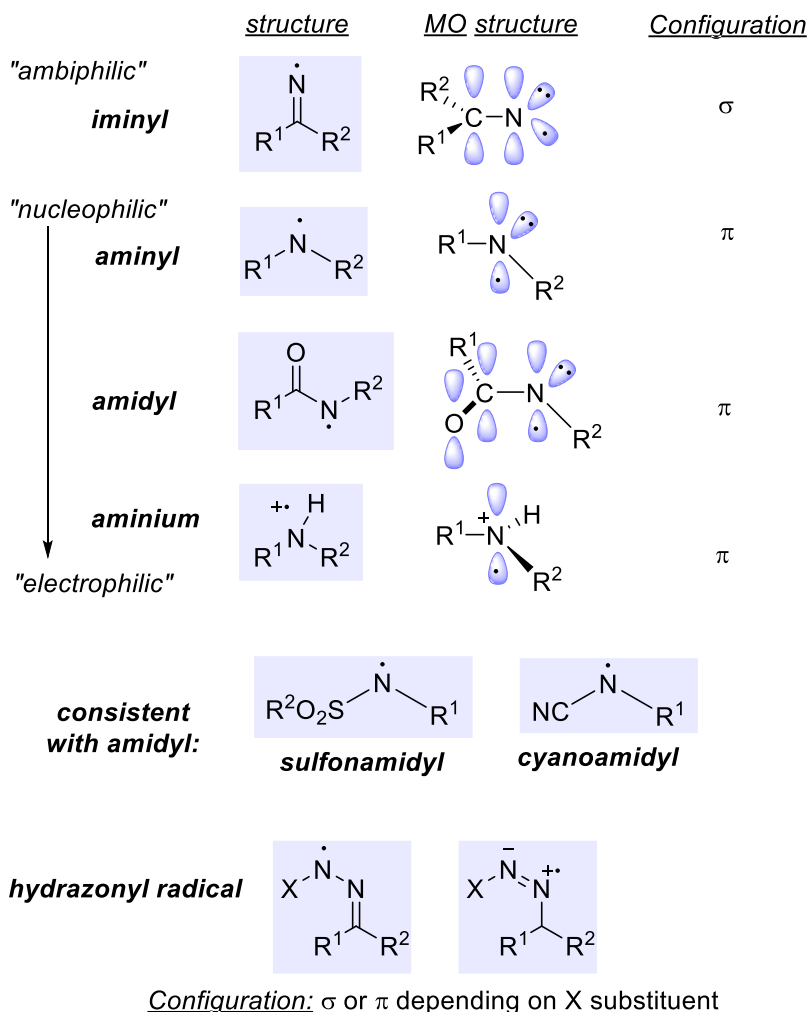
Scheme 1.32 Classification of NCRs

Nevertheless, for hydrazonyl radicals, such features are strongly influenced by the substituent on the sp^3 nitrogen atom of the starting hydrazones and

---

[113] Stella, L., _Nitrogen-Centered Radicals_. **2001**.

affect also the σ/π configuration.[114] However, to the aim of this dissertation, only arylsulfonyl-hydrazonyl radicals are studied, and they might be considered as a subgroup of amidyl radicals. Besides, sulfonamidyl and arylsulfonylhydrazonyl radicals will be analyzed in detail with dedicated introduction in the next chapters.

1.3.2.1 Radical philicity of NCRs and subsequent reaction outcome predictions

The concept of radical philicity is mainly employed to predict and design the most favored reactive partner for a radical species. An exemplar application of such concept is to anticipate the outcome of a reaction between a radical and an olefine, disclosing which alkene correspond to the best reactive partner. To the aim of this dissertation, where reaction of NCRs with carbon based unsaturated systems is the focus, this analysis is perfectly suited. To provide such observation, frontier molecular orbitals of the involved radical species and of the unsaturated system are contemplated (Scheme 1.33).
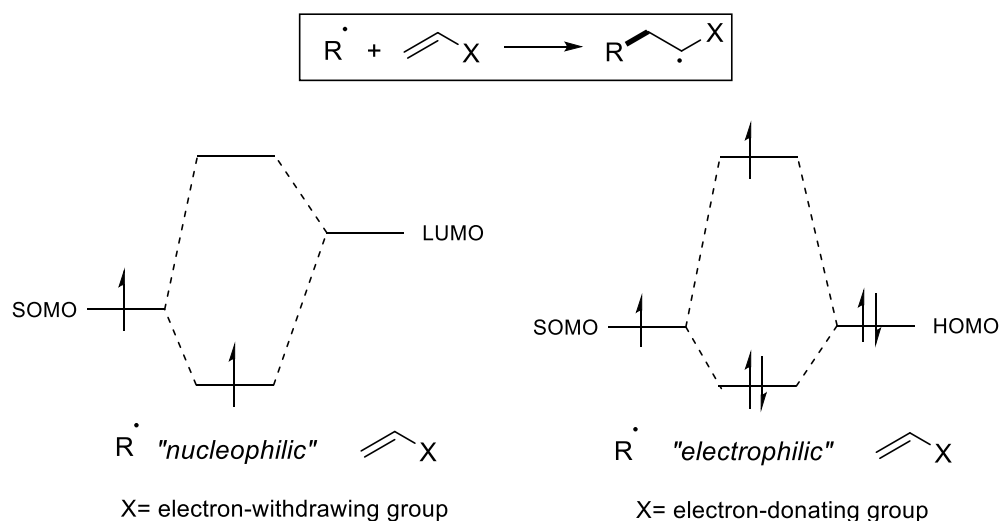
Scheme 1.33 Orbital interaction diagrams between the SOMO of the radical and the LUMO of an electrophilic alkene acceptor (left) and between the HOMO of a nucleophilic alkene acceptor (right)

---

[114] Duan, X. Y.; Zhou, N. N.; Fang, R.; Yang, X. L.; Yu, W.; Han, B. *Angew. Chem. Int. Ed.* **2014,** *53*, 3158-3162.

The energy of the SOMO of a radical is evaluated, to determine its radical philicity, since this latter is correlated to the electronegativity.[115] Once established, a coupling partner providing a successful reaction outcome can be anticipated. Such coupling partner must be chosen to match the polarity of NCRs radical so electron poor olefin will react with more nucleophilic radicals (like aminyl) whereas electron rich alkenes will prefer more electrophilic radicals. However, the determination of the philicity for a given radical is not trivial. A critical help in the determination of radical philicity is provided by computation studies, a further tool in reaction design in modern organic synthesis.[111,112] Besides, the recent review work by Welin research group furnished a didactic approach to elucidate radical philicity thus predicting radical reactivity.[116]

1.3.3 General reactivities of NCRs

The main modes of transformation observed for NCRS are the β-scission (or α-carbon cleavage), the addition to unsaturated system both in intra- and inter-molecular fashion and the 1,5 HAT (Scheme 1.34).

a) *α-carbon cleavage*
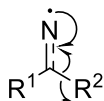
b) *intramolecular addition to π-systems*

c) *intermolecular addition to π-systems*
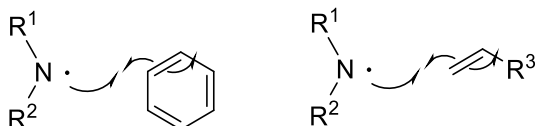
d) *1,5-HAT*
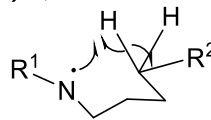
Scheme 1.34 General reactivities of NCRs

β-scission corresponds to the homolysis of the bond between the carbon atom directly connected to the nitrogen center and the substituent on such carbon (Scheme 1.34a). It can also be considered a Norrish type I reactivity. It is typically observed for iminyl NCRs leading to the generation of

---

[115] Laird, E. R.; Jorgensen, W. L. *J. Org. Chem.* **1990,** *55,* 9-27.
[116] Parsaee, F.; Senarathna, M. C.; Kannangara, P. B.; Alexander, S. N.; Arche, P. D. E.; Welin, E. R. *Nat. Rev. Chem.* **2021,** *5,* 486-499.

a nitrile derivative and R• radical,[117] while, for aminium radical, it was first reported by Minisci and Galli (with the generation of R• and iminium $R^1C(R^2)=N^+-R^3$ ion).[118]

Crucial to the aim of this dissertation is the reactivity of NCRs with unsaturated systems (Scheme 1.34c). The mechanism is the same of a radical addition. For NCR intramolecular addition systems (Scheme 1.34b), 5-*exo trig* cyclization are observed, although 6-*endo trig* might also be observed shaping the transition state of such reaction by the appropriate tuning of the olefin substituents.[119] This cyclization mode is a straightforward synthetic strategy to deliver functionalized heterocycles, as emphasized throughout this whole thesis. Intermolecular addition to π-systems, on the other hand, is a powerful tool for the installation of nitrogen-based functionalities on preformed organic scaffolds. It is indeed widely employed as exemplar late-stage functionalization strategy.

Finally, concerning addition to unsaturated system, NCR adding to arenes and aromatic systems are also reported systems This typically leads to homolytic aromatic substitution (HAS, in Scheme 1.34b and Scheme 1.34c example with benzene). HAS is a formal hydrogen atom substitution, it is initiated by the addition of NCR to the aromatic system delivering a delocalized radical species. Thus, aromaticity is either repristinated upon the loss of a hydrogen atom completing the substitution or *via* oxidation SET event delivering a cation species that evolves with deprotonation and N-C functionalization.[120]

However, in some cases a dearomatization process following the generation of the delocalized radical might also occur. Despite being predominantly observed for carbon centered radical attacking an arene moiety,[121] direct NCR promoted intramolecular dearomatization leading to C-N bond formation might be observed.[122,123] Only when the spirocyclic scaffold resulting as an outcome of this reaction *ipso*-HAS might represent a stable alternative (e.g.

---

[117] Boivin, J.; Fouquet, E.; Zard, S. Z. *J. Am. Chem. Soc.* **1991,** *113*, 1055-1057.

[118] Minisci, F.; Galli, R. *Tetrahedron Lett.* **1966,** *7*, 2531-2533.

[119] Beckwith, A. L. J.; Schiesser, C. H. *Tetrahedron* **1985,** *41*, 3925-3941.

[120] Bowman, W. R.; Storey, J. M. D. *Chem. Soc. Rev.* **2007,** *36*, 1803-1822. Augood, D. R.; Hey, D. H.; Nechvatal, A.; Williams, G. H. *Nature* **1951,** *167*, 725-725.

[121] Cheng, Y.-Z.; Feng, Z.; Zhang, X.; You, S.-L. *Chem. Soc. Rev.* **2022**.

[122] Han, Y.; Jin, Y.; Jiang, M.; Yang, H.; Fu, H. *Org. Lett.* **2019,** *21*, 1799-1803.

[123] Wu, L.; Hao, Y.; Liu, Y.; Song, H.; Wang, Q. *Chem. Commun.* **2020,** *56*, 8436-8439.

formation of a cyclohexadienone instead of aromaticity repristination).[122] Dearomatization will be discussed in detail in Chapter 4 of this dissertation.

1,5-HAT is a reactive path that provide peripheral functionalization of the molecule bearing the nitrogen functionality. A NCRs might indeed operate a hydrogen atom abstraction on a distal (tipically) carbon center. The newly formed radical is generated on the δ-position since the transition state for this transformation is a favored 6-membered cyclic intermediate systems (Scheme 1.34d).[124]

These three main classes of reactivities are then subjected to other general considerations. First, all of them lead to the evolution of another radical species, typically carbon centered one from a NCR one. Such consequence should be wisely exploited to achieve multiple bond construction, so that after a first N-C bond formation other C-C or C-X bond formation might occur. This would trigger cascade processes by the initial generation of a NCR.

Moreover, concerning radical additions to unsaturated system, it must be remarked that differently from polar electrophilic addition to olefins, being governed by the stability of the intermediate carbocation, the radical mechanism might be exploited to dictate addition with anti-Markovnikov selectivity.[125]

As a general statement, increased reactivity is proportional to the electrophilicity of the NCR species considered. However, experiments on 5-*exo trig* cyclization rate determined that amidyl radicals constitute an exception, being the most reactive (2×10^9 s^{-1} and 5×10^8 s^{-1}). Decreasing rate of cyclization are then coherently reported for aminium radical (1×10^8 s^{-1}), followed by aminyl (2×10^4 s^{-1}) and finally iminyl (1×10^4 s^{-1}, Scheme 1.35).[126] Aminyl radicals are the most nucleophilic in nature, being burdened with both a lone pair and the unpaired electron on the same nitrogen. However, comparing their reduction rate constant for reaction with Bu$_3$SnH with that of carbon centered and alkoxy radicals they appear as the least reactive (from most to least: alkoxy>carbon>aminyl).[113] Among the four classes of NCR, aminyl radicals are the ones showing reversibility in addition to unsaturated bonds. Thus, their use is typically avoided when a radical

---

[124] Stateman, L. M.; Nakafuku, K. M.; Nagib, D. A. *Synthesis* **2018,** *50*, 1569-1586.

[125] Gasc, M. B.; Lattes, A.; Perie, J. J. *Tetrahedron* **1983,** *39*, 703-731.

[126] Horner, J. H.; Musa, O. M.; Bouvier, A.; Newcomb, M. *J. Am. Chem. Soc.* **1998,** *120*, 7738-7748.

amination of an olefin is planned, nevertheless, they exhibit preference for hydrogen abstraction, becoming suitable candidates to promote carbon centered radical formation upon 1,5-HAT.[127]

Rates of cyclisation (k_c)

NCR

$k_c(s^{-1})$: 2×10^9 5×10^8 1×10^8 2×10^4 1×10^4

decrease in rate of cyclisation
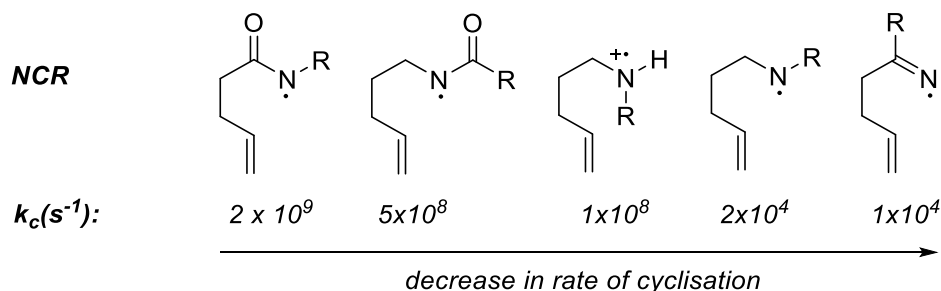
Scheme 1.35 Comparison of the rate of cyclization for NCRs adding intramolecularly to unsaturated alkenes.

1.3.4 Visible-light mediated generation of NCRs

This general introduction on NCRs' generation and reactivity provided the basic premises of this dissertation. The use of visible light induces modes of radical generation to deliver NCRs for cyclization reactions thus affording complex saturated heterocyclic scaffolds.

The peculiar reactivity of NCRs is certainly not unprecedented, and many thermal strategies towards such intermediates have been reported since the beginning of the 20th century.[128] The thermal and historical methods leading to NCRs relies on high temperature, strong oxidative or reductive environment, use of hypervalent iodine compounds, use of radical initiators and UV irradiation that dramatically limited the scope and applications of these otherwise intriguing transformation towards NCRs. Moreover, the control on the reaction outcomes of the radical chain initiated by the generation of NCR resulted extremely difficult in such harsh conditions.

However, among these methods a groundbreaking idea in the development of sp² functionalization by NCR was disclosed. Such milestone is represented by the Hoffman-Loffer-Freytag (HLF) reaction that also laid the foundation for NCR-mediated strategies for the synthesis of heterocycles. The HLF corresponds to the first uses of NCRs in organic synthesis and dates to 1883

---

[127] Walton, J. C. *Acc. Chem Res.* **2014,** *47*, 1406-1416.
[128] Pratley, C.; Fenner, S.; Murphy, J. A. *Chem. Rev.* **2022,** *122*, 8181–8260.

and 1909,[129,130] however the radical nature of the process was confirmed decades later with mechanistic studies by Corey.[131] The first NCR generated in HFL was a radical aminium ion **24**. Indeed, upon the protonation of a haloamine **23** the N-Cl bond is cleaved by UV irradiation or under thermal initiator, delivering the NCR **24**. As the reaction was conducted with aliphatic haloamines, no addition reaction was observed. However, 1,5-HAT remains a possible reactive pathway. The abstraction of the δ-hydrogen delivers the carbon centered radical **25**, that is halogenated upon interaction with another molecule of chloroamine **23**. The radical attack of the carbon centered radical to the N-Cl in acidic mean leads to the regeneration of the aminium species **24**, thus propagating the radical chain while concomitantly forging a C-Cl bond. The new species carrying C-Cl bond **26** undergoes intramolecular ionic cyclization in basic conditions furnishing a nitrogen heterocycle **27** (Scheme 1.36).
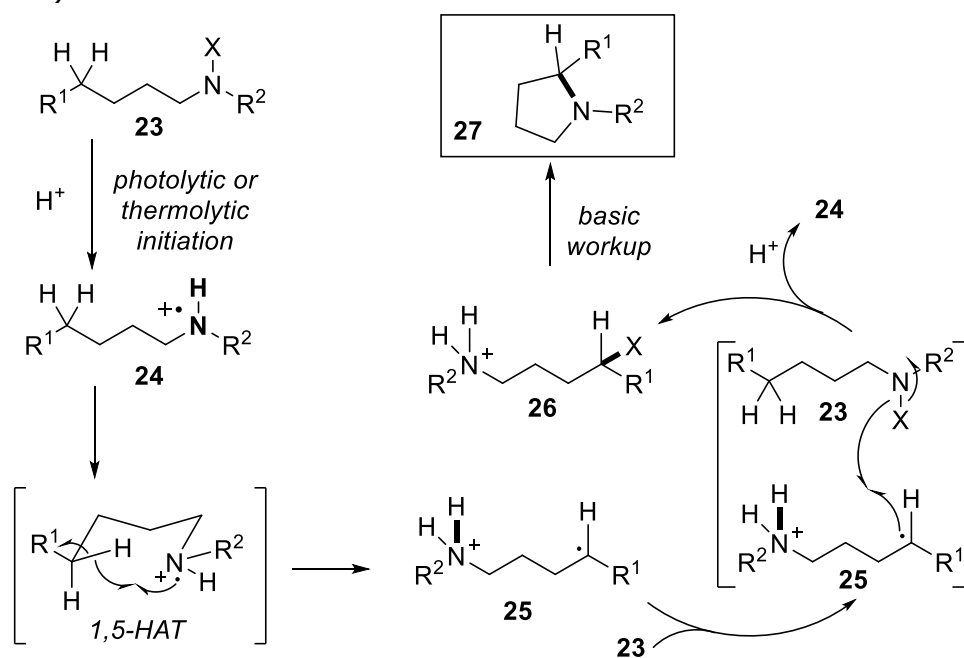
Scheme 1.36 General mechanism of the HFL reaction

Since the discovery and application of HFL reaction, the use of light was already contemplated among the methods of NCR generation. However, the

[129] Hofmann, A. W. *Ber. Dtsch. Chem. Ges.* **1883,** *16*, 558-560.
[130] Löffler, K.; Freytag, C. *Ber. Dtsch. Chem. Ges.* **1909,** *42*, 3427-3431.
[131] Corey, E. J.; Hertler, W. R. *J. Am. Chem. Soc.* **1960,** *82*, 1657-1668.

use of UV light limited these applications since many organic structures might encounter degradation under such conditions. The recent reviewing work by Murphy summarizes the methods of N-X radical generation that relies both on thermal conditions and on UV-light irradiation. Most of the methods based on irradiation were developed in the absence of the actual technology concerning light sources. Indeed, some of these molecules carrying the N-X functionalities might undergo photolysis even under visible light irradiation, however the light sources employed in traditional chemistry, covering both visible and UV wavelengths did not consent to observe such discrimination. Given the technological advances concerning light sources, that provide sharper and more accurate emissive band, some of these methods might be reconsidered since they might also occur under mild visible light irradiation.

Nevertheless, it is only with the advent of photoredox catalysis that the visible light has been definitely implemented as an indispensable and essential tool to generate NCRs. Recently, an extensive work on reviewing all the photoredox methods that provide NCRs and their associated reactivity has been accomplished by Roizen and co-workers.[132] First, the authors report how the breaking of N-X on functionalized nitrogen center has become available in mild conditions using photoredox catalysis (cleavage of *N*-Halogen bond in chloramines, cleavage of N-N bond of aminopyridinium salts and cleaveage of N-S bond in tosylamides and sulfoximines are considered, Scheme 1.37).
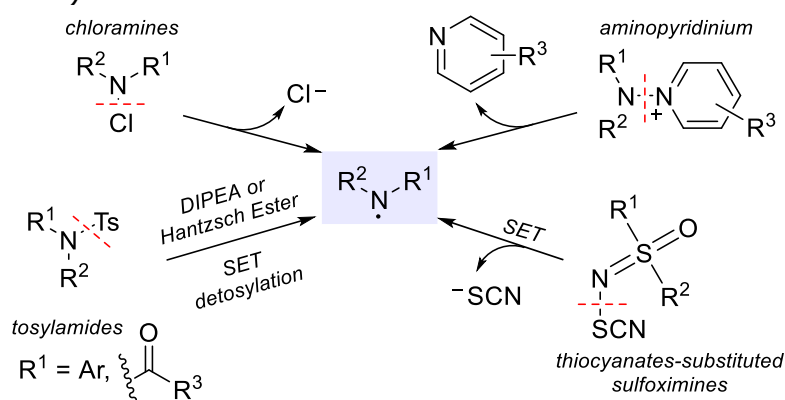
Scheme 1.37 Photoredox mediated generation of NCRs from N-X cleavage when X=Cl, S, N [132]

---

[132] Kwon, K.; Simons, R. T.; Nandakumar, M.; Roizen, J. L. *Chem. Rev.* **2022,** *122*, 2353-2428.
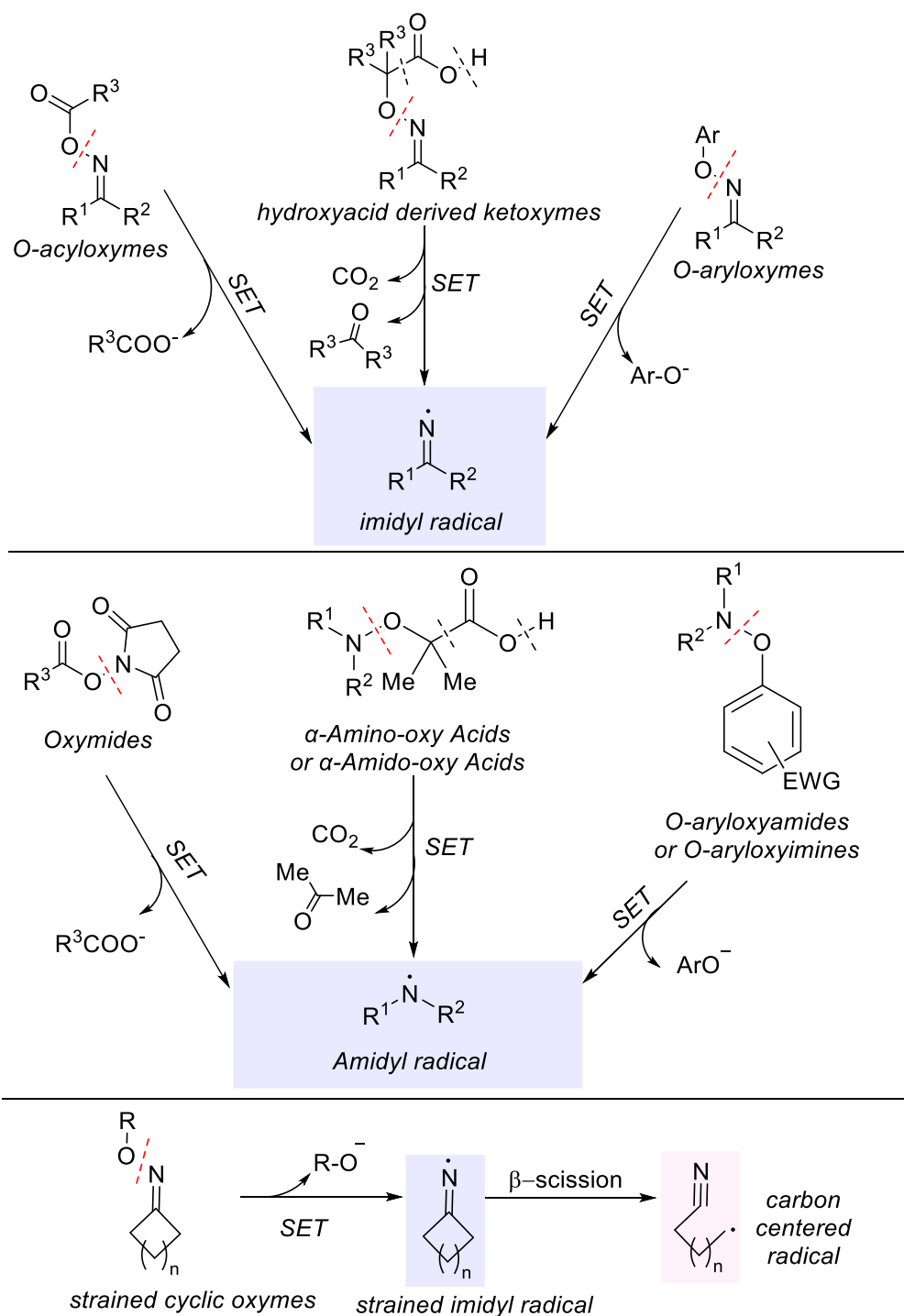
Scheme 1.38 Photoredox mediated generation of NCRs by N-O cleavage[132]

Concerning instead N-O bond cleavage in photoredox conditions, a recent renaissance (driven in particular by Leonori's research group[110]) has been witnessed, particularly using oxymes to provide neutral iminyl radical. However, neutral aminyl or neutral amidyl radicals might also be obtained starting from α-Amino-oxy Acids or α-Amido-oxy Acids) and *O*-aryloxyimides or *O*-aryloxyamides (Scheme 1.38).

Finally, coherently with the aim of this dissertation, a critical focus was set on N-H bond cleavage. Indeed, only the extensive development of photoredox catalysis provides the ultimate mean to convert light into chemical energy that would selectively break the N-H bond. This instrument is revolutionary since it allows to work directly on the nitrogen center without prefunctionalization. N-H conversion into charged NCR (like aminium) only requires the direct oxidation of the nitrogen center in an oxidative SET mechanism. This is a straightforward strategy to obtain a radical cation species centered on nitrogen. The broad range of applications of this electrophilic radical intermediate for C-N bond formation is not included in the aim of this dissertation, having neutral NCRs as focus, it has been comprehensively recently discussed by Knowles.[133] However, photoredox catalysis also enabled the generation of neutral NCRs with the direct activation of such N-H bond. This mainly occurs exploiting PCET mechanism or *via* sequential proton transfer (deprotonation of N-H) followed by oxidative SET, and this strategy can be applied to amides, sulfonamides, sulfamates and hydrazones (Scheme 1.39).

Such neutral NCRs might then react in all the modes listed in paragraph 1.3.3. To the aim of this dissertation, the reactivity of neutral hydrazonyl radical and neutral sulfonamidyl radical will be analyzed. Particularly, the addition of hydrazonyl and sulfonamidyl radicals to unsaturated systems leading to cyclization and thus triggering further functionalization in a cascade fashion will be discussed.

---

[133] Ganley, J. M.; Murray, P. R. D.; Knowles, R. R. *ACS Catal.* **2020,** *10*, 11712-11738.
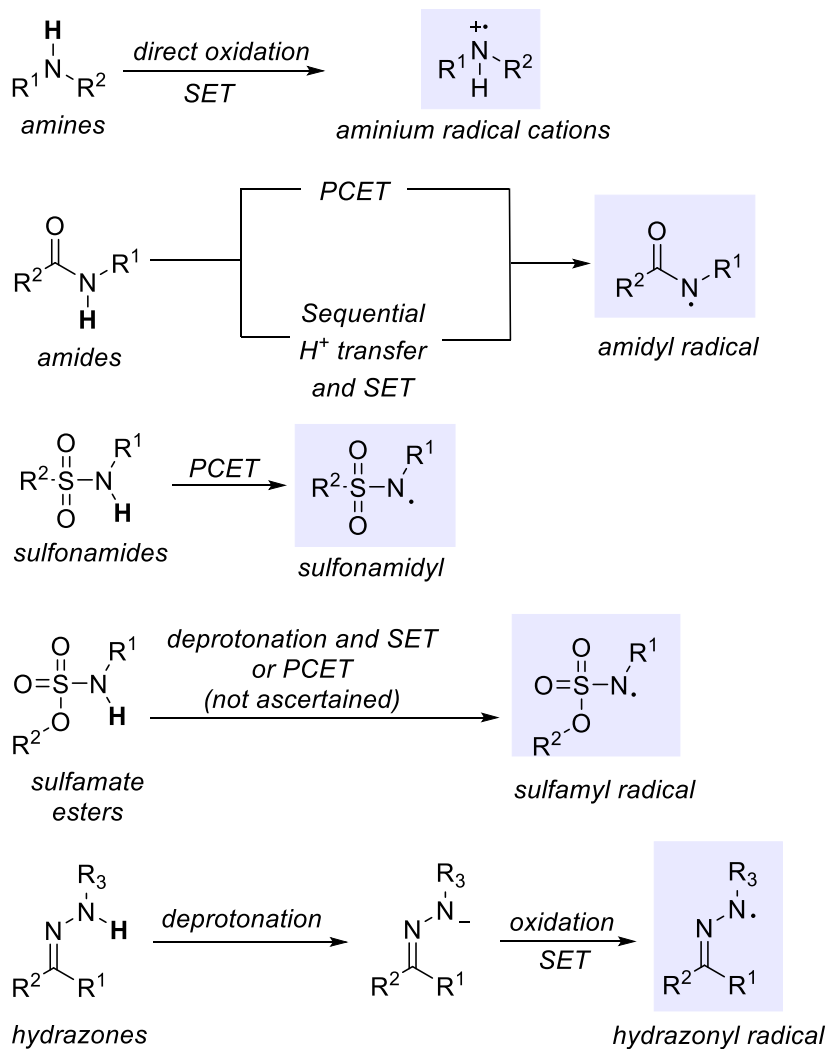
Scheme 1.39 Photoredox mediated generation of NCRs by direct N-H cleavage[132]

CHAPTER TWO:

INTRODUCTION

SATURATED NITROGEN HETEROCYCLES

CHAPTER 2 INTRODUCTION – SATURATED NITROGEN HETEROCYCLES

The final aim of this dissertation is demonstrating the potentiality of photocatalysis in the construction and functionalization of nitrogen containing saturated heterocycles through cascade processes. To achieve such goal, the construction of heterocycles is provided by the formation of new C-N bond between a nitrogen center and an unsaturated moiety. In this chapter, the interest for saturated or partially saturated nitrogen containing heterocycles in medicinal chemistry is explained and evaluated. Finally, a brief overview of the most employed synthetic strategies for intramolecular cyclization by C-N bond formation between nitrogen centers and unsaturated moiety (mostly hydroamination and arylamination strategies) leading to nitrogen heterocycles are presented.

2.1 Nitrogen-based heterocycles in medicinal chemistry

Cyclic structures containing a heteroatom are among the most important structures in organic chemistry. When such heteroatom is a nitrogen, the heterocycle also acquires a crucial significance in medicinal chemistry. Indeed, nitrogen-based heterocycles characterize life science, being found both in natural products (alkaloids, vitamins, hormones, and antibiotics)[134] but also as active core in synthetic products like drugs and pharmaceuticals.[135] The reason of such vast diffusion might be imputed to the features imparted to molecules by the nitrogen atom. Considering the simplest heterocycles, cyclic amines, an immediate observation concerns the ability of this functional group accepting or donating protons at value of pH like the ones found living systems. Many biomolecular motors are based on H^+ shuttle mechanisms, thus the ability of influencing them determines a direct biological effect. Moreover, nitrogen can be easily involved in intermolecular interactions, mainly hydrogen bonds. Consequently, even nitrogen functionalities that are not as basic as amines, impact on interaction with biological macromolecules, typically through interaction with the active site of enzymes. Research in last decades reported examples of how nitrogen

---

[134] Walsh, C. T. *Tetrahedron Lett.* **2015,** *56*, 3075-3081.
[135] Heravi, M. M.; Zadsirjan, V. *RSC Adv.* **2020,** *10*, 44247-44311.

atoms can readily bind DNA through hydrogen bonding thus explaining anti-cancer activities[136] of some *N*-based heterocycles.[137]

Another factor that derives from the presence of the nitrogen atoms and therefore determines the prevalence of *N*-heterocycles in biologically active compounds is their stability inside human body. Indeed, once again, the great number of interactions due to the suitable pKa values of nitrogen functionalities and the ability of interacting with proteins allows the permanence and prevents degradation of the cyclic molecule in such systems.

A general trend in medicinal chemistry also suggests that a drug candidate would be more successfully achieved replacing aromatic ring with heteroaromatic and heteroaliphatic rings. And even in the comparison among individual hetero-rings, nitrogen-based ones (*versus* oxygen- and sulphur-based) it ensures the most desirable behavior in terms of solubility or protein binding ability.[138]

The replacement of a carbon atom with a nitrogen one triggers dramatic effects in terms of pharmaceutical characteristics in a molecule. Thus, observing that more than 85% of all biologically active compounds comprise a heterocycle and among them 60% of FDA approved drugs possess at least one nitrogen-based heterocycle in their structures, it is not surprising. This represents a crucial point even in the years of modern organic synthesis. Indeed, as outlined by a *Nature Chemistry* perspective of 2018[139] that analyses which opportunities and challenges are left in modern organic synthesis (both in academic and industrial fields) to transform drug discovery, two of the "key messages" of the author still concern the synthesis of nitrogen heterocycles. The first remarks the urgence for developing more synthetic methods which tolerate polar groups and among them especially amines and *N*-heterocycles. Second, new reactions are needed, particularly non-traditional disconnections that would also allow aliphatic heterocyclic ring synthesis. The new photochemical methodologies studied throughout this dissertation were also envisaged to meet these purposes.

---

[136] Hosseinzadeh, Z.; Ramazani, A.; Razzaghi-Asl, N. *Curr. Org. Chem.* **2018,** *22*, 2256-2279.
[137] Özkay, Y.; Işıkdağ, İ.; İncesu, Z.; Akalın, G. *Eur. J. Med. Chem.* **2010,** *45*, 3320-3328.
[138] Ritchie, T. J.; Macdonald, S. J. F.; Peace, S.; Pickett, S. D.; Luscombe, C. N. *Med. Chem. Commun.* **2012,** *3*, 1062-1069.
[139] Blakemore, D. C.; Castro, L.; Churcher, I.; Rees, D. C.; Thomas, A. W.; Wilson, D. M.; Wood, A. *Nat. Chem.* **2018,** *10*, 383-394.

2.2 Importance of saturated three-dimensional structures in medicinal chemistry

In 2009 Lovering and coworkers established a fundamental paradigm for medicinal chemistry, the concept of "*escape from Flatland*".[140] To identify the parameters that determines the success of a molecule as a drug candidate, they examined the variation of physical chemical properties of main interest in drug efficiency: molecular weight, topological polar surface area, rotatable bonds, and hydrogen bond donors and acceptors. The groundbreaking results of these studies confirmed that complexity enhances the possibilities of clinical success, and this complexity is dictated by of the presence of saturated sp^3 carbon structure considered.

Indeed, moving from an aromatic planar structure to a three-dimensional saturated cyclic structure implies new conformations for the molecules, that might increase their interaction with the cavity of the active site. Besides, three-dimensionality might not only enhance the possibility of complementing the spatial cavities of target protein, but also exclude the possibility of non-desired interactions with other sites, thus allowing a higher specificity and fewer side effects for potential pharmaceuticals. Saturation is also directly correlated with the creation of new chiral centers whose presence was crucial for drug candidates progressing through clinical testing. Moreover, saturation influences the increase in molecular weight and the solubility of a molecular scaffold.

In conclusion, the molecular complexity imparted by saturation represents a factor of success for molecules as drug candidates in medicinal chemistry.[141] It is with this goal in mind that my PhD project focuses on the synthesis of saturated or partially saturated nitrogen containing heterocycles, in the attempt of tuning photochemical methodology that provide molecular products with a desirable level of complexity.

2.3 Synthesis of heterocycles by C-N bond formation between a nitrogen center and an unsaturated moiety

The main strategy that will be described throughout this dissertation is the transformation of a linear molecule (an acyclic amide or hydrazone)

---

[140] Lovering, F.; Bikker, J.; Humblet, C. *J. Med. Chem.* **2009,** *52*, 6752-6756.
[141] Lovering, F. *Med. Chem. Commun.* **2013,** *4*, 515-519.

into a cyclic nitrogen functionalized molecule provided by the formation of a C-N bond between a nitrogen functionality and an unsaturated moiety. My PhD project focuses on the exploitation of NCRs' reactivity to achieve such goal. Instead, traditional methods for C−N bond formation typically relies on polar chemistry. Among them, the most employed exploit transition metal catalysis. Mandatory examples are transition metal catalyzed hydroaminations. However even catalysts based on rare earth-, actinide-, lanthanide -and alkali-metals are employed for hydroamination. Besides, among transition metal catalysts, Buchwald−Hartwig amination/amidation and the copper-based Ullman-Goldberg and Cham-Lam couplings are essential examples of strategies for aminoarylation.

2.3.1 Intramolecular metal mediated hydroamination and carboamination of unsaturated moiety

Hydroamination (hydroamidation) and carboamination (carboamidation) reactions between an amine and an unsaturated moiety (typically olefins) are thermodynamically hampered by an activation barrier determined by the electrostatic repulsion between the electron pair of the nucleophilic nitrogen atom and the π electrons of the double bond. To overcome such barrier one of these two functional group requires "activation".

Catalysts based on group 1–5 metals[142,143,144] are reported to activate the amine through a protonolysis reaction. Such reaction is achieved employing a metal salt with a X moiety, typically an alkyl or an amido group, that imparts ionic character to such M-X bond. Indeed, the M-X species deprotonate the N-H bond while forming a metal amido (or imido) complex (Scheme 2.1, top right). This latter is now able to interact with the olefin portion as described in detail in following paragraphs.

Late transition metals instead, might activate either the amine or the unsaturated portion. In the first case, oxidative addition of N-H bond to the metal in low oxidation state provides a metal hydride complex (Scheme 2.1, bottom right). The subsequent insertion of the unsaturated bond into such metal complex followed by reductive elimination reaction delivers the

---

[142] Brinkmann, C.; Barrett, A. G. M.; Hill, M. S.; Procopiou, P. A. *J. Am. Chem. Soc.* **2012,** *134*, 2193-2207.
[143] Hill, M. S.; Liptrot, D. J.; Weetman, C. *Chem. Soc. Rev.* **2016,** *45*, 972-988.
[144] Hannedouche, J.; Schulz, E. *Chem. Eur. J.* **2013,** *19*, 4972-4985.

hydroamination product. In the second case, the olefin is activated and the metal acts as a Lewis acid and provides π-activation, thus making nucleophilic attack of nitrogen lone pair possible (Scheme 2.1 left). The final hydroamination product is then obtained upon protonolysis of the carbon-metal bond.
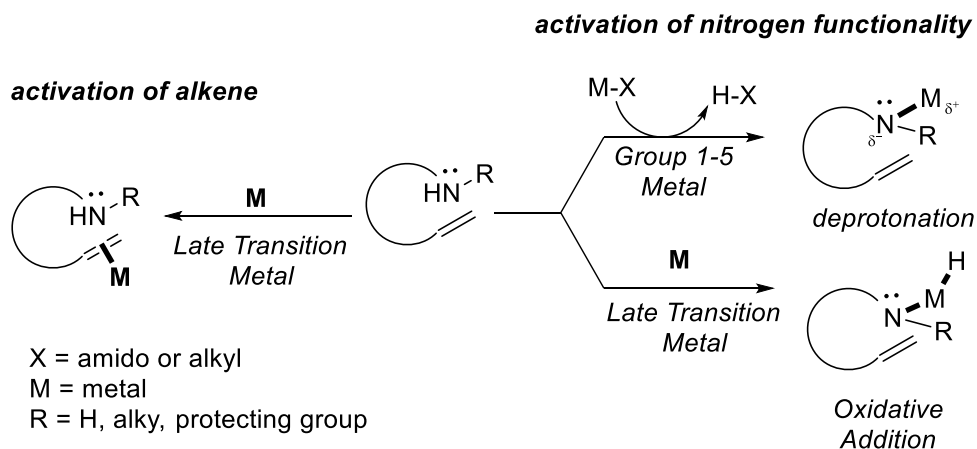
Scheme 2.1 Metal catalyzed activation of substrates for intramolecular hydroamination

An overview of the most common metal-mediated methods for the intramolecular synthesis of saturated heterocycles *via* hydroamination or carboamination (typically arylamination) of the double bond is provided below.

2.3.1.1 Late transition metal mediated intramolecular hydroamination and arylamination

Palladium, Rhodium, Gold, Copper, Platinum, and Iridium are reported as catalysts for intramolecular hydroamination reactions and their use for the synthesis of aliphatic amines have been reviewed in detail.[145,146] Particularly, Rh(I), Ir(I), Pt(II), and Au(I), relies on the instauration of strong transition metal/π-alkene complexes, providing the activation of the unsaturated moiety toward nucleophilic attack by the amine. For most of these transformations regioselectivity issues and rationalization of enantioselectivity was also studied, however to the aim of this introduction such topic is not discussed.

---

[145] Huang, L.; Arndt, M.; Gooßen, K.; Heydt, H.; Gooßen, L. J. *Chem. Rev.* **2015,** *115*, 2596-2697.
[146] Trowbridge, A.; Walton, S. M.; Gaunt, M. J. *Chem. Rev.* **2020,** *120*, 2613-2692.
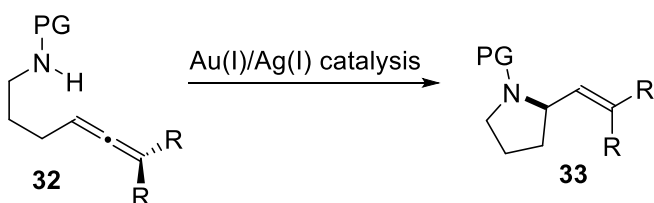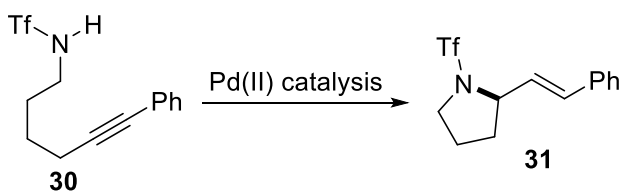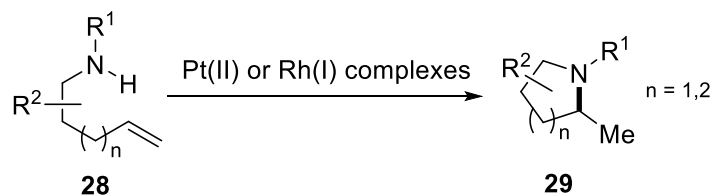
Scheme 2.2 Examples of intramolecular hydroamination strategies for the synthesis of saturated nitrogen heterocycles[146]

2.3.1.2 Palladium(0) mediated intramolecular hydroamination and arylamination

Among late transition metals, Pd employment is limited to intramolecular hydroaminations of alkenes given the β-hydride elimination mechanism that occurs upon the generation of alkyl–palladium intermediates. This is the reason why the most employed reactivity of Pd(0) towards the synthesis of *N*-saturated heterocycles involves arylaminations or transformations proceeding *via* allylpalladium intermediates **35** (yielding vinyl functionalized heterocycles **36**). Even in these cases, given the wide use of Pd(0) catalysis in total synthesis and the possibility for asymmetric reactive outcomes, the topic has been extensively reviewed[147,148] and only intramolecular

---

[147] Wolfe, J. P.; Neukom, J. D.; Mai, D. H., *Catalyzed Carbon-Heteroatom Bond Formation*. Wiley-VCH Verlag GmbH: Weinheim **2010**.
[148] Schultz, D. M.; Wolfe, J. P. *Synthesis* **2012,** *44*, 351-361.

transformations leading to saturated cyclic amines **36** and **39** are considered in Scheme 2.3.
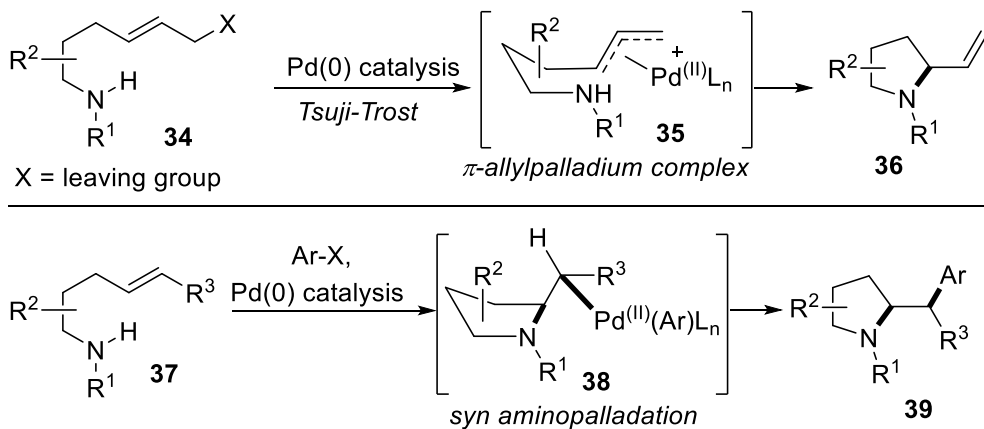
Scheme 2.3 Pd catalyzed cycloamination *via* allylpalladium complex and arylamination via *syn* aminopalladiation leading to saturated nitrogen heterocycles[147]

Concerning the addition of amine to unsaturated system like arenes, strategies widely employed in total synthesis and drug synthesis are represented by palladium catalyzed intramolecular Buchwald-Hartwig[149] and copper catalyzed Ullman-Goldberg[149] and Cham Lam[150] transformations. These are arylation reactions, however an intramolecular variation might lead to the synthesis of saturated heterocycles. Indeed, when an haloarene **40** or an arylboronic acid **41** bears another substituent on the aromatic ring which is an alkyl chain with a nitrogen center (Scheme 2.4), such reagent might undergo an intramolecular cyclization. For the haloarenes, in the presence of the base and the metal catalyst, the oxidative addition of the aryl moiety occurs at the metal center, and the subsequent amine ligation on the metal complex anticipates the product that is formed by reductive elimination. For Chan-Lam transformation with arylboronic acids instead, a formation of a copper-aryl complex is hypothesized and the subsequent evolution to a copper(III)-aryl-amide precedes the formation of the product upon reductive elimination. In all cases, the final product is a saturated or partially saturated

[149] Seifinoferest, B.; Tanbakouchian, A.; Larijani, B.; Mahdavi, M. *Asian J. Org. Chem.* **2021,** *10*, 1319-1344.
[150] Sanjeeva Rao, K.; Wu, T.-S. *Tetrahedron* **2012,** *68*, 7735-7754.

nitrogen heterocycle fused to the aromatic moiety **42** resulting from arylation of the amine (Scheme 2.4).
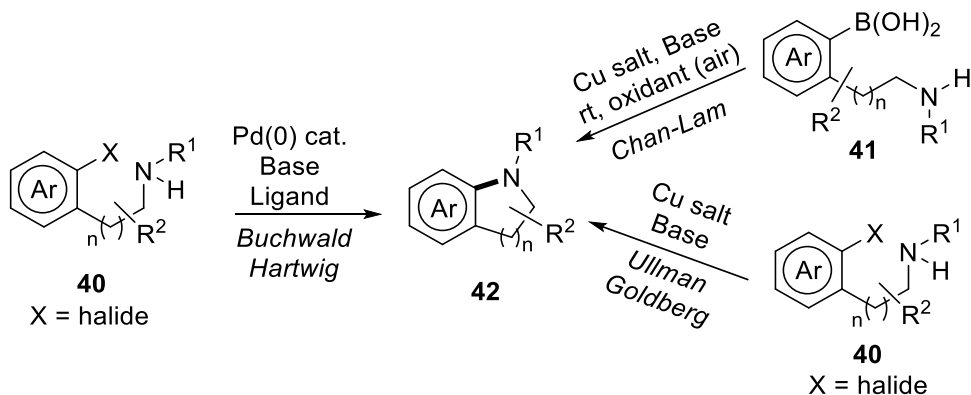
Scheme 2.4 Buchwald Hartwig, Ullman Goldberg and Chan Lam arylamination transformation providing a saturated nitrogen heterocycle fused to an arene **42**

2.3.1.3 Lanthanide, Actinide, rare earth, and alkali metals-catalyzed hydroamination

The general mechanism for lanthanide catalyzed hydroamination is also comparable to catalysis mediated by other rare earth-, actinide-, and alkali(earth)-metals.[142,143] The active catalyst **45** is provided by exchange on the metal center of the complex **43** between the nitrogen functionality of the reagent **44** and the silyl ether **49** acting as the leaving group. The subsequent insertion of the olefin into the M-N provides the intermediate **47** that upon protonolysis and concomitant exchange with another molecule of starting reagent **44** delivers the cyclized product **48** and regenerate the active catalyst **45**.[151,152]

The rapid protonolysis by another amine molecule **43** enabled using rare earth, actinide, and alkali (earth) metals is a powerful tool to avoid the β-hydride elimination mechanism that might occur when Pd is employed.

---

[151] Hong, S.; Marks, T. J. *Acc. Chem Res.* **2004,** *37*, 673-686.
[152] Dong, S.; Chen, J.; Qiao, K.; Fang, J.; Yang, Y.; Maron, L.; Liu, B. *ACS Catal.* **2021,** *11*, 3790-3800.
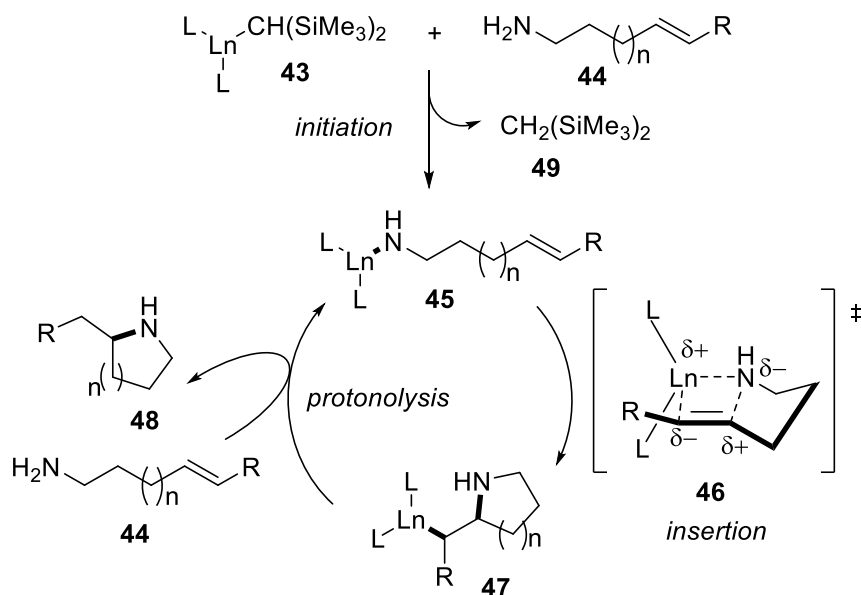
Scheme 2.5 Simplified general catalytic cycle for organolanthanide mediated hydroamination/cyclization of aminoalkenes **43**

2.4 Baldwin's Rules for intramolecular cyclizations

As highlighted in the introduction, one of the final aims of this dissertation is to provide access to saturated nitrogen heterocycles upon cyclization of linear molecules. In 1976 Jack Baldwin first proposed a series of empirically derived guidelines describing the favorabilities of ring closure reactions in alicyclic compounds.[153] These observations represent a powerful tool both for the nomenclature (the classification) and the outcome prediction of a cyclization process. Indeed ring closures are classified and nominated considering three aspects:

- the *number* of atoms in the newly formed ring;
- the *exo* or the *endo* closures, depending whether the bond broken during the ring closure is incorporated (*endo*) or located outside (*exo*) the ring formed as product;
- the *tet* (tetrahedral *sp³* hybridized), *trig* (trigonal *sp²* hybridized) and *dig* (diagonal *sp²* hybridized) geometry of the atom being attacked.

---

[153] Baldwin, J. E. *J. Chem. Soc., Chem. Commun.* **1976**, 734-736.

Baldwin reported that only certain combinations of ring size and the *exo/endo/dig/trig/tet* favored the formation of a ring. These outcomes were mostly reconducted to orbital overlap considerations. Nevertheless, the term "favored" must be used carefully. The author aimed to indicate a reaction exhibiting a rate that is not able to compete effectively with an alternative mode of cyclization as disfavored with respect to the second one that is favoured (fast). However, the disfavored product may be observed when a faster alternative reaction is not possible.

Table 2.1 Baldwin dis/favoured ring closures, where X = disfavoured and $\checkmark$ = favoured, -=not predicted

type	3		4		5		6		7	
	exo	*endo*	*exo*	*endo*	*exo*	*endo*	*exo*	*endo*	*exo*	*endo*
tet	✓	-	✓	-	✓	X	✓	X	✓	X
trig	✓	X	✓	X	✓	X	✓	✓	✓	✓
dig	X	✓	X	✓	✓	✓	✓	✓	✓	✓

In this dissertation, *6-exo-trig* and *5-exo-trig* cyclization are discussed (see Chapter 3, 4, 5).

CHAPTER THREE:

CASCADE RADICAL PROCESSES OF γ,δ-UNSATURATED HYDRAZONES: CYCLIZATION AND DEAROMATIZATION

CHAPTER 3 CASCADE RADICAL PROCESSES OF γ,δ-UNSATURATED HYDRAZONES: CYCLIZATION AND DEAROMATIZATION

3.1 Introduction: hydrazones as precursors to hydrazonyl radicals

Hydrazones are a class of organic compounds readily accessible upon the treatment of a carbonyl compound with hydrazine. The nucleophilic addition of the nitrogen of the hydrazine to the carbon center of the carbonyl results in net elimination of water and installation of a C=N double bond, with this nitrogen center bearing the amino functionality (the other N center of the hydrazine) as a substituent. Since modern organic chemistry is continuously in search for the development of safe and readily available materials for synthesis, the most employed kind of hydrazones nowadays are *N*-tosylhydrazones. Indeed, the direct treatment of aldehydes and ketones **50** with an equivalent of *para*-toluenesulfonyl hydrazide **51** at room temperature in an alcoholic solvent leads to the precipitation of the desired *N*-tosylhydrazone **52** (Scheme 3.1).
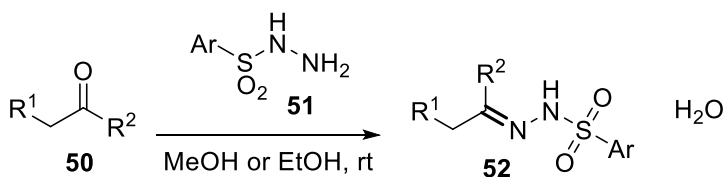
Scheme 3.1 General synthesis of *N*-arylsulfonylhydrazones **52**

Differently from the corresponding product obtained using hydrazine, this synthesis avoids the use of such toxic reagent while *N*-tosylhydrazones also demonstrate better stability and can be safely handled and prepared in large scale (Scheme 3.1). Hydrazones (particularly, *N*-substituted hydrazones) are useful substrates in synthesis, whose employment in polar chemistry has been deeply explored. However, their use in synthetic radical processes has only flourished in the last decade, with first seminal works

dating back to 2013.[154,155,156] The corresponding hydrazonyl NCR **54** are easily accessed upon the treatment of hydrazones **53** with stoichiometric or excess amounts of oxidants such as azodicarboxylates,[154,155] TEMPO[114,156,157] or alkyl peroxides as radical initiators. Indeed, a radical initiator might operate a hydrogen atom abstraction from the N-H functionality of the hydrazone thus yielding the NCR **54**.

In most cases, these reported processes require also high temperature in addition to the use of the initiator. Once the NCR hydrazonyl radical is generated, it is exploited to conduct an addition to an unsaturated moiety of the hydrazone molecule, thus performing an intramolecular radical cyclization reaction. The radical initiator can also be successfully replaced in cyclization processes using a copper catalyst and the strong oxidant properties of molecular oxygen. Such combination, exploiting the ability of nitrogen and of π-located electrons for complexing copper, together with the Cu(I)-Cu(II) cycle inducted by O_2, favors the radical mediated cyclization of hydrazones (Scheme 3.2).[158,159]

R[1] = alkyl, aryl   R[2] = H, alkyl
R[3] = H, alkyl   R[4] = aryl or Tosyl
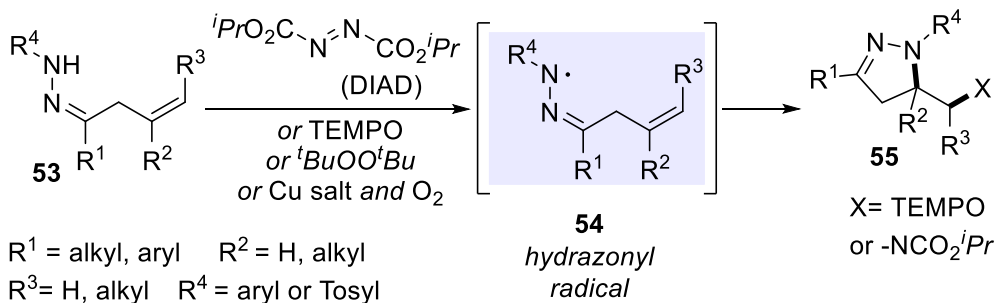
Scheme 3.2 Generation of hydrazonyl radicals **54** using radical initiators to trigger cyclization reactions

Similar strategies for the cyclization of hydrazones promoted by the combination of copper salts and oxidants, but also with other transition

[154] Duan, X. Y.; Yang, X. L.; Fang, R.; Peng, X. X.; Yu, W.; Han, B. *J. Org. Chem.* **2013,** *78*, 10692-10704.
[155] Zhu, M.-K.; Chen, Y.-C.; Loh, T.-P. *Chem. Eur. J.* **2013,** *19*, 5250-5254.
[156] Zhu, X.; Wang, Y.-F.; Ren, W.; Zhang, F.-L.; Chiba, S. *Org. Lett.* **2013,** *15*, 3214-3217.
[157] Zhu, X.; Chiba, S. *Org. Biomol. Chem.* **2014,** *12*, 4567-4570.
[158] Pünner, F.; Sohtome, Y.; Sodeoka, M. *Chem. Commun.* **2016,** *52*, 14093-14096.
[159] Fan, Z.; Feng, J.; Hou, Y.; Rao, M.; Cheng, J. *Org. Lett.* **2020,** *22*, 7981-7985.

metals, are reported and have been recently gathered in a review paper in which both polar and radical strategies were analyzed.[160]

Regardless of the methods adopted to generate the hydrazonyl radical, if the hydrazone bears a distal unsaturated moiety, this latter is exploited as a site of radical addition to obtain heterocycles containing two adjacent nitrogen atoms such as pyrazoline, pyrazole, dihydropyridazine, and pyridazine analogues.

3.1.1 Features of the hydrazonyl radical

As previously noted in the introduction, conversion of the starting hydrazone to the corresponding hydrazonyl radical **57** generates a sp^2 hybridized species with the unpaired electron located in the p orbital of the nitrogen of the amine functionality). However, the spin density is located both on the N of the sulfonamidyl moiety atom and on the conjugated C atom, thus determining two limit resonance structures **57**. Once the NCR is generated, the radical addition to the unsaturated moiety occurs from the nitrogen atom and a new C-N bond will form between this nitrogen and one of the two carbon atoms of the alkene. The outcome of cyclization yielding *exo-trig* or *endo-trig* products depends on the nature of the substituent on the olefin and on the reaction conditions (as described in following paragraphs).

An exception to this description is represented by those hydrazones in which the substituent on N-sp^3 is a trifluoroacetyl or a trichloroacetyl group. In these cases, as reported by Duan and co-workers,[114] the radical **59** assumes a σ configuration, since the spin density is localized on the two nitrogens, but not on the carbon atom. For such hydrazonyl radicals, cyclization might occur establishing a bond between the N-sp^2 and one of the two carbon atoms of the alkene, leading to the formation of azomethyne imines **60** with C-N bond incorporated in the cycle (Scheme 3.3).

To the aim of this dissertation, arylsulfonylhydrazonyl NCRs are concerned. Their behavior, being the substituent group on the N-sp^3 atom a sulfonyl group, corresponds to that of amidyl NCRs, since the proximity of the SO_2 bestows properties like that determined by the carbonyl in amides to the N-sp^3 atom.

---

[160] Lv, Y.; Meng, J.; Li, C.; Wang, X.; Ye, Y.; Sun, K. *Adv. Synth. Catal.* **2021,** *363*, 5235-5265.
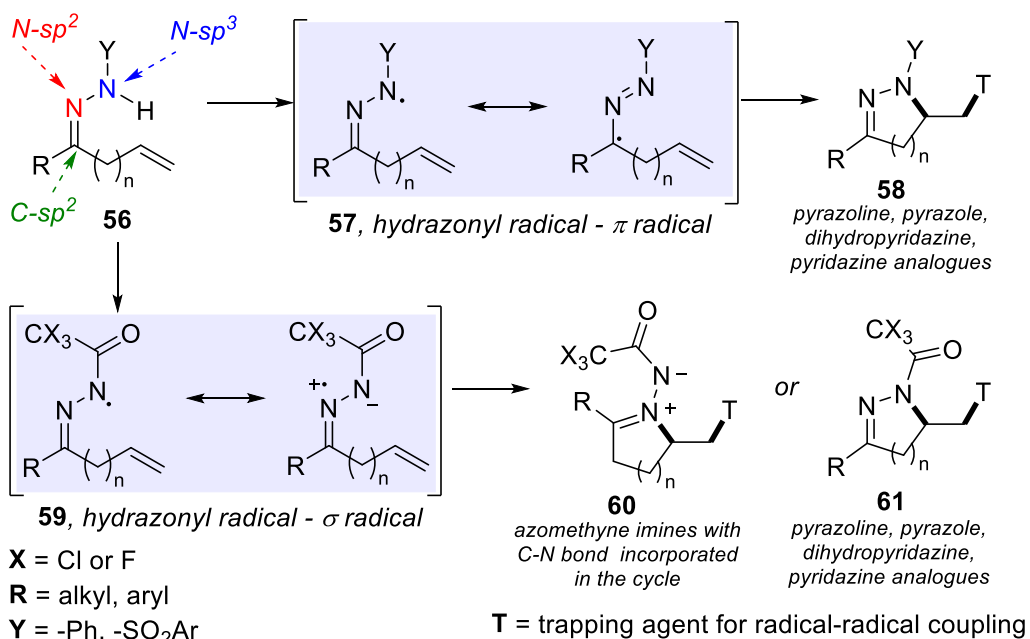
Scheme 3.3 Hydrazonyl radicals (with resonance structures) **57**, **59** from unsaturated hydrazones **56**, and their products of cyclization **58**, **60**, **61**

3.1.2 Photoredox generated hydrazonyl radicals

In 2014, Chen, Xiao and co-workers reported the first generation of tosylhydrazonyl radical **64** under photoredox conditions to promote intramolecular cyclization reactions.[161] This methodology relied on a sequential deprotonation and SET oxidation, achieved using an excess of a strong base (NaOH) and the classical PC Ru(bpy)$_3$Cl$_2$ in a 2 mol% loading under blue light irradiation. The starting unsaturated hydrazone **62** is converted to the corresponding hydrazonyl anion **63** by sodium hydroxide. Calculations claim that this anion possesses an E$_{ox}$ (N$^-$/N$^•$)=+0.56 V *versus* SCE in DMF which, compared with the reduction potential for the excited state of Ru PC that is E$_{1/2}$(*PC/PC$^-$)=+0.77 V *vs* SCE in CH$_3$CN, confirms that a SET event between the anion **63** and *Ru(II) might be possible. **63** yields the hydrazonyl radical **64** with concomitant reduction of the PC. Thus, the photoredox generated neutral hydrazonyl NCR **64** is afforded and exploited for an intramolecular cyclization reaction (Scheme 3.4)

---

[161] Hu, X.-Q.; Chen, J.-R.; Wei, Q.; Liu, F.-L.; Deng, Q.-H.; Beauchemin, A. M.; Xiao, W.-J. *Angew. Chem. Int. Ed.* **2014,** *53*, 12163-12167.
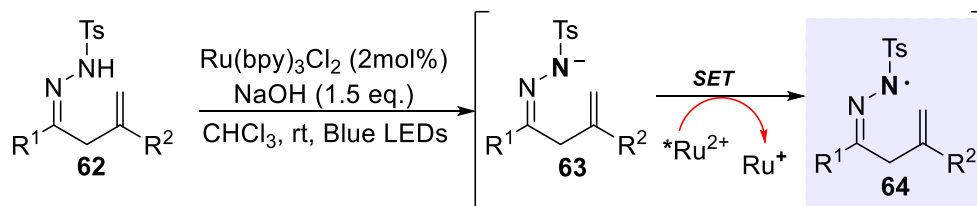
Scheme 3.4 Photoredox generation of hydrazonyl radical from unsaturated *N*-tosylhydrazones proposed by Xiao[161]

3.1.2.1 Photoredox reactivity of β,γ-unsaturated *N*-tosylhydrazones
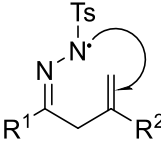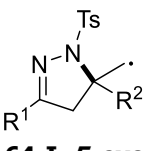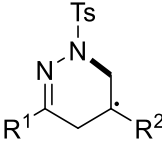
Despite the huge importance of the works of 2014,[161] the generation of hydrazonyl radicals **64** and its further cyclization under photoredox conditions was only investigated for substrates **62** bearing an unsaturation in the β,γ position. However, Chen's and Xiao's research groups further contributed to this topic in following years highlighting how starting from β,γ-unsaturated tosylhydrazones **62** both *5-exo-trig* and *6-endo-trig* cyclization might be observed.[162,163] The hydrazonyl radical **64** is always produced with a sequential deprotonation and SET oxidation, a mechanism that the authors identified as oxidative deprotonation electron transfer (ODET).[164] Such NCR **64** attacked then the unsaturated portion to perform the cyclization yielding a carbon centered radical **64-I** or **64-II** (Scheme 3.5 and Table 3.1). The regioselectivity towards *5-exo-trig* and *6-endo-trig* cyclization is dictated by two factors: reaction conditions and stability of the carbon radical **64-I** or **64-II**. *5-exo-trig* cyclization is the preferred pathway when the resulting carbon radical intermediate **64-I** is β-unsubstituted or alkylated. The calculation of the activation free energy for *5-exo-trig* vs *6-endo-trig* cyclization was confirmed by experimental observation and resulted to be lower for the former (Table 3.1).

---

[162] Hu, X.-Q.; Chen, J.; Chen, J.-R.; Yan, D.-M.; Xiao, W.-J. *Chem. Eur. J.* **2016,** *22*, 14141-14146.

[163] Hu, X.-Q.; Qi, X.; Chen, J.-R.; Zhao, Q.-Q.; Wei, Q.; Lan, Y.; Xiao, W.-J. *Nat. Commun..* **2016,** *7*, 11188.

[164] Yu, X.-Y.; Zhao, Q.-Q.; Chen, J.; Xiao, W.-J.; Chen, J.-R. *Acc. Chem Res.* **2020,** *53*, 1066-1083.

Table 3.1 Free energies calculated for the radical products of *5-exo-trig* and *6-endo-trig* cyclization of β,γ-unsaturated *N*-tosylhydrazones **62**[163]

	62	**64-I, 5-exo**	**64-II, 6-endo**

R²	**ΔG (kcal/mol)[a]**	**ΔG (kcal/mol)[a]**
H	8.8	13.5
Me	7.5	11.2
Ph	11.4	8.7

a) Gibbs free energies calculated in CHCl₃ using N-12//6-311+G(d,p)//B3LYP/6-31G(d)
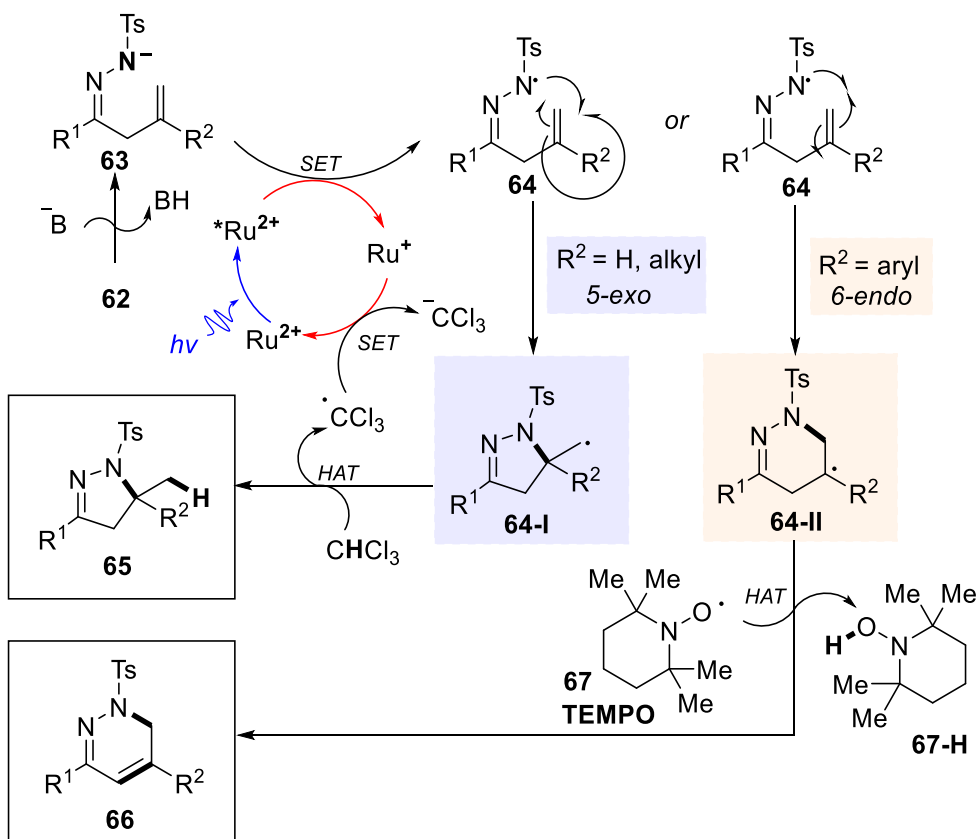
Scheme 3.5 Mechanism of intramolecular addition for photoredox generated hydrazonyl radical **64** from β,γ-unsaturated *N*-tosylhydrazones **62**

However, this regioselectivity is reversed using both an oxidative reaction environment (like the combination of TEMPO **67** and O_2[162] or TEMPO **67** in stoichiometric quantity[163]) and tailoring the starting hydrazone so that the *6-endo-trig* cyclization yields a benzyl radical **64-II**. Indeed, with an aryl substituent in the β position, the energy associated with the transition state resulting in a *6-endo-trig* cyclization is largely diminished by the possibility of formation of a relatively stable benzyl radical **64-II**. The carbon centered radicals **64-I** or **64-II** yield the final products **65** or **66** terminating the radical chain by hydrogen abstraction from an HAT donor. This latter might be the solvent $CHCl_3$ for *5-exo-trig* cyclization, thus delivering a $^\bullet CCl_3$ species that engage the PC in a turnover step, regenerating the PC cycle and furnishing a $^-CCl_3$ anion that can act as a base. On the other hand, in oxidative conditions, the interaction of TEMPO **67** with PC or with radical species leads it to act as a H shuttle, becoming an HAT catalyst that allows the product of *6-endo-trig* cyclization **66** to be delivered upon H-quenching of the carbon radical intermediate **64-II** formed following cycle formation (Scheme 3.5).

With *5-exo-trig* cyclization the authors disclosed access to 4,5-dihydropyrazoles **65** whereas with *6-endo-trig* cyclization 1,6-dihydropyridazines **66** were isolated (Scheme 3.6).

The idea of intercepting or trapping the carbon radical intermediate **64-I** or **64-II** formed following the cyclization process, obtaining carboamination or oxiamination of the olefin, was exploited to install functionalization on such heterocycles. Several coupling partners were tested to achieve different lateral derivatizations. In one of the previously cited works,[162] oxyamination of 4,5-dihydropyrazoles **68** and 1,6-dihydropyridazines **69** was obtained since the presence of TEMPO in combination with molecular oxygen allowed the oxidation of the carbon radical with the installation of hydroxyl functionality. To install an allylic moiety on the products **71** instead, activated allylsulfones **70** with arylsulfonyl moiety as the leaving group were used as coupling partners,[165] and recently even α-(trifluoromethyl)styrenes **72** were employed in a defluorinative alkylation to attach an allylic moiety with *gem*-difluoro functionality on the resulting heterocycle **73**.[166] Umemoto's reagent

[165] Zhao, Q.-Q.; Chen, J.; Yan, D.-M.; Chen, J.-R.; Xiao, W.-J. *Org. Lett.* **2017,** *19*, 3620-3623.

[166] Gao, Q.-S.; Niu, Z.; Chen, Y.; Sun, J.; Han, W.-Y.; Wang, J.-Y.; Yu, M.; Zhou, M.-D. *Org. Lett.* **2021,** *23*, 6153-6157.

74 was also successfully employed as the source of perfluoroalkyl radicals to forge C-C bonds between the latter and the newly formed heterocycle.[167] Remarkably, in the last case, despite the presence of the phenyl functionality in the β-position, the 5-membered heterocycle **75** was always observed, indicating that in the absence of an oxidative environment the structural conditions are not sufficient to dictate the *endo* selectivity. However, authors confirmed that the mechanistic studies were still ongoing, in fact, a different cyclization pathway (not mediated by hydrazonyl radical formation and subsequent addition to the unsaturation) was theorized (Scheme 3.7).[167]
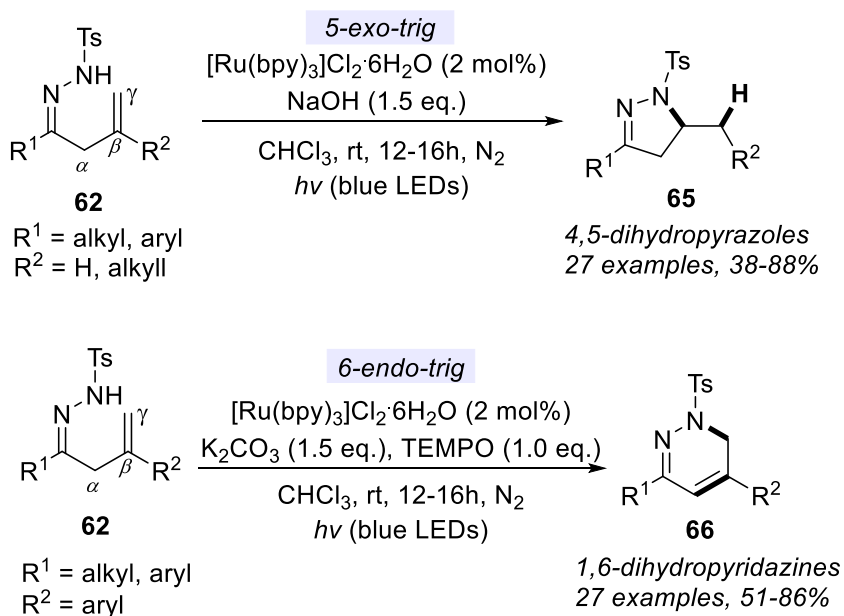
Scheme 3.6 Photoredox mediated hydroamination and carboamination of β,γ-unsaturated *N*-tosylhydrazones yielding dihydropyrazoles **65** by *5-exo-trig* cyclization[161] and dihydropyridazines **66** by *6-exo-trig* cyclization[163]

---

[167] Wei, Q.; Chen, J.-R.; Hu, X.-Q.; Yang, X.-C.; Lu, B.; Xiao, W.-J. *Org. Lett.* **2015,** *17*, 4464-4467.

62
R^1 = alkyl, aryl
R^2 = H, alkyl, aryl

[Mes-Acr]ClO$_4$ (5 mol%)
TEMPO (20 mol%)
K$_2$CO$_3$ (1.5 eq.)
CH$_3$CN, rt, 1.5-12h, O$_2$
hv (blue LEDs);
then PPh$_3$ (1.0 eq.)

68
when R^2 = H, alkyl
21 examples
51-93%

or

69
when R^2 = aryl
8 examples,
59-91%

62a
R^1 = alkyl, aryl
R^2 = Ts or Ms

MeOOC ... S(O)$_2$Ph **70** (3.0 eq.)
Ir(ppy)$_2$(bpy)PF$_6$ (2 mol%)
K$_2$CO$_3$ (2.0 eq.)
CH$_3$CN, rt, 10h, N$_2$, *hv* (blue LEDs)

71a
COOMe
15 examples, 33-75%

62b
R^1 = Ph
or 4-CF$_3$-C$_6$H$_4$

MeOOC ... S(O)$_2$Ph **70** (3.0 eq.)
Ir(ppy)$_2$(bpy)PF$_6$ (2 mol%)
K$_2$CO$_3$ (2.0 eq.)
CH$_3$CN, rt, 10h, N$_2$, *hv* (blue LEDs)

71b
CO$_2$Me
2 examples, 52-72%

62c
R^1 = aryl
R^2 = various
substituents

72 CF$_3$ (0.66 eq.)
Rose Bengal (3 mol%)
Cs$_2$CO$_3$ (1.0 eq.)
CH$_3$CN, rt, 10h, N$_2$
hv (blue LEDs)

73
35 examples, 40-96%

62
R^1 = alkyl, aryl
R^2 = Ph

74 CF$_3$ BF$_4$ (1.1 eq.)
Ru(bpy)$_3$(PF$_6$)$_2$ (1 mol%)
NaHCO$_3$ (2.0 eq.)
CH$_3$CN, rt, 12-18h, N,
hv (blue LEDs)

75
CF$_3$
15 examples
26-95%

Scheme 3.7 Photoredox reactivity of β,γ-unsaturated *N*-tosylhydrazones

3.2 A study on the general reactivity of unsaturated *N*-tosylhydrazones

3.2.1 General aim: broadening the scope of unsaturated hydrazones in photoredox transformations

As emerged from the previous paragraph, a wide research branch has been dedicated to the investigation of the reactivity of β,γ-unsaturated *N*-tosylhydrazones **62** under photoredox conditions. Regardless how detailed the studies about this reactivity are, one cannot avoid but wonder whether moving the unsaturation might result in a variation of such reactive pattern. Even if the transformation would occur with the same outcome, especially for intramolecular cyclization, such olefinic shift would provide access to heterocycles of different sizes. Besides, only tosylhydrazones were typically investigated in the previously mentioned studies, while investigations about how the reactivity would be affected by a change in the substituent of N-sp^3 still seems to lack in literature. Thus. It appeared that there still was a wide range of transformations for unsaturated hydrazones under photoredox conditions that need to be disclosed and explored yet.

3.2.1.1 Photoredox reactivity of α,β-unsaturated *N*-tosylhydrazones

With the main goal of broadening the scope of unsaturated hydrazones that can be employed under photoredox conditions, our research group started its research in the field of visible light induced reactions. Given the large availability of readily accessible α,β-unsaturated carbonyl compounds, the first photochemical study of our group was conducted on the photoredox behavior of α,β-unsaturated *N*-tosylhydrazones **76**.[168]

To our delight a first divergence from the typical cyclization mechanism observed for β,γ-unsaturated *N*-tosylhydrazones was reported. Indeed, α,β-unsaturated *N*-mesitylsulfonyl- (mesityl=2,4,6-trimethylphenyl Mes), *N*-trisylsulfonyl- (trisyl=2,4,6-triisopropylphenyl Tris) and *N*-tosylhydrazones **76** obtained from the corresponding enales yielded allylic sulfones **80** in moderate yields under photoredox catalysis by blue LEDs irradiation of Ru(bpy)$_3$Cl$_2$ as the catalyst, with K$_2$CO$_3$ as the base and a 1:1 mixture of DMF and CHCl$_3$ as the solvents. The process occurs upon SET mediated generation

---

[168] Parisotto, S.; Garreffa, G.; Canepa, C.; Diana, E.; Pellegrino, F.; Priola, E.; Prandi, C.; Maurino, V.; Deagostino, A. *ChemPhotoChem* **2017,** *1*, 56-59.

of the corresponding hydrazonyl radical **78** from the hydrazone anion **77**, following concomitant nitrogen loss and 1,5-shift of the arylsulfonyl moiety providing a carbon centered vinyl radical intermediate **79**, precursor to the final allylic sulfone **80** (Scheme 3.8).[168]
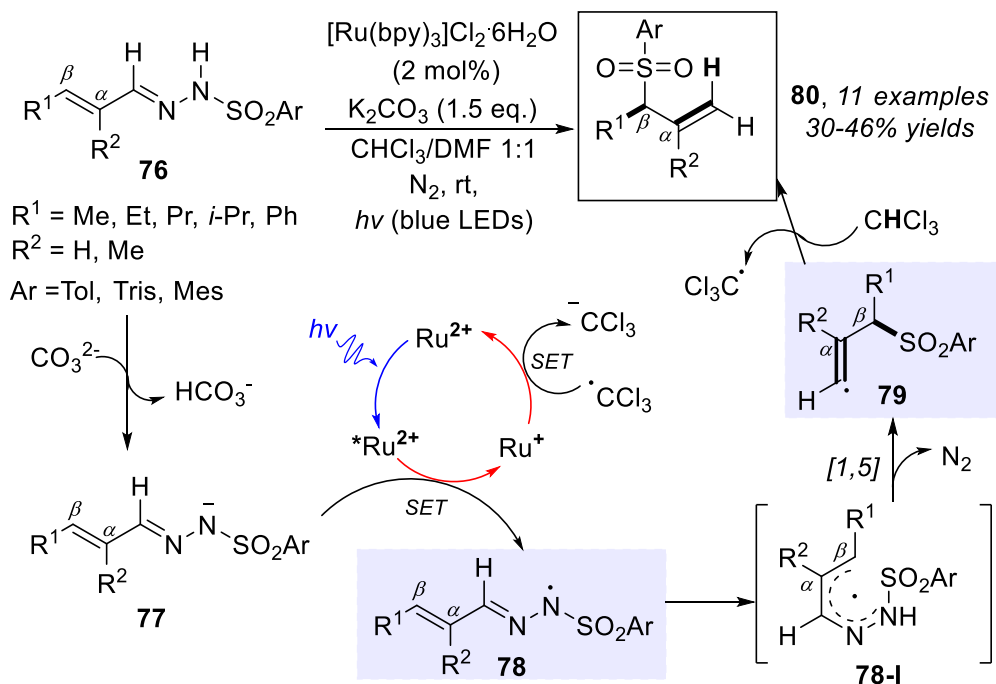
Scheme 3.8 Photoredox reactivity of α,β-unsaturated N-arylsulfonylhydrazones from enals leading to allylic sulfones[168]

The reaction conducted from enones tosylhydrazones resulted in the decomposition of the starting material or in a not-photomediated polar intramolecular cyclization (conjugate addition of the sulfonamidyl nitrogen on the alkene moiety, providing aromatization to the corresponding pyrazole by base-promoted detosylation).

Surprisingly, with the first attempt of our research group, we immediately remarked that α,β-unsaturated *N*-arylsulfonylhydrazones expressed a different reactivity under photoredox conditions when compared to β,γ-unsaturated *N*-tosylhydrazones.

My PhD project in this group started with these premises, driven by the curiosity of evaluating which other perturbations of the typical reactivity

would be observed with a further shift of the unsaturation to γ,δ-unsaturated *N*-tosylhydrazones.

3.2.2 Tetrahydropyridazines

Pyridazine **81** is a six-membered aromatic heterocycle with two adjacent nitrogen atoms. Since Wermuth[169] defined this scaffold as "privileged structure" for medicinal chemistry, these molecules have gained interest and popularity among both medicinal and synthetic chemists. The medicinal interest is driven by the unique physicochemical properties of such heterocycles. The localization of two polar nitrogen atoms on the same side of the molecule determines an elevated dipolar moment of 3.9 Debye units that combined with a highly π-deficient aromatic skeleton and a pKa of 2.3 endow the molecule with several desirable features. Protonation and hydrogen bond formation with such scaffold are favored, directly enhancing the ability of being involved in H bond with receptor proteins where carbocycles could not bind. That immediately affects their successful employment as bioisosters of the aromatic ring. Besides, the increased polarity determines a better solubility in water and biological systems while the two nitrogen atoms are also optimal ligands to chelate metal core like Pt for Pt-based medicines. Pyridazines based molecules have emerged in the last decade as promising candidates exhibiting analgesic, anti-inflammatory, antimicrobial, antithrombotic, antidepressant, diuretics, antihypertensive, antidiabetic, anti-Alzheimer, *anti*-HIV and anticancer activities.[170,171]

When Lovering[140,141] expressed the trailblazing concept of moving from aromatic to saturated and three-dimensional structures to achieve improved clinical successes in medicinal chemistry candidates, hydrogenated analogues of privileged scaffolds in medicinal chemistry have also gained particular attention. Tetrahydropyridazines **82** are the hydrogenated analogues of pyridazines. They share similar desirable physicochemical properties with their aromatic counterparts due to the presence of the two adjacent nitrogen atoms and have demonstrated promising pharmacological and biological activities in several domains (Figure 3.1).[172]

[169] Wermuth, C. G. *Med. Chem. Commun.* **2011,** *2*, 935-941.
[170] Jaballah, M. Y.; Serya, R. T.; Abouzid, K. *Drug. Res.* **2017,** *67*, 138-148.
[171] He, Z.-X.; Gong, Y.-P.; Zhang, X.; Ma, L.-Y.; Zhao, W. *Eur. J. Med. Chem.* **2021,** *209*, 112946.
[172] Nagle, P.; Pawar, Y.; Sonawane, A.; Bhosale, S.; More, D. *Med. Chem. Res.* **2014,** *23*, 918-926. Lange, J. H. M.; den Hartog, A. P.; van der Neut, M. A. W.; van Vliet,

81
pyridazine

82
1,4,5,6-tetrahydropyridazine

Human Bone cell PR binder

Bemoradan (Cardiotonic Agent)
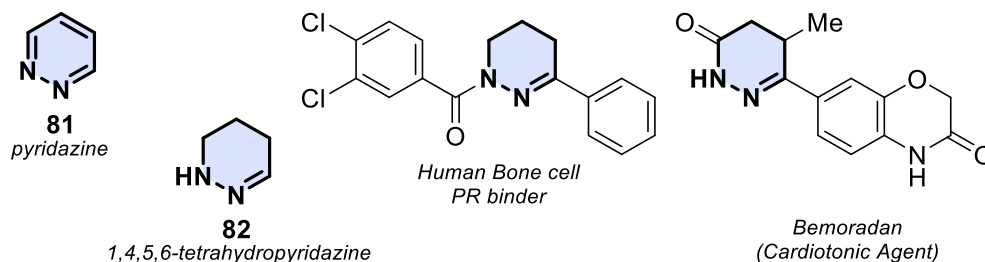
Figure 3.1 Pyridazine **81**, Tetrahydropyridazine **82** and biologically active 1,4,5,6-tetrahydropyridazines.

The common pathways to both dihydrogenated and tetrahydrogenated analogues of pyridazines are represented by the direct hydrogenation of the aromatic compounds[173] or cycloaddition reactions, in particular aza-Diels-Alder reactions of 1,2-diaza-1,3-dienes[174] and other [4+2] cycloaddition of diazocompounds and alkenes[175] and [3+3] formal cycloadditions exploiting

B. J.; Kruse, C. G. *Bioorg. Med. Chem. Lett.* **2009,** *19*, 5675-5678. Palmer, S.; Campen, C. A.; Allan, G. F.; Rybczynski, P.; Haynes-Johnson, D.; Hutchins, A.; Kraft, P.; Kiddoe, M.; Lai, M.-T.; Lombardi, E.; Pedersen, P.; Hodgen, G.; Combs, D. W. *J. Steroid Biochem. Mol. Biol.* **2000,** *75*, 33-42. Zhi, L.; Marschke, K. B. *Expert Opin. Ther. Pat.* **1999,** *9*, 695-700. Rybczynski, P. J.; Combs, D. W.; Jacobs, K.; Shank, R. P.; Dubinsky, B. *J. Med. Chem.* **1999,** *42*, 2403-2408. Lijun, Z.; Williams, M. A.; Mendel, D. B.; Escarpe, P. A.; Xiaowu, C.; Wang, K.-Y.; Graves, B. J.; Lawton, G.; Kim, C. U. *Bioorg. Med. Chem. Lett.* **1999,** *9*, 1751-1756. Combs, D. W.; Reese, K.; Phillips, A. *J. Med. Chem.* **1995,** *38*, 4878-4879. Combs, D. W.; Reese, K.; Cornelius, L. A. M.; Gunnet, J. W.; Cryan, E. V.; Granger, K. S.; Jordan, J. J.; Demarest, K. T. *J. Med. Chem.* **1995,** *38*, 4880-4884.
[173] Wang, W.; Meng, W.; Du, H. *Dalton Trans.* **2016,** *45*, 5945-5948.
[174] Shen, L.-W.; Li, T.-T.; You, Y.; Zhao, J.-Q.; Wang, Z.-H.; Yuan, W.-C. *J. Org. Chem.* **2021,** *86*, 11472-11481. Arroyo, Y.; Rodríguez, J. F.; Santos, M.; Sanz Tejedor, M. A.; Vaca, I.; García Ruano, J. L. *Tetrahedron Asymmet.* **2004,** *15*, 1059-1063. Rossi, E.; Abbiati, G.; Attanasi, O. A.; Rizzato, S.; Santeusanio, S. *Tetrahedron* **2007,** *63*, 11055-11065. Lopes, S. M. M.; Brigas, A. F.; Palacios, F.; Lemos, A.; Pinho e Melo, T. M. V. D. *Eur. J. Org. Chem.* **2012,** *2012*, 2152-2160. Tong, M.-C.; Chen, X.; Li, J.; Huang, R.; Tao, H.; Wang, C.-J. *Angew. Chem. Int. Ed.* **2014,** *53*, 4680-4684. Yang, X.-L.; Peng, X.-X.; Chen, F.; Han, B. *Org. Lett.* **2016,** *18*, 2070-2073.
[175] Du, Y. L.; Zhao, F.; Han, Z. Y.; Gong, L. Z. *Synthesis* **2016,** *49*, 151. Wu, Q.; Shao, P. L.; He, Y. *RSC Adv.* **2019,** *9*, 21507. Yin, W. H.; Fang, L.; Wang, Z. Y.; Gao, F.; Li, Z. F.; Wang, Z. Y. *Org. Lett.* **2019,** *21*, 7361. Huang, R.; Tao, H. Y.; Wang, C. J. *Org. Lett.* **2017,** *19*, 1176. Deng, Y. M.; Pei, C.; Arman, H.; Dong, K. Y.; Xu, X. F.; Doyle, M. P. *Org. Lett.* **2016,** *18*, 5884.

cyclopropyl derivatives and hydrazones.[176] Even intramolecular strategies which relies on transition metal-mediated (typically Pd[177] and Cu[178]) or on base-mediated anionic cyclizations were reported.[179] However, for these strategies, supplementary efforts are devoted to obtaining the required starting materials (olefins with appropriate substituents to promote cycloadditions and stable diazacompounds) and matching them with sometimes harsh reaction conditions (Scheme 3.9).
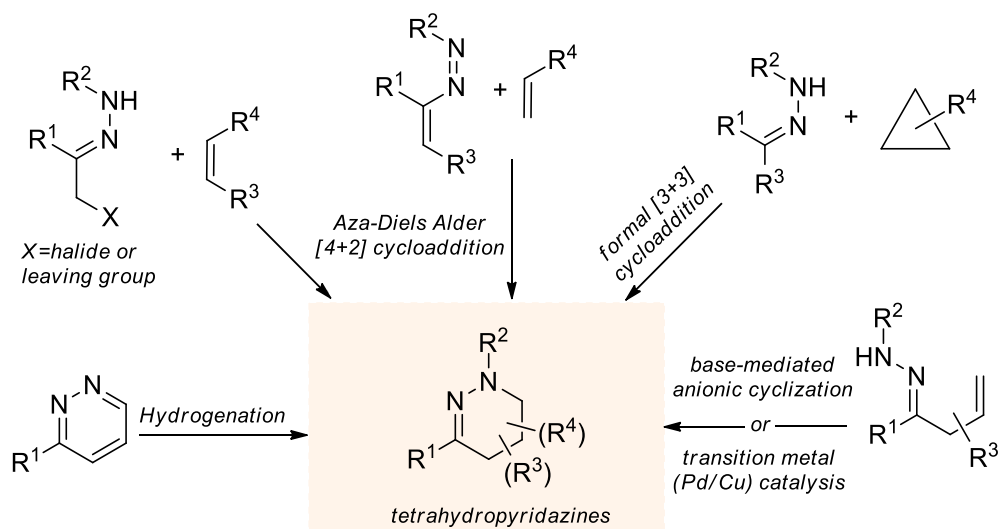
Scheme 3.9 Synthetic strategies towards tetrahydropyridazines (photoredox catalysis excluded)

In this context, the radical pathways disclosed by photoredox catalysis with the generation of hydrazonyl radicals appear as an intriguing alternative, especially for the mild conditions and the availability of the starting materials (unsaturated carbonyl compounds to be converted in hydrazones). Besides, in a preliminary hypothesis, avoiding the oxidative conditions proposed by Xiao[162,163] might also provide a broader scope of the starting materials, since also those functional groups that could not tolerate such oxidative reaction

[176] Mishra, M.; De, P. B.; Pradhan, S.; Punniyamurthy, T. *J. Org. Chem.* **2019,** *84*, 10901. Huo, H. R.; Runa, A.; Gong, Y. F. *J. Org. Chem.* **2019,** *84*, 2093.
[177] Mboyi, C. D.; Abdellah, I.; Duhayon, C.; Canac, Y.; Chauvin, R. *ChemCatChem* **2013,** *5*, 3014. Guo, Y. J.; Zhao, J. B.; Zhang, Q. *Adv. Synth. Catal.* **2020,** *362*, 1208.
[178] Guo, Y. Q.; Zhao, M. N.; Ren, Z. H.; Guan, Z. H. *Org. Lett.* **2018,** *20*, 3337.
[179] Peng, X.; Kaga, A.; Hirao, H.; Chiba, S. *Org. Chem. Front.* **2016,** *3*, 609-613.

mean could be employed. In this case, γ,δ-unsaturated *N*-tosylhydrazones emerged as a good starting point.

3.2.3 Photoredox reactivity of γ,δ-unsaturated *N*-tosylhydrazones

Given the rising biological importance of tetrahydropyridazines and driven by the opportunity of discovering a new photoredox mediated reactivity for unsaturated hydrazones, we began our investigation on γ,δ-unsaturated *N*-tosylhydrazones **83**. Indeed, anticipating the same reactivity observed for β,γ-unsaturated *N*-tosylhydrazones we expected an alternative pathway *via 6-exo-trig* cyclization towards tetrahydropyridazines **84** avoiding oxidative conditions or structural requirements like the aromatic substituent in the β position (Scheme 3.10).
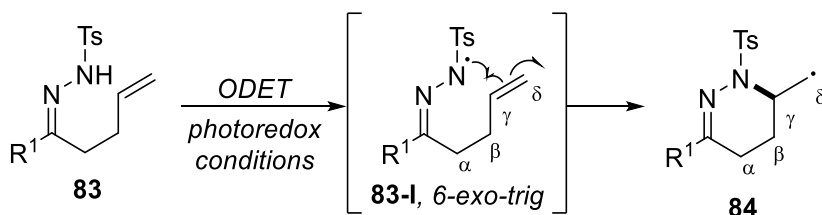
Scheme 3.10 Expected cyclization mode yielding carbon radical intermediate **84** for γ,δ-unsaturated *N*-tosylhydrazones **83**
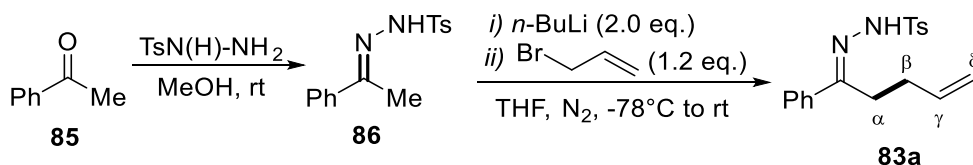
Scheme 3.11 Synthesis of γ,δ-unsaturated *N*-tosylhydrazones **83a**

To synthetize the desired γ,δ-unsaturated *N*-tosylhydrazones **83a**, we started from acetophenone **85**, treated with tosylhydrazide to obtain the corresponding hydrazone **86**. The unsaturated moiety was then installed upon treatment with 2 equivalents of *n*-BuLi, yielding the deprotonation of both the sulfonamide nitrogen and the α-carbon, and the subsequent addition of allyl bromide as the electrophile (Scheme 3.11). Thus, we proceeded with the first attempt of providing the tetrahydropyridazine product **87**, using KOH as the base, [Ru(bpy)$_3$]Cl$_2$·6H$_2$O as the catalyst in CHCl$_3$ as the solvent and a 9W blue lamp as the light source. Despite the attempted optimization, the

first conditions reported remained the best and we did not manage to achieve yields over 24%, even when a LEDs blue lamp (blue LEDs Kessil A160 Tuna Blue 40W) was used (Table 3.2, entry 20).

Table 3.2 The optimization of photoredox catalysed cyclization of γ,δ-unsaturated *N*-tosylhydrazones **83a**

Entry	Base	Catalyst	Solvent	Conv.	Yield[a]	Light Source
1	KOH	[Ru(bpy)$_3$]Cl$_2$	CHCl$_3$	100	24 (18)	9W, 450 nm, blue
2	KOH	[Ru(bpy)$_3$]Cl$_2$	CHCl$_3$	0	0	dark
3	-	[Ru(bpy)$_3$]Cl$_2$	CHCl$_3$	0	0	9W, 450 nm, blue
4	KOH	-	CHCl$_3$	0	0	9W, 450 nm, blue
5	KOH	[Ru(bpy)$_3$]Cl$_2$	CH$_3$CN	100	Degrad.	9W, 450 nm, blue
6	KOH	[Ru(bpy)$_3$]Cl$_2$	DMSO	0	0	9W, 450 nm, blue
7	KOH	[Ru(bpy)$_3$]Cl$_2$	DMF	0	0	9W, 450 nm, blue
8	KOH	[Ru(bpy)$_3$]Cl$_2$	CHCl$_3$/DMF 1:1	30	5	9W, 450 nm, blue
9	KOH	[Ru(bpy)$_3$]Cl$_2$	CH$_3$OH	0	0	9W, 450 nm, blue
10	KOH	[Ru(bpy)$_3$]Cl$_2$	DCM	0	0	9W, 450 nm, blue
11	KOH	[Ru(bpy)$_3$]Cl$_2$	THF	0	0	9W, 450 nm, blue
12	KOH	[Ru(bpy)$_3$][PF$_6$]$_2$	CHCl$_3$	100	4	9W, 450 nm, blue
13	KOH	[Ru(bpz)$_3$][PF$_6$]$_2$	CHCl$_3$	0	0	9W, 450 nm, blue
14	KOH	Eosin Y	CHCl$_3$	0	0	9W, 550 nm, green
15	KOH	[Ir(ppy)$_2$(dtbpy)][PF$_6$]	CHCl$_3$	100	12 (10)[b]	9W, 365 nm, purple
16	KOH	Rhodamine B	CHCl$_3$	0	0	9W, 550 nm, green
17	K$_2$CO$_3$	[Ru(bpy)$_3$]Cl$_2$	CHCl$_3$	100	16 (13)[b]	9W, 450 nm, blue
18	NaOH	[Ru(bpy)$_3$]Cl$_2$	CHCl$_3$	25	8	9W, 450 nm, blue
19	Cs$_2$CO$_3$	[Ru(bpy)$_3$]Cl$_2$	CHCl$_3$	30	13	9W, 450 nm, blue
20	KOH	[Ru(bpy)$_3$]Cl$_2$	CHCl$_3$	100	24	40 W, 456 nm, blue

Reactions conditions: tosylhydrazone **83a** (0.3 mmol), anhydrous solvent (5 mL), base (1.2 eq; 0.36 mmol), catalyst (3% mol; 0.009 mmol) *a)* Determined by NMR spectroscopy using nitromethane as the internal standard; *b)* Yields determined on isolated product

We imputed such poor yield to a competitive hydrogen atom transfer process. Indeed, given the reactivity of NCRs, 1,5-HAT process constitutes a competitive pathway that interferes with the desired intramolecular olefin addition (see paragraph 1.3.3 General reactivities of NCRs). Besides, in our

case the 1,5-HAT would lead to the formation of a stable radical intermediate, namely an allyl radical **88**. This putative species might then be involved in degradation pathways (Scheme 3.12).
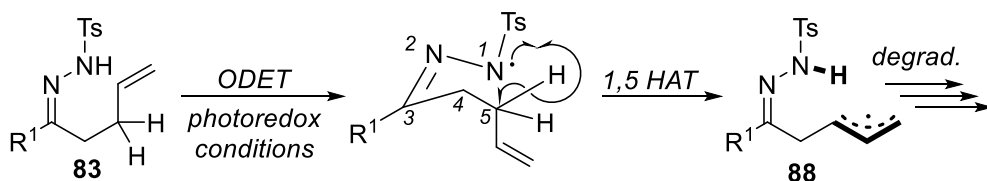
Scheme 3.12 Competitive putative 1,5-HAT pathway towards allyl radical **88**

3.2.3.1 Engineering the starting material to enhance yield

Facing the impossibility of enhancing the efficiency of the cyclization process with the optimization of reaction conditions, we envisaged an overcoming strategy to such obstacle by imposing variations on the starting material. A different starting material was designed to avoid the presumed 1,5-HAT a β-hindered γ,δ-unsaturated *N*-tosylhydrazones.
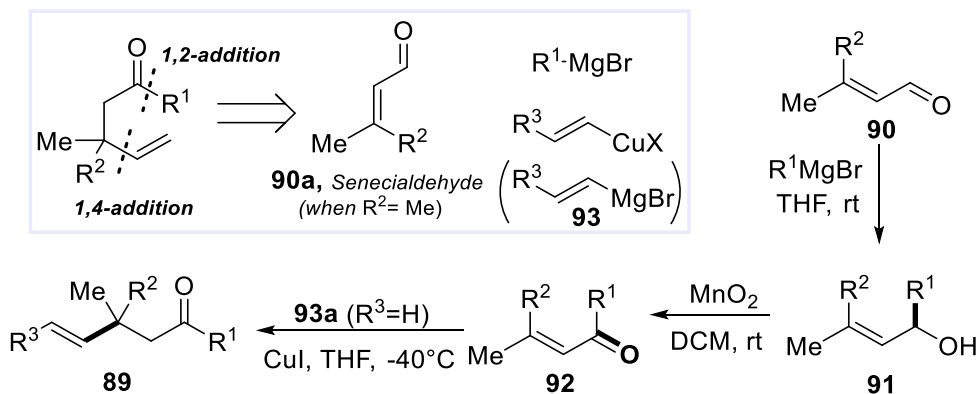
Scheme 3.13 Synthesis of β-Hindered γ,δ-unsaturated ketones **89**

Such synthetic targets required a sequential application of 1,2- and 1,4-conjugate nucleophilic additions. A direct strategy was proposed starting from the commercially available conjugated senecialdehyde **90a** (3-methylcrotonaldehyde), carrying two geminal methyl substituents on the terminal sp² carbon. The suitable Grignard reagent with the appropriate halide led to the installation of an α-substituent on the carbonyl, yielding a secondary alcohol **91**. Restoring the carbonyl moiety upon oxidation to the corresponding β-*gem* disubstituted conjugated ketone **92** provided an ideal substrate for 1,4 addition of vinylmagnesiumbromide **93a** (or another

available alkenylmagnesiumbromide **93**), yielding the β-hindered γ,δ-unsaturated ketone **89.** This latter was finally converted in the desired hydrazone **94**. Commercially available conjugated ketones **92** bearing two *identical* substituents on the terminal carbon of the alkene moiety were also considered for the 1,4-addition with **93** (Scheme 3.13). This simple modification providing the installation of these two geminal substituents in the β position accomplished two tasks. Primary, it impeded the 1,5-HAT, removing the putative competitive pathway towards cyclization. Second, it could induce a Thorpe-Ingold effect[180] facilitating the ring closure.

3.2.4 Photoredox reactivity of β-hindered γ,δ-unsaturated *N*-tosylhydrazones

For our first attempt, the analogue of the hydrazones **83a** used for optimization in Table 3.2 was synthesized, a β-hindered γ,δ-unsaturated *N*-tosylhydrazones with two geminal methyl groups on the β carbon **94a**. Such species, once reacted in the optimized conditions, provided complete conversion with recovery of a single product in 35% yield and in 52% yield when the 40W light source was employed. NMR studies, confirming the absence of the multiplet ^{1}H-NMR signal characterizing the C-H for the carbon of the newly formed C-N bond in cycle **87** as well as the absence of the doublet integrating 3 protons for the methyl substituent on the same carbon center, suggested that the generation of carbon radical intermediate **94a-II**, (similarly to **84**, Scheme 3.10), and precursor to the product, occurred without subsequent HAT quenching. Indeed, the carbon radical intermediate **94a-II** deriving from the cyclization of β-hindered γ,δ-unsaturated *N*-tosylhydrazone further reacted with the aromatic ring of the tosyl moiety delivering a tricyclic structure **95a** (Scheme 3.14). Such radical attack on arene resulted in the reduction of the latter and provided dearomatization with the formation of a fused 1,4-dienic moiety **95a** as a single diasteroisomer (^{1}H-NMR signals for alkenyl sp^2 protons at 5.35 and at 6.75 broad singlet and multiplet respectively,and three DEPT-135 ^{13}C-NMR methylene signals at 31.4, 31.5, and 34.6 ppm; Figure 3.3 and Figure 3.4). The simple introduction of two geminal methyl groups in β position induced a cascade process involving two consecutive 6-*exo-trig* cyclizations. Such structural hypothesis was confirmed both by NMR studies (the HMQC

---

[180] Jung, M. E.; Piizzi, G. *Chem. Rev.* **2005,** *105*, 1735-1766. Beesley, R. M.; Ingold, C. K.; Thorpe, J. F. *J. Chem. Soc., Trans.* **1915,** *107*, 1080-1106.

experiment particularly helped the structure elucidation, Figure 3.4) and single crystal X-ray diffraction (Figure 3.2). Moreover NMR analysis both of the crude and of the isolated product confirmed that a single diasteroisomer was formed as product.
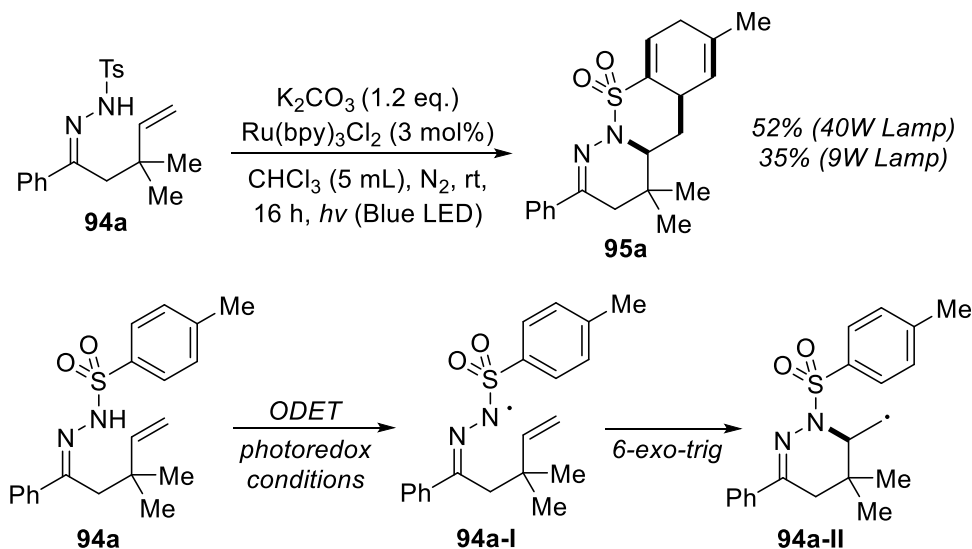
Scheme 3.14 Observed photoredox reactivity for β-hindered γ,δ-unsaturated *N*-tosylhydrazone **94a** yielding tricyclic product **95a**
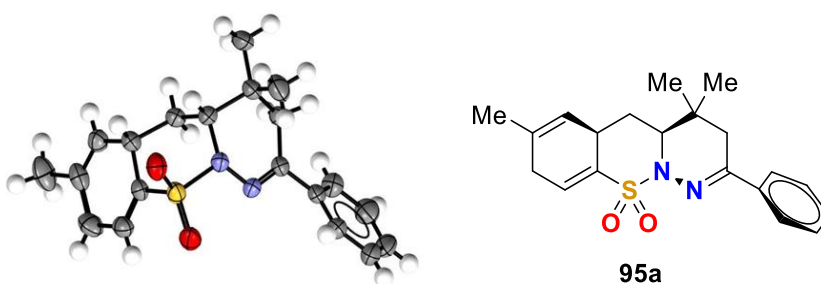
Figure 3.2 Structure of product **95a** as determined by single crystal X-ray diffraction (right) and ORTEP plot of the asymmetric unit of **95a** in the crystal structure (left; color code gray: carbon; blue: nitrogen; red: oxygen; yellow: sulfur; 50% of probability represented). X-ray analysis by Dr. E. Priola.

Figure 3.3 Stacked H^1-NMR spectra of **87** and **95a** demonstrating the effect of the geminal methyl groups on the outcome of the photoredox transformation
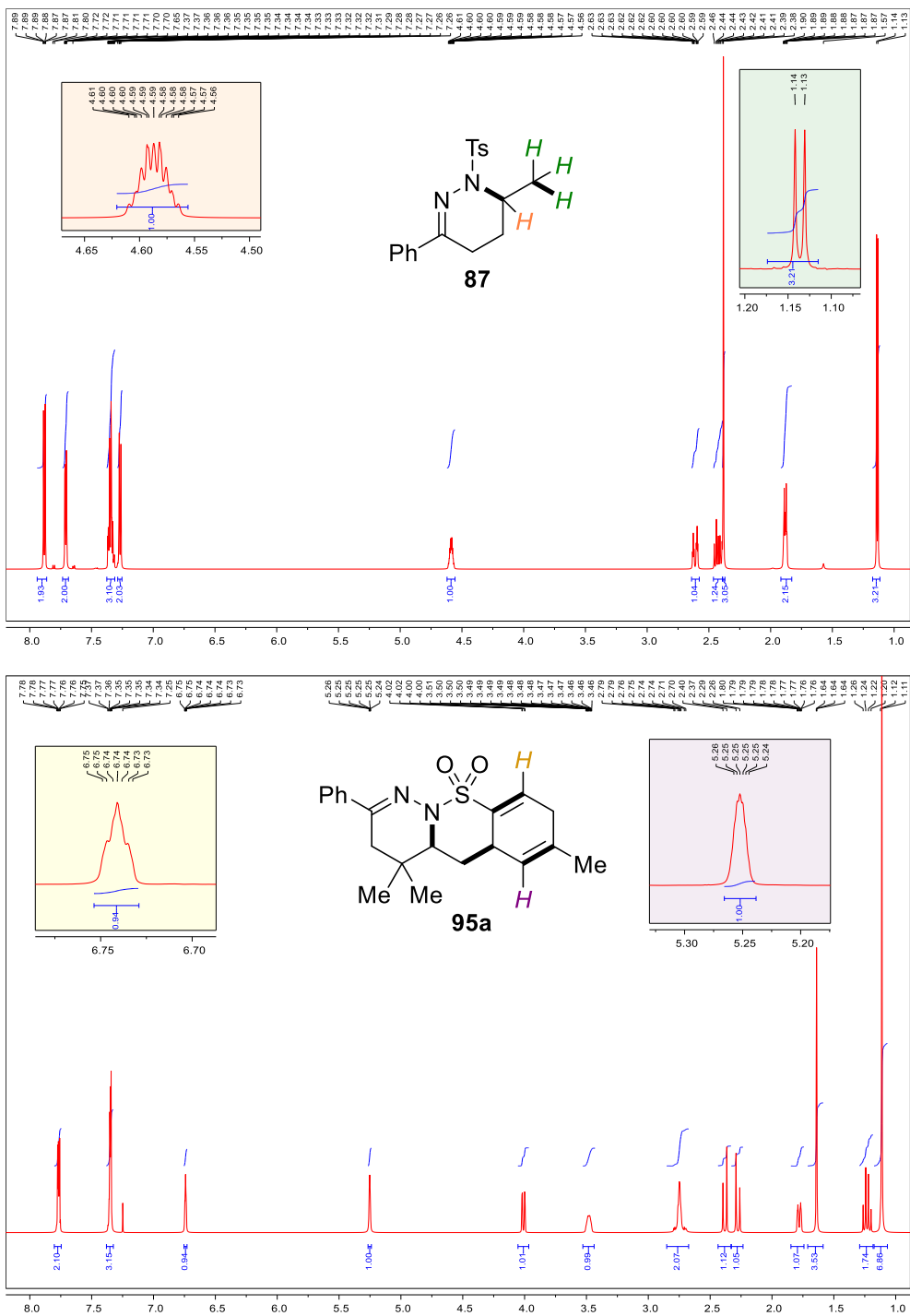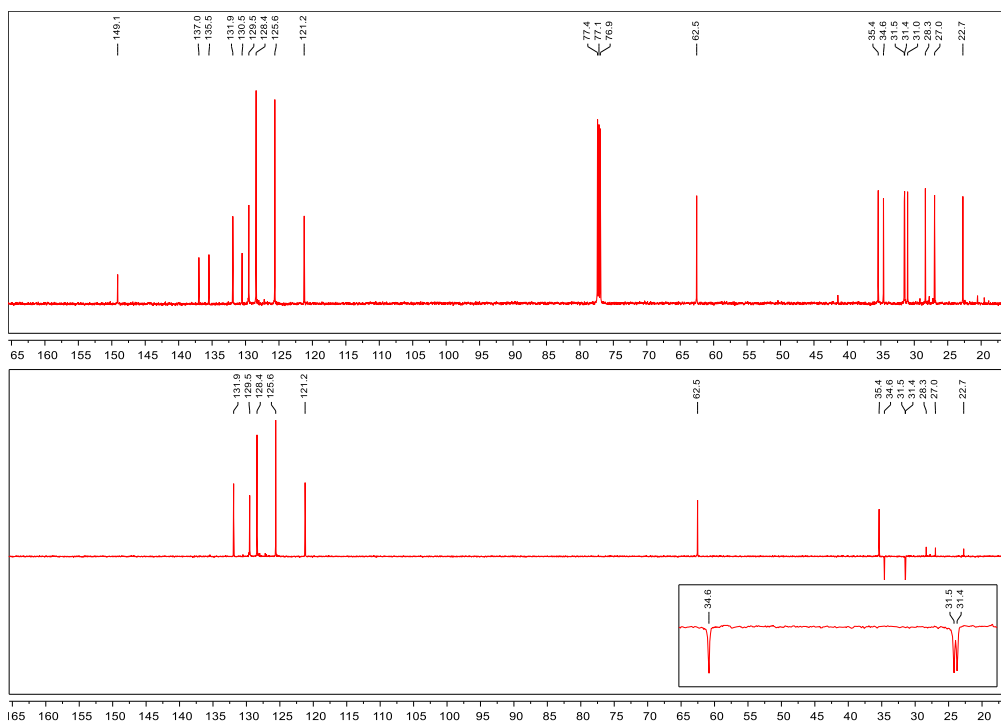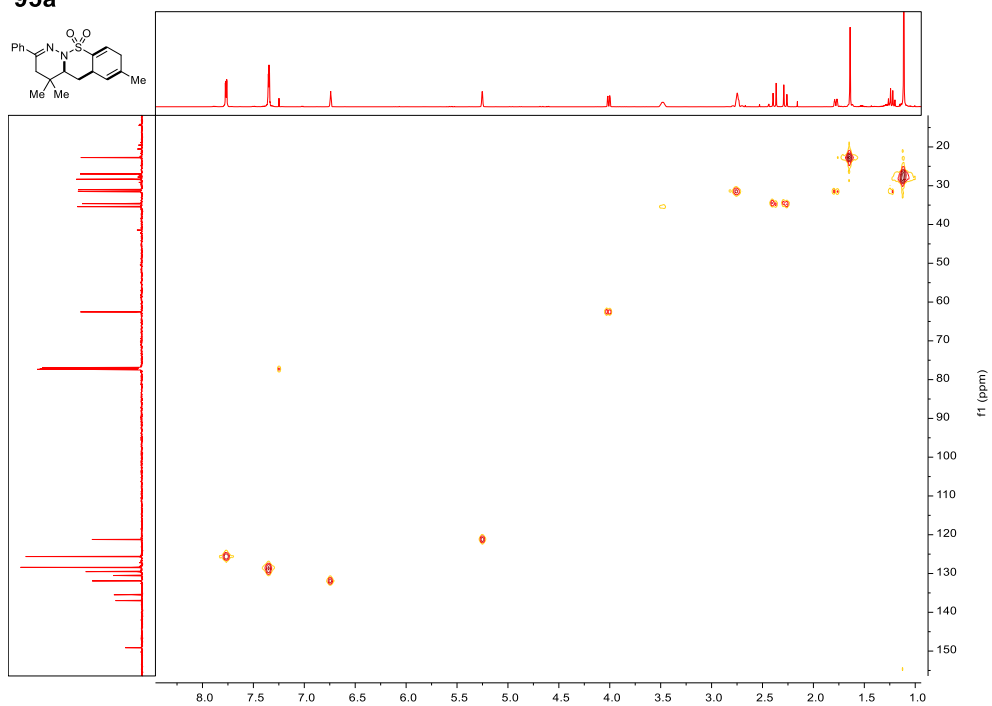
Figure 3.4 ^{13}C-NMR, 135-DEPT and HET-COR (HMQC: ^{1}H-NMR vs ^{13}C-NMR) spectra of compound **95a** used for structure determination

106

3.2.4.1 Dearomatization

The dearomatization of 6-membered carbon aromatic ring furnishes a 1,4-cyclohexadienyl structure. The Birch reduction of arenes is the organic chemistry textbook strategy that provides such transformation with a radical mediated mechanism. The unexpected yet interesting reaction outcome that we reported, allowed a dearomatization process in mild conditions and employing photoredox catalysis as source of electrons for such reduction (Scheme 3.15).

Birch Reduction for dearomatization

$$\text{Arene} \xrightarrow[\text{ROH, low T}]{\text{Na/NH}_3} \text{1,4-Cyclohexadiene}$$

$\bullet = C_{sp}^2$ $\bullet = C_{sp}^3$
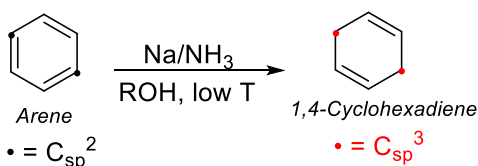
Photoredox induced cyclization and dearomatization: *4 C_{sp}^2 become 4 C_{sp}^3*

Simple, linear, achiral building blocks

$C_{sp}^2 \bullet \longrightarrow \bullet \; C_{sp}^3$

Complex, 3-D, chiral molecular scaffolds
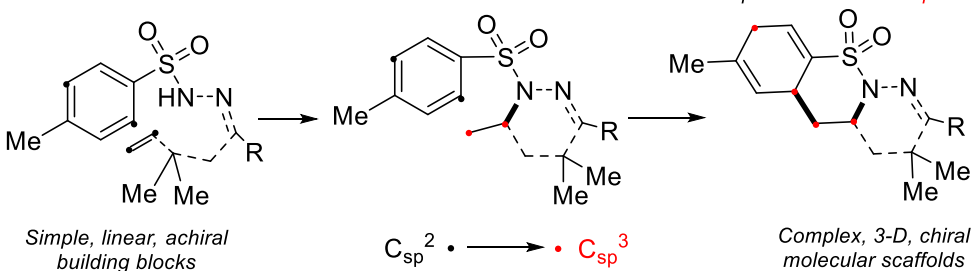
Scheme 3.15 Comparison between the classic Birch reduction for arene dearomatization and the photoredox induced dearomatization observed.

Selective dearomatization has proven to be a powerful tool in total synthesis to achieve complex natural product frameworks in a stereocontrolled fashion.[181] Indeed, dearomatization allows to shift from the chemistry of aromatic compounds to the chemistry of olefins, opening path towards the incorporation of otherwise incompatible functional groups. In addition, dearomatization strategies might represent an alternative to achieve olefins (especially intriguing scaffolds like skipped dienes) from natural occurring aromatic molecules.[182]

---

[181] Wertjes, W. C.; Southgate, E. H.; Sarlah, D. *Chem. Soc. Rev.* **2018,** *47*, 7996-8017.

[182] Roche, S. P.; Porco Jr., J. A. *Angew. Chem. Int. Ed.* **2011,** *50*, 4068-4093.

The photoredox transformation of a β-hindered γ,δ-unsaturated *N*-tosylhydrazones promoted a cascade process leading to dearomatization propelled by the previous cyclization. To our delight, this synthetic outcome of such ring formation met the initial expectations of this investigation. Indeed, the unsaturation shift towards γ,δ-unsaturated *N*-tosylhydrazones led to the disclosure of a new mode of reactivity, providing both a cyclization to a tetrahydropyridazine scaffold and a subsequent intramolecular radical dearomatization process delivering a tricyclic structure (ring sizes: 6/6/6).

A similar reactivity was observed by Xiao for β,γ-unsaturated *N*-tosylhydrazones **62** (Scheme 3.16a).[183] In that case, dual catalysis was exploited to obtain a tricyclic structure **96** (ring sizes: 5/6/6). Indeed, the dearomatized benzosultams obtained were unstable, spontaneously reacting to yield the aromatized product. Thus, to prevent degradation and anticipate the aromatized product, a cobalt cocatalyst was required. Occasional examples of a similar reactivity were also reported as byproducts **97** in another work by Xiao[165], when 4-halophenylsulfonylhydrazones **62d** instead of *N*-tosylhydrazones were employed (Scheme 3.16b).

For γ,δ-unsaturated *N*-tosylhydrazones **94** such reactivity furnishing stable dearomatized tricyclic products **95**, was yet unprecedented. Nevertheless, while the Covid pandemic was hitting the hardest and we were struggling to return to the laboratories and complete the scope of the reaction, Stephenson's group reported the first arene dearomatization under photoredox conditions (Scheme 3.16c).[184] In this case, an amidyl radical, generated under photoredox conditions from a *N*-tosyl-4,5-unsaturated amides **98**, initiates a *5-exo-trig* cyclization yielding a carbon radical intermediate that subsequently leads to the intramolecular dearomatization (yielding a 5/6/6 tricycle **99**). Dearomatization meets the concept of "escaping flatland" promoted by Lovering,[140,141] and recently a renewed interest for such process has raised, especially when it can be performed under photoredox conditions.[121] Our discovery, albeit conceptually slightly anticipated by these previous works, was still unprecedented for this class of hydrazones. Moreover, the new dearomatized tricyclic 6/6/6 observed structure represented a complementary contribution to this field of research.

---

[183] Zhao, Q.-Q.; Hu, X.-Q.; Yang, M.-N.; Chen, J.-R.; Xiao, W.-J. *Chem. Commun.* **2016,** *52*, 12749-12752.

[184] McAtee, R. C.; Noten, E. A.; Stephenson, C. R. J. *Nat. Commun.* **2020,** *11*, 2528.

a) Xiao's synthesis of dihydropyrazole-fused benzosultams

Ru(bpy)$_3$Cl$_2$·6H$_2$O (2 mol%)
[Co(dmgH)$_2$ClPy] (8 mol%)
K$_2$CO$_3$ (1.5 eq.)
CH$_3$CN, rt, 24-48h, blue LEDs

21 examples
31-77% yields

62

96
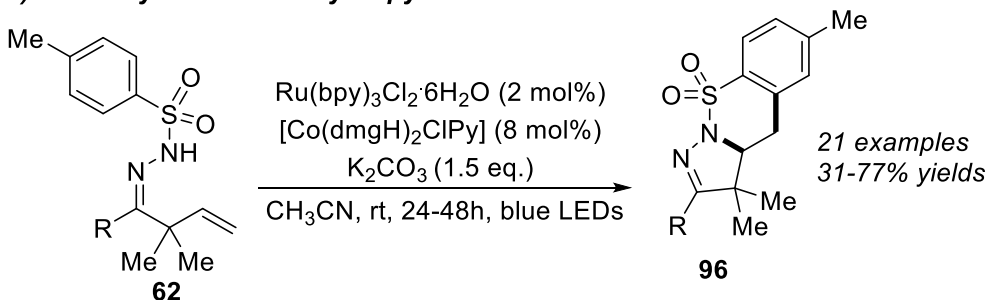
b) Xiao's observed byproducts of dearomatization

MeO$_2$C **70**

Ir(ppy)$_2$(bpy)PF6 (2 mol%)
K$_2$CO$_3$ (2.0 eq.)
CH$_3$CN, rt, 10h, blue LEDs

X = F,Cl

97

2 examples
26-36% yields

observed as intramolecular
transformation byproducts

62d

X = F,Cl
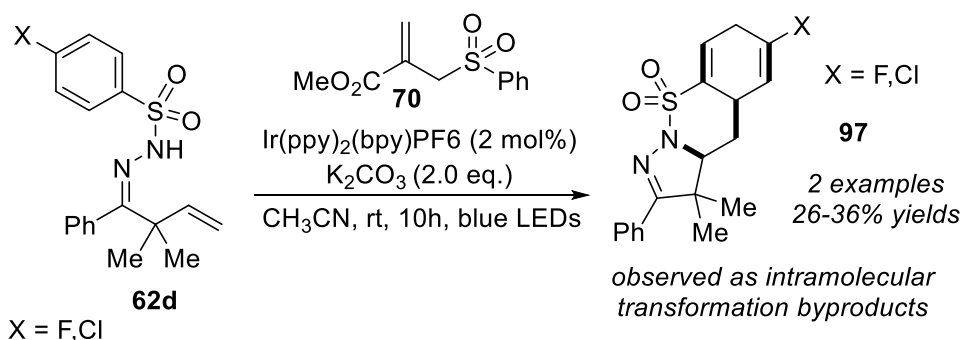
c) Stephenson's synthesis of benzosultams by dearomatization

[Ir(dF(CF$_3$ppy)$_2$)(5,5′-CF$_3$-bpy)]PF$_6$
(1 mol%)
NBu$_4$OP(O)(OBu$_2$) (0.65 eq.)
PhCF$_3$/*t*-BuOH (0.05 M),
rt, 14h, blue LEDs

98

99

21 examples
27-80% yields

R^3 = R^4 = Me, -(CH$_2$)$_3$-
R^5 = H, Me
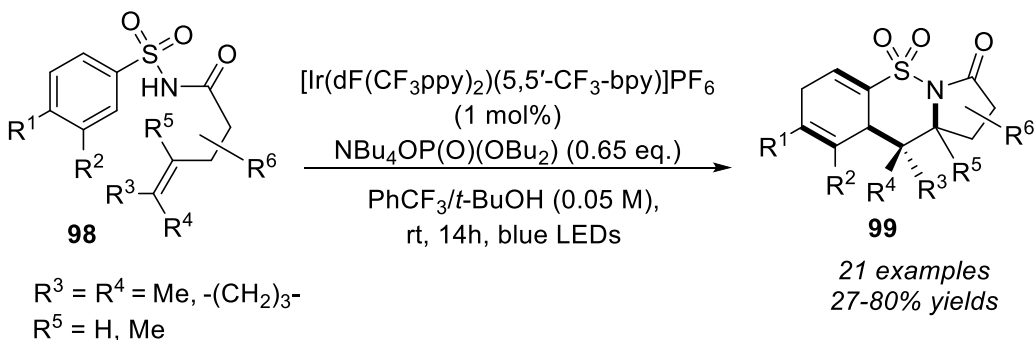
Scheme 3.16 Previous reported examples of reactivities with NCRs generated under photoredox conditions triggering a similar cascade process with carbon radical attack to arene to form tricyclic structures **96, 97, 99**.

3.2.5 Radical cyclization and dearomatization of β-Hindered γ,δ-unsaturated *N*-arylsulfonylhydrazones

Thanks to the employment of the β-hindered γ,δ-unsaturated *N*-tosylhydrazone **94a** we observed an unprecedented photoredox transformation. Such transformation was initiated by a *N*-hydrazonyl radical whose subsequent evolution through a domino carboamination/dearomatization yielded a tricyclic structure containing both the tetrahydropyridazine scaffold, a benzosultam functionality and a 1,4-cyclohexadienyl moiety **95a**. Given both the methodological appeal for dearomatization processes and the biological importance of tetrahydropyridazines and 1,4-skipped dienes, we pursued the investigation of such reaction.

3.2.5.1 Optimization

To identify the conditions for high yielding transformation of **94a** in **95a**, an optimization based on the variation of the base, the solvent, the PC, and the light source was conducted and is reported in Table 3.3. The starting point were the optimized conditions for tetrahydropyridazines **87**. The Kessil A160 Blue LEDs Lamp with potency of 40W enhanced the yield from 35% (entry 1) to 52% (entry 2). The combination of base and light sources was studied. With strong bases like KOH and NaOH the transformation was effective with the weaker 9W lamp but led to degradation when the 40W lamp was used (entries 1-6). The use of a weaker lamp and weaker bases led to incomplete or absent conversion of the starting material (entries 7-9). With 40W lamp, instead, we reported the best yield of 73% (70% on the isolated product, entry 10) although the increase of the base from 1.2 to 1.5 equivalent and the change of the solvent from chloroform to acetonitrile were required. Once again, the power of the light source was determining, the reaction is completed in 16h with 40W lamp, while with 9W lamp, even after 72h the reaction was unfinished (85% conversion, 50% yield, entry 9). To evaluate the effect of the PC on the process, a screening of some common PCs was conducted with the weaker 9W lamps in the same conditions of entry 9. Despite the weaker lamps, Iridium based PCs provided complete conversion of the reagents (entries 14, 15). Nevertheless, yields were still lower than the one obtained with [Ru(bpy)$_3$]Cl$_2$·6H$_2$O despite the uncomplete conversion. Eosin Y and Ru(bpz)$_3$ resulted inefficient (entries 13, 16) and the unreacted starting material was recovered. Control experiments were conducted removing the reaction participants one at the time.

Table 3.3 Optimization of photoredox catalysed cyclization and dearomatization of β-Hindered γ,δ-unsaturated *N*-tosylhydrazones **94a**
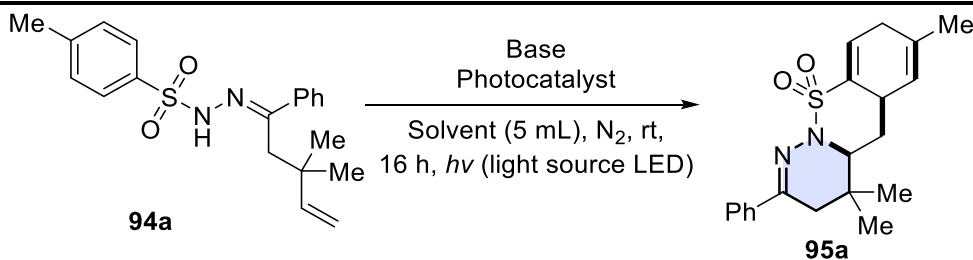
Entry	Base	Catalyst	Solvent	Yield %	Light Source
1	KOH (1.2 eq)	[Ru(bpy)₃]Cl₂ (3% mol)	CHCl₃	35 (22)[b]	9W, 450 nm, blue
2	KOH (1.2 eq)	[Ru(bpy)₃]Cl₂ (3% mol)	CHCl₃	52 (45)[b]	40 W, 456 nm, blue
3	K₂CO₃ (1.5 eq)	[Ru(bpy)₃]Cl₂ (3% mol)	CHCl₃	40 (35)[b]	40 W, 456 nm, blue
4	KOH (1.2 eq)	[Ru(bpy)₃]Cl₂ (3% mol)	CH₃CN	0[d]	40 W, 456 nm, blue
5	KOH (1.5 eq)	[Ru(bpy)₃]Cl₂ (3% mol)	CH₃CN	0[d]	40 W, 456 nm, blue
6	NaOH (1.5 eq)	[Ru(bpy)₃]Cl₂ (3% mol)	CH₃CN	0[d]	9W, 450 nm, blue
7	Cs₂CO₃ (1.5 eq)	[Ru(bpy)₃]Cl₂ (3% mol)	CH₃CN	[0][c] 0	9W, 450 nm, blue
8	K₂CO₃ (1.2 eq)	[Ru(bpy)₃]Cl₂ (3% mol)	CH₃CN	[45][c] 43	9W, 450 nm, blue
9 [e]	K₂CO₃ (1.5 eq)	[Ru(bpy)₃]Cl₂ (3% mol)	CH₃CN	[85][c] 50	9W, 450 nm, blue
10	**K₂CO₃ (1.5 eq)**	**[Ru(bpy)₃]Cl₂ (3% mol)**	**CH₃CN**	**73 (70)[b]**	**40 W, 456 nm, blue**
11	K₂CO₃ (1.5 eq)	[Ru(bpy)₃]Cl₂ (2% mol)	CH₃CN	58	40 W, 456 nm, blue
12	K₂CO₃ (1.5 eq)	[Ru(bpy)₃]Cl₂ (1% mol)	CH₃CN	55	40 W, 456 nm, blue
13 [e]	K₂CO₃ (1.5 eq)	Eosyn Y (3% mol)	CH₃CN	[0][c] 0	9W, 550 nm, green
14	K₂CO₃ (1.5 eq)	[Ir(ppy)₂(dtbpy)][PF₆] (3% mol)	CH₃CN	37	9W, 365 nm, purple
15	K₂CO₃ (1.5 eq)	[Ir(dFCF₃ppy)₂(bpy)]PF₆ (3% mol)	CH₃CN	42 (36)[b]	9W, 365 nm, purple
16	K₂CO₃ (1.5 eq)	[Ru(bpz)₃][PF₆]₂ (3% mol)	CH₃CN	[0][c] 0	40 W, 456 nm, blue
17	–	[Ru(bpy)₃]Cl₂ (3% mol)	CH₃CN	[0][c] 0	40 W, 456 nm, blue
18	K₂CO₃ (1.5 eq)	–	CH₃CN	[0][c] 0	40 W, 456 nm, blue
19	K₂CO₃ (1.5 eq)	[Ru(bpy)₃]Cl₂ (3% mol)	CH₃CN	[0][c] traces	-

Reactions conditions: tosylhydrazone (0.3 mmol), anhydrous solvent (5 mL), base (1.2 eq; 0.36 mmol), catalyst (3% mol; 0.009 mmol) *a)* Determined by NMR spectroscopy using nitromethane as internal standard; *b)* Yields determined on isolated product; *c)* incomplete or no conversion observed, [calculated conversion reported]; *d)* mixture of degradation products was observed *e)* reaction time:72 hours

In the absence of the base the transformation did not occur (entry 17). Besides, the photoredox nature of the process was confirmed since when the PC was removed (entry 18) or when the reaction was run in the dark (entry 19) only traces or no product were obtained.

3.2.5.2 Generalization

Exploiting the synthesis of β-Hindered-γ,δ-unsaturated ketones **89** we synthesized a list of corresponding *N*-arylsulfonylhydrazones **94a-k** (where the aryl is a tosyl or a phenylsulfonyl group, Table 3.4). We considered the variations of the arene moiety of arylsulfonyl hydrazones (e.g. using phenylsulfonyl), to observe differently substituted cyclohexadienic structures. Thus, substrates **94a-k** were reacted in the optimized conditions to extend the scope of the transformation.

Table 3.4 Library of *N*-arylsulfonylhydrazone **94** synthesized for photoredox consecutive cyclization and dearomatization

R^2 = H, *benzenesulfonohydrazide*
R^2 = Me, *tosylhydrazide*

R	94a	94b	94c	94d	94e	94f	94g	94h	94i	94j	94k
1	Ph	2-Naphth	2-py	*m*-Tol	*m*-MeOPh	*p*-Tol	*o*-Tol	Ph	Me	Me	Ph
2	Me	Me	Me	Me	Me	Me	Me	Me	Me	H	H
3	Me	Me	Me	Me	Me	Me	Me	Ph	Me	Me	Me

Best yields were obtained with tosylhydrazones **94a** and **94i** and afforded hexahydrobenzo[e]pyridazino[1,6-b][1,2]thiazine-10,10-dioxide **95a** and **95i** in yields (70% and 73%, respectively). Notably, it is not required that the tosylhydrazones' α-substituent (R^1) is an aromatic group, thus the reaction can be successfully applied to arylsulfonylhydrazones derived from aliphatic ketones as confirmed by product **95i**. The same analysis was conducted on the corresponding *N*-phenylsulfonylhydrazones, to recover α-methyl product **95j** and the α-phenyl product **95k** with the unsubstituted cyclohexadienic portion (55% and 40% yield, respectively) with a general decrease in yield observed when compared with the corresponding products from tosyl derivatives. Subsequently, we moved the evaluation to the electronic properties of the α-substituent R^1 using both electron poor aromatics like 2-pyridinyl (**95c,** 37%) and electron rich aromatics like 2-naphthyl (**95b**, 43%), 3-methoxyphenyl (**95e**, 50%), and tolyl substituents. For the latter, a further analysis was conducted to evaluate both electronic and steric effects (**95d** *meta* 60%, **95f** *para* 62%, **95g** *ortho* 52%).

Table 3.5 Scope of the synthesis of **95**
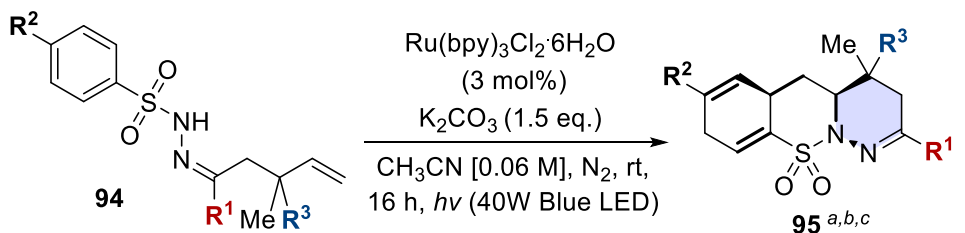
from N-tosylhydrazones

95a: *70%*

95b: *43%*

95c: *37%*
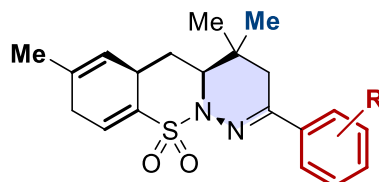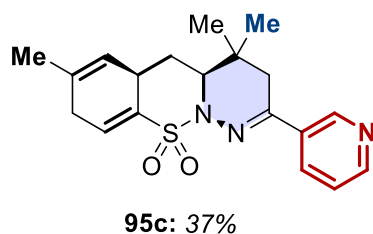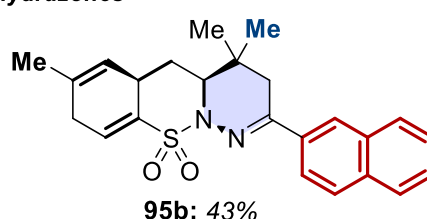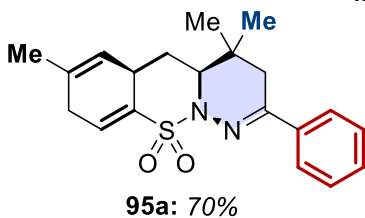
R=*m*-M**e** **95d:** *60%*   R=*p*-M**e** **95f:** *62%*
R=*m*-OM**e** **95e:** *50%* R=*o*-M**e** **95g:** *52%*

95h: *34%*

95i: *73% (51%)*[d]
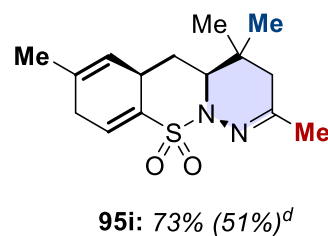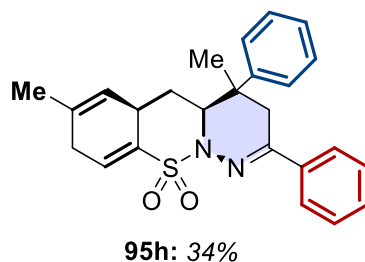
from N-benzenesulfonylhydrazones

95j: *55%*

95k: *40%*
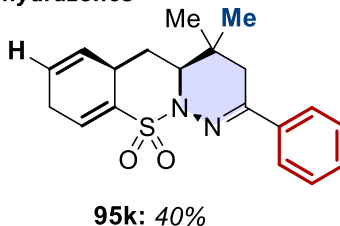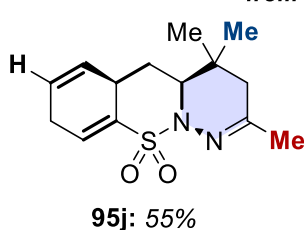
a) Reaction conditions: *N*-arylsulfonylhydrazone **94** 0.3 mmol, K₂CO₃ 0.45 mmol, anhydrous CH₃CN 5 mL, [Ru(bpy)₃]Cl₂·6H₂O 0.09 mmol, 40W blue lamp, 16 h, inert atm. *b)* Yields determined on isolated product. *c)* Relative configurations of products assigned by analogy to **95a**. *d)* Yields for reaction scaled on 2 mmol of **94i**, 72 h reaction time

While *meta* and *para* derivatives resulted comparable in yields, *ortho* substitution limits the process outcome, thus demonstrating an influence of steric effects. Concerning β substitution, increasing the steric congestion using a phenyl instead of another geminal methyl resulted in 34% yield for product **95h**. The reaction, proven by X-ray diffraction to be totally diastereoselective (Figure 3.2), was also scaled up to 2 mmol for **94i** (readily obtainable in 2 steps from commercially available ketone mesityl oxide), thus product **95i** was obtained in 51% yield after 72 hours (Table 3.5).

Finally, we tested the possibility of obtaining a (partially) saturated tetracyclic core 6/6/6/6 structure, exploiting a naturally occurring starting material. Pulegone **96**, a monoterpene ketone from the flowering plants *Lamiaceae* (mint family) was converted into the desired structure **95l**, in three steps (organocuprate addition, tosylhydrazide condensation and photoredox cyclization followed by the unique chromatography purification step of the whole synthesis, with an overall yield of 17.5%, Scheme 3.17)

96 (*R*)-(+)-*pulegone*
naturally occurring
β-hindered ketone

94l

95l, *17,5% overall*
tetracyclic structure (6/6/6/6)
obtained in 3 steps from **96**
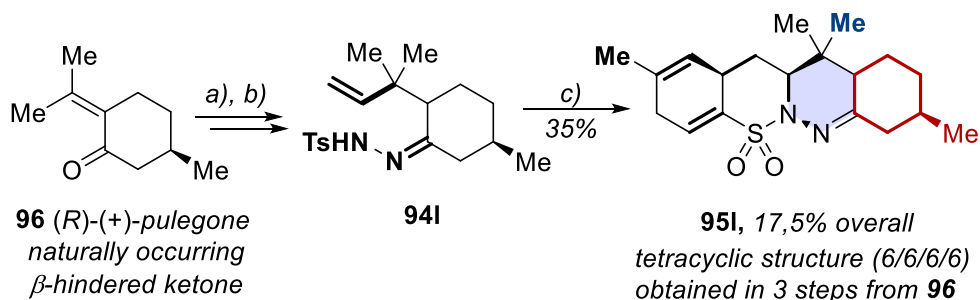
Scheme 3.17 Three-steps synthesis of a tetracyclicic tetrahydropyridazine **95l** from naturally occurring Pulegone **96**; *a)* CuI, $H_2C=CH_2$-MgBr, THF, -40°C, inert atm. (83%); *b)* tosylhydrazide, CH_3OH, rt (57%); *c)* K_2CO_3, [Ru(bpy)$_3$]Cl$_2$·6H$_2$O, anhydrous CH_3CN, 40W blue lamp, 16 h, inert atm (35%).

3.2.5.3 Studies of reaction mechanism

Mechanistic suggestion concerning the deprotonation and subsequent photoredox mediated oxidation of the starting hydrazones (ODET process), are corroborated by the literature about previously reported photoredox transformation of β,γ-unsaturated *N*-tosylhydrazones.[164] However, since we were facing a new reactivity, we provided detailed mechanistic investigation on our process.

3.2.5.3.1 Stern-Volmer Plot and Cyclic Voltammetry
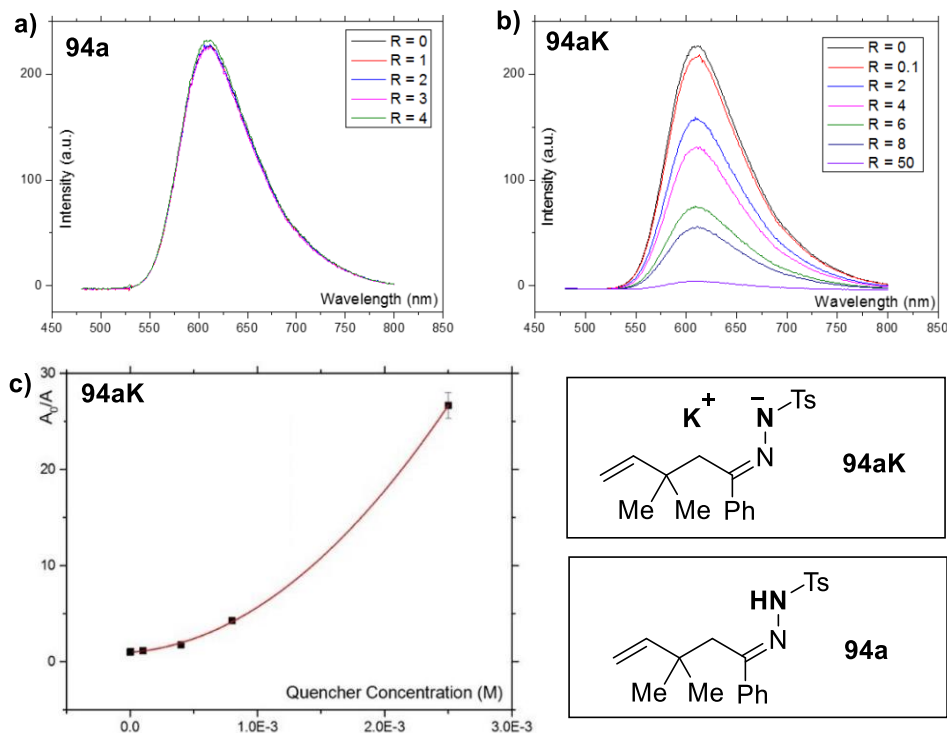
Figure 3.5 *a)* Fluorescence spectra of a 50μM solution of Ru(bpy)$_3$Cl$_2$·6H$_2$O in presence of different concentrations of *N*-tosylhydrazone **94a**, R=ratio between **94a** and Ru(bpy)$_3$Cl$_2$·6H$_2$O concentrations; *b)* Fluorescence spectra of a 50μM solution of Ru(bpy)$_3$Cl$_2$·6H$_2$O in the presence of different concentrations of *N*-tosylhydrazone potassium salt **94aK**, R=ratio between **94aK** and Ru(bpy)$_3$Cl$_2$·6H$_2$O concentrations; *c)* Stern–Volmer plot for the [Ru(bpy)$_3$]$^{2+}$ luminescence quenching in the presence of *N*-tosylhydrazone **94aK**

To confirm the ODET hypothesis, in collaboration with Dr. F. Pellegrino of University of Turin, Chemistry Department, we performed Stern–Volmer luminescence quenching studies to discover which species worked as a quencher of the photoexcited state of Ru(II) PC. Tosylhydrazone **94a** was not able to accomplish such task (Figure 3.5a), differently from its K$^+$ salt **94aK** (formed upon deprotonation by K$_2$CO$_3$) that act as a quencher of Ru(II) fluorescence (Figure 3.5b), performing both static and dynamic quenching as highlighted by the nonlinear Stern-Volmer Plot (Figure 3.5c). Such dual behavior was coherent with the formation of an ion pair between the tosylhydrazone anion **94aK** and Ru(II), as previously observed.

This demonstrated that a photoexcited PC involved **94aK** in a SET event and cyclovoltammetries (CVs, performed again in collaboration with Dr. Pellegrino) of Ru(II) and **94aK** showed that the PC possessed the potential to oxidize the anion, ultimately demonstrating that the formation of hydrazonyl NCR by ODET is truthfully. Besides, we also accomplished the electrochemical characterization of the final isolated product **95a**, confirming that such species was stable in the employed photoredox reaction conditions. Thus, knowing the CV profile of the species involved (**94aK**, **95a** and Ru(bpy)$_3$Cl$_2$, we could even implement a complete electrochemical study following the whole reaction by CV (Figure 3.6).
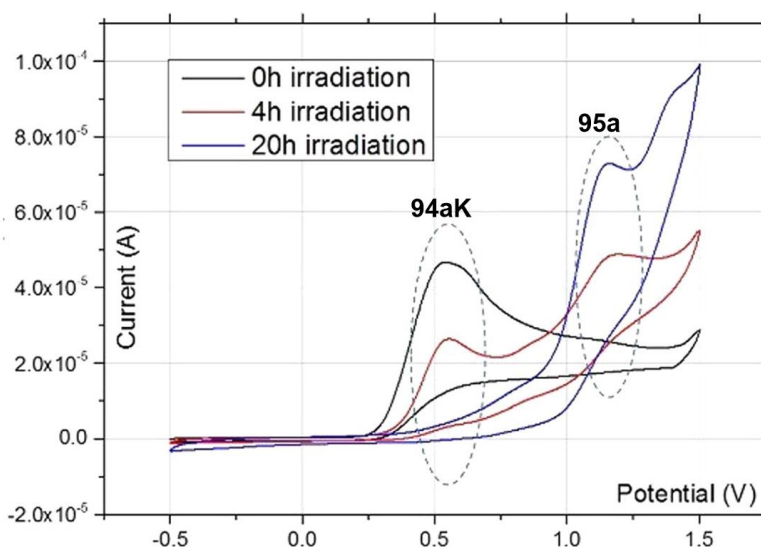
Figure 3.6 Electrochemical characterization of the reaction. CVs performed at three different times during the reaction: $t_0 = 0$ h, immediately after irradiation, black line; $t_1 = 4$ h of irradiation, red line; $t_2 = 20$ h of irradiation, blue.

A 0.1 mM Ru(bpy)$_3$Cl$_2$·6H$_2$O and 3 mM **94aK** solution in CH$_3$CN was irradiated for 20 h, under nitrogen atmosphere and CV were registered three times: after 0 minutes (t_0, immediately after irradiation began), after 4 hours and after 20 hours. At the t_0, only the peak of **94aK** characterized the CV of the reaction mixture (+0.52 V, black line, Figure 3.6). This also occurred because the low concentration of the PC did not allow to detect its voltammogram, covered by the more intense one of **94aK**. After 4 h under irradiation, as the reaction proceeded, CV shows the decreasing of the substrate **94aK** and presence of the product **95a** was detected. Indeed, the peak of the substrate **94aK** decreased in intensity (lowering of current intensity value at +0.52 V, red line, Figure 3.6) while a new peak, corresponding to the oxidation of **95a**

116

appeared (+1.23 V, red line, Figure 3.6). After 20 h of irradiation completeness was achieved, showing exclusively one intense peak (located at 1.23 V, with disappearance of the peak at +0.52 V, blue line, Figure 3.6).

3.2.5.3.2 TEMPO trapping experiment and forced radical initiation

Being the ODET process confirmed, further experiments were conducted to assess the radical nature of the process and to validate the hypothesis of the radical cyclization with the formation of carbon centered radical intermediates.
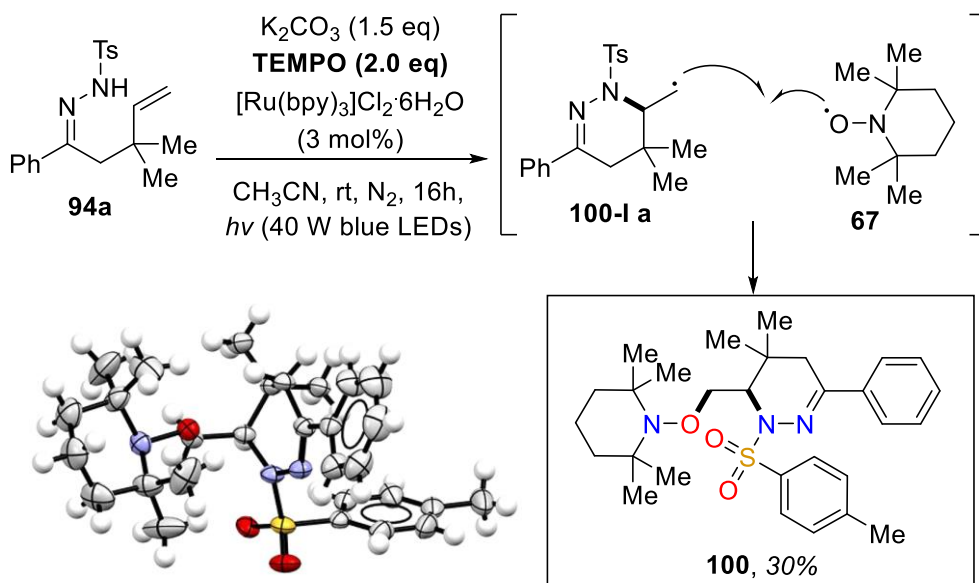
Scheme 3.18 TEMPO **67** Trapping Experiment yielding adduct **100** and ORTEP plot of the asymmetric unit of **100** in the crystal structure (bottom left; color code gray: carbon; blue: nitrogen; red: oxygen; yellow: sulfur; 50% of probability represented). X-ray analysis by Dr. E. Priola.

Thus, the model reaction studied for optimization was carried out in the presence of 2.0 equivalents of TEMPO radical. The reactive outcome was a tetrahydropyridazine **100** that did not undergo the second cyclization and dearomatization. Indeed, a six membered cycle formed, and the radical located on the exocyclic carbon centered was trapped by TEMPO **67**, with the formation of a C-O bond affording 1-phenyl-*N*-tosyl-6-(2,2,6,6-tetramethyl-*N*-methylenoxy)1,4,5,6-tetrahydropyridazine **100-I** in 30% yield. The structure of such adduct was confirmed by HRMS, NMR

spectroscopy, and single crystal X-ray diffraction, leading to the unquestionable hypothesis that a key carbon radical intermediate **100-I** was involved in the process (Scheme 3.18).

3.2.5.3.3 Proposed Mechanism
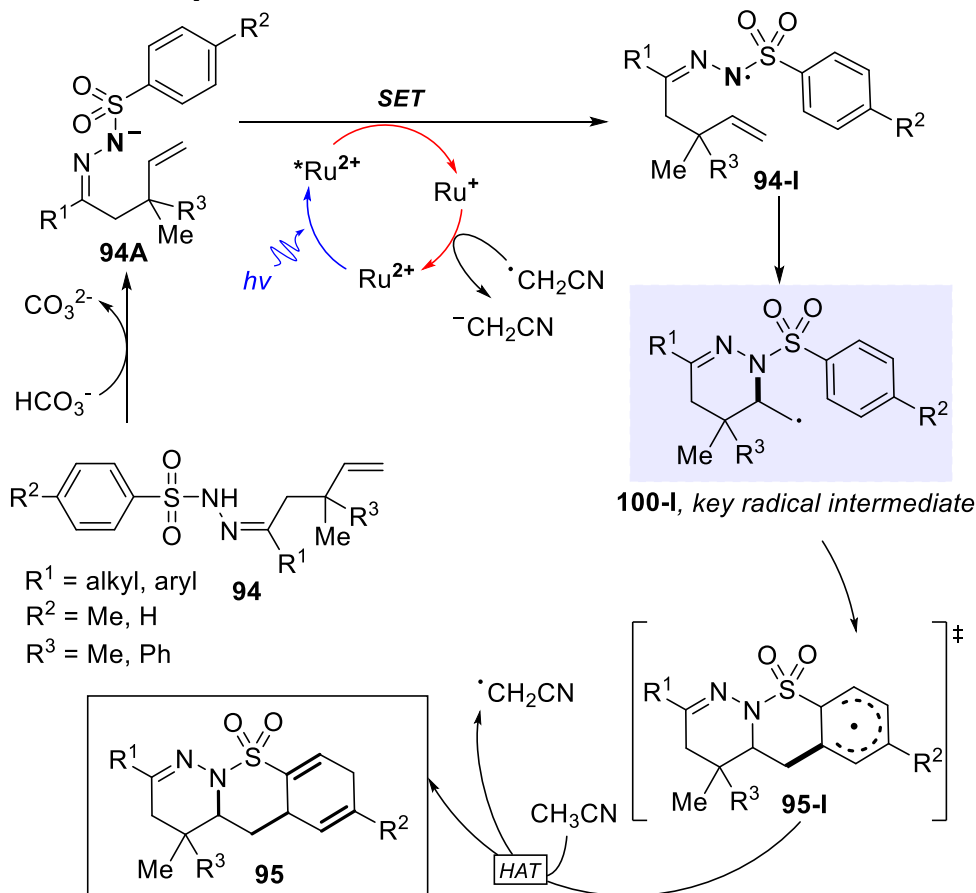
Scheme 3.19 Proposed mechanism for photoredox catalyzed yielding dearomatized tryciclic tetrahydropyridazine product **95**

A mechanism is proposed considering the experimental findings (Scheme 3.19). The starting hydrazone substrate **94** is deprotonated yielding the corresponding anion **94-A** that is further oxidized by the excited state of the PC, in a typical ODET process delivering the hydrazonyl NCR **94-I**. The intramolecular radical attack of the latter to the alkene promotes the first *6-exo-trig* cyclization with the formation of a new C-N bond providing the key carbon centered radical intermediate **100-I**. This carbon radical undergoes the second cyclization attacking the arene moiety of the arylsulfonyl moiety

118

of the molecule, establishing a new C-C bond and providing the dearomatized tricyclic product **95** upon a postulated HAT from the solvent quenching the cyclic radical intermediate **95-I**. Since the reactivity of the key radical intermediate **100-I** was further exploited in following studies to achieve other reactive outcomes, a more detailed mechanism hypothesis, with further explanation and computational studies in support, will be provided in the next chapter.

3.2.5.4 Conclusion

In this Chapter a photoredox catalyzed reaction of β-hindered γ,δ-unsaturated *N*-arylsulfonylhydrazones leading to two consecutive intramolecular 6-*exo-trig* cyclizations with the formation a new C-N and a new C-C bond has been described. Such transformation provided a tetrahydropyridazine core embedded in a tricyclic 6/6/6 structure that also contain the intriguing 1,4 dienes moiety. The fused cycles originated as the outcome of a radical dearomatization of the tosyl moiety and the final product was obtained as single diasteromer.

Our findings highlighted the importance of a generalization in the study of the reactivity of unsaturated hydrazones under photoredox conditions. Indeed, the simple shift of the unsaturated moiety, combined with slight structural modifications, allowed us to observe a significantly different reactive outcome.

The control of the reactivity of the key carbon radical intermediate **100-I** might be the mainspring of new and different chemical pathways. Thus, we envisaged that a structural modification either of the arylsulfonyl moiety or of the olefin might direct the reactivity towards new outcomes. The photoredox reactivity leading to the synthesis of simple, monocyclic tetrahydropyridazines that will be described in next chapter is a direct consequence of the methodological achievement of this one.

CHAPTER FOUR:
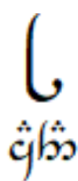
ს

ქსა

PHOTOINDUCED CYCLIZATION AND RADICAL SMILES REARRANGEMENT OF γ,δ-UNSATURATED *N*-ARYLSULFONYLHYDRAZONES

CHAPTER 4 PHOTOINDUCED CYCLIZATION AND RADICAL SMILES REARRANGEMENT OF γ,δ-UNSATURATED *N*-ARYLSULFONYLHYDRAZONES

4.1. Introduction

Rearrangement reactions are exploited in synthesis to obtain complex structures from more available precursors. Since increasing the structural complexity of the target molecule is part of the aim of this dissertation, this synthetic approach was not ignored. Indeed, throughout this chapter it will be explained how the Smiles Rearrangement provides access to other classes of tetrahydropyridazines from unsaturated hydrazones.

4.1.1 Smiles Rearrangement

The general definition of the Smiles rearrangement is a polar transformation where an intramolecular migration of an aryl ring acting as an electrophile is observed. From a mechanistic point of view, a nucleophilic aromatic substitution reaction (SNAr) occurs.
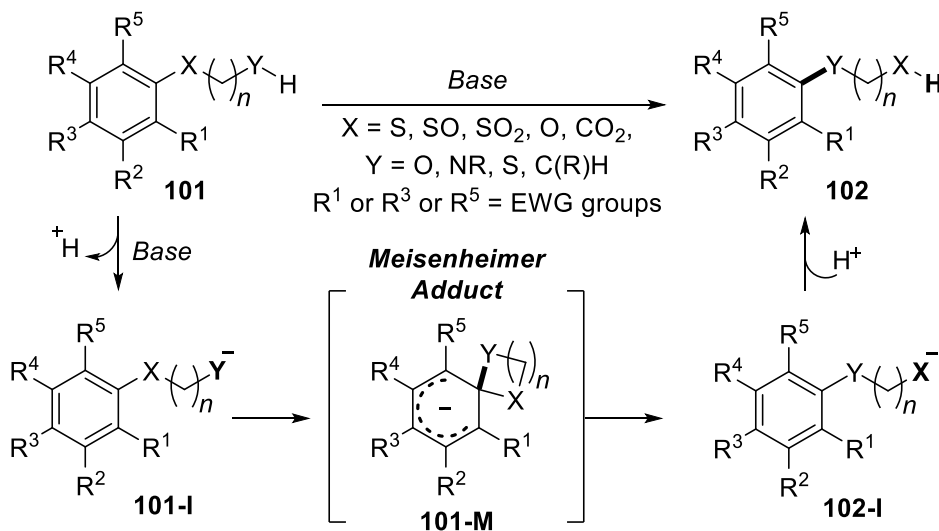
Scheme 4.1 Generalized mechanism of Smiles rearrangement of arene **101** into arene **102**

Generally, aromatic substitution might follow two pathways. The first is a stepwise mechanism *via* formation of a stable cyclohexadienyl anionic intermediate σ-adduct, the Meisenheimer adduct. Alternatively, it proceeds in

a concerted fashion, in which the Meisenheimer adduct is observed only as a transition state. The two components of such adduct are an arene bearing an electron withdrawing group (EWG) and a pronucleophile group as the substituents. Particularly, the Smiles rearrangement (originally reported in at the end of the 19th century for naphtholsulfones[185] but generalized only in the 1930 by Smiles[186]) is intramolecular *ipso* directed SNAr. The substrate of this substitution reaction is an arene **101** characterized by a substituent group with a X group directly linked to the aromatic ring and another distal group Y-H. The Y, typically a heteroatom, is part of a pronucleophile moiety Y-H that will be converted into the nucleophile Y⁻ operating the attack. The X group is instead a chemical entity able to dislodge the negative charge from the ring and act as the leaving group. Arene **101** is also characterized by other EWG substituent at the *ortho* or the *para* position with respect to the reaction center (that is the carbon of the C-X bond). Such EWGs stabilize the Meisenheimer adduct **101-M** and promote nucleophilic aromatic substitution at the *ipso* position. Typically, the nucleophile **101-I** is generated upon treatment with base. Given the intramolecular nature of this process, the Meisenheimer adduct **101-M** is a spirocycle. Thus, X assumes a double function both assisting the linkage of the nucleophile to the aromatic ring and working as the leaving group during the elimination that delivers the substituted molecule **102-I** yielding the product **102** upon protonation (Scheme 4.1).

In the 1970s, Truce developed a variation of such rearrangement, later known as Truce-Smiles rearrangement.[187] When an organolithium compound is used as the base, a carbon nucleophile **103A** can be generated, thus a new C-C bond is forged as the result of the intramolecular SNAr (Scheme 4.2).

---

[185] Henriques, R. *Ber. Dtsch. Chem. Ges.* **1894,** *27*, 2993-3005. Hinsberg, O. *J. Prakt. Chem.* **1916,** *93*, 277-301. Hinsberg, O. *J. Prakt. Chem.* **1914,** *90*, 345-353.
[186] McClement, C. S.; Smiles, S. *J. Chem. Soc.* **1937**, 1016-1021. Galbraith, F.; Smiles, S. *J. Chem Soc.* **1935**, 1234-1238. Evans, W. J.; Smiles, S. *J. Chem. Soc.* **1935**, 181-188. Levi, A.; Warren, L. A.; Smiles, S. *J. Chem. Soc.* **1933**, 1490-1493. Warren, L. A.; Smiles, S. *J. Chem. Soc.* **1932**, 2774-2778. Warren, L. A.; Smiles, S. *J. Chem. Soc.* **1930**, 1327-1331. .
[187] Truce, W. E.; VanGemert, B.; Brand, W. W. *J. Org. Chem.* **1978,** *43*, 101-105. Truce, W. E.; Robbins, C. R.; Kreider, E. M. *J. Am. Chem. Soc.* **1966,** *88*, 4027-4033. Truce, W. E.; Hampton, D. C. *J. Org. Chem.* **1963,** *28*, 2276-2279. Truce, W. E.; Ray, W. J. *J. Am. Chem. Soc.* **1959,** *81*, 481-484. Truce, W. E.; Ray, W. J.; Norman, O. L.; Eickemeyer, D. B. *J. Am. Chem. Soc.* **1958,** *80*, 3625-3629.

Scheme 4.2 *a)* Generalized mechanism of Truce-Smiles Rearrangement of arene **103** into arene **104** *b)* Typical tandem Truce–Smiles rearrangement – SO₂ extrusion reaction studied by Dohmori

Besides, this variation circumvents the need for an activating substituent in the *ortho* or *para* position of the migrating aryl unit. Recently, the term Truce-Smiles rearrangement has been extended to indicate every intramolecular nucleophilic aromatic substitution operated by a carbanion nucleophile in which a $C(sp^2)$–X bond is broken and a new $C(sp^2)$–C bond is formed by *ipso* substitution. However, similar rearrangements involving a carbanion enolate **105-A** obtained upon treatment with a hydroxide base were reported for a decade since 1954 by Dohmori.[188] In those cases, a heterocyclic Meisenheimer adduct **105-I** was formed, and SO_2 was extruded from this cycle to deliver the product **106**. This tandem sequence, combining the Truce–Smiles rearrangement and SO_2 extrusion, exploited the ability of the sulfonyl group to act both as excellent leaving group and as an electron density withdrawer by inductive effect (Scheme 4.2).

The development of Truce-Smiles variation, allowing the synthesis of C-C bonds, widely expanded the employment of such reaction in organic chemistry.[189,190] The preparation of the carbanion nucleophile has been extensively studied and other tandem reaction sequences have been disclosed.[191] Asymmetric variations were also defined, with the notable example of the Clayden rearrangement of lithiated ureas, carbamates and thiocarbamates **107**, providing enantioenriched tertiary amines, alcohols, and thiols **108** upon 1,4-aryl shift (Scheme 4.3).[192]

[188] Naito, T.; Dohmori, R.; Shimoda, M. *Pharm. Bull.* **1955,** *3*, 34-37. Naito, T.; Dohmori, R. *Pharm. Bull.* **1955,** *3*, 38-42. Naito, T.; Dohmori, R.; Kotake, T. *Chem. Pharm. Bull.* **1964,** *12*, 588-590. Dohmori, R. *Chem. Pharm. Bull.* **1964,** *12*, 591-594. Dohmori, R. *Chem. Pharm. Bull.* **1964,** *12*, 595-601. Dohmori, R. *Chem. Pharm. Bull.* **1964,** *12*, 601-606.
[189] Snape, T. J. *Chem. Soc. Rev.* **2008,** *37*, 2452-2458.
[190] Truce, W. E.; Kreider, E. M.; Brand, W. W., *Organic Reactions. The Smiles and Related Rearrangements of Aromatic Systems*. **2011**.
[191] Henderson, A. R. P.; Kosowan, J. R.; Wood, T. E. *Can. J. Chem.* **2017,** *95*, 483-504.
[192] Zawodny, W.; Montgomery, S. L.; Marshall, J. R.; Finnigan, J. D.; Turner, N. J.; Clayden, J. *J. Am. Chem. Soc.* **2018,** *140*, 17872-17877. Maury, J.; Zawodny, W.; Clayden, J. *Org. Lett.* **2017,** *19*, 472-475. Tait, M.; Donnard, M.; Minassi, A.; Lefranc, J.; Bechi, B.; Carbone, G.; O'Brien, P.; Clayden, J. *Org. Lett.* **2013,** *15*, 34-37. Tetlow, D. J.; Hennecke, U.; Raftery, J.; Waring, M. J.; Clarke, D. S.; Clayden, J. *Org. Lett.* **2010,** *12*, 5442-5445. Clayden, J.; Dufour, J.; Grainger, D. M.; Helliwell, M. *J. Am. Chem. Soc.* **2007,** *129*, 7488-7489.

Scheme 4.3 Generalized mechanism for the Clayden rearrangement

4.1.2 The radical Smiles rearrangement

Despite the excellent results obtained by Clayden[192] in the construction of chiral centers, the employment of organolithium bases and the required cryogenic conditions moved the interest of organic chemists towards radical variation of such rearrangement. Given the need of modern organic synthesis for greener and milder operative conditions, radical chemistry is being living its renaissance. Indeed, thanks to the new protocols developed to generate radical species in mild conditions (photochemical and electrochemical ones above all), many polar transformations are experiencing their conversion to the corresponding radical variations, even Smiles and Truce-Smiles rearrangement.[193,194] The first seminal examples date back to 1972[195] and 1991[196] but in the last decade, the field of radical aryl migration has flourished. These radical methodologies prevented the use of strong basic conditions and enabled the migration of aryl groups onto C atoms. Interestingly, such reported examples typically concerned the migration of arylsulfonates and arylsulfonamides leading to the extrusion of SO_2 drawing a sort of continuity line with the first reported examples of the polar variation (the Truce-Smiles reactivity actually disclosed by Dohmory[188]).

As described in the seminal examples by Gérard-Sapi's group[197] and Nevado's group,[198] the use of a radical initiator in the presence of a conjugated sulfonylamides precursors **109** leads to an initial radical addition to the unsaturated portion generating a carbon radical intermediate **109-I**.

---

[193] Holden, C. M.; Greaney, M. F. *Chem. Eur. J.* **2017,** *23*, 8992-9008.
[194] Allart-Simon, I.; Gérard, S.; Sapi, J. *Molecules* **2016,** *21*, 878.
[195] Loven, R.; Speckamp, W. N. *Tetrahedron Lett.* **1972,** *13*, 1567-1570.
[196] Motherwell, W. B.; Pennell, A. M. K. *J. Chem. Soc., Chem. Commun.* **1991**, 877-879.
[197] Pudlo, M.; Allart-Simon, I.; Tinant, B.; Gérard, S.; Sapi, J. *Chem. Commun.* **2012,** *48*, 2442-2444.
[198] Kong, W.; Casimiro, M.; Merino, E. b.; Nevado, C. *J. Am. Chem. Soc.* **2013,** *135*, 14480-14483.

Such species, like the Truce-Smiles carbanion, intramolecularly attack the *ipso* position of the aromatic moiety triggering a cascade process with the formation of a strained spirocyclic **109-II**, followed by subsequent C-S and final S-N bond cleavage providing SO$_2$ extrusion.[199] Quenching of the delivered NCR **110-I**, typically by HAT, furnishes the final product **110** (Scheme 4.4).
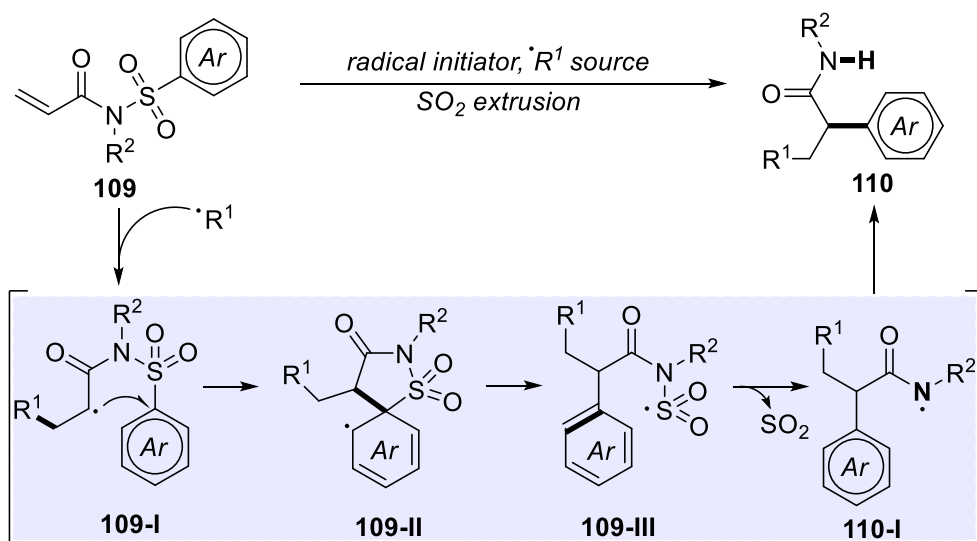
Scheme 4.4 Generalized mechanism of radical Smiles rearrangement (focus on seminal examples concerning sulfonylamides substrates **109**)

4.1.2.1 Photoinduced Smiles Rearrangement

The radical Smiles rearrangement is classified as an aryl migration reaction and the protocols developed have been extensively reviewed as part of this larger class of transformation,[200] or as a specific topic.[193,194] Recently, Stephenson and co-workers gathered all the examples of aryltransfer strategies mediated by photoredox catalysis.[201] To the aim of this chapter introduction, given the importance of arylsulfonyl moiety for this dissertation,

[199] Khartabil, H.; Doudet, L.; Allart-Simon, I.; Ponce-Vargas, M.; Gérard, S.; Hénon, E. *Org. Biomol. Chem.* **2020,** *18*, 6840-6848.
[200] Chen, Z.-M.; Zhang, X.-M.; Tu, Y.-Q. *Chem. Soc. Rev.* **2015,** *44*, 5220-5245.
[201] Allen, A. R.; Noten, E. A.; Stephenson, C. R. J. *Chem. Rev.* **2022,** *122*, 2695-2751.

transformations classified by the authors as aryl transfer from S to C[201] are described.
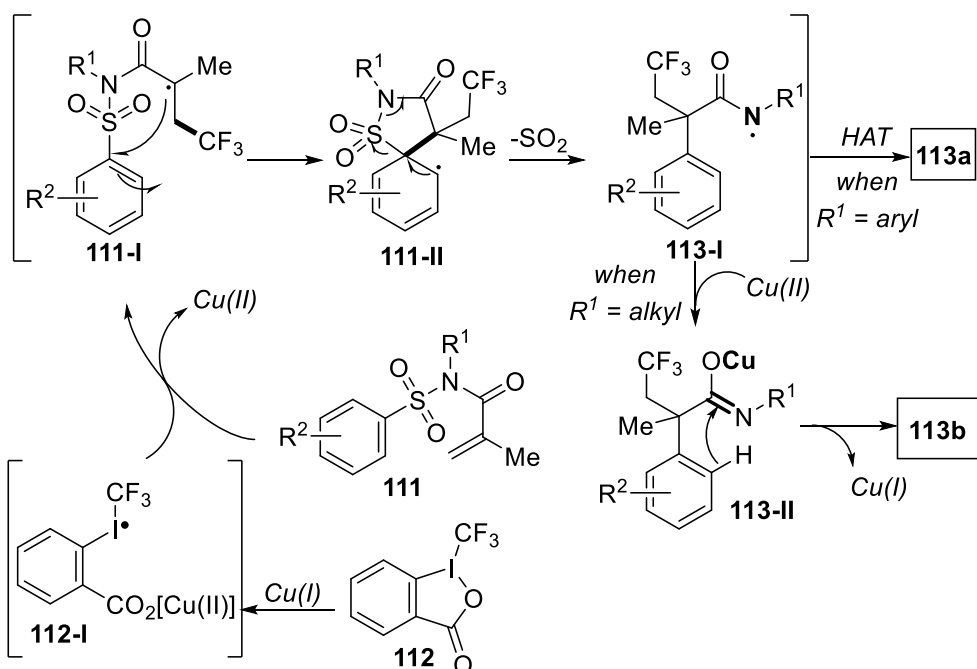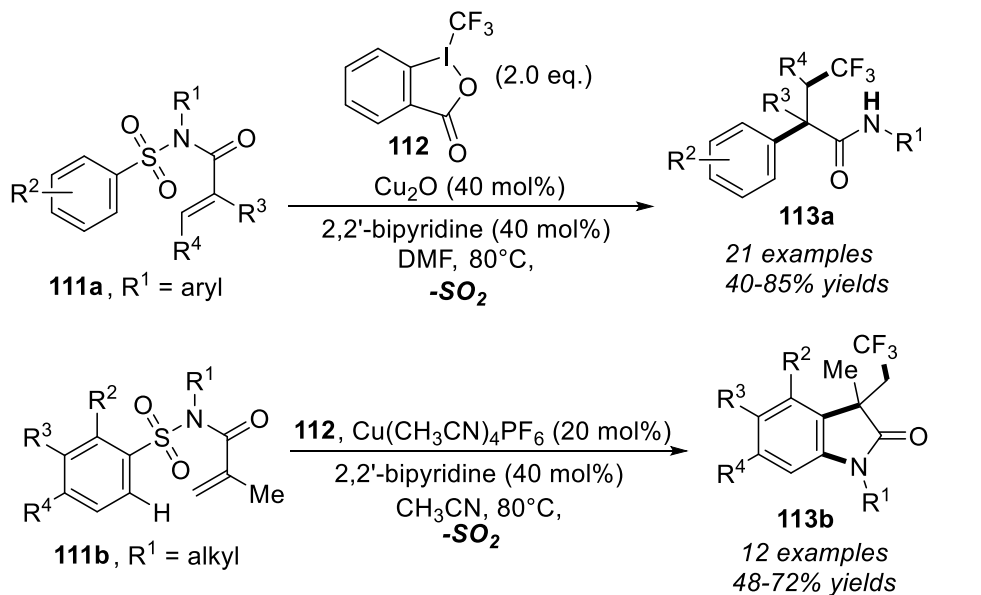
Scheme 4.5 Nevado's seminal work on thermal radical Smiles Rearrangement of arylsulfonamides **111**

A focus is dedicated to those transformations initiated by a NCR that triggers the formation of a C centered radical radical species (*via* addition to an unsaturated moiety) which ultimately acts as radical initiator of the Smiles rearrangement.

However, albeit not photoredox catalyzed, it is unavoidable to remark the importance of seminal work concerning aryl transfer from S to C by Nevado in 2013.[198] In this paper the authors described a cascade process triggered by the conjugate addition of a trifluoromethyl radical (generated by the combined use of a copper catalyst and Togni's reagent **112**) to a *N*-arylsulfonyl acrylamide **111**. As reported by the author, the copper catalyst seems to activate Togni's reagent **112**, generating a highly reactive CF_3-Cu^{II} containing radical **112-I** which interacts with the starting material, the activated alkene **111**, to give a new $C(sp^3)-CF_3$ providing the alkyl radical intermediate **111-I** that initiates the rearrangement. The Giese-type alkyl radical **111-I** performs radical Smiles rearrangement resulting in a formal 1,4-aryl transfer upon SO_2 extrusion delivering either trifluoromethylated oxindoles **113b** or amides **113a** (Scheme 4.5). This aryl transfer from S to C proved its efficacy in the construction of complex molecular architecture from simple substrates and inspired other researcher to define other protocols involving different radical precursors or radical generation strategies.

Indeed, two years later, Yang, Xia, and co-workers developed an analogous transformation under photoredox conditions employing trifluoromethanesulfonyl chloride in the presence of photoexcited $Ru(bpy)_3Cl_2$ to access the trifluoromethyl radical undergoing the same conjugate addition to acrylamides **111.** The result was the conversion of **111 to** oxindoles **113bc** or amides **113ac** upon 1,4-aryl migration and loss of SO_2.[202] This protocol enshrined the employment of photoredox catalysis to perform radical smiles rearrangements. Stephenson's research group in 2015,[203] followed by Wan and Zhang's research group in 2016,[204] adapted this concept to intramolecular reactivity with alkyl radicals (generated upon C-Br homolysis under photoredox conditions) able to trigger a Smiles rearrangement to delivering 2,2-difluoroarylethanols **115** from bromodifluoroethyl sulfonate

---

[202] Zheng, L.; Yang, C.; Xu, Z.; Gao, F.; Xia, W. *J. Org. Chem.* **2015,** *80*, 5730-5736.
[203] Douglas, J. J.; Albright, H.; Sevrin, M. J.; Cole, K. P.; Stephenson, C. R. J. *Angew. Chem. Int. Ed.* **2015,** *54*, 14898-14902.
[204] Li, Y.; Hu, B.; Dong, W.; Xie, X.; Wan, J.; Zhang, Z. *J. Org. Chem.* **2016,** *81*, 7036-7041.

esters **114** and *N*-aryl-2-arylacetamides **117** from *N*-arylsulfonyl 2-bromoacetamides **116** respectively (Scheme 4.6).
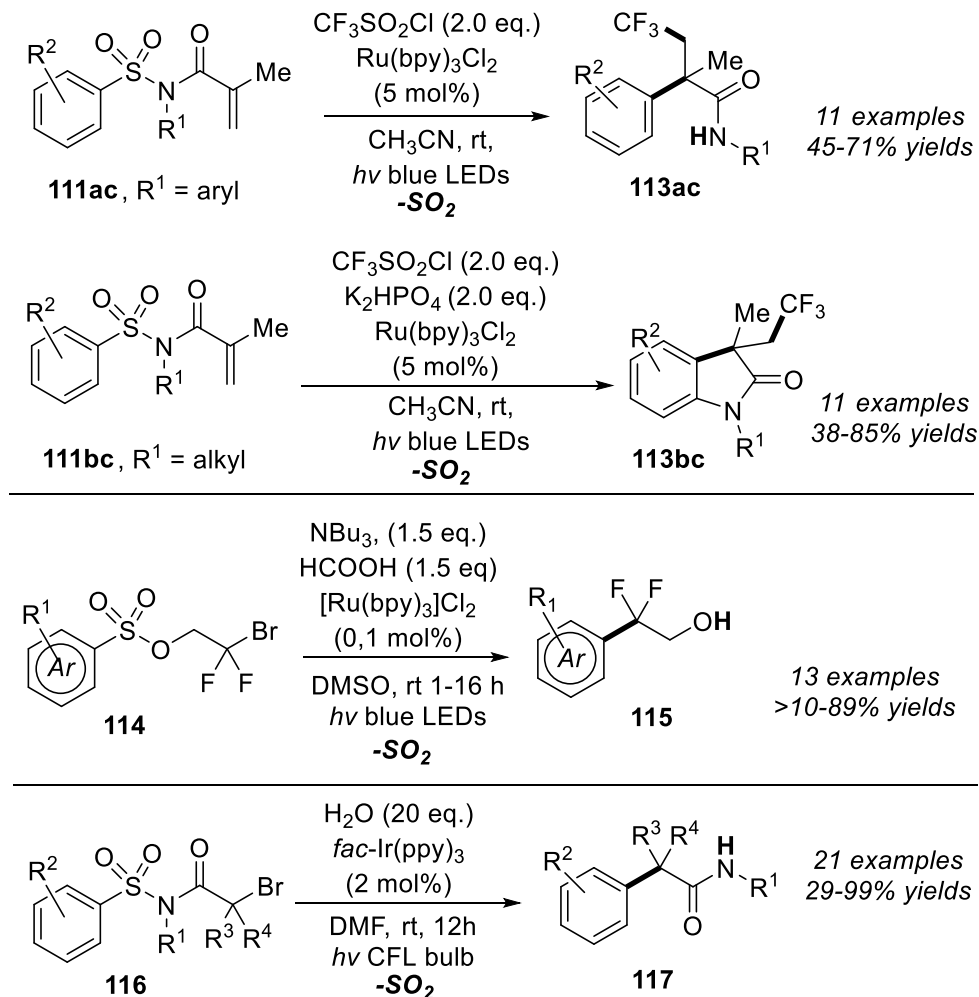
Scheme 4.6 Examples of photoredox induced radical Smiles rearrangement resulting in aryl transfer from S to C.

In 2016 a crucial paper to the aim of this introduction was published by Brachet and Belmont's group reporting an aryl transfer from S to C initiated by the generation of a hydrazonyl radical.[205] In this case, β,γ unsaturated *N*-arylsulfonylhydrazones **118** were employed, however, the unsaturated moiety was a terminal alkyne.

---

[205] Brachet, E.; Marzo, L.; Selkti, M.; König, B.; Belmont, P. *Chem. Sci.* **2016**, *7*, 5002-5006.
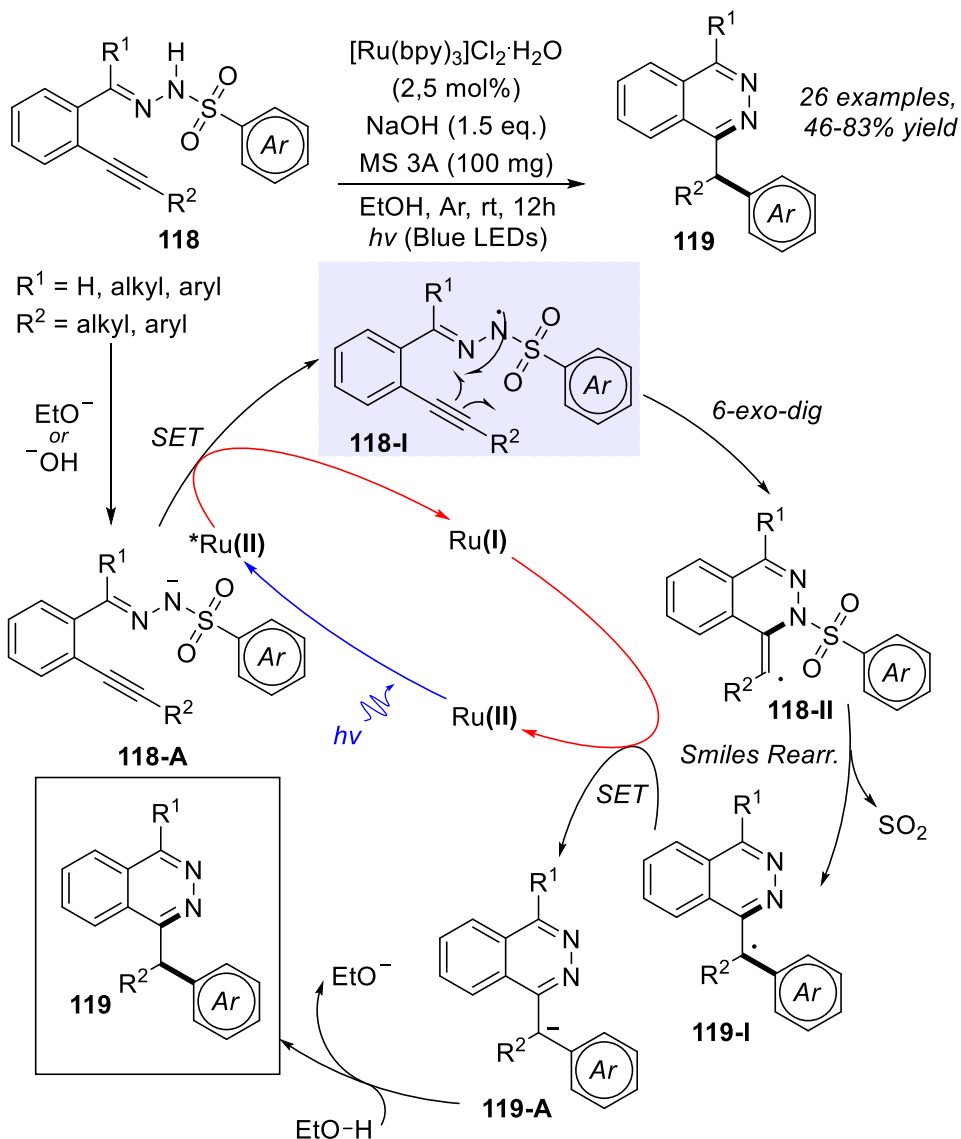
Scheme 4.7 Sequential intramolecular *6-Exo-dig* cyclization and radical Smiles rearrangement triggered by the formation of a hydrazonyl NCR **118-I**.

The hydrazonyl NCR **118-I** was generated upon ODET mechanism, and attack to the unsaturated portion resulted in *6-exo-dig* cyclization with the formation of a vinyl radical **118-II** that promoted the Smiles rearrangement. The alkyl radical **119-I** obtained is reduced to the corresponding anion **119-A** in the turnover step of the oxidative quenching cycle of the PC and it is finally protonated by the alcohol solvent to yield phthalazine **119**. This

method tolerates a good selection of aryl or heteroaryl migrating groups and would even allow the formation of a carbon stereocenter (Scheme 4.7).

Recently, the same research group demonstrated the versatility of such methodology reporting the first radical "phospho"-Smiles-Truce rearrangement, utilizing a migration from the C_{Ar}–P bond of an arylphosphonohydrazone **120**.[206] The mechanism is identical with C–N/C–C bond-forming cascade providing benzohydrylphthalazines **119**, however the phenylphosphinoxi moiety acts as the leaving group in this case and the ethanolysis of the P–N bond is required to obtain the product **119**, since a simple extrusion of a neutral molecule like sulfur dioxide is not possible (Scheme 4.8).
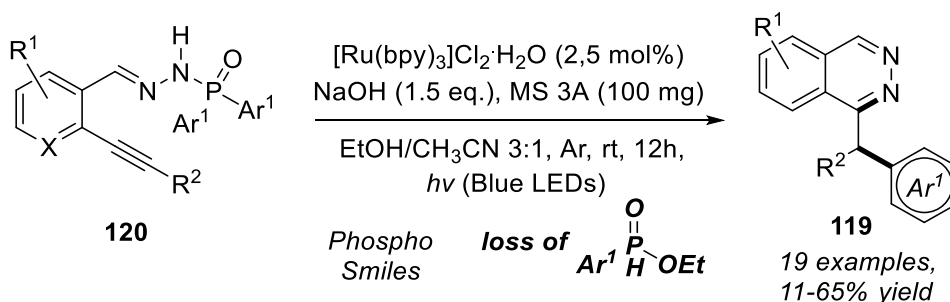
Scheme 4.8 Photoinduced "phospho"-Smiles rearrangement, utilizing a migration from the C_{Ar}–P bond of an arylphosphonohydrazone **120**

To conclude, the photoinduced Smiles Rearrangement is becoming a more and more appealing strategy for the synthesis of high complex molecular scaffold, in particular since 2021 and thanks to the groundbreaking discovery of Nevado's research group.[207] The authors unveiled an asymmetric variation of this visible light induced transformation (Scheme 4.9). This paper highlines once again the complementarity of photoredox catalysis to the common thermal chemistry. First, it allows the synthesis of all-carbon quaternary stereocenter with Smiles rearrangement. Second, the developed photoredox and radical pathways allowed disclosure of a new mechanistic paradigm. Indeed, according to the calculation of the authors, the rearrangement occurs *via* a spirocyclic transition state, whereas the expected radical intermediate

[206] De Abreu, M.; Belmont, P.; Brachet, E. *J. Org. Chem.* **2021,** *86*, 3758-3767.
[207] Hervieu, C.; Kirillova, M. S.; Suárez, T.; Müller, M.; Merino, E.; Nevado, C. *Nat. Chem.* **2021,** *13*, 327-334.

corresponding to the classical Meisenheimer intermediate of polar reactions was never localized along the potential energy surface of the reaction.[207,208]
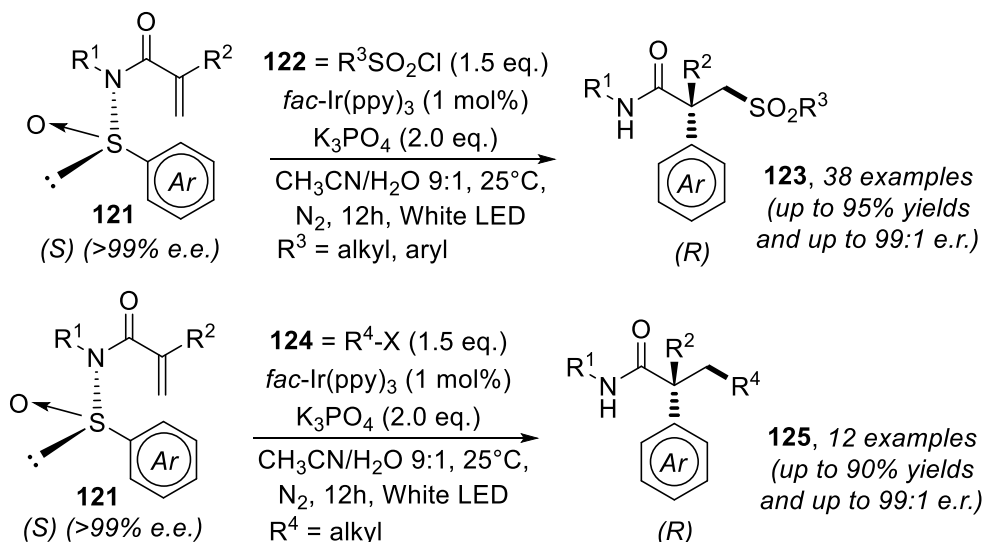
Scheme 4.9 Asymmetric, visible light-mediated radical sulfinyl-Smiles rearrangement providing access to all-carbon quaternary stereocenters

4.2 Photoinduced synthesis of "monocyclic" tetrahydropyridazines from γ,δ-unsaturated *N*-arylsulfonylhydrazones

4.2.1 Objectives and general considerations

Once identified the radical **100-I** as the protagonist of the reactivity disclosed in the previous chapter, we started reconsidering our synthetic approach to tetrahydropyridazines. Indeed, we persisted in our efforts to deliver the tetrahydropyridazine scaffold under photoredox conditions, this time as a single heterocycle instead of embedded in a tricyclic structure.

Two alternatives were considered to direct the reactivity towards such desired outcome, and both relied on substrate tailoring to alter the reactivity

---

[208] Lennox, A. J. J. *Angew. Chem. Int. Ed.* **2018,** *57*, 14686-14688.

of the intermediate **100-I** (obtained after the first *6-exo-trig* cyclization and C-N bond formation).

First, to prevent the carbon radical **100-I** attack to the aromatic moiety molecule, we envisaged that an *ortho*-substituted arene moiety of the hydrazone might serve the purpose. The position occupied by a substituent should impede the carbon radical attack leading to aromatization, directing the fate of the carbon intermediate **100-I** towards HAT instead. Commercially available 2,4,6-trimethylbenzenesulfonohydrazide (or Mesitylene-2-sulfonylhydrazide, Mes = 2,4,6-Trimethylbenzene) could be employed to replace tosylhydrazide or benzenesulfonohydrazide. Second, we figured that the stability of the intermediate **100-I** could be enhanced, instead of preventing the radical attack with modification on the arene moiety. If such stability enhancement was enough to disadvantage the radical addition to the arene, a radical termination *via* HAT would be favored (Scheme 4.10).
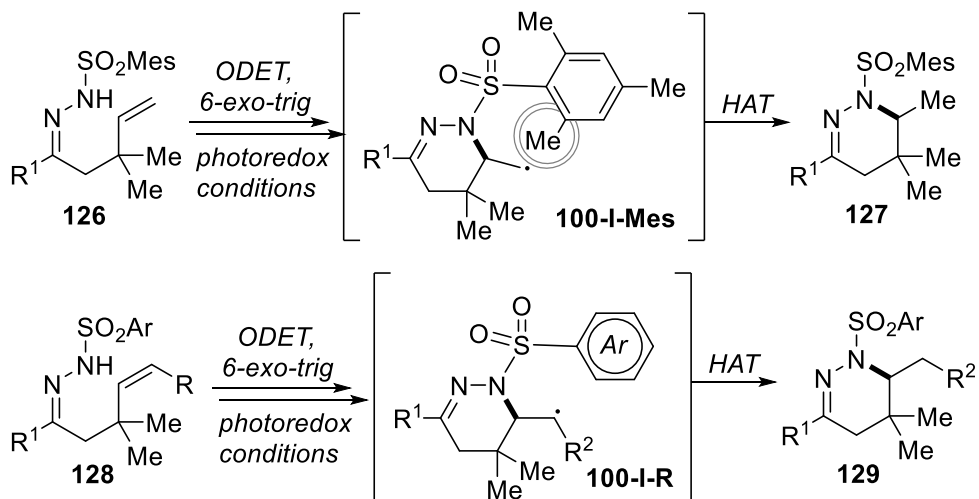
Scheme 4.10 Hypothesis on the photoredox reactivity of γ,δ unsaturated *N*-arylsulfonylhydrazones to achieve "monocyclic" tetrahydropyridazine scaffold **127** and **129** as outcome

Nevertheless, both these strategies implied the stabilization of the carbon radical intermediate **100-I** that might contribute to set the ideal condition for a Smiles Rearrangement as observed by Brachet and Belmont's group (Scheme 4.7).[205] Indeed, if the carbon radical intermediate **100-I-SR** is characterized by a stability similar to that of the vinyl radical hypothesized by Brachet and Belmont (intermediate **118-II**, Scheme 4.7), the Smiles

rearrangement becomes a desired pathway, yielding a tetrahydropyridazine **131** with a free N-H functionality **131** (Scheme 4.11).
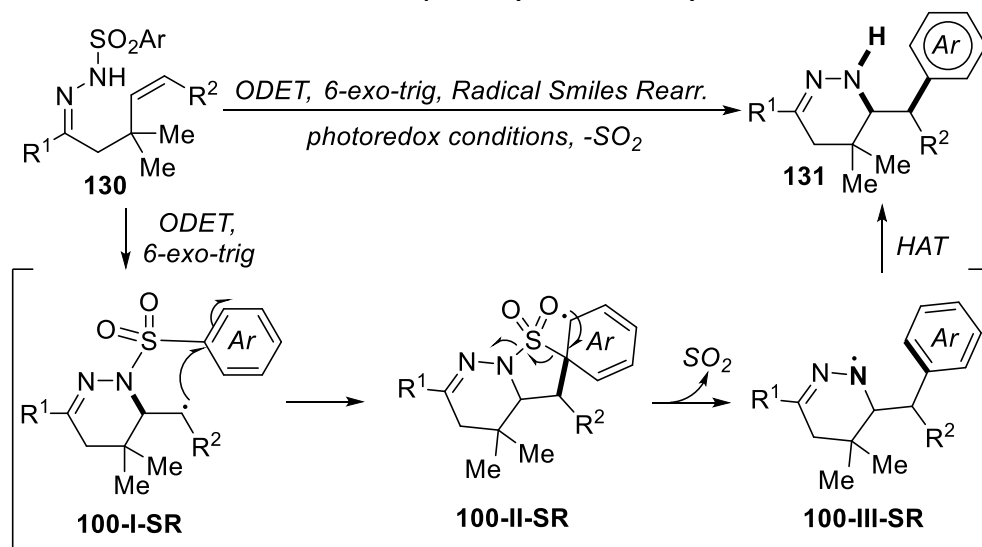
Scheme 4.11 Expected outcome of a photoredox mediated radical Smiles rearrangement of γ,δ unsaturated *N*-arylsulfonylhydrazones

As remarked in the previous chapter, our study on photoredox reactivity of γ,δ-unsaturated *N*-arylsulfonylhydrazones was driven not only by the appealing synthetic targets achievable, but also by a strong pulse in accomplishing a generalized study on the reactivity. With this goal in mind, we progressed in the experimental and computational investigation that characterize this chapter.

4.2.2 Generalization

To synthetize hydrazones **132** with an *ortho* hampered arene moiety (mesitylsulfonyl hydrazones), we recovered the β-Hindered γ,δ-unsaturated ketones **89a**, **89b**, **89f**, **89g**, **89i** and **89l**) synthetized as depicted in the previous chapter (Scheme 3.13 and Chapter 6, experimental procedures, for labeling) and we reacted them with mesitylsulfonyl hydrazide (Table 4.1).

Concerning the synthesis of precursors that would stabilize the carbon radical intermediate, we focused on internal alkenes, following the same route used for β-Hindered γ,δ-unsaturated ketones **89** (Scheme 3.13), but employing propenylmagnesium bromide **93b** to convert **92** into the β-hindered γ,δ-unsaturated ketones with a substituent on the terminal carbon of the alkene.

Alkenes **89j-k** were then reacted both with tosylhydrazide and with mesitylsulfonylhydrazide to obtain the corresponding hydrazones **133a-c**. (Scheme 4.12).

Table 4.1 List of *N*-mesitylsulfonylhydrazones **132** synthesized

	132a	**132b**	**132c**	**132d**	**132e**	**132f**
R	Ph	2-Naphth	*p*-Tol	*o*-Tol	Me	
	from **89a**	from **89b**	from **89f**	from **89g**	from **89i**	**89l** = (from *pulegone*)
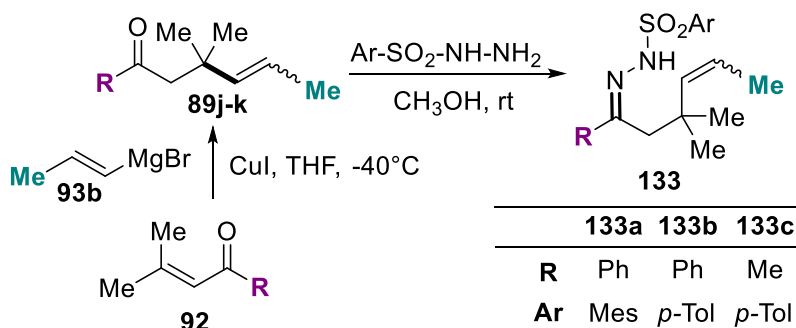
Scheme 4.12 The synthesis of *N*-mesitylsulfonylhydrazones **133a-c** (Mes=2,4,6-trimethylphenyl)

Once accomplished the synthesis of arylsulfonylhydrazones **132a-g** and **133a-c**, we tested their reactivity to verify our hypothesis on the chemoselectivity dictated by substrate tailoring. We started reacting the mesitylsulfonylhydrazones **132** in the optimized condition for the dearomatization reaction (Table 3.3, entry 10) and a completely different outcome was observed (Table 4.2). As anticipated, the hydroamination product **134** derived from the *6-exo-trig* cyclization of the *N*-hydrazonyl radical (where the *ortho* substituent prevented the second cyclization) was observed. However, together with this latter, a second carboamination

product derived from a photoredox promoted Smiles rearrangement **135** was also observed. Best yields were reported with 2,2-dimethylbut-3-enylphenylmesitylsulfonylhydrazone **132a** and 2,2-dimethylbut-3-enylmethylmesitylsulfonylhydrazone **132e** with a yield of 95% and a ratio of 53:47 and 61:39 between products **134a/135a** and **134a/135a**, respectively. This confirmed once again no significant difference between aromatic and aliphatic derivatives for such transformations of hydrazones (Table 4.2). Other aromatic substituents were also evaluated: the 2-naphthyl substrate **132b** afforded **134b/135b** with a yield of 72% with a ratio of 58:42.

Even for this reactivity tolyl derivative were tested to determine steric hindrance effect, and *ortho*-tolyl derivative **132d** (62% yield for **134d/135d**, ratio 69:31) decreased the efficiency of the process compared to *para*-substituted **132c** (87% yield for **134e/135e**, ratio 61:39). Finally, access to the hydrocinnoline scaffold was gauged when hydrazone **132f,** derived from Pulegone **96,** was subjected to irradiation. Only product **134f** was recovered in 35% yield, while the corresponding Smiles rearrangement was observed in traces (Table 4.2). We imputed such observation to the rigidity determined by the two fused six membered cycles (almost completely saturated), one from the pulegone scaffold and the other derived from the radical cyclization. Such hampered structure would prevent an easy attack of the alkyl radical to the aromatic moiety impeding the Smiles rearrangement.

To complete this general study of reactivity, we assessed the effect of an internal double bond in the reactivity of hydrazones under these photoredox conditions. *N*-arylsulfonylhydrazones **133** were reacted in the same conditions used for *N*-mesitylsulfonylhydrazone **132** and, to our delight, this modification of the starting material directed the reactivity towards a single product (Table 4.3).

In all cases, regardless of the arylsulfonyl moiety (whether tosyl or mesitylsulfonyl), only the Smiles rearrangement product was recovered. Moreover, no substantial difference was dictated by the arene substituents since both mesitylsulfonyl hydrazone **133a** and the corresponding tosyl derivatives **133b** yielded products **136a** and **136b** in 72% yield (Table 4.3). Besides, once again difference among aliphatic and aromatic substituents in the tosylhydrazones were neglectable (72% for phenyl product **136b** *versus* 70% for aliphatic **136c**, Table 4.3).

Table 4.2 Scope of the synthesis of **134a-f** and **135a-e**.

Reaction scheme: **132** (*c*) with Ru(bpy)₃Cl₂·6H₂O (3 mol%), K₂CO₃ (1.5 eq.), CH₃CN [0.06 M], N₂, rt, 16 h, *hv* (40W Blue LED) → **134** (a,b,c) + **135** (a,b,c)

Starting material **132** shows R¹ group, SO₂Mes, NH, N hydrazone, vinyl, Me, Me substituents.

Products:
- **134a** / **135a** : 53/47; 95%
- **134b** / **135b** : 58/42; 72%
- **134c** / **135c** : 71/29; 87%
- **134d** / **135d** : 69/31; 62%

R¹ = aliphatic substituent

- **134e** / **135e** : 61/39; 95%
- **134f**, 35%
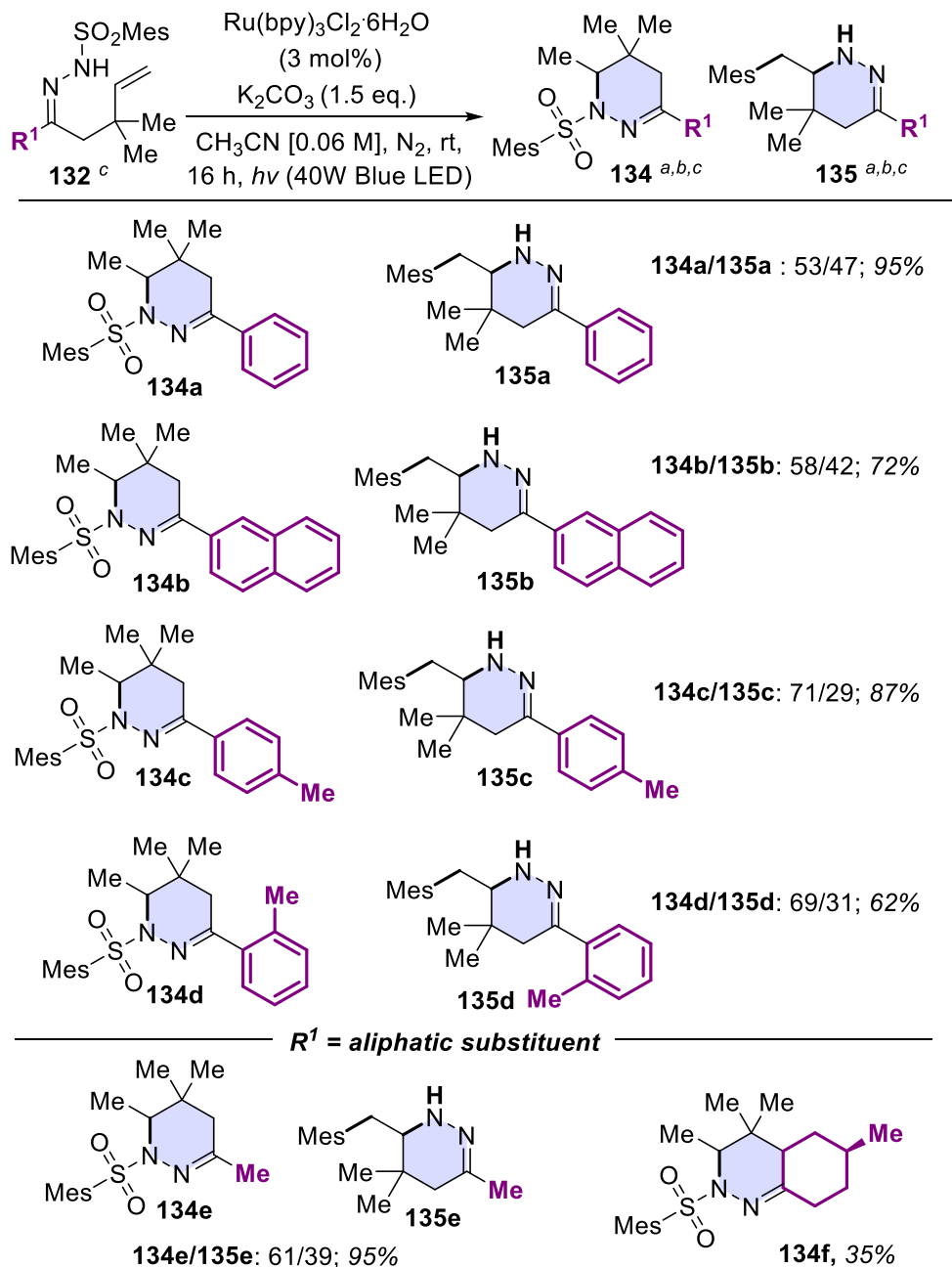
a) Reaction conditions: *N*-mesitylsulfonylhydrazone **132** 0.3 mmol, K₂CO₃ 0.45 mmol, anhydrous CH₃CN 5 mL, [Ru(bpy)₃]Cl₂·6H2O 0.09 mmol, 40W blue lamp, 16 h, inert atm; *b)* Yields determined on isolated product; *c)* Mes=2,4,6-trimethylphenyl

Table 4.3 Scope of the synthesis of **136**.
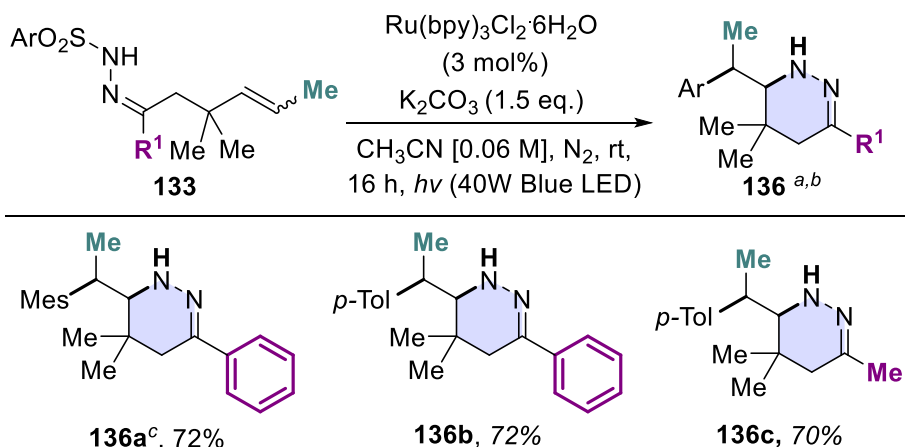
a) Reaction conditions: N-arylsulfonylhydrazone **133** 0.3 mmol, K$_2$CO$_3$ 0.45 mmol, anhydrous CH$_3$CN 5 mL, [Ru(bpy)$_3$]Cl$_2$·6H$_2$O 0.09 mmol, 40W blue lamp, 16 h, inert atm; *b)* Yields determined on isolated product; *c)* Mes=2,4,6-trimethylphenyl

To conclude, for products **134a-f**, **135a-e**, and **136a-c**, only one diastereoisomer was recovered. As described in detail in the next paragraph, concerning mechanistic investigation, the employment of a substituted olefin like substrate **133** and its subsequent effect on the stabilization of the alkyl radical imposed the chemoselectivity of the transformation towards a single pathway: the Smiles rearrangement. Indeed, two months after the publication of our paper with the results reported in chapter 3 and 4 of this dissertation, Liu's group[209] reported exactly the same transformation, using various γ,δ unsaturated *N*-arylsulfonylhydrazones with two geminal alkyl substituents on the δ carbon of the unsaturated moiety, observing only the Smiles rearrangement product yielding 1,4,5,6-tetrahydropyridazines. Besides, Stephenson's research group also accomplished a similar discovery, following a similar extension of their work concerning the dearomatization of *N*-tosyl-4,5-unsaturated amides under photoredox conditions.[184] Indeed the authors reported (in may 2022) a photoredox-induced aminoarylation of *N*-arylsulfonyl-4,5-unsaturated amide**s** *via* Smiles-Truce rearrangement following cyclization.[210]

[209] Tu, J.-L.; Tang, W.; Liu, F. *Org. Chem. Front.* **2021,** *8*, 3712-3717.
[210] Noten, E. A.; McAtee, R. C.; Stephenson, C. R. J. *Chem. Sci.* **2022**.

4.2.3 Proposed Mechanism

Our final aim being providing a general study of the reactivity of γ,δ-unsaturated *N*-arylsulfonylhydrazones, a comprehensive explanation for the three different reactive pathways originating from the hydrazonyl NCR was needed. The experiments performed in chapter 3 (CVs, Fluorescence Quenching, Stern-Volmer Plot, Radical Trapping) proved the photoredox initial trigger, the radical nature of the process and the centrality of the carbon radical **100-I**. However, to provide elucidation on the different fates of such radical intermediate species determining three different outcomes (dearomatization *via* two consecutive *6-exo-trig* cyclization, single *6-exo-trig* cyclization, Smiles rearrangement following *6-exo-trig* cyclization) also a computational analysis was contrived. A collaboration with professor G. Ghigo of the Department of Chemistry of Turin was established, and the main results of the computational studies that allowed mechanism rationalization are reported (the detailed discussion of computational methods and results is not part of this dissertation since it was accomplished by Dr. G. Ghigo). The computational DFT studies analyzed the transformation of the species in CH_3CN and the energy values commented are Gibbs free energies at room temperature (ΔG, in kcal/mol). The computational DFT studies analyzed the transformation of the species in CH_3CN and the energy values commented are Gibbs free energies at room temperature (ΔG, in kcal/mol). The structures of reactants, intermediate adducts, and transition states were optimized using the density functional method (DFT), with the functional M06-2X and the basis sets 6-311+G(d,p) for H, C, N, and O atoms and 6-311+G(2df) for S atoms. Solvent effects of CH_3CN were introduced in all calculations using the universal solvation model density method (SMD).

Calculations analyzed the reaction pathway of three species: *N*-tosylhydrazone **94i**, *N*-mesitylsulfonylhydrazone **132e**, *N*-tosylhydrazone of internal alkene **133c**. As stated in the previous chapter, mechanism starts with ODET process and the generation of the hydrazonyl NCR. Subsequent intramolecular attack provides cyclization delivering the radical **100-I**. Computation analysis confirmed these observations, clarifying that this latest step occurs through several conformations of TSA. However, all of them eventually yield the same number of radical intermediates **100-I.** For the three hydrazones, the lowest activation energies concerning the formation of the corresponding radical **100-I** are similar, moreover, since the *6-exo-trig* cyclization is monomolecular, the Eyring equation can be applied to furnish

an estimation of the rate constants of cycle formation. Thus, we confirmed that the fast formation of radicals **100-I** is irreversible, being exoergic in all cases (Table 4.4).

Table 4.4 Calculated values for radical *6-exo-trig* cyclization of γ,δ-unsaturated-*N*-arylsulfonylhydrazones (calculation by Dr. G. Ghigo).

	94i	132e	133c
Ar	*p*-Tol	Mes	*p*-Tol
R′	H	H	Me
$\Delta G^{\ddagger}_{TS\text{-}A}$	10.8 kcal/mol	12.2 kcal/mol	9.2 kcal/mol
$k_{TS\text{-}A}$	2×10^5 s^{-1}	1×10^4 s^{-1}	1×10^6 s^{-1}
ΔG_{reac}	−9.7 kcal/mol	−7.6 kcal/mol	−11.1 kcal/mol

From radical **100-I** three possible pathways generates:

i) The hydrogen atom transfer (HAT) from the solvent CH$_3$CN generating products **134**;

i) the intramolecular attack of the radical centers to the *ortho* (with respect to the sulfur) position of the arene moiety yielding, after the HAT, from CH$_3$CN, dearomatization products **95**;

iii) the intramolecular attack of the primary radical centers to the *ipso* positions of the aromatic triggering a radical Smiles rearrangement and followed by the final HAT from the solvent, yielding products **135** or **136**.

This generalized mechanism, based both on experimental evidence gathered in Chapter 3 and 4 and on computational findings described below is summarized in Scheme 4.13.
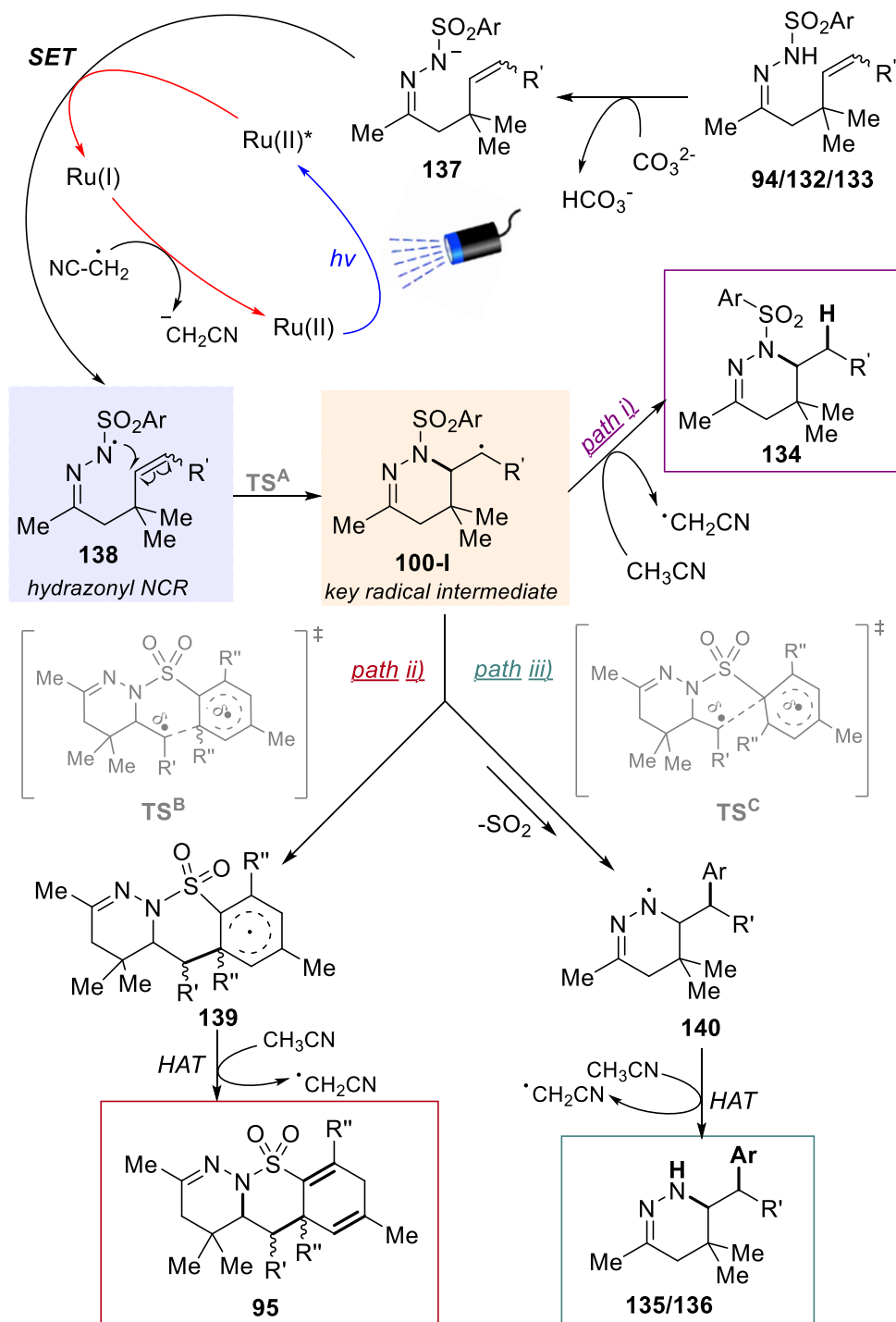
Scheme 4.13 General reaction mechanism for the synthesis of tetrahydropyridazines from γ,δ-unsaturated-*N*-arylsulfonylhydrazones

First, the investigation was focused on how the arene moiety of the arylsulfonylhydrazones might affect the choice between the two different monomolecular pathways *ii* and *iii* (Scheme 4.13). The pathway *ii* (Scheme 4.13), passing through TS^B, is required to overcome a barrier (values calculated for this barrier for the three species is indicated as **ΔG‡$_{TS-B}$**, Table 4.5) as well as pathway *iii* (Scheme 4.13), passing through TS^C (**ΔG‡$_{TS-C}$**, Table 4.5).

Table 4.5 Calculated values for radical monomolecular reactions (pathway *ii* and *iii*) of carbon radical **100-I** (calculation by Dr. G. Ghigo).

	94i	132e	133c
Ar	*p*-Tol	Mes	*p*-Tol
R'	H	H	Me
ΔG‡$_{TS-B}$	**14.4 kcal/mol**	17.1 kcal/mol	17.2 kcal/mol
ΔG‡$_{TS-C}$	16.0 kcal/mol	**14.7 kcal/mol**	15.8 kcal/mol
$k$$_{TS-B}$	$4×10^2$ s^{-1}	3 s^{-1}	5 s^{-1}
$k$$_{TS-C}$	$2×10^1$ s^{-1}	$2×10^2$ s^{-1}	$3×10^1$ s^{-1}
$k$$_{HAT-CH3CN}$:$1×10^2$ s^{-1}			

Tosyl derivative **94i** has the lowest activation barrier towards the tricyclic products (**ΔG‡$_{TS-B}$**= 14.4 kcal mol^{-1}, Table 4.5), whereas its counterpart with a not terminal olefin **133c** is characterized by a barrier towards dearomatization (**ΔG‡** = 17.2 kcal mol^{-1}, Table 4.5), that is as high as the one for the *ortho* hindered mesitylsulfonylhydrazones **132e** (**ΔG‡$_{TS-B}$**= 17.1 kcal mol^{-1}, Table 4.5). Concerning this latter, intramolecular attack of the

primary radical centers **100-I** to the *ortho* positions of the aromatics (TS^B) is more difficult than that in the tolyl derivatives presumably due the steric hindrance of the *ortho* methyl groups.

By contrast, when the attack to the *ipso* positions is considered for all the three species, the same methyl groups in the mesityl derivatives **132e** concur to stabilize the incipient delocalized aromatic radicals formed in TS^C, which, in fact, presents the lowest barrier (**ΔG$^‡_{TS-C}$**= 14.7 kcal mol^{-1}, Table 4.5). These results are qualitatively applicable to all the experimental observations with the terminal γ,δ-unsaturated hydrazones. In fact, computational determinations of the ΔG$^‡_{TS}$ confirmed that the choice between pathways *ii* and *iii* (Scheme 4.13) is uniquely due to the nature of the arene moiety. Thus, Ar can be both a phenyl (*N*-phenylsulfonylhydrazones) or a tolyl (*N*-tosylhydrazones), but the lack of the *para*-methyl does not change the preferential choice towards pathways *ii* and all tosylhydrazones **94a-i** and **94l** follow the same pathway as phenylsulfonylhydrazones **94j-k** yielding **95a-l**. The presence of an aryl or alkyl group linked to C=N is also irrelevant for reactivity. Further confirmation of such experimental evidence is provided by the analysis of the rate constant for the two monomolecular processes (Table 4.5). For the tosyl derivative **94i**, the attack to the *ortho* positions (TS^B) is favored. Accordingly, the rate constant k_{TS-B} that was estimated by the Eyring equation is 4×10^2 s^{-1} (whereas the same constant for an *ipso* attack i k_{TS-C} =2×10^1 s^{-1}, Table 4.5). For the mesitylsulfonyl derivative **132e** instead, the attack to the *ipso* positions is favored given the rate constant k_{TS-C}=2×10^2 s^{-1} (compared to the value k_{TS-B}=3 s^{-1}, Table 4.5, for attack to the *ortho* positions).

Process *i* is a radical termination by HAT, hence is bimolecular in nature and involves a molecule taken from the solvent, while pathways *ii* and *iii* are monomolecular (Scheme 4.13). Therefore, the rate constant calculated for bimolecular pathway *i* cannot be confidentially compared with those calculated for the other two pathways to establish or rationalize the chemoselectivity. However, since the rate constant for the HAT of triplet benzophenone with CH$_3$CN has been measured,[211] (value reported as k_{HAT-CH_3CN}=1×10^2 s^{-1}), it can cautiously be used as an indication for a comparison with the two other monomolecular pathways reported in detail in Table 4.5. Indeed, the reaction constant k_{TS-B}=4×10^2 s^{-1} for the formation of product

---

[211] Naguib, Y. M. A.; Steel, C.; Cohen, S. G.; Young, M. A. *J. Phys. Chem.* **1987,** *91*, 3033-3036.

95 (*i.e.*, **95i**) from **94i** is twice the one calculated for the theoretical formation of product **135** (*i.e.*, **135e**) from **132e** that is in a semiquantitative agreement with the experimental finding. For tosylderivatives **94** the dearomatized product **95** is the unique product given the high rate of *ortho* attack. Mesitylsulfonyl derivative **132e**, instead, characterized by rate constants for HAT and for *ortho* attacks that are lower and are also comparable in values, evolves towards the generation of the radical smiles rearrangement product **135** (*i.e.* **135e** 29%, for $k_{TS-C}=2\times10^2$ s^{-1}, Table 4.5). along with the HAT product **134** from path *i* (*i.e.,* **134e** 58%).

Finally, the effect of the olefin on the reaction outcome was evaluated. For the tosyl derivatives, when the γ,δ-unsaturated hydrazone contains an internal double bond (*i.e* **133c**) instead of a terminal one (*i.e* **94i**), the main product is uniquely a Smiles rearrangement product **136c** (pathway *iii*). Such transformation is favored over the second cyclization (pathway *ii* yielding **95**) by almost 2 kcal/mol (**ΔG‡$_{TS-C}$**=15.8 kcal/mol *vs* **ΔG‡$_{TS-B}$**=17.2 kcal/mol, Table 4.5). Therefore, the competition seems to occur only between pathways *i* (the HAT yielding **134**) and *iii*.

As discussed above, this implies comparison between rate constants calculated for mono- and bimolecular processes that should be avoided. However, the rate constant of the same process of HAT for different radicals might be evaluated. Calculated **k$_{HAT}$** reported in Table 4.6 are derived as if all the radicals **100-I** originated from the corresponding three hydrazones **94i**, **132e**, **133c** and terminating their reaction with the bimolecular process *i* (HAT from CH$_3$CN).

Table 4.6 Calculated constant rate values for HAT from CH$_3$CN (pathway *i*) to radical **100-I** generated from the corresponding γ,δ-unsaturated-*N*-arylsulfonylhydrazones **94i, 132e**, **133c** (calculation by Dr. G. Ghigo).

	94i	132e	133c
Ar	*p*-Tol	Mes	*p*-Tol
R'	H	H	Me
k$_{HAT}$	1.9x10^2 s^{-1}	7.5x10^{2}s^{-1}	**2.6x10^{-1} s^{-1}**

For terminal alkenes **94i** and **132e**, k_{HAT} are in the order of 10^2 s^{-1}, while that for the more stable secondary carbon radical **100-I** generated from a not terminal alkene **133c** is dramatically lower (k_{HAT}=2.6x10^{-1} s^{-1}, Table 4.6) thus motivating the preference for substrates **133** towards uniquely the pathway of Smiles rearrangement yielding **136**.

4.2.4 Conclusion

In this Chapter, we provided a generalization of the reactivity of β-hindered-γ,δ-unsaturated-*N*-arylsulfonylhydrazones under photoredox conditions.

Using the same catalytic system developed in Chapter 3, we demonstrated that with a wise tailoring of the substrate, two other different classes of tetrahydropyridazines (the hydroamination product of a single *6-exo-trig* cyclization and the carboamination product of a Smiles Rearrangement following initial *6-exo-trig* cyclization) can be obtained by intramolecular transformations. Experimental findings and computation calculations proved that modification of the starting material directly influenced the thermodynamics and stability of the key carbon radical **100-I** thus directing the chemoselectivity between the three photoredox transformation described in this chapter and in the previous one.

In our effort to perform a universal description of the reactivity of this peculiar class of hydrazones, we deduced that:

- *ortho* hindered arene moiety, like mesityl, prevent dearomatization, but both termination by HAT and termination by Smiles rearrangement occurs;
- an internal alkene moiety stabilizes the carbon radical intermediate following *6-exo-trig* cyclization; thus, the Smiles rearrangement becomes the preferred pathway, regardless of the arene moiety.
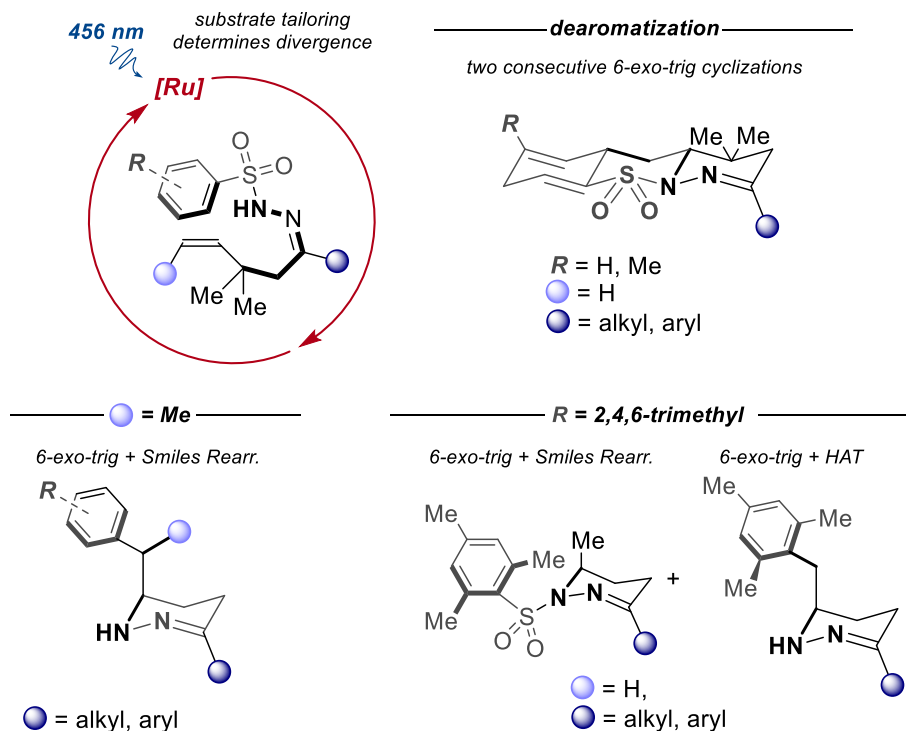
Scheme 4.14 Graphical Summary of Chapter 3 and 4

In summary, we outlined the unicity of γ,δ-unsaturated-*N*-arylsulfonylhydrazones as flexible platforms for photoredox mediated transformation. Using the same photocatalytic system, relying on Ru(bpy)$_3$Cl$_2$ as the PC, K$_2$CO$_3$ as the base, in CH$_3$CN as the solvent, and exploiting the formation a hydrazonyl NCR which always undergoes *6-exo-trig* cyclization, three different classes of biologically interesting tetrahydropyridazines were synthesized. These three products are 1,4-cyclohexadiene-fused tetrahydropyridazinylthiazines obtained by dearomatization, *N*-mesityltetrahydropyridazines obtained by HAT termination and functionalized tetrahydropyridazines with a new carbon stereocenter formed by Smiles rearrangement.

CHAPTER FIVE:
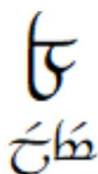
VISIBLE LIGHT PROMOTED DOMINO CYCLIZATION AND CHLOROVINYLATION OF LINEAR SULFONYLAMIDOALLENES

CHAPTER 5 VISIBLE LIGHT PROMOTED DOMINO CYCLIZATION AND CHLOROVINYLATION OF LINEAR SULFONYLAMIDOALLENES

5.1 Introduction

5.1.1 Pyrrolidines and Piperidines

As described in Chapter 2, saturated nitrogen heterocycles are relevant molecules with a leading role in pharmaceuticals witnessed by their percentage of FDA approvals. Among these alkaloids, those belonging to pyrrolidine and piperidine families (five- and six-membered aliphatic heterocycles containing a single nitrogen atom, Figure 5.1) are the most common. As all the other *N*-heterocycles, their added value relies on the peculiarity of the amine functionality for biological system and on the cyclic structure, which, combined both with sp^3-hybridization and non-planarity of this ring, directly relates to the enhanced possibility of exploration of the pharmacophore space due to the contained three-dimensional shape.[212,213]

The pyrrolidine **141** scaffold is characterized by biological versatility due to the chemical possibility of generating structural diversity and specific interactions. Indeed, given the odd number of atoms of the heterocycle, a single substituent placed on any of the four carbons of pyrrolidines mutates that atom into a stereogenic center. Thus, such compounds have proven their utility in contrasting cancer and microbial infections, as well as immune disorders, and against metabolic and neurodegenerative diseases. Similarly, the class of piperidines **142**, whose archetype is the molecule responsible for the spicy taste gives of black pepper, is the family of the 6-membered saturated cyclic amines and share a lot of biologically relevant features with pyrrolidines.

Moreover, this class of compound is ubiquitous in natural occurring alkaloids and corresponds to the most encountered heterocycle in pharmaceutical agents. The development of efficient protocols for the preparation of both pyrrolidines and piperidines is therefore essential.

---

[212] Li Petri, G.; Raimondi, M. V.; Spanò, V.; Holl, R.; Barraja, P.; Montalbano, A. *Top. Curr. Chem.* **2021,** *379*, 34.

[213] Vardanyan, R., *Piperidine-Based Drug Discovery*. Elsevier: **2017**.
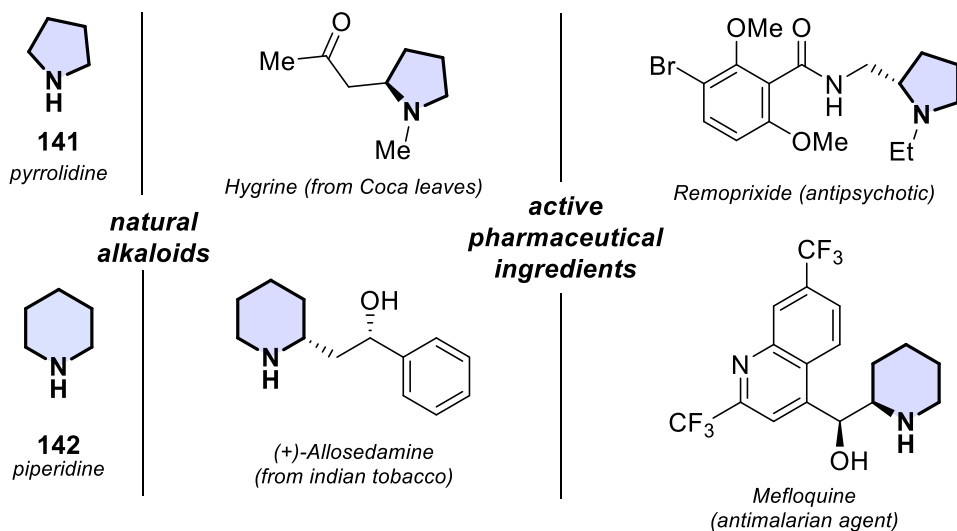
Figure 5.1 Pyrrolidine **141**, piperidine **142** and examples of biologically relevant molecules containing these scaffolds

5.1.1.1 Modification of saturated *N*-heterocycles

Modification of saturated heterocyclic molecules or synthesis of functionalized saturated heterocycle remains a major challenge in synthetic chemistry.[214,215] Strategies for the functionalization of their aromatic counterparts are widespread and work efficiently with tolerance of different functional groups with the main examples represented by cross coupling reactions. Similarly, exploiting the aromaticity as a strong driving force, protocol based on sequential condensation reactions leading to a final heteroarene with attached substituents were known and developed since last decades of 19th century (most iconic examples being Paal-Knorr pyrrole synthesis and Hantzsch pyridine synthesis).[216] Instead, the functionalization of saturated heterocycles is cumbersome and limited number of protocols have been developed for such aim. The first main category of protocol was deepened in Chapter 2 dealing with the cyclization of suitable linear unsaturated amine.

[214] Vo, C.-V. T.; Bode, J. W. *J. Org. Chem.* **2014,** *79*, 2809-2815.
[215] He, Y.; Zheng, Z.; Yang, J.; Zhang, X.; Fan, X. *Org. Chem. Front.* **2021,** *8*, 4582-4606.
[216] Hantzsch, A. *Ber. Dtsch. Chem. Ges.* **1881,** *14*, 1637-1638. Paal, C. *Ber. Dtsch. Chem. Ges.* **1884,** *17*, 2756-2767. Knorr, L. *Ber. Dtsch. Chem. Ges.* **1884,** *17*, 2863-2870.

a) α-lithiation with diamine ligands

addition to electrophile

$E^{\delta+}$

L = diamine ligands:
TMEDA, (-)-sparteine,
(+)-sparteine surrogate

CuCN·2LiCl

[Cu] $\xrightarrow{E^{\delta+}}$

sBuLi / L

Li L

transmetalation

cross coupling

ZnCl₂

ZnCl

$\xrightarrow[\text{ArBr}]{Pd^0}$

Ar

PG   PG   PG   PG

E

PG

b) radical based C-H functionalization

1,5-translocation

BEt₃ / O₂ or air

·R²

$\xrightarrow{h\nu}$ *photoredox conditions*

R¹   R¹   R¹   R¹   R²
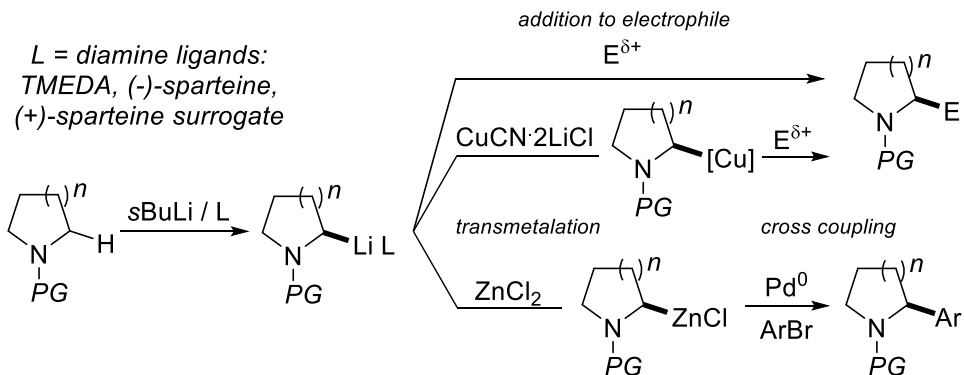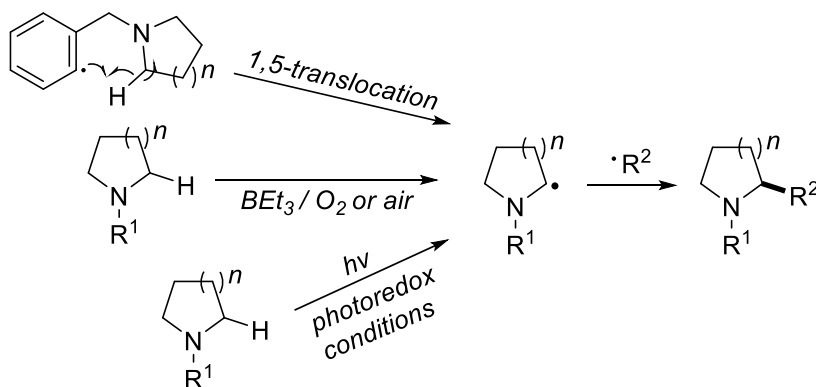
Scheme 5.1 Summary of typical strategies for saturated nitrogen heterocycles functionalization

      The second group is instead represented by the modification of preformed pyrrolidines and piperidines (Scheme 5.1). Since the cyclization has already occurred, the functionalization of an available heterocycles may seem easier. However, placing a substituent on the carbon atom of a saturate cyclic amine is one of the most difficult synthetic tasks. It corresponds to the selective activation of an aliphatic C-H bond. Indeed, the methylene units not adjacent to the heteroatom are indicated as remote or unactivated, and only a selected number of functionalization strategies were developed for such sites. Typically, these protocols require high substrate specificity and the presence of an intricated directing group to direct the effect of the (protected) nitrogen atom and to control the conformation of the cycle towards a

productive interaction with the Pd-based catalytic system.[217] Thus, most of the protocols based on heterocycle modifications benefit from the presence of the heteroatom[218] and exploit its activating effect on the adjacent α position.[214] These approaches mainly include metal-catalyzed carbene C–H insertions,[219] $C(sp^3)$–H activation by α-lithiation[214] or radical based C–H functionalization.[220] However, even these methods imply the presence of directing groups correctly positioned on the cycle or radical mechanisms whose scope is limited by scarce tolerance towards those functional groups that might trap free radicals.

Consequently, to avoid the limitation of both general strategies, we started researching an ideal transformation to perform both cyclization of a linear molecule and its concomitant functionalization. Our final aim became the synthesis of pyrrolidines and piperidines with a lateral functionalization on the carbon atom. This functional group should be a very reactive moiety easing further derivatizations, so that the saturated *N*-heterocycle obtained is prone to several kind of different manipulations. To comply with such requirement, we envisaged the incorporation of a halogen atom, specifically chlorine, into this lateral moiety.

5.1.2 Chlorinated molecules

Halogenated molecules are fundamental not only in biological science, being widespread in nature (especially from marine sources) and used as pesticides,[221,222] but also because they are a mainstay both in organic chemistry and medicinal chemistry,[223] meeting therefore the aim of this dissertation. They are used as precursors to alcohol, amines, ethers and thioethers obtained by nucleophilic substitution, they can be converted to the corresponding iodinated product by Finkelstein reaction[224] or transformed into organometallic species (e.g. Grignard and organolithium) and are exploited as starting materials towards radical intermediates obtained by halogen atom

[217] Antermite, D.; Bull, J. A. *Synthesis* **2019,** *51*, 3171-3204.
[218] Li, C.-J. *Acc. Chem. Res.* **2009,** *42*, 335-344.
[219] Doyle, M. P.; Duffy, R.; Ratnikov, M.; Zhou, L. *Chem. Rev.* **2010,** *110*, 704-724.
[220] Beatty, J. W.; Stephenson, C. R. J. *Acc. Chem. Res.* **2015,** *48*, 1474-1484.
[221] Jayaraj, R.; Megha, P.; Sreedev, P. *Interdiscip. Toxicol.* **2016,** *9*, 90-100.
[222] Gribble, G. W. *Environ. Chem.* **2015,** *12*, 396-405. Gribble, G. W. *Acc. Chem. Res.* **1998,** *31*, 141-152.
[223] Wilcken, R.; Zimmermann, M. O.; Lange, A.; Joerger, A. C.; Boeckler, F. M. *J. Med. Chem.* **2013,** *56*, 1363-1388.
[224] Finkelstein, H. *Ber. Dtsch. Chem. Ges.* **1910,** *43*, 1528-1532.

transfer (XAT).[225] Moreover, they are widespread in pharmaceuticals as precursors of drugs or as active substances themselves (e.g. chlorinated antibiotic dicloxacillin, anhestetic halothane or antinflammatory alcometasone).[226,227]

Detailed focus in this Chapter is dedicated to the chlorovinyl moiety. The smallest member of this family, vinyl chloride, is well-known given its employment in the plastic manufacture for the preparation of polyvinyl chloride (PVC) placing it at the top of the world production of petrochemicals.

Therefore, many synthetic efforts have been continuously dedicated to the incorporation of chlorine in organic molecules and the formation of C-Cl bonds. Typical approaches can be gathered in three macrofamilies: electrophilic addition to C-C multiple bonds, electrophilic aromatic substitution in aromatics, nucleophilic displacement of leaving groups or radical chlorination of C-H bonds (Scheme 5.2).
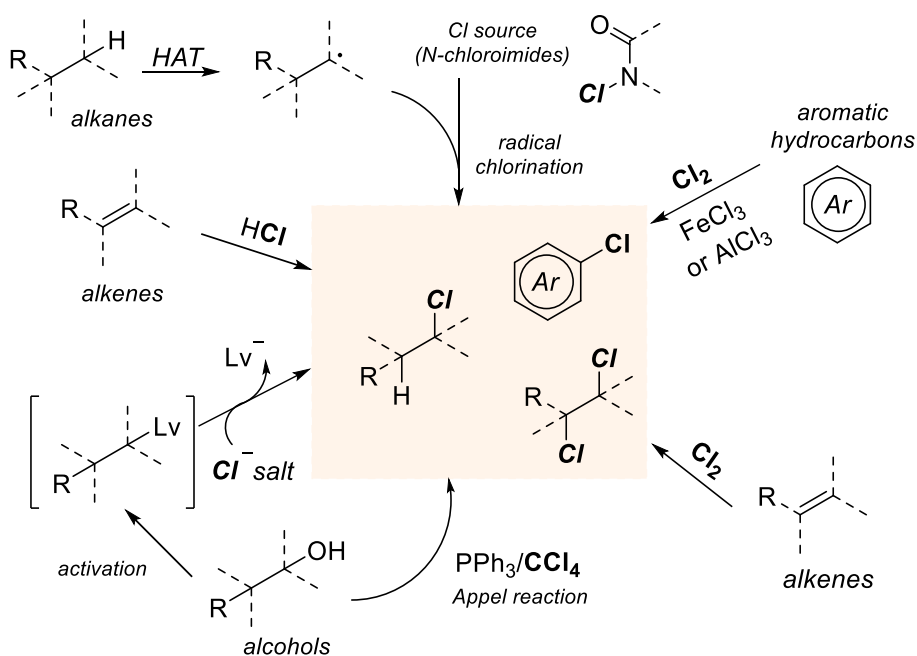
Scheme 5.2 Summary of C-Cl bond formation pathways towards chloroalkane and chloroarenes

225 Juliá, F.; Constantin, T.; Leonori, D. *Chem. Rev.* **2022,** *122*, 2292-2352.
226 Mendez, L.; Henriquez, G.; Sirimulla, S.; Narayan, M. *Molecules* **2017,** *22*, 1397.
227 Fang, W.-Y.; Ravindar, L.; Rakesh, K. P.; Manukumar, H. M.; Shantharam, C. S.; Alharbi, N. S.; Qin, H.-L. *Eur. J. Med. Chem.* **2019,** *173*, 117-153.

5.1.3 Synthesis of vinyl chlorides

The halovinyl and particularly chlorovinyl functionality is an extremely reactive group and a corner stone in organic chemistry. Besides the biological importance of natural occurring compounds containing this moiety, like the cytotoxic spongistatins[222] or the neuromodulator janthielamide A (and related lipoamides kimbeamides A–C and the ketide-extended pyranone kimbelactone A)[228] the chlorovinyl scaffold is also employed in fundamental transformations like cross-couplings.[229] However, strategies to access alkenyl chlorides are still limited. Among modern methodologies, the hydrochlorination of alkynes is a straightforward strategy typically employed. Hammond and Xu's research group studied this transformation employing *N,N*-Dimethylpropyleneurea (DMPU)/HCl as hydroalogenation reagent for ynones and ynamides **146**,[230] and also for terminal alkynes **143**,[231] where it was used in combination with nanogold particles. Tang's group provided an alternative study for the latter, achieving *E*-configured α-chloro enamides **148** (vinylamines or vinylamides), using only aqueous HCl (besides, authors described a photoredox mediated method for the *E*- to *Z*-isomerization).[232] Alternatively, both alkyl and aryl acid chlorides **149** were employed in the presence of alkynes **143** to achieve β-chlorovinyl ketones **150** and **151** (namely β-chloro-α,β-unsaturated ketones) either by Friedel-Crafts-type insertion reaction of acetylene with acid chlorides in chloroaluminate ionic liquids,[233] or by an iridium complex-catalyzed addition reaction.[234] Products **150** and **151** are the results of a double functionalization of the triple bond of alkynes, where chlorine and another functional group (instead of hydrogen) are installed on the two unsaturated carbon of the alkyne. Other examples of such dual functionalizations of alkynes **152** were also described.

---

[228] Nunnery, J. K.; Engene, N.; Byrum, T.; Cao, Z.; Jabba, S. V.; Pereira, A. R.; Matainaho, T.; Murray, T. F.; Gerwick, W. H. *J. Org. Chem.* **2012,** *77*, 4198-4208.

[229] Johansson Seechurn, C. C. C.; Kitching, M. O.; Colacot, T. J.; Snieckus, V. *Angew. Chem. Int. Ed.* **2012,** *51*, 5062-5085.

[230] Zeng, X.; Lu, Z.; Liu, S.; Hammond, G. B.; Xu, B. *J. Org. Chem.* **2017,** *82*, 13179-13187.

[231] Liang, S.; Ebule, R.; Hammond, G. B.; Xu, B. *Org. Lett.* **2017,** *19*, 4524-4527.

[232] Cao, W.; Chen, P.; Wang, L.; Wen, H.; Liu, Y.; Wang, W.; Tang, Y. *Org. Lett.* **2018,** *20*, 4507-4511.

[233] Iwai, T.; Fujihara, T.; Terao, J.; Tsuji, Y. *J. Am. Chem. Soc.* **2012,** *134*, 1268-1274.

[234] Yao, M.-L.; Quick, T. R.; Wu, Z.; Quinn, M. P.; Kabalka, G. W. *Org. Lett.* **2009,** *11*, 2647-2649.

Scheme 5.3 Summary of synthesis of vinyl chlorides from alkynes

When alkyne **152** was a terminal one, sulfonyl hydrazides in the presence of FeCl₃employed was employed to obtain the halosulfonylated product **153** (Scheme 5.3, pathway a)[235]. Another methodology achieved halotosyloxygenated product **156** using polymer **154** poly[(4-(hydroxy)(tosyloxy)iodo)styrene] in the presence of stoichiometric *N*-

---

235 Li, X.; Shi, X.; Fang, M.; Xu, X. *J. Org. Chem.* **2013,** *78*, 9499-9504.

chlorosuccinimide (NCS) **155** (Scheme 5.3, pathway b).[236] Moreover, since metal halides can behave as strong Lewis acid, they were employed as chlorine source for the functionalization of terminal arylacetylenes **152**. Indeed, reaction of the latter with lithium alkoxides **157** obtained from secondary alcohol provided the carbochlorination of the triple bound delivering product **158**. [237] In this case, the metal halide triggered the C-O bond rupture of **157**, providing an alkyl carbocation that intercepted the alkyne **152** with formation of a vinyl cation **157-I** that yielded the product **158** upon polar coupling with chloride ion (Scheme 5.3, pathway c).

However, since alkynes are more expensive and less widely available when compared to the corresponding alkenes, methods furnishing formal halogen atom addition to a preformed olefin were developed. These strategies typically required the multi-step synthesis of alkenylboron, alkenylsilane or organometallic species, followed by the conversion of the C–B, C–Si or C–metal moiety to the corresponding vinyl halides upon treatment with *N*-halo-succinimides or elemental halides.[238,239,240] Moreover, Buchwald exemplified how the use of Pd-catalysis allowed the conversion of aryl and vinyl triflates (C-O bond) to the corresponding halides.[241]

For the alkenylboron species yielding specifically chlorinated olefins, the chlorodeboronation of organotrifluoroborates using trichloroisocyanuric acid (TCCA) was observed by Molander and coworkers.[242] However, the other described methods typically provided access to vinyl bromides and vinyl iodides, with limited examples of vinyl chlorides synthesis. Evano's research group dedicated to this aim, developing protocols for a formal vinylic chlorine/halogen substitution, thus providing the less available chlorinated derivatives as products with retention of the double bond geometry (Scheme 5.4).[243,244]

[236] Chen, J.-M.; Huang, X. *Synthesis* **2004,** *2004*, 1577-1580.

[237] Snelders, D. J. M.; Dyson, P. J. *Org. Lett.* **2011,** *13*, 4048-4051.

[238] Morrill, C.; Grubbs, R. H. *J. Org. Chem.* **2003,** *68*, 6031-6034.

[239] Pawluć, P.; Hreczycho, G.; Szudkowska, J.; Kubicki, M.; Marciniec, B. *Org. Lett.* **2009,** *11*, 3390-3393.

[240] Bull, J. A.; Mousseau, J. J.; Charette, A. B. *Org. Lett.* **2008,** *10*, 5485-5488.

[241] Pan, J.; Wang, X.; Zhang, Y.; Buchwald, S. L. *Org. Lett.* **2011,** *13*, 4974-4976.

[242] Molander, G. A.; Cavalcanti, L. N. *J. Org. Chem.* **2011,** *76*, 7195-7203.

[243] Nitelet, A.; Kairouz, V.; Lebel, H.; Charette, A. B.; Evano, G. *Synthesis* **2019,** *51*, 251-257. Nitelet, A.; Evano, G. *Org. Lett,* **2016,** *18*, 1904-1907.

[244] Casitas, A.; Ribas, X., *Copper-Mediated Cross-Coupling Reactions (Chapter 6: Aromatic/Vinylic Finkelstein Reaction)*. John Wiley & Sons, Inc.: Hoboken, NJ **2013**.

Scheme 5.4 Summarized methods for synthesis of vinyl chlorides from sp^2 C=C bonds: conversion of vinyl-heteroatom bond into vinyl-Cl bond.

Styrene derivatives were converted to the styryl-chlorinated product with specifical protocols. A variation of the Hunsdiecker reactions with NCS **155** as Cl⁺ source was applied to cinnamic acids under microwave irradiation[245] or with NCS and triethylamine as the catalyst under thermal conditions delivering the corresponding *E* α-halostyrenes (Scheme 5.5).[246]

In the case of styrenes characterized by EWG group like α,β-unsaturated sulfones, nitrocompounds and nitriles) **161**, the α-chloro substitution of the hydrogen on the double bond was enabled by the presence of PhICl₂ **162** as the chlorinating agent in wet DMF (Scheme 5.5).[247]

[245] Kuang, C.; Senboku, H.; Tokuda, M. *Synlett* **2000,** *2000*, 1439-1442.
[246] Naskar, D.; Chowdhury, S.; Roy, S. *Tetrahedron Lett.* **1998,** *39*, 699-702. Das, J. P.; Roy, S. *J. Org. Chem.* **2002,** *67*, 7861-7864.
[247] Liu, L.; Zhang-Negrerie, D.; Du, Y.; Zhao, K. *Org. Lett.* **2014,** *16*, 436-439.
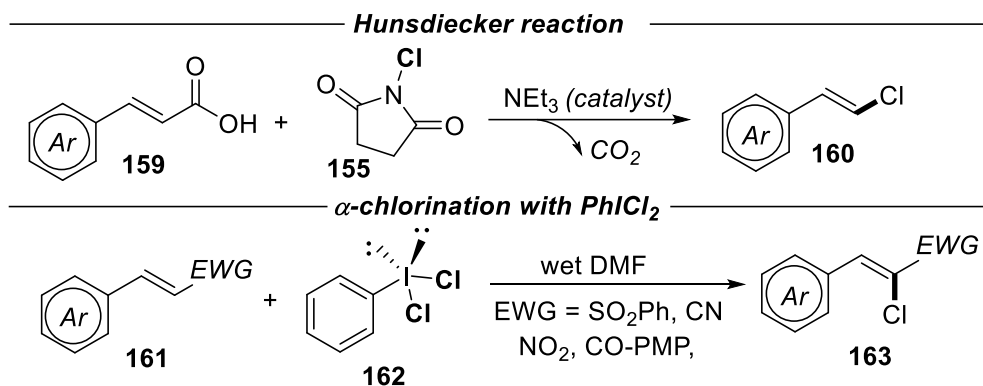
Scheme 5.5 Summarized methods for the synthesis of vinyl chlorides from sp^2 C=C bonds: synthesis from activated styrene moiety

Another methodology exploited unsaturated substrates like bis-activated cyclopropenes **164** as starting materials. Upon treatment with stoichiometric magnesium chloride ring-opening of cyclopropane was triggered and subsequent chlorination delivered multisubstituted alkenyl chlorides (Scheme 5.6).[248] Moreover, concerning alkenes as starting materials, olefin metathesis was not ignored. Hoveyda's research group developed the first protocol for a high-yielding cross metathesis of terminal alkenes and commercially available *Z*-dichloroethene **167** providing 1,2-disubstitued *Z*-alkenyl chlorides **169**.[249] The transformation occurred employing the highly reactive halo-substituted Molybdenum alkylidene species generated *in situ* from **168** (Scheme 5.6). A different approach starting from unsaturated compounds consisted of a double chlorination of a conjugated carbonyl compound **170** and a subsequent elimination of a single molecule of HCl. This transformation, reported by Kim and Park,[250] delivered α-chloro-α,β-unsaturated carbonyl compounds **172**. Treatment of a conjugated carbonyl compounds **170** with HCl and Oxone in CH_2Cl_2 provided the corresponding dihalides **171,** whose dehalogenation promoted by Et₃N, delivered **172**.

---

[248] Wang, Y.; Lam, H. W. *J. Org. Chem.* **2009,** *74*, 1353-1355.
[249] Koh, M. J.; Nguyen, T. T.; Zhang, H.; Schrock, R. R.; Hoveyda, A. H. *Nature* **2016,** *531*, 459-465.
[250] Kim, K.-M.; Park, I.-H. *Synthesis* **2004,** *2004*, 2641-2644.
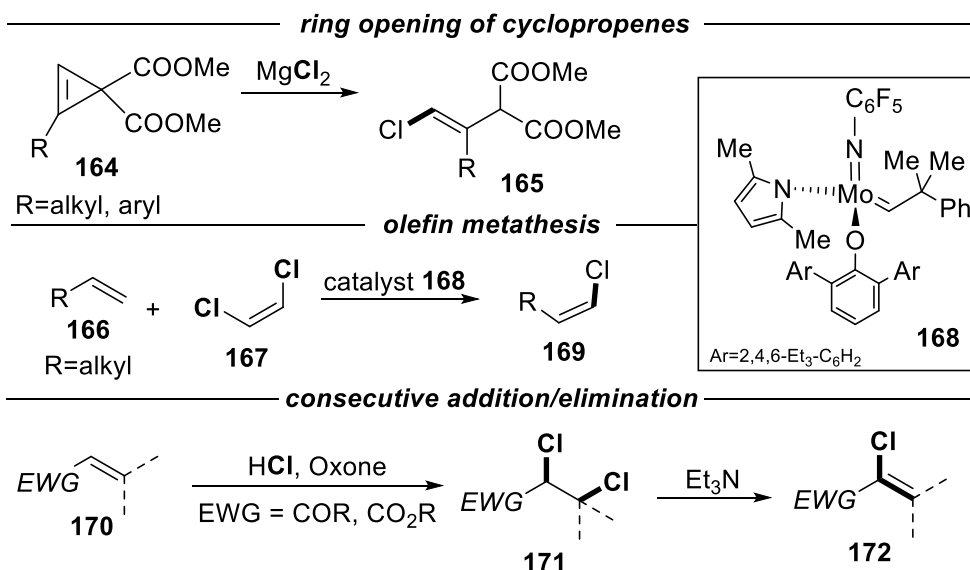
Scheme 5.6 Further methods for the synthesis of vinyl chlorides installing a chlorine atom into starting substrates containing sp^2 C=C bond.

Finally, in Scheme 5.7 some synthetic routes starting from saturated compounds containing a carbonyl moiety or a secondary alcohol were reported. The Wittig reaction of an aldehyde **173** with the appropriate halogen-substituted phosphonium salt **174** was employed for the formation of vinyl halides **178** already in early 90s.[251] However, the stereoselectivity was difficult to control with this method.[252] The chlorination of ketones **176** with triphosgene **180** (bis(trichloromethyl) carbonate, BTCC) was studied, too.[253] Aliphatic and aromatic vinyl chlorides **178** were prepared upon pyridine promoted E$_2$ elimination from an α-chloro pyridinium carbamate intermediate **177** formed *via* the triphosgene–pyridine activation of the corresponding ketones. A similar system for aromatic phenones **179** (1-phenylalkan-1-ones), was already reported to undergo an addition-elimination mechanism affording aryl-*Z*-vinyl chlorides **181** in the presence of a more elaborate catalytic system combining BTC **180**, scandium triflate, DMF, and benzoyl chloride. Here the acid chloride/scandium combination provided chlorine addition to the carbonyl followed by the *cis* elimination of

---

[251] Zhang, X.-p.; Schlosser, M. *Tetrahedron Lett.* **1993,** *34,* 1925-1928.
[252] Crane, E. A.; Zabawa, T. P.; Farmer, R. L.; Scheidt, K. A. *Angew. Chem. Int. Ed.* **2011,** *50,* 9112-9115.
[253] Saputra, M. A.; Ngo, L.; Kartika, R. *J. Org. Chem.* **2015,** *80,* 8815-8820.

benzoic acid delivering the product.[254] The Moffatt-Swern conditions for the oxidation of alcohols were adapted using excess DMSO and oxalyl chloride to exploit the resulting formation of chloronium ion and chloride anion as halogenating agents. This transformation was reported for aryl allylic alcohols **182**, which were converted to α-halogenated unsaturated ketones **183** in a tandem oxidation/halogenation reaction (Scheme 5.7).[255]
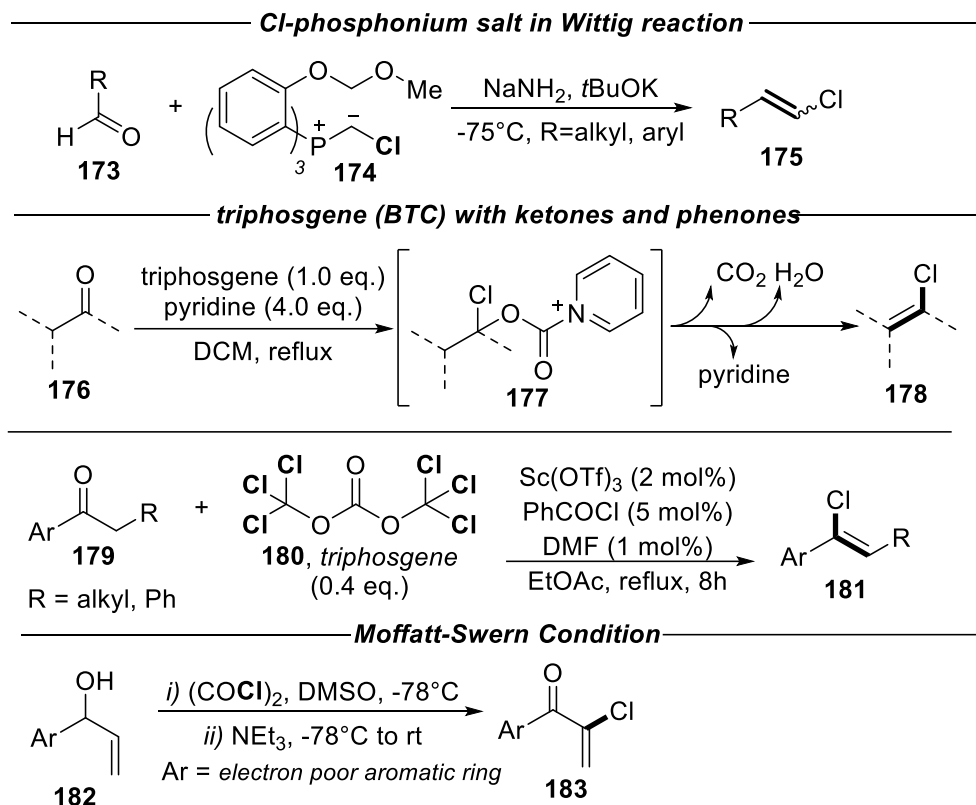
Scheme 5.7 The synthesis of vinyl chlorides from carbonyl compounds and secondary (aryl allyl) alcohols

BTC **180** and oxalyl chlorides, as many other chlorinating agents used in classical synthetic methodologies, are known for their toxicity by inhalation. To avoid the use of toxic and hazardous chlorinating reagents or harsh conditions, photocatalytic and electrocatalytic methods have been developed

[254] Su, W.; Jin, C. *Org. Lett.* **2007,** *9*, 993-996.
[255] Yin, J.; Gallis, C. E.; Chisholm, J. D. *J. Org. Chem.* **2007,** *72*, 7054-7057.

to install chlorine on organic molecules with radical mechanism in mild conditions. These protocols are discussed in the next chapter.

5.1.4 Photoredox and photocatalytic activation of NCS as chlorine donor

As describe above, photocatalysis and electrocatalysis allowed the use of mild conditions and safe reagents to provide chlorination of substrates *via* radical pathways. This year, our group has gathered the most recent protocols in such fields in a mini review.[256] However, to the aim of this introduction, the focus is dedicated to the activation of *N*-chloroimides under photocatalytic conditions. In 2016 König established that NCS **155** may undergo an electrophilic amplification due to photoredox conditions.[257]

As previously explained, NCS is a chlorinating agent, but it requires activation. Thanks to the two carbonyl moieties on the succinimide **155**, the nitrogen atom suffers the reduction of the electron density resulting in enhanced electrophilicity of the chlorine. Exploiting the oxidative quenching cycle of Ru(II) with the use of stoichiometric quantities of $(NH_4)_2S_2O_8$ as sacrificial oxidant, the Ru(III) complex is obtained, being able to oxidize NCS in the turnover step of PC cycle. The oxidation of NCS radical provided a cation intermediate **155-I**, the activated species which was sufficiently reactive to trigger SEAr even on arenes. Electron rich arene **184** were successfully chlorinated in the *para* position, nevertheless, electron-poor arenes such as acetanilide and acetophenone were unreactive under these conditions (Scheme 5.8).

Since this seminal work, the chlorination of arenes with *N*-chloroimides under photocatalytic or photoredox conditions has been further attempted, trying to disclose the electrophilic amplification of NCS even without a sacrificial oxidant. To achieve this goal, PCs possessing a photoexcited state more oxidant than Ru were investigated. Lamar's research group observed that organic dyes under aerobic conditions and white LED irradiation might be

---

[256] Parisotto, S.; Azzi, E.; Lanfranco, A.; Renzi, P.; Deagostino, A. *Reactions* **2022,** *3*, 233-253.
[257] Hering, T.; König, B. *Tetrahedron* **2016,** *72*, 7821-7825.

used lowering the loading of oxidant to a 10 mol% of $(NH_4)_2S_2O_8$ in acetonitrile (Scheme 5.9).[258]
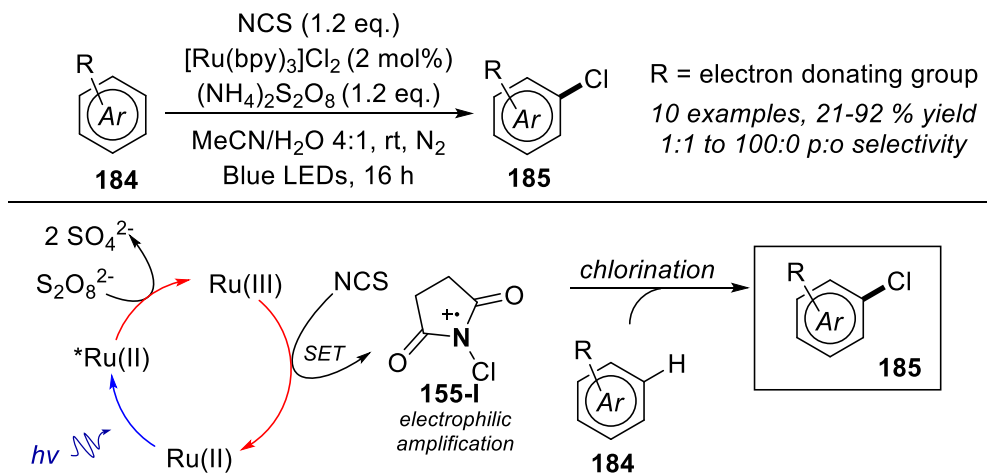
Scheme 5.8 Photoredox electrophilic amplification of NCS **155** as described by König[257]
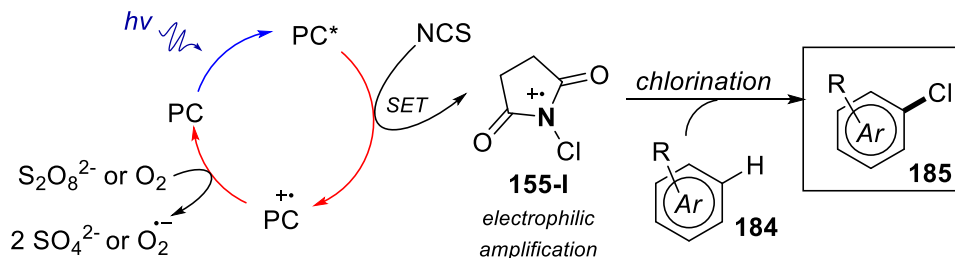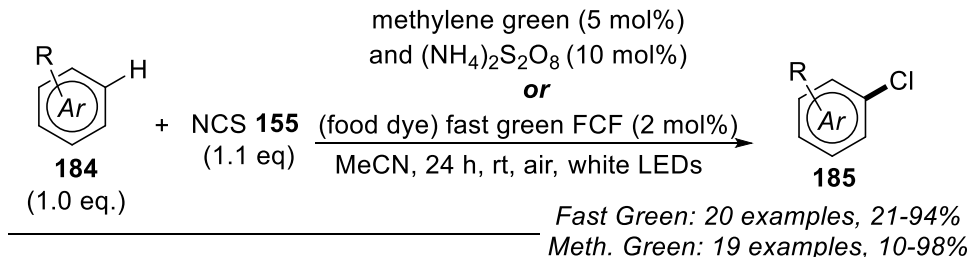
Scheme 5.9 Photoredox electrophilic amplification of NCS **155** with organic dyes as studied by Lamar[258-260]

---

[258] Rogers, D. A.; Gallegos, J. M.; Hopkins, M. D.; Lignieres, A. A.; Pitzel, A. K.; Lamar, A. A. *Tetrahedron* **2019,** *75*, 130498.

Oxygen was identified as the responsible for the regeneration of the ground-state PC, in accordance with reported formation of H_2O_2. This protocol was recently refined by the same group to achieve the chlorination of pharmaceuticals and agrochemicals with FDA-approved food dyes under aerobic conditions and white LED irradiation (Scheme 5.9).[259] In this case, the unique oxidant required to complete the PC cycle was oxygen from atmospheric air (Scheme 5.9). The same group also reported a further example of chlorine enhanced electrophilicity for halogenation of arene using trichloroisocyanuric acid TCAA.[260] Despite such halogenating reagent typically requires activation under acidic condition, the author reported how the same photoredox conditions previously honed might be applied to obtain the same effect. In this case, irradiation with white light using the inexpensive brilliant green as the PC in acetonitrile as the solvent afforded chlorination of electron poor arenes, too.

Despite the major contributes of Lamar and König to the chlorination of arenes, the versatility of the combination between the use of NCS and photocatalytic conditions enabled another crucial mechanism. Indeed, NCS was also employed to quench radical (cation) intermediates generated under photoredox conditions.

A recent example by Wu's research group in 2020, described a visible light chlorination of benzylic C-H bonds.[261] NCS was used in combination with Fukuzumi's dye **Mes-Acr**, an acridinium salt, as the PC. In this case, the pivotal role of photoredox catalysis was dual. First it provided an initial oxidation of a first equivalent of NCS by the photoexcited PC*. Second, to regenerate the ground state catalyst, Mes-Acr•⁻ reduced a second molecule of NCS affording the nitrogen radical NCS•⁺ (**155-I**). This latter was the activated species that delivered Cl⁻ and the succinimidyl radical **155-II** capable of providing HAT from the substrate **186** and generating a benzyl radical **186-I**. A third molecule of NCS trapped this carbon radical **186-I**, providing the product **187** and contributing to a chain propagation upon regeneration of the succinimidyl radical **155-II** (Scheme 5.10).

---

[259] Rogers, D. A.; Hopkins, M. D.; Rajagopal, N.; Varshney, D.; Howard, H. A.; LeBlanc, G.; Lamar, A. A. *ACS Omega* **2020,** *5*, 7693-7704.

[260] Rogers, D. A.; Bensalah, A. T.; Espinosa, A. T.; Hoerr, J. L.; Refai, F. H.; Pitzel, A. K.; Alvarado, J. J.; Lamar, A. A. *Org. Lett.* **2019,** *21*, 4229-4233.

[261] Xiang, M.; Zhou, C.; Yang, X.-L.; Chen, B.; Tung, C.-H.; Wu, L.-Z. *J. Org. Chem.* **2020,** *85*, 9080-9087.
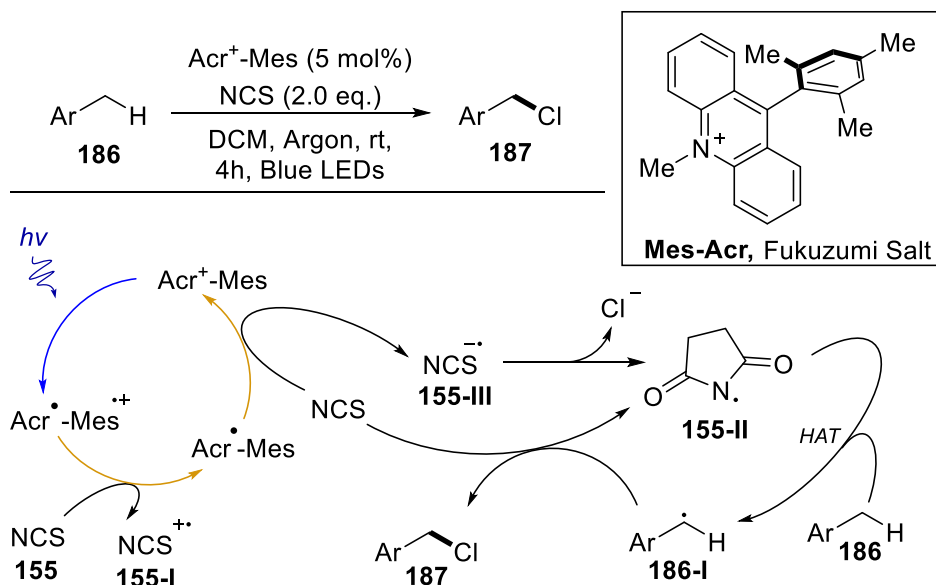
Scheme 5.10 Benzylic chlorination *via* NCS **155** activation with Fukuzumi's salt **188**

Recently, Mal and co-workers observed the formation of 3-chlorocoumarins **189** upon chlorinative cyclization of aryl alkynoates **188** under almost identical conditions (Scheme 5.11).[262]
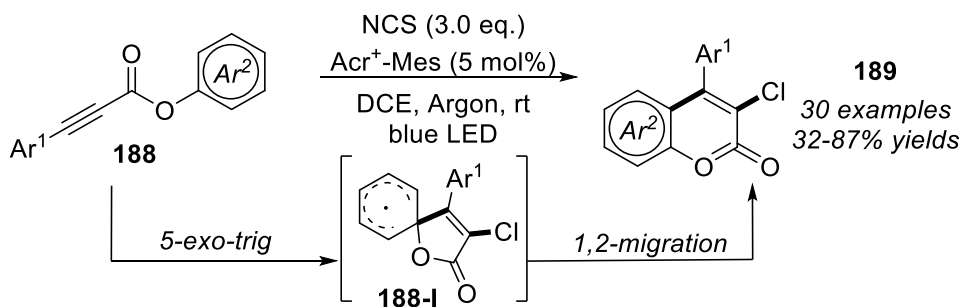
Scheme 5.11 Synthesis of chloroisocoumarins **189** *via* chlorinative cyclization upon photoredox conditions and use of NCS

This study stressed another aspect of the use of chlorinating agent under photoredox conditions, that is the possibility of chloro-induced cyclizations.

---

[262] Pramanik, M.; Mathuri, A.; Sau, S.; Das, M.; Mal, P. *Org. Lett.* **2021,** *23*, 8088-8092.

Since the rationalization of the HLF reaction, many efforts were devoted to the development of useful synthetic variations of this model transformation to afford the cyclization of amines. Nevertheless, recent literature highlights how, once again, the combination of NCS and photoredox catalysis represents a useful tool for the chlorination of aliphatic molecules avoiding their cyclization (as in HFL) or harsh conditions and the use of toxic Cl_2.

Indeed, in 2018 Leonori observed how oximes **190** provided remote halogenation achieving γ-chlorinated nitriles and imines **191** (depending on the structure of starting oximes, Scheme 5.12a).[263]
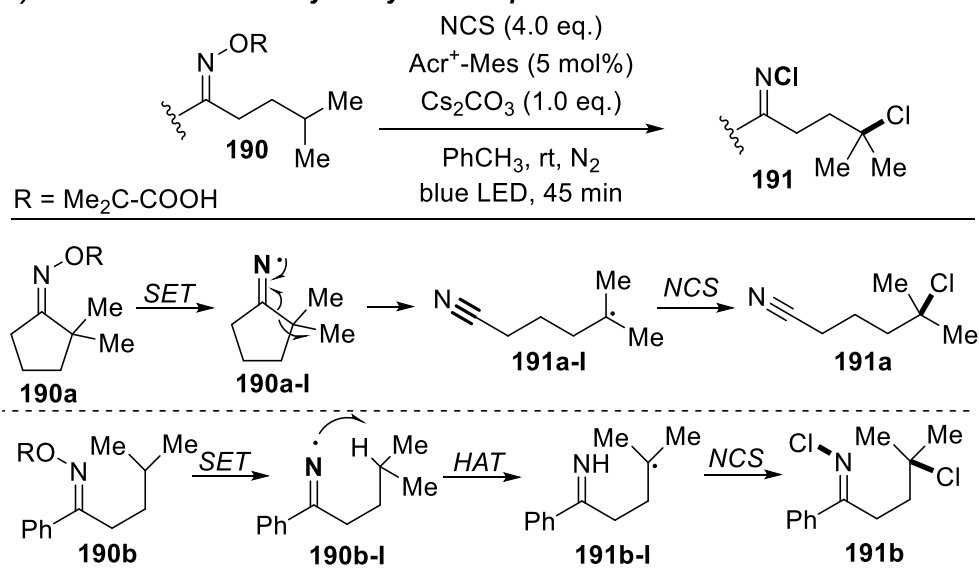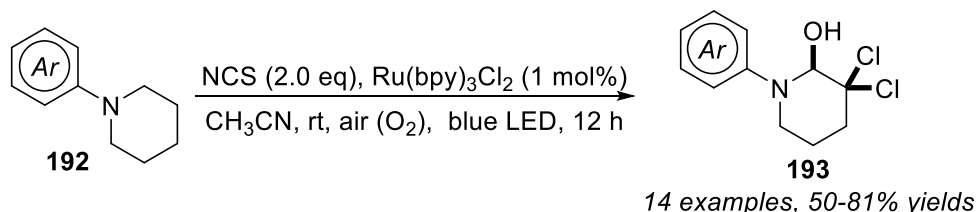
Scheme 5.12 Photoredox chlorination of nitrogen containing aliphatic molecules with NCS from iminyl radicals *(a)* and *N*-arylpiperidines *(b)*.

---

[263] Dauncey, E. M.; Morcillo, S. P.; Douglas, J. J.; Sheikh, N. S.; Leonori, D. *Angew. Chem. Int. Ed.* **2018,** *57*, 744-748.

Following an initial SET and N-O cleavage delivering the imidyl NCR **190a-I** or **190b-I**, this latter undergoes further homolytic rupture of either C-C or C-H bond. Being the starting oxime cyclic, C-C of **190a-I** is broken to open the ring, producing a terminal cyano group and a C-centered radical **191a-I** that is finally chlorinated by NCS working as the radical quencher. Otherwise, with linear oxyme, the imidyl radical **190b-I** provided a C-H bond cleavage due to 1,5-HAT affording a radical imine **191b-I**, that NCS quenches with a further chlorination of the nitrogen atom producing stable γ-Cl,*N*-Cl imine **191b** (Scheme 5.12a). The photocatalyst required to achieve such functionalization was again the **Mes-Acr** salt given its high values of redox potentials. Nevertheless, a recent work by Wang and co-workers confirmed that also Ru catalysts are suitable for the chlorination of cyclic amines, when used under oxidative conditions.[264]

The reaction of aryl piperidines **192** under aerobic conditions, in the presence of NCS in acetonitrile as the solvent and under blue light irradiation afforded 3,3-dichloro-2-hydroxy-piperidines **193** (Scheme 5.12b). Two subsequent chlorinations were observed, following the formation of an intermediate enamine generated upon interaction with the excited PC. The final capture of O_2 by the double chlorinated α-amino radical species delivered the dichloro-hydroxylated product **193**.

Finally, a relevant study to the aim of this introduction concerning the γ-chlorination of aliphatic amines despite not employing NCS was conducted by Wu's research group.[265] The authors discovered a methodology to functionalize sulfonamides **194** using sodium hypochlorite. The reactive *N*-chloroamine **196** was reported as produced *in situ* and such reactive species is subsequently reduced in a SET event by the excited [Ru(bpy)$_3$]Cl$_2$ delivering a chloride ion and a NCR **196-I**. This latter triggered a 1,5-HAT generating the carbon centered radical **196-II** which reacted with a second molecule of *N*-chloroamine **196** to obtain the product **195** and initiating a chain reaction regenerating the NCR species **196-I** (Scheme 5.13). Interestingly, chlorination at the allylic or benzylic position, but also across a cyclohexyl moiety, was not feasible.

---

[264] Wang, F.; Liu, X.; Wang, L. *Org. Biomol. Chem.* **2021,** *19*, 6141-6146.
[265] Zhu, Y.; Wang, J.-J.; Wu, D.; Yu, W. *Asian J. Org. Chem.* **2020,** *9*, 1650-1654.
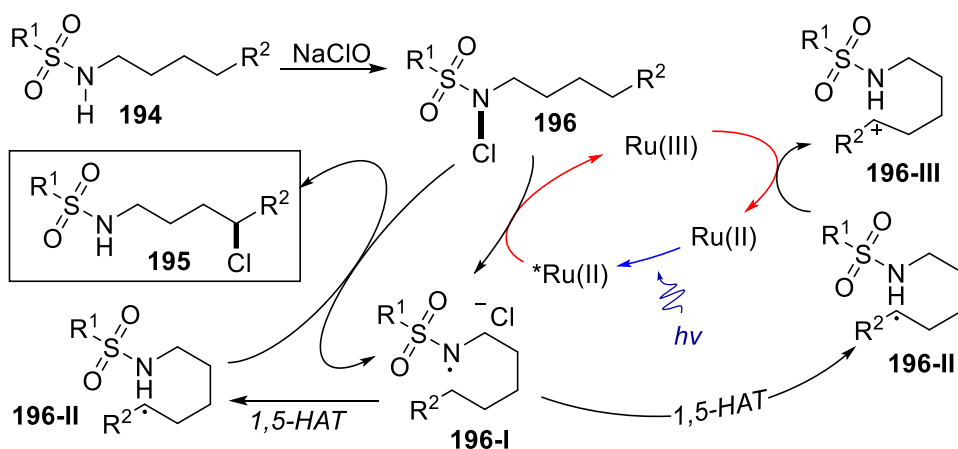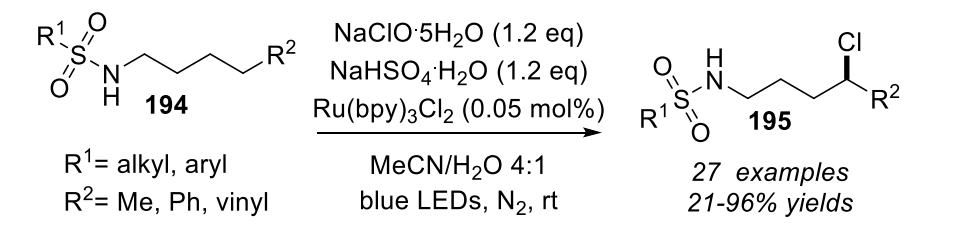
Scheme 5.13 Remote chlorination of aliphatic sulfonamides **194** with NaClO under photoredox conditions

All these recent efforts in chlorination reactions under photoredox conditions were gathered and combined with our interests in the synthesis of saturated nitrogen heterocycles containing a lateral vinyl chloride moiety. Thus, we conceived a domino process where the blend between NCS and photoredox conditions would provide the cyclization and chloro-functionalization of a linear amine.

5.2 Photoinduced cyclization and chlorination of allenes

5.2.1 Objectives and general considerations

Photoredox could be the key to provide a new strategy to obtain the cyclization of a linear molecule and the installation of a biologically and synthetically valuable chlorovinyl moiety. Once again, we relied on the possibility of generating a NCR under visible light irradiation to achieve a nitrogen promoted cyclization from a linear molecule. A cascade process, where both the cyclization and the lateral functionalization of the heterocycle

sequentially occurred was designed. To provide such dual functionalization the starting material should possess both an unsaturated site where the NCR could attack and a vicinal functional group that could undergo chlorination. Given the wide availability of chlorination method based on the modification of an unsaturated moiety (alkynes or alkenes) we identified the allene functionality as an ideal starting point. Indeed, the two adjacent double bonds of the allene supplied both the first unsaturated site for radical attack (delivering the cyclized scaffold) and a second olenific moiety where the chlorine could be attached generating a chlorovinyl heterocycle (Scheme 5.14).
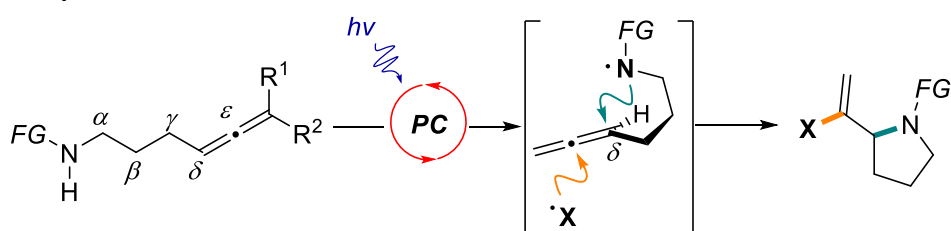
Scheme 5.14 Hypothesized reactivity for alkenes under photoredox conditions in the presence of a halogen donor

5.2.1.1 Visible light induced reactivity of allenes

Allenes have always been successfully addressed as substrates for the development of new methodologies in our group[266] (and reviewed in their synthetic utility).[267] Recently we successfully described how allenyl tosyl amines **197** could be employed in a room temperature Heck reaction with aryl halides thanks to the use of visible light irradiation.[268] A very simple Pd-based catalytic system, combined with light as the keystone to promote the carbo-palladation at room temperature, allowed to obtain arylated vinyl pyrrolidines and piperidines **198** from a linear tosylated amine **197** (Scheme 5.15).

[266] Parisotto, S.; Palagi, L.; Prandi, C.; Deagostino, A. *Chem. Eur. J.* **2018,** *24*, 5484-5488. Boi, T.; Deagostino, A.; Prandi, C.; Tabasso, S.; Toppino, A.; Venturello, P. *Org. Biomol. Chem.* **2010,** *8*, 2020-2027. Deagostino, A.; Prandi, C.; Toppino, A.; Venturello, P. *Tetrahedron* **2008,** *64*, 10344-10349.
[267] Deagostino, A.; Prandi, C.; Tabasso, S.; Venturello, P. *Curr. Org. Chem.* **2010,** *14*, 230-263. Deagostino, A.; Prandi, C.; Tabasso, S.; Venturello, P. *Molecules* **2010,** *15*, 2667-2685. Parisotto, S.; Deagostino, A. *Synthesis* **2019,** *51*, 1892-1912.
[268] Renzi, P.; Azzi, E.; Bessone, E.; Ghigo, G.; Parisotto, S.; Pellegrino, F.; Deagostino, A. *Org. Chem. Front.* **2022,** *9*, 906-916.

Scheme 5.15 Blue light enhanced Heck arylation at room temperature applied to allenes **197**

To outline a complementary study to this recent effort of ours, we intended to use the same starting materials to achieve different products and provide an alternative synthetic pathway to molecules that were not achievable *via* our Heck transformation. Nevertheless, regarding this project, differently from our previous report, we expected to design a reaction based on a radical mechanism promoted by visible light. Indeed, a recent review has gathered the successful achievements in UV-visible light mediated transformation of allenes *via* SET (determining addition of SET-generated radical intermediates to the central- or terminal carbon of the vicinal dienic moiety) or *via* EnT processes (typically [2+2] cycloaddition or intramolecular cyclization).[269] Moreover, the functionalization of allenes *via* radical processes even without the use of light has been extensively studied and reviewed.[270] However, all these studies agreed on focusing future investigations on visible light promoted radical functionalization of allenes, especially for heteroatom radical precursors. Indeed, only a limited number of strategies for the intramolecular cyclization of allenes driven by the generation of a NCR under visible light irradiation and subsequent functionalization were developed so far. These two protocols were discovered by Schomaker's group.[271-272] They rely on NCR formed upon N-O bond cleavage of *N*-aryloxyamide and *N*-aryloxycarbamates **199** (Scheme 5.16), with a wise exploitation of the previous discovery by Leonori concerning the behavior of aryloxyamides under photoredox conditions.[273]

---

[269] Singh, J.; Sharma, A.; Sharma, A. *Org. Chem. Front.* **2021,** *8*, 5651-5667.

[270] Liu, L.; Ward, R. M.; Schomaker, J. M. *Chem. Rev.* **2019,** *119*, 12422-12490. Qiu, G.; Zhang, J.; Zhou, K.; Wu, J. *Tetrahedron* **2018,** *74*, 7290-7301.

[271] Liu, L.; Ward, R. M.; Schomaker, J. M. *Chem. Eur. J.* **2020,** *26*, 13783-13787.

[272] Ward, R. M.; Schomaker, J. M. *J. Org. Chem.* **2021,** *86*, 8891-8899.

[273] Davies, J.; Svejstrup, T. D.; Fernandez Reina, D.; Sheikh, N. S.; Leonori, D. *J. Am. Chem. Soc.* **2016,** *138*, 8092-8095.
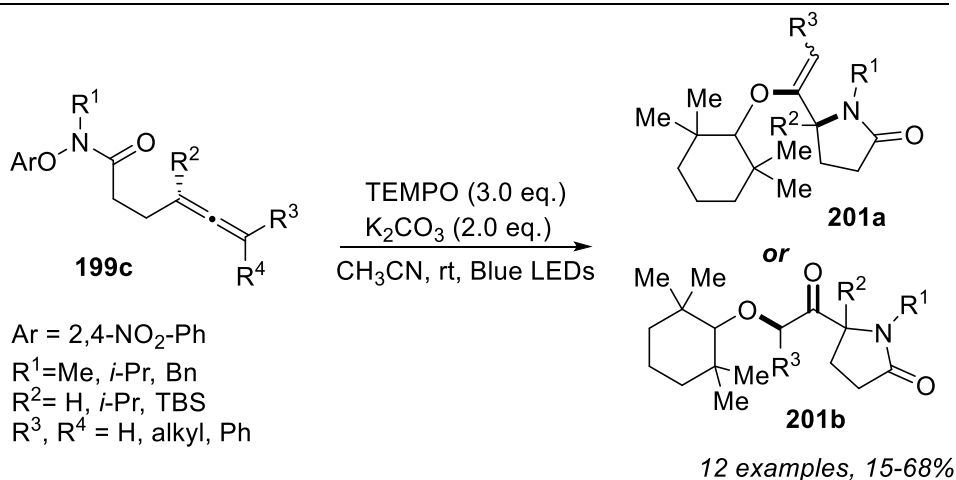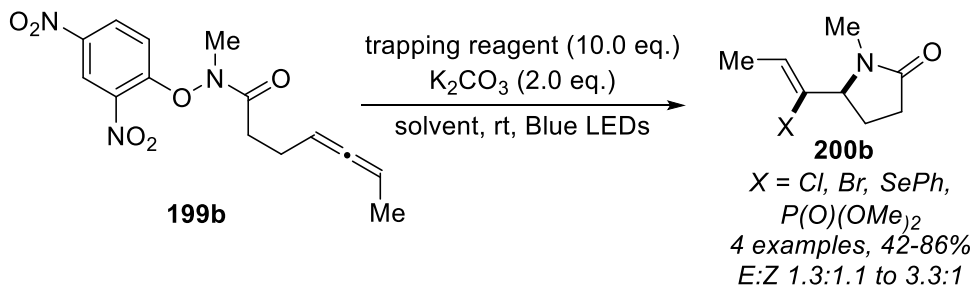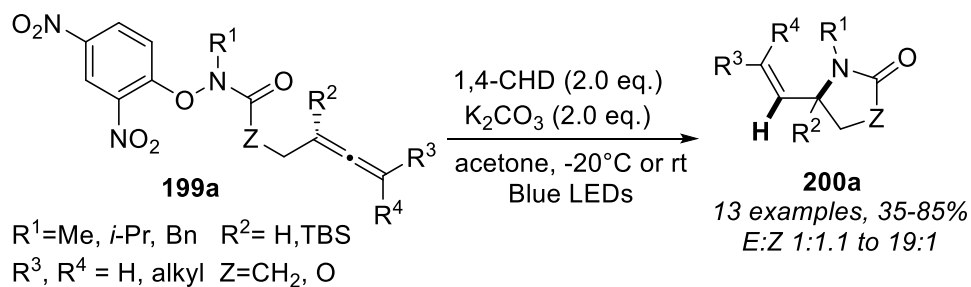
Scheme 5.16 Visible light promoted nitrogen driven cyclization of allenes

In the first work (Scheme 5.17 top), the regioselective addition of the amidyl radicals **199-II** to the allene moiety on the δ carbon furnished γ-lactams **200** with lateral alkyl vinyl functionality. This lateral vinyl functionality arose from a vinyl radical intermediate **200-I** which is finally quenched by a HAT reagent, in this case 1,4-cyclohexadiene (CHD). Additionally, the authors reported 4 examples of intermolecular trapping (one of them with Cl-functionalization from 10 equivalent of NCS as the coupling partner). The photoredox catalytic system providing this transformation relied on the formation of an EDA complex **199-EDA** between the K_2CO_3 and the 2,4-

dinitrophenoxy aryl substituent on the nitrogen atom of the reagent **199**. The absorption of light by this complex **199-EDA** delivered the NCR species **199-II** following the cleavage of the intermediate **199-I** with release of the phenoxide fragment.
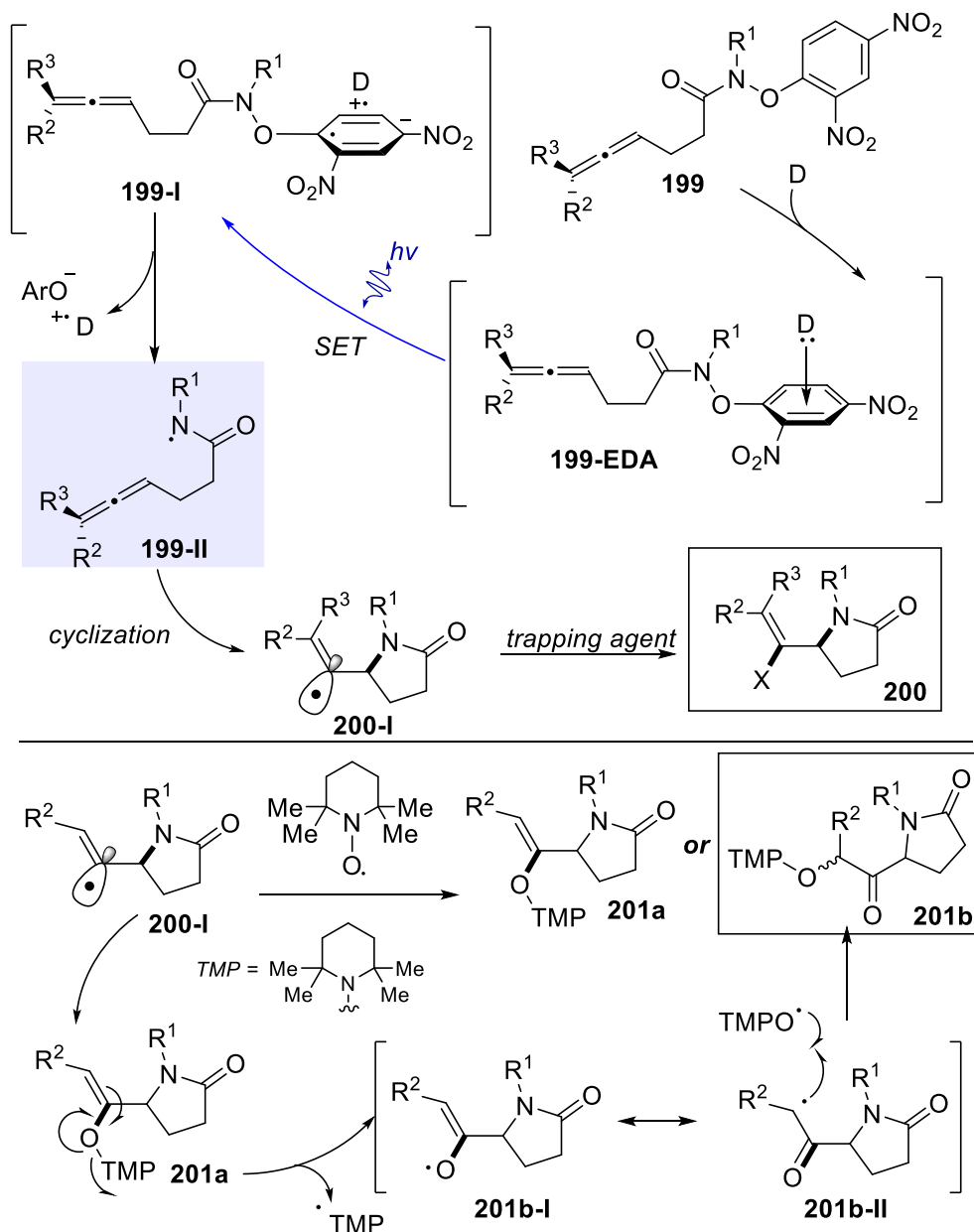
Scheme 5.17 Proposed mechanisms for the visible light induced allene functionalization described by Schomaker

171

The following work (Scheme 5.17 bottom), extended the same strategy employing TEMPO derivatives as trapping agent obtaining TEMPO enol ethers. Since this led to the generation of an intermediate enoxylated species **201a**, N-O bond cleavage might be observed, depending on the substitution pattern of the allene. This event delivered an α-keto radical **201b-I** that further recombined with TEMPO to give a α-ketoether **201b** (namely a latent 1,2 diketones) in moderate yields with good diastereoselectivity.

5.2.2 Photocatalytic chlorocyclization of linear sulfonylamidoallenes

As previously stated, the same cumulene substrates **197** studied in our previous work were used as the model molecules to develop the new protocol. A demanding task in their synthesis was represented by the installation of the allene functionality. However, we identified the commercially available 4-pentyn-1-ol **205** as the ideal starting material.
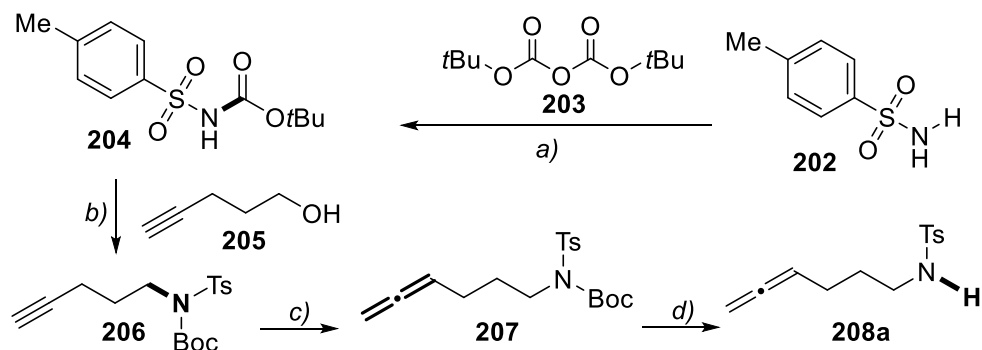
Scheme 5.18 Synthetic pathways towards N-tosylhexa-4,5-dien-1-ylamine **208a** a) Boc₂O **203** (1.15 eq.), Et₃N (1.10 eq), DMAP (0.10 eq), DCM, rt, 2h (91%); b) **205** (0.95 eq.), DIAD (1.2 eq.) PPh₃ (1.3 eq.), PhCH₃/THF 3:1, N₂, 0°C to rt (96%); c) CuBr (0.70 eq.), -(CH₂O)ₙ- (2.0 eq.) DIPA (2.0 eq.), 1,4-dioxane, N₂, 120°C, 16h; d) TFA (5.0 eq.), DCM, rt, 30-40 min (yield over c-d steps: 85%)

Indeed, the application of Ma's conditions to obtain the Crabbè(-Ma) homologation of the terminal alkynyl moiety resulted to be the best strategy to install the allene moiety.[274] The direct homologation of the starting alkynol and subsequent conversion into the corresponding allenol followed by the

---

[274] Brummond, K. M.; DeForrest, J. E. *Synthesis* **2007,** *2007*, 795-818. Huang, X.; Ma, S. *Acc. Chem Res.* **2019,** *52*, 1301-1312.

replacement of the hydroxy moiety with the tosylamide functionality is reported but resulted in low yields in our case. Thus, we optimized an alternative strategy based on a three-step large scale synthesis. The *Boc*-protected tosylamide **204** reacted under Mitsunobu conditions with 4-pentyn-1-ol **205** and furnished a 96% yield of the corresponding tosylamidocarbamate **206** upon crystallization. The protection on the amino functionality prevents any interaction of the nitrogen with the copper salt used in the following Crabbé homologation. This latter required high dilution conditions [0,1 M] and was conducted in small batches in parallel. The crude 4,5-dienic product **207** obtained was gathered and a TFA-mediated deprotection of the *Boc* yielded the desired *N*-tosylhexa-4,5-dien-1-ylamine **208a** following the unique silica gel chromatography purification required for this synthesis (Scheme 5.18)

Differently from the *N*-arylsulfonylhydrazones studied in Chapters 3 and 4, we expected the conversion of tosylamides to the corresponding neutral NCR to be more difficult. Thus, the groundbreaking results obtained by Leonori in 2019 with the coupling of amine and aromatics under photoredox conditions served as inspiration (Scheme 5.19)..[275]
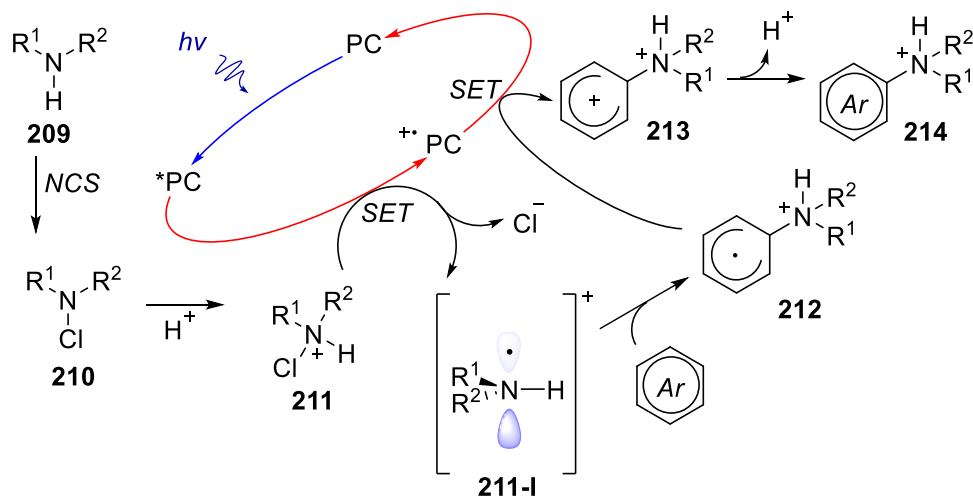
Scheme 5.19 *In situ* conversion of a primary and a secondary amine **209** into a *N*-chloramine **210** and following amination of arene as described by Leonori.[275]

[275] Ruffoni, A.; Juliá, F.; Svejstrup, T. D.; McMillan, A. J.; Douglas, J. J.; Leonori, D. *Nat. Chem.* **2019,** *11*, 426-433.

In this work, an aliphatic amine **209** was reacted in the presence of NCS under Brönsted acidic conditions to promote arene amination *via* a radical mediated transformation with the formation of an aminium radical intermediate **211-I**. Such combination provided *N*-chloramine **210**, with the subsequent protonation of nitrogen atom by the acid, resulting in a chloroammonium intermediate **211**, which, as all other chloroamine and NCS itself, displays an amplified electrophilic character at the chlorine atom. However, the work explained how the oxidative quenching of the excited state of the PC enabled to overcome this normal ionic reactivity upon the generation of an aminium radical **211-I** by the SET reduction of the precursor chloroammonium **211**. This protocol allowed the authors to avoid the chlorination of the arene coupling partner favoring instead the amination of the latter.

Thus, inspired by such findings, we tried to exploit similar conditions, except for the addition of a base. Indeed, tosylamide is not as basic as a free amine, and *N*-chlorination might be difficult. The presence of the base would instead ensure the deprotonation of the tosylamide and nitrogen chlorination.

5.2.2.1 Screening of the reaction conditions
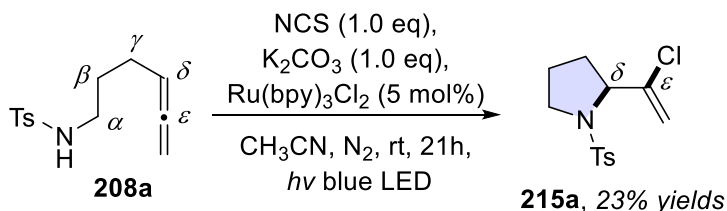
Scheme 5.20 First attempt of chloro-induced cyclization of allene **208a** for the synthesis of chlorovinylpyrrolidine **215a**

The allene **208a** was reacted in the presence of NCS (1.0 eq.) K_2CO_3 (1.0 eq.) and Ru(bpy)$_3$Cl$_2$ (5 mol%) in acetonitrile as the solvent under blue light irradiation. After 21 hours of irradiation a 2-chlorovinylpyrrolidine **215a** was recovered in 23% yield (Scheme 5.20).

We obtained both the cyclization with formation of the N-C bond with the δ carbon, and the installation of a lateral functionalization with the addition of a chlorine atom onto the sp carbon of the allene. NMR spectrum unambiguously confirmed this conversion as witnessed by the disappearance of the sp^2-H signals of the allene (triplet of triplets at 5.00 ppm and doublet of triplets at 4.62 ppm) and the occurrence of the disubstituted terminal vinyl

signal pattern (two peaks at 5.56 and 5.32 ppm, Figure 5.2 top) and of the C-H of the stereogenic center adjacent to the N, formed upon cyclization (multiplet at 4.32 ppm, Figure 5.2 bottom).
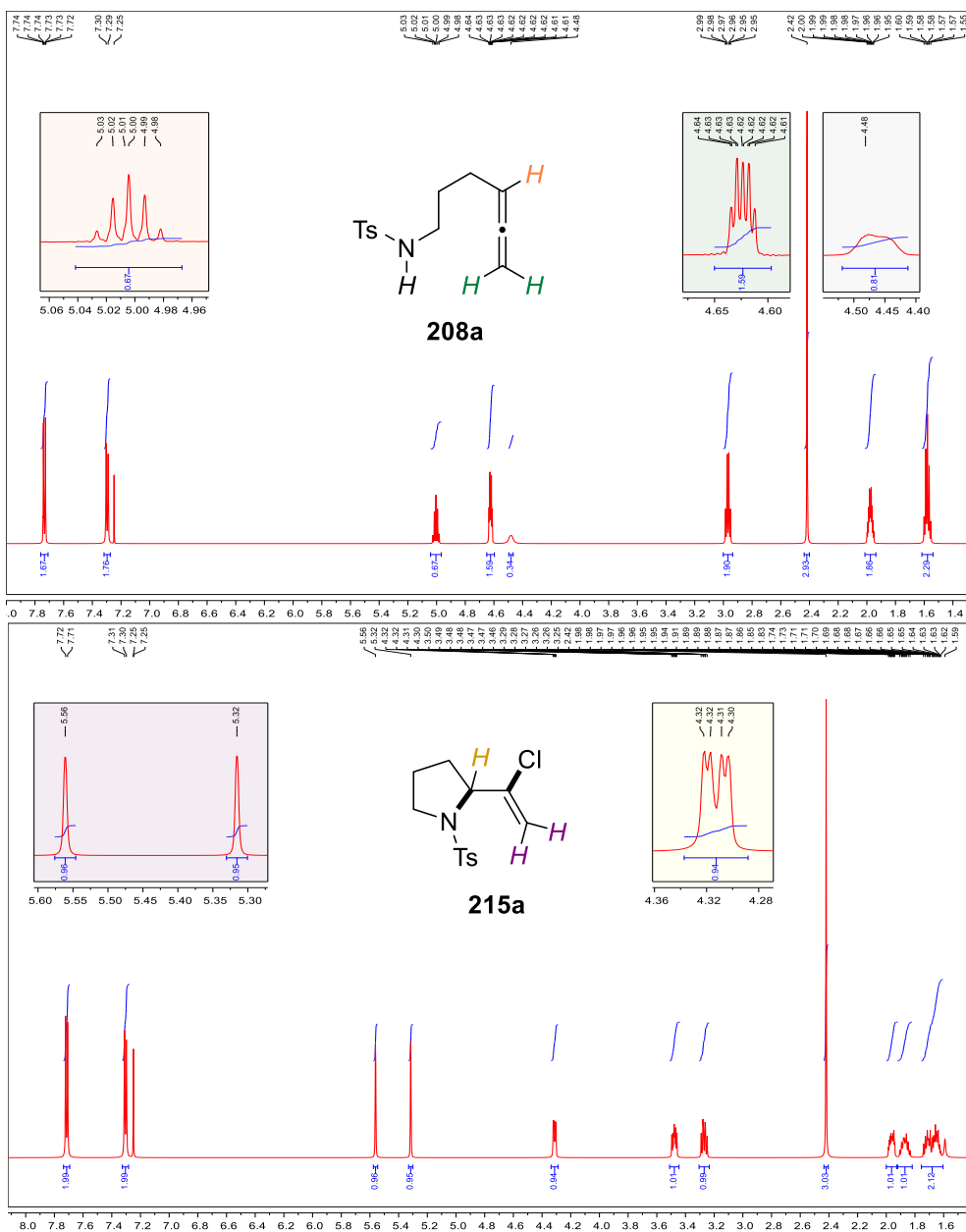
Figure 5.2 Stacked ^{1}H-NMR spectra of reagent **208a** and product **215a** demonstrating the cyclization and chlorovinylation of the substrate

Such results ventured our guess that NCS might serve both in the initial sulfonamide chlorination triggering the nitrogen radical formation and in the final halogenation of the allene.

However, prior to proceeding with description of the optimization results, (reported below in Table 5.1) some general observations are described.

Together with the principal aminochlorination product **215a**, we occasionally recovered traces (yield<5%) of an arylamination product of a second intramolecular cyclization **216**, providing a tricyclic structure upon radical attack on the tosyl moiety. This latter was similar to the ones observed for tosylhydrazones in Chapter 3-4 and might contribute as an indication for a radical mechanism, albeit never identified as the preferred product of this reaction. Moreover, even when low yields or no cyclization was observed, at the end of the reaction a species characterized by the typical ^{1}H-NMR signal pattern of a terminal allene (sp^2 signal in the 4.5-5.0 ppm region) was always identified. At first, we construed it as an indication of the presence of the unreacted starting material **208a**, nevertheless, the slight shift of NMR signals, when compared to signals of **208a** convinced us that another species, probably the *in situ* formed *N*-chloramide **208a-Cl** might be involved (Scheme 5.21).
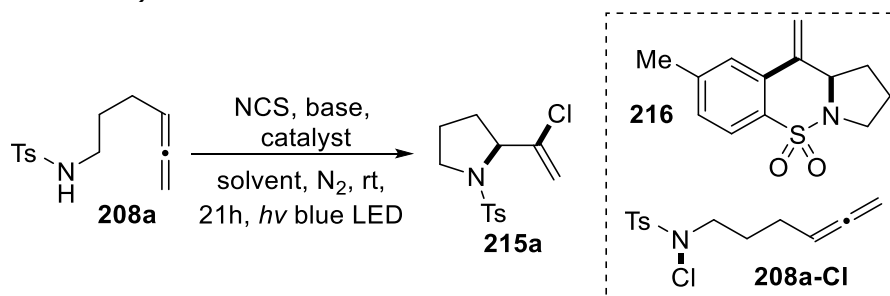
Scheme 5.21 Product **215a** and principal byproducts **216a** or other species **208a-Cl** observed during screening of the reaction conditions for the chloro-induced cyclization of allene **208a**
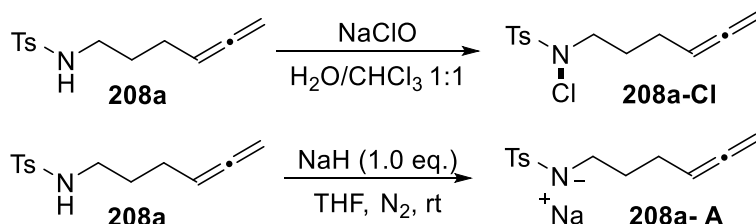
Scheme 5.22 Synthesis of **208a-A** and **208a-Cl**

Thus, we applied a typical procedure for the chlorination of tosylamides to synthesize the *N*-Cl analogue of the substrate **208a-Cl**. Then we used NaH to obtain its anionic sodium salt **208a-A** (Scheme 5.22).

The comparison of ^{1}H-NMR spectra of the three species with those obtained from the crudes of the reaction confirmed our assumption (Figure 5.3).
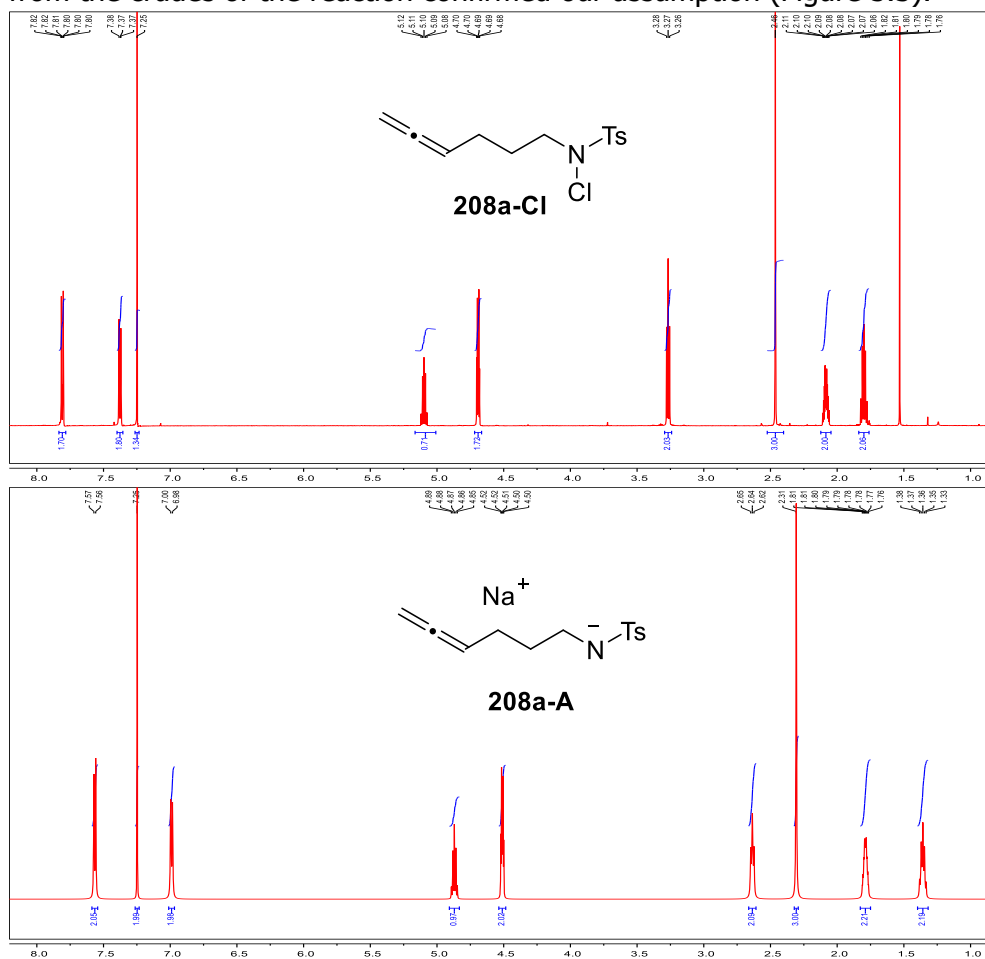
Figure 5.3 Stacked ^{1}H-NMR spectra of **208a**, **208a-Cl**, and **208a-A**

Thus, we could finally start the optimization of the reaction process using an excess of NCS (3.0 eq., excess used to guarantee both sulfonamide chlorination and allene halogenation) and evaluating the effects of variations of the catalyst, the base, and the solvent. The most relevant results of optimization are gathered in Table 5.1 (all detailed tables of optimization are reported in Chapter 6 -Experimental Procedures).

Table 5.1 Summary of screening and optimization of reaction conditions
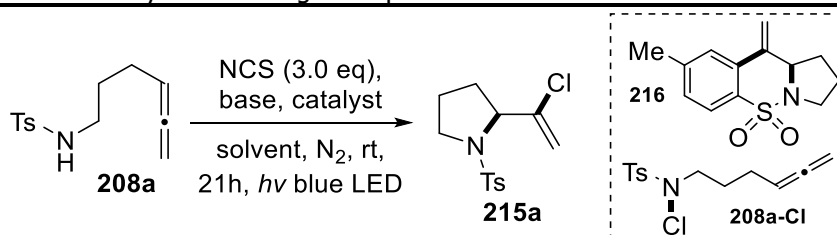
	solvent	Base	catalyst	208a [%][b]	215a [%][a]	216 [%][b]	208a-Cl [%][b]
1	CH₃CN	K₂CO₃ (1.0 eq.)	Ru(bpy)₃Cl₂ (5% mol)	0	33	2	0
2	CH₃CN	K₂CO₃ (1.0 eq.)	**Mes-(Acr)BF₄⁻ (5% mol)**	6	29	1	14
3	CH₃CN	K₂CO₃ (1.0 eq.)	**Ru(bpy)₃(PF₆)₂ (5% mol)**	0	43	4	0
4	CH₃CN	**KOH (1.0 eq.)**	Ru(bpy)₃(PF₆)₂ (5% mol)	0	29	1	0
5	CH₃CN	**Cs₂CO₃ (1.0 eq.)**	Ru(bpy)₃(PF₆)₂ (5% mol)	25	27	3	0
6	CH₃CN	**Na₂CO₃ (1.0 eq.)**	Ru(bpy)₃(PF₆)₂ (5% mol)	15	23	1	0
7	CH₃CN	**2,6-Lutidine (1.0 eq.)**	Ru(bpy)₃(PF₆)₂ (5% mol)	0	10	1<<	0
8	CH₃CN	**Et₃N (1.0 eq.)**	Ru(bpy)₃(PF₆)₂ (5% mol)	0	12	1<<	0
9	**CHCl₃**	K₂CO₃ (1.0 eq.)	Ru(bpy)₃(PF₆)₂ (5% mol)	0	28	2	0
10	**DMF**	K₂CO₃ (1.0 eq.)	Ru(bpy)₃(PF₆)₂ (5% mol)	0	28	0	0
11	**DMSO**	K₂CO₃ (1.0 eq.)	Ru(bpy)₃(PF₆)₂ (5% mol)	100	0	0	0
12	**PhCH₃**	K₂CO₃ (1.0 eq.)	Ru(bpy)₃(PF₆)₂ (5% mol)	0	47	1<<	0
13	**HCO₂Me**	K₂CO₃ (1.0 eq.)	Ru(bpy)₃(PF₆)₂ (5% mol)	0	31	4	0
14	**Acetone**	K₂CO₃ (1.0 eq.)	Ru(bpy)₃(PF₆)₂ (5% mol)	0	43	2	0
15	**PhCH₃/HCO₂CH₃ 3:1**	K₂CO₃ (1.0 eq.)	Ru(bpy)₃(PF₆)₂ (5% mol)	0	56	0	0
16	PhCH₃/**CH₃CN** 3:1	K₂CO₃ (1.0 eq.)	Ru(bpy)₃(PF₆)₂ (5% mol)	0	46	0	0
17	PhCH₃/**HCO₂CH₃** 3:1	K₂CO₃ **(0.5 eq.)**	Ru(bpy)₃(PF₆)₂ (5% mol)	0	52	0	0
18	PhCH₃/HCO₂CH₃ 3:1	K₂CO₃ **(0.2 eq)**	Ru(bpy)₃(PF₆)₂ (5% mol)	0	56	0	0
19	PhCH₃/ HCO₂CH₃ 3:1	K₂CO₃ (0.2 eq.)	Ru(bpy)₃(PF₆)₂ **(8% mol)**	0	56	0	0
20	PhCH₃/ HCO₂CH₃ 3:1	K₂CO₃ (0.2 eq.)	Ru(bpy)₃(PF₆)₂ **(1% mol)**	0	51	0	0

Reactions conditions: **208a** (0.20 mmol), base and catalyst as indicated. Anhydrous solvent(s) (4 mL total) under irradiation with 456 nm light source – blue light. *a)* Yield determined on isolated products. *b)* Yield determined after 2 repetitions with ¹H-NMR using dichloroethane and nitromethane as internal standards.

Ru-based PCs together with Fukuzumi's salt (Mes-Acr) furnished the best yield (entry 1-3). Thus, we investigated the behavior of Ru(bpy)$_3$Cl$_2$, Ru(bpy)$_3$(PF$_6$)$_2$Mes-(Acr)-BF$_4$ with different bases. Ru(bpy)$_3$(PF$_6$)$_2$, probably because of the different solubility dictated by the PF$_6^-$ provided the highest yield, thus variations were focused on this PC. M$_2$CO$_3$ and weaker inorganic bases (entry 3,5,6) seemed to allow product formation, however complete conversion was observed only with K as salt cation. When KOH was tested (entry 4), complete conversion but lower yields of the product were obtained (that is a general trend observed for other strong bases, see Chapter 6). Organic bases always provided complete conversion at the expense of lower yields (entry 7-8). A pivotal role was played by the solvent since it was unique factor whose variations allowed the observation of yield enhancement.

Polar solvent (acetonitrile and acetone as the best examples) both protic and aprotic ensured complete conversion (entry 3,9,10,13 and 14) nevertheless the best result was obtained with the apolar toluene (entry 12). In DMA complete conversion of the starting material was observed with no detection of the byproduct **216** not even in traces (entry 10). DMSO led to no reaction of the substrate most probably because of the interaction between NCS and DMSO disclosed by Jiao and co-workers[276] that prevent NCS interaction with the allene **208a**. The reaction seemed to work moderately good in toluene, however, due to the apolarity of this solvent, problems of solubility of the base and the catalyst were observed, and this might interfere with light propagation in the reaction mean. Thus, we explored some solvent mixture of toluene with other polar solvents to achieve the complete solubility of the reactants (entry 15-16).

Finally, a 3:1 combination of toluene/methyl formate allowed us to reach a 56% yield for the process (entry 16). Afterwards we tested the loading of the base and the catalyst (entry 17-20). To our delight, only a catalytic amount of base was necessary, while increasing the mol% of catalyst did not influence the yield (entry 19). On the other hand, it was possible to decrease such quantity to 1 mol% without significant loss in yield (entry 20).
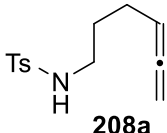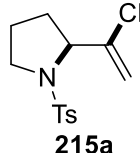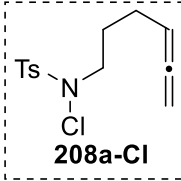
5.2.2.2 Control experiments

Once the optimization of the reaction conditions was completed, we performed the control experiments. The reaction was repeated in the absence

---

[276] Song, S.; Li, X.; Wei, J.; Wang, W.; Zhang, Y.; Ai, L.; Zhu, Y.; Shi, X.; Zhang, X.; Jiao, N. *Nat. Catal.* **2020,** *3*, 107-115.

of NCS, of the base, of the catalyst, in the dark and in the presence of water (Table 5.2).

Table 5.2 Control experiments

standard conditions:
NCS (3.0 eq), K$_2$CO$_3$ (0.2 eq), Ru(bpy)$_3$(PF$_6$)$_2$ (5 mol%)
PhCH$_3$/HCO$_2$CH$_3$ 3:1
N$_2$, rt, 21h, *hv* blue LED

208a → **215a** / **208a-Cl**

	208a [%]	Deviation from standard conditions	215a [%]	208a-Cl [%]
1	0	*None*	56	0
2	100	no Base	0	0
3	100	No NCS	0	0
4	13	nocatalyst (PC)	11	66
5	0	Presence of 1.00 eq of H$_2$O	29	0
6	18	no irradiation (in the dark)	traces	82
7	0	White LED instead of Blue LED	49	0

Standard reaction conditions: **208a** (0.20 mmol), K$_2$CO$_3$ (0.20 eq., 0.04 mmol), NCS (3.0 eq., 0.60 mmol) Ru(bpy)$_3$(PF$_6$)$_2$ (5 mol%, 0.01 mmol), anhydrous PhCH$_3$ (3 mL), anhydrous HCO$_2$CH$_3$ (1 mL) under irradiation with 456 nm light source – blue light. Yield determined after 2 repetitions with ^{1}H-NMR using dichloroethane and nitromethane as internal standards.

Both the base and the chlorinating agent were necessary for the reaction to occur, and no conversion of the starting material **208a** was observed whether one of this two reagents was absent (entry 2 and 3). Moreover, the role of the catalyst seemed to be important but not indispensable. Indeed, the formation of the desired product was observed under irradiation even in the absence of the PC, but the reaction proceeded slowly and with uncomplete conversion of the starting allene **208a** or its *N*-chlorinated analogue **208a-Cl** (entry 4). Thus, we concluded that the catalyst improved or at least accelerated the reaction process.

Besides, the presence of water was tolerated, despite an important decrease in yield was observed (entry 5). The experiment repeated in the absence of irradiation confirmed that a source of photons was required to observe cyclization and provided the hint that the *N*-chlorination of the substrate is not a light-dependent process (entry 6). Traces of the desired product were recovered probably due to the normal daylight irradiation during the set-up of the reaction. An additional test confirmed that even white LEDs promoted the transformation (entry 7).

Table 5.3 Thermal experiments

	208a [%]	solvent	temperature	catalyst	base	215a [%]	208a-Cl [%]
1	20	PhCH₃/HCO₂CH₃ 3:1	45°C	Ru(bpy)₃(PF₆)₂ (5% mol)	K₂CO₃ (0.20 eq.)	0	80
2	19	PhCH₃/HCO₂CH₃ 3:1	60°C	Ru(bpy)₃(PF₆)₂ (5% mol)	K₂CO₃ (0.20 eq.)	0	81
3	13	PhCH₃/HCO₂CH₃ 3:1	90°C	Ru(bpy)₃(PF₆)₂ (5% mol)	K₂CO₃ (0.20 eq.)	3	78
4	9	PhCH₃	45°C	Ru(bpy)₃(PF₆)₂ (5% mol)	K₂CO₃ (0.20 eq.)	0	91
5	9	PhCH₃	60°C	Ru(bpy)₃(PF₆)₂ (5% mol)	K₂CO₃ (0.20 eq.)	0	91
6	20	PhCH₃	90°C	Ru(bpy)₃(PF₆)₂ (5% mol)	K₂CO₃ (0.20 eq.)	7	25
7	9	PhCH₃	45°C	/	K₂CO₃ (1.0 eq.)	0	91
8	14	PhCH₃	60°C	/	K₂CO₃ (1.0 eq.)	0	86
9	27	PhCH₃	90°C	/	K₂CO₃ (1.0 eq.)	2	65

Reactions Conditions: **208a** (0.20 mmol), K₂CO₃ (0.20 eq., 0.04 mmol or 1.0 eq., 0.20 mmol), NCS (3.0 eq., 0.60 mmol) anhydrous PhCH₃ (4 mL) in a sealed 8 mL vial put in a drysin® heating plate at the desired T for 21h. Yield determined after 2 repetitions with ¹H-NMR, using dichloroethane and nitromethane as internal standards.

A possible influence of thermal heating due to lamp irradiation needed to be excluded to complete the control tests. The model reaction was repeated at 45°C, 60°C and 90°C for 21h but in the absence of light irradiation. A partial conversion of the starting material was reported only at 90°C, with the formation of the desired product **215a** in traces, thus we excluded a thermal pathway for **215a** in our conditions.

Nevertheless, the computational calculations (also in this case accomplished by Dr. Ghigo) suggested the possibility of a total polar mechanism that would be favored in a completely nonpolar solvent, as when uniquely toluene is used. The reaction was then repeated with only the base (both with 0.20 and with 1.0 eq.) and NCS (3.0 eq,) at four different temperatures (room temperature, 45°C, 60°C and 90°C) in dry toluene (Table 5.3). Traces of the desired product **215a** were found only in the 90°C batch. Also, in the 90°C batch with catalytic quantities of base the product was observed together with several unidentified byproducts.

5.2.2.3 Halogen Donor

Once we confirmed the photo-induced nature of the process, we investigated the coupling partner, namely the halogen donor. The amount of NCS and its effect on the reaction was evaluated (Table 5.4). The standard conditions with 3.0 eq ensured the best yield (entry 1), while substoichiometric quantities of chlorinating agent led to poor conversion and the reaction occurred with low yields and recovery of the starting material, most of which not *N*-chlorinated (entry 2-3). With 1.0 eq and 2.0 eq. (entry 4-5) the reaction occurs in moderate yields, although the complete conversion of the substrate is not observed.

Table 5.4 Evaluation of the influence of NCS

	208a [%]	Deviation from standard conditions	215a [%]	208a-Cl [%]	216 [%]
1	0	None	56	0	4
2	90	0.25 eq. NCS	5	0	7
3	72	0.50 eq. NCS	10	0	4
4	30	1.00 eq. NCS	41	8	8
5	29	2.00 eq. NCS	45	5	6
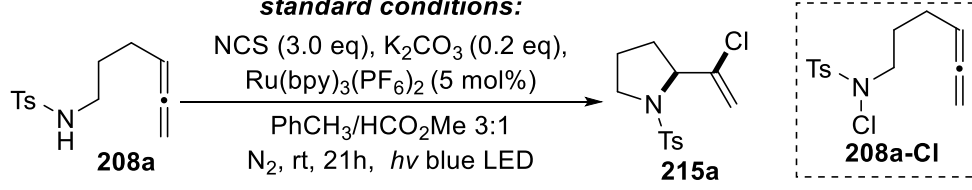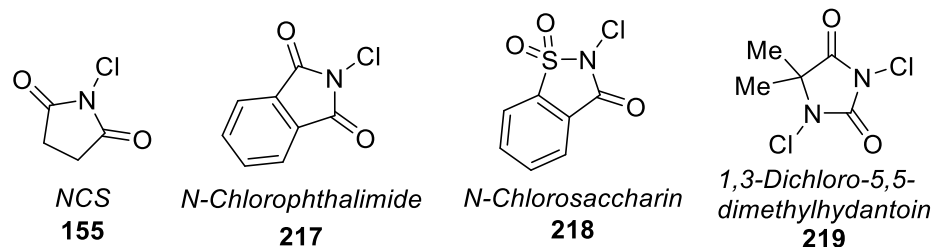
Standard reaction conditions: **208a** (0.20 mmol), K_2CO_3 (0.20 eq., 0.04 mmol), NCS (3.0 eq., 0.60 mmol) Ru(bpy)$_3$(PF$_6$)$_2$ (5 mol%, 0.01 mmol), anhydrous PhCH$_3$ (3 mL), anhydrous HCO$_2$CH$_3$ (1 mL) under irradiation with 456 nm light source – blue light. Yield determined after 2 repetitions with ^{1}H-NMR using dichloroethane and nitromethane as internal standards.

5.2.2.3.1 Chlorine Donors

Given the results obtained with the variation of the amount of NCS, we tried to enhance the yield investigating other *N*-chloramide species as halogenating agent (Table 5.5). Besides, as suggested by literature.[256,265] NaClO could also be employed under photoredox conditions as a chlorine donor. Among all the partner tested only 1,3-Dichloro-5,5-dimethylhydantoin **219** (DCDMH) gave comparable yield to the model reaction. Thus, control experiments were

conducted repeating the reaction in the dark and in the absence of the PC for this species. Differently from NCS, DCDMH provided the desired product **215a** with the same yield both with and without the PC. Moreover, no traces of starting material were recovered after 21h under irradiation, however unreacted **208a-Cl** was observed. Those data suggested that, as Lamar already observed,[259] the behavior under photocatalytic or photoredox conditions of NCS and DCDMH is different in mechanism despite yielding the same product. Albeit the commercial availability of NCS and DCDMH is comparable (also in terms of cost and toxicity), our study aimed to deepen the effect of light and/or photoredox catalysis specifically on NCS mechanism of action. Thus, findings related to DCMDH behavior are not further discussed in this dissertation.

Table 5.5 Different chlorine donors tested

standard conditions:
NCS (3.0 eq), K_2CO_3 (0.2 eq), Ru(bpy)$_3$(PF$_6$)$_2$ (5 mol%)
PhCH$_3$/HCO$_2$Me 3:1
N$_2$, rt, 21h, hv blue LED

208a → **215a** / **208a-Cl**

NCS **155** — N-Chlorophthalimide **217** — N-Chlorosaccharin **218** — 1,3-Dichloro-5,5-dimethylhydantoin **219**

	208a [%]	Deviation from standard conditions	215a [%]	208a-Cl [%]	216 [%]
1	0	None	56	0	4
2	0	3.00 eq. of **217**	41	0	7
3	0	3.00 eq. of **218**	30	0	4
4	0	3.00 eq. of DCDMH**219**	51	0	nd
5	92	3.00 eq. of NaClO (11-15% aq)	4	3	nd
6	0	3.00 eq. of DCDMH **219**; no catalyst	50	25	nd
7	91	3.00 eq. of DCDMH**219**; no irradiation (in the dark)	traces	19	nd

Standard reaction conditions: **208a** (0.20 mmol), K$_2$CO$_3$ (0.20 eq., 0.04 mmol), Chlorinating agent (3.0 eq., 0.60 mmol) Ru(bpy)$_3$(PF$_6$)$_2$ (5 mol%, 0.01 mmol), anhydrous PhCH$_3$ (3 mL), anhydrous HCO$_2$CH$_3$ (1 mL) under irradiation with 456 nm light source – blue light. Yield determined after 2 repetitions with ^{1}H-NMR using dichloroethane and nitromethane as internal standards.

5.2.2.3.2 *N*-halo succinimides

Table 5.6 Reactions with other *N*-halosuccinimides

standard conditions:
NXS (3.0 eq), K$_2$CO$_3$ (0.2 eq),
Ru(bpy)$_3$(PF$_6$)$_2$ (5 mol%)
PhCH$_3$/HCO$_2$Me 3:1
N$_2$, rt, 21h, *hv* blue LED

	X =	Deviation from standard conditions	208a [%]	220-X [%]
1	*Cl*	*None*	*0*	*56*
2	Br	3.00 eq. of NBS	0	58
3	Br	3.00 eq. of NBS, no base	0	57
4	Br	3.00 eq. of NBS, no catalyst	0	55
5	Br	3.00 eq. of NBS, no irradiation (in the dark)	0	58
6	I	3.00 eq. of NIS	0	66
7	I	3.00 eq. of NIS, no base	0	65
8	I	3.00 eq. of NIS, no catalyst	0	64
9	I	3.00 eq. of NIS, no irradiation (in the dark)	0	66

Standard reaction conditions: **208a** (0.20 mmol), K$_2$CO$_3$ (0.20 eq., 0.04 mmol), NXS (3.0 eq., 0.60 mmol) Ru(bpy)$_3$(PF$_6$)$_2$ (5 mol%, 0.01 mmol), anhydrous Toluene (3 mL), anhydrous methylformate (1 mL) under irradiation with 456 nm light source − blue light. Yields determined after 2 repetitions with ^{1}H-NMR using dichloroethane and nitromethane as internal standards.

Since NCS and all the other chlorinating agents based on *N*-chloroimides functionality, albeit with different yields, furnished the desired product **215a**, we assumed that the transformation might be extended to other commercially available *N*-halo succinimides. Thus, we tested the model reaction replacing NCS with *N*-bromo-(NBS) and *N*-iodo succinimide (NIS). Discussing the aim of this project, we anticipated the difficulty of chlorine and vinyl chloride moiety incorporation when compared to the corresponding transformation with Br- and I-derivatives. Accordingly, we expected these transformations to be more accessible and they indeed occurred with higher yields. Notwithstanding the control experiments (reactions repeated in the absence of PC, light irradiation, and base) all gave the same yields establishing the not photocatalytic nature of the process for NBS and NIS.

5.2.2.4 Coupling partners

Based on the assumption that the reaction with NCS was driven by the formation of NCR, we studied similar transformations in which an unsaturated moiety could serve both as the cyclization and the functionalization site. Given the paramount efforts of Leonori and coworkers in photoredox-generated NCR, we assumed that their findings about the imino-functionalization of olephins might provide guidance.[277] To prevent disadvantageous SET quenching between the PC* and the coupling partner **X-Y** (instead of the substrate) and an electronic mismatch between the generated species **Y•** (that is an electrophilic radical species) and **PC•+** resulting from oxidative quenching of the **PC*** and the *N*-oxime, they re-designed the starting oxime.
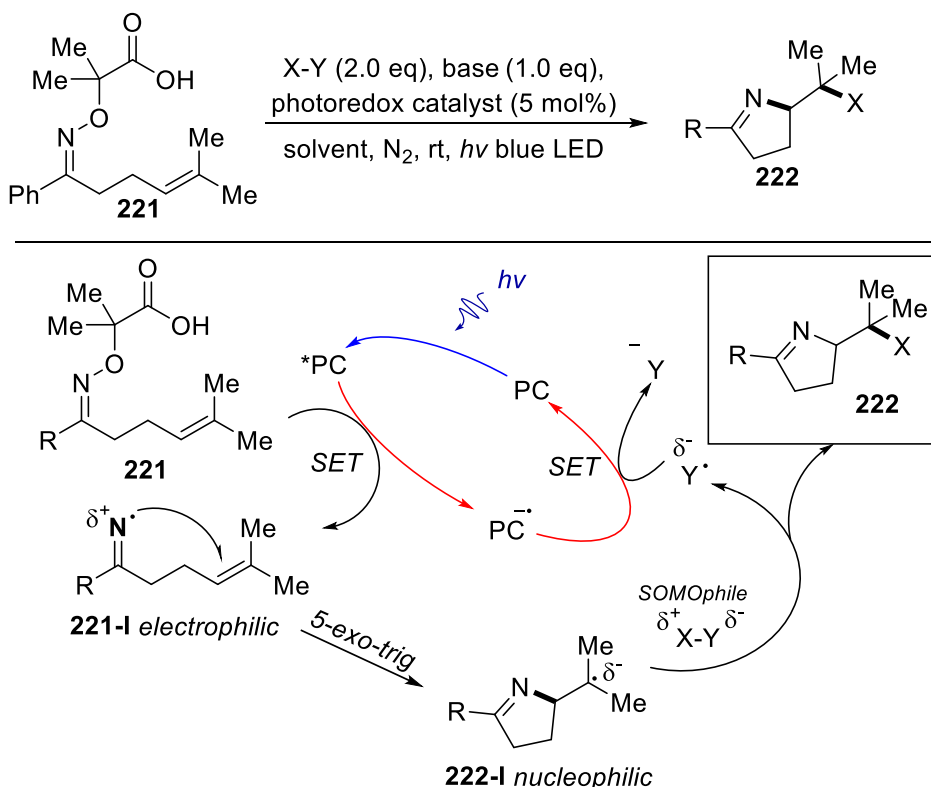
Scheme 5.23 Mechanism of photoredox imino-functionalization of olephins by Leonori[277]

---

[277] Davies, J.; Sheikh, N. S.; Leonori, D. *Angew. Chem. Int. Ed.* **2017,** *56*, 13361-13365.

Indeed, the typical NCR deriving from *N*-aryloxime results from a photoredox cycle starting where the oxidative quenching of **PC*** and the concomitant reductive SET of the oxime substrate provides NCR. The use of carboxylate-bearing alkyloximes **221** delivers the NCR **221-I** instead *via* reductive quenching of **PC***(and corresponding oxidative SET of the substrate). **221-I** spontaneously undergoes *5-exo-trig* cyclization with formation of **222-I** and the correct choice of a SOMOphile **X−Y** coupling partner provides the functionalization of **222-I** with the release of the product **222** and of the radical **Y•** that becomes the crucial species to regenerate the ground state upon the reduction to **Y⁻** in the turnover step (Scheme 5.23).

Since this transformation gave an olefin chloroamination in the presence of an excess of NCS and a base, we thought that it might be similar in mechanism to our reaction with the allene **208a** and the formation of **215a**. Moreover, the author successfully isolated an iodinated product employing NIS, but the brominated analogue was obtained using diethylbromomalonate **224** (instead of NBS). Thus, to extend the scope of our transformation, and postulating an analogy with this transformation, we tested diethyl bromomalonate **224**, (phenylthio)isoindoline-1,3-dione **225**, trimethylsilylethynyl IBX-derivative **226** employed by the authors and some typical HAT reagent like γ-Terpinene **227** and tributyltin hydride **228** as coupling partners instead of NCS (Scheme 5.24).
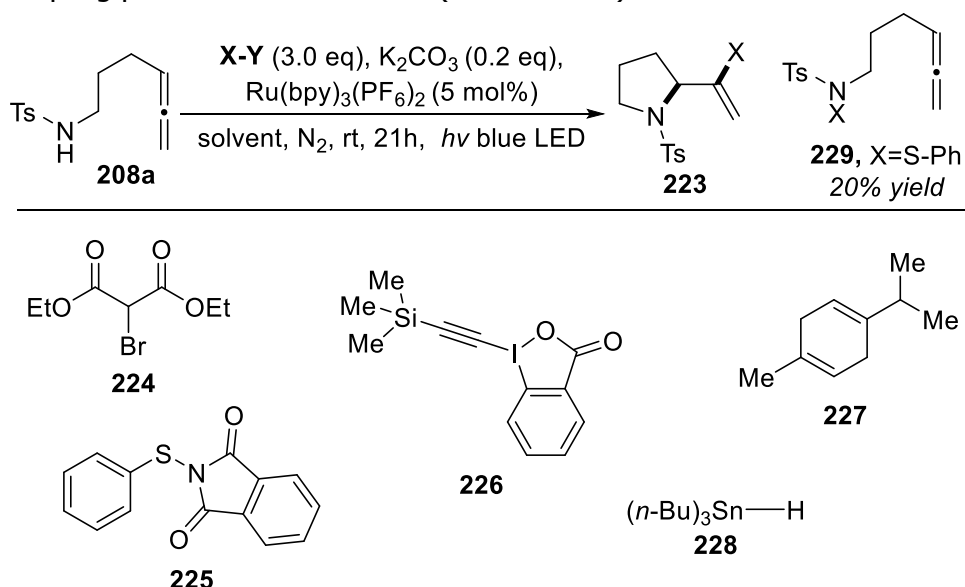
Scheme 5.24 Summary of coupling partners tested

However, none of the attempts proved successful and no reaction was observed. Only in one case, when X-Y was the thiophenol derivative **225**, a 20% yield of the corresponding *N*-phenylthioderivative **229** was recovered together with unreacted allene **208a**.

5.2.3 Mechanism investigation

Since our assumption were disproved by the experimental evidence and only the combination of NCS and base provided the cyclization and functionalization of the allene, we started the rationalization of such transformation.

5.2.3.1 NMR monitoring

First, we investigated the difference between the nature of the process involving NCS in comparison to the other *N*-halosuccinimide (NBS, NIS). We hypothesized that three main reactants deriving from the substrate might be involved, the allene starting material **208a** itself, the putative anionic species formed upon deprotonation by the base **208a-A** (obtained treating allene with NaH) and the *N*-chlorinated amide **208a-Cl** (obtained upon chlorination with NaClO). We compared the chemical shift of these three species (Figure 5.3) and used them as a reference to the study with ^{1}H-NMR monitoring the evolution of the reaction components when they are not subjected to irradiation Since the photocatalytic process led to complete conversion also in CHCl$_3$, we studied the transformation in CDCl$_3$. Test tube solutions were prepared replicating the reaction conditions of molarity and equivalent ratio and the spectra were acquired every 60 minutes (Figure 5.4). The solution of allene **208a** and NCS **155** provided no changes but when K$_2$CO$_3$ was present (given the poor solubility, excess of base was used) we witnessed the immediate formation of **208a-Cl** and the instauration of equilibrium among the two species **208a/208a-Cl**. No chemical shifts related to **208a-A** were detectable. When the same experiment was repeated with allene **208a** and NBS, the immediate formation of the corresponding bromovinylpyrrolidine was observed, and the allene was not converted to the corresponding *N*-brominated intermediate (the broad singlet of N-H proton is still observed). Conversion to the final pyrrolidine **220-Br** was accomplished after 1 h, confirming that the process is totally polar, and no irradiation or intermediate *N*-haloamidic species formation is required with the more reactive NBS (Figure 5.4).
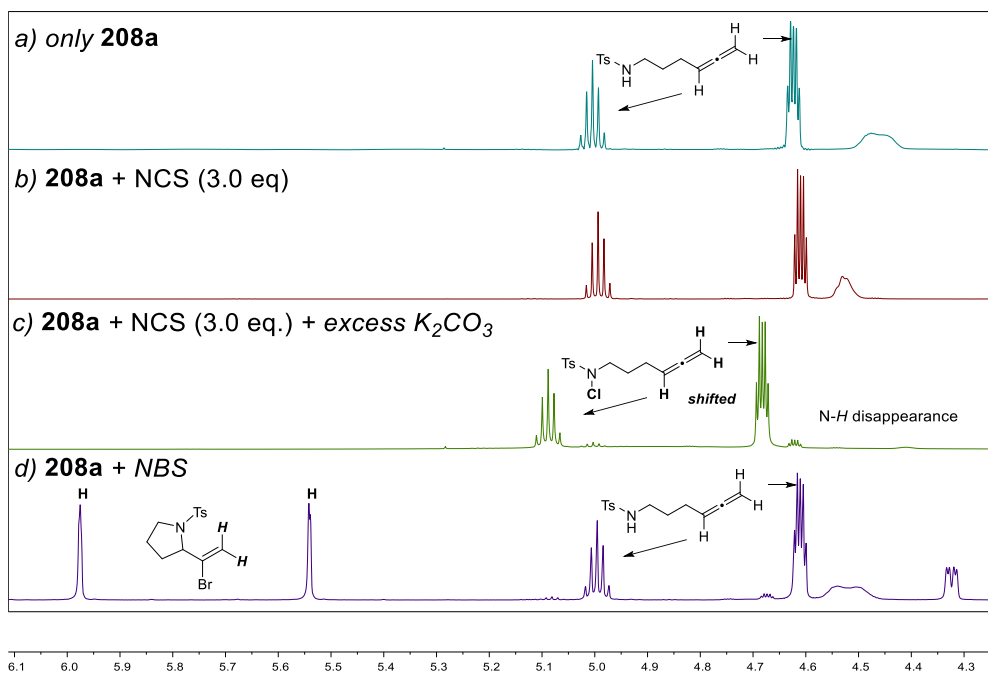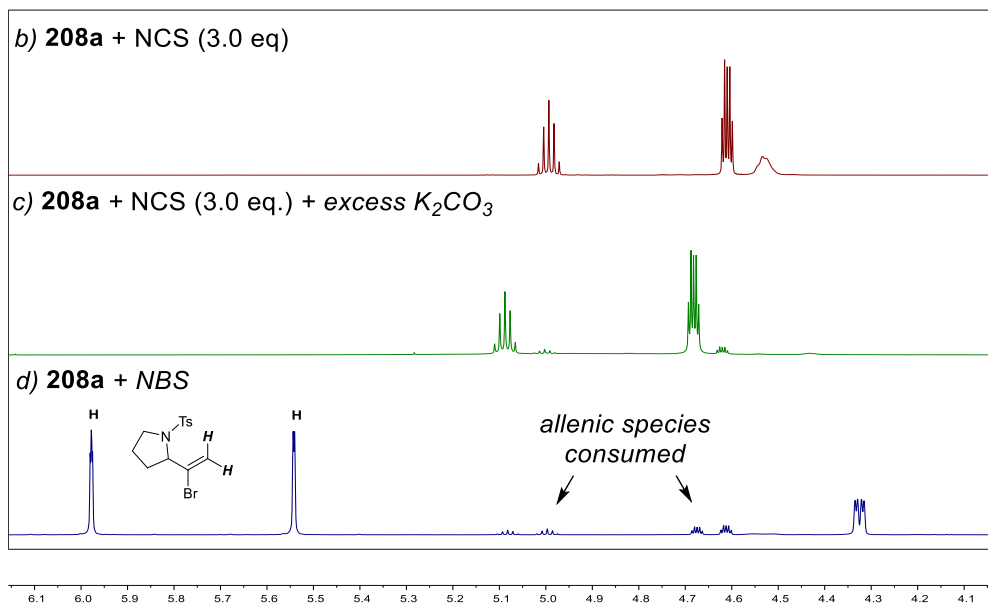
Figure 5.4 Details of stacked ^{1}H-NMR spectra of reactant mixtures in CDCl$_3$. Solutions preparation: in 750 µL of CDCl$_3$: allene **208a** [0.05 M], NXS (when present) [0.15 M], K$_2$CO$_3$ (when present: excess of 14 mg 0.100 mmol added as solid to the tube due to poor solubility in CDCl$_3$).

On the other hand, the mixture of allene **208a**, NCS **155** an K_2CO_3 was continuously monitored every 60 minutes for 6 hours but no signals ascribable to the product **215a** originated (Figure 5.4).

These findings confirmed that the NCS-based transformation is associated with the equilibrium between **208a** and the *in situ* formed **208a-Cl** which can be originated only under basic conditions. Besides, no evolution towards the final product is detected without light irradiation.

5.2.3.2 ON/OFF Experiments
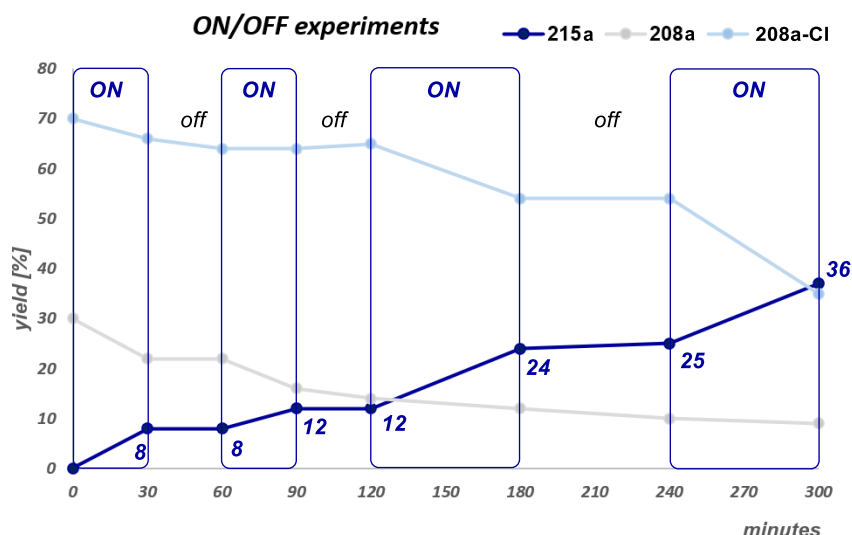
Figure 5.5 Chart summarizing the ON/OFF experiments. Yields determined by ^{1}H-NMR analysis using dichloroethane as internal standard

To prove the conclusion of NMR monitoring and demonstrate the fundamental role of the light irradiation to promote the product formation, we performed some ON/OFF experiments. The reaction mixture under stirring was subjected to light/dark cycles of variable time length and the resulting chart (Figure 5.5) demonstrated the proceeding of the reaction exclusively under continuous irradiation. Moreover, an equilibrium between **208a** and **208a-Cl** is established by the reaction conditions. Blue light seemed not to affect it, however irradiation results in consumption of allene (sum of the two species **208a** and **208a-Cl**) to provide **215a**.

5.2.3.3 Fluorescence quenching and Stern-Volmer experiments

Empirical evidence gathered so far confirmed the essential role of light in promoting the transformation, but also raised some doubts about the photoredox nature of the process. Stern-Volmer experiment were conducted using **208a**, **208a-Cl**, **208a-A**, and NCS **155** as the quenchers to identify a possible quencher of the photoexcited state of $Ru(bpy)_3(PF_6)_2$. Given the difficulty of replication of our reaction conditions in the fluorimeter cell, due to uncomplete solubility, the analyses were carried out in acetonitrile, since, complete conversion and modest yield of the product were recovered also with this more polar solvent, as reported in Table 5.1.
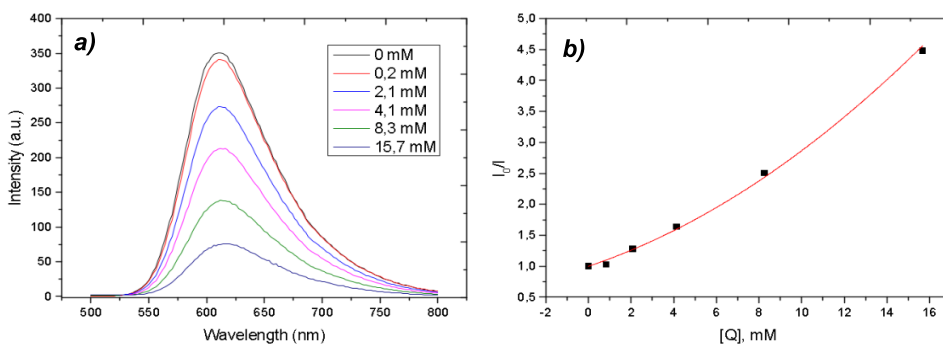
Figure 5.6 a) Fluorescence spectra of a 50μM solution of $Ru(bpy)_3(PF_6)_2$in the presence of different concentrations of allene sodium salt **208a-A** b) Stern–Volmer plot for the $[Ru(bpy)_3]^{2+}$ luminescence quenching in the presence of allene sodium salt **208a-A.**

NCS is not able to work as a quencher (as already demonstrated by Koenig and Lamar) and even when K_2CO_3 was added to the batch and the measure repeated attempting to replicate the reaction conditions, no quenching was reported. Thus, an electrophilic amplification promoted by SET from the PC* could be excluded. As expected, the starting allene **208a** proved not to be a quencher, whereas anionic **208a-A**, similarly as what observed in Chapter 3 for hydrazones, is a quencher of the PC* (Figure 5.6a). Thus, we assumed that **208a-A** can be oxidized to the corresponding NCR. Finally, differently from the study by Wu and coworkers (Scheme 5.13),[265] the *N*-chlorinated sulfonamide **208a-Cl** is not a quencher of the excited state of the PC in our case. Consequently, the **208a-Cl** species formed *in situ* that seems to promote our transformation might provide the corresponding NCR with a different mechanism, probably not photoredox mediated. Nevertheless,

contribution of the anion **208a-A** to the reaction mechanism as the active species in a photoredox process could not be excluded.

5.2.3.4 Radical Trapping Experiment

To confirm the formation of radical intermediates both TEMPO radical and BHT (3,5-di-tert-butyl-4-hydroxytoluene) were employed, adding 3.0 eq of scavenger to the reaction mixture, furnishing mixed results. Indeed, TEMPO radical partially suppressed the reactive process, and product **215a** was obtained in 15% yields, whereas unreacted starting material **208a** was recovered in 30-35% yield. Interestingly, after the workup of the reaction, the crude did not show any trace of *N*-chlorinated species **208a-Cl**. The experiment was repeated also with **208a-A** and **208a-Cl** as the starting materials and only poor yield of the product was observed (10-16% yield) while unreacted **208a** was recovered. Despite the starting materials being the sodium salt **208a-A** or the chlorinated species **208a-Cl**, even in this case no traces of other allene signals different from those belongings to the protonated **208a** were observed. In all experiments with TEMPO, no formation of adduct with the latter and a radical intermediate of the process was observed. On the other hand, when BHT was employed, the reaction was not influenced by its presence, and the product **215a** was recovered with the usual yield of 56% after the complete conversion of the substrate **208a**. These findings are not resolutive to confirm a radical pathway. They might suggest a pathway with an initial intramolecular radical process evolving towards a final intermolecular polar functionalization.

5.2.3.5 Empirical Identification of the reacting allene intermediate

The three species identified as possible reactant **208a**, **208a-Cl** and **208a-A** were then tested in different experimental conditions, trying to replicate the 56% yield of product **215a** of the model reaction.
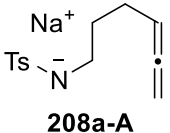
Given the results of Stern-Volmer Plot, we started with the study of the anionic species **208a-A** (Table 5.7). It might be an intermediate of the process since the reaction repeated in the standard conditions with **208a-A** instead of **208a** resulted in no loss in yield (entry 1, Table 5.7). However, even in this case, the presence of the catalyst is necessary to achieve a complete conversion (complete disappearance of every signal related to each of the three allene species **208a**, **208a-A**, and **208a-Cl**) of the starting material (entry 2-3, Table 5.7). In partial agreement with fluorescence quenching experiments, we assumed that part of the product is generated

via pathways starting upon PC* quenching by the anion **208a-A**. Both NCS and the base are mandatory for the reaction to occur, otherwise **208a-A** returned the protonated allene **208a** at the end of the irradiation (entry 4, Table 5.7). Since an already deprotonated species is used, the base is not necessary to provide the final product **215a**, albeit unconverted **208a-Cl** was recovered (entry 5, Table 5.7). The light is necessary to trigger the reactive process even starting from such anionic species, otherwise no transformation is observed, and all the anion **208a-A** is converted to the chlorinated **208a-Cl** (entry 6, Table 5.7). From these findings it was concluded that deprotonated allene **208a-A** might undergo two fates: either being chlorinated by NCS and converted to **208a-Cl** or quench the PC* to deliver the NCR intermediate that provided **215a**.
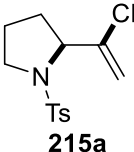
Table 5.7 Analysis of reactivity of **208a-A**
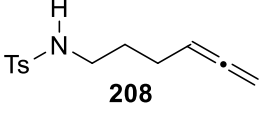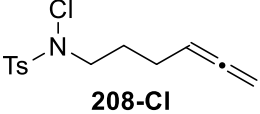
	208a-A [%]	Deviation from standard conditions	215a [%]	208a-Cl [%]	208a [%]
1	0	None	56	0	0
2	0	no catalyst	13	72	8
3	0	no base, no catalyst	13	70	6
4	0	no base, no NCS	0	0	100
5	0	no base	45	10	0
6	0	no base, no irradiation(in the dark)	0	100	0

Standard reaction conditions: **208a-A** (0.20 mmol), K_2CO_3 (0.20 eq., 0.04 mmol), NCS (3.0 eq., 0.60 mmol) Ru(bpy)$_3$(PF$_6$)$_2$ (5 mol%, 0.01 mmol), anhydrous PhCH$_3$ (3 mL), anhydrous HCO$_2$CH$_3$ (1 mL) under irradiation with 456 nm light source – blue light. Yield determined after 2 repetitions with ^{1}H-NMR using dichloroethane and nitromethane as internal standards.

It was then crucial to understand whether conversion to **208a-Cl** collateral or desirable effect was, since both literature and some experimental data evoked the *N*-chlorinated **208a-Cl** as the reactive species, thus we performed a similar investigation for the latter (Table 5.8).

Table 5.8 Analysis of reactivity of **208a-Cl**

standard conditions:
NCS (3.0 eq), K₂CO₃ (0.2 eq), Ru(bpy)₃(PF₆)₂ (5 mol%), PhCH₃/HCO₂CH₃ 3:1, N₂, rt, 21h, *hv* blue LED

	208a-Cl [%]	Deviation from standard conditions	215a [%]	208a [%]
1	0	None	56	0
2	0	no catalyst	55	0
3	25	no base, no NCS	25	0
4	19	no base, no NCS, no catalyst	45	0
5	0	irradiation with Kessil Purple Light no base, no NCS, no catalyst	32	0
6	24	irradiation with Kessil Blue 440 nm Light (NO UV tail), no base, no NCS, no catalyst	39	0
7	100	no base, no NCS, no irradiation (in the dark)	0	0
8	0	NCS (2.0 eq), no base, no catalyst	40	0
9	23	no NCS, no catalyst	26	16

Standard reaction conditions: **208a-Cl** (0.20 mmol), K₂CO₃ (0.20 eq., 0.04 mmol), NCS (3.0 eq., 0.60 mmol) Ru(bpy)₃(PF₆)₂ (5 mol%, 0.01 mmol), anhydrous toluene (3 mL), anhydrous methylformate (1 mL) under irradiation with 456 nm light source – blue light. Yield determined after 2 repetitions with ¹H-NMR using dichloroethane and nitromethane as internal standards

First, we reacted **208a-Cl** in the standard conditions and no deviation in yield from model reaction was observed (entry 1, Table 5.8). Surprisingly, the same result was obtained in the absence of the catalyst (entry 2, Table 5.8). Moreover, the reaction repeated with the catalyst but without base and NCS gave poor yield and uncomplete conversion (entry 3, Table 5.8). Thus, we assumed that **208a-Cl** was the actual reactive species in a not photoredox catalyzed process and we tested this possibility. Our hypothesis was that the homolysis of *N*-Cl bond of the chlorosulfonamide **208a-Cl** upon light absorption might provide both the reactive NCR species and the Cl atom source for the functionalization of the allene **208**. Indeed, Alexanian's research group has dedicated to the development of *N*-chloroamides **230** as reagents for site-selective C–H chlorination upon visible light cleavage of the N-Cl bond.[278,279] All the reported transformations proceeded with simple

---

[278] Quinn, R. K.; Könst, Z. A.; Michalak, S. E.; Schmidt, Y.; Szklarski, A. R.; Flores, A. R.; Nam, S.; Horne, D. A.; Vanderwal, C. D.; Alexanian, E. J. *J. Am. Chem. Soc.* **2016,** *138*, 696-702.
[279] Carestia, A. M.; Ravelli, D.; Alexanian, E. J. *Chem. Sci.* **2018,** *9*, 5360-5365.

irradiation (sometimes even light household irradiation) and PC was not required. Besides, in a recent report the authors investigated variations to the model *N*-chloroamide **230**, and a sulfonamidyl derivative **231** proved to be efficient for intermolecular chlorination (Scheme 5.25).[280]

Study on selective chlorination of alkanes applied to the synthesis of Chlorolissoclimide:

233 → **234**

230 (2.0 eq.)
Cs$_2$CO$_3$ (1.0 eq.)
PhH, 55°C, visible light,

235 + 1.0 equiv reagent

radical chlorination (thermal)
10 mol% BPO, Cs$_2$CO$_3$ (0.5 eq.)
PhCF$_3$, 65°C

→ **236**

N-chloroamides reagents

230, *75% yield*   **231**, *53% yield*   **232**, *32% yield*
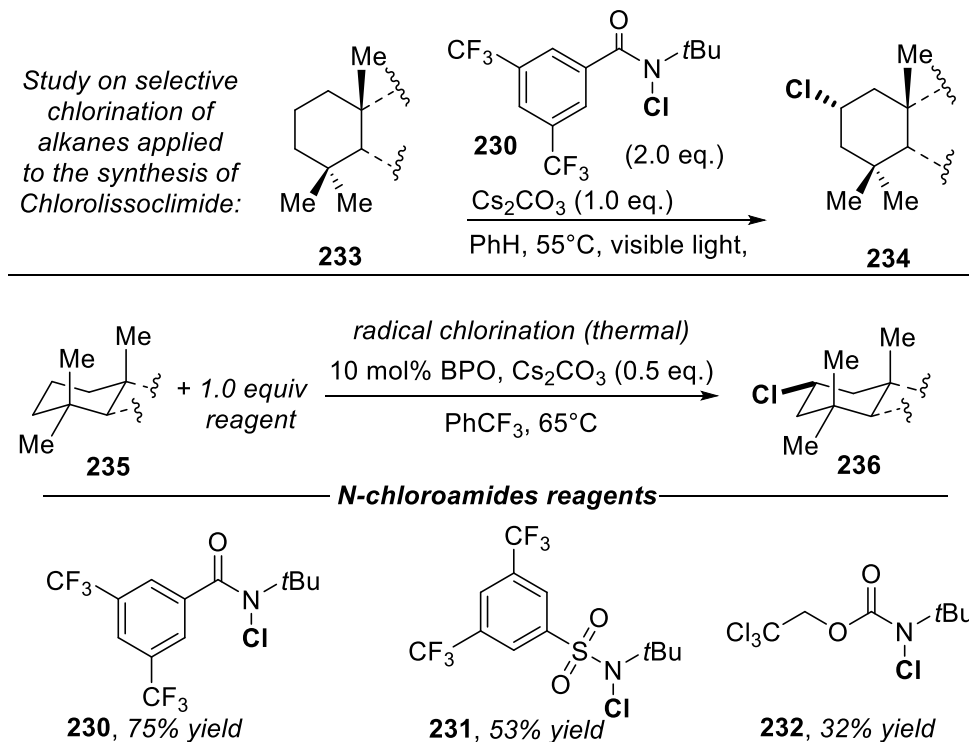
Scheme 5.25 Summary of selective chlorination using *N*-chloroamides **230-232** studied by Alexanian and co-workers[278-280]

The removal of every reactant except for the allene **208a-Cl** and the photons from light provided the final product **215a** in moderate yield (45%, entry 4, Table 5.8).

The light alone seemed sufficient to trigger the transformation, but incomplete conversion was still observed, suggesting a deficiency in recreating the conditions of the model reaction. Initially, we believe this might could be ascribable to the light source. Our light source employed so far was a A160WE Kessil Blue Lamp, with a maximum of emission at 460 nm but possessing a weak tail in the UV-A region (390 nm). UV-Vis absorption experiments confirmed that the chlorinated specie **208a-Cl** absorbs in the

---

[280] Tierney, M. M.; Crespi, S.; Ravelli, D.; Alexanian, E. J. *J. Org. Chem.* **2019,** *84*, 12983-12991.

UV region, consequently we repeated the reaction removing every reactant and using a Kessil Purple Lamp PR160. This lamp emits with a maximum centered at 390 nm with a wide range of the peak superimposing the UV region. Thus, we anticipated that such better overlap with the reactant would provide enhancement in yields. Despite the complete conversion observed, the purple lamp also led to partial degradation of either the substrate **208a-Cl** or the product **215a**, since only 32% yield was achieved (entry 5, Table **5.8**). A complementary experiment with a Kessil Blue Lamp PR160 (maximum 440 nm) which emits without residual UV tail, furnished higher yield (39%, entry 6, Table 5.8) but still uncomplete conversion. Consequently, we deduced that the actual missing factor enhancing the conversion rate is an additional source of chloride besides that coming from the reagent. Indeed, repeating the reaction with the A160WE Kessil Blue Lamp adding 2.0 equivalents of NCS provided a complete conversion of the starting material (49% yield, entry 8, Table 5.8). Repeating the reaction without NCS and catalyst to avoid complete conversion and adding the base allowed to observe the restoration of the equilibrium between **208a** and **208a-Cl** as witnessed by the recovery of the species **208a** (entry 9, Table 5.8).

The *N*-chlorinated amine **208a-Cl** appeared as a reactive species and not an interfering byproduct, but the role of PC in enhancing the yield was still elusive. Therefore, a final study was conducted to understand the role of the base in determining the equilibrium between **208a**, **208a-Cl** and **208a-A**. To test whether a complete conversion of **208a** in **208a-Cl** without residual equilibrium would provide the product **215a** using only light and avoiding photoredox conditions we explore further variations of the base in the absence of the catalyst (Table 5.9).
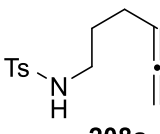
Stoichiometric and excess (1.90 eq.) loading of both inorganic bases and more soluble (in toluene) organic bases were considered, excluding the Ru salt from the reaction mixture. Only organic bases (entry 6-7, Table 5.9) or strong inorganic bases (entry 3, Table 5.9) provided complete conversion. Nevertheless, the product yield observed were always lower than the one of model reaction in standard conditions. This forced exclusion of the putative parallel photoredox-mediated pathway always resulted in diminished yields.

In conclusion, we confirmed that an excess of chlorinating reagent is required both to produce *in situ* **208a-Cl** (which is a reactive species in the process) and to provide a reagent for the chlorination of the resulting heterocycle **215a**. This *N*-chlorinated sulfonamide **208a-Cl** reacts due to light irradiation

but probably not mainly because of photoredox conditions. Nevertheless, a small enhancement in yield is probably due to a collateral photoredox process that involves the starting allene **208a** and its deprotonated species **208a-A**.
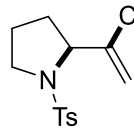
Table 5.9 Investigation of the role of the base
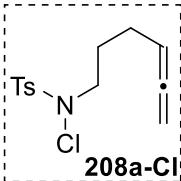
	208a [%]	Deviation from standard conditions	215a [%]	208a-Cl [%]
1	0	None	56	0
2	10	K₂CO₃ (1.00 eq.), no catalyst	10	68
3	0	KOH (1.00 eq.), no catalyst	28	0
5	8	K₂CO₃ (1.90 eq.), no catalyst	22	52
6	0	Pyridine (1.90 eq.), no catalyst	26	0
7	0	Lutidine (1.90 eq.), no catalyst	40	0

Standard reaction conditions: **208a** (0.20 mmol), K₂CO₃ (0.20 eq., 0.04 mmol), NCS (3.0 eq., 0.60 mmol) Ru(bpy)₃(PF₆)₂ (5 mol%, 0.01 mmol), anhydrous toluene (3 mL), anhydrous methylformate (1 mL) under irradiation with 456 nm light source – blue light. Yield determined after 2 repetitions with ¹H-NMR using dichloroethane and nitromethane as internal standards

5.2.3.6 Mechanism preliminary hypothesis

A preliminary hypothesis of mechanism was formulated based on the data collected by mechanistic investigations. Allene **208a** is subjected, under reaction conditions, to an equilibrium involving its transient anionic form **208a-A** and the *N*-chlorinated species **208a-Cl** derived from the consequent reaction of the deprotonated species with NCS. A main possible pathway involves the photolysis of N-Cl bond of **208a-Cl**, which delivers the NCR **208a-I** undergoing *5-exo-trig* cyclization and generation of the vinyl radical **215a-I**. Suggestion of the existence of such radical could not be witnessed by direct coupling with TEMPO, however the formation of byproduct **216** is justified only by a radical attack of the carbon radical to the tosyl moiety. 1,5-HAT is impeded; however, it might represent an alternative in longer allenes leading to collateral reactions. The allyl radical **215a-I** might then trap a chlorine atom from NCS (with release of a succinimidyl radical **155-II**) or by direct coupling with a •Cl from photolysis achieving the desired product.
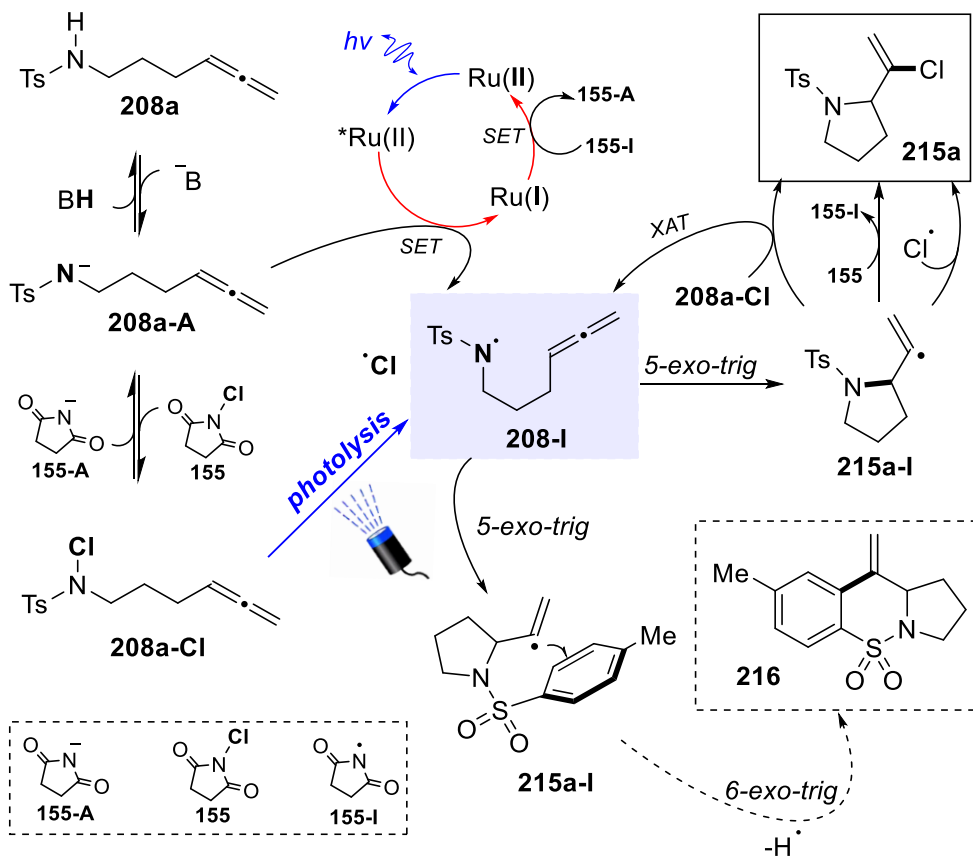
Scheme 5.26 Preliminary mechanism hypothesis

Besides, as proposed by Wu[265] and studied by Alexanian,[278-280] the *N*-chlorinated species **208a-Cl** might serve itself as a chlorinating agent. Indeed, DFT calculation by Dr. Ghigo confirmed that the vinyl radical might extract a chlorine atom more easily from this latter then from NCS. Alternatively, a parallel mechanism confirmed by DFT calculation might lead to **208a-I** *via the* reductive quenching of *Ru(II) by anion **208a-A**. The turnover step regenerating the catalyst might be operated by succinimidyl radical **155-II** reduction to the corresponding anion. However, DFT analysis are still progressing to entirely justify the mechanism, so these are just preliminary hypotheses (Scheme 5.26).

5.2.4 Preliminary scope investigation
Once all the experimental data providing insights into the mechanism were collected, computation analyses were started by Dr. Ghigo to solve the

remaining points of contention. In the meanwhile, given the awareness of the limitations of the transformation (only chlorination products provided uniquely by NCS) an exploration of the scope potentialities of our protocol was attempted (Table 5.10).

Table 5.10 Preliminary scope of the synthesis of **215a**

215a: 56%

215b: 20%

215c: 52%

215d: 30%

215e: 52%

215f: 51%

215g: 40%[d]

215h: 54%
only one isomer found

215j: 48%
isomer ratio 5:1

215k: 44%
isomer ratio 4:1
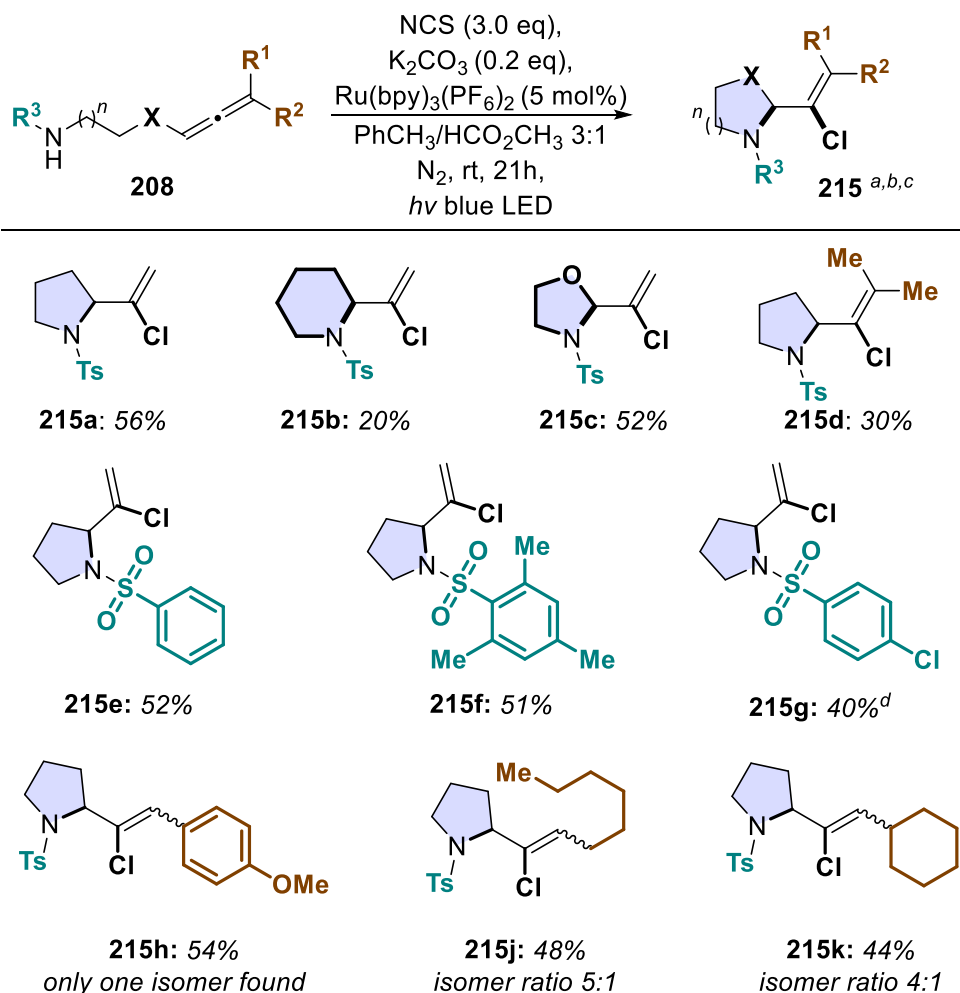
a) Reaction conditions: allene **208a** 0.2 mmol, K_2CO_3 0.04 mmol, NCS 0.60 mmol, Ru(bpy)$_3$(PF$_6$)$_2$ 0.01 mmol, anhydrous toluene (3 mL), anhydrous methylformate (1 mL), 40W blue lamp, 16 h, inert atm.; b) Yields determined on isolated product; c) analysis for E/Z are still ongoing; d) 32h reaction time.

A preliminary investigation considered variations in the ring size and in the characteristic of the cycle obtained: three- and four-membered rings seemed

to be inaccessible, whereas 6-membered piperidine **215b** could be obtained in low yield. We imputed this poor results due to competing pathways arising from 1,5-HAT (possible for alkyl chains with 5 methylenic units) as witnessed by the total degradation of unreactive 8-carbon allene (synthetized attempting to achieve 7 membered cycle). Variations in the atoms of the linear chain were also considered: installation of a γ-oxygen did not affect the yield and oxazolidine **215c** was obtained in 52% yield. Then we explored the effect of the arene moiety. Different arylsulfonylamides were tested and yields were comparable to that of the model reaction (e.g. **215e** and **215f**) although deactivated 4-chlorosulfonylamide needed longer reaction time and provided **215g** in moderately lower yield (40%). Finally, envisaging a new synthetic protocol towards tri- or tetra-substituted chloro-olefins, we examined the reaction of internal allenes. The tetrasubstituted product **215d** was isolated in lower yield, probably because of the increased hindrance factor, while preliminary analysis of the reactivity achieving trisubstituted alkenes **215h-k** showed a general tolerance for aliphatic (both linear and cyclic) and aromatic substituents. A general preference for one of the two possible geometric isomers is observed, with major isomer presence of about 75-80%. Attribution of *E* or *Z* geometry of such predominant product is still under analysis.

5.2.5 Conclusions

In this chapter, a new reactivity of sulfonylamides bearing a lateral chain functionalized with an allene moiety has been studied. The use of visible light disclosed access to chlorovinyl nitrogen heterocycles in moderate yield *via* C-N and C-C bond formation. The main radical process involved, seemed not to be photoredox mediated. However, the loading of a PC enhanced the yield and provided higher conversion rate of the transformation. Importantly, it was demonstrated that, differently from more reactive analogous NBS and NIS, the halogenations using NCS cannot be observed under common thermal conditions, while blue light disclosed this pathway. Finally, the importance of allenes as the starting material has been highlighted since their treatment under irradiation could provide access to various tri- and tetra-substituted chlorolefins with an attached *N*-heterocycle.

CHAPTER SIX:

ॐ
हिन्दी
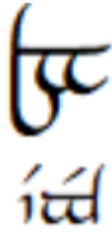
EXPERIMENTAL SECTION

CHAPTER 6 – Experimental section

6.1 Materials and methods

Flasks and all equipment used for the generation and reaction of moisture-sensitive compounds were dried by electric heat gun under vacuum and back filled with N_2, then used under N_2 atmosphere.

All commercially available reagents and solvents were used as received. Anhydrous solvents were purchased by Sigma-Aldrich or distilled as indicated by Armarego.[281] ZnI, NaI, aldehydes and NCS were purified as indicated by Armarego.[281]

Products were purified by preparative column chromatography on Sigma-Aldrich silica-gel for flash chromatography, 0.04–0.063 mm/230–400 mesh. Reactions were monitored by TLC using silica-gel on TLC-PET foils Sigma-Aldrich, 2–25 μm, layer thickness 0.2 mm, medium pore diameter 60 Å.

NMR spectra were recorded employing a Jeol ECZR instrument. ^{1}H NMR spectra were recorded in $CDCl_3$ or DMSO-d^6 at 600 MHz. ^{13}C NMR spectra were recorded in $CDCl_3$ at 150 MHz. Chemical shifts were reported in ppm relative to the resonance of $CHCl_3$ (δ= 7.26) for ^{1}H NMR, or referred to the central peak of $CDCl_3$ (δ= 77.0) for ^{13}C NMR. ^{13}C NMR spectra were measured with complete proton decoupling. DEPT experiments were carried out with a DEPT-135 sequence.

UV–vis spectra were carried out with a Varian Cary "100 Scan" spectrophotometer. The extinctions were measured on freshly prepared and previously N_2 sparged solutions. Optical path length: 1 cm. The solutions were stable during the timescales necessary for the measurements, and the results of repeated measures were reproducible.

Fluorescence emission spectra were collected with a Cary Eclipse Fluorescence Spectrophotometer, with excitation at 415 and 450 nm. Excitation and emission slits set both at 5 nm. Spectra were taken in a fluorescence fused silica cuvette with 1 cm optical path length.

IR spectra were recorded on a BrukerVertex 70 FT-IR.

The electrochemical measurements were performed using a standard photo-electrochemical setup, composed of a computer-controlled potentiostat, AUTOLAB PGSTAT12. The electrochemical cell was a conventional three-

---

[281] Armarego, W. L. F., *Purification of laboratory chemicals*. Butterworth-Heinemann: **2017**.

electrode cell with a 1 mm thick fused silica window. Cyclic Voltammetry (CV) was carried out in the following conditions:

- Electrodes: Pt (W), Glassy Carbon (A), Ag/AgCl/TEACl (C)
- 0.1 M Bu4NPF6 in DMF solution
- Scan Rate: 100 mV s^{-1}
- Irradiation: KESSIL LAMP 1170 W m^{-2} and λ = 456 nm
- Nitrogen Atmosphere

HRMS spectra were obtained on a mass selective detector Agilent 5970 B operating at an ionizing voltage of 70 eV connected to a HP 5890 GC equipped with a HP-1 MS capillary column (25 m length, 0.25 mm I.D., 0.33 μm film thickness). The MS flow-injection analyses were run on a high resolving power hybrid mass spectrometer (HRMS) Orbitrap Fusion (Thermo Scientific, Rodano, Italy) and a Bruker Daltonics microTOF Mass Spectrometer equipped with an h-ESI ion source. The samples were analysed in methanol or acetonitrile solution using a syringe pump at a flow rate of 10 μL/min. The tuning parameters adopted for the ESI source were as follows: source voltage 3.5 kV, RF lens 60% (positive ion mode MH$^+$, MNa$^+$); source voltage 2.5 kV, RF lens 60%. The ion transfer tube was maintained at 270 °C. The mass accuracy of the recorded ions (vs the calculated ones) was <5 ppm. Analyses were run using full MS (50-500 m/z range) acquisition, at 240 000 resolution (200 m/z).

Photochemical reactions of Chapter 3 and 4 were carried out in a cylinder-shaped photochemical reactor (40 mm as ID and 25 mm height for general procedures and reactions, 65 mm as ID and 50 mm height for gram-scale reaction). Photochemical reactions of Chapter 5 were carried out in a 10 mL Schlenk tube. A Kessil Blue Lamp was used as irradiation source, which emits a band centered at 450 nm and of about 55 nm width to half height. The irradiation source was located at 4 cm from the reaction solution surface for the cylinder shape reactor, and at 3 cm from the glass wall for the Schlenk tube.

Cristal analysis: measured by Dr. E. Priola, University of Turin, Chemistry Department. Crystal of compounds **95a** and **100** were obtained by slow precipitation from CHCl$_3$ at room temperature. Data of single crystals of compound have been collected on a Gemini R Ultra diffractometer (Agilent Technologies U.K. Ltd., Oxford, U.K.). All the data were collected using graphite monochromated Mo Kα radiation (*k* = 0.71073 Å) with the x-scan method. Cell parameters were retrieved using CrysAlisPro (Agilent

Technologies CrysAlisProSoftare system, version 1.171.35.11 Agilent Technologies U.K. Ltd., Oxford, U.K. (2012)) software, and the same program has been used for performing data reduction, with corrections for Lorenz and polarizing effects. Scaling and absorption corrections were applied by the CrysAlisPro (Agilent Technologies CrysAlisProSoftare system, version 1.171.35.11 Agilent Technologies U.K. Ltd., Oxford, U.K. (2012)) multiscan technique. All the structures were solved by direct methods using SHELXS-14[282] and refined with full-matrix least-squares method on F^2 inserted in SHELXL-14[283] using the program Olex^2.[284] All non-hydrogen atoms were anisotropically refined. Hydrogen atoms were located in the final Fourier-difference maps and refined with coordinates and U^{iso} calculated and riding on the corresponding atom. Structural illustrations have been drawn with Mercury.[285]

New compounds were fully characterized, for known compounds characterized with different procedures, the reference with full characterization is cited and only ^{1}H-NMR characterization is reported. Complete characterization of the instrumentation used for photochemical processes, emission profile of the lamps and photon flows are omitted. Same for the complete description of the X-ray analysis. For a complete report please refer to the published paper.

New compounds of Chapter 5: given the preliminary nature of the data presented concerning the scope of the reaction, some of the new compounds introduced in Chapter 5 and described in Paragraph 6.4 are characterized only by NMR spectroscopy (^{1}H, ^{13}C) and may lack HRMS and IR analysis.

[282] Sheldrick, G. *Acta Cryst.* **2008,** *64*, 112-122.
[283] Sheldrick, G. *Acta Cryst.* **2015,** *71*, 3-8.
[284] Macrae, C. F.; Bruno, I. J.; Chisholm, J. A.; Edgington, P. R.; McCabe, P.; Pidcock, E.; Rodriguez-Monge, L.; Taylor, R.; van de Streek, J.; Wood, P. A. *J. Appl. Cryst.* **2008,** *41*, 466-470.
[285] Dolomanov, O. V.; Bourhis, L. J.; Gildea, R. J.; Howard, J. A. K.; Puschmann, H. *J. Appl. Cryst.* **2009,** *42*, 339-341.

6.2 Cascade Radical Processes of γ,δ-unsaturated *N*-arylsulfonylhdyrazones: cyclization and dearomatization

6.2.1 Two steps synthesis of 6-Methyl-3-phenyl-1-tosyl-1,4,5,6-tetrahydropyridazine (87)
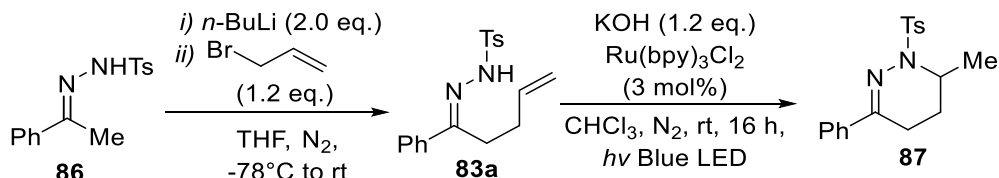
1-Phenyl-4-penten-1-one N-Tosylhydrazone (83a)
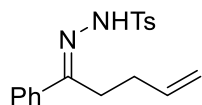
Under a N$_2$ atmosphere in a dried Schlenk bottle, acetophenone *N*-tosylhydrazone **86** (1.44 g, 5.0 mmol) was dissolved in 10 mL of THF. The resulting mixture was vigorously stirred for 5 min, cooled to −78 °C, then *n*-BuLi (2.5 M solution, 4.4 mL, 11.0 mmol) was added dropwise over 30 min. Turning of the solution from yellow to orange (after addition of 1 equiv) then from orange to red (after addition of 2 equiv of *n*-BuLi) was observed. The reaction was stirred at −78 °C for 45 min. Subsequently allyl bromide was added (0.73 g, 6.0 mmol), temperature allowed to raise and stirring maintained until complete consumption of the reactant (monitored by TLC). The reaction was then quenched with a NH$_4$Cl saturated solution (20 mL) and diluted with Et$_2$O (30 mL). The aqueous phase was extracted with CH$_2$Cl$_2$ (3 × 15 mL) then the organic phase reunited, washed with brine (30 mL), dried over Na$_2$SO$_4$, and filtered. The obtained crude was then purified by flash chromatography on silica gel (PE/EE 65/35) and subsequently crystallized from methanol to obtain 1.42 g of 1-phenyl-4-penten-1-one *N*-tosylhydrazone **83a** as cubic-shaped colorless crystals (yield 86%). A mixture of isomers was found. Spectral data are coherent with those previously reported in literature.[286] 1H NMR (600 MHz, CDCl$_3$, Me$_4$Si) δ mixture of isomers (51:49) 7.96 (s, 1H, N−*H*, isomer A), 7.95 (s, 1H, N−*H*, isomer B), 7.89 (d, *J* = 8.0 Hz, 2H, Ar−*H*, isomer A), 7.78 (d, *J* = 8.0 Hz, 2H, Ar−*H*, isomer B), 7.44 (m, 4H, Ar−*H* both isomers), 7.32 (m, 8H, Ar−*H*, both isomers), 7.06 (m, 2H, Ar−*H*, both isomers), 5.67 (*J* = 16.9, 10.2, 6.5 Hz, 1H, C*H*=CH$_2$, both

---

[286] Li, L.; Liu, P.; Su, Y.; Huang, H. *Org. Lett.* **2016,** *18*, 5736-5739.

isomers), 4.96 (dd, J = 17.4, 1.1 Hz, 1H, CH=CH_2, *H trans*, both isomers); 4.92 (dd, J = 10.7, 1.1 Hz, 1H, CH=CH_2, *H cis*, both isomers), 2.66 (t, J = 7.6 Hz, 2H, N=C(Ph)–CH_2 isomer A), 2.57 (t, J = 7.6 Hz, 2H, N=C(Ph)–CH_2 isomer B), 2.42 (s, 3H, Ar–CH_3 isomer A), 2.41 (s, 3H, Ar–CH_3 isomer B), 2.21 (m, 4H, N=C(Ph)–CH$_2$–CH_2 both isomers).

6-Methyl-3-phenyl-1-tosyl-1,4,5,6-tetrahydropyridazine (87)
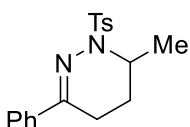
In a sealed photochemical reactor, 6.8 mg of [Ru(bpy)$_3$]Cl$_2$·6H$_2$O (0.009 mmol) were dissolved in 5 mL of anhydrous CHCl$_3$ and the solution was degassed with N$_2$ for 15 min. Then phenylprop-3-enyl-*N*-tosylhydrazone **83a** (98.5 mg, 0.300 mmol) and KOH (20.0 mg, 0.360 mmol) were added in one portion and the solution degassed for additional 10 min. The mixture was then stirred at 4 cm from the irradiation source at room temperature until reaction completion. The solution was then filtered on a short pad of silica gel using CH$_2$Cl$_2$ as eluent and Et$_2$O to wash the column. The crude product was purified by flash chromatography on silica gel (PE/EE 65/35) to obtain 24.1 mg of a greenish solid **87** (24%). ^{1}H NMR (600 MHz, CDCl$_3$, Me$_4$Si) δ 7.88 (d, J = 8.3 Hz, 2H, Ar–*H*), 7.71 (dd, J = 8.1, 1.7 Hz, 2H, Ar–*H*), 7.38–7.31 (m, 3H, Ar–*H*), 7.27 (d, J = 8.1 Hz, 2H, Ar–*H*), 4.59 (m, 1H, N–C*H*–CH$_3$), 2.61 (dt, J = 18.2, 3.4 Hz, 1H, N=C(Ph)—C(H)*H*), 2.42 (dt, J = 18.3, 10.2 Hz, 1H, N=C(Ph)—C(H)*H*), 2.38 (s, 3H, Ar–C*H$_3$*), 1.88 (dt, J = 9.3, 2.9 Hz, 2H, CH$_2$–C*H$_2$*-CH), 1.14 (d, J = 6.8 Hz, 3H, N–CH–C*H$_3$*). ^{13}CNMR (151 MHz, CDCl$_3$, Me$_4$Si) δ 147.3 (Cq), 143.6 (Cq), 137.1 (Cq), 135.4 (Cq), 129.5 (2 × CH), 129.2 (CH), 128.4 (2 × CH), 128.2 (2 × CH), 125.3 (2 × CH), 47.4 (CH), 24.4 (CH$_2$), 21.7 (CH$_3$), 18.3 (CH$_2$), 17.5 (CH$_3$). mp 142–145 °C. v_{max} (neat)/cm^{-1} 3060, 2926, 2866, 1603, 1444, 1238, 907, 839, 762, 690. HRMS (ESI) m/z [M + H]$^+$ Calcd for C$_{18}$H$_{21}$N$_2$O$_2$S 329.1318, found 329.1310.

6.2.2 General Procedure for the Synthesis of dimethyl α,β-unsaturated Ketones (92)
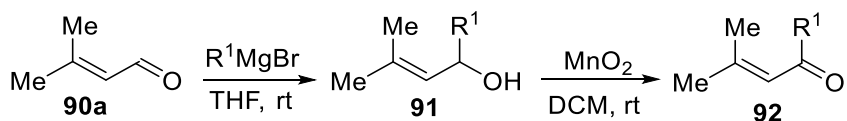
A dried three-necked round-bottom flask connected with a drip funnel and a reflux condenser was dried under N$_2$ atmosphere. Magnesium (290 mg, 12.0 mmol) and a small crystal of double sublimed Iodine was added to the flask,

covered with anhydrous THF, and vigorously stirred. A small aliquot of the solution of the appropriate aryl bromide R^1MgBr (10.0 mmol, 1 M in THF) was added, and the resulting orange mixture was stirred until a turning to gray or colorless was observed. At this point, the rest of the aryl bromide solution was added dropwise through funnel and heated to reflux for 6 h. The solution was then cooled to rt and 3-methylbut-2-enal **90a** (930 mg, 11.0 mmol, 1 M in THF) was added dropwise. Stirring was maintained until complete consumption of the aldehyde **90a** (about 2 h) then the reaction was cooled to 0 °C and quenched diluting with NH_4Cl saturated solution (30 mL) and Et_2O (30 mL). The aqueous layer was extracted with Et_2O (2 × 30 mL) and the collected organic phases were washed with brine (30 mL) and finally dried over Na_2SO_4. Filtration of the solids and removal of the volatiles under reduced pressure afforded an oil corresponding to α,β-unsaturated alcohol **91** that was then poured in a 250 mL round-bottom flask and dissolved in 150 mL of CH_2Cl_2. MnO_2 (7.00 g, 80.0 mmol) was added to the mixture in small portions every hour until complete oxidation of the alcohol **91**. The resulting mixture was filtered over a thin pad of Celite that was then washed with CH_2Cl_2 and AcOEt. The solvents were removed under reduced pressure to give an orange oil, whose purification by flash chromatography (PE/AcOEt 97.5/2.5, 1% Et_3N) afforded the desired α,β-unsaturated ketone **92** as a yellowish oil.

2-Methylprop-1-enylphenone (92a)
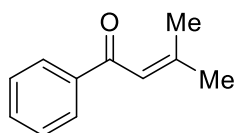
Following the described procedure, 1.59 g (10.0 mmol) of bromobenzene were reacted with magnesium and 3-methylbut-2-enal**90a**, then subsequently with MnO_2 to afford 1.04 g (6.5 mmol) of 2-methylprop-1-enylphenone (**92a**) as a yellowish oil (yield 65%). Spectral data are coherent with those reported in literature.[287] ^1H NMR (600 MHz, $CDCl_3$, Me_4Si) δ 7.96–7.90 (m, 2H, Ar*H*); 7.41–7.56 (m, 3H, Ar*H*); 6.75 (sept, *J* = 1.3 Hz, 1H, CO–C*H*); 2.21 (d, *J* = 1.3 Hz, 3H, CH=C—(C*H₃*)₂); 2.03 (d, *J* = 1.3 Hz, 3H, CH=C—(C*H₃*)₂).

---

[287] Otera, J.; Fujita, Y.; Sakuta, N.; Fujita, M.; Fukuzumi, S. *J. Org. Chem.* **1996,** *61*, 2951-2962.

2-Methylprop-1-enylnaphtone (92b)
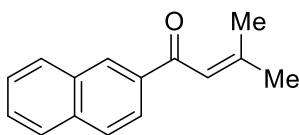
Following the described procedure, 2.05 g (10.0 mmol) of 2-bromonaphtalene were reacted with magnesium and 3-methylbut-2-enal **90a**, then subsequently with MnO$_2$ to afford 1.22 g (5.8 mmol) of 3-methyl-1-(naphthalen-2-yl)but-2-en-1-one **92b** (58%). Spectral data are coherent with those reported in literature.[288] ^{1}H NMR (600 MHz, CDCl$_3$, Me$_4$Si δ 8.43–8.40 (m, 1H, Ar–*H*); 8.03 (dd, *J* = 8.7, 1.8 Hz, 1H, Ar–*H*); 7.95 (d, *J* = 8.3 Hz, 1H, Ar–*H*); 7.87 (ddt, *J* = 7.5, 5.4, 0.7 Hz, 2H, Ar–*H*); 7.57 (t, *J* = 7.5 Hz, 1H, Ar–*H*); 7.53 (t, *J* = 7.5 Hz, 1H, Ar–*H*); 6.90 (bs, 1H, CO–C*H*); 2.26 (d, *J* = 1.3 Hz, 3H, CH=C—(C*H*$_3$)$_2$); 2.05 (d, *J* = 1.3 Hz, 3H, CH=C—(C*H*$_3$)$_2$).

2-Methylprop-1-enyl-2-pyridylketone (92c)
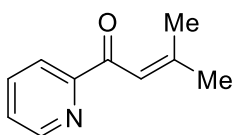
According to the described procedure, 1.57 g (10.0 mmol) of 2-bromopyridine were reacted with magnesium. Differently from the general procedure, turning from yellow to black was observed. After complete formation of the Grignard reagent, 3-methylbut-2-enal **90a** was added and the obtained crude was subsequently reacted with MnO$_2$ to afford 0.61 g of 2-methylprop-1-enyl-2-pyridylketone **92c** as a brown oil (38%). ^{1}H NMR (600 MHz, CDCl$_3$, Me$_4$Si) δ 8.66 (ddd, *J* = 4.8, 1.8, 1.0 Hz, 1H. Ar–*H*); 8.08 (dt, *J* = 7.9, 1.1 Hz, 1H, Ar–*H*); 7.83 (tt, *J* = 7.7, 1.4 Hz, 1H, Ar–*H*); 7.45 (sept, *J* = 1.3 Hz, 1H, CO–C*H*); 7.42 (ddt, *J* = 7.4, 4.8, 1.2 Hz, 1H, Ar–*H*); 2.30 (d, *J* = 1.3 Hz, 3H, CH=C—(C*H*$_3$)$_2$); 2.06 (d, *J* = 1.3 Hz, 3H, CH=C—(C*H*$_3$)$_2$). ^{13}CNMR (151 MHz; CDCl$_3$, Me$_4$Si) δ 190.22 (Cq); 159.71 (Cq); 155.35 (Cq); 148.63 (CH); 137.13 (CH); 126.46 (CH); 122.65 (CH); 119.74 (CH); 28.57 (CH$_3$); 21.51 (CH$_3$). HRMS (ESI) *m/z* [M + H]$^+$ Calcd for C$_{10}$H$_{12}$NO 162.0913, found 162.0909. IR v$_{max}$ (neat)/cm^{-1} 3082, 2960, 1688, 1639, 1583, 1353, 994.

---

[288] Harris, M. R.; Konev, M. O.; Jarvo, E. R. *J. Am. Chem. Soc.* **2014,** *136*, 7825-7828.

2-Methylprop-1-enyl-*m*-tolylketone (92d)
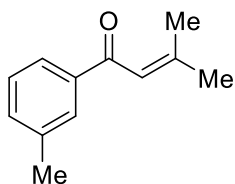
Following the described procedure, 1.70 g (10.0 mmol) of *m*-tolyl bromide were reacted with magnesium and 3-methylbut-2-enal **90a**, then subsequently with MnO_2 to afford 0.71 g of 2-methylprop-1-enyl-*m*-tolylketone **92d** as yellowish oil (41%). ^{1}H NMR (600 MHz, $CDCl_3$, Me_4Si) δ 7.73 (s, 1H, Ar*H*); 7.70 (m, 1H, Ar*H*) 7.34 (d, *J* = 1.1 Hz, 1H, Ar*H*); 7.32 (m, 1H, Ar*H*); 6.72 (quin, *J* = 1.3 Hz, 1H, CO–C*H*); 2.40 (s, 3H, Ar–C*H₃*); 2.19 (d, *J* = 1.3 Hz, 3H, CH=C—(C*H₃*)₂); 2.01 (d, *J* = 1.3 Hz, 3H, CH=C—(C*H₃*)₂). ^{13}CNMR (151 MHz; $CDCl_3$, Me_4Si) δ 191.9 (Cq); 156.4(Cq); 139.4 (Cq); 138.3 (Cq); 133.1 (CH); 128.9 (CH); 128.4 (CH); 125.5 (CH); 121.5 (CH); 28.0 (CH_3); 21.58 (CH_3); 21.2 (CH_3). HRMS (ESI) *m/z* [M + H]⁺ Calcd for $C_{12}H_{15}O$ 175.1117, found 175.1111. IR v_{max} (neat)/cm⁻¹ 3019, 2942, 1659, 1610, 1495, 899 cm⁻¹.

2-Methylprop-1-enyl-*m*-methoxyphenone (92e)
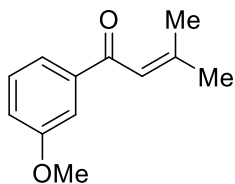
Following the described procedure, 1.86 g (10.0 mmol) of *m*-bromoanisole were reacted with magnesium and 3-methylbut-2-enal **90a**, then subsequently with of MnO_2 to afford 1.05 g of 2-methylprop-1-enyl-*m*-methoxyphenylketone **92f** as a yellowish oil (55%). ^{1}H NMR (600 MHz, $CDCl_3$, Me_4Si) δ 7.49 (ddd, *J* = 7.7, 1.5, 0.9 Hz, 1H, Ar–*H*); 7.46 (dd, *J* = 2.7, 1.5 Hz, 1H, Ar–*H*); 7.34 (t, *J* = 7.9 Hz, 1H, Ar–*H*); 7.06 (ddd, *J* = 8.2, 2.7, 1.0 Hz, 1H, Ar–*H*); 6.72 (sept, *J* = 1.3 Hz, 1H, CO–C*H*); 3.85 (s, 3H, O–C*H₃*); 2.20 (d, *J* = 1.3 Hz, 3H, CH=C—(C*H₃*)₂); 2.01 (d, *J* = 1.4 Hz, 3H, CH=C—(C*H₃*)₂). ^{13}C NMR (151 MHz; $CDCl_3$, Me_4Si) δ 191.3 (Cq); 159.9 (Cq); 156.9 (Cq); 140.8 (Cq); 129.5 (CH); 121.3 (CH); 120.9 (CH); 118.9 (CH); 112.6 (CH); 55.5 (CH_3); 28.1 (CH_3); 21.3 (CH_3). HRMS (ESI) *m/z* [M + H]⁺ Calcd for $C_{12}H_{15}O_2$ 191.1067, found 191.1062. IR v_{max} (neat)/cm⁻¹ 3022, 2899, 1658, 1612, 1495, 1249, 1043, 899 cm⁻¹.

2-Methylprop-1-enyl-*p*-tolylketone (92f)
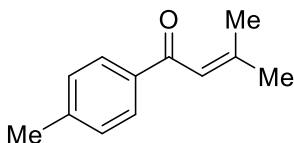
Following the described procedure, 1.70 g (10.0 mmol) of *p*-tolyl bromide were reacted with magnesium and 3-methylbut-2-enal **90a**, then subsequently with MnO_2 to afford 1.01 g of 2-

methylprop-1-enyl-*m*-tolylketone **92f** as yellowish oil (59%).[289]1H NMR (600 MHz, CDCl$_3$, Me$_4$Si) δ 7.26 (d, *J* = 7.8, 2H, Ar*H*); 7.15 (d, *J* = 7.8, 2H, Ar*H*); 5.41 (m, CO–C*H*); 2.32 (s, 3H, Ar–C*H$_3$*); 1.78 (s, 3H, CH=C—(C*H$_3$*)$_2$); 1.73 (s, 3H, CH=C—(C*H$_3$*)$_2$).

2-Methylprop-1-enyl-*o*-tolylketone (92g)
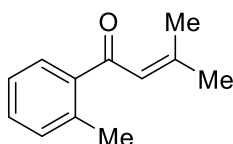
Following the described procedure, 1.70 g (10.0 mmol) of *o*-tolyl bromide were reacted with magnesium and 3-methylbut-2-enal **90a**, then subsequently with MnO$_2$ to afford 0.96 g of 2-methylprop-1-enyl-*o*-tolylketone **92g** as yellowish oil (55%).[290]1H NMR (600 MHz, CDCl$_3$, Me$_4$Si) δ 7.49 (dm, *J* = 9 Hz, 1H, Ar*H*); 7.31 (td, *J* = 7.2, 1.2 Hz, 1H, Ar*H*) 7.22 (t, *J* = 7.0 Hz, 2H, Ar*H*); 7.32 (m, 1H, Ar*H*); 6.42 (m, 1H, CO–C*H*); 2.45 (s, 3H, Ar–C*H$_3$*); 2.16 (s, 3H, CH=C—(C*H$_3$*)$_2$); 1.96 (s, 3H, CH=C—(C*H$_3$*)$_2$).

6.2.3 One step synthesis of 2-Phenylprop-1-enylphenone (92h)
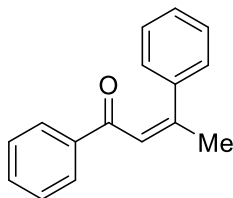
Following a modified procedure to that reported by Luo,[291] acetophenone (2.4 g, 20 mmol) and ethyl orthotitanate (2.4 g, 10 mmol) in 100 mL of heptane were heated to reflux in a bottomed flask equipped with a Dean–Stark trap which was filled with 5 mL of sulfuric acid (96% solution) to absorb the liberating alcohol. When the reaction was complete, the mixture was cooled to room temperature, then 30 mL of acetonitrile were added, and the resulting mixture stirred for 1 h. The mixture was then transferred to a separatory funnel and the bottom layer was separated and moved to a 50 mL round bottomed flask where it was further treated with 4 mL of hydrochloric acid 37% solution. This mixture was stirred for 10 min then heated to reflux and cooled to rt. A precipitate formed which was separated from the filtrated solution. The accumulated precipitate was washed with cold acetonitrile and the resulting organic phase was united with the filtrated solution and the

---

[289] Ma, W.; Xue, D.; Yu, T.; Wang, C.; Xiao, J. *Chem. Commun.* **2015,** *51*, 8797-8800.
[290] Wittenberg, R.; Srogl, J.; Egi, M.; Liebeskind, L. S. *Org. Lett.* **2003,** *5*, 3033-3035.
[291] Yu, T.; Zhu, Q.; Luo, S. *Tetrahedron Lett.* **2020,** *61*, 151887.

solvent evaporated. The obtained residue was purified on silica gel column chromatography to afford the desired product **92h** as a yellow solid (63% yield, PE/AcOEt 99/1). ^{1}H NMR (600 MHz, CDCl$_3$, Me$_4$Si) δ 7.98 (dm, J = 6.0 Hz, 2H. Ar–H), 7.54–7.58 (m, 3H, Ar–H), 7.47 (tm, J = 7.8 Hz, 2H, Ar–H), 7.39–7.42 (ddt, J = 7.4, 4.8, 1.2 Hz, 3H, Ar–H), 2.16 (s, 3H, CH=C—CH_3).

6.2.4 General Procedure for the Synthesis of γ,δ-Unsaturated Ketones (89)
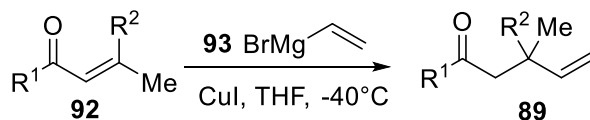
According to the procedure reported by Von Fraunberg[292] with slight modifications, under a N$_2$ atmosphere in a dried Schlenk bottle, copper iodide (190 mg, 0.5 mmol) was added at −40 °C to vinylmagnesium bromide **93a** (11.0 mL, commercial 1.0 M solution in THF). The resulting mixture was vigorously stirred for 15 min, then a cooled 0.5 M solution of the appropriate α,β-unsaturated ketone **92** (10.0 mmol) in THF was added dropwise over 30 min keeping temperature of the bath below −40 °C. Once the addition was completed, temperature was allowed to raise up to rt and stirring was maintained until complete consumption of the reactant. The reaction was then quenched with a NH$_4$Cl/NH$_4$OH 9:1 solution (30 mL) and diluted with Et$_2$O (30 mL). The organic phase was washed with NH$_4$Cl (10 mL aliquots) until the aqueous phase stopped turning blue. It was then washed with brine (30 mL), dried over Na$_2$SO$_4$, and filtered. The volatiles were removed under reduced pressure to give a colorless oil, that was used without further purification.

2,2-Dimethylbut-3-enylphenone (89a)
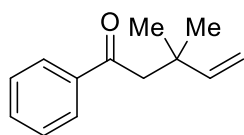
Following the described procedure, 1.60 g (10.0 mmol) of 2-methylprop-1-enylphenone **92a** were reacted with CuI and vinylmagnesium bromide **93a** to afford 1.64 g (8.7 mmol) of 2,2-dimethylbut-3-enylphenone **89a** (87%) as a colorless oil. ^{1}H NMR (600 MHz, CDCl$_3$, Me$_4$Si) δ 7.93–7.89 (m, 2H, Ar–H); 7.53 (ddt, J = 7.9, 6.9, 1.3 Hz, 1H, Ar–H); 7.46–7.40 (m, 2H, Ar–H); 5.95 (dd, J = 17.4, 10.7 Hz, 1H, CH=CH$_2$); 4.95 (dd, J =

---

[292] Von Fraunberg, K. *Ger. Patent* **1976**.

17.5, 1.1 Hz, 1H, CH=CH_2); 4.90 (dd, J = 10.7, 1.1 Hz, 1H, CH=CH_2); 2.96 (s, 2H, CO–CH_2); 1.17 (s, 6H, CH$_2$–(CH_3)$_2$–CH). ^{13}CNMR (151 MHz; CDCl$_3$, Me$_4$Si) 199.6 (Cq); 147.5 (CH); 138.4 (Cq); 132.9 (CH); 128.6 (2 × CH); 128.3 (2 × CH); 110.7 (CH$_2$); 49.2 (CH$_2$); 36.8 (Cq); 27.4 (2 × CH$_3$). HRMS (ESI) m/z [M + H]$^+$ Calcd for C$_{13}$H$_{17}$O 189.1274, found 189.1268. IR v$_{max}$ (neat)/cm^{-1} 3082, 2960, 1676, 1618, 1240.

2,2-Dimethylbut-3-enylnaphtone (89b)

Following the described procedure, 2.10 g (10.0 mmol) of 2-methylprop-1-enylnaphtone **92b** were reacted with CuI and vinylmagnesium bromide **93a** to afford 1.48 g 2,2-dimethylbut-3-enylnaphtone **89b** (62%) as a colorless oil which crystallize as a white-yellowish solid after cooling. ^{1}H NMR (600 MHz, CDCl$_3$, Me$_4$Si) δ 8.43–8.40 (m, 1H, Ar–H); 8.00 (dd, J = 8.7, 1.8 Hz, 1H, Ar–H); 7.95 (ddq, J = 8.2, 1.4, 0.7 Hz, 1H, Ar–H); 7.89–7.84 (m, 2H, Ar–H); 7.58 (ddd, J = 8.2, 6.9, 1.3 Hz, 1H, Ar–H); 7.54 (ddd, J = 8.1, 6.9, 1.3 Hz, 1H, Ar–H); 6.00 (dd, J = 17.4, 10.7 Hz, 1H, CH=CH$_2$); 4.98 (dd, J = 17.4, 1.1 Hz, 1H, CH=CH_2); 4.92 (dd, J = 10.7, 1.1 Hz, 1H, CH=CH_2); 3.09 (s, 2H, CO–CH_2); 1.22–1.20 (s, 6H, CH$_2$–(CH_3)$_2$–CH). ^{13}CNMR (151 MHz; CDCl$_3$, Me$_4$Si) δ 199.6 (Cq); 147.6 (CH); 135.8 (Cq); 135.5 (Cq); 132.6 (Cq); 130.1 (CH); 129.7 (CH); 128.5 (CH); 128.4 (CH); 127.8 (CH); 126.8 (CH); 124.2 (CH); 110.7 (CH$_2$); 49.3 (CH$_2$); 37.0 (Cq); 27.4 (2 × CH$_3$). HRMS (ESI) m/z [M + H]$^+$ Calcd for C$_{17}$H$_{19}$O 239.1430, found 239.1426. IR v$_{max}$ (neat)/cm^{-1} 3226, 1639, 1381, 1305, 1164. mp 53–56 °C.

2,2-Dimethylbut-3-enyl-pyridyl ketone (89c)

Following the described procedure, 1.61 g (10.0 mmol) of 2-methylprop-1-enyl-2-pyridylketone **92c** were reacted with CuI and vinylmagnesium bromide **93a** to afford 1.66 g of 2,2-dimethylbut-3-enyl-pyridyl ketone **89c** (88%) as a colorless oil. ^{1}H NMR (600 MHz, CDCl$_3$, Me$_4$Si) δ 8.64 (ddq, J = 4.4, 1.7, 0.9 Hz, 1H, Ar–H); 7.97 (dq, J = 7.9, 1.2 Hz, 1H, Ar–H); 7.81–7.75 (m, 1H, Ar–H); 7.41 (ddt, J = 7.5, 4.8, 1.4 Hz, 1H, Ar–H); 5.97 (ddd, J = 17.4, 10.7, 1.2 Hz, 1H, CH=CH$_2$); 4.92 (dt, J = 17.4, 1.3 Hz, 1H, CH=CH_2); 4.85 (dt, J = 10.7, 1.3 Hz, 1H, CH=CH_2); 3.26 (s, 2H, CO–CH_2); 1.15 (d, J = 1.4 Hz, 6H, CH$_2$–(CH_3)$_2$–CH). ^{13}C NMR (151 MHz; CDCl$_3$, Me$_4$Si)

δ 201.1 (Cq); 154.4 (Cq); 148.7 (CH); 147.6 (CH); 136.9 (CH); 126.9 (CH); 121.8 (CH); 110.4 (CH_2); 47.6 (CH_2); 36.80 (Cq); 27.34 (2 × CH_3). HRMS (ESI) m/z [M + H]$^+$ Calcd for $C_{12}H_{16}NO$ 190.1226, found 190.1222. IR v_{max} (neat)/cm^{-1} 3038, 2961, 1689, 1583, 1328, 1013.

2,2-Dimethylbut-3-enyl-*m*-tolyl ketone (89d)

Following the described procedure, 1.74 g (10.0 mmol) of 2-methylprop-1-enyl-*m*-tolylketone **92d** were reacted with CuI and vinylmagnesium bromide **93a** to afford 1.69 g (8.4 mmol) of 2,2-dimethylbut-3-enyl-*m*-tolyl ketone **89d** (84%) as a colorless oil. ^{1}H NMR (600 MHz, CDCl$_3$, Me$_4$Si) δ 7.7 (dq, J = 1.8, 0.9 Hz, 1H, Ar–*H*); 7.69 (dt, J = 7.4, 1.7 Hz, 1H, Ar–*H*); 7.34 (ddq, J = 7.7, 1.8, 0.8 Hz, 1H, Ar–*H*); 7.33–7.29 (m, 1H, Ar–*H*); 5.95 (dd, J = 17.4, 10.7 Hz, 1H, C*H*=CH$_2$); 4.95 (dd, J = 17.4, 1.1 Hz, 1H, CH=C*H*$_2$); 4.90 (dd, J = 10.7, 1.1 Hz, 1H, CH=C*H*$_2$); 2.94 (s, 2H, CO–C*H*$_2$); 2.39 (d, J = 0.8 Hz, 3H, Ar–C*H*$_3$); 1.16 (s, 6H, CH$_2$–(C*H*$_3$)$_2$–CH). ^{13}CNMR (151 MHz; CDCl$_3$, Me$_4$Si) δ 199.8 (Cq); 147.6 (CH); 138.5 (Cq); 138.3 (Cq); 133.6 (CH); 128.8 (CH); 128.4 (CH); 125.6 (CH); 110.6 (CH_2); 49.3 (CH_2); 36.8 (Cq); 27.4 (CH_3); 21.5 (2 × CH_3). HRMS (ESI) m/z [M + H]$^+$ Calcd for $C_{14}H_{19}O$ 203.1430, found 203.1427. IR v_{max} (neat)/cm^{-1} 3082, 2961, 2871, 1673, 1603, 1249.

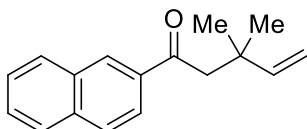## 2,2-Dimethylbut-3-enyl-*m*-methoxyphenone (89e)
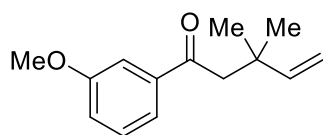
Following the described procedure, 1.90 g (10.0 mmol) of 2-methylprop-1-enyl-*m*-methoxyphenone **92e** were reacted with CuI and vinylmagnesium bromide **93a** to afford 1.57 g of 2,2-dimethylbut-3-enyl-*m*-methoxyphenone **89e** (72%) as a colorless oil. ^{1}H NMR (600 MHz, CDCl$_3$, Me$_4$Si) δ 7.52 (dm, J = 7.8 Hz, 1H, Ar–*H*); 7.44 (dd, J = 3.0, 1.2 Hz, 1H, Ar–*H*); 7.34 (t, J = 7.8 Hz, 2H, Ar–*H*); 7.07 (ddd, J = 7.8, 3.0, 1.2 Hz, 2H, Ar–*H*); 5.91 (dd, J = 17.4, 10.8 Hz, 1H, C*H*=CH$_2$); 4.95 (dd, J = 17.4, 1.2 Hz, 1H, CH=C*H*$_{2a}$); 4.89 (d, J = 10.8, 1.2 Hz, 1H, CH=C*H*$_{2b}$); 4.08 (s, 3H, Ar-OC*H*$_3$); 2.94 (s, 2H, CO–C*H*$_2$); 1.16 (s, 6H, CH$_2$–(C*H*$_3$)$_2$–CH). ^{13}CNMR (151 MHz; CDCl$_3$, Me$_4$Si) δ199.3 (Cq); 159.8 (Cq); 147.5 (CH); 139.8 (Cq); 129.5 (CH); 121.0 (CH); 119.4 (CH); 112.5 (CH); 110.7 (CH_2); 55.5 (CH_3); 49.4 (CH_2); 36.8 (Cq); 27.4 (CH_3). HRMS (ESI) m/z [M +

H]$^+$ Calcd for $C_{14}H_{19}O_2$ 219.1380, found 219.1379. IR v_{max} (neat)/cm^{-1} 3073, 2937, 1614, 1593, 1260.

2,2-Dimethylbut-3-enyl-*p*-tolyl ketone (89f)
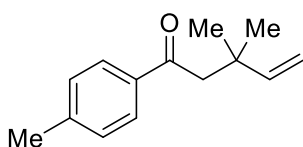
Following the described procedure, 1.74 g (10.0 mmol) of 2-methylprop-1-enyl-*p*-tolylketone **92f** were reacted with CuI and vinylmagnesium bromide **93a** to afford 1.71 g (8.4 mmol) of 2,2-dimethylbut-3-enyl-*p*-tolyl ketone **89f** (85%) as a colorless oil.[293] ^{1}H NMR (600 MHz, CDCl$_3$, Me$_4$Si) δ 7.82 (d, *J* = 7.8 Hz, 2H, Ar–*H*); 7.22 (d, *J* = 7.8 Hz, 2H, Ar–*H*); 5.97 (dd, *J* = 17.4, 10.8 Hz, 1H, C*H*=CH$_2$); 4.94 (d, *J* = 17.4 Hz, 1H, CH=C*H*$_{2a}$); 4.89 (d, *J* = 10.8 Hz, 1H, CH=C*H*$_{2b}$); 2.94 (s, 2H, CO–C*H*$_2$); 2.39 (s, 3H, Ar–C*H*$_3$); 1.16 (s, 6H, CH$_2$–(C*H*$_3$)$_2$–CH).

2,2-Dimethylbut-3-enyl-*o*-tolyl ketone (89g)
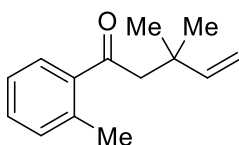
Following the described procedure, 1.74 g (10.0 mmol) of 2-methylprop-1-enyl-*o*-tolylketone **92g** were reacted with CuI and vinylmagnesium bromide **93a** to afford 1.09 g (8.4 mmol) of 2,2-dimethylbut-3-enyl-*o*-tolyl ketone **89g** (54%) as a colorless oil. ^{1}H NMR (600 MHz, CDCl$_3$, Me$_4$Si) δ 7.52 (d, *J* = 7.2 Hz, 1H, Ar–*H*); 7.52 (td, *J* = 7.2, 1.2 Hz, 1H, Ar–*H*); 7.22 (t, *J* = 7.8 Hz, 2H, Ar–*H*); 5.91 (dd, *J* = 17.4, 11.4 Hz, 1H, C*H*=CH$_2$); 4.93 (dd, *J* = 17.4, 0.6 Hz, 1H, CH=C*H*$_{2a}$); 4.89 (d, *J* = 11.4, 0.6 Hz, 1H, CH=C*H*$_{2b}$); 2.89 (s, 2H, CO–C*H*$_2$); 2.43 (s, 3H, Ar–C*H*$_3$); 1.14 (s, 6H, CH$_2$–(C*H*$_3$)$_2$–CH). ^{13}CNMR (151 MHz; CDCl$_3$, Me$_4$Si) δ204.4 (Cq); 147.4 (CH); 140.0 (Cq); 137.4 (Cq); 131.9 (CH); 130.8 (CH); 128.3 (CH); 125.6 (CH); 110.6 (CH$_2$); 52.9 (CH$_2$); 37.2 (Cq); 27.4 (CH$_3$); 21.0 (2 × CH$_3$). HRMS (ESI) *m*/*z* [M + H]$^+$. Calcd for $C_{14}H_{19}O$ 203.1430, found 203.1428. IR v_{max} (neat)/cm^{-1} 3082, 2962, 1678, 1640, 1456, 1346, 1235.
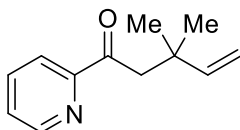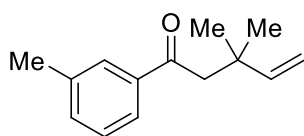
2-Phenyl-2-methylbut-3-enylphenone (89h)
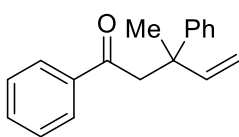
Following the described procedure, 2.08 g (10.0 mmol) of 2-phenylprop-1-enylphenone **92h** were reacted with CuI and vinylmagnesium bromide **93a** to afford 2.07 g of 2-phenyl-2-methylbut-3-enylphenone **89h**. (83%) as

[293] Duan, X.-Y.; Yang, X.-L.; Jia, P.-P.; Zhang, M.; Han, B. *Org. Lett.* **2015,** *17*, 6022-6025.

colorless oil. ^{1}H NMR (600 MHz, CDCl$_3$, Me$_4$Si) δ 7.85 (dm, J = 8.4 Hz, 2H, Ar–H); 7.51 (tm, 1H, J = 9.0 Hz, Ar–H); 7.39 (tm, 2H, J = 7.8 Hz, Ar–H); 7.33 (dm, J = 8.4 Hz, 2H, Ar–H); 7.23 (tm, 2H, J = 9.0 Hz, Ar–H); 7.16 (tm, 1H, J = 7.8 Hz, Ar–H); 6.26 (dd, J = 17.4, 10.2 Hz, 1H, CH=CH$_2$); 5.13 (dd, J = 10.2, 1.8 Hz, 1H, CH=CH_{2a}); 5.06 (dd, J = 17.4, 1.8 Hz, 1H, CH=CH_{2b}); 3.48 (s, 2H, CO–CH_2); 1.58 (s, 3H, CH_3). ^{13}CNMR (151 MHz; CDCl$_3$, Me$_4$Si) δ 198.4 (Cq); 146.0 (CH); 132.8 (CH); 129.2 (Cq); 128.7 (2 × CH) ; 128.5 (2 × CH); 128.4 (Cq); 128.3 (2 × CH); 128.1 (2 × CH); 126.3 (2 × CH); 112.4 (CH$_2$); 48.4 (CH$_2$); 43.8 (Cq); 26.0 (CH$_3$). HRMS (ESI) m/z [M + H]$^+$. Calcd for C$_{18}$H$_{19}$O 251.1430, found 251.1430. IR v$_{max}$ (neat)/cm^{-1} 2829, 2667, 2554, 1678, 1452, 1288, 1154, 925.

4,4-Dimethylhex-5-en-2-one (89i)
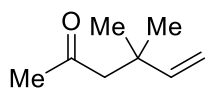
Following the described procedure, 0.98 g (10.0 mmol) of mesityl oxide **92i** (4-methylpent-3-en-2-one) were reacted with CuI and vinylmagnesium bromide **93a** to afford 1.12 g of 4,4-dimethylhex-5-en-2-one **89i** (89%) as a colorless oil. Spectral data are coherent with those reported in literature.[294] ^{1}H NMR (600 MHz, CDCl$_3$, Me$_4$Si) δ 5.90 (dd, J = 18.0, 10.81H, CH=CH$_2$); 4.94 (dd, J = 18.0, 1.1 Hz, 1H, CH=CH_2 (H trans)); 4.93 (dd, J = 10.8, 1.1 Hz, 1H, CH=CH_2 (H cis)); 2.41 (s, 2H, CO–CH_2); 2.09 (s, 3H, CH_3-CO); 1.10 (s, 6H, CH$_2$–(CH_3)$_2$–CH).

(2*S*,5*R*)- and (2*R*,5*R*)-5-Methyl-2-(2,2-dimethylprop-2-enyl)cyclohexanone (89l)
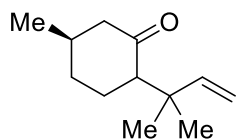
Following the described procedure, 1.52 g (10.0 mmol) of commercially available *R*-pulegone (4-methylpent-3-en-2-one)**96** were reacted with CuI and vinylmagnesium bromide **93a** to afford 1.49 g of (2*S*,5*R*) and(2*R*,5*R*)-5-methyl-2-(2,2-dimethylprop-2-enyl)cyclohexanone **89l** (83%) as a colorless oil. ^{1}H NMR (600 MHz, CDCl$_3$, Me$_4$Si) (isomer A) δ 5.95 (ddd, J = 16.3, 10.8, 1.1 Hz, 1H, CH=CH$_2$), 4.98–4.88 (m, 2H, CH=CH_2), 2.45 (dd, J = 13.0, 5.5 Hz, 1H, CH-C(H)H-CO), 2.25 (m, 2H, CO–CH, CO–CH–C(H)H), 2.00 (m, J = 2H, CH-C(H)H-CO with CO–CH–C(H)H), 1.88–1.83 (m, 2H, CH–CH_2–CH$_2$–CH), 1.56 (m, 1H, CH$_3$–CH), 0.98 (d, J = 6.2 Hz, 6H, CH-C-(CH_3)$_2$), 0.92 (d, J = 7.0 Hz, 3H, CH–CH_3). (isomer B) δ 5.94 (ddd, J = 16.3, 10.8, 1.1 Hz, 1H, CH-CH$_2$), 4.98–4.88 (m, 2H, CH=CH_2), 2.18 (m, 1H, CH-C(H)H-CO), 2.10–2.02

---

[294] Morita, M.; Sakaguchi, S.; Ishii, Y. *J. Org. Chem.* **2006,** *71*, 6285-6286.

(m, 2H, CH-C(H)*H*-CO), 1.86 (m, 2H, CH–C*H₂*–CH₂–CH), 1.80–1.70 (m, 1H, CH₃–C*H*), 1.40 (qdd, *J* = 12.9, 3.0, 1.1 Hz, 1H, CH-C(H)*H*-CH₂), 1.30 (qd, *J* = 13.2, 12.8, 2.7 Hz, 1H, CH-C(H)*H*-CH₂), 1.16–1.04 (m, 9H, CH–C*H₃* with CH-C-(C*H₃*)₂). ^{13}CNMR (151 MHz; CDCl₃, Me₄Si) (mixture of isomers) δ 212.6 (Cq), 211.6 (Cq), 147.4 (CH), 147.2 (CH), 111.3 (CH₂), 111.0 (CH₂), 58.9 (CH), 58.8 (CH), 52.5 (CH₂), 50.4 (CH₂), 38.4 (CH), 37.9 (Cq), 36.4 (Cq), 34.7 (CH2), 32.7 (CH), 31.3 (CH₂), 29.0 (CH₂), 25.9 (CH), 25.4 (CH), 25.0 (CH2), 24.3 (CH₃), 23.7 (CH₃), 22.4 (CH₃), 19.8 (CH₃).

6.2.5 General Procedures for the Synthesis of γ,δ-Unsaturated N-Arylsulfonylhydrazones (94)
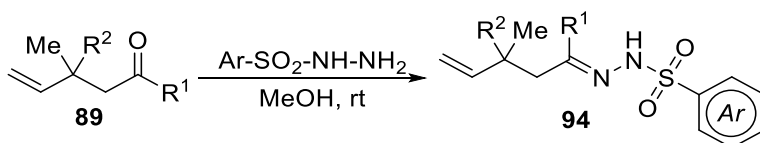
To a vigorously stirred suspension of arylsulfonylhydrazide Ar-SO₂-NH-NH₂(5.6 mmol, 1.12 equiv) in MeOH (3.0 mL); the appropriate ketone or **89** (5.0 mmol, 1.0 equiv) was added dropwise. The mixture was reacted to completion (about 18 h); then cooled to 0 °C. When the product precipitated it was removed by filtration and used without any further purification, otherwise the solvent was removed under reduced pressure and the crude purified by flash chromatography on deactivated silica gel (PE/AcOEt 90/10) to afford in both cases the *N*-arylsulfonylhydrazone **94** as a mixture of isomers (precipitation usually afforded one single stereoisomer or a mixture clearly enriched in only one of the possible stereoisomers).

2,2-Dimethylbut-3-enylphenone-*N*-tosylhydrazone (94a)
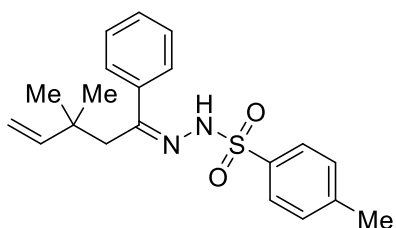
Following the described procedure 2,2-dimethylbut-3-enylphenone **89a**, (0.95 g, 5.0 mmol) was reacted with tosylhydrazide (1.00. g, 5.4 mmol) in methanol (3.0 mL) to obtain 1.03 g (2.9 mmol) of 2,2-dimethylbut-3-enylphenone-*N*-tosylhydrazone **94a** (mixture of isomers, 1.2:1) as a white powder (58%, PE/EE 7/3). ^{1}H NMR (600 MHz, CDCl₃, Me₄Si) (*major isomer*) δ 7.89 (d, *J* = 8.3 Hz, 2H, Ar–*H*), 7.87 (s, 1H, N–*H*), 7.49 (dm, *J* = 6.3, 2H, Ar–*H*), 7.35–7.29 (m, 5H, Ar–*H*), 5.58 (dd, *J* = 17.5, 10.6

Hz, 1H, C*H*=CH₂), 4.97 (dd, *J* = 17.5, 0.9 Hz, 1H, CH=CH*H* *trans*), 4.88 (dd, *J* = 10.6, 0.9 Hz, 1H, CH=CH*H* *cis*), 2.67 (s, 2H, N=C(Ar)–C*H₂*), 2.44 (s, 3H, Ar–C*H₃*), 0.91 (s, 6H, C(C*H₃*)₂); (*minor isomer*) δ 7.78 (d, *J* = 8.3 Hz, 2H, Ar–*H*), 7.54 (s, 1H, N–*H*), 7.42–7.36 (m, 5H, Ar–*H*), 7.04–7.00 (m, 2H, Ar–*H*), 5.54 (dd, *J* = 17.5, 10.7 Hz, 1H, C*H*=CH₂), 4.67 (dd, *J* = 17.4, 1.3 Hz, 1H, CH=CH*H* *trans*), 4.60 (dd, *J* = 10.7, 1.2 Hz, 1H, CH=CH*H* *cis*), 2.53 (s, 2H, s, 2H, N=C(Ar)–C*H₂*), 2.43 (s, 3H, Ar–C*H₃*), 0.85 (s, 6H, C(C*H₃*)₂). ^{13}CNMR (151 MHz; CDCl₃, Me₄Si) (*major isomer*) δ 155.2 (Cq), 146.8 (CH), 144.2 (Cq), 138.6 (Cq), 135.5 (Cq), 129.6 (CH), 129.6 (2 × CH), 128.4 (2 × CH), 128.2 (2 × CH), 127.0 (2 × CH), 113.4 (CH₂), 39.6 (CH₂), 38.0 (Cq), 27.9 (CH₃), 21.8 (2 × CH₃); (*minor isomer*) 156.8 (Cq), 147.2 (CH), 144.0 (Cq), 139.2 (Cq), 136.7 (Cq), 129.8 (CH), 129.5 (2 × CH), 128.3 (2 × CH), 128.0 (2 × CH), 127.2 (2 × CH), 110.5 (CH₂), 50.4(CH₂), 37.4 (Cq) 27.2 (CH₃), 21.7(2 × CH₃). HRMS (ESI) *m/z* [M + H]⁺ Calcd for C₂₀H₂₅N₂O₂S 357.1631, found 357.1626.

2,2-Dimethylbut-3-enylnaphtone-*N*-tosylhydrazone (94b)
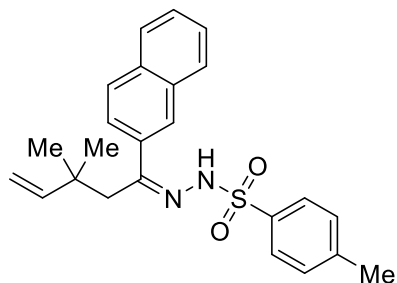
Following the described procedure 2,2-dimethylbut-3-enylnaphtone **89b** (1.02 g, 4.3 mmol) was reacted with tosylhydrazide (0.87g, 4.7 mmol) in methanol (6.0 mL) refluxed at 50 °C overnight. The reaction was then cooled to rt to obtain 1.01 g (2.5 mmol) of 2,2-dimethylbut-3-enylnaphtone-*N*-tosylhydrazone **94b** (only one isomer found) as a white powder (58%, PE/EE 7/3). ¹H NMR (600 MHz, CDCl₃, Me₄Si) δ 7.99 (s, 1H, N–*H*), 7.93 (dt, *J* = 8.3, 1.7 Hz, 2H, Ar–*H*), 7.90 (d, *J* = 1.3 Hz, 1H, Ar–*H*), 7.83–7.80 (m, 2H, Ar–*H*), 7.78 (d, *J* = 8.7 Hz, 1H, Ar–*H*), 7.74 (dd, *J* = 8.6, 1.8 Hz, 1H, Ar–*H*), 7.51–7.46 (m, 2H), 7.36 (d, *J* = 8.0 Hz, 2H, Ar–*H*), 5.64 (dd, *J* = 17.5, 10.6 Hz, 1H, C*H*=CH₂), 5.00 (dd, *J* = 17.5, 0.7 Hz, 1H, CH=CH*H* *trans*), 4.90 (dd, *J* = 10.7, 0.8 Hz, 1H, CH=CH*H* *cis*), 2.79 (s, 2H, N=C(Ar)–C*H₂*), 2.45 (s, 3H, Ar–C*H₃*), 0.95 (s, 6H, C(C*H₃*)₂). ^{13}CNMR (151 MHz; CDCl₃, Me₄Si) δ 154.7 (Cq), 146.9 (CH), 144.3 (Cq), 136.0 (Cq), 135.5 (Cq), 133.9 (Cq), 132.9 (Cq), 129.6 (2 × CH), 128.7 (CH), 128.3 (2 × CH), 128.2 (CH), 127.7 (CH), 126.9 (CH), 126.9 (CH), 126.7 (CH), 124.4 (CH), 113.4 (CH₂), 39.4 (CH₂), 38.1 (Cq), 28.0 (CH₃), 21.8 (2 × CH₃). HRMS (ESI) *m/z* [M + H]⁺ Calcd for C₂₄H₂₇N₂O₂S

407.1788, found 407.1777. IR v_{max} (neat)/cm^{-1} 3057, 2958, 1599, 1445, 1179.

2,2-Dimethylbut-3-enyl-pyridyl ketone-*N*-tosylhydrazone (94c)
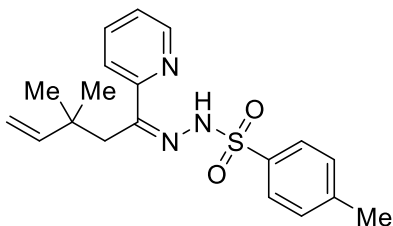
Following the described procedure 2,2-dimethylbut-3-enyl-pyridyl ketone **89c** (0.57 g, 3.0 mmol) was reacted with tosylhydrazide (0.61 g, 3.3 mmol) in methanol (5.0 mL) refluxed at 50 °C for 16h. The reaction was cooled to rt to obtain 0.450 g (1.26 mmol) of 2,2-dimethylbut-3-enyl-pyridyl ketone-*N*-tosylhydrazone **94c** as a white powder (42%, PE/AcOEt 98/2, mixture of isomers 1.3:1). ^{1}H NMR (600 MHz, CDCl$_3$, Me$_4$Si) (isomer A) δ 8.60 (dm, *J* = 4.9 Hz, 1H, Ar–*H*), 8.19–8.09 (bs, 1H, N–*H*), 7.87 (dd, *J* = 8.4, 1.9 Hz, 1H, Ar–*H*), 7.88–7.85 (m, 2H, Ar–*H*), 7.43 (d, *J* = 8.1 Hz, 1.1 Hz, 1H, Ar–*H*), 7.43 (dt, *J* = 8.1, 1.1 Hz, 1H, Ar–*H*), 7.31–7.26 (m, 2H, Ar–*H*), 5.52 (dd, *J* = 17.5, 10.7 Hz, 1H, C*H*=CH$_2$), 4.62 (dd, *J* = 17.5, 1.2 Hz, 1H, CH=C*H*$_2$, *H trans*), 4.52 (dd, *J* = 10.7, 1.2 Hz, 1H, CH=C*H*$_2$, *H cis*), 2.65 (s, 2H, N=C—C*H*$_2$), 2.42 (s, 3H Ar–CH$_3$), 0.77 (s, 6H, C(C*H*$_3$)$_2$). (isomer B) δ 8.49 (dd, *J* = 4.9, 1.8, 0.9 Hz, 1H, Ar–*H*), 8.19–8.09 (bs, 1H, N–*H*), 7.90 (dd, *J* = 8.4, 1.9 Hz, 1H, Ar–*H*), 7.64 (td, *J* = 7.7, 1.8 Hz, 1H), 7.32 (d, *J* = 8.1 Hz, 2H, Ar–*H*), 7.31–7.26 (m, 2H, Ar–*H*), 7.21 (ddd, *J* = 7.5, 4.8, 1.2 Hz, 1H, Ar–*H*), 5.66 (dd, *J* = 17.5, 10.6 Hz, 1H, C*H*=CH$_2$), 4.93 (dt, *J* = 17.4, 1.1 Hz, 1H, CH=C*H*$_2$, *H trans*), 4.87 (dt, *J* = 10.7, 1.4 Hz, 1H, CH=C*H*$_2$, *H cis*), 2.98 (2H, N=C—C*H*$_2$), 2.40 (s, 3H, Ar–C*H*$_3$), 0.92 (s, 6H, C(C*H*$_3$)$_2$). ^{13}C NMR (151 MHz; CDCl$_3$, Me$_4$Si) (mixture of isomers) δ 155.6 (Cq), 155.0 (Cq), 153.6 (Cq), 148.2 (CH), 147.8 (CH), 147.6 (CH), 147.5 (CH), 144.9 (Cq), 144.3 (Cq), 143.5 (Cq), 137.4 (CH), 136.6 (Cq), 136.5 (Cq), 135.5 (Cq), 129.7 (2 × CH), 129.5 (2 × CH), 128.1 (2 × CH), 128.1 (2 × CH), 124.0 (CH), 124.0 (CH), 123.9 (CH), 121.3 (CH), 112.9 (CH$_2$), 110.4 (CH$_2$), 46.6 (CH$_2$), 38.15 (Cq), 37.6 (Cq), 37.3 (CH$_2$), 27.6 (CH$_3$), 26.9 (CH$_3$), 21.7 (2 × CH$_3$), 21.6 (2 × CH$_3$). HRMS (ESI) *m/z* [M + H]$^+$ Calcd for C$_{19}$H$_{25}$N$_3$O$_2$S 358.1584, found 358.1582.

2,2-Dimethylbut-3-enyl-*m*-tolyl ketone-*N*-tosylhydrazone (94d)
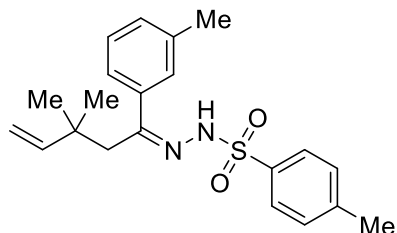
Following the described procedure 2,2-dimethylbut-3-enyl-*m*-tolyl ketone **89d** (0.46 g, 2.3 mmol) was reacted with tosylhydrazide (0.47 g, 2.5 mmol) in methanol (2 mL) to obtain 0.366 g (1.0 mmol) of 2,2-dimethylbut-3-enyl-*m*-tolyl ketone-*N*-tosylhydrazone **94d** (only one isomer found) as a white powder (43%, PE/EE 7/3). ^{1}H NMR (600 MHz, CDCl$_3$, Me$_4$Si) δ 7.90 (dt, J = 8.4, 1.8 Hz, 2H, Ar–*H*), 7.85 (s, 1H, N–*H*), 7.34 (d, J = 8.4 Hz, 2H, Ar–*H*), 7.28 (m, 1H, Ar–*H*), 7.19 (t, J = 7.8 Hz, 2H, Ar–*H*), 7.15 (bd, J = 7.8 Hz, 1H, Ar–*H*), 5.58 (dd, J = 17.4, 10.8 Hz, 1H, C*H*=CH$_2$), 4.99 (dd, J = 17.4, 0.6 Hz, 1H, CH=CH*H trans*), 4.90 (dd, J = 10.8, 0.6 Hz, 1H, CH=CH*H cis*), 2.65 (s, 2H, N=C(Ar)–C*H$_2$*), 2.44 (s, 3H, Ar–C*H$_3$*), 2.34 (s, 3H, Ar–C*H$_3$*), 0.89 (s, 6H, C(C*H$_3$*)$_2$). ^{13}CNMR (151 MHz; CDCl$_3$, Me$_4$Si) δ 155.3 (Cq), 146.9 (CH), 144.2 (Cq), 138.6 (Cq), 137.9 (Cq), 135.5 (Cq), 130.3 (CH), 129.5 (CH), 128.3 (2 × CH), 128.2 (2 x CH), 127.7 (CH), 124.2 (CH), 113.4 (CH$_2$), 39.7 (CH$_2$), 37.9 (Cq), 27.9 (CH$_3$), 21.7 (CH$_3$), 21.6 (2 × CH$_3$). mp 120–123 °C. IR v$_{max}$ (neat)/cm^{-1} 3284, 3186, 2961, 1641, 1597, 1341, 1164, 792. HRMS (ESI) *m/z* [M + H]$^+$ Calcd for C$_{21}$H$_{27}$N$_2$O$_2$S 371.1793, found 371.1779.

2,2-Dimethylbut-3-enyl-*m*-methoxyphenone-*N*-tosylhydrazone (94e)

Following the described procedure, 2,2-dimethylbut-3-enyl-*m*-methoxy phenone **89e** (0.48 g, 2.2 mmol) was reacted with tosylhydrazide in methanol (0.45 g, 2.4 mmol) to obtain (0.64 g, 1.5 mmol) of 2,2-dimethylbut-3-enyl-*m*-methoxyphenone-*N*-tosylhydrazone **94e** as a white powder (70%,). ^{1}H NMR (600 MHz, CDCl$_3$, Me$_4$Si) (mixture of isomers 2.6:1) δ 7.95 (bs, 1H, N–*H*, major isomer), 7.89 (d, J = 8.4, Hz, 2H, Ar–*H*, major isomer), 7.78 (d, J = 8.4 Hz, 2H, Ar–*H*, minor isomer), 7.61 (bs, 1H, N–*H*, minor isomer), 7.29 (m, 4H, Ar–*H*, both isomers), 7.20 (t, J = 7.8 Hz, 1H, Ar–*H*, major isomer), 7.07 (dm, J = 7.8 Hz, 1H, Ar–H, major isomer), 7.03 (m, 1H, Ar–H, major isomer), 6.57 (dt, J = 7.2, 0.6 Hz, 2H, Ar–H, minor isomer), 6.52 (m, 2H, Ar–H, minor isomer), 5.58 (dd, J = 17.4, 10.8 Hz, 1H,

C*H*=CH₂, major isomer), 5.52 (dd, *J* = 17.4, 10.2 Hz, 1H, CH=C*H*₂, major isomer), 4.98 (d, *J* = 17.4 Hz, 1H, CH=C*H*₂, *H trans*, major isomer), 4.86 (d, *J* = 10.2 Hz, 1H, CH=C*H*₂, *H cis*, major isomer), 4.67 (dd, *J* = 17.4, 1.8 Hz, 1H, CH=C*H*₂, *H trans*, minor isomer), 4.61 (dd, *J* = 10.8, 1.2 Hz, 1H, CH=C*H*₂, *H cis*, minor isomer), 3.78 (s, 3H, OC*H*₃, minor isomer), 3.77 (s, 3H, OC*H*₃, minor isomer), 2.64 (s, 2H, N=C—C*H*₂, major isomer), 2.51 (s, 2H, N=C—C*H*₂, minor isomer), 2.42 (s, 3H Ar–C*H*₃, both isomers), 0.90 (s, 6H, C(C*H*₃)₂, major isomer), 0.85 (s, 6H, C(C*H*₃)₂, minor isomer). ^{13}C NMR (151 MHz; CDCl₃, Me₄Si) (mixture of isomers) δ 160.3 (Cq), 159.4 (Cq), 156.0 (Cq), 154.9 (Cq), 147.2 (CH), 146.8 (CH), 144.2 (Cq), 144.0 (Cq), 140.0 (Cq), 135.7 (Cq), 135.5 (Cq), 134.9 (Cq), 130.8 (CH), 129.6 (2 × CH), 129.5 (2 × CH), 128.2 (2 × CH), 128.0 (2 × CH), 119.6 (CH), 119.1 (CH), 115.2 (CH), 115.0 (CH), 113.3 (CH₂), 112.9 (CH), 112.5 (CH), 110.5 (CH₂), 55.4 (CH₃), 55.3 (CH₃), 50.3 (CH₂), 39.6 (CH₂), 38.1 (Cq), 38.0 (Cq), 27.9 (CH₃), 27.2 (CH₃), 21.7 (2 × CH₃), 21.7 (2 × CH₃). HRMS (ESI) *m/z* [M + H]⁺ Calcd for C₂₁H₂₇N₂O₃S 387.1737, found 387.1728.

2,2-Dimethylbut-3-enyl-*p*-tolyl ketone-*N*-tosylhydrazone (94f)
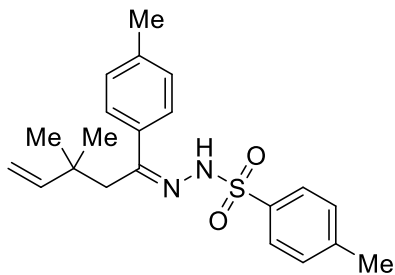
Following the described procedure 2,2-dimethylbut-3-enyl-*p*-tolyl ketone **89f** (1.01 g, 5.0 mmol) was reacted with tosylhydrazide (1.04 g, 5.6 mmol) in methanol (2 mL) to obtain 1.48 g (4.0 mmol) of 2,2-dimethylbut-3-enyl-*p*-tolyl ketone-*N*-tosylhydrazone **94f** as a white powder (80%, PE/EE 7/3). ^{1}H NMR (600 MHz, CDCl₃, Me₄Si) (mixture of isomers, 1.4:1) δ7.87 (d, *J* = 7.8 Hz, 2H, Ar–*H*, major isomer), 7.78 (d, *J* = 8.4 Hz, 2H, Ar–*H*, minor isomer), 7.52 (bs, 1H, N–*H*), 7.40 (d, *J*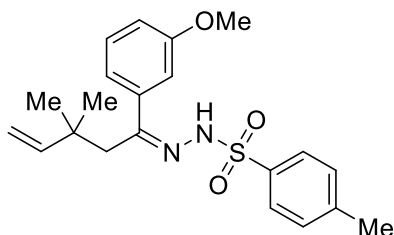 = 8.4 Hz, 1H, Ar–*H*, major isomer), 7.33 (d, *J* = 8.4 Hz, 1H, Ar–*H*, minor isomer), 7.31 (d, *J* = 7.8 Hz, 2H, Ar–*H*, minor isomer), 7.22 (d, *J* = 7.8 Hz, 2H, Ar–*H*, minor isomer), 7.19 (d, *J* = 7.8 Hz, 2H, Ar–*H*, major isomer), 7.11 (d, *J* = 7.8 Hz, 2H, Ar–*H*, major isomer), 6.91 (d, *J* = 8.4 Hz, 2H, Ar–*H*, major isomer), 5.58 (dd, *J* = 14.4, 10.8 Hz, 1H, C*H*=CH₂, major isomer), 5.56 (dd, *J* = 15.0, 10.8 Hz, 1H, CH=C*H*₂, minor isomer), 4.97 (d, *J* = 16.8 Hz, 1H, CH=C*H*₂, *H trans*, major isomer), 4.88 (dd, *J* = 10.8, 1.2 Hz, 1H, CH=C*H*₂, *H cis*, major isomer), 4.68 (dd, *J* = 17.4, 1.2 Hz, 1H, CH=C*H*₂, *H trans*, minor isomer), 4.61 (dd, *J* = 10.8, 1.2 Hz, 1H, CH=C*H*₂, *H cis*, minor isomer), 2.92

(s, 2H, N=C—CH_2, minor isomer), 2.64 (s, 2H, N=C—CH_2, major isomer), 2.44 (s, 3H Ar–CH$_3$, major isomer), 2.43 (s, 3H Ar–CH$_3$, minor isomer), 2.36 (s, 3H Ar–CH$_3$, minor isomer), 2.33 (s, 3H Ar–CH$_3$, major isomer), 0.91 (s, 6H, C(CH_3)$_2$, major isomer), 0.84 (s, 6H, C(CH_3)$_2$, minor isomer). ^{13}CNMR (151 MHz; CDCl$_3$, Me$_4$Si) (mixture of isomers 59:41) δ 156.4 (Cq), 156.1 (Cq), 147.3 (CH), 146.9 (CH), 144.2 (Cq), 143.9 (Cq), 139.9 (Cq), 139.7 (Cq), 135.8 (Cq), 135.5 (Cq), 130.6 (2 × CH), 130.2 (2 × CH), 129.6 (2 × CH), 129.6 (2 × CH), 129.2 (2 × CH), 129.1 (2 × CH), 128.5 (2 × CH), 128.2 (2 × CH), 128.0 (2 × CH), 127.1 (Cq), 126.9 (Cq), 113.4 (CH$_2$), 110.4 (CH$_2$), 50.3 (CH$_2$), 39.5 (CH$_2$), 37.9 (Cq), 37.3 (Cq), 28.0 (CH$_3$), 27.4 (CH$_3$), 27.2 (CH$_3$), 21.8 (2 × CH$_3$), 21.7 (2 × CH$_3$). HRMS (ESI) m/z [M + H]$^+$ Calcd for C$_{21}$H$_{27}$N$_2$O$_2$S 371.1793, found 371.1781.

2,2-Dimethylbut-3-enyl-*o*-tolyl ketone-*N*-tosylhydrazone (94g)

Following the described procedure 2,2-dimethylbut-3-enyl-*o*-tolyl ketone **89g** (1.01 g, 5.0 mmol) was reacted with tosylhydrazide (1.04 g, 5.6 mmol) in methanol (2 mL) to obtain 1.48 g (4.0 mmol) of 2,2-dimethylbut-3-enyl-*o*-tolyl ketone-*N*-tosylhydrazone **94g** as a white powder (56%, PE/EE 7/3). ^{1}H NMR (600 MHz, CDCl$_3$, Me$_4$Si) δ 7.89 (bs, 1H, N–H), 7.83 (d, J = 8.3 Hz, 2H, Ar–H), 7.31 (d, J = 7.8 Hz, 2H, Ar–H), 7.17 (dt, J = 7.8, 1.6 Hz, 1H, Ar–H), 7.10 (m, 3H, Ar–H), 5.68 (dd, J = 17.4, 10.8 Hz, 1H, CH=CH$_2$), 5.01 (dd, J = 17.4, 0.6 Hz, 1H, CH=CH_2H trans*), 4.92 (dd, J = 10.8, 0.6 Hz, 1H, CH=CH_2H cis*), 2.64 (s, 2H, N=C(Ar)–CH_2), 2.44 (s, 3H, Ar–CH_3), 2.03 (s, 3H, Ar–CH_3), 0.88 (s, 6H, C(CH_3)$_2$). ^{13}CNMR (151 MHz; CDCl$_3$, Me$_4$Si) 156.7 (Cq), 146.7 (CH), 144.2 (Cq), 139.1 (Cq), 136.0 (Cq), 135.8 (Cq), 131.3 (CH), 129.6 (2 × CH), 128.5 (CH), 128.4 (2 × CH), 128.4 (CH), 125.5 (CH), 113.2 (CH$_2$), 43.3 (CH$_2$), 38.5 (Cq), 27.7 (CH$_3$), 21.7 (2 × CH$_3$), 20.5 (CH$_3$). mp 98–102 °C. IR v$_{max}$ (neat)/cm^{-1} 3280, 3179, 2960, 1645, 1598, 1340, 1167, 768. HRMS (ESI) m/z [M + H]$^+$ Calcd for C$_{21}$H$_{27}$N$_2$O$_2$S 371.1793, found 371.1779.

2-Phenyl-2-methylbut-3-enylphenone *N*-tosylhydrazone (94h)
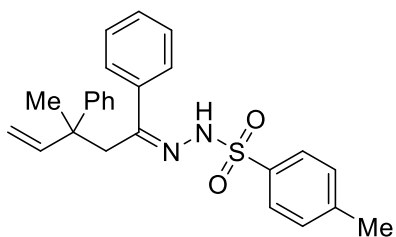
Following the described procedure 2-phenyl-2-methylbut-3-enylphenone, **89h** (1.27 g, 5.1 mmol) was reacted with tosylhydrazide (1.05 g, 5.6 mmol) in methanol (3.0 mL) to obtain 1.07 g (3.3 mmol) 2-phenyl-2-methylbut-3-enylphenone *N*-tosylhydrazone **94h** (mixture of isomers 1.1:1) as a white powder (64%). ^{1}H NMR (600 MHz, CDCl$_3$, Me$_4$Si) (mixture of isomers) δ 7.75 (d, *J* = 7.8 Hz, 1H, Ar–*H*), 7.69 (d, *J* = 8.4 Hz, 1H, Ar–*H*), 7.47 (m, 1H, Ar–*H*), 7.33 (m, 4H, Ar–*H*), 7.18–7.26 (m, 4H, Ar–*H*), 7.08 (m, 3H, Ar–*H*), 6.73 (bs, 1H, N–*H*, isomer 1), 6.47 (bs, 1H, N–*H*, isomer 2), 6.00 (dd, *J* = 17.4, 10.8, 1H, C*H*=CH$_2$, isomer 1), 5.97 (dd, *J* = 17.4, 10.2, 1H, C*H*=CH$_2$, isomer 2), 5.15 (d, *J* = 17.4, 1H, CH=C*H*$_2$, isomer 1), 5.13 (d, *J* = 10.8, 1H, CH=C*H*$_2$, isomer 1), 4.90 (d, *J* = 17.4, 1H, CH=C*H*$_2$, isomer 2), 4.88 (d, *J* = 10.2, 1H, CH=C*H*$_2$, isomer 2), 3.18 (d, *J* = 13.2, 1H, N=C(Me)—C*H*$_{2a}$, isomer 1), 3.12 (d, *J* = 13.2, 1H, N=C(Me)—C*H*$_{2b}$, isomer 1), 3.07 (d, *J* = 13.8, 1H, N=C(Me)—C*H*$_{2a}$, isomer 2), 2.98 (d, *J* = 13.8, 1H, N=C(Me)—C*H*$_{2b}$, isomer 2), 2.46 (m, 3H, Ar–C*H*$_3$, both isomers), 1.27 (s, 3H, C*H*$_3$, isomer 1), 1.16 (s, 3H, C*H*$_3$, isomer 2). ^{13}CNMR (151 MHz; CDCl$_3$, Me$_4$Si) (mixture of isomers) δ 156.2 (Cq), 155.5 (Cq), 146.1 (CH), 146.1 (Cq), 146.0 (Cq), 145.5 (Cq), 144.0 (Cq), 144.0 (Cq), 139.0 (Cq), 135.7 (Cq), 135.0 (Cq), 133.5 (Cq), 129.7 (2 × CH), 129.6 (2 × CH), 129.4 (2 × CH), 129.1 (2 × CH), 128.6 (2 × CH), 128.4 (2 × CH), 128.1 (2 × CH), 128.0 (2 × CH), 128.0 (2 × CH), 127.7 (CH), 127.5 (CH), 127.1 (CH), 126.9 (CH), 126.6 (CH), 126.3 (CH), 126.0 (CH), 126.0 (CH), 113.0 (CH$_2$), 112.3(CH$_2$), 49.1 (CH$_2$), 44.7 (Cq), 44.3 (Cq), 39.4 (CH$_2$), 25.9 (CH$_3$), 25.3 (CH$_3$), 21.8 (CH$_3$), 21.8 (CH$_3$). HRMS (ESI) *m*/*z* [M + H]$^+$ Calcd for C$_{25}$H$_{28}$N$_2$O$_2$S 419.1788, found 419.1789.

4,4-Dimethylhex-5-en-2-one-*N*-tosylhydrazone (94i)
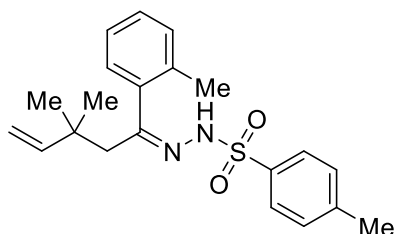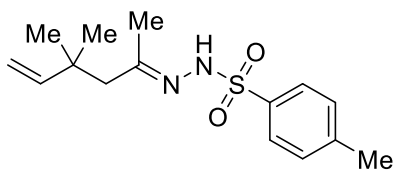
Following the described procedure 4,4-dimethylhex-5-en-2-one, **89i** (0.640 g, 5.1 mmol) was reacted with tosylhydrazide (1.05 g, 5.6 mmol) in methanol (3.0 mL) to obtain 0.720 g (2.45 mmol) of 4,4-dimethylhex-5-en-2-one-*N*-tosylhydrazone **94i** (mixture of isomers 3.8:1) as a white powder (48%). ^{1}H NMR (600 MHz, CDCl$_3$, Me$_4$Si)

(major isomer) δ 7.82 (d, J = 8.3 Hz, 2H, Ar–H), 7.79 (bs, 1H, N–H), 7.29 (d, J = 7.9 Hz, 2H, Ar–H), 5.69 (dd, J = 17.3, 10.8 Hz, 1H, CH=CH$_2$), 4.76 (dd, J = 10.8, 1.6 Hz, 1H, CH=CH_2 (*H cis*)), 4.73 (dd, J = 17.3, 1.2 Hz, 1H, CH=CH_2 (*H trans*)), 2.42 (s, 3H, Ar–CH_3), 2.21 (s, 2H, CH_2), 1.71 (s, 3H, N=C—CH_3), 0.84 (s, 6H, C(CH_3)$_2$); (*minor isomer*) δ 7.79 (d, J = 8.3 Hz, 2H, Ar–H), 7.5 (s, 1H, N–H), 7.34 (d, J = 7.9 Hz, 2H, Ar–H), 5.90 (dd, J = 17.3, 10.8 Hz, 1H, CH=CH$_2$), 4.98 (bd, J = 10.8 Hz, 1H, CH=CH_2 (*H cis*)), 4.94 (bd, J = 17.4 Hz, 1H, CH=CH_2 (*H trans*)), 2.41 (s, 3H, Ar–CH_3), 2.19 (s, 2H, CH_2), 1.91 (s, 3H, N=C—CH_3), 1.04 (s, 6H, C(CH_3)$_2$). ^{13}CNMR (151 MHz; CDCl$_3$, Me$_4$Si) (mixture of isomers) δ 147.5 (CH), 144.0 (Cq), 135.5 (Cq), 130.1 (2 × CH), 129.5 (2 × CH), 128.4 (2 × CH), 128.2 (2 × CH), 128.1 (Cq), 110.9 (CH$_2$), 51.4 (CH$_2$), 37.2 (Cq), 27.8 (CH$_3$), 27.1 (CH$_3$), 26.9 (CH$_3$), 21.7 (CH$_3$), 18.0 (2 × CH$_3$). HRMS (ESI) m/z [M + H]$^+$ Calcd for C$_{15}$H$_{23}$N$_2$O$_2$S 295.1475, found 295.1477.

4,4-Dimethylhex-5-en-2-one-*N*-phenylsulfonylhydrazone (94j)
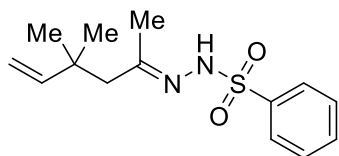
Following the described procedure 4,4-dimethylhex-5-en-2-one, **89i** (0.50 g, 4.0 mmol) was reacted with phenylsulfonylhydrazide (0.770 g, 4.5 mmol) in methanol (2.5 mL) to obtain 0.762 g (2.72 mmol) of 4,4-dimethylhex-5-en-2-one-*N*-phenylsulfonylhydrazone **94j** (mixture of isomers 1:1) as a white powder (68%). ^{1}H NMR (600 MHz, CDCl$_3$, Me$_4$Si) (major isomer) δ 7.96 (d, J = 1.2 Hz, 2H, Ar–H), 7.95 (t, J = 1.7 Hz, 1H, Ar–H), 7.74 (bs, 1H, N–H), 7.57 (tt, J = 7.4, 1.2 Hz, 2H, Ar–H), 5.66 (dd, J = 17.4, 10.8 Hz, 1H, CH=CH$_2$), 4.73 (dd, J = 10.8 1.2 Hz, 1H, CH=CH_2, *H cis*), 4.71 (dd, J = 17.4, 1.3 Hz, 1H, CH=CH_2, *H trans*), 2.19 (s, 2H, N=C(Me)—CH_2), 1.72 (s, 3H, N=C—CH_3), 0.81 (s, 6H, C(CH_3)$_2$); (*minor isomer*) δ 7.96 (d, J = 1.2 Hz, 2H, Ar–H), 7.92 (t, J = 1.7 Hz, 1H, Ar–H), 7.74 (s, 1H, N–H), 7.59 (tt, J = 7.4, 1.2 Hz, 2H, Ar–H), 5.67 (dd, J = 17.4, 10.8 Hz, 1H, CH=CH$_2$), 4.96–4.81 (m, 2H, CH=CH_2), 2.19 (s, 2H, N=C(Me)—CH_2), 1.91 (s, 3H, N=C—CH_3), 1.02 (s, 6H, C(CH_3)$_2$). ^{13}C NMR (151 MHz; CDCl$_3$, Me$_4$Si) (mixture of isomers) δ 156.9 (Cq), 156.8 (Cq), 147.4 (CH), (147.1 (CH), 138.5 (Cq), 133.1 (CH), 129.4 (2 × CH), 129.0 (2 × CH), 128.3 (CH), 128.2 (2 × CH), 128.0 (2 × CH), 112.9 (CH$_2$), 110.9 (CH$_2$), 51.4(CH$_2$), 43.8 (CH$_2$), 37.7 (Cq), 37.2 (Cq), 27.7 CH$_3$), 26.8 (CH$_3$), 26.3 (2 × CH$_3$), 18.2 (2 × CH$_3$). HRMS (ESI) m/z [M + H]$^+$. Calcd for C$_{14}$H$_{21}$N$_2$O$_2$S 281.1318, found 281.1324.

2,2-Dimethylbut-3-enylphenone-*N*-phenylsulfonylhydrazone (94k)
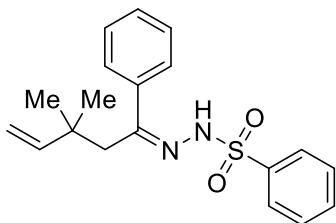
Following the described procedure 2,2-dimethylbut-3-enylphenone **89a** (0.38 g, 2.0 mmol) was reacted with phenylsulfonylhydrazide (0.38 g, 2.2 mmol) in methanol (2 mL) to obtain 1.13 g (3.5 mmol) of 2,2-dimethylbut-3-enylphenone-*N*-phenylsulfonylhydrazone **94k** (only one isomer found) as a white powder (50%). ^{1}H NMR (600 MHz, CDCl$_3$, Me$_4$Si) δ 8.04–7.99 (m, 2H, Ar–*H*), 7.88 (s, 1H, N–*H*), 7.63 (tt, *J* = 7.4, 1.8 Hz, 1H, Ar–*H*), 7.57 (ddt, *J* = 8.2, 6.7, 1.1 Hz, 2H, Ar–*H*), 7.48 (dt, *J* = 6.6, 1.7, 1.3 Hz, 2H, Ar–*H*), 7.37–7.28 (m, 3H, Ar–*H*), 5.57 (dd, *J* = 17.5, 10.6 Hz, 1H, C*H*=CH$_2$), 4.96 (dd, *J* = 17.5, 0.9 Hz, 1H, CH=CH$_2$,*H trans*), 4.87 (dd, *J* = 10.6, 0.9 Hz, 1H, CH=CH$_2$,*H cis*), 2.70–2.64 (m, 2H, N=C(Ph)–C*H$_2$*), 0.91–0.88 (bs, 6H, C-(C*H$_3$*)$_2$). ^{13}C NMR (151 MHz; CDCl$_3$, Me$_4$Si) δ 155.4 (Cq), 146.8 (CH), 138.6 (Cq), 138.4 (Cq), 133.4 (CH), 129.7 (CH), 129.0 (2 × CH), 128.4 (2 × CH), 128.2 (2 × CH), 128.0 (2 × CH), 113.5 (CH$_2$), 39.7 (CH$_2$), 37.9 (Cq), 27.9 (2 × CH$_3$). HRMS (ESI) *m/z* [M + H]$^+$. Calcd for C$_{19}$H$_{23}$N$_2$O$_2$S 343.1475, found 343.1485. IR v$_{max}$ (neat)/cm^{-1} 3059, 2956, 1641, 1445, 1349, 1160. mp 104–107 °C.

(5*R*)-5-Methyl-2-(1,1-dimethylprop-2-enyl)cyclohexanone *N*-tosylhydrazone (94l)
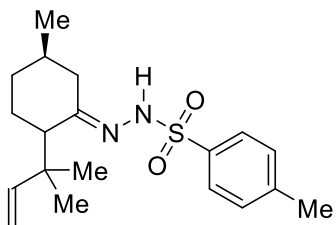
Following the described procedure pulegone derivative **94l**, (1.2 g, 6.7 mmol) was reacted with tosylhydrazide (1.4 g, 7.5 mmol) in methanol (5.0 mL) to obtain 1.3 g (3.8 mmol) upon precipitation with water of pulegone tosylhydrazone **95l** as a white powder (57%). Only 2 isomers observed. ^{1}H NMR (600 MHz, CDCl$_3$, Me$_4$Si) (mixture of 2 isomers 85/15), (major isomer) δ 7.84 (d, *J* = 8.2 Hz, 2H, Ar–*H*), 7.46 (s, 1H, N–*H*), 7.29 (d, *J* = 8.2 Hz, 2H, Ar–*H*), 5.83 (dd, *J* = 17.6, 10.8 Hz, 1H, C*H*=CH$_2$), 4.79 (dd, *J* = 17.6, 1.5 Hz, 1H, CH–C*H$_2$*,*H trans*), 4.76 (dd, *J* = 10.8, 1.5 Hz, 1H, CH–C*H$_2$*,*H cis*), 2.56 (dd, 1H, *J* = 13.5, 4.0 Hz, N=C—C(H)*H*—C(Me)H), 2.41 (s, 3H, Ar–C*H$_3$*), 1.91–1.85 (m, 2H, CH–C*H$_2$*–CH$_2$–C(Me)H), 1.76–1.71 (m, 1H, C*H*–CH$_2$–CH$_2$–C(Me)H), 1.59–1.53 (m, 1H, CH$_2$–C(Me)*H*–CH$_2$), 1.41 (dd, 1H, *J* = 13.5, 11.5 Hz, N=C—C(H)*H*—C(Me)H), 1.22 (ddd, *J* = 14.5, 12.8, 4.0 Hz, 1H, CH–CH$_2$–C(H)*H*–

C(Me)H), 1.03 (ddm, J = 13.5, 11.5, 1H, CH–CH$_2$–C(H)H–C(Me)H), 0.98 (s, 3H, C(CH$_3$) CH_3), 0.97 (s, 3H, C(CH$_3$) CH_3), 0.91 (d, J = 6.5 Hz, 3H, CH$_2$–CH–CH_3); (*minor isomer*) δ 7.79 (d, J = 8.2 Hz, 2H, Ar–H), 7.35 (d, J = 8.0 Hz, 2H, Ar–H), 5.75 (dd, J = 17.3, 11.0 Hz, 1H, CH=CH$_2$), 5.60 (s, 1H, N–H), 4.76 (dd, 1H, J = 17.5, 1.5 Hz, CH–CH_2H *trans*), 4.75 (dd, 1H, J = 10.8, 1.5 Hz, CH–CH_2H *cis*), 2.44 (s, 3H, Ar–CH_3), 2.35–2.29 (m, 1H, N=C—C(H)H—C(Me)H), 2.15 (t, 1H, J = 5.8 Hz, N=C—C(H)H—C(Me)H), 1.95–1.83 (m, 2H, CH–CH_2–CH$_2$–C(Me)H), 1.78–1.67 (m, 2H, CH$_2$–C(Me)H–CH$_2$ with CH–CH$_2$–CH$_2$–C(Me)H), 1.36–1.27 (m, 1H, CH–CH$_2$–C(H)H–C(Me)H), 1.10 (d, 1H, J = 12.2 Hz, CH–CH$_2$–C(H)H–C(Me)H), 0.90 (s, 3H, C(CH$_3$)–CH_3), 0.89 (s, 3H, C(CH$_3$)–CH_3), 0.87 (d, J = 6.2 Hz, 3H, CH$_2$–CH–CH_3). ^{13}C NMR (151 MHz; CDCl$_3$, Me$_4$Si) (mixture of isomers), δ 162.1 (Cq), 148.0 (CH), 144.0 (Cq), 135.6 (Cq), 130.0 (CH), 129.5 (2 × CH), 128.5 (2 × CH), 128.4 (2 × CH), 110.9 (CH$_2$), 110.5 (CH$_2$), 53.9 (CH), 51.8 (CH), 39.7 (Cq), 38.8 (Cq), 36.2 (CH$_2$), 34.4 (CH$_2$), 34.0 (CH), 32.1 (Cq), 31.2 (Cq), 28.9 (CH$_2$), 27.0 (CH$_2$), 25.8 (CH$_3$), 25.4 (CH$_3$), 23.9 (CH$_3$), 22.2 (CH$_3$), 21.4 (CH$_3$), 21.7 (CH$_3$). HRMS (ESI) m/z [M + H]$^+$ Calcd for C$_{19}$H$_{29}$N$_2$O$_2$S 349.1944, found 349.1952.

6.2.6 Synthesis of 2,2-Dimethylbut-3-enylphenone-*N*-tosylhydrazone-K+ salt (94aK)
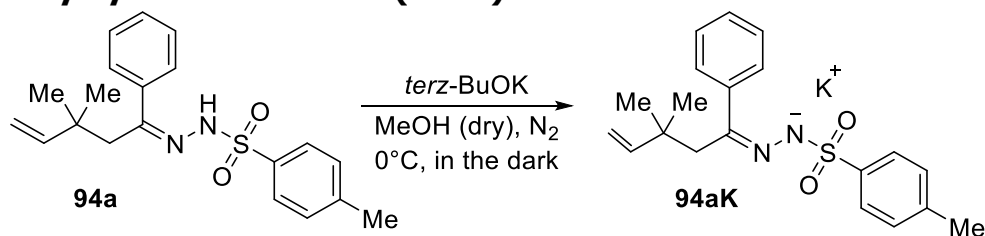
According to our previously reported procedure,[168] 1682,2-dimethylbut-3-enylphenone-*N*-tosylhydrazone **94a** (1 mmol, 0.360 g) was dissolved in the minimal amount of anhydrous MeOH at 0 °C and under N$_2$ atmosphere, then sublimed *tert*-BuO$^-$K$^+$ (1 mmol, 0.112 g) was added, and the solution was stirred in the dark for 30 min. Solvent evaporation afforded 0.39 g of 2,2-dimethylbut-3-enylphenone-*N*-tosylhydrazone-K$^+$ salt **94aK** (>99%). ^{1}H NMR (600 MHz, Methanol-d_4) δ 7.75 (d, J = 8.2 Hz, 2H, Ar–H), 7.39–7.35 (m, 2H, Ar–H), 7.21 (d, J = 7.9 Hz, 3H, Ar–H), 7.18 (t, J = 7.4 Hz, 2H, Ar–H), 7.14 (d, J = 7.0 Hz, 1H, Ar–H), 5.73 (dd, J = 17.4, 10.7 Hz, 1H, CH=CH$_2$), 4.63 (dd, J = 17.5, 1.7 Hz, 1H, CH=CH_2H *trans*), 4.49 (dd, J = 10.7, 1.6 Hz, 1H, CH=CH$_2$$H$ *cis*), 2.88 (s, 2H, N=C(Ph)–CH_2), 2.34 (s, 3H, Ar–CH_3), 0.80 (s,

6H, C(CH_3)$_2$). ^{13}C NMR (151 MHz, Methanol-d_4) δ 150.3 (Cq), 149.0 (CH), 142.1 (Cq), 141.9 (Cq), 140.3 (Cq), 128.3 (2 × CH), 127.4 (2 × CH), 126.9 (2 × CH), 126.8 (2 × CH), 126.6 (CH), 108.1 (CH$_2$), 37.9 (Cq), 37.2 (CH$_2$), 29.9 (CH$_3$), 26.71 (2 × CH$_3$). HRMS (ESI) m/z [M−]$^-$ Calcd for C$_{20}$H$_{23}$N$_2$O$_2$S 355.1486, found 355.1483. IR ν$_{max}$ (neat)/cm^{-1} 2957, 2923, 2053, 1636, 1441, 1279, 1078.

6.2.7 General procedure for the photoredoxsynthesis of tricyclic dearomatized products (95)
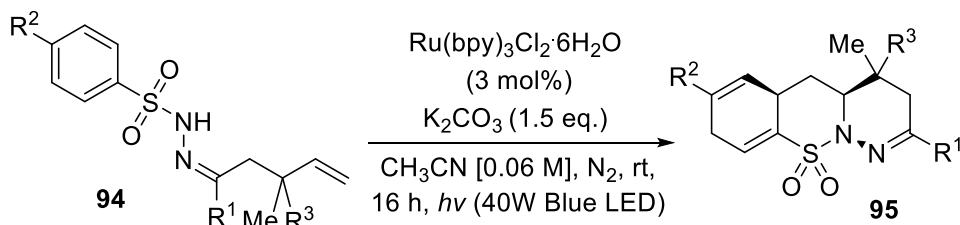
In a sealed photochemical reactor, 6.75 mg of [Ru(bpy)$_3$]Cl$_2$·6H$_2$O (0.009 mmol) were dissolved in 5 mL of anhydrous CH$_3$CN, the solution was degassed with N$_2$ for 15 min then the suitable tosylhydrazone **94a-i**, **94l** or phenylsulfonylhydrazone **94j-k** (0.30 mmol) and 62.2 mg of K$_2$CO$_3$ (0.45 mmol) were added. The solution was then stirred at 4 cm from the irradiation source (see above) at room temperature until the reaction was completed as monitored by TLC analysis. The solution was then filtered on a short pad of silica gel using CH$_2$Cl$_2$ as eluent. The crude product was purified by flash chromatography on silica gel (hexane/acetone 92/8) to obtain the dearomatized product **95**.

4,4,7-Trimethyl-2-phenyl-3,4,4a,5,5a,8-hexahydrobenzo[e] pyridazino[1,6-b][1,2]thiazine 10,10-dioxide (95a)
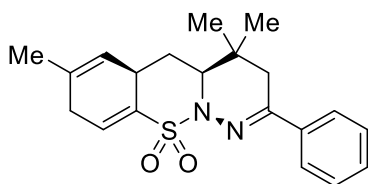
Following the general procedure9, 107 mg (0.30 mmol) of 2,2-dimethylbut-3-enylphenone-N-tosylhydrazone **94a** were reacted with K$_2$CO$_3$ and [Ru(bpy)$_3$]Cl$_2$·6H$_2$O for 16 h under blue light irradiation to obtain 75 mg (0.210 mmol) of 4,4,7-trimethyl-2-phenyl-3,4,4a,5,5a,8-hexahydrobenzo[e]pyridazino[1,6-b][1,2]thiazine 10,10-dioxide **95a** (70%) as a white solid. ^{1}H NMR (600 MHz, CDCl$_3$, Me$_4$Si) δ 7.80–7.75 (m, 2H, Ar–H), 7.38–7.32 (m, 3H, Ar–H), 6.74 (tm, J = 3.5, Hz, 1H, CH$_2$—CH=C), 5.25

(dq, J = 3.1, 1.6 Hz, 1H, CH₃CH=CH), 4.01 (dd, J = 12.6, 2.4 Hz, 1H, N–CH), 3.48 (bs,CH₂—CH—CH=), 2.75 (m, 2H, CH–CH_2–C(CH₃)₂), 2.38 (d, J = 18.4 Hz, 1H, CH-C(H)H-C(CH₃)), 2.28 (d, J = 18.3 Hz, 1H, CH-C(H)H-C(CH₃)), 1.78 (ddd, J = 13.5, 4.0, 1.8 Hz, 1H, CH-C(H)H-CH), 1.64 (t, J = 1.5 Hz, 3H, CH_3CH=CH), 1.23 (q, J = 12.7 Hz, 1H, CH-C(H)H-CH), 1.11 (s, 6H, CH₂–C(CH_3)₂). ¹³CNMR (151 MHz, CDCl₃, Me₄Si) δ 149.1 (Cq), 137.0 (Cq), 135.5 (Cq), 131.9 (CH), 130.5 (Cq), 129.5 (CH), 128.4 (2 × CH), 125.6 (2 × CH), 121.2 (CH), 62.5 (CH), 35.4 (CH), 34.6 (CH₂), 31.5 (CH₂), 31.4 (CH₂), 31.0 (Cq), 28.3 (CH₃), 27.0 (CH₃), 22.7 (CH₃). mp 169.2–170.5 °C, degradation. ν_max (neat)/cm⁻¹ 2966, 2921, 2908, 1448, 1345, 1159, 1060, 1021. HRMS (ESI) m/z [M + Na]⁺ Calcd for C₂₀H₂₄N₂O₂SNa 379.1451, found 379.1451.

Table 6.1 Crystal data and structure refinement for **95a**

Empirical formula	C₂₀H₂₄N₂O₂S
Formula weight	356.47
Temperature/K	298
Crystal system	monoclinic
Space group	P21/c
a/Å	12.233(2)
b/Å	9.6374(9)
c/Å	15.666(2)
α/°	90
β/°	100.026(14)
γ/°	90
Volume/Å3	1818.8(4)
Z	4
ρcalcg/cm3	1.302
μ/mm-1	0.194
F(000)	760.0
Crystal size/mm3	0.35 × 0.32 × 0.15
Radiation	MoKα (λ = 0.71073)
2Θ range for data collection/°	6.75 to 52.744
Index ranges	-15 ≤ h ≤ 14, -12 ≤ k ≤ 9, -19 ≤ l ≤ 19
Reflections collected	13976
Independent reflections	3644 [Rint = 0.0906, Rsigma = 0.1054]
Data/restraints/parameters	3644/33/237
Goodness-of-fit on F2	0.994
Final R indexes [I>=2σ (I)]	R1 = 0.0593, wR2 = 0.0991
Final R indexes [all data]	R1 = 0.1392, wR2 = 0.1267
Largest diff. peak/hole / e Å-3	0.21/-0.25
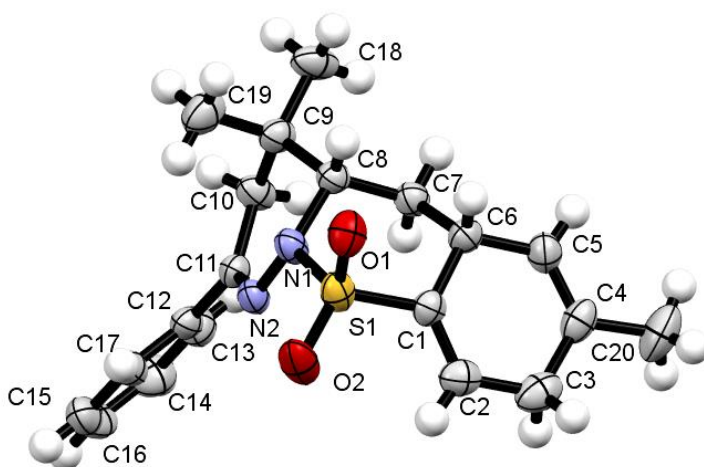
Figure 6.1 ORTEP plot for Asymmetric unit of compound **95a**.

Table 6.2 Crystal data and structure refinement for **95a**

Atom	Atom	Length/Å	Atom	Atom	Length/Å
S1	C1	1.751(3)	C11	C10	1.506(3)
S1	O1	1.439(2)	C12	C13	1.389(4)
S1	O2	1.424(2)	C12	C17	1.386(4)
S1	N1	1.663(2)	C4	C5	1.321(4)
C1	C6	1.508(4)	C4	C3	1.497(5)
C1	C2	1.319(4)	C4	C20	1.501(5)
N2	N1	1.399(3)	C9	C10	1.521(4)
N2	C11	1.292(3)	C9	C18	1.528(4)
C8	N1	1.488(3)	C9	C19	1.533(5)
C8	C7	1.525(4)	C2	C3	1.480(5)
C8	C9	1.540(4)	C16	C15	1.369(5)
C6	C7	1.543(4)	C16	C17	1.371(4)
C6	C5	1.486(4)	C13	C14	1.389(4)
C11	C12	1.478(4)	C15	C14	1.376(5)

Table 6.3 Bond Angles for **95a**

Atom	Atom	Atom	Angle/°	Atom	Atom	Atom	Angle/°
O1	S1	C1	107.42(16)	C12	C11	C10	118.9(3)
O1	S1	N1	104.88(13)	C13	C12	C11	120.5(3)
O2	S1	C1	111.68(16)	C17	C12	C11	120.6(3)
O2	S1	O1	119.40(16)	C17	C12	C13	118.9(3)
O2	S1	N1	109.70(14)	C5	C4	C3	122.3(4)
N1	S1	C1	102.21(15)	C5	C4	C20	122.7(4)
C6	C1	S1	112.9(2)	C3	C4	C20	115.1(3)
C2	C1	S1	121.7(3)	C10	C9	C8	107.4(3)
C2	C1	C6	125.4(4)	C10	C9	C18	111.7(3)
C11	N2	N1	118.2(2)	C10	C9	C19	108.9(3)
N1	C8	C7	111.5(2)	C18	C9	C8	110.7(3)
N1	C8	C9	107.1(3)	C18	C9	C19	108.9(3)
C7	C8	C9	116.1(3)	C19	C9	C8	109.2(3)
N2	N1	S1	113.39(18)	C1	C2	C3	122.4(3)
N2	N1	C8	120.0(2)	C4	C5	C6	125.8(3)
C8	N1	S1	114.0(2)	C2	C3	C4	113.7(3)
C1	C6	C7	110.5(3)	C11	C10	C9	112.5(3)
C5	C6	C1	110.2(3)	C15	C16	C17	120.1(4)
C5	C6	C7	113.5(3)	C14	C13	C12	119.8(4)
C8	C7	C6	112.3(3)	C16	C15	C14	120.4(4)
N2	C11	C12	116.3(3)	C15	C14	C13	119.9(4)
N2	C11	C10	124.8(3)	C16	C17	C12	120.8(4)

4,4,7-Trimethyl-2-(naphthalen-2-yl)-3,4,4a,5,5a,8-hexahydro benzo[*e*]pyridazino[1,6-*b*][1,2]thiazine 10,10-dioxide (95b)
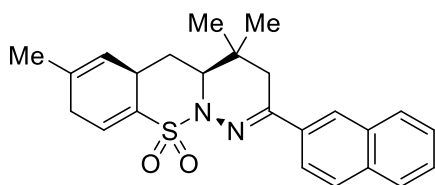
Following the general procedure, 122 mg (0.30 mmol) of 2,2-dimethylbut-3-enylnaphtone-*N*-tosylhydrazone (**10b**) were reacted with K_2CO_3 and [Ru(bpy)$_3$]Cl$_2$·6H$_2$O under blue light irradiation for 16 h to obtain 52.5 mg (0.13 mmol) of 2,4,4-trimethyl-3,4,4a,5,5a,8-hexahydrobenzo [*e*]pyridazino[1,6-*b*][1,2]thiazine 10,10-dioxide **13b** (43%) as a white solid. ¹H NMR (600 MHz, CDCl₃, Me₄Si) δ 8.11 (dd, *J* = 8.7, 1.8 Hz, 1H, Ar–*H*), 8.01 (s, 1H, Ar–*H*), 7.82 (ddd, *J* = 9.0, 5.6, 3.4 Hz, 2H Ar–*H*), 7.79 (d, *J* = 9.0 Hz, 1H, Ar–*H*), 7.47 (tt, *J* = 5.8, 4.7 Hz, 2H, Ar–*H*), 6.78 (m, 1H, CH₂— C*H*=C), 5.26 (m, 1H, CH₃CH=C*H*), 4.06 (dd, *J* = 12.7, 2.4 Hz, 1H, N–C*H*), 3.51 (bs, 1H, CH₂–C*H*–CH), 2.75 (m, 2H, CH–C*H*₂–C(CH₃)₂), 2.54 ((d, *J* = 18.0 Hz, 1H, CH-C(H)*H*–C(CH₃)), 2.42 (d, *J* = 18.2 Hz, 1H, CH-C(H)*H*–C(CH₃)), 1.81

(ddd, J = 13.3, 4.2, 2.4 Hz, 1H, CH-C(H)H-CH), 1.64 (s, 3H, CH_3CH=CH) 1.29 (q, J = 12.7 Hz, 1H, CH-C(H)H-CH), 1.16 (s, 6H, CH_2–C(CH_3)$_2$). ^{13}CNMR (151 MHz, CDCl$_3$, Me$_4$Si) δ 148.9 (Cq), 135.5 (Cq), 134.5 (Cq), 133.9 (Cq), 133.0 (Cq), 132.0 (CH), 130.5 (Cq), 128.5 (CH), 128.0 (CH), 127.8 (CH), 126.8 (CH), 126.4 (CH), 125.0 (CH), 123.4 (CH), 121.2 (CH), 62.7 (CH), 35.4 (CH), 34.5 (CH_2), 31.6 (CH_2), 31.4 (CH_2), 31.1 (Cq), 28.4 (CH_3), 27.0 (CH_3), 22.7 (CH_3). mp 63.4–67.2 °C. v_{max} (neat)/cm^{-1} 3057, 2958, 2923, 1599, 1445, 1349, 1349, 1179, 1158, 1018. HRMS (ESI) m/z [M + H]$^+$ Calcd for $C_{24}H_{27}N_2O_2S$ 407.1788, found 407.1773.

4,4,7-Trimethyl-2-(pyridin-2-yl)-3,4,4a,5,5a,8-hexahydrobenzo[*e*]pyridazino[1,6-*b*][1,2]thiazine 10,10-dioxide (95c)

Following the general procedure, 107 mg (0.30 mmol) of 2,2-dimethylbut-3-enyl-pyridyl ketone-*N*-tosylhydrazone **94c** were reacted with K$_2$CO$_3$ and [Ru(bpy)$_3$]Cl$_2$·6H$_2$O under blue light irradiation for 16 h to obtain 40 mg (0.11 mmol) of 4,4,7-trimethyl-2-(pyridin-2-yl)-3,4,4a,5,5a,8-hexahydrobenzo[*e*]pyridazino[1,6-*b*][1,2]thiazine 10,10-dioxide **95c** (37%) as a white solid. ^{1}H NMR (600 MHz, CDCl$_3$, Me$_4$Si) δ 8.52 (ddd, J = 4.8, 1.8, 0.9 Hz, 1H, Ar–H), 8.11 (dt, J = 8.1, 1.1 Hz, 1H, Ar–H), 7.66 (ddd, J = 8.1, 7.4, 1.8 Hz, 1H, Ar–H), 7.24 (ddd, J = 7.4, 4.8, 1.2 Hz, 1H, Ar–H), 6.74 (td, J = 3.5, 1.5 Hz, 1H, CH_2—CH=C), 5.26 (dq, J = 3.2, 1.6 Hz, 1H, CH$_3$CH=CH), 4.02 (ddd, J = 12.7, 2.5, 1.2 Hz, 1H, N–CH), 3.52–3.45 (m, 1H, CH_2–CH-CH), 2.75 (m, 2H, CH–CH_2–C(CH$_3$)$_2$), 2.73 (dd, J = 19.3, 1.0 Hz, 1H, CH-C(H)H-C(CH$_3$)), 2.38 (dd, J = 19.3, 1.0 Hz, 1H, CH-C(H)H-C(CH$_3$)), 1.81 (ddd, J = 13.4, 4.2, 2.5 Hz, 1H, CH-C(H)H-CH), 1.64 (dd, J = 1.9, 1.0 Hz, 3H, CH_3CH=CH), 1.26 (dt, J = 13.4, 12.5 Hz, 1H, CH-C(H)H-CH), 1.11 (s, 3H, CH_2–CH$_3$(CH_3)), 1.09 (s, 3H, CH_2–CH$_3$(CH_3)). ^{13}C NMR (151 MHz, CDCl$_3$, Me$_4$Si) δ 154.8 (Cq), 150.6 (Cq), 148.4 (CH), 136.3 (CH), 135.7 (Cq), 131.8 (CH), 130.4 (Cq), 124.0 (CH), 121.2 (CH), 120.6 (CH), 63.0 (CH), 35.4 (CH), 33.6 (CH_2), 31.7 (CH_2), 31.4 (CH_2), 30.7 (Cq), 28.3 (CH_3), 26.8 (CH_3), 22.7 (CH_3). mp 55.0–58.7 °C. v_{max} (neat)/cm^{-1} 3053, 2964, 1581, 1434, 1349, 1179. HRMS (ESI) m/z [M + H]$^+$ Calcd for $C_{19}H_{24}N_3O_2S$ 358.1584, found 358.1573.

4,4,7-Trimethyl-2-(*m*-tolyl)-3,4,4a,5,5a,8-hexahydrobenzo[*e*]pyridazino[1,6-*b*][1,2]thiazine 10,10-dioxide (95d)
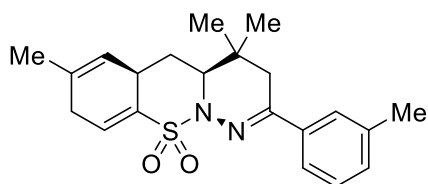
Following the general procedure, 111 mg (0.30 mmol) of 2,2-dimethylbut-3-enyl-*m*-tolyl ketone-*N*-tosylhydrazone **94d** were reacted with K_2CO_3 and [Ru(bpy)$_3$]Cl$_2$·6H$_2$O under blue light irradiation for 16 h to obtain 66.6 mg (0.18 mmol) of 4,4,7-trimethyl-2-(*m*-tolyl)-3,4,4a,5,5a,8-hexahydrobenzo[*e*]pyridazino[1,6-*b*][1,2]thiazine 10,10-dioxide **95d** (60%) as a white solid. ^{1}H NMR (600 MHz, CDCl$_3$, Me$_4$Si) δ 7.58 (s, 1H, Ar–*H*), 7.55 (d, *J* = 8.4 Hz, 1H, Ar–*H*), 7.25 (dd, *J* = 7.8, 7.2 Hz, 1H, Ar–*H*), 7.18 (d, *J* = 7.2 Hz, 1H, Ar–*H*), 6.76 (bs, 1H, CH$_2$—C*H*=C), 5.26 (m, 1H, CH$_3$CH=C*H*), 4.02 (dd, *J* = 12.5, 2.4 Hz, 1H, N–C*H*), 3.49 (m, 1H, CH$_2$–C*H*–CH), 2.76 (m, 1H, CH–C*H$_2$*–C(CH$_3$)$_2$), 2.37 (s, 3H, Ar–C*H$_3$*), 2.36 (s, 1H, CH-C(H)*H*-C(CH$_3$)), 2.29 (d, *J* = 18.2 Hz, 1H, CH-C(H)*H*-C(CH$_3$)), 1.78 (ddd, *J* = 13.3, 4.2, 2.5 Hz, 1H, CH-C(H)*H*-CH), 1.65 (s, 3H, C*H$_3$*CH=CH), 1.24 (q, *J* = 12.7 Hz, 2H, CH-C(H)*H*-CH), 1.12 (s, 6H, CH$_2$–C(C*H$_3$*)$_2$). ^{13}CNMR (151 MHz, CDCl$_3$, Me$_4$Si) δ 149.2 (Cq), 138.1 (Cq), 137.0 (Cq), 135.4 (Cq), 131.9 (CH), 130.5 (Cq), 130.3 (CH), 128.3 (CH), 126.2 (CH), 122.8 (CH), 121.2 (CH), 62.5 (CH), 35.4 (CH), 34.7 (CH$_2$), 31.5 (CH$_2$), 31.4 (CH$_2$), 31.0 (Cq), 28.3 (CH$_3$), 27.0 (CH$_3$), 22.7 (CH$_3$), 21.6 (CH$_3$). mp 73.0–75.2 °C. v$_{max}$ (neat)/cm^{-1} 2957, 2921, 2854, 1604, 1446, 1349, 1159, 1157, 1021. HRMS (ESI) *m/z* [M + H]$^+$ Calcd for C$_{21}$H$_{27}$N$_2$O$_2$S 371.1788, found 371.1783.

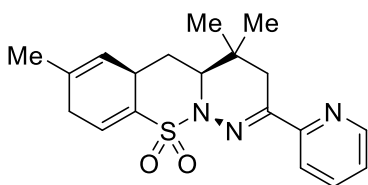## 2-(3-Methoxyphenyl)-4,4,7-trimethyl-3,4,4a,5,5a,8-hexahydrobenzo[*e*]pyridazino[1,6-*b*][1,2]thiazine 10,10-dioxide (95e)

Following the general procedure, 116 mg (0.30 mmol) of 2,2-dimethylbut-3-enyl-*m*-methoxyphenone-*N*-tosylhydrazone **94e** were reacted with K_2CO_3 and [Ru(bpy)$_3$]Cl$_2$·6H$_2$O under blue light irradiation for 16 h to obtain 58 mg (0.15 mmol) of 2-(3-methoxyphenyl)-4,4,7-trimethyl-3,4,4a,5,5a,8-hexahydrobenzo[*e*]pyridazino[1,6-*b*][1,2]thiazine 10,10-dioxide **95e** (50%) as a white solid. ^{1}H NMR (600 MHz, CDCl$_3$, Me$_4$Si) δ 7.34 (d, 1H, *J* = 1.8 Hz, Ar–H), 7.32 (dm, 1H, *J* = 6.6 Hz, Ar–*H*), 7.28 (d, 1H, *J* = 8.4 Hz, Ar–*H*), 7.24 (t, 1H, *J* = 7.8

Hz, Ar–*H*), 6.90 (dd, *J* = 7.8, 2.0, 1H, Ar–*H*), 6.74 (td, *J* = 3.6, 1.5 Hz, 1H, CH$_2$—C*H*=C), 5.25 (q, *J* = 1.8 Hz, 1H, CH$_3$CH=C*H*), 4.01 (dd, *J* = 13.0, 2.4 Hz, 1H, N–C*H*), 3.82 (s, 3H, O–C*H*$_3$), 3.48 (m, 1H, CH$_2$—C*H*—CH=), 2.75 (m, 2H, C*H*$_2$-C(CH$_3$)$_2$), 2.35 (d, *J* = 18.3 Hz, 1H, CH-C(H)*H*-C(CH$_3$)), 2.26 (d, *J* = 18.5 Hz, 1H, CH-C(H)*H*-C(CH$_3$)), 1.77 (ddd, *J* = 13.4, 4.3, 2.5 Hz, 1H, CH-C(H)*H*-CH), 1.64 (s, 3H, C*H*$_3$CH=CH), 1.22 (m, 1H, CH-C(H)*H*-CH), 1.11 (d, *J* = 3.0 Hz, 6H, CH$_2$–C(C*H*$_3$)$_2$). ^{13}C NMR (151 MHz, CDCl$_3$, Me$_4$Si) δ 159.7 (Cq), 148.9 (Cq), 138.5 (Cq), 135.5 (Cq), 131.9 (CH), 130.5 (Cq), 129.4 (CH), 121.2 (CH), 118.1 (CH), 115.1 (CH), 111.1 (CH), 62.5 (CH), 55.5 (CH$_3$), 35.4 (CH), 34.7 (CH$_2$), 31.5 (CH$_2$), 31.4 (CH$_2$), 31.0 (Cq), 28.3 (CH$_3$), 26.9 (CH$_3$), 22.7 (CH$_3$). mp 85.0–89.5 °C v_{max} (neat)/cm^{-1} 3030, 2961, 1598, 1449, 1349, 1287. HRMS (ESI) *m*/*z* [M + H]$^+$ Calcd for C$_{21}$H$_{27}$N$_2$O$_3$S 387.1737, found 387.1726.

4,4,7-Trimethyl-2-(*p*-tolyl)-3,4,4a,5,5a,8-hexahydrobenzo[*e*] pyridazino[1,6-*b*][1,2]thiazine 10,10-dioxide (95f)

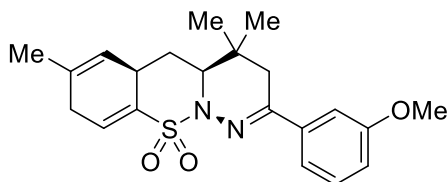

Following the general procedure, 111 mg (0.30 mmol) of 2,2-dimethylbut-3-enyl-*p*-tolyl ketone-*N*-tosylhydrazone **94f** were reacted with K$_2$CO$_3$ and [Ru(bpy)$_3$]Cl$_2$·6H$_2$O under blue light irradiation for 16 h to obtain 68.8 mg (0.18 mmol) of 4,4,7-trimethyl-2-(*p*-tolyl)-3,4,4a,5,5a,8-hexahydrobenzo [*e*]pyridazino[1,6-*b*][1,2]thiazine 10,10-dioxide **95f** (62%) as a white solid. ^{1}H NMR (600 MHz, CDCl$_3$, Me$_4$Si) δ 7.66 (dd, *J* = 8.4, 1.8 Hz, 2H, Ar–*H*), 7.26 (bd, *J* = 8.4 Hz, 2H, Ar–*H*), 6.74 (td, *J* = 3.6, 1.8 Hz, 1H, CH$_2$—C*H*=C), 5.26 (dd, *J* = 12.6, 1.8 Hz, 1H, CH$_3$CH=C*H*), 4.01 (dd, *J* = 13.0, 2.4 Hz, 1H, N–C*H*), 3.47 (m, 1H, CH$_2$–C*H*–CH), 2.76 (m, 1H, C*H*$_2$-C(CH$_3$)$_2$), 2.37 (dd, *J* = 18.0, 0.6 Hz, 1H, CH-C(H)*H*-C(CH$_3$), 2.34 (s, 3H, Ar–C*H*$_3$), 2.25 (bd, *J* = 18.0, 1H, CH-C(H)*H*-C(CH$_3$), 1.76 (ddd, *J* = 13.2, 4.2, 2.4 Hz, 1H, CH-C(H)*H*-CH), 1.63 (s, 3H, C*H*$_3$CH=CH), 1.24 (d, *J* = 12.0 Hz, 1H, CH-C(H)*H*-CH), 1.20 (d, *J* = 12.0 Hz, 1H, CH-C(H)*H*-CH), 1.11 (s, 3H, CH$_2$–C(C*H*$_3$)$_2$), 1.10 (s, 3H, CH$_2$–C(C*H*$_3$)$_2$). ^{13}C NMR (151 MHz, CDCl$_3$, Me$_4$Si) δ 149.1 (Cq), 139.6 (Cq), 135.4 (Cq), 134.2 (Cq), 131.8 (CH), 130.5 (Cq), 129.1 (2 × CH), 125.5 (2 × CH), 121.2 (CH), 62.5 (CH), 35.4 (CH), 34.6 (CH$_2$), 31.4 (2 × CH$_2$), 31.0 (Cq), 28.3 (CH$_3$), 27.0 (CH$_3$), 22.7 (CH$_3$), 21.3 (CH$_3$). mp degradation 172.5–180 °C. v_{max} (neat)/cm^{-1} 2971, 2916, 2862, 1449, 1344,

1177, 1159. HRMS (ESI) m/z [M + H]$^+$ Calcd for $C_{21}H_{27}N_2O_2S$ 371.1788, found 371.1777.

4,4,7-Trimethyl-2-(*o*-tolyl)-3,4,4a,5,5a,8-hexahydrobenzo[*e*] pyridazino[1,6-*b*][1,2]thiazine 10,10-dioxide (95g)

Following the general procedure, 111 mg (0.30 mmol) of 2,2-dimethylbut-3-enyl-*o*-tolyl ketone-*N*-tosylhydrazone **94g** were reacted with K_2CO_3 and [Ru(bpy)$_3$]Cl$_2$·6H$_2$O under blue light irradiation for 16 h to obtain 57.7 mg (0.16 mmol) of 4,4,7-trimethyl-2-(*o*-tolyl)-3,4,4a,5,5a,8-hexahydrobenzo [*e*]pyridazino[1,6-*b*][1,2]thiazine 10,10-dioxide **95g** (52%) as a white solid. ^{1}H NMR (600 MHz, CDCl$_3$, Me$_4$Si) δ 7.17–7.21 (m, 4H, Ar–*H*), 6.74 (td, J = 3.6, 1.8 Hz, 1H, CH$_2$—C*H*=C), 5.26 (m, 1H, CH$_3$CH=C*H*), 3.99 (dd, J = 12.6, 1.8 Hz, 1H, C=CHC*H*), 3.51 (m, 1H, C*H$_2$*-C(CH$_3$)$_2$), 2.77 (dm, J = 6.6 Hz, 2H, C*H$_2$*—CH=C), 2.34 (s, 3H, Ar–C*H$_3$*), 2.22 (dd, J = 19.0 1.2 Hz, 1H, CH-C(H)*H*-C(CH$_3$)), 2.15 (d, J = 18.7 Hz, 1H, CH-C(H)*H*- C(CH$_3$)), 2.15 (ddd, J = 13.2, 4.8, 3.0 Hz, 1H, CH-C(H)*H*-CH), 1.69 (s, 3H, C*H$_3$*CH=CH), 1.37 (d, J = 12.6 Hz, 1H, CH-C(H)*H*-CH), 1.33 (d, J = 12.6 Hz, 1H, CH-C(H)*H*- CH), 1.17 (s, 3H, CH$_2$–C(C*H$_3$*)$_2$), 1.06 (s, 3H, CH$_2$–C(C*H$_3$*)$_2$). ^{13}CNMR (151 MHz, CDCl$_3$, Me$_4$Si) δ 153.2 (Cq), 137.8 (Cq), 136.1 (Cq), 135.5 (Cq), 132.1 (CH), 131.1 (CH), 130.5 (Cq), 128.6 (CH), 127.8 (CH), 125.8 (CH), 121.3 (CH), 62.0 (CH), 38.3 (CH$_2$), 35.4 (CH), 31.6 (CH$_2$), 31.4 (CH$_2$), 31.2 (Cq), 28.3 (CH$_3$), 26.7 (CH$_3$), 22.8 (CH$_3$), 20.8 (CH$_3$). mp degradation 165.0–169.2 °C. v_{max} (neat)/cm^{-1} 2961, 2942, 2871, 2114, 1734, 1346, 1156, 1176. HRMS (ESI) m/z [M + H]$^+$ Calcd for $C_{21}H_{27}N_2O_2S$ 371.1788, found 371.1776.

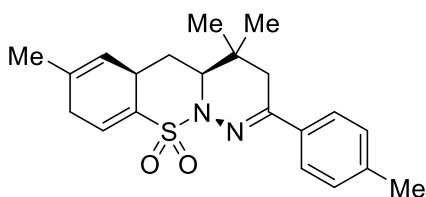## 4,7-Dimethyl-2,4-diphenyl-3,4,4a,5,5a,8-hexahydrobenzo[*e*] pyridazino[1,6-*b*][1,2]thiazine 10,10-dioxide (95h)
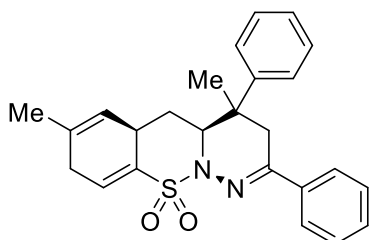
Following the general procedure, 125 mg (0.30 mmol) of 2-phenyl-2-methylbut-3-enylphenone *N*-tosylhydrazone **94h** were reacted with K_2CO_3 and [Ru(bpy)$_3$]Cl$_2$·6H$_2$O for 16 h under blue light irradiation to obtain 43 mg (0.10 mmol) of 4,4,7-trimethyl -2-phenyl-3,4,4a,5,5a,8-hexahydrobenzo[*e*] pyridazino[1,6-*b*][1,2]thiazine 10,10-dioxide **95h** (34%) as a white solid. ^{1}H

NMR (600 MHz, CDCl$_3$, Me$_4$Si) δ 7.85 (m, 2H, Ar–*H*), 7.40 (m, 3H, Ar–*H*), 7.30 (m, 2H, Ar–*H*), 7.25 (m, 3H, Ar–*H*), 6.76 (tm, *J* = 3.0, Hz, 1H, CH$_2$—C*H*=C), 5.23 (q, *J* = 1.2 Hz, 1H, CH$_3$CH=C*H*), 4.47 (dd, *J* = 12.6, 1.8 Hz, 1H, N–C*H*), 3.51 (bs, 1 H, CH$_2$—C*H*—CH=), 3.21 (d, *J* = 18.4 Hz, 1H, CPhMe–C*H*$_{2a}$), 2.78 (m, 2H, CH–C*H*$_2$–C(CH$_3$Ph), 2.54 (d, *J* = 18.4 Hz, 1H, CPhMe–C*H*$_{2b}$), 1.88 (ddd, *J* = 13.8, 4.2, 3.0 Hz, 1H, CH-C(H)*H*-CH), 1.67 (s, 3H, C*H*$_3$CH=CH), 1.43 (q, *J* = 13.0 Hz, 1H, CH-C(H)*H*-CH), 1.43 (s, 3H, -C(Ph)C*H*$_3$). ^{13}C NMR (151 MHz, CDCl$_3$, Me$_4$Si) δ 149.3 (Cq), 145.2 (Cq), 135.6 (Cq), 135.5 (Cq), 132.0 (CH), 130.7 (Cq), 129.7 (CH), 128.8 (2 × CH), 128.5 (2 × CH), 127.1 (CH), 125.7 (2 × CH), 125.4 (2 × CH), 121.1 (CH), 62.6 (CH), 35.3 (CH), 34.0 (CH$_2$), 32.2 (CH$_2$), 31.4 (CH$_2$), 29.8 (Cq), 26.5 (CH$_3$), 22.7 (CH$_3$). mp 113.0–117.0 °C. ν$_{max}$ (neat)/cm^{-1} 2964, 2929, 2256, 1498, 1412, 1338, 1180, 1157. HRMS (ESI) *m*/*z* [M + Na]$^+$ Calcd for C$_{25}$H$_{26}$N$_2$O$_2$SNa 441.1607, found 441.1614.

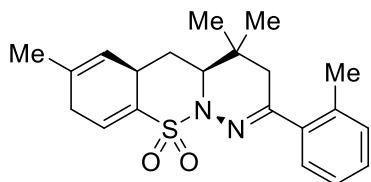## 2,4,4,7-tetramethyl-3,4,4a,5,5a,8-hexahydrobenzo[e]pyridazino[1,6-b][1,2]thiazine 10,10-dioxide (95i)

Following the general procedure A, 88 mg (0.30 mmol) of 4,4-dimethylhex-5-en-2-one-*N*-tosylhydrazone **94i** were reacted with K$_2$CO$_3$ and [Ru(bpy)$_3$]Cl$_2$·6H$_2$O for 16 h under blue light irradiation to obtain 65 mg (0.22 mmol) of 2,4,4,7-tetramethyl-3,4,4a,5,5a,8-hexahydrobenzo[*e*]pyridazino[1,6-*b*][1,2] thiazine 10,10-dioxide **95i** (73%) as a white solid. ^{1}H NMR (600 MHz, CDCl$_3$, Me$_4$Si) δ 6.74 (t, *J* = 3.8 Hz, 1H, CH$_2$—C*H*=C); 5.26 (q, *J* = 2.1 Hz 1H, CH$_3$CH=C*H*); 3.87 (dd, *J* = 12.8, 2.3 Hz, 1H, N–C*H*); 3.43 (bs, 1H, CH$_2$–C*H*–CH); 2.83 (ddd, *J* = 23.3, 7.8, 3.5 Hz, 1H, CH-C(H)*H*-C(CH$_3$)); 2.75 (dd, *J* = 22.7, 8.6, 1H, CH-C(H)*H*-C(CH$_3$)), 1.95 (s, 3H, C*H*$_3$—C=N); 1.88 (d, *J* = 18.9 Hz, 1H, CH-C(H)*H*-C(CH$_3$)$_2$); 1.84 (d, *J* = 19.0 Hz, 1H, CH-C(H)*H*-C(CH$_3$)$_2$), 1.72 (ddd, *J* = 13.5, 4.5, 2.3 Hz, 1H, CH-C(H)*H*-CH), 1.69 (s, 3H, C*H*$_3$CH=CH); 1.17 (q, *J* = 12.9 Hz, 1H, CH-C(H)*H*-CH); 1.05 (s, 3H, CH$_2$–C(CH$_3$)C*H*$_3$); 1.00 (s, 3H, CH$_2$–C(CH$_3$) (C*H*$_3$)). ^{13}C NMR (151 MHz, CDCl$_3$, Me$_4$Si) δ 152.7 (Cq); 135.1 (Cq); 131.8 (CH); 130.6 (Cq); 121.4 (CH); 62.0 (CH); 38.6 (CH$_2$); 35.41 (CH); 31.5(CH$_2$); 31.01 (Cq); 30.9 (CH$_2$); 28.3(CH$_3$); 26.7(CH$_3$); 24.3(CH$_3$); 22.9(CH$_3$). mp degradation 192.0–195 °C. ν$_{max}$ (neat)/cm^{-1} 2962, 1637, 1343, 1177, 1155. HRMS (ESI) *m*/*z* [M + Na]$^+$ Calcd for C$_{15}$H$_{22}$N$_2$O$_2$SNa 317.1294, found 317.1294.

2,4,4-Trimethyl-3,4,4a,5,5a,8-hexahydrobenzo[*e*]pyridazino[1,6-*b*][1,2]thiazine 10,10-dioxide (95j)

Following the general procedure A, 84 mg (0.30 mmol) of 4,4-dimethylhex-5-en-2-one-*N*-phenylsulfonylhydrazone **94j** were reacted with K_2CO_3 and [Ru(bpy)$_3$]Cl$_2$·6H$_2$O under blue light irradiation for 16 h to obtain 46 mg (0.165 mmol) of 2,4,4-trimethyl-3,4,4a,5,5a,8-hexahydrobenzo[*e*]pyridazino[1,6-*b*][1,2]thiazine 10,10-dioxide **95j** (55%) as a white solid. ^{1}H NMR (600 MHz, CDCl$_3$, Me$_4$Si) δ 6.74 (bs, 1H, CH$_2$—C*H*=C), 5.67 (dm, *J* = 10.2 Hz, 1H, CH—C*H*=CH—CH$_2$), 5.54 (dm, *J* = 10.1 Hz, 1H, CH–CH=C*H*-CH$_2$), 3.87 (dd, *J* = 12.8, 2.3 Hz, 1H, N–C*H*), 3.45 (m, 1H, CH$_2$–C*H*-CH), 2.94 (dm, *J* = 23.9 Hz, 1H, CH-C(H)*H*-C(CH$_3$)), 2.85 (ddq, *J* = 23.9, 8.7, 3.3 Hz, 1H, CH-C(H)*H*-C(CH$_3$)), 1.95 (s, 3H, C*H$_3$*—C=N), 1.87 (d, *J* = 6.5 Hz, 2H, CH–C*H$_2$*–C(CH$_3$)$_2$), 1.72 (ddd, *J* = 13.3, 4.2, 2.4 Hz, 1H, CH-C(H)*H*-CH), 1.22 (q, *J* = 12.8 Hz, 1H, CH-C(H)*H*-CH), 1.05 (s, 3H, CH$_2$–C(C*H$_3$*)$_2$), 0.99 (s, 3H, CH$_2$–C(C*H$_3$*)$_2$). ^{13}C NMR (151 MHz, CDCl$_3$, Me$_4$Si) δ 152.7 (Cq), 135.2 (Cq), 131.7 (CH), 126.7 (CH), 123.0 (CH), 62.0 (CH), 38.5 (CH$_2$), 34.3 (CH), 30.9 (Cq), 30.6 (CH$_2$), 28.2 (Cq), 26.8 (CH$_2$), 26.6 (CH$_3$), 24.2 (CH$_3$). mp degradation 185.0–190.2 °C. v$_{max}$ (neat)/cm^{-1} 2975, 712, 1639, 1341, 1171. HRMS (ESI) *m*/*z* [M + H]$^+$ Calcd for C$_{14}$H$_{21}$N$_2$O$_2$S 281.1318, found 281.1312.
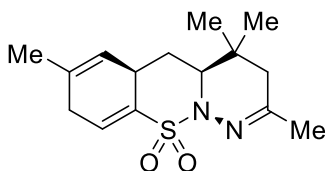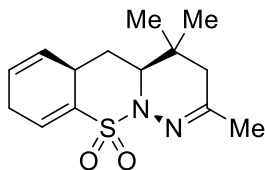
4,4-Dimethyl-2-phenyl-3,4,4a,5,5a,8-hexahydrobenzo[*e*]pyridazino[1,6-*b*][1,2]thiazine 10,10-dioxide (95k)
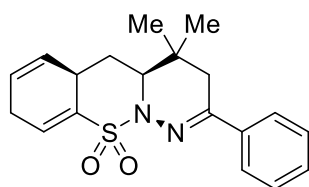
Following the general procedure A, 103 mg (0.30 mmol) of 2,2-dimethylbut-3-enylphenone-*N*-phenylsulfonylhydrazone **94k** were reacted with K_2CO_3 and [Ru(bpy)$_3$]Cl$_2$·6H$_2$O for 16 h under blue light irradiation to obtain 41 mg (0.120 mmol) of 4,4-dimethyl-2-phenyl-3,4,4a,5,5a,8-hexahydrobenzo[*e*]pyridazino[1,6-*b*][1,2]thiazine 10,10-dioxide **95k** (40%) as a white solid. ^{1}H NMR (600 MHz, CDCl$_3$, Me$_4$Si) δ 7.80–7.74 (m, 2H, Ar–*H*), 7.38–7.33 (m, 3H, Ar–*H*), 6.76 (bm, 1H, CH$_2$—C*H*=C), 5.63 (dm, *J* = 10.1, 1H, CH—C*H*=CH—CH$_2$, 1H), 5.54 (dm, *J* = 10.2, 3.3, 2.0 Hz, 1H, CH$_3$CH=C*H*), 4.03 (dd, *J* = 12.7, 2.5 Hz, 1H, N–C*H*), 3.52 (m, 1H, CH$_2$–C*H*-CH), 2.87 (tm, *J* = 8.6 Hz, 2H), 2.39 (dd, *J* = 18.3, 1.1 Hz, 1H, CH-C(H)*H*-C(CH$_3$ 2.29 (dd, *J* =

18.4, 0.9 Hz, 1H, CH-C(H)H-C(CH$_3$)), 1.79 (ddd, J = 13.3, 4.2, 2.5 Hz, 1H, CH-C(H)H-CH), 1.29 (q, J = 12.8 Hz, 1H, CH-C(H)H-CH), 1.12 (d, J = 1.8 Hz, 6H, CH$_2$–C(CH_3)$_2$). ^{13}CNMR (151 MHz, CDCl$_3$, Me$_4$Si) δ 149.1 (Cq), 136.9 (Cq), 135.5 (Cq), 131.8 (CH), 129.5 (CH), 128.4 (2 × CH), 126.6 (CH), 125.6 (2 × CH), 123.0 (CH), 62.5 (CH), 34.6 (CH$_2$), 34.4 (CH), 31.2 (CH$_2$), 31.0 (Cq), 28.3 (CH$_3$), 27.0 (CH$_3$), 26.8 (CH$_2$). mp 141.9–144.5 °C. v$_{max}$ (neat)/cm^{-1} 3059, 2956, 2922, 2868, 1445, 1349, 1169, 1019, 955. HRMS (ESI) m/z [M + Na]$^+$ Calcd for C$_{19}$H$_{22}$N$_2$O$_2$SNa 365.1294, found 365.1285.

2,9,12,12-Tetramethyl-3,8,9,10,11,11a,12,12a,13,13a-decahydro benzo[5,6][1,2]thiazino[2,3-*b*]cinnoline 5,5-dioxide (95l)
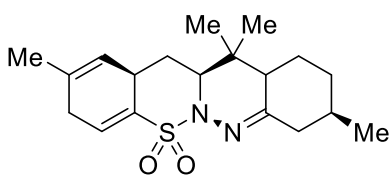
Following the general procedure A, 101 mg (0.300 mmol) of pulegone tosylhydrazone **94l** were reacted with K$_2$CO$_3$ and [Ru(bpy)$_3$]Cl$_2$·6H$_2$O under blue light irradiation for 16 h to obtain 36,5 mg (0.105 mmol) of 2,9,12,12-tetramethyl-3,8,9,10,11,11a,12,12a,13,13a-decahydrobenzo[5,6][1,2]thiazino[2,3-*b*]cinnoline 5,5-dioxide **95l** (35%) as a white solid. ^{1}H NMR (600 MHz, CDCl$_3$, Me$_4$Si) δ 6.72 (bs, 1H, CH$_2$—CH=C), 5.25 (bs, 1H, CH$_3$CH=CH), 3.90 (dd, J = 12.7, 2.3 Hz, 1H, N–CH), 3.40 (m, 1H, CH$_2$–CH–C(CH$_3$)$_2$), 2.81 (dm, J = 22.2 Hz, 1H, CH_{2a}-CH-C(CH$_3$)$_2$), 2.74 (dd, J = 22.2 Hz, 7.4 Hz, 1H, CH_{2b}-CH–C(CH$_3$)$_2$), 2.58 (dt, J = 14.5, 2.4 Hz, 1H, CH-CH_{2a}-C(CH$_3$)), 1.84 (m, 2H, CH(CH$_3$)–CH_2–C=N), 1.72 (d, J = 13.7 Hz, 1H, CH–CH_{2a}–CH$_2$), 1.68 (m, 1H, CH(CH$_3$)-CH$_2$-C(H)H-CH), 1.67 (s, 3H, CH_3CH=CH), 1.55 (s, 2H, CH_3CH=CH), 1.32–1.19 (m, 2H, CH(CH$_3$)-CH$_2$-C(H)H-CH with CH$_2$–C(CH)=N), 1.06 (qd, J = 12.5, 11.4, Hz, 1H, CH(CH$_3$)–C(H)H-CH$_2$–CH), 1.00 (s, 3H, (CH_3)$_{2a}$), 0.99 (s, 3H, (CH_3)$_{2b}$), 0.93 (d, J = 6.5 Hz, 3H, CH–CH_3). ^{13}CNMR (151 MHz, CDCl$_3$, Me$_4$Si) δ 158.3 (Cq), 135.1 (Cq), 132.0 (CH), 130.5 (CH), 121.3 (CH), 64.7 (CH), 43.3 (Cq), 42.5 (Cq), 35.5 (CH), 34.1 (CH$_2$), 33.8 (Cq), 33.2 (CH), 31.4 (CH$_2$), 30.0 (CH$_2$), 25.6 (CH$_2$), 25.1 (CH$_3$), 24.9 (CH$_3$), 22.8 (CH$_3$), 22.1 (CH$_3$). mp degradation 118.0–124.0 °C. v$_{max}$ (neat)/cm^{-1} 2949, 1737, 1630, 1453, 1352, 1150. HRMS (ESI) m/z [M + H]$^+$ Calcd for C$_{19}$H$_{29}$N$_2$O$_2$S 349.1944, found 349.1936.

6.2.8 Scaled-up Procedure for the Synthesis of 2,4,4,7-Tetramethyl-3,4,4a,5,5a,8-hexahydrobenzo [*e*]pyridazino[1,6-*b*][1,2]thiazine 10,10-dioxide (95i)

94i, *2.0 mmol*

Ru(bpy)$_3$Cl$_2$·6H$_2$O
(3 mol%)
K$_2$CO$_3$ (1.5 eq.)
CH$_3$CN [0.06 M], N$_2$, rt,
72h, *hv* (40W Blue LED)

95i, *51%*
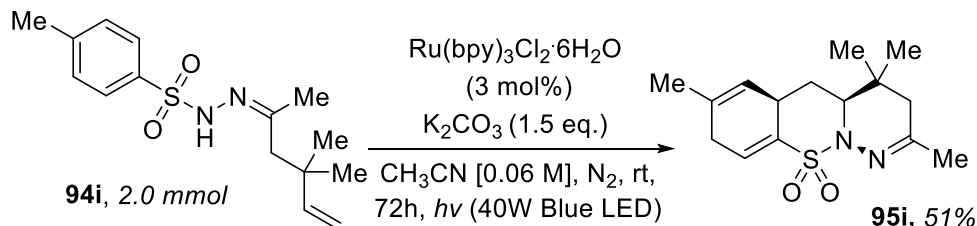
In a large-sized sealed photochemical reactor (65 mm as ID and 50 mm height), 40 mg of [Ru(bpy)$_3$]Cl$_2$·6H$_2$O (0.06 mmol) were dissolved in 25 mL of anhydrous CH$_3$CN, and the solution was degassed with N$_2$ for 15 min. Then 4,4-dimethylhex-5-en-2-one-*N*-tosylhydrazone **94i** (0.590 g, 2.00 mmol) and K$_2$CO$_3$ (0.415 g, 3.00 mmol) were added in one portion and the solution degassed for additional 10 min. The mixture was then stirred at 4 cm from the irradiation source at room temperature until reaction completion, which occurred in 72 h. The solution was then filtered on a pad of silica gel and Celite using CH$_2$Cl$_2$ as eluent and Et$_2$O to wash the column. The crude product was purified by flash chromatography on silica gel (hexane/acetone 92/8) to obtain 0.300 g of 2,4,4,7-tetramethyl-3,4,4a,5,5a,8-hexahydrobenzo[*e*]pyridazino[1,6-*b*][1,2]thiazine 10,10-dioxide **95i** as a white solid (yield = 51%).

6.2.9 TEMPO-Trapping Experiment: Isolation of TEMPO Adduct (100)

94a

K$_2$CO$_3$ (1.5 eq)
TEMPO (2.0 eq)
[Ru(bpy)$_3$]Cl$_2$·6H$_2$O
(3 mol%)
CH$_3$CN, rt, N$_2$, 16h,
hv (40 W blue LEDs)

100, *30%*
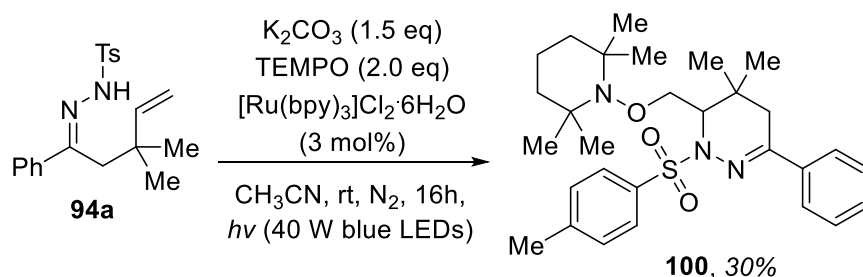
In a sealed photochemical reactor 6.8 mg (0.009 mmol) of [Ru(bpy)$_3$]Cl$_2$·6H$_2$O were dissolved in 5 mL of anhydrous CH$_3$CN, and the solution was degassed with N$_2$ for 15 min. Then 2,2-dimethylbut-3-enylphenonetosylhydrazone **94a** (107.0 mg, 0.300 mmol), TEMPO radical (2,2,6,6-tetramethylpiperidin-1-yl)oxyl) (94.0 mg, 0.600 mmol) and

K$_2$CO$_3$ (62.5 mg, 0.45 mmol) were added in one portion and the solution degassed for additional 10 min. The mixture was then stirred at 4 cm from the irradiation source (see above) at room temperature for 16 h. The solution was then filtered on a pad of silica gel and Celite using CH$_2$Cl$_2$ as eluent and Et$_2$O to wash the column. The crude product was purified by flash chromatography on silica gel (hexane/acetone 92/8) to obtain 46.4 mg (0.009 mmol) of the TEMPO-adduct (5,5-dimethyl-3-phenyl-6-(((2,2,6,6-tetramethylpiperidin-1-yl)oxy)methyl)-1-tosyl-1,4,5,6-tetrahydropyridazine) **100** as light pink crystals (yield = 30%). ^{1}H NMR (600 MHz, CDCl$_3$, Me$_4$Si) δ 7.88 (d, J = 8.3 Hz, 2H, Ar-*H*), 7.68 (m, 2H, Ar-*H*), 7.33 (m, 3H, Ar-*H*), 7.25 (m, 2H, Ar-*H*), 4.04 (s, 2H, O-C*H*$_2$), 4.04 (m, 1H, N-N(Ts)-C*H*) 2.60 (dd, J = 17.5, 1.2 Hz, 1H, (CH$_3$)$_2$-CH-C(H)*H*), 2.37 (s, 3H, Ar-C*H*$_3$), 2.23 (dd, J = 17.5, 1.2 Hz, 1H, (CH$_3$)$_2$-CH-C(H)*H*), 1.52 − 1.33 (m, 4H, C(C*H*$_2$)H$_2$), 1.23 (s, 3H, (s, 3H, N-C-C(CH$_3$)-C*H*$_3$), 1.17 (s, 3H, C(CH$_3$)$_2$-N-C(CH$_3$)C*H*$_3$), 1.12 (s, 3H, C(CH$_3$)$_2$-N-C(CH$_3$)C*H*$_3$), 1.08 (s, 3H, C(CH$_3$)$_2$-N-C(CH$_3$)C*H*$_3$), 0.90 (s, 3H, C(CH$_3$)$_2$-N-C(CH$_3$)C*H*$_3$), 0.97 − 0.79 (m, 2H, CH$_2$-C*H*$_2$-CH$_2$), 0.56 (s, 3H, N-C-C(CH$_3$)-C*H*$_3$). ^{13}CNMR (151 MHz, CDCl$_3$, Me$_4$Si) δ. 146.1 (Cq), 143.4 (Cq), 137.6 (Cq), 136.6 (Cq), 129.3 (2 x CH), 128.9 (CH), 128.3 (2 x CH), 128.1 (2 x CH), 125.4 (2 x CH), 60.7 (CH), 60.2 (Cq), 60.0 (Cq), 40.0 (CH$_2$), 39.9 (CH$_2$), 34.9 (CH$_2$), 33.4 (CH$_3$), 32.7 (Cq), 29.8 (CH$_2$), 29.0 (CH$_3$), 28.7 (CH$_3$), 26.8 (CH$_3$), 21.6 (CH$_3$), 20.7 (CH$_3$), 20.3 (CH$_3$), 17.1 (CH$_2$) . HRMS (ESI) m/z [M + H]$^+$ Calcd for C$_{29}$H$_{42}$N$_3$O$_3$S 512.2941, found 512.2938. IR v$_{max}$ (neat)/cm^{-1} 3002, 2951, 1733, 1598, 1493, 1344, 1167, 1092.
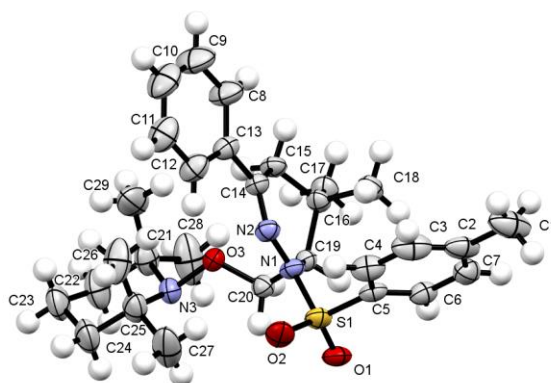
Figure 6.2 ORTEP plot of the Asymmetric unit of **100** (50 % probability)

Table 6.4 Crystal data and structure refinement for **100**

Empirical formula	$C_{29}H_{41}N_3O_3S$
Formula weight	511.71
Temperature/K	298
Crystal system	triclinic
Space group	P-1
a/Å	8.0001(6)
b/Å	10.6949(10)
c/Å	18.4042(17)
α/°	100.362(8)
β/°	101.543(8)
γ/°	98.215(7)
Volume/Å³	1491.3(2)
Z	2
ρ_{calc}g/cm³	1.140
μ/mm⁻¹	0.140
F(000)	552.0
Crystal size/mm³	0.3 × 0.25 × 0.22
Radiation	MoKα (λ = 0.71073)
2Θ range for data collection/°	6.548 to 52.744
Index ranges	-9 ≤ h ≤ 9, -13 ≤ k ≤ 13, -22 ≤ l ≤ 22
Reflections collected	26087
Independent reflections	6077 [R_{int} = 0.0958, R_{sigma} = 0.0910]
Data/restraints/parameters	6077/816/332
Goodness-of-fit on F²	1.005
Final R indexes [I>=2σ (I)]	R_1 = 0.0757, wR_2 = 0.1620
Final R indexes [all data]	R_1 = 0.1603, wR_2 = 0.2036
Largest diff. peak/hole / e Å⁻³	0.19/-0.20

Table 6.5 Bond Angles for **100**

Atom	Atom	Atom	Angle/°	Atom	Atom	Atom	Angle/°
O1	S1	N1	105.38(14)	C18	C16	C17	109.6(3)
O1	S1	C5	108.63(17)	C17	C16	C19	110.7(3)
N1	S1	C5	106.47(15)	C7	C6	C5	120.4(4)
O2	S1	O1	119.79(16)	O3	C20	C19	109.9(3)
O2	S1	N1	107.89(15)	C3	C2	C7	117.3(5)
O2	S1	C5	107.95(18)	C3	C2	C1	121.5(5)
C20	O3	N3	110.7(2)	C7	C2	C1	121.2(6)
N2	N1	S1	113.0(2)	C5	C4	C3	120.8(5)
N2	N1	C19	124.0(2)	C13	C12	C11	121.6(5)
C19	N1	S1	121.5(2)	C2	C3	C4	121.6(4)
C14	N2	N1	119.2(3)	C6	C7	C2	121.7(5)
O3	N3	C25	107.2(3)	N3	C25	C24	106.0(4)
O3	N3	C21	106.8(3)	N3	C25	C26	114.3(4)
C21	N3	C25	118.7(3)	N3	C25	C27	106.6(4)
C6	C5	S1	120.4(3)	C26	C25	C24	112.2(4)
C4	C5	S1	121.3(3)	C26	C25	C27	108.7(5)
C4	C5	C6	118.2(4)	C27	C25	C24	108.8(4)
N1	C19	C16	108.8(3)	N3	C21	C29	116.4(4)
N1	C19	C20	109.1(3)	N3	C21	C22	106.5(4)
C20	C19	C16	118.2(3)	N3	C21	C28	105.4(4)
N2	C14	C15	124.2(3)	C29	C21	C22	111.3(4)
N2	C14	C13	115.7(3)	C29	C21	C28	109.4(5)
C13	C14	C15	120.0(3)	C22	C21	C28	107.3(4)
C14	C15	C16	112.4(3)	C13	C8	C9	120.7(5)
C12	C13	C14	120.9(4)	C23	C24	C25	112.9(4)
C12	C13	C8	117.2(4)	C23	C22	C21	113.4(4)
C8	C13	C14	121.8(4)	C22	C23	C24	107.0(4)
C15	C16	C19	109.5(3)	C10	C11	C12	119.7(5)
C15	C16	C17	109.5(3)	C11	C10	C9	120.4(5)
C18	C16	C19	108.4(3)	C10	C9	C8	120.4(5)
C18	C16	C15	109.1(3)				

Table 6.6 Bond Lengths for **100**

Atom	Atom	Length/Å	Atom	Atom	Length/Å
S1	O1	1.432(2)	C18	C16	1.524(5)
S1	N1	1.643(3)	C16	C17	1.531(5)
S1	O2	1.421(3)	C6	C7	1.371(5)
S1	C5	1.730(4)	C2	C3	1.373(7)
O3	N3	1.450(3)	C2	C7	1.375(6)
O3	C20	1.411(4)	C2	C1	1.497(6)
N1	N2	1.379(4)	C4	C3	1.372(6)
N1	C19	1.482(4)	C12	C11	1.385(6)
N2	C14	1.286(4)	C25	C24	1.525(6)
N3	C25	1.489(5)	C25	C26	1.517(6)
N3	C21	1.483(5)	C25	C27	1.523(6)
C5	C6	1.380(5)	C21	C29	1.505(6)
C5	C4	1.369(5)	C21	C22	1.528(6)
C19	C16	1.533(4)	C21	C28	1.542(6)
C19	C20	1.509(4)	C8	C9	1.389(6)
C14	C15	1.497(4)	C24	C23	1.507(7)
C14	C13	1.469(5)	C22	C23	1.506(6)
C15	C16	1.527(5)	C11	C10	1.349(7)
C13	C12	1.379(5)	C10	C9	1.353(7)
C13	C8	1.380(5)			

6.3. Photoinduced cyclization and radical Smiles Rearrangement of γ,δ-unsaturated *N*-arylsulfonylhydrazones

6.3.1 General Procedure for the Synthesis of γ,δ-Unsaturated Ketones with Not Terminal Unsaturated Moiety (89j-89k)
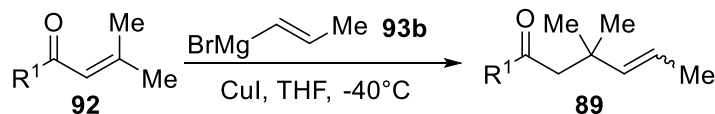
Ketones **89j** and **89k** were synthesized according to the procedure reported in chapter 6, paragraph 6.2.4) with a single modification: propenylmagnesium bromide **93b** (22.0 mL, commercial 0.5 M solution in THF) was used instead of vinylmagnesiumbromide **93a** and the products were obtained as a mixture of *E/Z* isomers.

2,2-Dimethylpent-3-enylphenone (89j)
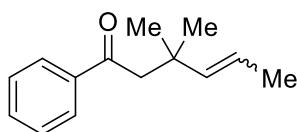
Following the described procedure, 1.60 g (10.0 mmol) of 2-methylprop-1-enylphenone **92a** (4-methylpent-3-en-2-one) were reacted with CuI and propenylmagnesium bromide **93b** to afford 1.75 g of 2,2-dimethylpent-3-enylphenone **89j** (87%) as a colorless oil. ^{1}H NMR (600 MHz, CDCl$_3$, Me$_4$Si), mixture of isomers (75:25) δ 7.91(dm, *J* = 7.2 Hz, 2H, Ar–*H*, *Z* isomer); 7.88(dm, *J* = 7.2 Hz, 2H, Ar–*H*, *E* isomer); 7.50 (m, 3H, Ar–*H*, both isomers); 7.41 (m, 3H, Ar–*H*, both isomers); 5.52 (dq, *J* = 15.6, 1.8 Hz, 1H, C*H*=CHCH$_3$, *E* isomer); 5.42 (dq, *J* = 12.0, 1.8 Hz, 1H, C*H*=CHCH$_3$, *Z* isomer); 5.33 (dq, *J* = 15.6, 6.0 Hz, 1H, CH=C*H*CH$_3$, *E* isomer); 5.31 (dq, *J* = 12.0, 7.2 Hz, 1H, CH=C*H*CH$_3$, *Z* isomer); 3.08 (s, 2H, CO–C*H*$_2$, *Z* isomer); 2.91 (s, 2H, CO–C*H*$_2$, *E* isomer); 1.68 (dd, *J* = 7.2, 1.8 Hz, 1H, CH=C*H*CH$_3$, *Z* isomer); 1.57 (dd, *J* = 6.0, 1.8 Hz, 1H, CH=C*H*CH$_3$, *E* isomer); 1.27 (s, 6H, CH$_2$–(C*H*$_3$)$_2$–CH, *Z* isomer), 1.13 (s, 6H, CH$_2$–(C*H*$_3$)$_2$–CH, *E* isomer). ^{13}C NMR (151 MHz; CDCl$_3$, Me$_4$Si), mixture of isomers (75:25) 199.9 (Cq, *E* isomer); 199.5 (Cq, *Z* isomer); 140.4 (CH, *E* isomer); 138.9 (CH, *Z* isomer); 138.6 (Cq, *E* isomer); 138.4 (Cq, *Z* isomer); 132.8 (2 × CH, *Z* isomer); 132.7 (2 × CH, *E* isomer); 128.5 (2 × CH, *Z* isomer); 128.5 (2 × CH, *E* isomer); 128.4 (CH, *E* isomer); 128.2 (CH, *Z* isomer); 123.0 (CH, *Z* isomer); 121.0

(CH, E isomer); 50.2 (CH$_2$, Z isomer); 50.0 (CH$_2$, E isomer); 36.1 (Cq, Z isomer); 36.1 (Cq, E isomer); 29.3 (CH$_3$, Z isomer), 27.9 (CH$_3$, E isomer), 18.0 (2 × CH$_3$, E isomer), 14.4 (2 × CH$_3$, Z isomer).

4,4-Dimethylhept-5-en-2-one (89k)
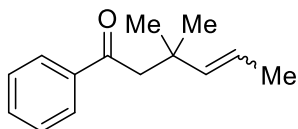
Following the described procedure, 0.98 g (10.0 mmol) of mesityl oxide **92i** (4-methylpent-3-en-2-one) were reacted with CuI and propenylmagnesium bromide **93b** to afford 0.97 g of 4,4-dimethylhept-5-en-2-one **89k** (69%) as a colorless oil. ^{1}H NMR (600 MHz, CDCl$_3$, Me$_4$Si), mixture of isomers (60:40) δ 5.52 (dq, J = 15.6, 1.8 Hz, 1H, CH=CHCH$_3$, E isomer); 5.34–5.38 (m, 3H, CH=CHCH$_3$, Z isomer, CH=CHCH$_3$, E and Z isomer); 2.53 (s, 2H, CO–CH_2, Z isomer); 2.37 (s, 2H, CO–CH_2, E isomer); 2.11 (s, 2H, CO–CH_3, Z isomer); 2.07 (s, 2H, CO–CH_3, E isomer); 1.71 (dd, J = 6.0, 3.0 Hz, 1H, CH=CHCH$_3$, Z isomer); 1.65 (dd, J = 6.6, 1.2 Hz, 1H, CH=CHCH$_3$, E isomer); 1.20 (s, 6H, CH$_2$–(CH_3)$_2$–CH, Z isomer), 1.07 (s, 6H, CH$_2$–(CH_3)$_2$–CH, E isomer). ^{13}C NMR (151 MHz; CDCl$_3$, Me$_4$Si), mixture of isomers (75:25) 208.8 (Cq, E isomer); 208.5 (Cq, Z isomer); 140.0 (CH, E isomer); 138.5 (CH, Z isomer); 123.6 (CH, Z isomer); 121.4 (CH, E isomer); 56.0 (CH$_2$, Z isomer); 55.8 (CH$_2$, E isomer); 35.8 (Cq, Z isomer); 35.4 (Cq, E isomer); 32.4 (CH$_3$, Z isomer), 32.0 (CH$_3$, E isomer), 29.2 (CH$_3$, Z isomer), 27.7 (CH$_3$, E isomer), 18.1 (2 × CH$_3$, E isomer), 14.4 (2 × CH$_3$, Z isomer).

6.3.2 General Procedure for the Synthesis of γ,δ-Unsaturated N-Mesitylsulfonylhydrazones (132)
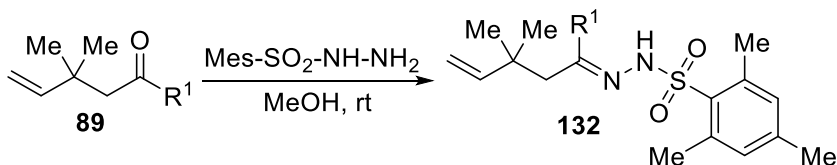
Mesitylsulfonylhydrazones **132** were synthesized according to the procedure reported in chapter 6, paragraph 6.2.5) with a single modification: commercially available 2,4,6-trimethylbenzenesulfonolhydrazide (mesitylsulfonylhydrazide) was employed instead of other arylsulfonylhydrazide.

2,2-Dimethylbut-3-enylphenone-*N*-mesitylsulfonylhydrazone (132a)
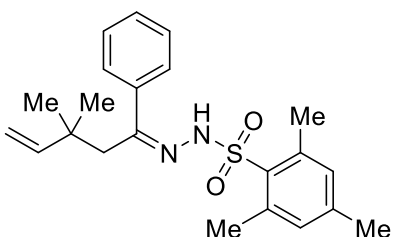
Following the described procedure 2,2-dimethylbut-3-enylphenone **92a** (0.75 g, 4.0 mmol) was reacted with mesitylsulfonylhydrazide (0.96 g, 4.5 mmol) in methanol (2.5 mL) to obtain 0.81 g (2.1 mmol) of 2,2-dimethylbut-3-enylphenone-*N*-2,4,6-mesitylsulfonylhydrazone **132a** (only one isomer found) as a white powder (53%, PE/EE 9/1). ^{1}H NMR (600 MHz, CDCl$_3$, Me$_4$Si) δ 7.93–7.96 (bs, 1H, N–*H*), 7.47 (dd, *J* = 8.0, 1.6 Hz, 2H, Ar–*H*), 7.34–7.25 (m, 3H, Ar–*H*), 6.97 (s, 2H, Ar–*H*), 5.78 (dd, *J* = 17.5, 10.6 Hz, 1H, C*H*=CH$_2$), 5.01 (d, *J* = 17.4 Hz, 1H, C*H*=CH$_2$*H trans*), 4.95 (dd, *J* = 10.8, 0.7 Hz, 1H, C*H*=CH$_2$*H cis*), 2.71 (s, 6H, *ortho* Ar -C*H$_3$*), 2.68 (s, 2H, N=C—C*H$_2$*), 2.30 (s, 3H, *para* Ar -C*H$_3$*), 0.97 (s, 6H, C(C*H$_3$*)$_2$). ^{13}C NMR (151 MHz; CDCl$_3$, Me$_4$Si) δ 154.2 (Cq), 146.8 (CH), 143.0 (Cq), 140.6 (2 × Cq), 138.8 (Cq), 132.5 (Cq), 131.9 (2 × CH), 129.3 (CH), 128.3 (2 × CH), 127.0 (2 × CH), 113.0 (CH$_2$), 39.0 (CH$_2$), 38.1(Cq), 28.0 (CH$_3$), 23.6 (2 × CH$_3$), 21.1 (2 × CH$_3$). mp 76–82 °C. HRMS (ESI) *m/z* [M + H]$^+$ Calcd for C$_{22}$H$_{29}$N$_2$O$_2$S 385.1944, found 385.1951. IR ν$_{max}$ (neat)/cm^{-1} 3201, 2962, 1602, 1444, 1377, 1159.

2,2-Dimethylbut-3-enylnaphtone-*N*-mesitylsulfonylhydrazone (132b)
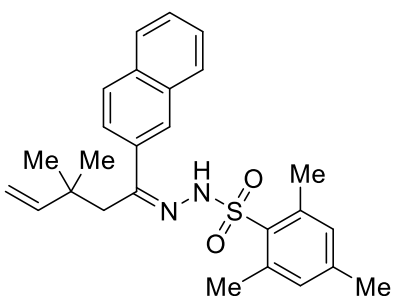
Following the described procedure 2,2-dimethylbut-3-enylnaphtone **92b**, (0.480 g, 2.0 mmol) was reacted with mesitylsulfonylhydrazide (0.47 g, 2.2 mmol) in methanol (2 mL) at rt to obtain 0.312 g of 2,2-dimethylbut-3-enylnaphtone-*N*-2,4,6-mesitylsulfonylhydrazone **132b** (0.72 mmol) as a white powder (36%, PE/AcOEt 99/1). ^{1}H NMR (600 MHz, CDCl$_3$, Me$_4$Si) δ 8.02 (s, 1H, N–*H*), 7.89 (m, 1H, Ar–*H*), 7.87 (m, 1H, Ar–*H*), 7.80 (m, 2H, Ar–*H*), 7.75 (dd, *J* = 8.7, 3.3 Hz, 1H, Ar–*H*), 7.66 (m, 1H, Ar–*H*) 7.47 (m, 1H, Ar–*H*), 6.99 (s, 2H, Ar–*H*), 5.83 (dd, *J* = 17.4, 10.6 Hz, 1H, C*H*=CH$_2$), 5.07 (d, *J* = 17.4 Hz, 1H, C*H*=CH$_2$*H trans*), 4.99 (dd, *J* = 10.8, 0.7 Hz, 1H, C*H*=CH$_2$*H cis*), 2.80 (s, 2H,

N=C—C*H₂*), 2.75 (s, 6H, *ortho* Ar-C*H₃*), 2.31 (s, 3H, *para* Ar-C*H₃*), 1.01 (s, 6H, C(C*H₃*)₂). ^{13}C NMR (151 MHz; CDCl₃, Me₄Si) 153.9 (Cq), 146.9 (CH), 143.1 (Cq), 140.6 (2 × Cq), 136.2 (Cq), 133.8 (Cq), 132.9 (Cq), 132.5 (Cq), 132.0 (2 × CH), 128.6 (CH), 128.0 (CH), 127.7 (CH), 126.8 (CH), 126.7 (Cq), 126.4 (CH), 124.5 (CH), 113.2 (CH₂), 39.0 (CH₂), 38.2 (Cq), 28.1 (CH₃), 23.5 (CH₃), 21.2 (2 × CH₃). mp 59–65 °C. HRMS (ESI) *m/z* [M + H]⁺ Calcd for C₂₆H₃₁N₂O₂S 435.2101, found 435.2107. IR ν$_{max}$ (neat)/cm⁻¹ 3228, 2960, 1602, 1467, 1376, 1331, 1187, 1161, 1052.

2,2-Dimethylbut-3-enyl-*p*-tolyl ketone-*N*-mesitylsulfonylhydrazone (132c)

Following the described procedure 2,2-dimethylbut-3-enyl-*p*-tolyl ketone **89f**, (0.85 g, 4.0 mmol) was reacted with mesitylsulfonylhydrazide (0.95 g, 4.5 mmol) in methanol (2 mL) to obtain 0.98 g (2.5 mmol) of 2,2-dimethylbut-3-enyl-*p*-tolyl ketone-*N*-mesitylsulfonylhydrazone **132c** as a white powder (62%, PE/AcOEt 98/2). ^{1}H NMR (600 MHz, CDCl₃, Me₄Si) (mixture of isomers 83:17). ^{1}H NMR (600 MHz, Chloroform-*d*) δ 7.93 (s, 1H, N–*H*, major isomer), 7.63 (bs, 1H, N–*H* minor isomer), 7.37 (d, *J* = 8.3 Hz, 2H, Ar–*H*, minor isomer), 7.34 (d, *J* = 8.1 Hz, 2H, Ar–*H* major isomer), 7.22 (d, *J* = 7.8 Hz, 2H, Ar–*H*, both isomers), 7.09 (m, 4H, Ar–*H*, both isomers), 6.96 (d, *J* = 4.0 Hz, 2H, Mes–*H*, both isomers), 5.79 (dd, *J* = 17.4, 10.2 Hz, 1H, C*H*=CH₂ major isomer), 5.54 (dd, *J* = 17.4, 10.2 Hz, 1H, C*H*=CH₂ minor isomer), 5.02 (dd, *J* = 17.4, 0.6 Hz, 1H, CH=C*H₂*, *H trans* major isomer), 4.96 (dd, *J* = 10.2, 1.2 Hz, 1H, CH=C*H₂*, *H cis* major isomer) 4.66 (dd, *J* = 17.4, 1.2 Hz, 1H, CH=C*H₂*, *H trans*, minor isomer), 4.59 (dd, *J* = 10.8, 1.2 Hz, 1H, CH=C*H₂*, *H cis*, minor isomer), 2.70 (m, 12H Ar–CH₃, both isomers), 2.59 (s, 2H, N=C—C*H₂*, major isomer), 2.45 (s, 2H, N=C—C*H₂*, major isomer), 2.31 (s, 3H, *p*-tolyl C*H₃* major isomer), 2.30 (s, 3H, *p*-tolyl C*H₃*, minor isomer), 2.29 (s, 3H Ar–CH₃ major isomer), 2.29 (s, 3H Ar–CH₃,minor isomer), 0.97 (s, 6H, C(C*H₃*)₂, minor isomer), 0.76 (s, 6H, C(C*H₃*)₂ major isomer). ^{13}C NMR (151 MHz; CDCl₃, Me₄Si) (mixture of isomers) δ154.7 (Cq), 154.3 (Cq), 147.0 (CH), 142.9 (CH), 140.6 (Cq), 140.5 (Cq), 139.4 (CH), 136.1 (CH), 132.6 (CH), 131.9 (2 × CH), 130.2 (2 × CH), 129.0 (2 × CH), 126.9 (2 × CH), 126.8

(2 × CH), 113.0 (CH$_2$), 110.4 (CH$_2$), 39.0 (CH$_2$), 38.1 (Cq), 37.7 (Cq), 36.2 (CH$_2$); 35.9 (CH); 28.0 (CH$_3$), 27.4 (CH$_3$), 23.6 (CH$_3$), 23.5 (CH$_3$), 21.3 (2 × CH$_3$) 21.1 (2 × CH$_3$). HRMS (ESI) *m/z* [M + H]$^+$ Calcd for C$_{23}$H$_{31}$N$_2$O$_2$S 399.2101, found 399.2104.

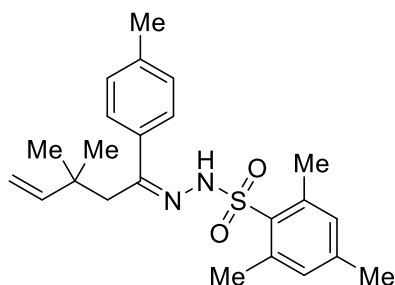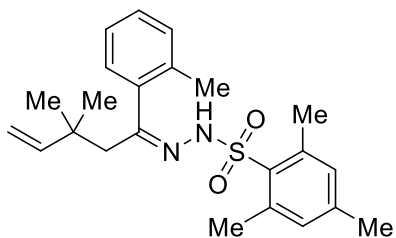## 2,2-Dimethylbut-3-enyl-*o*-tolyl ketone-*N*-mesitylsulfonylhydrazone (132d)

Following the described procedure 2,2-dimethylbut-3-enyl-*o*-tolyl ketone **89g**, (0.40 g, 2.0 mmol) was reacted with mesitylsulfonylhydrazide (0.45 g, 2.2 mmol) in methanol (2 mL) to obtain 139 mg (0.35 mmol) of 2,2-dimethylbut-3-enyl-*o*-tolyl ketone-*N*-mesitylsulfonylhydrazone **132d** as a white powder (15%, PE/AcOEt 98/2). Due to poor yield of the process and probable instability of the product obtained, only ^{1}H NMR spectrum was recorder to confirm the identity of the product that was then immediately subjected to irradiation in the following step, the photoredox reaction of cyclization. ^{1}H NMR (600 MHz, CDCl$_3$-*d*) δ 7.30 (m, 1H, Ar–*H*), 7.27 (m, 2H, Ar–*H*), 7.20 (m, 1H, Ar–*H*), 6.96 (s, 2H, Ar–*H*), 5.62 (dd, *J* = 17.5, 10.7 Hz, 1H, C*H*=CH$_2$), 4.70 (dd, *J* = 17.5, 1.3 H, 1H, CH=C*H*$_2$*H* trans), 4.64 (dd, *J* = 10.7, 1.3 Hz, 1H, CH=C*H*$_2$*H* cis), 2.57 (s, 2H, N=C(Ar)–C*H*$_2$), 2.56 (s, 6H, 2 × Ar–C*H*$_3$), 2.31 (s, 3H, *o*-tolyl C*H*$_3$), 2.30 (s, 3H, Ar–C*H*$_3$), 0.90 (s, 6H, C(C*H*$_3$)$_2$).

4,4-Dimethylhex-5-en-2-one-*N*-mesitylsulfonylhydrazone (132e)
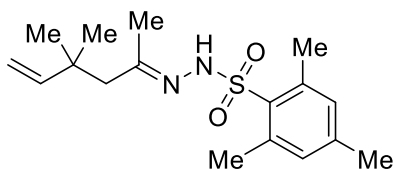
Following the described procedure 4,4-dimethylhex-5-en-2-one, **89i** (0.630 g, 5.0 mmol) was reacted with mesitylsulfonylhydrazide (1.070 g, 5.00 mmol) in methanol (3.1 mL) to obtain 1.13 g (3.5 mmol) 4,4-dimethylhex-5-en-2-one-*N*-mesitylhydrazone **132e** (mixture of isomers) as a white powder (70%, PE/EE 95/5). ^{1}H NMR (600 MHz, CDCl$_3$, Me$_4$Si) (major isomer) δ 7.37 (bs, 1H, N–*H*), 6.94 (s, 2H, Ar–*H*), 5.64 (dd, *J* = 17.4, 10.7 Hz, 1H, C*H*=CH$_2$), 4.74 (bd, *J* = 10.7, 1H, CH=C*H*$_2$, *H* cis), 4.70 (dd, *J* = 17.5, 1.2 Hz, 1H, CH=C*H*$_2$*H* trans), 2.64 (s, 6H, *ortho* Ar–C*H*$_3$), 2.28 (s, 3H, *para* Ar–C*H*$_3$), 2.13 (s, 2H,

N=C(Me)—C*H₂*), 1.71 (s, 3H, N=C—C*H₃*), 0.79 (s, 6H, C(C*H₃*)₂); (*minor isomer*) δ 7.37 (bs, 1H, N–*H*), 6.97 (s, 2H, Ar–*H*), 5.82 (dd, J = 17.5, 10.7 Hz, 1H, C*H*=CH₂), 5.04 (d, J = 10.7, 1H, CH=C*H₂*, *H cis*), 5.02 (d, J = 17.5, 1H, CH=CH₂*H trans*), 2.66 (s, 6H, *ortho* Ar–C*H₃*), 2.29 (s, 3H, *para* Ar–C*H₃*), 1.89 (s, 2H, N=C(Me)—C*H₂*), 1.78 (s, 3H, N=C—C*H₃*), 1.09 (s, 6H, C(C*H₃*)₂). ^{13}C NMR (151 MHz; CDCl₃, Me₄Si) (mixture of isomers) δ 154.6 (Cq), 147.5 (CH), 142.8 (Cq), 140.4 (2 × Cq), 140.2 (2 × Cq), 132.6 (Cq), 131.8 (2 × CH), 131.8 (2 × CH), 110.8 (CH₂), 51.3 (CH₂), 37.2 (Cq), 27.9 (Cq), 27.0 (2 × CH₃), 26.7 (2 × CH₃), 23.2 (CH₃), 21.0 (CH₃), 17.8 (2 × CH₃). HRMS (ESI) m/z [M + H]⁺ Calcd for C₁₇H₂₇N₂O₂S 323.1788, found 323.1780.

(5*R*)-5-Methyl-2-(1,1-dimethylprop-2-enyl)cyclohexanone *N*-mesitylsulfonylhydrazone (132f)
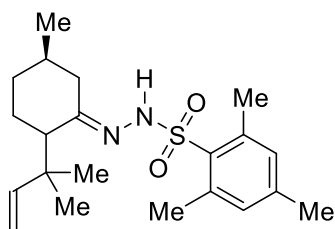
Following the described procedure, pulegone derivative **89l** (0.61 g, 3.4 mmol) was reacted with mesitylsulfonylhydrazide (0.79 g, 3.7 mmol) in methanol (2.5 mL) to obtain 0.68 g (1.8 mmol) of (5*R*)-5-methyl-2-(1,1-dimethylprop-2-enyl)cyclohexanone *N*-mesitylsulfonylhydrazone **132f** after column

chromatography, affording a white solid product as a mixture of the 4 isomer (54%, PE/EE 9/1). ^{1}H NMR (600 MHz, CDCl₃, Me₄Si) (mixture of 4 isomers) 6.97 (s, 2H, Ar–*H*, isomers 1), 6.93 (s, 2H, Ar–*H* isomer 2 and 3), 6.83 (s, 2H, Ar–*H* isomer 4), 5.95 (dd, J = 17.4, 10.9 Hz, 1H, C*H*=CH₂ isomer 1), 5.81 (dd, J = 17.5, 10.6 Hz, 1H, C*H*=CH₂ isomer 2 and 3), 5.70 (dd, J = 17.6, 10.7 Hz, H, C*H*=CH₂ isomer 4), 4.94 (bm, 2H, CH=C*H₂* isomer 1 and 4), 4.70 (bm, 2H, CH=C*H₂* isomer 2 and 3), 2.64 (s, 6H, *ortho* Ar–C*H₃* all isomers), 2.56 (dd, J = 13.4, 4.3, 1.7 Hz, 1H, N=C—C(H)*H*—C(Me)H, isomer 2), 2.53 (m, 1 H, isomer 3), 2.33 (m, 1H,) 1.41 (dd, 1H, J = 13.4, 11.5 Hz, N=C—C(H)*H*—C(Me)H, isomer 2), 2.27 (s, 6H, *para* Ar–C*H₃* all isomers), 2.56 ((dd, 1H, J = 13.5, 4.0 Hz, isomer 2), 2.35–2.31 (m, 1H, N=C—C(H)*H*—C(Me)H isomer 3), 2.29 (d, J = 14.8 Hz, 2H N=C—C(H)*H*—C(Me)H, isomer 2), 2.17 (ddd, J = 13.0, 4.9, 1.3 Hz, 2H, CH–C*H₂*–CH₂–C(Me)H isomer 2), 2.07 (t, 1H, J = 5.8 Hz, N=C—C(H)*H*—C(Me)H isomer 3), 1.99 (dd, J = 12.5, 1.3 Hz, CH–C*H₂*–CH₂–C(Me)H isomer 2), 1.95–1.83 (m, 2H, CH–C*H₂*–CH₂–C(Me)H isomer 3), 1.80–1.72 (m, 6H, CH₂–C(Me)*H*–CH₂ with C*H*–CH₂–CH₂–C(Me)H with C*H*–CH₂–CH₂–C(Me)H all isomers), 1.59 (ddt, J = 10.9, 8.7, 3.2 Hz, 1H, isomer

2), 1.55–1.49 (m, 0H), 1.43 (dm, J = 11.5, 1H, CH–CH$_2$–C(H)H–C(Me)H isomer 2), 1.41 (d, J = 11.4 Hz, 1H, CH–CH$_2$–C(H)H–C(Me)H, isomer 1) 1.34–1.29 (m, 1H, CH–CH$_2$–C(H)H–C(Me)H), isomer 3), 1.24–1.15 (m, 2H, CH–CH$_2$–C(H)H–C(Me)H, all isomers), 1.19 (ddd, J = 14.5, 12.8, 4.0 Hz, 1H, CH–CH$_2$–C(H)H–C(Me)H isomer 2), 1.10 (d, 1H, J = 12.2 Hz, CH–CH$_2$–C(H)H–C(Me)H isomer 3), 1.05 (dt, J = 8.0, 2.0 Hz, 2H, CH–CH$_2$–C(H)H–C(Me)H, isomer 2), 0.98 (d, J = 6.5 Hz, 3H, CH$_2$–CH–CH_3, isomer 1), 0.94 (d, J = 6.5 Hz, 3H, CH$_2$–CH–CH_3, isomer 2 and 3), 0.91 ((d, J = 6.5 Hz, 3H, CH$_2$–CH–CH_3), 0.87 (s, 3H, C(CH$_3$) CH_3 isomer 1), 0.86 (s, 3H, C(CH$_3$) CH_3 isomer 2 and 3), 0.84 (s, 3H, C(CH$_3$) CH_3 isomer 4), 0.73 (s, 3H, C(CH$_3$) CH_3 isomer 1), 0.71 (s, 3H, C(CH$_3$) CH_3 isomer 2), 0.70 (s, 3H, C(CH$_3$) CH_3 isomer 3), 0.69 (s, 3H, C(CH$_3$) CH_3 isomer 4). ^{13}C NMR (151 MHz; CDCl$_3$, Me$_4$Si) (mixture of 4 isomers) δ 159.8 (Cq), 159.8 (Cq), 147.9 (CH), 147.7 (CH), 147.4 (CH), 147.2 (CH), 142.7 (Cq), 142.7 (Cq), 140.1 (2 × Cq), 140.0 (2 × Cq), 137.5 (Cq), 132.7 (CH), 132.2 (CH), 131.9 (2 × CH), 131.8 (2 × CH), 130.7 (CH$_2$), 112.8(CH$_2$), 111.0(CH$_2$), 110.9(CH$_2$), 110.0(CH$_2$), 58.8 (CH), 53.8 (CH), 52.1 (CH), 51.8 (CH), 39.6 (Cq), 38.7 (Cq), 36.4 (CH), 35.7 (CH$_2$), 35.6 (CH$_2$), 34.7 (CH$_2$), 34.4 (CH$_2$), 34.3 (CH) 34.1 (CH) 33.6 (CH$_2$), 31.8 (CH), 31.2 (CH$_2$), 29.0 (CH$_2$), 28.9 (CH$_2$), 26.8 (CH$_3$), 25.6(CH$_2$), 25.5(CH$_3$), 25.4(CH$_3$), 25.0 (CH$_3$), 23.7 (CH$_3$), 23.5, (CH$_3$), 23.2 (CH$_3$), 23.1 (CH$_3$), 23.0 (CH$_3$), 22.4 (CH$_3$), 22.3 (CH$_3$), 21.4 (CH$_3$), 21.2 (2 × CH$_3$), 21.1 (2 × CH$_3$), 21.0 (2 × CH$_3$), 19.1 (2 × CH$_3$). HRMS (ESI) m/z [M + H]$^+$ Calcd for C$_{21}$H$_{33}$N$_2$O$_2$S 377.2257, found 377.2248.

6.3.3 General Procedures for the Synthesis of γ,δ-Unsaturated N-Mesitylsulfonylhydrazones (133)
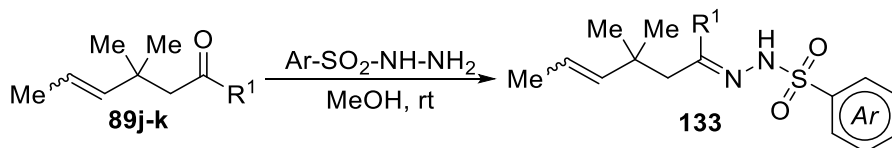
Hydrazones**133** were synthesized according to the procedure reported in chapter 3, paragraph 3.3.5 (General Procedures for the Synthesis of γ,δ-Unsaturated *N*-Arylsulfonylhydrazones (94)) with two modifications: not terminal alkenes **89j** and **89k** were employed as reagents and commercially available *p*-Toluenesulfonyl hydrazide (tosylhydrazide) or 2,4,6-trimethylbenzenesulfonolhydrazide (mesitylsulfonylhydrazide) were

employed as arylsulfonylhydrazides reaction partners. The products were always recovered as a mixture of isomers.

2,2-Dimethylpent-3-enylphenone-*N*-tosylhydrazone (133a)
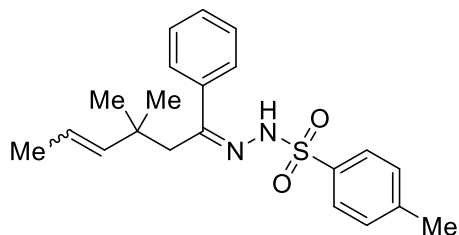
Following the described procedure 2,2-dimethylpent-3-enylphenone **89j** (1.01 g, 5.0 mmol) was reacted with tosylhydrazide (1.00. g, 5.4 mmol) in methanol (3.0 mL) to obtain 1.07 g (2.9 mmol) of 2,2-dimethylbut-3-enylphenone-*N*-tosylhydrazone **133a**
(mixture of isomers) as a white powder (58%). ^{1}H NMR (600 MHz, DMSO-d_6, Me$_4$Si) (mixture of isomers) δ 10.58 (s, 1H, NH, isomer 1), 10.56 (s, 1H, NH, isomer 2), 9.90 (s, 1H, NH, isomer 3), 9.89 (s, 1H, NH, isomer 4), 7.70–7.72m, 4H, Ar–*H*), 7.47 (m, 2H, Ar–*H*), 7.45 (m, 1H, Ar–*H*), 7.32–7.39 (m, 4H, Ar–*H*), 7.23–7.28 (m, 6H, Ar–*H*), 5.23 (dq, *J* = 15.6, 1.8 Hz, 1H, C*H*=CH—CH$_3$, isomer 1), 5.23 (dq, *J* = 12.0, 1.8 Hz, 1H, C*H*=CH—CH$_3$, isomer 2), 4.93–5.03 (bm, 2H, CH=C*H*CH$_3$ *all isomers*, C*H*=CH—CH$_3$, isomer 3 and 4), 2.85 (s, 2H, N=C(Ar)–C*H$_2$*, isomers 1 and 2), 2.75 (s, 2H, N=C(Ar)–C*H$_2$*),isomers 3 and 4), 2.30 (s, 3H, Ar–C*H$_3$*, isomer 1 and 2), 2.29 (s, 3H, Ar–C*H$_3$*, isomer 3 and 4), 1.49 (dd, *J* = 6.6, 1.2 Hz, 1H, CH=CHC*H$_3$*, isomer 3), 1.47 (dd, *J* = 7.2, 1.8 Hz, 1H, CH=CHC*H$_3$*, isomer 1), 1.28 (m, 1H, CH=CHC*H$_3$*, isomer 2 and 4), 0.91 (s, 6H, C(C*H$_3$*)$_2$, isomer 1), 0.89 (s, 6H, C(C*H$_3$*)$_2$, isomer 4), 0.80 (s, 6H, C(C*H$_3$*)$_2$, isomer 2), 0.77 (s, 6H, C(C*H$_3$*)$_2$, isomer 3). ^{13}C NMR (151 MHz; DMSO-d_6, Me$_4$Si) (mixture of isomers) δ 154.9 (Cq), 154.5 (Cq), 143.5 (CH), 143.4 (Cq), 143.2 (Cq), 140.9 (CH), 139.7 (Cq), 139.6 (CH), 138.8 (CH), 138.6 (CH), 136.8 (Cq), 136.6 (Cq), 136.5 (Cq), 129.7 (CH), 129.5 (2 × CH), 129.2 (2 × CH), 129.0 (2 × CH), 128.8 (2 × CH), 128.6 (2 × CH), 128.5 (2 × CH), 128.3 (2 × CH), 128.2 (2 × CH), 128.0 (2 × CH), 127.6 (2 × CH), 127.6 (2 × CH), 127.2 (2 × CH), 127.1 (2 × CH), 122.8 (2 × CH), 120.1 (CH), 120.0 (CH), 50.7 (CH$_2$), 46.0 (CH$_2$), 38.3 (CH$_2$), 38.3 (CH$_2$), 38.0 (Cq), 37.6 (Cq), 29.2 (CH$_3$), 29.2 (CH$_3$), 27.7 (CH$_3$), 21.3 (CH$_3$), 17.9 (2 × CH$_3$), 17.8 (2 × CH$_3$), 14.3 (2 × CH$_3$), 14.2 (2 × CH$_3$). HRMS (ESI) *m*/*z* [M + H]$^+$ Calcd for C$_{21}$H$_{27}$N$_2$O$_2$S 371.1788, found 371.1792.

2,2-Dimethylpent-3-enylphenone-*N*-mesitylsulfonylhydrazone (133b)

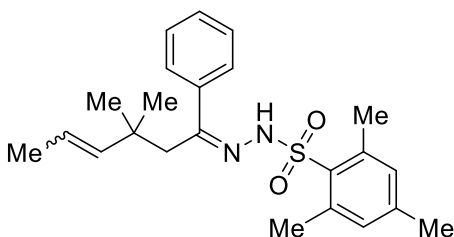Following the described procedure 2,2-dimethylpent-3-enylphenone **89j**, (1.01 g, 5.0 mmol) was reacted with mesitylsulfonylhydrazide (1.00. g, 5.4 mmol) in methanol (3.0 mL) to obtain 1.43 g (2.9 mmol) of 2,2-dimethylbut-3-enylphenone-*N*-tosylhydrazone **133b** (mixture of 4 isomers) as a white powder (72%). ^{1}H NMR (600 MHz, CDCl$_3$, Me$_4$Si) (mixture of isomers) δ 7.93 (s, 1H, NH, isomer 1), 7.93 (s, 1H, NH, isomer 2), 7.92 (s, 1H, NH, isomer 3), 7.91 (s, 1H, NH, isomer 4), 7.50 (m, 4H, Ar–*H*), 7.41–7.43 (m, 3H, Ar–*H*), 7.29 (m, 3H, Ar–*H*), 7.13 (dm, *J* = 7.2 Hz, 2H, Ar–*H*, isomer 1), 7.06 (dm, *J* = 6.6 Hz, 2H, Ar–*H*, isomer 1 and 2), 7.03 (dm, *J* = 6.6 Hz, 2H, Ar–*H*, isomer 1 and 2), 6.93–6.96 (m, 2H, Mes–*H*, all isomers), 4.97–5.00 (bm, 1H, C*H*=CH—CH$_3$, all isomers), 4.93–5.03 (bm, 2H, CH=C*H*CH$_3$,all isomers), 2.71 (s, 2H, N=C(Ar)–C*H*$_2$, isomers 1 and 2), 2.60 (s, 2H, N=C(Ar)–C*H*$_2$), isomers 3 and 4), 2.30 (s, 3H, Ar–C*H*$_3$, isomer 1 and 2), 2.29 (s, 3H, Ar–C*H*$_3$, isomer 3 and 4), 1.70 (dd, *J* = 6.6, 1.2 Hz, 1H, CH=CHC*H*$_3$, isomer 3), 1.68 (dd, *J* = 7.2, 1.8 Hz, 1H, CH=CHC*H*$_3$, isomer 1), 1.66 (bd, *J* = 7.2 Hz, 1H, CH=CHC*H*$_3$, isomer 12), 1.58 (dd, *J* = 6.0, 1.8 Hz, 1H, CH=CHC*H*$_3$, isomer 4), 1.07 (s, 6H, C(C*H*$_3$)$_2$, isomer 1), 0.98 (s, 6H, C(C*H*$_3$)$_2$, isomer 4), 0.93 (s, 6H, C(C*H*$_3$)$_2$, isomer 2), 0.66 (s, 6H, C(C*H*$_3$)$_2$, isomer 3). ^{13}C NMR (151 MHz; CDCl$_3$, Me$_4$Si) (mixture of isomers) δ 155.6 (Cq), 155.0 (Cq), 154.0 (Cq), 142.9 (CH), 142.9 (Cq), 142.7 (Cq), 140.7 (Cq), 140.5 (Cq), 140.3 (CH), 140.1 (Cq), 140.0 (CH), 139.2 (Cq), 139.0 (CH), 138.2 (CH), 134.0 (Cq), 132.7 (Cq), 131.9 (CH), 131.8 (2 × CH), 129.6 (2 × CH), 129.6 (2 × CH), 129.5 (2 × CH), 129.5 (2 × CH), 129.4 (2 × CH), 129.3 (2 × CH), 128.3 (2 × CH), 128.2 (2 × CH), 127.2 (2 × CH), 127.0 (2 × CH), 124.0 (CH), 123.4 (2 × CH), 120.8 (2 × CH), 51.0 (CH$_2$), 50.7 (CH$_2$), 44.7 (CH$_2$), 39.7 (CH$_2$), 39.4 (CH$_2$), 37.8 (Cq), 37.3 (Cq), 36.7 (Cq), 36.6 (Cq), 30.6 (CH$_3$), 29.3 (CH$_3$), 28.6 (CH$_3$), 27.7 (CH$_3$), 23.6 (CH$_3$), 23.2 (CH$_3$), 21.1 (2 × CH$_3$), 18.0 (2 × CH$_3$), 17.8 (2 × CH$_3$), 17.1 (2 × CH$_3$), 14.7 (2 × CH$_3$), 14.3 (2 × CH$_3$). HRMS (ESI) *m*/*z* [M + H]$^+$ Calcd for C$_{23}$H$_{31}$N$_2$O$_2$S 399.2101, found 399.2096.

4,4-Dimethylhept-5-enone-*N*-tosylhydrazone (133c)
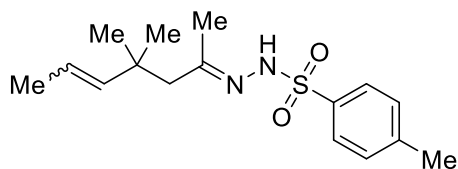
Following the described procedure 4,4-dimethylhept-5-en-2-one, **89k** (0.71 g, 5.1 mmol) was reacted with tosylhydrazide (1.05 g, 5.6 mmol) in methanol (3.0 mL) to obtain 1.01 g (3.3 mmol) of 4,4-dimethylhex-5-en-2-one-*N*-tosylhydrazone **133b** (mixture of isomers) as a white powder (64%). ^{1}H NMR (600 MHz, DMSO-d_6, Me$_4$Si) (mixture of isomers) δ 9.90 (bs, 1H, N−*H*, isomer 1), 9.88 (bs, 1H, N−*H*, isomer 2), 7.62 (d, *J* = 8.4 Hz, 2H, Ar−*H*, both isomers), 7.33 (d, *J* = 8.4 Hz, 2H, Ar−*H*, isomer 1), 7.31 (d, *J* = 8.4 Hz, 2H, Ar−*H*, isomer 1), 5.29 (dq, *J* = 13.8, 1.8 Hz, 1H, C*H*=CHCH$_3$, isomer 1), 5.10 (m, 3H, C*H*=CHCH$_3$, isomer 2 and CH=C*H*CH$_3$, both isomers), 2.46 (m, 3H, Ar−C*H$_3$*, isomer 2), 2.33 (m, 3H, Ar−C*H$_3$*, isomer 1), 2.12 (s, 2H, N=C(Me)—C*H$_2$*, isomer 1), 2.02 (s, 2H, N=C(Me)—C*H$_2$*, isomer 2), 1.73 (s, 3H, N=C—C*H$_3$*, isomer 1), 1.69 (s, 3H, N=C—C*H$_3$*, isomer 2), 1.50 (m, 1H, CH=CHC*H$_3$*, isomer 1), 1.45 (m, 3H, CH=CHC*H$_3$*, isomer 2), 0.88 (s, 6H, C(C*H$_3$*)$_2$, isomer 1), 0.72 (s, 6H, C(C*H$_3$*)$_2$, isomer 2). ^{13}C NMR (151 MHz; DMSO-d_6, Me$_4$Si) (mixture of isomers) δ 157.8 (Cq), 157.6 (Cq), 143.4 (Cq), 141.1 (CH), 139.0 (CH), 136.9 (Cq), 129.7 (2 × CH), 129.7 (2 × CH), 128.1 (2 × CH), 128.1 (2 × CH), 123.3 (CH), 120.5 (CH), 51.4 (CH$_2$), 51.3 (CH$_2$), 39.6 (Cq), 36.7 (Cq), 29.1 (CH$_3$), 27.7 (CH$_3$), 21.5 (CH$_3$), 19.5 (CH$_3$), 19.2 (CH$_3$), 18.2 (2 × CH$_3$), 14.5 (2 × CH$_3$). HRMS (ESI) *m*/*z* [M + H]$^+$ Calcd for C$_{16}$H$_{25}$N$_2$O$_2$S 309.1631, found 309.1638.

6.3.4 General procedure for the photoinduced reaction of β-hindered-γ,δ-Unsaturated *N*-Mesitylsulfonylhydrazones (132) yielding Tetrahydropyridazines (134 and 135).
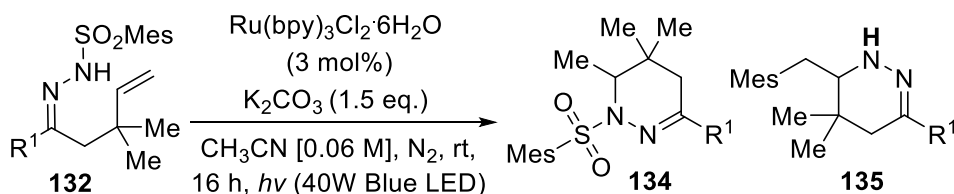
In a sealed photochemical reactor, 6.75 mg of [Ru(bpy)$_3$]Cl$_2$·6H$_2$O (0.009 mmol) were dissolved in 5 mL of anhydrous CH$_3$CN, the solution was degassed with N$_2$ for 15 min then the suitable mesitylsulfonylhydrazone **132** (0.30 mmol) and 62.2 mg of K$_2$CO$_3$ (0.45 mmol) were added. The solution was then stirred at 4 cm from the irradiation source (see above) at room

temperature until the reaction was completed as monitored by TLC analysis. Then, it was filtered on a short pad of silica gel using CH_2Cl_2 as eluent and Et_2O to wash the column. The crude product was purified by flash chromatography on silica gel (hexane/Et_2O 9/1).

1-(Mesitylsulfonyl)-4,5,5-trimethyl-3-phenyl-1,4,5,6-tetrahydropyridazine (134a)
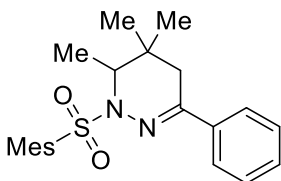
According to general procedure 115 mg (0.30 mmol) of 2,2-dimethylbut-3-enylphenone-*N*-2,4,6-mesityl sulfonylhydrazone **132a** were reacted with K_2CO_3 and [Ru(bpy)$_3$]Cl$_2$·6H$_2$O under blue light irradiation for 16 h to obtain 57.5 mg (0.15 mmol) of 1-(mesitylsulfonyl)-4,5,5-trimethyl-3-phenyl-1,4,5,6-tetrahydropyridazine **134a** (50%) as a white solid. ^{1}H NMR (600 MHz, CDCl$_3$, Me$_4$Si) δ 7.56 (d, J = 6.8 Hz, 2H, Ar–*H*), 7.30 (m, 3H, Ar–*H*), 6.97 (s, 2H, Ar–*H*), 4.14 (q, J = 6.6 Hz, 1H, N–C*H*), 2.74 (s, 6H, *ortho* Ar-(C*H₃*)), 2.40 (d, J = 18.0 Hz, 1H, (CH$_3$)$_2$-CH-C(H)*H*)), 2.30 (s, 3H, *para* Ar-(C*H₃*)), 2.26 (d, J = 18.0, 1H, (CH$_3$)$_2$-CH-C(H)*H*), 1.30 (d, J = 6.6 Hz, 3H, N–CH–C*H₃*), 1.11 (s, 3H, CH(CH$_3$)–C(C*H₃*)$_2$), 0.94 (s, 3H, CH(CH$_3$)–C(C*H₃*)$_2$). ^{13}CNMR (151 MHz, CDCl$_3$, Me$_4$Si) δ 145.3 (Cq), 142.7 (Cq), 141.0 (2 × Cq), 137.3 (Cq), 133.1 (Cq), 131.8 (2 × CH), 129.0 (CH), 128.3 (2 × CH), 125.3 (2 × CH), 56.5 (CH), 33.4 (CH$_2$), 30.9 (Cq), 28.5 (CH$_3$), 27.0 (CH$_3$), 23.5 (2 × CH$_3$), 21.1 (CH$_3$), 15.1 (CH$_3$). mp 136.5–139.4 °C. v_{max} (neat)/cm^{-1} 2964, 2930, 2873, 1598, 1461, 1443, 1327, 1162. HRMS (ESI) *m*/*z* [M + H]$^+$ Calcd for C$_{22}$H$_{29}$N$_2$O$_2$S 385.1944, found 385.1942.

5,5-Dimethyl-3-phenyl-6-(2,4,6-trimethylbenzyl)-1,4,5,6-tetrahydropyridazine (135a)
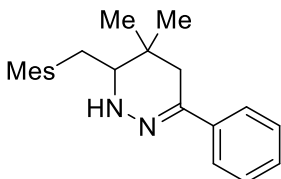
According to general procedure 115 mg (0.30 mmol) of 2,2-dimethylbut-3-enylphenone-*N*-2,4,6-mesitylsulfonylhydrazone **132a** were reacted with K_2CO_3 and [Ru(bpy)$_3$]Cl$_2$·6H$_2$O under blue light irradiation for 16 h to obtain 43 mg (0.13 mmol) of 5,5-dimethyl-3-phenyl-6-(2,4,6-trimethylbenzyl)-1,4,5,6-tetrahydropyridazine **135a** (45%) as a greenish oil. ^{1}H NMR (600 MHz, CDCl$_3$, Me$_4$Si) δ 7.62 (d, J = 7.2 Hz, 2H, Ar–*H*), 7.31 (tm, J = 7.5, 2H, Ar–*H*), 7.24 (m, 1H, Ar–*H*), 6.85 (s, 2H, Ar–*H*), 5.39 (bs,

1H, N–H), 3.06 (dm, J = 11.5 Hz, 1H, NH–CH–C(H)H–CH), 2.89 (dd, J = 13.8, 3.5 Hz, 1H, NH–CH–C(H)H–CH), 2.77 (tm, J = 12.5, 1H, NH–CH), 2.43 (d, J = 17.6 Hz, 1H, N=C(Ph)—C(H)H), 2.38 (d, J = 17.7 Hz, 1H, N=C(Ph)—C(H)H), 2.33 (s, 6H, *ortho* Ar-(CH_3)), 2.25 (s, 3H, *para* Ar-(CH_3)), 1.18 (s, 3H C(CH₃)–CH_3), 1.11 (s, 3H, C(CH₃)–CH_3). ^{13}C NMR (151 MHz, CDCl₃, Me₄Si) δ 141.6 (Cq), 138.8 (Cq), 137.3 (2 × Cq), 136.0 (Cq), 131.5 (Cq), 129.5 (2 × CH), 128.3 (2 × CH), 127.6 (CH), 124.2 (2 × CH), 59.0 (CH), 39.1 (CH₂), 30.6 (Cq), 27.4 (2 × CH₃), 26.8 (CH₂), 22.4 (CH₃), 20.9 (CH₃), 20.6 (CH₃). v_{max} (neat)/cm^{-1} 3064, 2978, 1598, 1428, 1379, 1065. HRMS (ESI) m/z [M + H]$^+$ Calcd for C₂₂H₂₉N₂ 321.2325, found 321.2330.

1-(Mesitylsulfonyl)-5,5,6-trimethyl-3-(naphthalen-2-yl)-1,4,5,6-tetrahydropyridazine (134b)

According to the general procedure, 130 mg (0.30 mmol) of 2,2-dimethylbut-3-enylnaphtone-*N*-2,4,6-mesitylsulfonylhydrazone **132b** were reacted with K₂CO₃ and [Ru(bpy)₃]Cl₂·6H₂O under blue light irradiation for 16 h to obtain 54 mg (0.12 mmol) of 1-(mesitylsulfonyl)-5,5,6-trimethyl-3-(naphthalen-2-yl)-1,4,5,6-tetrahydropyridazine **134b** (42%) as a white solid. ^{1}H NMR (600 MHz, CDCl₃, Me₄Si) δ 7.90 (s, 1H, Ar–H), 7.79 (m, 3H, Ar–H), 7.74 (d, J = 8.7 Hz, 1H, Ar–H), 7.45 (m, 2H, Ar–H), 6.99 (s, 2H, Ar–H), 4.17 (q, J = 6.6 Hz, 1H, N–CH), 2.78 (s, 6H, *ortho* Ar-(CH_3)), 2.52 (d, J = 17.7 Hz, 1H, (CH₃)₂-CH-C(H)H))), 2.42 (d, J = 17.7 Hz, 1H, (CH₃)₂-CH-C(H)H)), 2.31 (s, 3H, *para* Ar-(CH_3)), 1.34 (d, J = 6.6 Hz, 3H, N–CH–CH_3)), 1.16 (s, 3H, CH(CH₃)–C(CH_3)₂), 0.98 (s, 3H, CH(CH₃)–C(CH_3)₂). ^{13}C NMR (151 MHz, CDCl₃, Me₄Si) δ 145.2 (Cq), 142.8 (Cq), 141.0 (2 × Cq), 134.9 (Cq), 133.6 (Cq), 133.1 (Cq), 133.0 (Cq), 131.8 (2 × CH), 128.4 (CH), 127.9 (CH), 127.7 (CH), 126.6 (CH), 126.4 (CH), 124.7 (CH), 123.1 (CH), 56.6 (CH), 33.3 (CH₂), 30.9 (Cq), 28.6 (CH₃), 27.1 (CH₃), 23.5 (2 × CH₃), 21.1 (CH₃), 15.1 (CH₃). mp 136.2–139.8 °C. v_{max} (neat)/cm^{-1} 3052, 2958, 1602, 1503, 1321, 1160. HRMS (ESI) m/z [M + H]$^+$ Calcd for C₂₆H₃₁N₂O₂S 435.2101, found 435.2090.
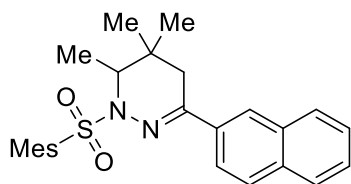
5,5-Dimethyl-3-(naphthalen-2-yl)-6-(2,4,6-trimethylbenzyl)-1,4,5,6-tetrahydropyridazine (135b)
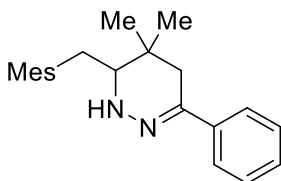
According to general Procedure B, 130 mg (0.30 mmol) of 2,2-dimethylbut-3-enylnaphtone-*N*-2,4,6-mesitylsulfonylhydrazone **132b** were reacted with K_2CO_3 and [Ru(bpy)$_3$]Cl$_2$·6H$_2$O under blue light irradiation for 16 h to obtain 35 mg (0.093 mmol) of 5,5-dimethyl-3-(naphthalen-2-yl)-6-(2,4,6-trimethylbenzyl)-1,4,5,6-tetrahydropyridazine**135b** (30%) as a greenish solid. ^{1}H NMR (600 MHz, CDCl$_3$, Me$_4$Si) δ 7.94 (dd, *J* = 8.8, 1.8 Hz, 1H, Ar–*H*), 7.86 (s, 1H, Ar–*H*), 7.76 (m, *J* = 15.9, 7.7 Hz, 3H, Ar–*H*), 7.43 (q, *J* = 6.6 Hz, 2H, Ar–*H*), 6.86 (s, 2H, Ar–*H*), 5.48 (s, 1H, N–*H*), 3.09 (dd, *J* = 11.6, 2.7 Hz, 1H, NH–CH–C(H)*H*–CH), 2.89 (dd, *J* = 13.7, 3.1 Hz, 1H, NH–C*H*), 2.80 (dd, *J* = 13.7, 11.6 Hz, 1H, NH–CH–C(H)*H*–CH), 2.51 (d, *J* = 2.8 Hz, 2H, N=C(Ar)–C*H*$_2$), 2.32 (s, 6H, *ortho* Ar-(C*H*$_3$)), 2.23 (s, 3H, *para* Ar-(C*H*$_3$), 1.20 (s, 3H, C(CH$_3$)–C*H*$_3$), 1.13 (s, 3H, C(CH$_3$)–C*H*$_3$). ^{13}C NMR (151 MHz, CDCl$_3$, Me$_4$Si) δ 141.3 (Cq), 137.3 (2 × Cq), 136.3 (Cq), 136.0 (Cq), 133.5 (Cq), 133.0 (Cq), 131.4 (Cq), 129.5 (2 × CH), 128.2 (CH), 127.7 (CH), 127.7 (CH), 126.1 (CH), 125.8 (CH), 122.9 (CH), 122.7 (CH), 59.1 (CH), 39.0 (CH$_2$), 30.6 (Cq), 27.5 (2 × CH$_3$), 26.9 (CH$_2$), 22.4 (CH$_3$), 20.9 (CH$_3$), 20.6 (CH$_3$). mp 124.5–128.7 °C. v$_{max}$ (neat)/cm^{-1} 3052, 2961, 1606, 1479, 1365, 1260. HRMS (ESI) *m*/*z* [M + H]$^+$ Calcd for C$_{26}$H$_{31}$N$_2$ 371.2482, found 371.2490.

1-(Mesitylsulfonyl)-5,5,6-trimethyl-3-(*p*-tolyl)-1,4,5,6-tetrahydropyridazine (134c)

According to the general procedure, 119 mg (0.30 mmol) of 2,2-dimethylbut-3-enyl-*p*-tolyl ketone-*N*-mesitylsulfonylhydrazone **132c** were reacted with K_2CO_3 and [Ru(bpy)$_3$]Cl$_2$·6H$_2$O under blue light irradiation for 16 h to obtain 74 mg (0.19 mmol) of 1-(mesitylsulfonyl)-5,5,6-trimethyl-3-(*p*-tolyl)-1,4,5,6-tetrahydropyridazine **134c** (62%) as a white solid. ^{1}H NMR (600 MHz, CDCl$_3$, Me$_4$Si) δ 7.46 (d, *J* = 7.8 Hz, 1H, Ar–*H*), 7.10 (d, *J* = 7.8 Hz, 1H, Ar–*H*), 6.95 (s, 2H, Ar–*H*), 4.12 (q, *J* = 6.6 Hz, 1H, N–C*H*), 2.76 (s, 6H, *ortho* Ar-(C*H*$_3$)$_2$), 2.38 (d, *J* = 18.0 Hz, 1H, (CH$_3$)$_2$-CH-C(H)*H*), 2.32 (s, 3H, *para* Ar–C*H*$_3$), 2.29 (s, 3H, Ar–C*H*$_3$, tolyl), 2.23 (d, *J* = 18.0 Hz, 1H, (CH$_3$)$_2$-CH-C(H)*H*), 1.29 (d, *J* = 6.6 Hz, 3H, N–CH–C*H*$_3$), 1.10 (s,

3H, CH(CH₃)–C(C*H₃*)₂), 0.92 (s, 3H, CH(CH₃)–C(C*H₃*)₂). ^{13}C NMR (151 MHz, CDCl₃, Me₄Si) δ 145.4 (Cq), 142.6 (Cq), 141.0 (2 × Cq), 138.9 (Cq), 134.6 (Cq), 133.2 (Cq), 131.7 (2 × CH), 129.0 (2 × CH), 125.2 (2 × CH), 54.4 (CH), 33.4 (CH₂), 30.9 (Cq), 28.5 (CH₃), 27.0 (CH₃), 23.5 (2 × CH₃), 21.3 (CH₃), 21.1 (CH₃), 15.0 (CH₃). mp 142.0–147.0 °C. ν$_{max}$ (neat)/cm⁻¹ 3020, 2958, 1682, 1611, 1511, 1324, 1109. HRMS (ESI) *m/z* [M + Na]⁺ Calcd for C₂₃H₃₀N₂O₂SNa 421.1920, found 421.1919.
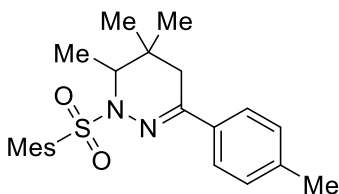
5,5-Dimethyl-3-(*p*-tolyl)-6-(2,4,6-trimethylbenzyl)-1,4,5,6-tetrahydropyridazine (135c)

According to the general procedure, 119 mg (0.30 mmol) of 2,2-dimethylbut-3-enyl-*p*-tolyl ketone-*N*-mesitylsulfonylhydrazone **132c** were reacted with K₂CO₃ and [Ru(bpy)₃]Cl₂·6H₂O under blue light irradiation for 16 h to obtain 25 mg (0.075 mmol) of 5,5-dimethyl-3-(*p*-tolyl)-6-(2,4,6-trimethylbenzyl)-1,4,5,6-tetrahydropyridazine **135c** (25%) as a greenish oil. ^{1}H NMR (600 MHz, CDCl₃, Me₄Si) δ 7.52 (dm, *J* = 8.4, 2H, Ar–*H*), 7.13 (d, *J* = 8.4 Hz, 2H, Ar–*H*), 6.86 (s, 2H, Ar–*H*), 5.34 (bs, 1H, N–*H*), 3.05 (dd, *J* = 11.4, 3.0 Hz, 1H, NH–CH–C(H)*H*–CH), 2.89 (dd, *J* = 13.8, 3.6 Hz, 1H, NH–C*H*), 2.80 (dd, *J* = 13.8, 11.4 Hz, 1H, NH–CH–C(H)*H*–CH), 2.43 (d, *J* = 17.4 Hz, 1H, N=C(Ar)–C*H₂a*), 2.36 (d, *J* = 17.4 Hz, 1H, N=C(Ar)–C*H₂b*), 2.34 (s, 6H, *ortho* Ar–C*H₃*), 2.33 (s, 3H, *para* Ar-(C*H₃*), 2.25 (s, 3H, *para* Ar-(C*H₃*), 1.18 (s, 3H, C(CH₃)–C*H₃*), 1.12 (s, 3H, C(CH₃)–C*H₃*). ^{13}C NMR (151 MHz, CDCl₃, Me₄Si) δ 142.1 (Cq), 137.2 (2 × Cq), 136.0 (2 × Cq), 131.7 (Cq), 131.5 (2 × Cq), 129.5 (2 × CH), 129.2 (Cq), 129.0 (2 × CH), 124.3 (2 × CH), 59.0 (CH), 39.2 (CH₂), 30.6 (Cq), 27.4 (2 × CH₃), 26.8 (CH₂), 22.3 (CH₃), 21.2 (CH₃), 20.9 (CH₃), 20.5 (CH₃). ν$_{max}$ (neat)/cm⁻¹ 3372, 2958, 2916, 2885, 1511, 1460, 1366, 1324. HRMS (ESI) *m/z* [M + H]⁺ Calcd for C₂₃H₃₁N₂ 335.2482, found 335.2481.

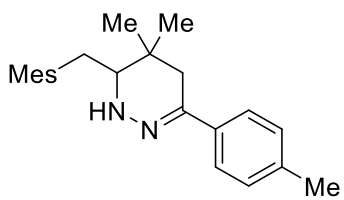## 1-(Mesitylsulfonyl)-5,5,6-trimethyl-3-(*o*-tolyl)-1,4,5,6-tetrahydropyridazine (134d)

According to the general procedure, 119 mg (0.30 mmol) of 2,2-dimethylbut-3-enyl-*o*-tolyl ketone-*N*-mesitylsulfonylhydrazone **132d** were reacted with K₂CO₃ and [Ru(bpy)₃]Cl₂·6H₂O under blue light

irradiation for 16 h to obtain 49 mg (0.13 mmol) of 1-(mesitylsulfonyl)-5,5,6-trimethyl-3-(o-tolyl)-1,4,5,6-tetrahydropyridazine **134d** (42.5%) as a white solid. ^{1}H NMR (600 MHz, CDCl$_3$, Me$_4$Si) δ 7.13 (m, 4H), 6.89 (s, 2H, Ar–H), 4.10 (q, J = 6.6 Hz, 1H), 2.76 (s, 6H, *ortho* Ar-(CH_3)$_2$), 2.43 (d, J = 18.0 Hz, 1H, (CH$_3$)$_2$-CH-C(H)H), 2.27 (s, 3H, *para* Ar–CH_3), 2.01 (s, 3H, *ortho* tolyl), 1.99 (d, J = 18.0 Hz, 1H, (CH$_3$)$_2$-CH-C(H)H),), 1.35 (d, J = 6.6 Hz, 3H, N–CH–CH_3), 1.06 (s, 3H, CH(CH$_3$)–C(CH_3)$_2$), 0.99 (s, 3H, CH(CH$_3$)–C(CH_3)$_2$). ^{13}C NMR (151 MHz, CDCl$_3$, Me$_4$Si) δ 148.1 (Cq) 141.0 (2 × Cq), 138.3 (Cq), 136.0 (Cq), 133.3 (Cq) 131.7 (2 × CH), 131.0 (CH), 128.1 (CH), 127.7 (CH), 125.5 (CH), 56.1 (CH), 37.0 (CH$_2$), 31.0 (Cq), 29.8 (CH$_3$), 28.4 (CH$_3$), 26.8 (CH$_3$), 23.3 (CH$_3$), 21.0 (CH$_3$), 20.1 (CH$_3$), 15.2 (CH$_3$). mp 112.0–116.7 °C. v$_{max}$ (neat)/cm^{-1} 2992, 2958, 1602, 1456, 1317, 1161, 1032, 776. HRMS (ESI) m/z [M + H]$^+$ Calcd for C$_{23}$H$_{31}$N$_2$O$_2$S 399.2101, found 399.2087.
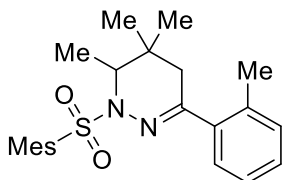
5,5-Dimethyl-3-(o-tolyl)-6-(2,4,6-trimethylbenzyl)-1,4,5,6-tetrahydropyridazine (135d)
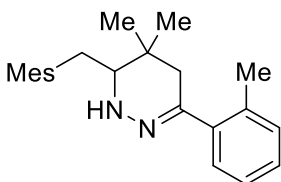
According to the general procedure, 119 mg (0.30 mmol) of 2,2-dimethylbut-3-enyl-o-tolyl ketone-N-mesitylsulfonylhydrazone **132d** were reacted with K$_2$CO$_3$ and [Ru(bpy)$_3$]Cl$_2$·6H$_2$O under blue light irradiation for 16 h to obtain 16 mg (0.06 mmol) of 5,5-dimethyl-3-(o-tolyl)-6-(2,4,6-trimethylbenzyl)-1,4,5,6-tetrahydropyridazine **135d** (19%) as a greenish oil. ^{1}H NMR (600 MHz, CDCl$_3$, Me$_4$Si) δ 7.15 (m, 4H, Ar–H), 6.85 (s, 2H, Ar–H), 5.04 (bs, 1H, N–H), 3.07 (dd, J = 11.4, 3.0 Hz, 1H, NH–CH–C(H)H–CH), 2.89 (dd, J = 13.8, 3.6 Hz, 1H, NH–CH), 2.78 (dd, J = 13.8, 11.4 Hz, 1H, NH–CH–C(H)H–CH), 2.36 (d, J = 17.4 Hz, 1H, N=C(Ar)–CH_{2a}), 2.34 (s, 6H, *ortho* Ar–CH_3), 2.33 (s, 3H, *ortho* tolyl), 2.24 (s, 3H, *para* Ar-(CH_3)), 2.23 (d, J = 17.4 Hz, 1H, N=C(Ar)–CH_{2b}), 1.24 (s, 3H, C(CH$_3$)–CH_3), 1.16 (s, 3H, C(CH$_3$)–CH_3). ^{13}C NMR (151 MHz, CDCl$_3$, Me$_4$Si) δ 141.8 (Cq), 137.3 (Cq), 137.3 (Cq), 137.2 (2 × Cq), 136.0 (2 × Cq), 135.6 (Cq), 130.8 (CH), 129.5 (2 × CH), 127.8 (CH), 125.7 (CH), 59.1 (CH), 42.7 (CH$_2$), 30.7 (Cq), 27.2 (CH$_3$), 27.0 (CH$_2$), 24.2 (CH$_3$), 22.4(CH$_3$), 20.9(CH$_3$), 20.6 (CH$_3$), 20.4 (CH$_3$). v$_{max}$ (neat)/cm^{-1} 3371, 2975, 2920, 1611, 1484, 1453, 1384, 1319, 1259, 1014. HRMS (ESI) m/z [M + H]$^+$ Calcd for C$_{23}$H$_{31}$N$_2$ 335.2482, found 335.2476.

1-(Mesitylsulfonyl)-3,5,5,6-tetramethyl-1,4,5,6-tetrahydropyridazine (134e)

According to the general procedure, 97 mg (0.30 mmol) of 4,4-dimethylhex-5-en-2-one-*N*-mesitylhydrazone **132e** were r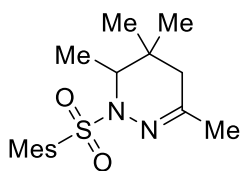eacted with K_2CO_3 and [Ru(bpy)$_3$]Cl$_2$·6H$_2$O under blue light irradiation for 16 h to obtain 53 mg (0.165 mmol) of 1-(mesitylsulfonyl)-3,5,5,6-tetramethyl-1,4,5,6-tetrahydropyridazine **134e** (55%) as a white solid. ^{1}H NMR (600 MHz, CDCl$_3$, Me$_4$Si) δ 6.92 (s, 2H, Ar–*H*), 3.97 (qd, *J* = 6.6, 1.5 Hz, 1H, N–C*H*), 2.68 (s, 6H, *ortho* Ar-(C*H$_3$*)), 2.28 (s, 3H, *para* Ar-(C*H$_3$*)), 2.00 (d, *J* = 18.5 Hz, 1H, (CH$_3$)$_2$-CH-C(H)*H*)), 1.82 (s, 3H, N≡C—C*H$_3$*), 1.67 (dd, *J* = 18.5, 1.5 Hz, 1H, (CH$_3$)$_2$-CH-C(H)*H*)), 1.21 (d, *J* = 6.6 Hz, 3H, N–CH–C*H$_3$*)), 0.98 (s, 3H, CH(CH$_3$)–C(C*H$_3$*)$_2$), 0.88 (d, *J* = 0.9 Hz, 3H, CH(CH$_3$)–C(C*H$_3$*)$_2$). ^{13}C NMR (151 MHz, CDCl$_3$, Me$_4$Si) δ 148.3 (Cq), 142.3 (Cq), 141.0 (2 × Cq), 133.6 (Cq), 131.6 (2 × CH), 55.9 (CH), 37.2 (CH$_2$), 31.0 (Cq), 28.4 (CH$_3$), 26.8 (CH$_3$), 24.1 (CH$_3$), 23.4 (2 × CH$_3$), 21.1 (CH$_3$), 14.5 (CH$_3$). mp degradation 150–170 °C. ν$_{max}$ (neat)/cm^{-1} 2967, 1712, 1602, 1314, 1080. HRMS (ESI) *m/z* [M + H]$^+$ Calcd for C$_{17}$H$_{27}$N$_2$O$_2$S 323.1788, found 323.1776.
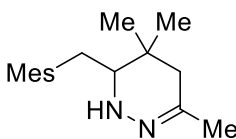
3,5,5-Trimethyl-6-(2,4,6-trimethylbenzyl)-1,4,5,6-tetrahydropyridazine (15e)

According to the general procedure, 97 mg (0.30 mmol) of 4,4-dimethylhex-5-en-2-one-*N*-mesitylhydrazone **12e** were reacted with K_2CO_3 and [Ru(bpy)$_3$]Cl$_2$·6H$_2$O under blue light irradiation for 16 h to obtain 53 mg (0.165 mmol) of 31 mg (0.120 mmol) of 3,5,5-trimethyl-6-(2,4,6-trimethylbenzyl)-1,4,5,6-tetrahydropyridazine **15e** (40%) as a greenish oil. ^{1}H NMR (600 MHz, CDCl$_3$, Me$_4$Si) δ 6.81 (s, 2H, Ar–*H*), 4.80 (s, 1H, N–*H*), 2.84 (dd, *J* = 11.5, 3.3 Hz, 2H, NH–CH–C(H)*H*–CH), 2.80 (dd, *J* = 13.8, 3.3 Hz, 2H, NH–CH–C(H)*H*–CH), 2.66 (dd, *J* = 13.7, 11.5 Hz, 1H, NH–CH–C(H)*H*–CH), 2.30 (s, 6H, *ortho* Ar-(C*H$_3$*)), 2.22 (s, 3H *para* Ar-(C*H$_3$*)), 1.99 (d, *J* = 18.2 Hz, 1H, N≡C(Me)-C(H)*H*), 1.83 (d, *J* = 18.3 Hz, 1H, N≡C(Me)-C(H)*H*), 1.77 (s, 3H, N≡C—C(CH$_2$)*H$_3$*), 1.06 (s, 3H, C(CH$_3$)–C*H$_3$*), 1.03 (s, 3H, C(CH$_3$)–C*H$_3$*). ^{13}C NMR (151 MHz, CDCl$_3$, Me$_4$Si) δ 145.0 (Cq), 137.2 (2 × Cq), 136.0 (Cq), 131.8 (Cq), 129.4 (2 × CH), 59.0 (CH), 43.2 (CH$_2$), 30.9 (Cq), 27.2 (2 × CH$_3$), 26.6 (CH$_2$), 23.6 (CH$_3$), 22.0 (CH$_3$), 20.8 (CH$_3$), 20.5 (CH$_3$). ν$_{max}$ (neat)/cm^{-1} 3377, 2950 2916, 1593, 1480, 1447,

1264, 1127, 1067. HRMS (ESI) m/z [M + H]$^+$. Calcd for $C_{17}H_{27}N_2$ 259.2169, found 259.2170.

(7*R*)-2-(Mesitylsulfonyl)-3,4,4,7-tetramethyl-2,3,4,4a,5,6,7,8-octahydrocinnoline (134f)
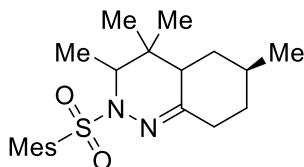
According to the general procedure, 105 mg (0.30 mmol) of pulegone derivative *N*-mesitylsulfonylhydrazone **132f** were reacted with K_2CO_3 and [Ru(bpy)$_3$]Cl$_2$·6H$_2$O under blue light irradiation for 16 h to obtain 37 mg (0.124 mmol) of (7*R*)-2-(mesitylsulfonyl)-3,4,4,7-tetramethyl-2,3,4,4a,5,6,7,8-octahydrocinnoline **134f** (35%) as a white solid. ^{1}H NMR (600 MHz, CDCl$_3$, Me$_4$Si) δ 6.92 (s, 2H, Ar–*H*), 3.97 (q, *J* = 6.6 Hz, 1H, N–C(CH$_3$)*H*), 2.68 (s, 6H, *ortho* Ar–C*H*$_3$), 2.35 (ddd, *J* = 14.7, 4.1, 2.3 Hz, 1H, CH–C*H*$_2$-C(CH$_3$)H), 2.28 (s, 3H, *para* Ar-(C*H*$_3$)), 1.86 (dd, *J* = 12.0, 4.4 Hz, 1H, C(H)*H*—C=N); 1.81–1.77 (m, 2H, CH–C(H)*H*–CH$_2$–CH), 1.72 (t, *J* = 12.6, 1H, CH-C(H)*H*C(CH$_3$)H), 1.49–1.42 (m, 1H, CH–CH$_2$–C(H)*H*–CH), 1.18 (d, *J* = 6.6 Hz, 3H, N–CH–C*H*$_3$), 1.17–0.98 (m, 2H, CH–C(H)*H*–CH$_2$–CH with CH–CH$_2$–C(H)*H*–CH), 0.96 (s, 3H, −C(CH$_3$)–C*H*$_3$), 0.90 (d, *J* = 6.5 Hz, 3H, CH$_2$–C*H*(CH$_3$)–CH$_2$), 0.84 (s, 3H, −C(CH$_3$)–C*H*$_3$). ^{13}C NMR (151 MHz, CDCl$_3$, Me$_4$Si) δ 153.9 (Cq), 142.3 (Cq), 141.1 (2 × Cq), 133.6 (Cq), 131.6 (2 × CH), 58.4 (CH), 42.9 (CH$_2$), 41.03 (CH), 34.0 (CH$_2$), 32.8 (CH), 25.3 (CH$_3$), 25.1 (CH$_2$), 24.9 (CH$_3$), 23.4 (2 × CH$_3$), 22.2 (CH$_3$), 21.1 (CH$_3$), 13.2 (CH$_3$). mp degradation 106–115 °C. ν$_{max}$ (neat)/cm^{-1} 3001, 2937, 1627, 1602, 1379, 1159. HRMS (ESI) m/z [M + H]$^+$ Calcd for $C_{21}H_{33}N_2O_2S$ 377.2257, found 377.2244.

6.3.5 General procedure for the photoinduced reaction of β-Hindered-γ,δ-Unsaturated *N*-arylsulfonylhydrazones (133) yielding Tetrahydropyridazines (136).
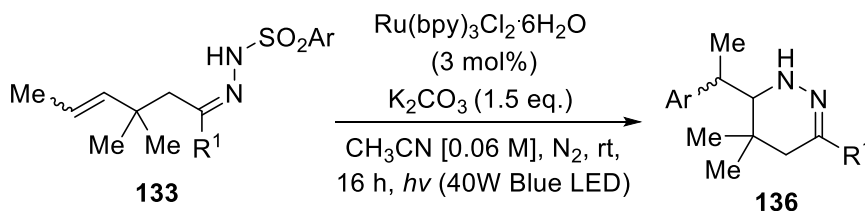
Tetrahydropyridazines **136** were synthesized as single product according to the procedure reported above in this chapter, paragraph 6.3.4 General procedure for the photoinduced reaction of β-hindered-γ,δ-Unsaturated N-Mesitylsulfonylhydrazones (132) yielding Tetrahydropyridazines (134 and 135) using hydrazones with a not terminal alkene moiety **133**.

5,5-Dimethyl-3-phenyl-6-(1-mesityllethyl)-1,4,5,6-tetrahydro pyridazine (136a)
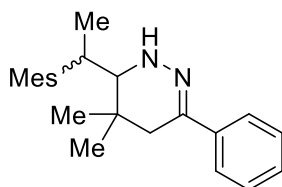
According to the general procedure, 119 mg (0.30 mmol) of 2,2-dimethylpent-3-en-2-one-*N*-mesitylsulfonylhydrazone **133a** were reacted with K_2CO_3 and [Ru(bpy)$_3$]Cl$_2$·6H$_2$O under blue light irradiation for 16 h to obtain 66 mg (0.22 mmol) 5,5-dimethyl-3-phenyl-6-(2,4,6-trimethylbenzyl)-1,4,5,6-tetrahydropyridazine **136a** (72%) as a yellow solid. ^{1}H NMR (600 MHz, CDCl$_3$, Me$_4$Si) δ 7.58 (dd, *J* = 7.2, 1.8 Hz, 2H, Ph*H*), 7.31 (tm, *J* = 7.2 Hz, 2H, Ph*H*), 7.24 (tm, *J* = 7.2 Hz, 1H, Ph*H*, isomer A), 7.22 (tm, *J* = 7.2 Hz, 1H, Ph*H*, isomer B), 6.83 (s, 2H, Mes–*H*, isomer A), 6.82 (s, 2H, Mes–*H*, isomer B), 5.31 (s, 1H, N–*H*), 3.51 (quin, *J* = 7.2 Hz, 1H, Tol–C*H*–CH$_3$), 3.32 (d, *J* = 9.0 Hz, 1H, C*H*-ring), 2.52 (d, *J* = 17.4 Hz, 1H, C(H)*H*-ring), 2.39 (s, 3H, Ar–C*H$_3$*), 2.34 (s, 3H, Ar–C*H$_3$*), 2.28 (d, *J* = 17.4 Hz, 1H, C(H)*H*-ring), 2.24 (s, 3H, Ar–C*H$_3$*), 1.45 (d, *J* = 7.2 Hz, 3H, *J* = 7.2 Hz, 1H, tol-CH–C*H$_3$*), 1.25 (s, 3H, CH$_3$ ring), 1.10 (s, 3H, CH$_3$ ring). ^{13}C NMR (151 MHz, CDCl$_3$, Me$_4$Si) (mixture of isomers) δ 140.3 (Cq), 138.8 (Cq), 137.4 (Cq), 136.1 (Cq), 135.9 (Cq), 131.4 (CH), 129.8 (2 × CH), 128.3 (2 × CH), 127.4 (CH), 124.1 (2 × CH), 63.5 (CH), 40.7 (CH$_2$), 40.2 (Cq), 34.2 (CH), 31.5 (Cq), 29.5 (CH$_3$), 22.6 (CH$_3$), 21.9 (CH$_3$), 21.4 (CH$_3$), 20.7 (CH$_3$), 20.2 (CH$_3$). ν$_{max}$ (neat)/cm^{-1} 3394, 3010, 2992, 1608, 1572, 1445, 1307, 1131. mp 85.4–89.7 °C. HRMS (ESI) *m/z* [M + H]$^+$ Calcd for C$_{23}$H$_{31}$N$_2$ 335.2482, found 335.2482.

5,5-Dimethyl-3-phenyl-6-(1-tolylethyl)-1,4,5,6-tetrahydropyridazine (136b)
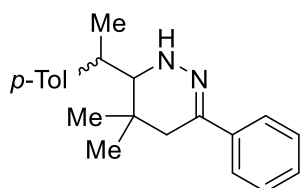
According to the general procedure, 119 mg (0.30 mmol) of 2,2-dimethylpent-3-en-2-one-*N*-tosylhydrazone **133b** were reacted with K_2CO_3 and [Ru(bpy)$_3$]Cl$_2$·6H$_2$O under blue light irradiation for 16 h to obtain 66 mg (0.22 mmol) 5,5-dimethyl-

3-phenyl-6-(2,4,6-trimethylbenzyl)-1,4,5,6-tetrahydropyridazine **136b** (72%) as a yellow solid. ^{1}H NMR (600 MHz, CDCl$_3$, Me$_4$Si) δ7.55 (dd, J = 8.4 Hz, 2H, PhH), 7.55 (tm, J = 7.2 Hz, 2H, PhH), 7.22 (tt, J = 7.2 Hz, 1.2, 1H, PhH), 7.15 (dm, J = 6.6 Hz, 2H, Ar–H), 7.11 (dm, J = 6.6 Hz, 2H, Ar–H), 5.40 (s, 1H, N–H), 2.99 (d, J = 7.8 Hz, 1H, CH-ring), 2.92 (quin, J = 7.2 Hz, 1H, tol–CH–CH$_3$), 2.40 (d, J = 18.0 Hz, 1H, C(H)H-ring), 2.32 (s, 3H, Ar–CH_3), 2.20 (d, J = 18.0 Hz, 1H, C(H)H-ring), 1.41 (d, J = 7.2 Hz, 3H, J = 7.2 Hz, 1H, Tol-CH–CH_3), 1.20 (s, 3H, CH$_3$ring), 0.90 (s, 3H, CH$_3$ring). ^{13}C NMR (151 MHz, CDCl$_3$, Me$_4$Si) δ 141.2 (Cq), 140.9 (Cq), 138.8 (Cq), 136.4 (Cq), 129.5 (2 × CH), 128.2 (2 × CH), 128.0 (2 × CH), 127.4 (CH), 124.2 (2 × CH), 65.4 (CH), 40.3 (CH$_2$), 40.2 (CH), 31.0 (Cq), 29.4 (CH$_3$), 22.7 (CH$_3$), 22.5 (CH$_3$), 21.1 (CH$_3$). mp 89.0–95.8 °C. ν$_{max}$ (neat)/cm^{-1} 3381, 3010, 2990, 1591, 1514, 1467, 1338, 1324, 1071. HRMS (ESI) m/z [M + H]$^+$ Calcd for C$_{21}$H$_{27}$N$_2$ 307.2169, found 307.2175.

3,5,5-Trimethyl-6-(1-tolylethyl)-1,4,5,6-tetrahydropyridazine (136c)
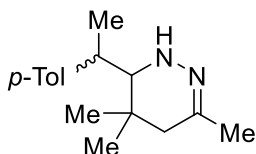
According to the general procedure, 92 mg (0.30 mmol) of 4,4-dimethylhept-5-enone-N-tosylhydrazone **133c** were reacted with K$_2$CO$_3$ and [Ru(bpy)$_3$]Cl$_2$·6H$_2$O under blue light irradiation for 16 h to obtain 51.2 mg (0.21 mmol) 5,5-dimethyl-3-phenyl-6-(2,4,6-trimethylbenzyl)-1,4,5,6-tetrahydropyridazine **136c** (70%) as a yellowish oil. ^{1}H NMR (600 MHz, CDCl$_3$, Me$_4$Si) δ 7.11 (m, J = 6.6 Hz, 2H, Ar–H), 7.06 (dm, J = 6.6 Hz, 2H, Ar–H), 5.40 (s, 1H, N–H), 2.92 (q, J = 7.2 Hz, 1H, Tol–CH–CH$_3$), 2.74 (d, J = 7.2 Hz, 1H, CH-ring), 2.31 (s, 3H, Ar–CH_3), 1.98 (d, J = 16.8 Hz, 1H, C(H)H-ring), 1.73 (s, 3H, N≡C—CH_3), 1.67 (d, J = 16.8 Hz, 1H, C(H)H-ring), 1.34 (d, J = 7.2 Hz, 3H, J = 7.2 Hz, 1H, Tol-CH–CH_3), 1.08 (s, 3H, CH$_3$ring), 0.88 (s, 3H, CH$_3$ring). ^{13}C H NMR (151 MHz, CDCl$_3$, Me$_4$Si) δ 144.8 (Cq), 141.5 (Cq), 136.2 (Cq), 129.3 (2 × CH), 128.0 (2 × CH), 65.3 (CH), 44.4 (CH$_2$), 40.0 (CH), 31.6 (Cq), 29.2 (CH), 23.2 (CH$_3$), 22.7 (CH$_3$), 22.4 (CH$_3$), 21.1 (CH$_3$). ν$_{max}$ (neat)/cm^{-1} 3060, 2964, 1498, 1338, 1260, 1157. HRMS (ESI) m/z [M + H]$^+$ Calcd for C$_{16}$H$_{25}$N$_2$ 245.2012, found 245.2006.

6.4 Visible light promoted domino cyclization and chlorovinylation of linear sulfonylamidoallenes

6.4.1 Optimization of the reaction conditions
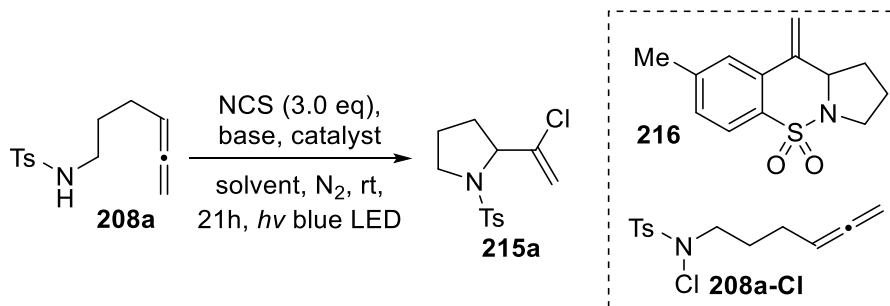
General procedure: A 10 mL Schlenk tube (with screwing cap) containing a magnetic stirring bar was dried with a heat gun under vacuum then the tube was backfilled with N_2. 4 mL of solvent were added *via* syringe and degassed with N_2 bubbling for 20 minutes, then NCS, the catalyst and the base (when solid) were added in one portion, otherwise, the base was subsequently added *via* syringe under N_2 atmosphere. The resulting mixture was stirred and degassed with N_2 for 2 minutes and the allene **208a** (50 mg, 0.2 mmol) was added *via* syringe under N_2 atmosphere and the mixture was stirred and degassed with N_2 for additional 2 minutes. Finally, the bottle was sealed and placed under irradiation with Kessil A160PR Blue LED (456 nm) light placed at 3 cm distance for 21 h with continuous stirring. The reaction was then filtered through a thin pad of silica and eluted with EtOAc. The solvent was evaporated, and the crude purified with SiO_2 gel chromatography (Eluent: EP 9/1 Acetone).

Table 6.7 Optimization of the catalyst

Entry	catalyst	208 [%][b]	215 [%][a]	216 [%][a]	208-Cl [%][a]
1	Mes-(Acr)-Me$^+$ BF$_4^-$	6	29	1	14
2	Ru(bpy)$_3$Cl$_2$	0	33	2	0
3	**Ru(bpy)$_3$(PF$_6$)$_2$**	**0**	**43**	**4**	**0**
4	[Ir(dtbbpy)(ppy)$_2$][PF$_6$]	0	15	1<<	0
5	[Ir(dFCF$_3$ppy)$_2$(bpy)]PF$_6$	0	9	1<<	0
6	Rhodamine 6G	17	17	3	26
7	Eosin Y (Green Light used)	18	12	4	12
8	Rhodamine B (Green Light used)	15	30	2	37
9	4-CzIPN	0	24	1	0

Reactions conditions: **208a** (1.0 eq, 0.20 mmol, 50 mg), catalyst (0.05 eq., as indicated), K$_2$CO$_3$ (1.0 eq, 0.20 mmol, 28 mg) as indicated, in anhydrous CH$_3$CN 4 mL under irradiation with 456 nm light source – blue light. *a)* Yield determined on isolated products. *b)* Yield determined by ^{1}H-NMR analysis, using dichloroethane and nitromethane as internal standards

Table 6.8 Optimization of the base

Entry	base	208 [%][b]	215 [%][a]	216 [%][a]	208-Cl [%][a]
1	**K$_2$CO$_3$**	**0**	**43**	**4**	**0**
2	Cs$_2$CO$_3$	25	27	3	0
3	Na$_2$CO$_3$	15	23	1	0
4	NaHCO$_3$	13	25	1<<	0
5	Li$_2$CO$_3$	4	27	2	0
6	KOH	0	29	1	0
7	NaOH	0	17	1<<	0
8	K$_3$PO$_4$	0	27	0	0
9	Na$_2$HPO$_4$	0	16	0	0
10	NaH$_2$PO$_4$	0	8	0	0
11	2,6-Lutidine	10	10	1<<	0
12	Et$_3$N	0	12	1<<	0

Reactions conditions: **208a** (1.0 eq, 0.20 mmol, 50 mg), Ru(bpy)$_3$(PF$_6$)$_2$ (0.05 eq., 0.01 mmol, 8 mg), base (1.0 eq, 0.20 mmol) as indicated, in anhydrous CH$_3$CN 4 mL under irradiation with 456 nm light source – blue light. *a)* Yield determined on isolated products. *b)* Yield determined by ^{1}H-NMR analysis, using dichloroethane and nitromethane as internal standards

Table 6.9 Optimization of the solvent and solvent mixtures

Entry	solvent	208 [%][b]	215 [%][a]	216 [%][a]	208-Cl [%][a]
1	CH$_3$CN	0	43	4	0
2	CHCl$_3$	0	28	2	0
3	CH$_2$Cl$_2$	0	34	3	0
4	PhCl	0	34	3	0
5	1,2-Dichloroethane	0	26	1	0
6	DMF	0	28	Not obs	0
7	DMA	0	20	Not obs	0
8	DMSO	100	0	0	0
9	1,4-Dioxane	0	5	6	0
10	THF	0	15	6	0
11	CH$_3$OH	0	14	1	0
12	PhCH$_3$	0	47	5	0
13	HCO$_2$CH$_3$	0	31	4	0
14	Acetone	0	43	2	0

Entry	Solvent mixture [solvent 1/ solvent 2] ratio [1:2]	215 [%]
M-1	PhCH$_3$/CH$_3$CN 3:1	46
M-2	PhCH$_3$DMSO 3:1	0%
M-3	PhCH$_3$/PhCl 3:1	49
M-4	**PhCH$_3$/ HCO$_2$Me 3:1**	**56**
M-5	PhCH$_3$/ DMF 3:1	32
M-6	PhCH$_3$/Acetone 3:1	45
M-7	PhCH$_3$/Acetone 2:2	42

Reactions conditions: **208a** (1.0 eq, 0.20 mmol, 50 mg), Ru(bpy)$_3$(PF$_6$)$_2$ (0.05 eq., 0.01 mmol, 8 mg), K$_2$CO$_3$ (1.0 eq, 0.20 mmol, 28 mg) in anhydrous solvent (4 mL in total) as indicated under irradiation with 456 nm light source – blue light. *a)* Yield determined on isolated products. *b)* Yield determined by ^{1}H-NMR analysis, using dichloroethane and nitromethane as internal standards

Table 6.10 Optimization of loading of the base and of the catalyst

Entry	Ru(bpy)$_3$(PF$_6$)$_2$	K$_2$CO$_3$	215 [%]
1	5% mol	1.0 eq.	56%
2	5% mol	0.5 eq.	52%
3	5% mol	0.3 eq.	53%
4	**5% mol**	**0.2 eq.**	**56%**
5	5% mol	0.1 eq.	51%
6	8% mol	0.2 eq.	56%
7	4% mol	0.2 eq.	49%
8	3% mol	0.2 eq.	49%
9	2% mol	0.2 eq.	49%
10	1% mol	0.2 eq.	51%
11	0.5% mol	0.2 eq.	39%

Reactions conditions: **208a** (1.0 eq, 0.20 mmol, 50 mg), Ru(bpy)$_3$(PF$_6$)$_2$ and K$_2$CO$_3$ as indicated in anhydrous solvent (PhCH$_3$ 3 mL and HCO$_2$Me 1mL) under irradiation with 456 nm light source – blue light. *a)* Yield determined on isolated products. *b)* Yield determined by ^{1}H-NMR analysis, using dichloroethane and nitromethane as internal standards

Table 6.11 Optimization of Catalyst/Base Combination (less efficient catalysts)

Base	208 [%][b]	215 [%][a]	216 [%][a]	208-Cl [%][a]
Catalyst: Ru(bpy)₃Cl₂				
K_2CO_3	0	**33**	2	0
Cs_2CO_3	20	**22**	1	0
KOH	0	**12**	1<<	0
NaOH	0	**18**	1<<	0
2,6-Lutidine	10	**10**	1	0
Catalyst: Mes-(Acr)-Me⁺ BF₄⁻				
K_2CO_3	6	**29**	1<<	14
Cs_2CO_3	17	**11**	1<<	0
KOH	0	**0**	0	0
NaOH	0	**14**	0	0
2,6-Lutidine	0	**13**	1	0
Catalyst: Rhodamine B (using green lamp)				
K_2CO_3	15	**30**	2	37
Cs_2CO_3	20	**5**	5	0
2,6-Lutidine	80	**9**	traces	0
Catalyst: [Ir(dtbbpy)(ppy)₂][PF₆]				
K_2CO_3	0	15	1<<	0
K_3PO_4	0	13	1<<	0
Na_2HPO_4	0	traces	0	0
NaH_2PO_4	0	traces	0	0
Catalyst: potassium 5-bromo-1H-indole-1-carbodithioate				
2,6-lutidine	0	**18**	0	0
Catalyst: 4Cz-IPN				
K_2CO_3	0	**18**	0	0
K_3PO_4	0	**traces**	0	0

Note: With Na₂CO₃ NaHCO₃ and Li₂CO₃ degradation of the starting material was observed and not even traces of product recovered

Reactions conditions: **208a** (1.0 eq, 0.20 mmol, 50 mg), catalyst (0.05 eq., 0.01 mmol) and base (1.0 eq, 0.20 mmol) as indicated in anhydrous CH_3CN 4 mL under irradiation with 456 nm light source – blue light. *a)* Yield determined on isolated products. *b)* Yield determined by ^{1}H-NMR analysis, using dichloroethane and nitromethane as internal standards

6.4.2 General Procedures for the synthesis of allenes (208)

6.4.2.1 General Procedure A: synthesis of allenes (208a and 208b)
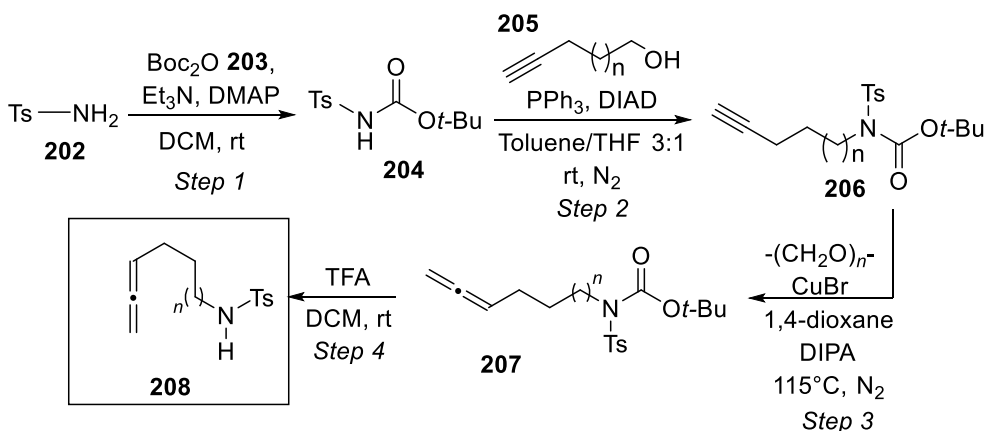
Allenes **208a, 208b** were synthesized according to our previously reported procedure[268] from the corresponding commercially available alkynols **205**. For allenes **208a** and **208b** slight modifications to our previously described procedure were applied to achieve a larger scale preparation:

Step 1: **t-Butyl N-tosylcarbamate (204)**

Following the reported procedure, *t*-Butyl *N*-tosylcarbamate **204** was obtained as a white solid (yield 91%). Spectral data are coherent with those reported in literature.[295] ^{1}H-NMR (600 MHz, CDCl$_3$, Me$_4$Si) δ = 7.89 (d, J= 8.3 Hz, 2H, Ar-*H*), 7.33 (d, *J* = 8.3 Hz, 2H, Ar-*H*), 2.44 (s, 3H; Ar-C*H$_3$*), 1.38 (s, 9H; C(C*H$_3$*)$_3$).

Step 2: Reaction was scaled to 30 mmol (1.0 eq. of alkyne **205**, 30.00 mmol; 1.05 eq. of *t*-butyl tosylcarbamate **204**, 8.80 g, 32 mmol; 1.22 eq of DIAD, 7.30 g, 36 mmol; 1.30 eq. of PPh$_3$, 10.45 g, 40 mmol; in 60 mL of a 3:1 mixture of anhydrous PhCH$_3$/THF). The crude white solid was purified by crystallization from ethanol (3 mL/mmol) to obtain the desired product in 92% yield from pent-4-yn-1-ol **205a** and in 90% yield from hex-5-yn-1-ol **205b**.

---

[295] Shaw, P.; Hassell-Hart, S. J.; Douglas, G. E.; Malcolm, A. G.; Kennedy, A. R.; White, G. V.; Paterson, L. C.; Kerr, W. J. *Org. Lett.* **2022**, *24*, 2750-2755.

t-Butyl pent-4-yn-1-yl(*N*-tosyl)carbamate (206a)
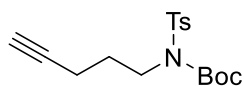
Following the described procedure, 2.60 g (30 mmol) of pent-4-yn-1-ol **205a** were reacted to afford 9.30 g of *t*-butyl pent-4-yn-1-l(*N*-tosyl)carbamate **206a** as a white solid after crystallization. Spectral data are coherent with those reported in literature.[296] ^{1}H-NMR (600 MHz, CDCl$_3$, Me$_4$Si) δ 7.78 (dm, *J* = 8.2 Hz, 2H, Ar-*H*), 7.30 (dm, *J* = 8.2, 2H, Ar-*H*), 3.92 (m, 2H, N-C*H*$_2$-CH$_2$), 2.44 (s, 3H, Ar-C*H*$_3$), 2.28 (td, *J* = 7.1, 2.7 Hz, 2H, C*H*$_2$-C≡CH), 2.02-1.96 (m, 3H, CH$_2$-CH$_2$-CH$_2$ and CH$_2$-C≡C*H*), 1.35 (s, 9H, C(C*H*$_3$)$_3$).

t-Butyl hex-5-yn-1-yl(*N*-tosyl)carbamate (206b)

Following the described procedure, 3.0 g (30 mmol) of hex-5-yn-1-ol **206a** were reacted to afford 9.5 g of *t*-Butyl hex-5-yn-1-yl(*N*-tosyl)carbamate **206b** as a white solid. Spectral data are coherent with those reported in literature.[268] ^{1}H-NMR (600 MHz, CDCl$_3$, Me$_4$Si) δ: 7.78 (d, *J* = 8.3 Hz, 2H,Ar-*H*), 7.30 (dm, *J* = 8.3 Hz, 2H, Ar-*H*), 3.85 (m, 2H, N-C*H*$_2$-CH$_2$), 2.43 (s, 3H; Ar-C*H*$_3$), 2.26 (td, *J*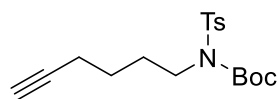 = 7.0, 2.6 Hz, 2H,CH$_2$-C*H*$_2$-C≡), 1.97 (t, *J* =2.7 Hz, 1H, C≡C*H*), 1.90-1.85 (m, 2H, CH$_2$-C*H*$_2$-CH$_2$), 1.59 (quin, *J* = 7.1 Hz, 2H, CH$_2$-C*H*$_2$-CH$_2$-C≡), 1.34 (s, 9H, C(C*H*$_3$)$_3$).

Step 3: reaction was scaled to 1.70 mmol of alkyne for each Pyrex tube (1.0 eq. of alkyne, 1.70 mmol; 2.0 eq. of paraformaldehyde, 100 mg, 3.35 mmol; 0.70 eq. of CuBr, 168 mg, 1.17 mmol; 2.0 eq. of DIPA, 340 mg, 0.470 mL, 3.35 mmol; in 17 mL of anhydrous 1,4-dioxane). The crudes were gathered, and the crude red oil obtained as product was used without further purification in the next step

t-butyl hexa-4,5-dien-1-yl(*N*-tosyl)carbamate (207a)
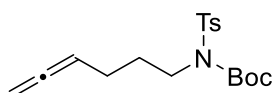
Following the described procedure, 1.90 g (5.64 mmol) of *t*-Butyl pent-4-yn-1-yl(*N*-tosyl)carbamate **206a** were reacted to afford *t*-butyl hexa-4,5-dien-1-yl(tosyl)carbamate **207a** as a red oil (yield 91% on the crude). Spectral data are coherent with those reported in literature.[268] ^{1}H-NMR (600 MHz, CDCl$_3$,

---

[296] Campbell, C. D.; Greenaway, R. L.; Holton , O. T.; Walker, P. R.; Chapman, H. A.; Russell, C. A.; Carr, G.; Thomson, A. L.; Anderson, E. A. *Chem. Eur. J.* **2015,** *21*, 12627-12639.

Me$_4$Si): δ 7.77 (d, J = 8.3 Hz, 2H, Ar-H), 7.30 (d, J = 8.3 Hz, 2H, Ar-H), 5.14 (quin, J = 6.4 Hz, 1H, CH$_2$-CH=C=CH$_2$), 4.70 (dt, J = 6.3, 3.1 Hz, 2H, CH=C=CH_2), 3.87-3.83 (m, 2H, N-CH_2-CH$_2$), 2.43 (s, 3H, Ar-CH_3), 2.07 (m, 2H, CH$_2$-CH_2-CH), 1.88 (quin, J = 7.9 Hz, 2H,CH$_2$-CH_2-CH$_2$), 1.33 (s, 9H, C(CH$_3$)$_3$).

t-Butyl hepta-5,6-dien-1-yl(N-tosyl)carbamate (207b)
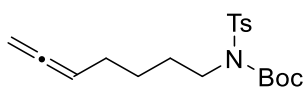
Following the described procedure, 1.98 g (5.64 mmol) of t-butyl hexa-4,5-dien-1-yl(tosyl)carbamate **206b** were reacted with paraformaldehyde to afford t-butyl hepta-5,6-dien-1-yl(N-tosyl)carbamate **207b** as a red oil which was used without further purification in step 4 (yield 63% on the crude). Spectral data are coherent with those reported in literature.[268] ^{1}H-NMR (600 MHz, CDCl$_3$, Me$_4$Si): crude reaction mixture; δ 7.77 (d, J = 8.4 Hz, 2H, Ar-H), 7.29 (d, J = 8.4 Hz, 2H, Ar-H), 5.10 (quin, J = 6.7 Hz, 1H, CH$_2$-CH=C=CH$_2$), 4.67 (dt, J = 6.7, 3.3 Hz, 2H, =C=CH_2), 3.82 (m, 2H, N-CH_2-CH$_2$), 3.70 (residue of dioxane), 2.44 (s, 3H, Ar-CH_3), 2.08-2.03 (m, 2H, CH$_2$-CH_2-CH), 1.82-1.77 (m, 2H, N-CH_2-CH$_2$), 1.50-1.45 (m, 2H, CH$_2$-CH_2-CH$_2$), 1.33 (s, 9H, C(CH$_3$)$_3$).

Step 4:

N-tosylhexa-4,5-dien-1-ylamine (208a)
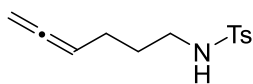
Following the described procedure, 1.80 g (5.11 mmol) of t-butyl hexa-4,5-dien-1-yl(tosyl)carbamate **207a** were reacted with TFA to afford 1.09 g of N-tosylhexa-4,5-dien1-ylamine **208a** as a yellowish oil after flash silica gel chromatography purification with EP/Acetone 85/15 (yield 94% on the crude, yield 85% over the two steps 3-4). Spectral data are coherent with those reported in literature.[268] ^{1}H-NMR (600 MHz, CDCl$_3$, Me$_4$Si): δ= 7.74 (d, J = 8.3 Hz, 2H, Ar-H), 7.31 (d, J = 8.3 Hz, 2H, Ar-H), 5.02 (quin, J = 6.7 Hz, 1H, CH$_2$-CH=C=CH$_2$), 4.64 (dt, J = 6.7, 3.2 Hz, 2H, CH=C=CH_2), 4.30 (s broad, 1H, NH), 2.99 (q, J = 7.0 Hz, 2H, NH-CH_2-CH$_2$), 2.43 (s, 3H, Ar-CH_3), 1.99 (m, 2H, CH$_2$-CH_2-CH), 1.59 (quin, J = 7.1 Hz, 2H, CH$_2$-CH_2-CH$_2$).
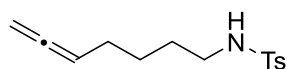
N-tosylhepta-5,6-dien-1-ylamine (208b)

Following the described procedure, 1.86 g (5.11 mmol) of *t*-butyl hepta-5,6-dien-1-yl(tosyl)carbamate **207b** were reacted with TFA to afford 0.771 mg of *N*-tosylhepta5,6-dien-1-ylamine **208b** as a yellow oil after chromatography purification with EP/Acetone 85/15 (yield 93% on the crude, yield 57% over the two steps 3-4). Spectral data are coherent with those reported in literature.[268] ^{1}H-NMR (600 MHz, CDCl$_3$, Me$_4$Si): δ 7.74 (d, *J* = 8.3 Hz, 2H, Ar-*H*), 7.31 (d, *J* = 8.3 Hz, 2H, Ar-*H*), 5.02 (quin, *J* = 6.7 Hz, 1H, CH$_2$-C*H*=C), 4.64 (dt, 2H, *J* = 6.7, 3.3 Hz, =C=C*H$_2$*), 4.27 (t, *J* = 6.2 Hz, 1H, NH), 2.95 (q, *J* = 6.8 Hz, 2H, NH-C*H$_2$*-CH$_2$), 2.43 (s, 3H, Ar-C*H$_3$*), 1.94 (m, 2H, CH$_2$-C*H$_2$*-CH), 1.50 (quin, *J* = 7.1 Hz, 2H, NH-CH$_2$-C*H$_2$*-CH$_2$), 1.39 (quin, *J* = 7.1 Hz, 2H, CH$_2$-C*H$_2$*-CH$_2$).

6.4.2.2 General Procedure B: synthesis of alkoxy-allene (208c)
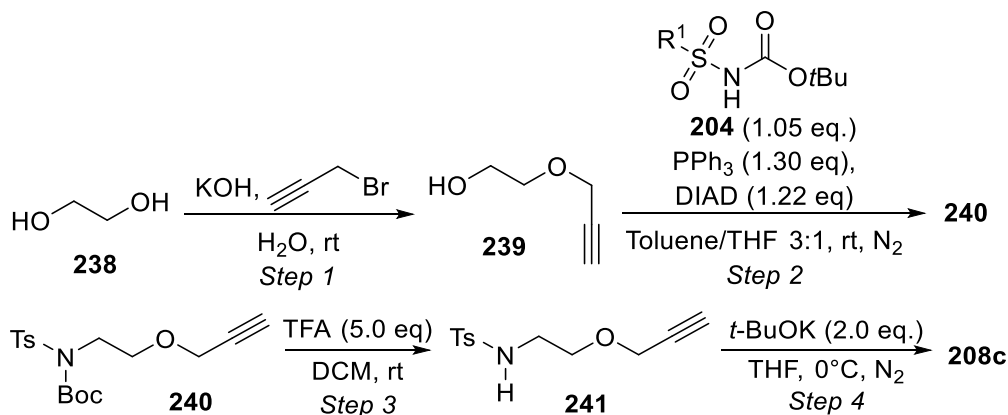
Step 1: 2-(prop-2-yn-1-yloxy)ethanol (239)

Following a procedure by Finn[297] ethylene glycol **238** (6.98 mL, 7.76 g, 125 mmol, 5.0 eq.) was reacted with propargyl bromide (2.79 mL of 80% w/w solution in PhCH$_3$, 25 mmol, 1.0 Eq.) and KOH (2.81 g, 50 mmol, 2.0 eq.) in water (4.40 mL) to obtain 2,90 g of 2-(prop-2-yn-1-yloxy)ethan-1-ol **239** (yield 58%). Spectral data are coherent with those reported in literature.[297] ^{1}H-NMR (600 MHz, CDCl$_3$,

---

[297] Kislukhin, A. A.; Higginson, C. J.; Hong, V. P.; Finn, M. G. *J. Am. Chem. Soc.* **2012,** *134*, 6491-6497.

Me$_4$Si) δ 4.20 (d, J = 2.4 Hz, 2H, CH_2C≡CH), 3.77 (m, 2H, CH_2), 3.65 (m, 2H, CH_2), 2.45 (t, j = 2.4 Hz, 1H, C≡CH), 2.08 (s, 1H, OH).

Step 2: *t*-butyl (2-(prop-2-yn-1-yloxy)ethyl)(*N*-tosyl)carbamate (240)

Ts—N(Boc)—CH₂CH₂—O—CH₂C≡CH
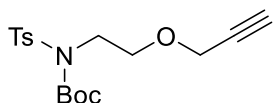
Employing our conditions for Mitsunobu reaction (see above, general procedure A, step 2) alcohol **239** (1.0 eq., 8.0 mmol, 0.80 g) were reacted with 1 *t*-butyl tosylcarbamate **204** (1.05 eq, 9.6 mmol, 2.60 g), DIAD (1.22 eq, 9.76 mmol, 1.98 g) and PPh$_3$ (1.30 eq., 10.4 mmol, 2.73 g); in 24 mL of a 3:1 mixture of anhydrous PhCH$_3$/THF. The crude obtained was purified by column chromatography (EP/EE 9:1), to obtain *t*-butyl (2-(prop-2-yn-1-yloxy)ethyl)(*N*-tosyl)carbamate **240** as a colorless oil. Spectral data are coherent with those reported in literature.[298] ^{1}H-NMR (600 MHz, CDCl$_3$, Me$_4$Si) δ 7.85 (d, J = 8.1 Hz, 2H, Ar-H), 7.28 (d, J = 8.1 Hz, 2H, Ar-H), 4.19 (d, J = 2.4 Hz, 2H, O-CH_2-C≡), 4.06 (t, J = 5.8 Hz, 2H, O-(CH_2)$_2$-N), 3.78 (t, J = 5.8 Hz, , O-(CH_2)$_2$-N), 2.44-2.39 (m, 4H, Ar-CH_3, CH$_2$-C≡CH), 1.32 (s, 9H, (CH_3)$_3$).

Step 3: 4-methyl-*N*-(2-(prop-2-yn-1-yloxy)ethyl)benzenesulfonamide (241)

Ts—N(H)—CH₂CH₂—O—CH₂C≡CH
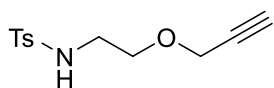
Following the general procedure A, step 4) carbamate **240** (1.0 eq., 2.5 mmol, 0.88g) was deprotected using TFA (5.0 eq, 12.5 mmol, 1.40 g) to afford 0.600 g of 4-methyl-*N*-(2-(prop-2-yn-1-yloxy)ethyl)benzenesulfonamide **241** (yield 95%) as a colorless oil that was used without further purification in the following step. Spectral data match previous report. Spectral data are coherent with those reported in literature.[298] ^{1}H-NMR (600 MHz, CDCl$_3$, Me$_4$Si) δ 7.72 (d, J = 8.4 Hz, 2H, Ar-H), 7.28 (d, J = 8.4 Hz, 2H, Ar-H), 5.00 (t, 1H, NH), 4.04 (d, J = 2.3 Hz, 2H, O-CH_2-C≡), 3.52 (t, J = 5.1 Hz, 2H, O-(CH_2)$_2$-N), 3.14 − 3.09 (m, 2H, O-(CH_2)$_2$-N), 2.42-2.38 m, 4H, Ar-CH_3, CH$_2$-C≡CH), 1.32 (s, 9H, (CH_3)$_3$).

---

[298] Broggini, G.; Poli, G.; Beccalli, E. M.; Brusa, F.; Gazzola, S.; Oble, J. *Adv. Synth. Catal.* **2015,** *357*, 677-682.

Step 4: **4-methyl-*N*-(2-(propa-1,2-dien-1-yloxy)ethyl)benzene sulfonamide (208c)**
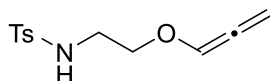
A 10 mL Schlenk tube (with screwing cap) containing a magnetic stirring bar was dried with a heat gun under vacuum then the tube was backfilled with N_2. The alkyne **241** (1.0 eq., 1 mmol, 250 mg) and 4 mL of dry THF were poured into the flask under N_2 atmosphere and the solution was cooled to -10 °C. *t*BuOK commercial solution 1M in THF was added dropwise (2.1 eq., 2.1 mmol, 2 mL) under N_2 atmosphere with continuous stirring. The reaction was sealed and kept a -10°C for 35 minutes, then quenched with 3mL of water. The water phase was extracted with Et_2O (3x10 mL), then the organic phase was collected, dried with Na_2SO_4, filtered and the solvent evaporated. The crude yellow oil obtained (a mixture containing 60:40 ratio of **208c/241**) was purified with silica gel flash chromatography (SiO_2 deactivated with 1% w/w of Et_3N, eluent EP:EE 9:1) to obtain 125 g of **208c** (50% yield, conversion ratio ignored) as a yellow oil. ^{1}H-NMR (600 MHz, $CDCl_3$, Me_4Si) δ 7.73 (d, *J* = 8.1 Hz, 2H, Ar-*H*), 7.30 (d, *J* = 8.1 Hz, 2H, Ar-*H*), 6.62 (t, *J* = 6.0 Hz, 1H, O-C*H*=C=), 5.40 (d, *J* = 6.0 Hz, 2H, O-CH=C=C*H$_2$*), 4,76 (m, 1H, N*H*), 3.56 (t, *J* = 5.1 Hz, 2H, C*H$_2$*-O), 3.19 (m, 2H, C*H$_2$*-NH), 2.42 (s, 3H, Ar-C*H$_3$*). ^{13}C-NMR (150 MHz, $CDCl_3$, Me_4Si) 200.8 (Cq), 143.8 (Cq), 137.0 (Cq), 129.9 (2 x CH), 127.2 (2 x CH), 121.2 (CH), 91.6 (CH_2), 66.8 (CH_2), 42.5 (CH_2), 21.6 (CH_3)

6.4.2.3 General Procedure C: synthesis of internal allenes (208d, 208h, 208j and 208k)

A procedure reported by Ma and coworkers was adapted.[299]
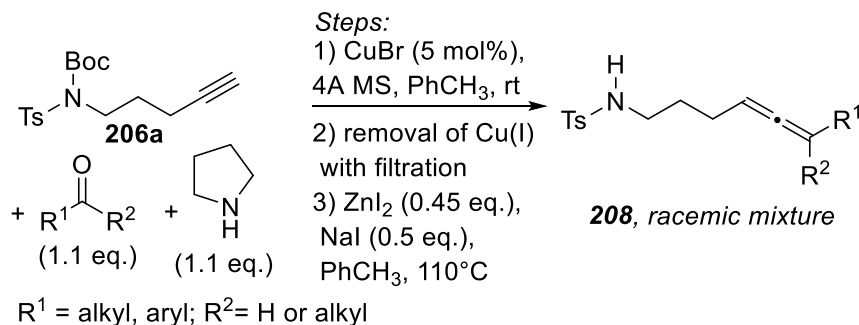
R^1 = alkyl, aryl; R^2= H or alkyl

---

[299] Ye, J.; Li, S.; Chen, B.; Fan, W.; Kuang, J.; Liu, J.; Liu, Y.; Miao, B.; Wan, B.; Wang, Y.; Xie, X.; Yu, Q.; Yuan, W.; Ma, S. *Org. Lett.* **2012,** *14*, 1346-1349.

The reaction seemed to be sensitive to scale up, so it was repeated on maximum 1 mmol of substrate (larger scale preparation performed by parallel repetitions).

Step 1: A 10 mL Schlenk tube (with screwing cap) containing a magnetic stirring bar was dried with a heat gun under vacuum then the tube was backfilled with N_2. CuBr (0.05 eq., 7.4 mg, 0.05 mmol), activated 4 Å molecular sieves (305 mg), and the alkyne **206a** (1.0 eq, 340 mg, 1.0 mmol) were added and subjected to two vacuum/N_2 cycles. Anhydrous $PhCH_3$ (2 mL), the appropriate carbonyl compound (ketone or aldehyde, 1.1 eq., 1.1 mmol) and the pyrrolidine (1.1 eq., 78 mg, 1.1 mmol) were added sequentially under N_2 atmosphere. The solution was then stirred at room temperature until completion (24h for aldehydes, 72 h for ketones).

Step 2: The crude reaction mixture was then filtered through a short pad of silica and eluted with AcOEt (40 mL). Then the solvent was evaporated, and the crude yellowish oil obtained subjected to the following step.

Step 3: A 10 mL Schlenk tube (with screwing cap) containing a magnetic stirring bar was dried with a heat gun under vacuum then the tube was backfilled with N_2. Anhydrous ground ZnI_2 (0.45 eq., 147.0 mg, 0.45 mmol) and NaI (0.5 eq., 75.2 mg, 0.5 mmol) were added. Subsequently the Schlenk tube was heated with a heating gun (350°C) and subjected to two vacuum/N_2 cycles. The crude oil product was then dissolved in $PhCH_3$ (5 mL) and added *via* syringe to the Schlenk tube and the tube sealed to be immerged in a pre-heated oil bath at 110 °C with vigorous stirring for 6 h. The resulting reaction mixture was then filtered through a short pad of silica gel and eluted with AcOEt (40 mL). The crude obtained after evaporation of the solvent was finally purified with flash silica gel chromatography to isolate the racemic mixture of not terminal allene.

4-methyl-*N*-(6-methylhepta-4,5-dien-1-yl)benzenesulfonamide (208d).
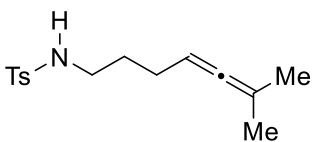
Following the described procedure, 0.360 g of *t*-butyl pent-4-yn-1- yl(tosyl)carbamate **206a** was reacted with 175 mg an excess of anhydrous acetone (3.0 eq, 3.0 mmol) to afford 70 mg of 4-

methyl-*N*-(6-methylhepta-4,5-dien-1-yl)benzenesulfonamide **208d** as colorless oil (EP/Acetone 9/1, yield 25%). Spectral data are coherent with those reported in literature.[300] ^{1}H-NMR (600 MHz, CDCl$_3$, Me$_4$Si): δ 7.74 (d, *J* = 8.3 Hz, 2H, Ar-*H*), 7.29 (d, *J* = 8.3 Hz, 2H, Ar-*H*)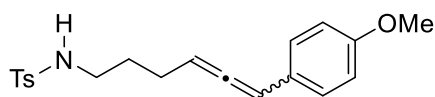, 4.83 (m, 1H, C*H*=C), 4.75 (t, *J* = 6.2 Hz, 1H, N*H*), 2.98 (m, 2H; NH-C*H$_2$*-CH$_2$), 2.40 (s, 3H, Ar-C*H$_3$*), 1.95 − 1.85 (m, 2H, CH$_2$-C*H$_2$*-CH), 1.60 (s, 3H, =C(C*H$_3$*)$_2$), 1.59 (S, 3H, =C(C*H$_3$*)$_2$) 1.52 (quin, *J* = 7.2 Hz, 2H, CH$_2$-C*H$_2$*-CH$_2$).

N-(6-(4-methoxyphenyl)hexa-4,5-dien-1-yl)-4-methylbenzene sulfonamide (208h).

Following the described procedure, 0.360 g of *t*-butyl pent-4-yn-1-yl(tosyl)carbamate **206a** was reacted with 150 mg of 4-methoxybenzaldehyde to afford 147 mg of *N*-(6-(4-methoxyphenyl)hexa-4,5-dien-1-yl)-4-methylbenzenesulfonamide **208h** as a yellow oil (EP/Acetone 9/1, yield 40%). Spectral data are coherent with our previous report.[268] ^{1}H-NMR (600 MHz, CDCl$_3$, Me$_4$Si): δ 7.71 (d, *J* = 8.3 Hz, 2H,Ts-*H*), 7.25 (d, *J* = 8.3 Hz, 2H, Ts-*H*), 7.14 (d, *J* = 8.8 Hz, 2H, Ar-*H*), 6.82 (d, *J* = 8.8 Hz, 2H, Ar-*H*), 6.05 (dt, *J* = 6.4, 3.1 Hz, 1H, C=C*H*-Ph), 5.46 (q, *J* = 6.4 Hz, 1H, CH$_2$-C*H*=C), 4.69 (t, *J* = 6.3 Hz, 1H, N*H*), 3.01-2.93 (m, 2H; NH-C*H$_2$*-CH$_2$), 3.78 (s, 3H; OC*H$_3$*), 2.39 (s, 3H; Ar-C*H$_3$*), 2.20-2.05 (m, 2H; CH$_2$-C*H$_2$*-CH), 1.66-1.58 (m, 2H; CH$_2$-C*H$_2$*-CH$_2$).

4-methyl-*N*-(undeca-4,5-dien-1-yl)benzenesulfonamide (208j)
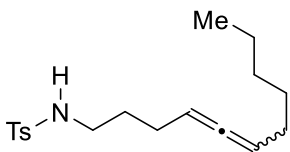
Following the described procedure, 0.360 g of *t*-butyl pent-4-yn-1- yl(tosyl)carbamate **206a** were reacted with 100 mg of hexanal to afford 100 mg of 4-methyl-*N*-(undeca-4,5-dien-1-yl)benzenesulfonamide **208j** as a yellow oil (EP/Acetone 9/1, 30%). Spectral data are coherent with those reported in literature.[300] ^{1}H NMR (600 MHz, CDCl$_3$, Me$_4$Si): δ 7.73 (d, *J* = 8.3 Hz, 2H, Ar-*H*), 7.28 (d, *J* = 8.3 Hz, 2H, Ar-*H*), 5.01 (m, 1H, CH$_2$-C*H$_a$*=C), 4.95 (m, 1H, C=C*H$_b$*-CH$_2$), 4.83 (t, *J* = 6.2 Hz, 1H, N*H*), 2.94 (td, *J* = 7.0, 6.0 Hz, 1H, NH-C*H$_2$*-CH$_2$), 2.40 (s, 3H, Ar-C*H$_3$*), 2.02 − 1.84 (m, 4H, CH$_2$-C*H$_2$*-CH$_2$ and C*H$_2$*-

---

[300] Jonasson, C.; Horváth, A.; Bäckvall, J.-E. *J. Am. Chem. Soc.* **2000,** *122*, 9600-9609.

CH$_3$), 1.60-1.49 (m, 2H, CH$_2$-CH_2-CH$_2$), 1.35-1.30 (m, 2H, CH$_2$-CH_2-CH$_2$), 1.30-1.20 (m, 4H, CH$_2$-CH_2-CH$_2$), 0.85 (t, J = 7.0 Hz, 3H, CH$_2$-CH_3).

N-(6-cyclohexylhexa-4,5-dien-1-yl)-4-methylbenzenesulfonamide (208j)

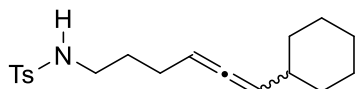Following the described procedure, 0.360 g of *t*-butyl pent-4-yn-1- yl(tosyl)carbamate **206a** were reacted with 110 mg of hexanal to afford 135 mg of *N*-(6-cyclohexylhexa-4,5-dien-1-yl)-4-methylbenzenesulfonamide **208j** as a yellow oil (EP/Acetone 9/1, 40%). ^{1}H NMR (600 MHz, CDCl$_3$, Me$_4$Si): δ 7.73 (d, J = 8.3 Hz, 2H, Ar-H), 7.29 (d, J = 8.3 Hz, 2H, Ar-H), 5.02 (m, 2H, CH$_2$-CH=C=CH-Cy), 4.50 (t, J = 6.2 Hz, 1H, NH), 2.97 (dq, J = 7.1, 1.6 Hz, 2H, NCH$_2$-CH_2-CH$_2$), 2.41 (s, 3H, Ar-CH_3), 1.99-1.92 (m, 2H, Cy=C=CH-CH_2), 1.92-1.85 (m, 1H, CH=C=CH-C$_a$(C$_b$H$_2$)H_bH$_a$), 1.71-1.65 (m, 5H, (CH$_2$)$_2$-CH_2-(CH$_2$)$_2$, C$_b$$H_bH_a$-CH$_2$-CH$_2$-CH$_2$-C$_aH_2$, C$_a$$H_bH_a$-CH$_2$-CH$_2$-CH$_2$-C$_bH_2$), 1.56 (quin, J = 7.1 Hz, 2H, NCH$_2$-CH_2-CH$_2$), 1.28-1.19 (m, 2H, CH=C=CH-C$_a$(C$_b$H$_2$)H$_b$$H_a$, C$_aH_b$$H_a$-CH$_2$-CH$_2$-CH$_2$-C$_bH_2$), 1.18-1.09 (m, 1H, CH=C=CH-C$_b$(C$_a$H$_2$)H$_b$$H_a$), 1.06-0.96 (m, 2H, CH=C=CH-C$_b$(C$_a$H$_2$)H_bH$_a$, C$_b$H$_b$$H_a$-CH$_2$-CH$_2$-CH$_2$-C$_aH_2$). ^{13}C NMR (151 MHz, CDCl$_3$, Me$_4$Si): δ 202.8 (Cq), 143.4 (Cq), 137.1 (Cq), 129.8 (2 x CH), 127.2 (2 x CH), 98.0 (CH), 90.5 (CH), 42.8 (CH$_2$), 37.24 (CH), 33.2 (CH$_2$), 33.2 (CH$_2$), 33.1 (CH$_2$), 28.9 (CH$_2$), 26.2 (CH$_2$), 26.1 (CH$_2$), 26.0 (CH$_2$), 21.6 (CH$_3$).

6.4.2.4 General Procedure D: synthesis of allenes (208e, 208f, 208g)
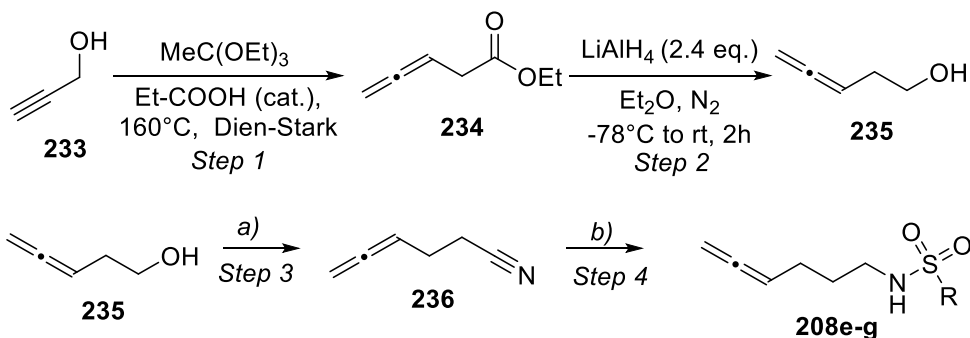
a)
i) Et$_3$N, MsCl, N$_2$, Et$_2$O, 0°C to rt, 1h
ii) NaCN, DMSO, 50°C, 72h

b)
i) LiAH$_4$ (1.5 eq), Et$_2$O, 0 °C to rt, 12 h
ii) RSO$_2$Cl **237** (1.10 eq), KOH (5.00 eq), Et$_2$O, rt, 24 h.

For allenes **208e**, **208f**, and **208g** the general synthetic route was adapted from two different previous reports[301,302] defining 4 steps:

Step 1: Ethyl penta-3,4-dienoate (234)

A procedure by Breit[303] from propargyl alcohol **233** was followed and the obtained product **234** was purified by distillation (bp: 46 mbar, 75 °C, yield 80%).^{1}H-NMR (600 MHz, CDCl$_3$, Me$_4$Si) δ 5.26 (tt, J = 7.4, 6.7 Hz, 1H, C*H*=C=CH$_2$), 4.75 (dt, *J* = 6.7, 2.9 Hz, 2H, CH=C=C*H*$_2$), 4.15 (q, *J* = 7.1 Hz, 2H, O-C*H*$_2$), 3.04 (dt, *J* = 7.4, 2.9 Hz, 2H, CH-C*H*$_2$-C(O)), 1.26 (t, *J* = 7.1 Hz, 3H, CH$_2$-C*H*$_3$).

Step 2: penta-3,4-dien-1-ol (235)

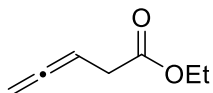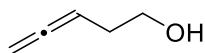A reported procedure of reduction with LiAlH$_4$ was adapted to penta-3,4-dienoate **234** (instead of Ethyl 3-(((tert-butyldiphenylsilyl)oxy)methyl)penta-3,4-dienoate).[304]   Penta-3,4-dienoate **234** (24 mmol, 1.0 eq, 3.03 g), LiAlH$_4$ (33.6 mmol, 1.4 eq, 1.30 gr) and dry Et$_2$O (70 mL distilled from sodium benzophenone) were used. The reaction was monitored by GC-MS. The product penta-3,4-dien-1-ol **235** obtained in 84% yield and was used without further purification in the next step. Spectral data are coherent with those reported in literature.[301] ^{1}H-NMR (600 MHz, CDCl$_3$, Me$_4$Si) δ 5.11 (q, *J* = 6.7 Hz, 1H, CH$_2$-C*H*=C=CH$_2$), 4.72 (td, *J* = 3.0, 6.7 Hz, 2H, CH=C=C*H*$_2$), 3.70 (t, *J* = 6.4 Hz, 2H, O-C*H*$_2$), 2.26 (tq, *J* = 3.0, 6.4 Hz, 2H, O-CH$_2$-C*H*$_2$), 1.60 (bs, 1H, O-*H*)

Step 3: Hexadi-4,5-enenitrile (236)
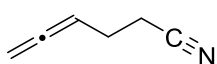
The procedure reported by Díez-González[301] was followed, but after the addition of NaCN the reaction was heated in dry sin at 50°C so that total conversion was achieved in 68 hours. The product Hexadi-4,5-enenitrile **236** obtained in 60% yield (on the crude product) was used without further purification in the next step. Spectral data are coherent with those reported in literature.[301] ^{1}H NMR (600 MHz, CDCl$_3$) δ 5.19 (quin, *J*

---

[301] Zelenay, B.; Munton, P.; Tian, X.; Díez-González, S. *Eur. J. Org. Chem.* **2019,** *2019*, 4725-4730.
[302] Berthold, D.; Geissler, A. G. A.; Giofré, S.; Breit, B. *Angew. Chem. Int. Ed.* **2019,** *58*, 9994-9997.
[303] Schmidt, J. P.; Breit, B. *Angew. Chem. Int. Ed.* **2020,** *59*, 23485-23490.
[304] Joseph E. Burchick. Jr., S. M. W., Kay M. Brummond. *Org. Synth.* **2017**, 109-122.

= 6.6 Hz, 1H, CH$_2$-CH=C=CH$_2$), 4.84 (J = 6.6, 3.3 Hz, 2H, CH=C=CH_2), 2.45 (t, J = 6.7 Hz, 2H, NC-CH_2), 2.34 (m, 2H, CH$_2$-CH_2).

Step 4: Adapting the procedure by Breit[302], a round-bottomed flask dried under vacuum was filled with a suspension of LiAlH$_4$ (0.65 g, 17.2 mmol) in Et$_2$O (40 mL) under N$_2$ atmosphere. Then the solution was cooled at -78°C and a solution **236** (0.80 g, 8.6 mmol) in Et$_2$O (10 mL) was slowly added. The reaction mixture was stirred for 2 h, while temperature was allowed to reach -20°C. Monitoring of the reaction by GC-Ms confirmed reaction completion and the reaction was quenched at this temperature by a dropwise addition of aqueous 5M KOH until H$_2$ evolution stopped and a white precipitate formed. After stirring at 0°C for 30 min, the formed precipitate was filtered off and washed with Et$_2$O (10 mL). The aqueous layer was separated and extracted with Et$_2$O (3×10 mL). The combined organic phases were dried over Na$_2$SO$_4$, filtered, and concentrated under reduced pressure. The crude amine (typically 2 mmol) and 5.0 eq. KOH were suspended in Et$_2$O (5 mL) in a screwing cap vial to obtain a 0.4 M solution of the amine. 1.10 eq of the appropriate sulfonyl chloride R-SO$_2$Cl **237** was added in small portions (1 mmol every 30 minutes) at 0 °C. The suspension was continuously stirred and allowed to warm to rt overnight, then the reaction was carefully quenched with H$_2$O (5 mL) and the phases were separated. The aqueous phase was extracted with CH$_2$Cl$_2$ (3 × 5 mL). The organic phases were dried over Na$_2$SO$_4$ and concentrated under reduced pressure then the crude was purified with silica gel chromatography.

N-(penta-3,4-dien-1-yl)benzenesulfonamide (208e)
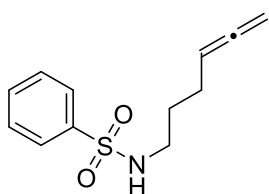
Following the described procedure, nitrile **236** (2.0 mmol, 190 mg) was reacted with benzenesulfonyl chloride **237a** (2.2 mmol, 390 mg) to obtain 260 mg of sulfonylamide **208e** as a colorless oil (Eluent: EP 95/5 Acetone. 55% yield). Spectral data match previous report.[305] ^{1}H-NMR (600 MHz, CDCl$_3$, Me$_4$Si): δ 7.87 (dm, J = 7.6 Hz, 2H, Ar-H), 7.59 – 7.55 (m, 1H, *p*-H-Ar), 7.50 (tm, J = 7.6 Hz, 2H, Ar-H), 4.97 (quin, J = 6.6 Hz, 1H, CH$_2$-CH=C=CH$_2$), 4.70 (m, 1H, N-H), 4.58 (dt, J = 6.7,

---

[305] Yang, C.-H.; Han, M.; Li, W.; Zhu, N.; Sun, Z.; Wang, J.; Yang, Z.; Li, Y.-M. *Org. Lett.* **2020,** *22*, 5090-5093.

3.3 Hz, 2H, CH=C=CH_2), 2.94 (q, J = 6.7 Hz, 2H, NH-CH_2-CH$_2$), 2.00 − 1.92 (m, 2H; CH$_2$-CH_2-CH), 1.63 − 1.55 (m, 2H, CH$_2$-CH_2-CH$_2$).

2,4,6-Trimethyl-*N*-(penta-3,4-dien-1-yl)benzenesulfonamide (208f)

Following the described procedure, nitrile **236** (2.0 mmol, 190 mg) was reacted with 2,4,6-trimethylbenzenesulfonyl chloride **237b** (2.2 mmol, 480 mg), to obtain 346 mg of sulfonylamide **208f** as a colorless oil (Eluent: EP 92/8 Acetone, yield 62%). ^{1}H NMR (600 MHz, CDCl$_3$, Me$_4$Si): δ 6.95 (s, 2H, Ar-*H*), 4.99 (q, J = 6.6 Hz, 1H, CH$_2$-C*H*=C=CH$_2$) 4.62 (dt, J = 6.7, 3.3 Hz, 2H, CH=C=CH_2), 4.47 (bt, J = 6.6 Hz, 1H, N-*H*) 2.93 (q, J = 6.8 Hz, 2H, NH-CH_2-CH$_2$), 2.62 (s, 6H, *o*-CH_3-*Ar*), 2.29 (s, 3H, *p*-CH_3-*Ar*), 1.96 (m, 2H; CH$_2$-CH_2-CH), 1.60 − 1.54 (m, 2H, CH$_2$-CH_2-CH$_2$). ^{13}C NMR (151 MHz, CDCl$_3$, Me$_4$Si) δ 208.8 (Cq), 142.2 (Cq), 139.2 (Cq), 133.7 (Cq), 132.1 (2 x CH), 88.8 (CH), 75.5 (CH$_2$), 42.0 (CH$_2$), 28.8 (CH$_2$), 25.2 (CH$_2$), 23.0 (CH$_3$), 21.0 (CH$_3$).

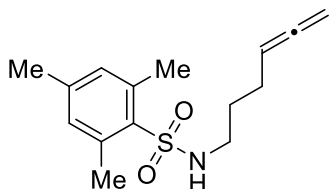## 4-Chloro-*N*-(penta-3,4-dien-1-yl)benzenesulfonamide (208g)
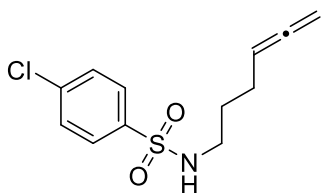
Following the described procedure, nitrile **236** (2.0 mmol, 190 mg) was reacted with 4-chlorolbenzenesulfonyl chloride **237c** (2.2 mmol, 464 mg), to obtain 245 mg of sulfonylamide **208g** as a colorless oil (Eluent: EP 92/8 Acetone, 45% yield). ^{1}H NMR (600 MHz, CDCl$_3$, Me$_4$Si): δ 7.80 (dm, J = 7.6 Hz, 2H, Ar-*H*), 7.50 (dm, J = 7.6 Hz, 2H, Ar-*H*), 5.03 (quin, J = 6.7 Hz, 1H, CH$_2$-C*H*=C=CH$_2$), 4.66 (dt, J = 6.7, 3.3 Hz, 2H, CH=C=CH_2), 4.39 (t, J = 6.6 Hz, 1H, N-*H*), 3.02 (q, J = 6.8 Hz, 2H, NH-CH_2-CH$_2$), 2.00 (m, 2H; CH$_2$-CH_2-CH), 1.61 (quin, J = 7.1 Hz, 2H, CH$_2$-CH_2-CH$_2$). ^{13}C NMR (151 MHz, CDCl$_3$, Me$_4$Si) δ 208.8 (Cq), 139.2 (Cq), 138.7 (Cq), 129.5 (2 x CH), 128.6 (2 x CH), 88.7 (CH), 75.8 (CH$_2$), 42.7 (CH$_2$), 28.8 (CH$_2$), 25.1 (CH$_2$).

6.4.2.5 Synthesis of allenes (208a-Cl and 208a-A)

N-chloro-N-(hexa-4,5-dien-1-yl)-tosylamide (208a-Cl)
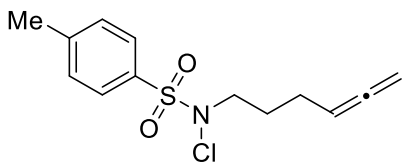
According to a modified procedure,[306] in a 100 mL round-bottomed flask, allene **208** (1.0 eq., 400 mg, 1.6 mmol) was dissolved in 30 mL of CHCl$_3$, then 30 mL of aqueous NaClO (11-15% available chlorine) was added and vigorously stirred until reaction completion (carefully monitored every 30 minutes by TLC in eluent Hexanes/AcOEt 3:1. The reaction mixture was then stopped, the aqueous fase removed and washed with CHCl$_3$ (3x30 mL) then the organic phase was collected, dried over Na$_2$SO$_4$ filtered and solvent evaporated under reduced pressure to obtain 458 mg of a colorless oil that resulted to be the pure product **208a-Cl** (98%), used without further purification, and stored under N$_2$ at -20°C (as a white solid). ^{1}H NMR (600 MHz, CDCl$_3$, Me$_4$Si) δ 7.81 (dm, J = 7.9 Hz, 2H, Ar-H), 7.38 (dm, J = 7.9 Hz, 2H, Ar-H), 5.10 (quin, J = 6.9, 6.9 Hz, 1H, CH$_2$-CH=C=CH$_2$), 4.69 (dt, 2H, CH=C=CH_2), 3.27 (br t, J = 6.9 Hz, 2H, N-CH_2), 2.46 (s, 3H, Ar-CH_3), 2.08 (m, 2H, CH_2-CH=C), 1.80 (quin, J = 6.9 Hz, 2H, CH$_2$-CH_2-CH$_2$). ^{13}C NMR (151 MHz, CDCl$_3$, Me$_4$Si) δ 208.7 (Cq), 145.5 (Cq), 130.0 (Cq), 129.8 (2xCH), 129.7 (2xCH), 88.8 (CH), 75.7 (CH$_2$), 56.0 (CH$_2$), 26.3 (CH$_2$), 24.6 (CH$_2$), 21.8 (CH$_3$).

Sodium hexa-4,5-dien-1-yl(tosyl)amide 208a-A
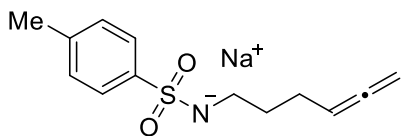
A 10 mL Schlenk tube (with screwing cap) containing a magnetic stirring bar was dried with a heat gun under vacuum then the tube was backfilled with N$_2$. NaH in mineral oil suspension (1.0 eq., 24 mg (40 mg of the suspension), 1.0 mmol), was added under N$_2$ to the flask and subjected to two vacuum/N$_2$ cycles. Anhydrous THF (3 mL/mmol of NaH) was added *via* syringe under N$_2$ atmosphere, then the allene **208** (1.1 eq, 1.1 mmol, 275 mg) was added dropwise at RT to this mixture. The solution was stirred for 2h, then upon

---

[306] Dzandzi, J. P. K.; Beckford Vera, D. R.; Genady, A. R.; Albu, S. A.; Eltringham-Smith, L. J.; Capretta, A.; Sheffield, W. P.; Valliant, J. F. *J. Org. Chem.* **2015,** *80*, 7117-7125.

completion verified by TLC, hexanes were added (5 ml/mmol of NaH) and a white precipitate formed. The precipitate was filtered and washed with hexanes and cold THF (1mL/mmol of NaH) to remove the unreacted amide **208**. 205 mg of white solid were recovered and resulted to be the desired sodium salt **208a-A.** ^{1}H NMR (600 MHz, CDCl$_3$, Me$_4$Si) δ 7.57 (d, J = 7.9 Hz, 2H, Ar-H), 6.99 (d, J = 7.9 Hz, 2H, Ar-H), 4.87 (quin, J = 6.7 Hz, 1H, CH$_2$=C=CH), 4.51 (dt, J = 6.7, 3.2 Hz, 2H) 2H, CH=C=CH_2), 2.64 (t, J = 6.9 Hz, 2H, N-CH_2), 2.31 (s, 3H, Ar-CH_3), 1.79 (m, 2H, CH_2-CH=C), 1.36 (quin, J = 6.9 Hz, 2H, CH$_2$-CH_2-CH$_2$). ^{1}H NMR (600 MHz, DMSO-d_6, Me$_4$Si) δ 7.44 (d, J = 7.9 Hz, 2H, Ar-H), 7.08 (d, J = 7.9 Hz, 2H, Ar-H), 5.09 (quin, J = 6.7, 1H, CH$_2$=C=CH), 4.65 (dt, J = 6.6, 3.3 Hz, 2H, CH=C=CH_2), 2.57 (t, J = 6.9 Hz, 2H, N-CH_2), 2.27 (s, 3H, Ar-CH_3), 1.89 (m, 2H, CH_2-CH=C), 1.33 (quin, J = 6.9, 2H, CH$_2$-CH_2-CH$_2$). ^{13}C NMR (151 MHz, DMSO-d_6, Me$_4$Si) δ 208.3 (Cq), 141.5 (Cq), 129.7 (2 x CH), 127.0 (2 x CH), 90.0 (CH), 79.7 (Cq) 75.9 (CH$_2$), 43.5 (CH$_2$), 30.1 (CH$_2$), 25.5 (CH$_2$), 21.4 (CH$_3$).

6.4.3 General procedure for the synthesis of 2-chlorovinyl saturated nitrogen heterocycles (215)
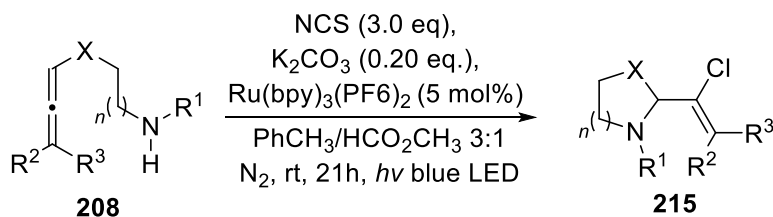

A 10 mL Schlenk tube (with screwing cap) containing a magnetic stirring bar was dried with a heat gun under vacuum then the tube was backfilled with N$_2$. 3 mL of PhCH$_3$ and 1 mL of HCO$_2$CH$_3$ were added *via* syringe and degassed with N$_2$ for 20 minutes, then NCS (3.0 eq., 0.60 mmol, 80 mg), Ru(bpy)$_3$(PF$_6$)$_2$ (0.05 eq., 0.01 mmol, 8 mg) and K$_2$CO$_3$ (0.20 eq., 0.04 mmol, 5 mg) were added in one portion. The resulting mixture was stirred and degassed for 2 minutes and the allene **208** (1.0 eq., 0.20 mmol) was added *via* syringe under N$_2$ and the mixture was stirred and degassed for additional 2 minutes. Finally, the bottle was sealed and placed under irradiation with Kessil A160PR Blue LED (456 nm) light placed at 3 cm distance for 21 h with continuous stirring. The reaction mixture was filtered through a thin pad of silica and eluted with EtOAc. The solvent was evaporated, then the crude was purified with silica gel chromatography.

2-(1-Chlorovinyl)-1-tosylpyrrolidine (215a)
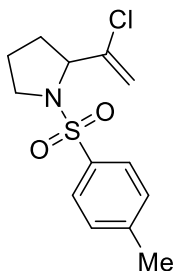
Following the described procedure, allene **208a** (0.2 mmol, 50 mg) was reacted to obtain, 32mg of 2-(1-chlorovinyl)-1-tosylpyrrolidine **215a** as a colorless oil (eluent: EP 92/8 Acetone, yield: 56%). ^{1}H NMR (600 MHz, CDCl$_3$, Me$_4$Si): δ 7.73 (d, J = 8.1 Hz, 2H, Ar-H), 7.32 (d, J = 7.8 Hz, 2H, Ar-H), 5.57 (s, 1H, CCl=CH$_a$H$_b$), 5.33 (s, 1H, CCl=CH$_a$H$_b$), 4.32 (m, 1H, N-CH-CCl), 3.49 (m, 1H, N-CH$_a$H$_b$-CH$_2$), 3.28 (m, 1H, N-CH$_a$H$_b$-CH$_2$), 2.43 (s, 3H, CH_3), 1.97 (m, 1H, N-CH$_2$-(CH_2)$_2$), 1.89 (m, 1H, N-CH$_2$-(CH_2)$_2$), 1.73 (m, 1H, N-CH$_2$-(CH_2)$_2$), 1.66 (m, 1H, N-CH$_2$-(CH_2)$_2$). ^{13}C NMR (151 MHz, CDCl$_3$, Me$_4$Si) δ 143.7 (Cq), 141.8 (Cq), 135.0 (Cq), 129.8 (2xCH), 127.6 (2xCH), 113.7 (CH$_2$), 64.3 (CH), 49.3 (CH$_2$), 31.1 (CH$_2$), 23.9 (CH$_2$), 21.6 (CH$_3$). HRMS (ESI) m/z [M + H]$^+$ Calcd for C$_{13}$H$_{17}$ClNO$_2$S 286.0663, found 286.0664.

8-methyl-10-methylene-2,3,10,10a-tetrahydro-1H-benzo [e]pyrrolo[1,2-b][1,2]thiazine 5,5-dioxide (216a)
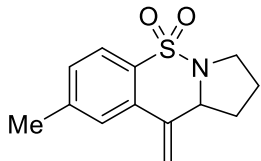
Following the described procedure, allene **208a** (0.2 mmol, 50 mg) was reacted to obtain. Byproduct **216a** was recovered in traces together with impurities (eluent: EP 92/8 Acetone), and preparative TLC (eluent EP 7:1 AcOEt) was necessary for characterization. ^{1}H NMR (600 MHz, CDCl$_3$, Me$_4$Si) δ 7.71 (d, J = 7.8 Hz, 1H, Ar-H), 7.32 (s, J = 1.7, 0.9 Hz, 1H, Ar-H), 7.27 − 7.23 (m, 1H, Ar-H), 5.57 (d, J = 1.3 Hz, 1H, C=CH$_a$H$_b$), 5.22 (d, J = 1.3 Hz, 1H, C=CH$_a$H$_b$), 4.75 (bt, J = 7.2, 1H, C-CH(CH$_2$)-N), 3.53 (m, 1H, N(CH)-CH$_a$H$_b$-CH$_2$), 2.95 (m, 1H, m, 1H, N(CH)-CH$_a$H$_b$-CH$_2$), 2.42 (s, 3H, Ar-CH_3), 2.39 − 2.29 (m, 1H, C-CH(CH_bH$_a$)-N), 1.92 − 1.80 (m, 1H, C-CH(CH$_b$$H_a$)-N), 1.77 − 1.63 (m, 2H, CH$_2$-CH_2-CH$_2$). ^{13}C NMR (151 MHz, CDCl$_3$, Me$_4$Si) δ 143.4 (Cq), 140.8 (Cq), 135.5 (Cq), 132.3 (Cq), 129.2 (CH), 127.5 (CH), 124.6 (CH), 115.2 (CH$_2$), 64.9 (CH), 50.3 (CH$_2$), 35.5 (CH$_2$), 24.2 (CH$_2$), 21.8 (CH$_3$). HRMS (ESI) m/z [M + H]$^+$ Calcd for C$_{13}$H$_{16}$NO$_2$S 250.0896, found 250.0897.

2-(1-Chlorovinyl)-1-tosylpiperidine (215b)
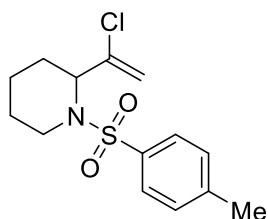
Following the described procedure, allene **208b** (0.2 mmol, 53 mg) was reacted to obtain, 12 mg of 2-(1-chlorovinyl)-1-tosylpiperidine **215b** as a colorless oil (eluent EP 95/5 Acetone, yield: 20%). ^{1}H NMR (600 MHz, CDCl$_3$, Me$_4$Si) δ 7.72 (dm, J = 8.1 Hz, 2H, Ar-H), 7.29 (dm, J = 8.1 Hz, 2H, Ar-H), 5.44 (t, J = 2.0 Hz, 1H, CCl=CH$_a$H$_b$), 5.38 (t, J = 2.0 Hz, 1H, CCl=CH$_a$H$_b$), 4.77 (m, 1H, N-CH-CCl), 3.74 (dm, J = 13.7, 1H, N-CH$_a$H$_b$-CH$_2$), 3.09 (tm, J = 13.7, 1H, 1H, N-CH$_a$H$_b$-CH$_2$), 2.43 (s, 3H, CH_3), 2.22 (m, 1H, N-CH$_2$-(CH_2)$_3$), 1.48 (m, 3H, m, 1H, N-CH$_2$-(CH_2)$_3$), 1.29 (m, 2H, m, 1H, N-CH$_2$-(CH_2)$_3$). ^{13}C NMR (151 MHz, CDCl$_3$) δ 143.3 (Cq), 139.6 (Cq), 138.1 (Cq), 129.7 (2xCH), 127.1 (2xCH), 115.2 (CH$_2$), 57.2 (CH), 41.8 (CH$_2$), 26.6 (CH$_2$), 24.4 (CH$_2$), 21.6 (CH$_3$), 18.8 (CH$_2$). HRMS (ESI) m/z [M+K]$^+$ Calcd for C$_{14}$H$_{19}$ClKNO$_2$S$^+$ 338.0378, found 338.0378.

## 2-(1-Chlorovinyl)-3-tosyloxazolidine (215c)
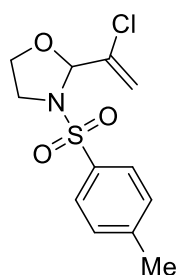
Following the described procedure, allene **208c** (0.2 mmol, 51 mg) was reacted to obtain, 30 mg of 2-(1-chlorovinyl)-3-tosyloxazolidine **215b** as a colorless oil (EP/Acetone 92/8, 52% yield). ^{1}H NMR (600 MHz, CDCl$_3$, Me$_4$Si) δ 7.75 (d, J=8.3 Hz, 2H, Ar-H), 7.33 (d, J = 8.0 Hz, 2H, Ar-H), 5.72 (dm, J = 1.7, 1H, CCl=CH$_a$H$_b$), 5.64 (s, 1H, N-CH-O), 5.49 (d, J = 1.7 Hz, 1H, CCl=CH$_a$H$_b$), 3.97 (m, 1H, N-(CH_2)$_2$-O), 3.58 (m, 2H, N-(CH_2)$_2$-O), 3.50 (m, 1H, N-(CH_2)$_2$-O), 2.43 (s, 3H, CH_3). ^{13}C NMR (151 MHz, CDCl$_3$, Me$_4$Si) δ 144.6 (Cq), 138.5 (Cq), 134.5 (Cq), 130.1 (2xCH), 127.9 (2xCH), 116.7 (CH$_2$), 90.8 (CH), 66.1 (CH$_2$), 46.5 (CH$_2$), 21.7 (CH$_3$).

2-(1-Chloro-2-methylprop-1-en-1-yl)-1-tosylpyrrolidine (215d)
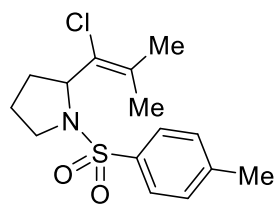
Following the described procedure, allene **208d** (0.2 mmol, 53 mg) was reacted to obtain, 19 mg of 2-(1-chloro-2-methylprop-1-en-1-yl)-1-tosylpyrrolidine **215d** as a colorless oil (EP/Acetone 90/10, 52% yield). ^{1}H NMR (600 MHz, CDCl$_3$, Me$_4$Si) δ 7.66 (dm, J = 8.1 Hz, 2H, Ar-H), 7.25 (dm, J = 8.1 Hz, 2H, Ar-H), 4.93 (m, 1H, N-CH-CCl), 3.62 (m, 1H, N-CH$_a$H$_b$-CH$_2$), 3.38 (m, 1H, N-CH$_a$H$_b$-CH$_2$), 2.40 (s, 3H, Ar-CH_3), 2.01 (m, 2H, N-CH$_2$-(CH_2)$_2$), 1.93 (m, 1H, m, 2H,

N-CH$_2$-(CH$_2$)$_2$), 1.89 (s, 3H, ClC=C(CH$_{3a}$)CH$_{3b}$), 1.73 (s, 3H, ClC=C(CH$_{3b}$)CH$_{3a}$), 1.64 (m, 2H, N-CH$_2$-(CH$_2$)$_2$). ^{13}C NMR (151 MHz, CDCl$_3$, Me$_4$Si) δ 143.1 (Cq), 136.8 (Cq), 131.0 (Cq), 129.3 (2xCH), 128.9 (Cq), 127.3 (2xCH), 59.4 (CH), 49.3 (CH$_2$), 31.4 (CH$_2$), 25.3(CH$_2$), 22.4 (CH$_3$), 21.6 (CH$_3$), 20.6 (CH$_3$).

2-(1-Chlorovinyl)-1-(phenylsulfonyl)pyrrolidine (215e)
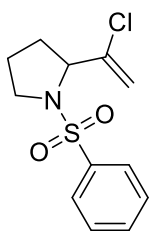
Following the described procedure, allene **208e** (0.2 mmol, 47 mg) was reacted to obtain, 28 mg of 2-(1-chlorovinyl)-1-(phenylsulfonyl)pyrrolidine **215e** as a colorless oil (EP/Acetone 90/10, 52% yield). ^{1}H NMR (600 MHz, CDCl$_3$, Me$_4$Si) δ 7.84 (m, 2H, Ar-H), 7.59 (m, 1H, Ar-H), 7.52 (m, 2H, Ar-H), 5.55 (t, J = 1.5 Hz, 1H, CCl=CH$_a$H$_b$), 5.32 (d, J = 1.5 Hz, 1H, CCl=CH$_a$H$_b$), 4.35 (m, 1H, m, 1H, N-CH-CCl), 3.50 (m, 1H, N-CH$_a$H$_b$-CH$_2$), 3.30 (m, 1H, N-CH$_a$H$_b$-CH$_2$), 1.98 (m, 1H, N-CH$_2$-(CH$_2$)$_2$), 1.89 (m, 1H, N-CH$_2$-(CH$_2$)$_2$), 1.74 (m, 1H, N-CH$_2$-(CH$_2$)$_2$), 1.67 (m, 1H, N-CH$_2$-(CH$_2$)$_2$). ^{13}C NMR (151 MHz, CDCl$_3$, Me$_4$Si) δ 141.7 (Cq), 138.0 (Cq), 132.9 (CH), 129.2 (2xCH), 127.50 (2xCH), 113.9 (CH$_2$), 64.4 (CH), 49.3 (CH$_2$), 31.1 (CH$_2$), 23.9 (CH$_2$).

## 2-(1-Chlorovinyl)-1-(mesitylsulfonyl)pyrrolidine (215f)
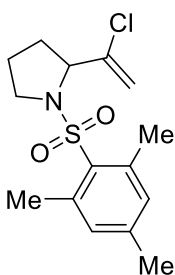
Following the described procedure, allene **208f** (0.2 mmol, 56 mg) was reacted to obtain 32 mg of 2-(1-chlorovinyl)-1-(mesitylsulfonyl)pyrrolidine **215e** as a colorless oil (EP/Acetone 95/5, yield 51%). ^{1}H NMR (600 MHz, CDCl$_3$, Me$_4$Si): δ 6.5 (m, 2H, Ar-H), 5.19 (t, J = 1.6 Hz, 1H, CCl=CH$_a$H$_b$), 4.98 (d, J = 1.6 Hz, 1H, CCl=CH$_a$H$_b$), 4.52 (m, 1H, m, 1H, N-CH-CCl), 3.58 (m, 1H, N-CH$_a$H$_b$-CH$_2$), 3.34 (m, 1H, N-CH$_a$H$_b$-CH$_2$), 2.61 (s, 6H, o-CH$_3$-Ar), 2.27 (s, 3H, p-CH$_3$-Ar), 2.18-2.10 (m, 1H, N-CH$_2$-(CH$_2$)$_2$), 2.09 – 1.94 (m, 2H, N-CH$_2$-(CH$_2$)$_2$), 1.93-1.85 (m, 1H, N-CH$_2$-(CH$_2$)$_2$). ^{13}C NMR (151 MHz, CDCl$_3$, Me$_4$Si) δ 142.7 (Cq), 141.8 (Cq), 140.3 (Cq), 133.2 (Cq), 131.9 (2 x CH), 113.6 (CH$_2$), 63.7 (CH), 48.8 (CH$_2$), 31.9 (CH$_2$), 24.5 (CH$_2$), 23.0 (2 x CH$_3$), 21.1 (CH$_3$).

1-((4-Chlorophenyl)sulfonyl)-2-(1-chlorovinyl)pyrrolidine (215g)
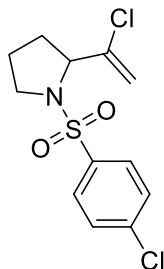
Following the described procedure, allene **208g** (0.2 mmol, 54 mg) was reacted to obtain, after 32 h, 24.5 mg of 1-((4-chlorophenyl)sulfonyl)-2-(1-chlorovinyl)pyrrolidine **215g** as a colorless oil (EP/Acetone 92/8, 40 % yield). ^{1}H NMR (600 MHz, CDCl$_3$, Me$_4$Si): 7.78 (dm, J = 8.1 Hz, 2H, Ar-*H*), 7.50 (dm, J = 8.1 Hz, 2H, Ar-*H*), 5.53 (d, J = 1.7 Hz, 1H, CCl=CH$_a$*H$_b$*), 5.32 (d, J = 1.7 Hz, 1H, CCl=C*H$_a$*H$_b$), 4.37 (m, 1H, m, 1H, N-C*H*-CCl), 3.48 (m, 1H, N-CH$_a$*H$_b$*-CH$_2$), 3.33 (m, 1H, N-C*H$_a$*H$_b$-CH$_2$), 2.05 − 1.98 (m, 1H, N-CH$_2$-(C*H$_2$*)$_2$), 1.98 − 1.88 (m, 1H, N-CH$_2$-(C*H$_2$*)$_2$), 1.86 − 1.77 (m, 1H, N-CH$_2$-(C*H$_2$*)$_2$), 1.77 − 1.69 (m, 1H, N-CH$_2$-(C*H$_2$*)$_2$). ^{13}C NMR (151 MHz, Chloroform-*d*) δ 141.6 (Cq), 139.5 (Cq), 136.9 (Cq), 129.5 (2 x CH), 128.9 (2 x CH), 114.2 (CH), 64.5 (CH), 49.3 (CH$_2$), 31.2 (CH$_2$), 24.0 (CH$_2$).

2-(1-Chloro-2-(4-methoxyphenyl)vinyl)-1-tosylpyrrolidine - (215h)

Following the described procedure, allene **208h** (0.2 mmol, 71 mg) was reacted to obtain, 40 mg 2-(1-chloro-2-(4-methoxyphenyl)vinyl)-1-tosylpyrrolidine **215h** as a colorless oil (EP/Acetone 90/10, 51% yield). Only one isomer was recovered. ^{1}H NMR (600 MHz, CDCl$_3$, Me$_4$Si) δ 7.80 (dm, J = 8.1 Hz, 2H, Ar^1-*H*), 7.56 (dm, J = 8.7 Hz, 2H, Ar^2-*H*)), 7.36 (dm, J = 8.1 Hz, 2H, Ar^1-*H*), 6.88 (dm, J = 8.7 Hz, 2H, Ar^2-*H*), 5.89 (s, 1H, CCl=C*H*-Ar^2), 4.74 (m, 1H, N-C*H*-CCl), 3.86 (m, 1H, N-CH$_a$*H$_b$*-CH$_2$) 3.82 (s, 3H, O-C*H$_3$*), 3.55 (m, 1H, N-C*H$_a$*H$_b$-CH$_2$), 2.45 (s, 3H, C*H$_3$*), 2.33 (m, 1H, N-CH$_2$-(C*H$_2$*)$_2$), 1.92 (m, 1H, N-CH$_2$-(C*H$_2$*)$_2$), 1.78 (m, 1H, N-CH$_2$-(C*H$_2$*)$_2$), 1.10 (m, 1H, N-CH$_2$-(C*H$_2$*)$_2$). ^{13}C NMR (151 MHz, CDCl$_3$, Me$_4$Si) δ 160.1 (Cq), 144.4 (Cq), 135.3 (Cq), 131.6 (2xCH), 130.2 (2xCH), 128.9 (Cq), 127.7 (2xCH), 113.2 (2xCH), 99.7 (Cq), 67.0 (CH), 66.7 (CH), 55.4 (CH$_3$), 52.3 (CH$_2$), 30.1 (CH$_2$), 24.8 (CH$_2$), 21.7 (CH$_3$).
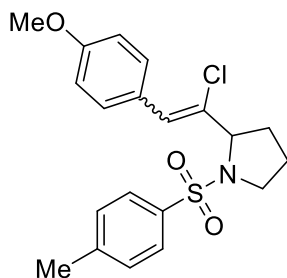
2-(1-Chlorohept-1-en-1-yl)-1-tosylpyrrolidine (215j)
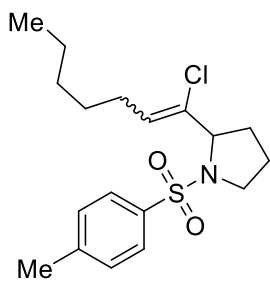
Following the described procedure, allene **208j** (0.2 mmol, 64 mg) was reacted to obtain 34 mg of 2-(1-chlorohept-1-en-1-yl)-1-tosylpyrrolidine **215j** as a colorless oil (EP/Acetone 90/10, yield 48%). Mixture of *E/Z* isomers, isomer A/B ratio 1:3.85. ^{1}H NMR (600 MHz, CDCl$_3$, Me$_4$Si) δ 7.70 (d, *J* = 8.2 Hz, 2H, Ar-*H* isomer A), 7.69 (d, *J* = 8.2 Hz, 2H, Ar-*H* isomer B), 7.27 (d, *J* = 8.2 Hz, 2H, Ar-*H* isomer B), 7.28 (d, *J* = 8.2 Hz, 2H, Ar-*H* isomer A), 5.82 (t, *J* = 7.8 Hz, 1H, CCl=C*H* isomer B), 5.63 (t, *J* = 7.8 Hz, 1H, CCl=C*H* isomer A), 4.81 (dd, *J* = 8.2, 3.5 Hz, 1 H, N-C*H*-CCl, isomer A), 4.35 (dd, *J* = 8.2, 3.5 Hz, 1 H, N-C*H*-CCl, isomer B), 3.60-3.53 (m, 1H, N-CH$_a$*H$_b$*-CH$_2$, isomer A), 3.47-3.40 (m, 1H, N-CH$_a$*H$_b$*-CH$_2$, isomer B), 3.39-3.31 (m, 1H, N-C*H$_a$*H$_b$-CH$_2$), 2.41 (s, 3H, Ar-C*H$_3$*), 2.26-2.10 (m, 2H, - C*H$_2$*-C*H*= isomer A), 2.12 (q, *J* = 7.3 Hz, 2H, C*H$_2$*-C*H*= isomer B), 2.04-1.84 (m, 3H, m, 1H, N-CH$_2$-(C*H$_2$*)$_2$), 1.80-1.71 (m, 2H, m, 1H, N-CH$_2$-(C*H$_2$*)$_2$), 1-70-1.61 (m, 2H, m, 1H, N-CH$_2$-(C*H$_2$*)$_2$), 1.51-1.22 (m, 6H, CH$_3$-C*H$_2$*-CH$_2$, CH$_2$-(C*H$_2$*)$_2$-CH$_2$ isomer A), 1.36 (quin, 2H, *J* = 7.3 Hz, CH$_3$-C*H$_2$*-CH$_2$ isomer B), 1.33-1.23 (m, 4H, CH$_2$-(C*H$_2$*)$_2$-CH$_2$ isomer B), 0.89 (t, *J* = 7.0 Hz, 3H, CH$_2$-C*H$_3$*), 0.88 (t, *J* = 7.0 Hz, 3H, CH$_2$-C*H$_3$*). ^{13}C NMR (151 MHz, CDCl$_3$, Me$_4$Si): *Isomer A* δ 143.3 (Cq), 136.4 (Cq), 134.0 (Cq), 131.1 (CH), 129.5 (2 x CH), 127.4 (2 x CH), 58.2 (CH), 49.4 (CH$_2$), 31.6 (CH$_2$), 31.5 (CH$_2$), 29.1 (CH$_2$), 28.5 (CH$_2$), 25.3 (CH$_2$), 24.1 (CH$_2$), 21.6 (CH$_3$), 14.1 (CH$_3$); *Isomer B* δ 143.4 (Cq), 135.7 (Cq), 133.7 (Cq), 129.6 (2 x CH), 127.9 (CH), 127.5 (2 x CH), 64.7 (CH), 49.2 (CH$_2$), 31.5 (CH$_2$), 31.3 (CH$_2$), 28.3 (CH$_2$), 28.1 (CH$_2$), 24.1 (CH$_2$), 22.5 (CH$_2$), 21.6 (CH$_2$), 14.1 (CH$_3$).
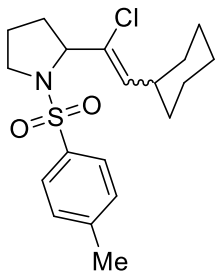
2-(1-Chloro-2-cyclohexylvinyl)-1-tosylpyrrolidine (215k)

Following the described procedure, allene **208k** (0.2 mmol, 65 mg) was reacted to obtain, 34 mg of 2-(1-chloro-2-cyclohexylvinyl)-1-tosylpyrrolidine **215k** as a colorless oil (EP/Acetone 90/10, yield 44%). Mixture of *E/Z* isomers, isomer A/B ratio 1:4.65. ^{1}H NMR (600 MHz, CDCl$_3$, Me$_4$Si) δ 7.70 (d, *J* = 8.2 Hz, 2H, Ar-*H* isomer A), 7.69 (d, *J* = 8.2 Hz, 2H, Ar-*H* isomer B), 7.28 (d, *J* = 8.2 Hz, 2H, Ar-*H* isomer B), 7.28 (d, *J* = 8.2 Hz, 2H, Ar-*H* isomer A), 5.63 (d, *J* = 8.8 Hz, 1H, CCl=C*H* isomer B), 5.49 (d, *J* = 8.8 Hz, 1H, CCl=C*H* isomer A), 4.80 (dd, *J* = 8.2, 3.5 Hz, 1 H, N-C*H*-CCl, isomer A),

4.33 (dd, J = 8.2, 3.5 Hz, 1 H, N-CH-CCl, *isomer B*), 3.62-3.52 (m, 1H, N-CH$_a$H$_b$-CH$_2$, *isomer A*), 3.47-3.41 (m, 1H, N-CH$_a$H$_b$-CH$_2$, *isomer B*), 3.41-3.32 (m, 1H, N-CH$_a$H$_b$-CH$_2$), 2.43 (s, 3H, Ar-CH_3 *isomer A*), 2.41 (s, 3H, Ar-CH_3 *isomer B*), 2.41-2.31 (m, 1H, -CH-CH=CCl), 2.06-1.83 (m, 1H, m, 1H, N-CH$_2$-(CH_2)$_2$), 1.81-1.72 (m, 2H, m, 1H, N-CH$_2$-(CH_2)$_2$), 1.71-1.59 (m, 5H, N-CH$_2$-(CH_2)$_2$, (CH$_2$)$_2$-CH_2-(CH$_2$)$_2$, cyclohexyl CH_2) 1.37-1.12 (m, 4H, cyclohexyl CH_2), 1.12-0.98 (m, 2H, CCl-C=CH-C(CH$_2$)H_2).

^{13}C NMR (151 MHz, CDCl$_3$, Me$_4$Si) *Isomer A:* δ 143.3 (Cq), 136.5 (CH), 136.4 (Cq), 135.8 (Cq), 129.6 (2 x CH), 127.4 (2 x CH), 58.5 (CH), 49.5 (CH$_2$), 38.1 (CH), 33.6 (CH$_2$), 32.7 (CH$_2$), 32.7 (CH$_2$), 25.9 (CH$_2$), 25.8 (2xCH$_2$), 25.3 (CH$_2$), 21.7 (CH$_3$). *Isomer B:* δ 143.4 (Cq), 135.8 (Cq), 133.0 (CH), 132.0 (Cq), 129.6 (2 x CH), 127.5 (2 x CH), 64.7 (CH), 49.3 (CH$_2$), 37.5 (CH), 31.9 (CH$_2$), 31.9 (CH$_2$), 31.3 (CH$_2$), 26.1 (CH$_2$), 25.7 (CH$_2$), 24.1 (CH$_2$), 21.7 (CH$_3$).

6.4.4 General procedure for the synthesis of 2-(1-halovinyl)-1-tosylpyrrolidines (220-X) under thermal conditions
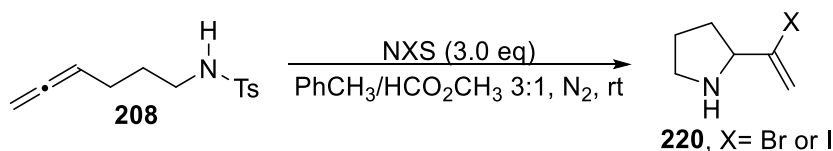
A 10 mL Schlenk tube (with screwing cap) containing a magnetic stirring bar was dried with a heat gun under vacuum then the tube was backfilled with N$_2$. 3 mL of PhCH$_3$ and 1 mL of HCO$_2$CH$_3$ were added *via* syringe and degassed with N$_2$ for 20 minutes, then the appropriate halosuccinimide NXS (3.0 eq., 0.60 mmol) was added. The resulting mixture was stirred and degassed for 2 minutes and the allene **208** (1.0 eq., 0.20 mmol, 50 mg) was added *via* syringe under N$_2$ and the mixture was stirred and degassed for additional 2 minutes. Finally, the bottle was sealed, and the solution kept under vigorous stirring until reaction completion as monitored by TLC. The reaction mixture was filtered through a thin pad of silica and eluted with EtOAc. The solvent was evaporated, then the crude was purified with silica gel chromatography (Eluent/Acetone 9:1).

2-(1-Bromovinyl)-1-tosylpyrrolidine (220-Br)
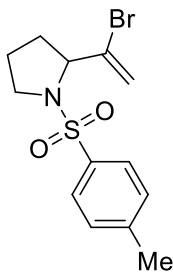
Following the described procedure, allene **208a** was reacted with NBS (3.0 eq, 0.60 mmol, 107 mg) to obtain, after purification, 42 mg of **200-Br** as a colorless solid in 58% yield. Spectral data match previous report.[300] ^{1}H NMR (600 MHz, CDCl$_3$, Me$_4$Si): δ 7.72 (d, J = 8.3 Hz, 2H, Ar-H), 7.31 (d, J = 8.3 Hz, 1H, Ar-H), 5.99 (dd, J = 2.0, 1.2 Hz, CBr=CH$_a$H$_b$), 5.56 (dd, J = 2.0, 0.7 Hz, 1H, CBr=CH_aH$_b$), 4.35 (dd, 1H, J = 8.3, 3.5 Hz, N-CH-CBr), 3.49 (m, 1H, N-CH$_a$H$_b$-CH$_2$), 3.28 (m, 1H, N-CH$_a$H$_b$-CH$_2$), 2.42 (s, 3H, CH_3), 1.99 (m, 2H, N-CH$_2$-(CH_2)$_2$), 1.72 (m, 1H, N-CH$_2$-(CH_2)$_2$), 1.64 (m, 1H, N-CH$_2$-(CH_2)$_2$).

2-(1-Iodovinyl)-1-tosylpyrrolidine (220-I)
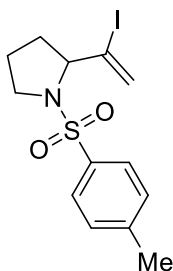
Following the described procedure, allene **208a** was reacted with NIS (3.0 eq, 0.60 mmol, 137 mg) to obtain, after purification 50 mg of **220-I** as a colorless solid in 66% yield. Spectral data match previous report.[307] ^{1}H NMR (600 MHz, CDCl$_3$, Me$_4$Si): δ 7.72 (d, J = 8.3 Hz, 2H, Ar-H), 7.31 (d, J = 8.3 Hz, 1H, Ar-H), 6.43 (dd, J = 1.9, 1.3 Hz, CI=CH$_a$H$_b$), 5.83 (dd, J = 2.0, 0.7 Hz, 1H, CI=CH_aH$_b$), 4.16 (dd, 1H, J = 8.3, 3.8 Hz, N-CH-CBr), 3.48 (m, 1H, N-CH$_a$H$_b$-CH$_2$), 3.31 (m, 1H, N-CH$_a$H$_b$-CH$_2$), 2.42 (s, 3H, CH_3), 1.89 (m, 2H, N-CH$_2$-(CH_2)$_2$), 1.74 (m, 1H, N-CH$_2$-(CH_2)$_2$), 1.62 (m, 1H, N-CH$_2$-(CH_2)$_2$).

---

[307] Shaw, R. W.; Gallagher, T. *J. Chem. Soc., Perkin Trans. 1* **1994**, 3549-3555.

CONCLUSIONS

In this Ph.D. thesis the results concerning the intramolecular cyclization of β-hindered-γ,δ-unsaturated-N-arylsulfonylhydrazones and the chlorocyclization of N-(allenyl)sulfonyllamides under blue light irradiation have been reported. In Chapter 3 and 4, the use of the same photoredox catalytic system allowed three different classes of tetrahydropyridazines from the same kind of γ,δ-unsaturated-N-arylsulfonylhydrazones to be achieved. Contrarily to the classical paradigm of an uncontrollable reactivity of radical species, the outcome of these radical transformations could be directed. Indeed, the mild conditions required by photoredox catalysis ensured reliable predictions of the evolution of the key radical intermediate involved, and the features of these radical species could be directly affected by convenient modifications of the starting material.

In chapter 5, the fundamental role of light provided both the generation of the nitrogen centered radical species and the availability of the halogen partner. A chloro-cyclization process was disclosed affording a chloro-vinyl saturated nitrogen heterocycle. Functionalization with chlorine atom of the obtained heterocycle was unachievable in thermal conditions but visible light revealed a new non-thermal pathway that expanded the possibility of chlorination reactions.

Despite the first examples being reported since early 20th century, the continuous efforts of researchers in the field of cyclizations promoted by nitrogen centered radical are persisting nowadays. This interest can be attributed also to photocatalysis and to the recent development of photoredox chemistry, which has helped and enhanced the understanding of the chemistry of the nitrogen centered radicals. The implementation of photocatalysis in industrial processes and technology advances in radical generation are maintaining this interest, therefore countless opportunities for new developments of this "classical" chemical transformation remain available.

APPENDIX I: Abbreviations and acronyms

A = acceptor

Acr = acridinium

Aq = aqueous

AIBN = azobisisobutyronitrile

Ar = aryl

BET = back electron transfer

Boc = tert-butoxycarbonyl

bpy = 2,2'-bipyridyl

bpz = 2,2'-bipyrazyl

BTCC = triphosgene or bis(trichloromethyl) carbonate

CHD = 1,4-cyclohexadiene

CI = conical intersection

CV = cyclic voltammetry

D = donor

DCDMH = 1,3-Dichloro-5,5-dimethylhydantoin

DCE = 1,2-dichloroethane

DFT = density functional theory

DMF = dimethylformamide

DMPU = N,N-Dimethylpropyleneurea

DMSO = dimethylsulfoxide

dtbbpy = di-*tert*-butylpyridyl

ΔG = Gibbs free energy

EDA = Electron donor-acceptor

EDG = Electron donating group

EWG = Electron withdrawing group

EnT = energy transfer

eq. = equivalents

Et = ethyl

HAS = homolytic aromatic substitution

HAT = hydrogen atom transfer

      d-HAT = direct hydrogen atom transfer

      i-HAT = indirect hydrogen atom transfer

HetAr = heteroaryl

HIV = human immunodeficiency virus

HLF = Hoffman-Loffler-Freytag

HOMO = highest occupied molecular orbital
IC = interconversion
ISC = intersystem crossing
i-Pr = *iso*-propyl
L = ligand
LED = light emitting diode
LUMO = lowest occupied molecular orbital
Mes = 2-mesityl or 2,4,6-trimethylphenyl
MLCT = metal to ligand charge transfer
NCR = nitrogen centered radical
NCS = *N*-chlorosuccinimide
NBS = *N*-bromosuccinimide
NMR = nuclear magnetic resonance
NIS = *N*-iodosuccinimide
NXS = *N*-halosuccinimide
ODET = oxidative deprotonation electron transfer
ORTEP = Oak Ridge thermal ellipsoid plot
PC = photoredox catalyst
PCET = proton coupled electron transfer
PET = photoinduced electron transfer
PVC = polyvinylchloride
RAE = redox active ester
RT = room temperature
SET = single electron transfer
$S_{n1}(v=n_2)$ = electronic singlet state of level n_1 associated with the vibration level n_2
SCRIP = singlet contact radical ion pair
SCE = standard calomel electrode
SNAr = nucleophilic aromatic substitution
SOMO = singlet occupied molecular orbital
t-Bu = *tert*-butyl
TCAA = trichloroisocyanuric acid
TCRIP = triplet contact radical ion pair
TEMPO = (2,2,6,6-Tetramethylpiperidin-1-yl)oxyl radical
TFA = trifluoroacetic acid
THF = tetrahydrofuran

$T_{n1}(v=n_2)$ = electronic triplet state of level n_1 associated with the vibration level n_2

tol = tolyl

Ts = tosyl

UV = ultraviolet

VR = vibrational relaxation

XAT = halogen atom transfer

BIBLIOGRAPHY

1. Wardle, B., *Principles and Applications of Photochemistry*. John Wiley & Sons: Manchester **2009**.
2. McNaught, M.; Wilkinson, A., *IUPAC. Compendium of Chemical Terminology ("Gold Book")*. Blackwell Scientific Publications: Oxford **1997**.
3. Braslavsky, S. E. *Pure Appl. Chem.* **2007,** *79*, 293-465.
4. Cox, A.; Kemp, T. J., *Introductory Photochemistry*. McGraw-Hill: London **1971**.
5. Wayne, C. E.; Wayne, R. P., *Photochemistry*. Oxford University Press: **2005**.
6. Jablonski, A. *Nature* **1933,** *131*, 839-840.
7. Zimmermann, J.; Zeug, A.; Röder, B. *Phys. Chem. Chem. Phys.* **2003,** *5*, 2964-2969.
8. Kasha, M. *Chem. Rev.* **1947,** *41*, 401-419.
9. Kasha, M. *Discuss. Faraday Soc.* **1950,** *9*, 14-19.
10. Kasha, M. *J. Chem. Educ.* **1984,** *61*, 204.
11. Braslavsky, S. E. *Pure Appl. Chem.* **2007,** *79*, 293-465.
12. Valeur, B., *Molecular Fluorescence: Principles and Applications*. Wiley-VCH Verlag GmbH: Weinheim **2001**.
13. Wilkinson, F. *J. Phys. Chem* **1962,** *66*, 2569-2574.
14. Arnaut, L.; Formosinho, S.; Burrows, H., *Chemical Kinetics. From Molecular Structure to Chemical Reactivity*. Elsevier: Amsterdam **2007**.
15. Főrster, T. *Discuss. Faraday Soc.* **1959,** *27*, 7-17.
16. Sahoo, H. *J. Photochem. Photobiol. C: Photochem. Rev.* **2011,** *12*, 20-30.
17. Dexter, D. L. *J. Chem. Phys.* **1953,** *21*, 836-850.
18. Scandola, F.; Indelli, M. T.; Chiorboli, C.; Bignozzi, C. A., *Photoinduced electron and energy transfer in polynuclear complexes*. Springer Berlin **1990**.
19. Marcus, R. A. *Angew. Chem. Int. Ed.* **1993,** *32*, 1111-1121.
20. Robb, M. A.; Bernardi, F.; Olivucci, M. *Pure Appl. Chem.* **1995,** *67*, 783-789.
21. Martinez, T. J. *Nature* **2010,** *467*, 412-413.
22. Polli, D.; Altoè, P.; Weingart, O.; Spillane, K. M.; Manzoni, C.; Brida, D.; Tomasello, G.; Orlandi, G.; Kukura, P.; Mathies, R. A.; Garavelli, M.; Cerullo, G. *Nature* **2010,** *467*, 440-443.
23. Albini, A.; Fagnoni, M., *Photochemically-Generated Intermediates in Synthesis*. John Wiley & Sons: Hoboken, New Jersey **2013**.
24. Noyori, R. *Tetrahedron* **2010,** *66*, 1028.
25. Ciamician, G. *Science* **1912,** *36*, 385-394.
26. Benrath, A. *Z. Phys. Chem.* **1910,** *74U*, 115-124.
27. Ravelli, D.; Protti, S.; Albini, A. *Molecules* **2015,** *20*, 1527-1542.
28. Ravelli, D.; Protti, S.; Fagnoni, M. *Chem. Rev.* **2016,** *116*, 9850-9913.
29. Segura, J. L.; Martín, N. *Chem. Rev.* **1999,** *99*, 3199-3246.
30. Toteva, M. M.; Richard, J. P. *Adv. Phys. Org. Chem.* **2011,** *45*, 39-91.
31. Curran, D. P. *Synthesis* **1988,** *1988*, 417-439.
32. O'Mahony, G. *Synlett* **2004,** *2004*, 572-573.
33. Cottrell, T. L., *The Strengths of Chemical Bonds*. Butterworth: London **1958**.
34. Kerr, J. A. *Chem. Rev.* **1966**, 465-500.
35. Benson, S. W. *J. Chem. Ed.* **1965,** *42*, 502-518.
36. Takeda, H.; Ishitani, O. *Coord. Chem. Rev.* **2010,** *254*, 346-354.
37. Lowry, M. S.; Bernhard, S. *Chem. Eur. J.* **2006,** *12*, 7970-7977.
38. Graetzel, M. *Acc. Chem Res.* **1981,** *14*, 376-384.
39. Kalyanasundaram, K.; Grätzel, M. *Coord. Chem. Rev.* **1998,** *177*, 347-414.
40. Van Bergen, T. J.; Hedstrand, D. M.; Kruizinga, W. H.; Kellogg, R. M. *J. Org. Chem.* **1979,** *44*, 4953-4962.
41. Pac, C.; Ihama, M.; Yasuda, M.; Miyauchi, Y.; Sakurai, H. *J. Am. Chem. Soc.* **1981,** *103*, 6495-6497.
42. Cano-Yelo, H.; Deronzier, A. *Tetrahedron Lett.* **1984,** *25*, 5517-5520. Cano-Yelo, H.; Deronzier, A. *J. Photochem.* **1987,** *37*, 315-321.
43. Fukuzumi, S.; Koumitsu, S.; Hironaka, K.; Tanaka, T. *J. Am. Chem. Soc.* **1987,** *109*, 305-316.
44. Okada, K.; Okamoto, K.; Morita, N.; Okubo, K.; Oda, M. *J. Am. Chem. Soc.* **1991,** *113*, 9401-9402.

45.   Nicewicz, D. A.; MacMillan, D. W. C. *Science* **2008,** *322*, 75-80.
46.   Ischay, M. A.; Anzovino, M. E.; Du, J.; Yoon, T. P. *J. Am. Chem. Soc.* **2008,** *130*, 12886-12887.
47.   Narayanam, J. M. R.; Tucker, J. W.; Stephenson, C. R. J. *J. Am. Chem. Soc.* **2009,** *131*, 8756-8757.
48.   Romero, N. A.; Nicewicz, D. A. *Chem. Rev.* **2016,** *116*, 10075-10166.
49.   Kozlowski, M.; Yoon, T. P. *J. Org. Chem.* **2016,** *81*, 6895-6897.
50.   Photoinduced Electron Transfer (PET) and Single Electron Transfer (SET) may appear as interchangeable along the dissertation. However, the use of PET will be related only to those ET involving the excited state of a molecule, with a direct interaction of the excited state of a PC. SET, as a more general definition indicating all kind of electron transfers, will be used to indicate a general redox event with the transfer of a single electron.
51.   Stephenson, C. R. J.; Yoon, T. P.; Macmillan, D. W. C., *Visible light photocatalysis in organic chemistry*. Wiley-VCH Verlag GmbH: Weinheim **2018**.
52.   Arias-Rotondo, D. M.; McCusker, J. K. *Chem. Soc. Rev.* **2016,** *45*, 5803-5820.
53.   Zeitler, K. *Angew. Chem. Int. Ed.* **2009,** *48*, 9785-9789.
54.   Crespi, S.; Jäger, S.; König, B.; Fagnoni, M. *Eur. J. Org. Chem.* **2017,** *2017*, 2147-2153.
55.   Maity, S.; Zhu, M.; Shinabery, R. S.; Zheng, N. *Angew. Chem. Int. Ed.* **2012,** *51*, 222-226.
56.   Demas, J. N.; Harris, E. W.; McBride, R. P. *J. Am. Chem. Soc.* **1977,** *99*, 3547-3551.
57.   Brunschwig, B.; Sutin, N. *J. Am. Chem. Soc.* **1978,** *100*, 7568-7577.
58.   McCusker, J. K. *Acc. Chem Res.* **2003,** *36*, 876-887.
59.   Campagna, S.; Puntoriero, F.; Nastasi, F.; Bergamini, G.; Balzani, V., *Photochemistry and Photophysics of Coordination Compounds I*. Springer: Berlin **2007**.
60.   Teegardin, K.; Day, J. I.; Chan, J.; Weaver, J. *Org. Process Res. Dev.* **2016,** *20*, 1156-1163.
61.   Larsen, C. B.; Wenger, O. S. *Chem. Eur. J.* **2018,** *24*, 2039-2058.
62.   Hockin, B. M.; Li, C.; Robertson, N.; Zysman-Colman, E. *Catal. Sci. Technol.* **2019,** *9*, 889-915.
63.   Glaser, F.; Wenger, O. S. *Coord. Chem. Rev.* **2020,** *405*, 213129.
64.   Nicewicz, D. A.; Nguyen, T. M. *ACS Catal.* **2014,** *4*, 355-360.
65.   Fukuzumi, S.; Ohkubo, K. *Org. Biomol. Chem.* **2014,** *12*, 6059-6071.
66.   Hari, D. P.; König, B. *Chem. Commun.* **2014,** *50*, 6688-6699.
67.   Majek, M.; Filace, F.; Wangelin, A. J. v. *Beilstein J. Org. Chem.* **2014,** *10*, 981-989.
68.   Albini, A. *Synthesis* **1981,** *1981*, 249-264.
69.   Zhao, J.; Wu, W.; Sun, J.; Guo, S. *Chem. Soc. Rev.* **2013,** *42*, 5323-5351.
70.   Ni, T.; Caldwell, R. A.; Melton, L. A. *J. Am. Chem. Soc.* **1989,** *111*, 457-464.
71.   Arceo, E.; Montroni, E.; Melchiorre, P. *Angew. Chem. Int. Ed.* **2014,** *53*, 12064-12068.
72.   Alonso, R.; Bach, T. *Angew. Chem. Int. Ed.* **2014,** *53*, 4368-4371.
73.   Metternich, J. B.; Gilmour, R. *J. Am. Chem. Soc.* **2015,** *137*, 11254-11257.
74.   Yasunao, K.; Tatsuo, A.; Hirochika, S.; Katsumi, T. *Chem. Lett.* **1988,** *17*, 1193-1196.
75.   Akaba, R.; Ohshima, K.; Kawai, Y.; Obuchi, Y.; Negishi, A.; Sakuragi, H.; Tokumaru, K. *Tetrahedron Lett.* **1991,** *32*, 109-112.
76.   Lin, S.; Ischay, M. A.; Fry, C. G.; Yoon, T. P. *J. Am. Chem. Soc.* **2011,** *133*, 19350-19353.
77.   Hamilton, D. S.; Nicewicz, D. A. *J. Am. Chem. Soc.* **2012,** *134*, 18577-18580.
78.   Mukherjee, S.; Yang, J. W.; Hoffmann, S.; List, B. *Chem. Rev.* **2007,** *107*, 5471-5569.
79.   Terrett, J. A.; Clift, M. D.; MacMillan, D. W. C. *J. Am. Chem. Soc.* **2014,** *136*, 6858-6861.
80.   Narayanam, J. M. R.; Stephenson, C. R. J. *Chem. Soc. Rev.* **2011,** *40*, 102-113.
81.   Xuan, J.; Xiao, W.-J. *Angew. Chem. Int. Ed.* **2012,** *51*, 6828-6838.
82.   Prier, C. K.; Rankic, D. A.; MacMillan, D. W. C. *Chem. Rev.* **2013,** *113*, 5322-5363.
83.   Skubi, K. L.; Blum, T. R.; Yoon, T. P. *Chem. Rev.* **2016,** *116*, 10035-10074.
84.   Shaw, M. H.; Twilton, J.; MacMillan, D. W. C. *J. Org. Chem.* **2016,** *81*, 6898-6926.
85.   Ravelli, D.; Fagnoni, M.; Albini, A. *Chem. Soc. Rev.* **2013,** *42*, 97-113.
86.   Twilton, J.; Le, C.; Zhang, P.; Shaw, M. H.; Evans, R. W.; MacMillan, D. W. C. *Nat. Rev. Chem.* **2017,** *1*, 0052 (0051-0018).
87.   *Photochemistry in Organic Synthesis [Special Issue]. Chem. Rev.,* American Chemical Society: **2016,** *116,* 17
88.   *Photoredox Catalysis in Organic Chemistry [Special Issue]. Acc. Chem. Res.,* American Chemical Society: **2016,** *49,* 7-10
89.   *Photochemical Catalytic Processes [Special Issue]. Chem. Rev.,* American Chemical Society: **2022,** *122,* 2
90.   Douglas, J. J.; Sevrin, M. J.; Stephenson, C. R. J. *Org. Process Res. Dev.* **2016,** *20*, 1134-1147.
91.   Marzo, L.; Pagire, S. K.; Reiser, O.; König, B. *Angew. Chem. Int. Ed.* **2018,** *57*, 10034-10072.

92. Petzold, D.; Giedyk, M.; Chatterjee, A.; König, B. *Eur. J. Org. Chem.* **2020,** *2020*, 1193-1244.
93. Pitre, S. P.; Overman, L. E. *Chem. Rev.* **2022,** *122*, 1717-1751.
94. Choi, G. J.; Knowles, R. R. *J. Am. Chem. Soc.* **2015,** *137*, 9226-9229.
95. Murarka, S. *Adv. Synth. Catal.* **2018,** *360*, 1735-1753.
96. Capaldo, L.; Ravelli, D.; Fagnoni, M. *Chem. Rev.* **2022,** *122*, 1875-1924.
97. Chu, L.; Ohta, C.; Zuo, Z.; MacMillan, D. W. C. *J. Am. Chem. Soc.* **2014,** *136*, 10886-10889.
98. Nguyen, J. D.; D'Amato, E. M.; Narayanam, J. M. R.; Stephenson, C. R. J. *Nat. Chem.* **2012,** *4*, 854-859.
99. Tarantino, K. T.; Liu, P.; Knowles, R. R. *J. Am. Chem. Soc.* **2013,** *135*, 10022-10025.
100. Prier, C. K.; MacMillan, D. W. C. *Chem. Sci.* **2014,** *5*, 4173-4178.
101. Chen, N.; Xu, H.-C. *Green Synth. Catal.* **2021,** *2*, 165-178.
102. Xiong, P.; Xu, H.-C. *Acc. Chem Res.* **2019,** *52*, 3339-3350.
103. Togo, H.; Harada, Y.; Yokoyama, M. *J. Org. Chem.* **2000,** *65*, 926-929. Togo, H.; Hoshina, Y.; Muraki, T.; Nakayama, H.; Yokoyama, M. *J. Org. Chem.* **1998,** *63*, 5193-5200.
104. Barton, D. H. R.; Beckwith, A. L. J.; Goosen, A. *J. Chem. Soc. (Resumed)* **1965**, 181-190.
105. Forrester, A. R.; Gill, M.; Sadd, J. S.; Thomson, R. H. *J. Chem. Soc., Chem. Commun.* **1975**, 291-292.
106. Callier-Dublanchet, A.-C.; Quiclet-Sire, B.; Zard, S. Z. *Tetrahedron Lett.* **1995,** *36*, 8791-8794. Boivin, J.; Callier-Dublanchet, A.-C.; Quiclet-Sire, B.; Schiano, A.-M.; Zard, S. Z. *Tetrahedron* **1995,** *51*, 6517-6528. Boivin, J.; Fouquet, E.; Schiano, A.-M.; Zard, S. Z. *Tetrahedron* **1994,** *50*, 1769-1776.
107. Neale, R. S. *Synthesis* **1971,** *1971*, 1-15.
108. Kärkäs, M. D. *ACS Catal.* **2017,** *7*, 4999-5022.
109. Gentry, E. C.; Knowles, R. R. *Acc. Chem Res.* **2016,** *49*, 1546-1556. Murray, P. R. D.; Cox, J. H.; Chiappini, N. D.; Roos, C. B.; McLoughlin, E. A.; Hejna, B. G.; Nguyen, S. T.; Ripberger, H. H.; Ganley, J. M.; Tsui, E.; Shin, N. Y.; Koronkiewicz, B.; Qiu, G.; Knowles, R. R. *Chem. Rev.* **2022,** *122*, 2017-2291.
110. Davies, J.; Morcillo, S. P.; Douglas, J. J.; Leonori, D. *Chem. Eur. J.* **2018,** *24*, 12154-12163.
111. Héberger, K.; Lopata, A. *J. Org. Chem.* **1998,** *63*, 8646-8653.
112. De Vleeschouwer, F.; Van Speybroeck, V.; Waroquier, M.; Geerlings, P.; De Proft, F. *Org. Lett.* **2007,** *9*, 2721-2724.
113. Stella, L., *Nitrogen-Centered Radicals.* **2001**.
114. Duan, X. Y.; Zhou, N. N.; Fang, R.; Yang, X. L.; Yu, W.; Han, B. *Angew. Chem. Int. Ed.* **2014,** *53*, 3158-3162.
115. Laird, E. R.; Jorgensen, W. L. *J. Org. Chem.* **1990,** *55*, 9-27.
116. Parsaee, F.; Senarathna, M. C.; Kannangara, P. B.; Alexander, S. N.; Arche, P. D. E.; Welin, E. R. *Nat. Rev. Chem.* **2021,** *5*, 486-499.
117. Boivin, J.; Fouquet, E.; Zard, S. Z. *J. Am. Chem. Soc.* **1991,** *113*, 1055-1057.
118. Minisci, F.; Galli, R. *Tetrahedron Lett.* **1966,** *7*, 2531-2533.
119. Beckwith, A. L. J.; Schiesser, C. H. *Tetrahedron* **1985,** *41*, 3925-3941.
120. Bowman, W. R.; Storey, J. M. D. *Chem. Soc. Rev.* **2007,** *36*, 1803-1822. Augood, D. R.; Hey, D. H.; Nechvatal, A.; Williams, G. H. *Nature* **1951,** *167*, 725-725.
121. Cheng, Y.-Z.; Feng, Z.; Zhang, X.; You, S.-L. *Chem. Soc. Rev.* **2022**.
122. Han, Y.; Jin, Y.; Jiang, M.; Yang, H.; Fu, H. *Org. Lett.* **2019,** *21*, 1799-1803.
123. Wu, L.; Hao, Y.; Liu, Y.; Song, H.; Wang, Q. *Chem. Commun.* **2020,** *56*, 8436-8439.
124. Stateman, L. M.; Nakafuku, K. M.; Nagib, D. A. *Synthesis* **2018,** *50*, 1569-1586.
125. Gasc, M. B.; Lattes, A.; Perie, J. J. *Tetrahedron* **1983,** *39*, 703-731.
126. Horner, J. H.; Musa, O. M.; Bouvier, A.; Newcomb, M. *J. Am. Chem. Soc.* **1998,** *120*, 7738-7748.
127. Walton, J. C. *Acc. Chem Res.* **2014,** *47*, 1406-1416.
128. Pratley, C.; Fenner, S.; Murphy, J. A. *Chem. Rev.* **2022,** *122*, 8181–8260.
129. Hofmann, A. W. *Ber. Dtsch. Chem. Ges.* **1883,** *16*, 558-560.
130. Löffler, K.; Freytag, C. *Ber. Dtsch. Chem. Ges.* **1909,** *42*, 3427-3431.
131. Corey, E. J.; Hertler, W. R. *J. Am. Chem. Soc.* **1960,** *82*, 1657-1668.
132. Kwon, K.; Simons, R. T.; Nandakumar, M.; Roizen, J. L. *Chem. Rev.* **2022,** *122*, 2353-2428.
133. Ganley, J. M.; Murray, P. R. D.; Knowles, R. R. *ACS Catal.* **2020,** *10*, 11712-11738.
134. Walsh, C. T. *Tetrahedron Lett.* **2015,** *56*, 3075-3081.
135. Heravi, M. M.; Zadsirjan, V. *RSC Adv.* **2020,** *10*, 44247-44311.
136. Hosseinzadeh, Z.; Ramazani, A.; Razzaghi-Asl, N. *Curr. Org. Chem.* **2018,** *22*, 2256-2279.

137. Özkay, Y.; Işıkdağ, İ.; İncesu, Z.; Akalın, G. *Eur. J. Med. Chem.* **2010,** *45*, 3320-3328.

138. Ritchie, T. J.; Macdonald, S. J. F.; Peace, S.; Pickett, S. D.; Luscombe, C. N. *Med. Chem. Commun.* **2012,** *3*, 1062-1069.

139. Blakemore, D. C.; Castro, L.; Churcher, I.; Rees, D. C.; Thomas, A. W.; Wilson, D. M; Wood, A. *Nat. Chem.* **2018,** *10*, 383-394.

140. Lovering, F.; Bikker, J.; Humblet, C. *J. Med. Chem.* **2009,** *52*, 6752-6756.

141. Lovering, F. *Med. Chem. Commun.* **2013,** *4*, 515-519.

142. Brinkmann, C.; Barrett, A. G. M.; Hill, M. S.; Procopiou, P. A. *J. Am. Chem. Soc.* **2012,** *134*, 2193-2207.

143. Hill, M. S.; Liptrot, D. J.; Weetman, C. *Chem. Soc. Rev.* **2016,** *45*, 972-988.

144. Hannedouche, J.; Schulz, E. *Chem. Eur. J.* **2013,** *19*, 4972-4985.

145. Huang, L.; Arndt, M.; Gooßen, K.; Heydt, H.; Gooßen, L. J. *Chem. Rev.* **2015,** *115*, 2596-2697.

146. Trowbridge, A.; Walton, S. M.; Gaunt, M. J. *Chem. Rev.* **2020,** *120*, 2613-2692.

147. Wolfe, J. P.; Neukom, J. D.; Mai, D. H., *Catalyzed Carbon-Heteroatom Bond Formation*. Wiley-VCH Verlag GmbH: Weinheim **2010**.

148. Schultz, D. M.; Wolfe, J. P. *Synthesis* **2012,** *44*, 351-361.

149. Seifinoferest, B.; Tanbakouchian, A.; Larijani, B.; Mahdavi, M. *Asian J. Org. Chem.* **2021,** *10*, 1319-1344.

150. Sanjeeva Rao, K.; Wu, T.-S. *Tetrahedron* **2012,** *68*, 7735-7754.

151. Hong, S.; Marks, T. J. *Acc. Chem Res.* **2004,** *37*, 673-686.

152. Dong, S.; Chen, J.; Qiao, K.; Fang, J.; Yang, Y.; Maron, L.; Liu, B. *ACS Catal.* **2021,** *11*, 3790-3800.

153. Baldwin, J. E. *J. Chem. Soc., Chem. Commun.* **1976**, 734-736.

154. Duan, X. Y.; Yang, X. L.; Fang, R.; Peng, X. X.; Yu, W.; Han, B. *J. Org. Chem.* **2013,** *78*, 10692-10704.

155. Zhu, M.-K.; Chen, Y.-C.; Loh, T.-P. *Chem. Eur. J.* **2013,** *19*, 5250-5254.

156. Zhu, X.; Wang, Y.-F.; Ren, W.; Zhang, F.-L.; Chiba, S. *Org. Lett.* **2013,** *15*, 3214-3217.

157. Zhu, X.; Chiba, S. *Org. Biomol. Chem.* **2014,** *12*, 4567-4570.

158. Pünner, F.; Sohtome, Y.; Sodeoka, M. *Chem. Commun.* **2016,** *52*, 14093-14096.

159. Fan, Z.; Feng, J.; Hou, Y.; Rao, M.; Cheng, J. *Org. Lett.* **2020,** *22*, 7981-7985.

160. Lv, Y.; Meng, J.; Li, C.; Wang, X.; Ye, Y.; Sun, K. *Adv. Synth. Catal.* **2021,** *363*, 5235-5265.

161. Hu, X.-Q.; Chen, J.-R.; Wei, Q.; Liu, F.-L.; Deng, Q.-H.; Beauchemin, A. M.; Xiao, W.-J. *Angew. Chem. Int. Ed.* **2014,** *53*, 12163-12167.

162. Hu, X.-Q.; Chen, J.; Chen, J.-R.; Yan, D.-M.; Xiao, W.-J. *Chem. Eur. J.* **2016,** *22*, 14141-14146.

163. Hu, X.-Q.; Qi, X.; Chen, J.-R.; Zhao, Q.-Q.; Wei, Q.; Lan, Y.; Xiao, W.-J. *Nat. Commun..* **2016,** *7*, 11188.

164. Yu, X.-Y.; Zhao, Q.-Q.; Chen, J.; Xiao, W.-J.; Chen, J.-R. *Acc. Chem Res.* **2020,** *53*, 1066-1083.

165. Zhao, Q.-Q.; Chen, J.; Yan, D.-M.; Chen, J.-R.; Xiao, W.-J. *Org. Lett.* **2017,** *19*, 3620-3623.

166. Gao, Q.-S.; Niu, Z.; Chen, Y.; Sun, J.; Han, W.-Y.; Wang, J.-Y.; Yu, M.; Zhou, M.-D. *Org. Lett.* **2021,** *23*, 6153-6157.

167. Wei, Q.; Chen, J.-R.; Hu, X.-Q.; Yang, X.-C.; Lu, B.; Xiao, W.-J. *Org. Lett.* **2015,** *17*, 4464-4467.

168. Parisotto, S.; Garreffa, G.; Canepa, C.; Diana, E.; Pellegrino, F.; Priola, E.; Prandi, C.; Maurino, V.; Deagostino, A. *ChemPhotoChem* **2017,** *1*, 56-59.

169. Wermuth, C. G. *Med. Chem. Commun.* **2011,** *2*, 935-941.

170. Jaballah, M. Y.; Serya, R. T.; Abouzid, K. *Drug. Res.* **2017,** *67*, 138-148.

171. He, Z.-X.; Gong, Y.-P.; Zhang, X.; Ma, L.-Y.; Zhao, W. *Eur. J. Med. Chem.* **2021,** *209*, 112946.

172. Nagle, P.; Pawar, Y.; Sonawane, A.; Bhosale, S.; More, D. *Med. Chem. Res.* **2014,** *23*, 918-926. Lange, J. H. M.; den Hartog, A. P.; van der Neut, M. A. W.; van Vliet, B. J.; Kruse, C. G. *Bioorg. Med. Chem. Lett.* **2009,** *19*, 5675-5678. Palmer, S.; Campen, C. A.; Allan, G. F.; Rybczynski, P.; Haynes-Johnson, D.; Hutchins, A.; Kraft, P.; Kiddoe, M.; Lai, M.-T.; Lombardi, E.; Pedersen, P.; Hodgen, G.; Combs, D. W. *J. Steroid Biochem. Mol. Biol.* **2000,** *75*, 33-42. Zhi, L.; Marschke, K. B. *Expert Opin. Ther. Pat.* **1999,** *9*, 695-700. Rybczynski, P. J.; Combs, D. W.; Jacobs, K.; Shank, R. P.; Dubinsky, B. *J. Med. Chem.* **1999,** *42*, 2403-2408. Lijun, Z.; Williams, M. A.; Mendel, D. B.; Escarpe, P. A.; Xiaowu, C.; Wang, K.-Y.; Graves, B. J.; Lawton, G.; Kim, C. U. *Bioorg. Med. Chem. Lett.* **1999,** *9*, 1751-1756. Combs, D. W.; Reese, K.; Phillips, A. *J. Med. Chem.* **1995,** *38*, 4878-4879. Combs, D. W.; Reese, K.; Cornelius, L. A. M.; Gunnet, J. W.; Cryan, E. V.; Granger, K. S.; Jordan, J. J.; Demarest, K. T. *J. Med. Chem.* **1995,** *38*, 4880-4884.

173. Wang, W.; Meng, W.; Du, H. *Dalton Trans.* **2016,** *45*, 5945-5948.

174. Shen, L.-W.; Li, T.-T.; You, Y.; Zhao, J.-Q.; Wang, Z.-H.; Yuan, W.-C. *J. Org. Chem.* **2021,** *86*, 11472-11481. Arroyo, Y.; Rodríguez, J. F.; Santos, M.; Sanz Tejedor, M. A.; Vaca, I.; García Ruano, J. L. *Tetrahedron Asymmet.* **2004,** *15*, 1059-1063. Rossi, E.; Abbiati, G.; Attanasi, O. A.; Rizzato, S.; Santeusanio, S. *Tetrahedron* **2007,** *63*, 11055-11065. Lopes, S. M. M.; Brigas, A. F.; Palacios, F.; Lemos, A.; Pinho e Melo, T. M. V. D. *Eur. J. Org. Chem.* **2012,** *2012*, 2152-2160. Tong, M.-C.; Chen, X.; Li, J.; Huang, R.; Tao, H.; Wang, C.-J. *Angew. Chem. Int. Ed.* **2014,** *53*, 4680-4684. Yang, X.-L.; Peng, X.-X.; Chen, F.; Han, B. *Org. Lett.* **2016,** *18*, 2070-2073.

175. Du, Y. L.; Zhao, F.; Han, Z. Y.; Gong, L. Z. *Synthesis* **2016,** *49*, 151. Wu, Q.; Shao, P. L.; He, Y. *RSC Adv.* **2019,** *9*, 21507. Yin, W. H.; Fang, L.; Wang, Z. Y.; Gao, F.; Li, Z. F.; Wang, Z. Y. *Org. Lett.* **2019,** *21*, 7361. Huang, R.; Tao, H. Y.; Wang, C. J. *Org. Lett.* **2017,** *19*, 1176. Deng, Y. M.; Pei, C.; Arman, H.; Dong, K. Y.; Xu, X. F.; Doyle, M. P. *Org. Lett.* **2016,** *18*, 5884.

176. Mishra, M.; De, P. B.; Pradhan, S.; Punniyamurthy, T. *J. Org. Chem.* **2019,** *84*, 10901. Huo, H. R.; Runa, A.; Gong, Y. F. *J. Org. Chem.* **2019,** *84*, 2093.

177. Mboyi, C. D.; Abdellah, I.; Duhayon, C.; Canac, Y.; Chauvin, R. *ChemCatChem* **2013,** *5*, 3014. Guo, Y. J.; Zhao, J. B.; Zhang, Q. *Adv. Synth. Catal.* **2020,** *362*, 1208.

178. Guo, Y. Q.; Zhao, M. N.; Ren, Z. H.; Guan, Z. H. *Org. Lett.* **2018,** *20*, 3337.

179. Peng, X.; Kaga, A.; Hirao, H.; Chiba, S. *Org. Chem. Front.* **2016,** *3*, 609-613.

180. Jung, M. E.; Piizzi, G. *Chem. Rev.* **2005,** *105*, 1735-1766. Beesley, R. M.; Ingold, C. K.; Thorpe, J. F. *J. Chem. Soc., Trans.* **1915,** *107*, 1080-1106.

181. Wertjes, W. C.; Southgate, E. H.; Sarlah, D. *Chem. Soc. Rev.* **2018,** *47*, 7996-8017.

182. Roche, S. P.; Porco Jr., J. A. *Angew. Chem. Int. Ed.* **2011,** *50*, 4068-4093.

183. Zhao, Q.-Q.; Hu, X.-Q.; Yang, M.-N.; Chen, J.-R.; Xiao, W.-J. *Chem. Commun.* **2016,** *52*, 12749-12752.

184. McAtee, R. C.; Noten, E. A.; Stephenson, C. R. J. *Nat. Commun.* **2020,** *11*, 2528.

185. Henriques, R. *Ber. Dtsch. Chem. Ges.* **1894,** *27*, 2993-3005. Hinsberg, O. *J. Prakt. Chem.* **1916,** *93*, 277-301. Hinsberg, O. *J. Prakt. Chem.* **1914,** *90*, 345-353.

186. McClement, C. S.; Smiles, S. *J. Chem. Soc.* **1937**, 1016-1021. Galbraith, F.; Smiles, S. *J. Chem Soc.* **1935**, 1234-1238. Evans, W. J.; Smiles, S. *J. Chem. Soc.* **1935**, 181-188. Levi, A.; Warren, L. A.; Smiles, S. *J. Chem. Soc.* **1933**, 1490-1493. Warren, L. A.; Smiles, S. *J. Chem. Soc.* **1932**, 2774-2778. Warren, L. A.; Smiles, S. *J. Chem. Soc.* **1930**, 1327-1331.

187. Truce, W. E.; VanGemert, B.; Brand, W. W. *J. Org. Chem.* **1978,** *43*, 101-105. Truce, W. E.; Robbins, C. R.; Kreider, E. M. *J. Am. Chem. Soc.* **1966,** *88*, 4027-4033. Truce, W. E.; Hampton, D. C. *J. Org. Chem.* **1963,** *28*, 2276-2279. Truce, W. E.; Ray, W. J. *J. Am. Chem. Soc.* **1959,** *81*, 481-484. Truce, W. E.; Ray, W. J.; Norman, O. L.; Eickemeyer, D. B. *J. Am. Chem. Soc.* **1958,** *80*, 3625-3629.

188. Naito, T.; Dohmori, R.; Shimoda, M. *Pharm. Bull.* **1955,** *3*, 34-37. Naito, T.; Dohmori, R. *Pharm. Bull.* **1955,** *3*, 38-42. Naito, T.; Dohmori, R.; Kotake, T. *Chem. Pharm. Bull.* **1964,** *12*, 588-590. Dohmori, R. *Chem. Pharm. Bull.* **1964,** *12*, 591-594. Dohmori, R. *Chem. Pharm. Bull.* **1964,** *12*, 595-601. Dohmori, R. *Chem. Pharm. Bull.* **1964,** *12*, 601-606.

189. Snape, T. J. *Chem. Soc. Rev.* **2008,** *37*, 2452-2458.

190. Truce, W. E.; Kreider, E. M.; Brand, W. W., *Organic Reactions. The Smiles and Related Rearrangements of Aromatic Systems*. **2011**.

191. Henderson, A. R. P.; Kosowan, J. R.; Wood, T. E. *Can. J. Chem.* **2017,** *95*, 483-504.

192. Zawodny, W.; Montgomery, S. L.; Marshall, J. R.; Finnigan, J. D.; Turner, N. J.; Clayden, J. *J. Am. Chem. Soc.* **2018,** *140*, 17872-17877. Maury, J.; Zawodny, W.; Clayden, J. *Org. Lett.* **2017,** *19*, 472-475. Tait, M.; Donnard, M.; Minassi, A.; Lefranc, J.; Bechi, B.; Carbone, G.; O'Brien, P.; Clayden, J. *Org. Lett.* **2013,** *15*, 34-37. Tetlow, D. J.; Hennecke, U.; Raftery, J.; Waring, M. J.; Clarke, D. S.; Clayden, J. *Org. Lett.* **2010,** *12*, 5442-5445. Clayden, J.; Dufour, J.; Grainger, D. M.; Helliwell, M. *J. Am. Chem. Soc.* **2007,** *129*, 7488-7489.

193. Holden, C. M.; Greaney, M. F. *Chem. Eur. J.* **2017,** *23*, 8992-9008.

194. Allart-Simon, I.; Gérard, S.; Sapi, J. *Molecules* **2016,** *21*, 878.

195. Loven, R.; Speckamp, W. N. *Tetrahedron Lett.* **1972,** *13*, 1567-1570.

196. Motherwell, W. B.; Pennell, A. M. K. *J. Chem. Soc., Chem. Commun.* **1991**, 877-879.

197. Pudlo, M.; Allart-Simon, I.; Tinant, B.; Gérard, S.; Sapi, J. *Chem. Commun.* **2012,** *48*, 2442-2444.

198. Kong, W.; Casimiro, M.; Merino, E. b.; Nevado, C. *J. Am. Chem. Soc.* **2013,** *135*, 14480-14483.

199. Khartabil, H.; Doudet, L.; Allart-Simon, I.; Ponce-Vargas, M.; Gérard, S.; Hénon, E. *Org. Biomol. Chem.* **2020,** *18*, 6840-6848.
200. Chen, Z.-M.; Zhang, X.-M.; Tu, Y.-Q. *Chem. Soc. Rev.* **2015,** *44*, 5220-5245.
201. Allen, A. R.; Noten, E. A.; Stephenson, C. R. J. *Chem. Rev.* **2022,** *122*, 2695-2751.
202. Zheng, L.; Yang, C.; Xu, Z.; Gao, F.; Xia, W. *J. Org. Chem.* **2015,** *80*, 5730-5736.
203. Douglas, J. J.; Albright, H.; Sevrin, M. J.; Cole, K. P.; Stephenson, C. R. J. *Angew. Chem. Int. Ed.* **2015,** *54*, 14898-14902.
204. Li, Y.; Hu, B.; Dong, W.; Xie, X.; Wan, J.; Zhang, Z. *J. Org. Chem.* **2016,** *81*, 7036-7041.
205. Brachet, E.; Marzo, L.; Selkti, M.; König, B.; Belmont, P. *Chem. Sci.* **2016,** *7*, 5002-5006.
206. De Abreu, M.; Belmont, P.; Brachet, E. *J. Org. Chem.* **2021,** *86*, 3758-3767.
207. Hervieu, C.; Kirillova, M. S.; Suárez, T.; Müller, M.; Merino, E.; Nevado, C. *Nat. Chem.* **2021,** *13*, 327-334.
208. Lennox, A. J. J. *Angew. Chem. Int. Ed.* **2018,** *57*, 14686-14688.
209. Tu, J.-L.; Tang, W.; Liu, F. *Org. Chem. Front.* **2021,** *8*, 3712-3717.
210. Noten, E. A.; McAtee, R. C.; Stephenson, C. R. J. *Chem. Sci.* **2022**.
211. Naguib, Y. M. A.; Steel, C.; Cohen, S. G.; Young, M. A. *J. Phys. Chem.* **1987,** *91*, 3033-3036.
212. Li Petri, G.; Raimondi, M. V.; Spanò, V.; Holl, R.; Barraja, P.; Montalbano, A. *Top. Curr. Chem.* **2021,** *379*, 34.
213. Vardanyan, R., *Piperidine-Based Drug Discovery*. Elsevier: **2017**.
214. Vo, C.-V. T.; Bode, J. W. *J. Org. Chem.* **2014,** *79*, 2809-2815.
215. He, Y.; Zheng, Z.; Yang, J.; Zhang, X.; Fan, X. *Org. Chem. Front.* **2021,** *8*, 4582-4606.
216. Hantzsch, A. *Ber. Dtsch. Chem. Ges.* **1881,** *14*, 1637-1638. Paal, C. *Ber. Dtsch. Chem. Ges.* **1884,** *17*, 2756-2767. Knorr, L. *Ber. Dtsch. Chem. Ges.* **1884,** *17*, 2863-2870.
217. Antermite, D.; Bull, J. A. *Synthesis* **2019,** *51*, 3171-3204.
218. Li, C.-J. *Acc. Chem. Res.* **2009,** *42*, 335-344.
219. Doyle, M. P.; Duffy, R.; Ratnikov, M.; Zhou, L. *Chem. Rev.* **2010,** *110*, 704-724.
220. Beatty, J. W.; Stephenson, C. R. J. *Acc. Chem. Res.* **2015,** *48*, 1474-1484.
221. Jayaraj, R.; Megha, P.; Sreedev, P. *Interdiscip. Toxicol.* **2016,** *9*, 90-100.
222. Gribble, G. W. *Environ. Chem.* **2015,** *12*, 396-405. Gribble, G. W. *Acc. Chem. Res.* **1998,** *31*, 141-152.
223. Wilcken, R.; Zimmermann, M. O.; Lange, A.; Joerger, A. C.; Boeckler, F. M. *J. Med. Chem.* **2013,** *56*, 1363-1388.
224. Finkelstein, H. *Ber. Dtsch. Chem. Ges.* **1910,** *43*, 1528-1532.
225. Juliá, F.; Constantin, T.; Leonori, D. *Chem. Rev.* **2022,** *122*, 2292-2352.
226. Mendez, L.; Henriquez, G.; Sirimulla, S.; Narayan, M. *Molecules* **2017,** *22*, 1397.
227. Fang, W.-Y.; Ravindar, L.; Rakesh, K. P.; Manukumar, H. M.; Shantharam, C. S.; Alharbi, N. S.; Qin, H.-L. *Eur. J. Med. Chem.* **2019,** *173*, 117-153.
228. Nunnery, J. K.; Engene, N.; Byrum, T.; Cao, Z.; Jabba, S. V.; Pereira, A. R.; Matainaho, T.; Murray, T. F.; Gerwick, W. H. *J. Org. Chem.* **2012,** *77*, 4198-4208.
229. Johansson Seechurn, C. C. C.; Kitching, M. O.; Colacot, T. J.; Snieckus, V. *Angew. Chem. Int. Ed.* **2012,** *51*, 5062-5085.
230. Zeng, X.; Lu, Z.; Liu, S.; Hammond, G. B.; Xu, B. *J. Org. Chem.* **2017,** *82*, 13179-13187.
231. Liang, S.; Ebule, R.; Hammond, G. B.; Xu, B. *Org. Lett.* **2017,** *19*, 4524-4527.
232. Cao, W.; Chen, P.; Wang, L.; Wen, H.; Liu, Y.; Wang, W.; Tang, Y. *Org. Lett.* **2018,** *20*, 4507-4511.
233. Iwai, T.; Fujihara, T.; Terao, J.; Tsuji, Y. *J. Am. Chem. Soc.* **2012,** *134*, 1268-1274.
234. Yao, M.-L.; Quick, T. R.; Wu, Z.; Quinn, M. P.; Kabalka, G. W. *Org. Lett.* **2009,** *11*, 2647-2649.
235. Li, X.; Shi, X.; Fang, M.; Xu, X. *J. Org. Chem.* **2013,** *78*, 9499-9504.
236. Chen, J.-M.; Huang, X. *Synthesis* **2004,** *2004*, 1577-1580.
237. Snelders, D. J. M.; Dyson, P. J. *Org. Lett.* **2011,** *13*, 4048-4051.
238. Morrill, C.; Grubbs, R. H. *J. Org. Chem.* **2003,** *68*, 6031-6034.
239. Pawluć, P.; Hreczycho, G.; Szudkowska, J.; Kubicki, M.; Marciniec, B. *Org. Lett.* **2009,** *11*, 3390-3393.
240. Bull, J. A.; Mousseau, J. J.; Charette, A. B. *Org. Lett.* **2008,** *10*, 5485-5488.
241. Pan, J.; Wang, X.; Zhang, Y.; Buchwald, S. L. *Org. Lett.* **2011,** *13*, 4974-4976.
242. Molander, G. A.; Cavalcanti, L. N. *J. Org. Chem.* **2011,** *76*, 7195-7203.
243. Nitelet, A.; Kairouz, V.; Lebel, H.; Charette, A. B.; Evano, G. *Synthesis* **2019,** *51*, 251-257. Nitelet, A.; Evano, G. *Org. Lett,* **2016,** *18*, 1904-1907.

244. Casitas, A.; Ribas, X., *Copper-Mediated Cross-Coupling Reactions (Chapter 6: Aromatic/Vinylic Finkelstein Reaction)*. John Wiley & Sons, Inc.: Hoboken, NJ **2013**.
245. Kuang, C.; Senboku, H.; Tokuda, M. *Synlett* **2000,** *2000*, 1439-1442.
246. Naskar, D.; Chowdhury, S.; Roy, S. *Tetrahedron Lett.* **1998,** *39*, 699-702. Das, J. P.; Roy, S. *J. Org. Chem.* **2002,** *67*, 7861-7864.
247. Liu, L.; Zhang-Negrerie, D.; Du, Y.; Zhao, K. *Org. Lett.* **2014,** *16*, 436-439.
248. Wang, Y.; Lam, H. W. *J. Org. Chem.* **2009,** *74*, 1353-1355.
249. Koh, M. J.; Nguyen, T. T.; Zhang, H.; Schrock, R. R.; Hoveyda, A. H. *Nature* **2016,** *531*, 459-465.
250. Kim, K.-M.; Park, I.-H. *Synthesis* **2004,** *2004*, 2641-2644.
251. Zhang, X.-p.; Schlosser, M. *Tetrahedron Lett.* **1993,** *34*, 1925-1928.
252. Crane, E. A.; Zabawa, T. P.; Farmer, R. L.; Scheidt, K. A. *Angew. Chem. Int. Ed.* **2011,** *50*, 9112-9115.
253. Saputra, M. A.; Ngo, L.; Kartika, R. *J. Org. Chem.* **2015,** *80*, 8815-8820.
254. Su, W.; Jin, C. *Org. Lett.* **2007,** *9*, 993-996.
255. Yin, J.; Gallis, C. E.; Chisholm, J. D. *J. Org. Chem.* **2007,** *72*, 7054-7057.
256. Parisotto, S.; Azzi, E.; Lanfranco, A.; Renzi, P.; Deagostino, A. *Reactions* **2022,** *3*, 233-253.
257. Hering, T.; König, B. *Tetrahedron* **2016,** *72*, 7821-7825.
258. Rogers, D. A.; Gallegos, J. M.; Hopkins, M. D.; Lignieres, A. A.; Pitzel, A. K.; Lamar, A. A. *Tetrahedron* **2019,** *75*, 130498.
259. Rogers, D. A.; Hopkins, M. D.; Rajagopal, N.; Varshney, D.; Howard, H. A.; LeBlanc, G.; Lamar, A. A. *ACS Omega* **2020,** *5*, 7693-7704.
260. Rogers, D. A.; Bensalah, A. T.; Espinosa, A. T.; Hoerr, J. L.; Refai, F. H.; Pitzel, A. K.; Alvarado, J. J.; Lamar, A. A. *Org. Lett.* **2019,** *21*, 4229-4233.
261. Xiang, M.; Zhou, C.; Yang, X.-L.; Chen, B.; Tung, C.-H.; Wu, L.-Z. *J. Org. Chem.* **2020,** *85*, 9080-9087.
262. Pramanik, M.; Mathuri, A.; Sau, S.; Das, M.; Mal, P. *Org. Lett.* **2021,** *23*, 8088-8092.
263. Dauncey, E. M.; Morcillo, S. P.; Douglas, J. J.; Sheikh, N. S.; Leonori, D. *Angew. Chem. Int. Ed.* **2018,** *57*, 744-748.
264. Wang, F.; Liu, X.; Wang, L. *Org. Biomol. Chem.* **2021,** *19*, 6141-6146.
265. Zhu, Y.; Wang, J.-J.; Wu, D.; Yu, W. *Asian J. Org. Chem.* **2020,** *9*, 1650-1654.
266. Parisotto, S.; Palagi, L.; Prandi, C.; Deagostino, A. *Chem. Eur. J.* **2018,** *24*, 5484-5488. Boi, T.; Deagostino, A.; Prandi, C.; Tabasso, S.; Toppino, A.; Venturello, P. *Org. Biomol. Chem.* **2010,** *8*, 2020-2027. Deagostino, A.; Prandi, C.; Toppino, A.; Venturello, P. *Tetrahedron* **2008,** *64*, 10344-10349.
267. Deagostino, A.; Prandi, C.; Tabasso, S.; Venturello, P. *Curr. Org. Chem.* **2010,** *14*, 230-263. Deagostino, A.; Prandi, C.; Tabasso, S.; Venturello, P. *Molecules* **2010,** *15*, 2667-2685. Parisotto, S.; Deagostino, A. *Synthesis* **2019,** *51*, 1892-1912.
268. Renzi, P.; Azzi, E.; Bessone, E.; Ghigo, G.; Parisotto, S.; Pellegrino, F.; Deagostino, A. *Org. Chem. Front.* **2022,** *9*, 906-916.
269. Singh, J.; Sharma, A.; Sharma, A. *Org. Chem. Front.* **2021,** *8*, 5651-5667.
270. Liu, L.; Ward, R. M.; Schomaker, J. M. *Chem. Rev.* **2019,** *119*, 12422-12490. Qiu, G.; Zhang, J.; Zhou, K.; Wu, J. *Tetrahedron* **2018,** *74*, 7290-7301.
271. Liu, L.; Ward, R. M.; Schomaker, J. M. *Chem. Eur. J.* **2020,** *26*, 13783-13787.
272. Ward, R. M.; Schomaker, J. M. *J. Org. Chem.* **2021,** *86*, 8891-8899.
273. Davies, J.; Svejstrup, T. D.; Fernandez Reina, D.; Sheikh, N. S.; Leonori, D. *J. Am. Chem. Soc.* **2016,** *138*, 8092-8095.
274. Brummond, K. M.; DeForrest, J. E. *Synthesis* **2007,** *2007*, 795-818. Huang, X.; Ma, S. *Acc. Chem Res.* **2019,** *52*, 1301-1312.
275. Ruffoni, A.; Juliá, F.; Svejstrup, T. D.; McMillan, A. J.; Douglas, J. J.; Leonori, D. *Nat. Chem.* **2019,** *11*, 426-433.
276. Song, S.; Li, X.; Wei, J.; Wang, W.; Zhang, Y.; Ai, L.; Zhu, Y.; Shi, X.; Zhang, X.; Jiao, N. *Nat. Catal.* **2020,** *3*, 107-115.
277. Davies, J.; Sheikh, N. S.; Leonori, D. *Angew. Chem. Int. Ed.* **2017,** *56*, 13361-13365.
278. Quinn, R. K.; Könst, Z. A.; Michalak, S. E.; Schmidt, Y.; Szklarski, A. R.; Flores, A. R.; Nam, S.; Horne, D. A.; Vanderwal, C. D.; Alexanian, E. J. *J. Am. Chem. Soc.* **2016,** *138*, 696-702.
279. Carestia, A. M.; Ravelli, D.; Alexanian, E. J. *Chem. Sci.* **2018,** *9*, 5360-5365.
280. Tierney, M. M.; Crespi, S.; Ravelli, D.; Alexanian, E. J. *J. Org. Chem.* **2019,** *84*, 12983-12991.
281. Armarego, W. L. F., *Purification of laboratory chemicals*. Butterworth-Heinemann: **2017**.

296

282. Sheldrick, G. *Acta Cryst.* **2008,** *64*, 112-122.

283. Sheldrick, G. *Acta Cryst.* **2015,** *71*, 3-8.

284. Macrae, C. F.; Bruno, I. J.; Chisholm, J. A.; Edgington, P. R.; McCabe, P.; Pidcock, E.; Rodriguez-Monge, L.; Taylor, R.; van de Streek, J.; Wood, P. A. *J. Appl. Cryst.* **2008,** *41*, 466-470.

285. Dolomanov, O. V.; Bourhis, L. J.; Gildea, R. J.; Howard, J. A. K.; Puschmann, H. *J. Appl. Cryst.* **2009,** *42*, 339-341.

286. Li, L.; Liu, P.; Su, Y.; Huang, H. *Org. Lett.* **2016,** *18*, 5736-5739.

287. Otera, J.; Fujita, Y.; Sakuta, N.; Fujita, M.; Fukuzumi, S. *J. Org. Chem.* **1996,** *61*, 2951-2962.

288. Harris, M. R.; Konev, M. O.; Jarvo, E. R. *J. Am. Chem. Soc.* **2014,** *136*, 7825-7828.

289. Ma, W.; Xue, D.; Yu, T.; Wang, C.; Xiao, J. *Chem. Commun.* **2015,** *51*, 8797-8800.

290. Wittenberg, R.; Srogl, J.; Egi, M.; Liebeskind, L. S. *Org. Lett.* **2003,** *5*, 3033-3035.

291. Yu, T.; Zhu, Q.; Luo, S. *Tetrahedron Lett.* **2020,** *61*, 151887.

292. Von Fraunberg, K. *Ger. Patent* **1976**.

293. Duan, X.-Y.; Yang, X.-L.; Jia, P.-P.; Zhang, M.; Han, B. *Org. Lett.* **2015,** *17*, 6022-6025.

294. Morita, M.; Sakaguchi, S.; Ishii, Y. *J. Org. Chem.* **2006,** *71*, 6285-6286.

295. Shaw, P.; Hassell-Hart, S. J.; Douglas, G. E.; Malcolm, A. G.; Kennedy, A. R.; White, G. V.; Paterson, L. C.; Kerr, W. J. *Org. Lett.* **2022,** *24*, 2750-2755.

296. Campbell, C. D.; Greenaway, R. L.; Holton , O. T.; Walker, P. R.; Chapman, H. A.; Russell, C. A.; Carr, G.; Thomson, A. L.; Anderson, E. A. *Chem. Eur. J.* **2015,** *21*, 12627-12639.

297. Kislukhin, A. A.; Higginson, C. J.; Hong, V. P.; Finn, M. G. *J. Am. Chem. Soc.* **2012,** *134*, 6491-6497.

298. Broggini, G.; Poli, G.; Beccalli, E. M.; Brusa, F.; Gazzola, S.; Oble, J. *Adv. Synth. Catal.* **2015,** *357*, 677-682.

299. Ye, J.; Li, S.; Chen, B.; Fan, W.; Kuang, J.; Liu, J.; Liu, Y.; Miao, B.; Wan, B.; Wang, Y.; Xie, X.; Yu, Q.; Yuan, W.; Ma, S. *Org. Lett.* **2012,** *14*, 1346-1349.

300. Jonasson, C.; Horváth, A.; Bäckvall, J.-E. *J. Am. Chem. Soc.* **2000,** *122*, 9600-9609.

301. Zelenay, B.; Munton, P.; Tian, X.; Díez-González, S. *Eur. J. Org. Chem.* **2019,** *2019*, 4725-4730.

302. Berthold, D.; Geissler, A. G. A.; Giofré, S.; Breit, B. *Angew. Chem. Int. Ed.* **2019,** *58*, 9994-9997.

303. Schmidt, J. P.; Breit, B. *Angew. Chem. Int. Ed.* **2020,** *59*, 23485-23490.

304. Joseph E. Burchick. Jr., S. M. W., Kay M. Brummond. *Org. Synth.* **2017**, 109-122.

305. Yang, C.-H.; Han, M.; Li, W.; Zhu, N.; Sun, Z.; Wang, J.; Yang, Z.; Li, Y.-M. *Org. Lett.* **2020,** *22*, 5090-5093.

306. Dzandzi, J. P. K.; Beckford Vera, D. R.; Genady, A. R.; Albu, S. A.; Eltringham-Smith, L. J.; Capretta, A.; Sheffield, W. P.; Valliant, J. F. *J. Org. Chem.* **2015,** *80*, 7117-7125.

307. Shaw, R. W.; Gallagher, T. *J. Chem. Soc., Perkin Trans. 1* **1994**, 3549-3555.

Acknowledgements

Affrontare un dottorato non è semplice. Non posso dire che sia la sfida più difficile della mia vita, anche per rispetto nei confronti dei veri momenti di difficoltà nella vita di ognuno. Tuttavia, è una sfida per la quale mi sono spesso sentito poco preparato, poco all'altezza, poco allenato.

Le persone che mi hanno istruito, che hanno fatto in modo che colmassi questa lacuna di preparazione, loro sono le ragioni per la quale sono riuscito ad affrontarla fino alla fine. Devo quindi ringraziare la mia relatrice, la professoressa Annamaria Deagostino *in primis* poiché ha creduto in me, affidandomi questa responsabilità, insegnandomi a gestirla e guidandomi fino alla fine, senza mai smettere di motivarmi. A lei accosto il Dottor Stefano Parisotto, il mio secondo mentore scientifico, colui che per primo mi ha avvicinato all'idea di un dottorato, della ricerca, colui che mi ha insegnato a trovare la passione nella chimica organica e, come Annamaria, ha davvero fatto in modo di fornirmi tutti gli strumenti necessari per affrontare il dottorato. Ringrazio la Dottoressa Polyssena Renzi, per il suo modello esemplare, che mi ha insegnato la vera professionalità in questo lavoro, la gestione della rigidità e del rigore necessari per portare a termine un compito con efficienza. Colgo questa occasione per scusarmi con tutti e tre i miei mentori scientifici qualora a volte possa essere sembrato irrispettoso, remissivo o semplicemente non abbia imparato abbastanza. Penso che fosse solo una conseguenza del fatto che non potessi piegare tramite la prepotenza le leggi della chimica a mio favore, come a volte riuscivo a fare con le leggi del gioco nello sport. Vi ringrazio per la pazienza comunque dimostrata nei miei confronti.

Ringrazio il Dottor Francesco Pellegrino, collaboratore e amico e ringrazio Alberto Lanfranco, prima tesista e poi dottorando nel gruppo di Annamaria, sempre in grado di portare la giusta dose di professionalità e risate nel gruppo. Entrambi ringrazio non solo come colleghi, ma anche e soprattutto per aver saputo essere dei grandi amici nei momenti in cui ne avevo bisogno, pur rimanendo all'interno delle mura dell'università.

Ultimi ma non meno importanti, coloro che fuori dal laboratorio hanno saputo sostenermi: le persone che non hanno mai potuto realmente prepararmi a ciò che stavo affrontando ma che hanno fornito ogni supporto fisico e morale. Ringrazio quindi i miei genitori, Rosa e Leo, e mio fratello Michele, le uniche vere ragioni per cui ho potuto continuare a coltivare il mio livello di istruzione fino al dottorato, anche loro hanno sempre creduto in me e in quello che facevo e senza il loro supporto e la loro educazione non sarei mai arrivato a questo punto. Ringrazio poi la mia ragazza Giorgia, sempre al mio fianco, l'unica in grado di rendere belli non solo i momenti migliori, ma soprattutto quelli più complicati di questi tre anni, un porto sicuro in ogni momento burrascoso, una compagna magnifica. Ringrazio nuovamente Stefano, questa volta in veste di amico, per tutte le volte (la maggior parte) in cui ha abbandonato il suo ruolo di mentore e abbracciato quello di amico disinteressato, fuori dal e dentro al laboratorio, per il supporto e la comprensione come e anche più di molti altri. Infine, al mio "fratello acquisito" Filippo, per il quale credo davvero non servano altro che le poche parole per dirgli "ti ringrazio".